

FINAL PHASE 1 RESEARCH REPORT

Federal Agency and Organization: DOE EERE – Geothermal Technologies Program

Recipient Organization: Cornell University

DUNS Number: 872612445

Recipient Address: Attn: Cathy Long
373 Pine Tree Road,
Office of Sponsored Programs,
Ithaca, NY 148502820

Award Number: DE-EE0006726

Project Title: Low Temperature Geothermal Play Fairway Analysis for the Appalachian Basin

Project Period: October 1, 2014 – September 30, 2016

Principal Investigator: Teresa E. Jordan
J. Preston Levis Professor of Engineering
tej1@cornell.edu
607-255-3596

Report Submitted by: Teresa E. Jordan

Date of Report Submission: November 18, 2016

Reporting Period: October 1, 2014 – September 30, 2016

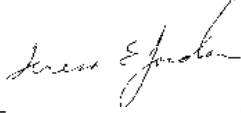
Report Frequency: Final (revised)

Project Partners: **Cornell University** – Teresa Jordan, Frank Horowitz, Jery Stedinger, Jefferson Tester, Erin Camp, Calvin Whealton, Jared Smith;

West Virginia University – Brian Anderson, Kelydra Welcker, Xiaoning He;

Southern Methodist University – Maria Richards, Cathy Chickering Pace, Matt Hornbach, Zachary Frone, Christine Ferguson, Rahmi Bolat, Maria Beatrice Magnani.

DOE Project Team: Contracting Officer – Michael A. Buck
Project Officer – Holly Thomas
Project Monitors – Eve Sprunt, Janell Edman, Dick Benoit

Signature  _____ **Date November 18, 2016**

*The Prime Recipient certifies that the information provided in this report is accurate and complete as of the date shown.

Distribution Limitations: This report may be distributed without limitation provided the Section of Phase 2 Recommendations with cost estimates has been removed.

TABLE OF CONTENTS

TABLE OF CONTENTS.....	2
LIST OF FIGURES AND TABLES.....	3
EXECUTIVE SUMMARY	7
Data Sources and Project Flow	9
Thermal Resource Quality	10
Natural Reservoir Quality	11
Seismicity.....	11
Utilization Opportunities.....	11
Combined Risk Metric	12
SUMMARY OF PROJECT ACTIVITIES	15
Original Project Hypotheses	15
Approaches Used	15
Accomplishments and Challenges	17
Task 1 Thermal Resource Quality Assessment.....	18
Task 2 Natural Reservoir Quality	28
Task 3 Risk of Seismicity	32
Task 4 Utilization Assessment.....	36
Task 5 Combined Risk Metric Analysis	40
Utility of the Methods for Application at other Sites.....	45
Commercial Viability of the Play	45
METHODOLOGY	47
DISCUSSION OF RESULTS.....	52
Primary Conclusions	52
Thermal Analysis	52
Reservoir Favorability/Productivity Analysis.....	52
Seismic Risk Analysis.....	54
Utilization Analysis	54
Combination of Risk Analysis	57
Comparison of Actual Accomplishments with Original Goals and Objectives	69
RECOMMENDATIONS FOR FURTHER ANALYSIS	71
Description of Objectives and Outcomes of Recommended Studies.....	71
Description of Recommended Activities	71
REFERENCES	75

LIST OF FIGURES AND TABLES

FIGURE 1: POPULATION DENSITY (U.S. CENSUS BUREAU, 2010) WITHIN THE APPALACHIAN BASIN REGION (SHUMAKER, 1996) HIGHLIGHTING THE LARGER CITIES. THE BLACK POLYGON SHOWS THE BOUNDARY OF THE NORTHERN PART OF THE APPALACHIAN BASIN.	8
FIGURE 2: APPALACHIAN BASIN GEOTHERMAL PLAY FAIRWAY ANALYSIS PROCESS. EACH OF FOUR KEY RISK FACTORS STUDIED IN THE CONTEXT OF FAVORABILITY AND UNCERTAINTY WERE COMBINED USING PLAY FAIRWAY METRICS (PFM) TO CREATE FINAL PLAY MAPS AND OVERALL BASIN RISK.	9
FIGURE 3: WELL LOCATIONS COLORED BY DEPTH OF THE BHT MEASUREMENT, AND BHT CORRECTION REGIONS USED IN THIS PROJECT. COUNTY AND STATE OUTLINES ARE SHOWN. FOR QUALITY REASONS, ONLY THOSE BHT MEASUREMENTS AT DEPTHS GREATER THAN 1000 M WERE RETAINED FOR ANALYSIS.	10
FIGURE 4: INDIVIDUAL RISK FACTOR MAPS AND THE COMBINED PLAY FAIRWAY METRIC MAPS ARE EXPRESSED AS A FIVE-POINT SCALE (SHOWN HERE) AND A SIMILAR THREE-POINT SCALE.	12
FIGURE 5: THE MOST FAVORABLE PLAY FAIRWAYS WITHIN THE APPALACHIAN BASIN BASED ON THIS PROJECT SYNTHESIS OF ALL RISK FACTORS AS OF PHASE 1. PLAY FAIRWAYS ARE NAMED FOR ONE OR MORE POPULATION CENTERS WITHIN THEM. ALL BUT THE PITTSBURGH PLAY FAIRWAY ARE SUBDIVIDED INTO AN INNER FAIRWAY (HIGH PRIORITY) AND OUTER FAIRWAY (MEDIUM PRIORITY) REGIONS, BASED ON THE COMBINED RISK ANALYSIS. INDIVIDUAL POTENTIAL USERS SHOULD REFER TO THE SET OF COMBINED RISK MAPS THAT BEST FITS THEIR CRITERIA BECAUSE THE COMBINED RISK FACTORS ARE HIGHLY HETEROGENEOUS WITHIN EACH FAIRWAY.	14
FIGURE 6: A) PREDICTED MEAN DEPTH TO 80 °C BASED UPON THERMAL ANALYSIS. THE SUB-REGIONS WITHIN THE BASIN ARE BOUNDARIES FOR THE SPATIALLY STRATIFIED KRIGING INTERPOLATION OF THE THERMAL FIELD PROPERTIES. B) UNCERTAINTY ON THE DEPTH TO 80 °C EXPRESSED AS STANDARD DEVIATION.	20
FIGURE 7: COUNTIES SELECTED FOR MORE DETAILED THERMAL MAPS BASED UPON HAVING FAVORABLE THERMAL PROPERTIES, AVAILABLE RESERVOIRS, AND POPULATION CENTERS.	20
FIGURE 8: ERIE, PA AND CHAUTAUQUA, NY (PREDICTED MEAN DEPTH TO 80 °C [M]) WITH CROSS SECTION.	21
FIGURE 9: VARIABILITY AND UNCERTAINTY IN THE PREDICTED MEAN DEPTH TO 80 °C ALONG CROSS SECTION C-C'. INTERPOLATION BOUNDARIES ARE MARKED BY VERTICAL DOTTED LINES. MEAN DEPTHS ARE SIGNIFICANTLY DIFFERENT WHEN UNCERTAINTY BARS DO NOT OVERLAP.	21
FIGURE 10: FAYETTE, PA AND PRESTON, WV (PREDICTED MEAN DEPTH TO 80 °C [M]) WITH CROSS SECTION.	22
FIGURE 11: VARIABILITY AND UNCERTAINTY IN THE PREDICTED MEAN DEPTH TO 80 °C ALONG CROSS SECTION D-D'. INTERPOLATION BOUNDARIES ARE MARKED BY VERTICAL DOTTED LINES. MEAN DEPTHS ARE SIGNIFICANTLY DIFFERENT WHEN UNCERTAINTY BARS DO NOT OVERLAP.	22
FIGURE 12: KANAWHA AND LINCOLN, WV (PREDICTED MEAN DEPTH TO 80 °C [M]) WITH CROSS SECTION.	23
FIGURE 13: VARIABILITY AND UNCERTAINTY IN THE PREDICTED MEAN DEPTH TO 80 °C ALONG CROSS SECTION E-E'. INTERPOLATION BOUNDARIES ARE MARKED BY VERTICAL DOTTED LINES. MEAN DEPTHS ARE SIGNIFICANTLY DIFFERENT WHEN UNCERTAINTY BARS DO NOT OVERLAP.	23
FIGURE 14: GILMER, WV (PREDICTED MEAN DEPTH TO 80 °C [M]) WITH CROSS SECTION.	24
FIGURE 15: VARIABILITY AND UNCERTAINTY IN THE PREDICTED MEAN DEPTH TO 80 °C ALONG CROSS SECTION F-F'. INTERPOLATION BOUNDARIES ARE MARKED BY VERTICAL DOTTED	

LINES. MEAN DEPTHS ARE SIGNIFICANTLY DIFFERENT WHEN UNCERTAINTY BARS DO NOT OVERLAP.....24

FIGURE 16: PREDICTED MEAN DEPTH TO 80 °C [M]) WITH CROSS SECTION FOR CHEMUNG, STEUBEN, AND TOMKINS COUNTIES OF NY AND POTTER AND TIOGA COUNTIES OF PA.25

FIGURE 17: VARIABILITY AND UNCERTAINTY IN THE PREDICTED MEAN DEPTH TO 80 °C ALONG CROSS SECTION G-G'. INTERPOLATION BOUNDARIES ARE MARKED BY VERTICAL DOTTED LINES. MEAN DEPTHS ARE SIGNIFICANTLY DIFFERENT WHEN UNCERTAINTY BARS DO NOT OVERLAP.25

FIGURE 18: WELLS CONSIDERED EQUILIBRIUM OR HAVING RELIABLE TEMPERATURE DATA ARE COMPARED TO PREDICTED TEMPERATURES AT 1.5 KM DEPTH. COLORS OF CIRCLES SHOW DIFFERENCES IN MEASURED AND PREDICTED TEMPERATURE AT 1.5 KM IN TERMS OF THE NUMBER OF STANDARD ERRORS THAT THE EQUILIBRIUM TEMPERATURE WAS FROM THE PREDICTED MEAN.26

FIGURE 19: PLAY FAIRWAY METRIC RISK SEGMENT MAP FOR THE THERMAL RESOURCE WITH A FIVE COLOR SCHEME. GREEN-FAVORABLE, RED-UNFAVORABLE.27

FIGURE 20: HISTOGRAMS OF THE P50 RPIW (BLUE) AND RPIG (BROWN) FREQUENCIES OF RESERVOIRS IN THE APPALACHIAN BASIN. THE P50 EXPRESSES THE MOST LIKELY CASE GIVEN THE SET OF 100,000 MONTE CARLO REALIZATIONS FOR EACH RESERVOIR. THE FREQUENCIES ARE ORDERED BY THE RESERVOIR PRODUCTIVITY INDICES (KG/MPA-S).29

FIGURE 21: DISTRIBUTION OF RESERVOIRS OF VARYING DEGREES OF FAVORABILITY AS MEASURED BY THE RESERVOIR FAVORABILITY METRICS: RPIW ON THE UPPER LEFT, RPIG IN THE UPPER RIGHT, AND RFC IN THE LOWER LEFT. THE GRAY AREAS INDICATE REGIONS WITHOUT SUITABLE DATA, BECAUSE OF THE DATA BIAS TOWARD OIL AND GAS PRODUCTION. WITHIN THE GRAY AREAS THERE MAY EXIST HIGH QUALITY NATURAL RESERVOIRS, AND UNDOUBTEDLY THERE EXIST REGIONS WITHOUT SUITABLE NATURAL RESERVOIRS. TO DISCRIMINATE THOSE TWO CASES IN THE AREAS WITHOUT OIL OR GAS FIELDS REQUIRES ANALYSIS BEYOND THE SCOPE OF PHASE 1.30

FIGURE 22: PLAY FAIRWAY METRIC RISK SEGMENT MAP FOR THE RESERVOIR RESOURCE WITH A FIVE COLOR SCHEME. GREEN-FAVORABLE, RED-UNFAVORABLE. THIS MAP DISPLAYS THE RESULT BASED ON THE METRIC RESERVOIR FLUID CAPACITY (RFC).31

FIGURE 23: MAP OF SPATIAL VARIABILITY OF THE RISK OF INDUCED SEISMICITY BASED ON THE PROXIMITY OF EACH LOCATION IN THE STUDY AREA TO A RECORDED SEISMIC EVENT AND/OR THE CO-OCCURRENCE OF A “WORM” AND A NEARBY SEISMIC EVENT. RED INDICATES HIGHEST RISK; GREEN IS LOWEST RISK.33

FIGURE 24: MAP OF THE SPATIAL VARIABILITY OF RISK OF INDUCED SEISMICITY ESTIMATED BASED ON SLIP-TENDENCY, AS CALCULATED BY THE PREMISES OF THE LOCATIONS OF PLANES OF WEAKNESS RELATIVE TO THE REGIONAL STRESS FIELD. FOR THIS ANALYSIS, THE “WORMS” ARE TREATED AS IF THEY ARE ALL PLANES OF WEAKNESS, AND BYERLEE’S LAW CRITERIA USED.34

FIGURE 25: PREFERRED MAP OF THE SPATIAL DISTRIBUTION OF RISK OF INDUCED SEISMICITY, CREATED BY AVERAGING THE PROXIMITY AND SLIP-TENDENCY TECHNIQUES.35

FIGURE 26: PLAY FAIRWAY METRIC RISK SEGMENT MAP FOR THE UTILIZATION OF RESOURCE WITH A FIVE COLOR SCHEME. GREEN-FAVORABLE, RED-UNFAVORABLE.39

FIGURE 27: EXAMPLE OF A PARALLEL AXIS PLOT FOR NINE ILLUSTRATIVE PROJECT LOCATIONS. THE RESERVOIR METRIC ILLUSTRATED IS RFC AND THE RISK FACTOR COMBINATION METHOD IS THE AVERAGE. THE PLOT EMPHASIZES WHICH SITES TEND TO PERFORM BETTER ON THE METRICS OR IF THERE ARE TRADEOFFS BETWEEN OBJECTIVES. THIS EXAMPLE ILLUSTRATES THE USE OF RESERVOIR FLUID CAPACITY AS THE RESERVOIR METRIC.42

FIGURE 28: BOXPLOTS OF THE ESTIMATED EMPIRICAL DISTRIBUTION OF FAVORABILITY FOR THE THREE GEOLOGIC VARIABLES FOR NINE ILLUSTRATIVE PROJECT LOCATIONS, FOR COMBINATIONS BASED ON AVERAGING THE INDIVIDUAL RISK FACTORS. THE RESERVOIR METRIC USED IS RFC. THE DISTRIBUTION AT EACH SITE REPORTS THE RESULTS OF A MONTE

CARLO SIMULATION. THE BOX IS DEFINED AS BETWEEN THE 25TH AND 75TH PERCENTILES WITH A LINE AT THE MEDIAN. THE WHISKERS EXTEND TO THE MOST EXTREME OBSERVATION THAT IS WITHIN 1.5 TIMES THE INTERQUARTILE RANGE FROM THE UPPER OR LOWER QUARTILE. POINTS OUTSIDE THE WHISKERS ARE PLOTTED INDIVIDUALLY.43

FIGURE 29: GRAPH SHOWING THE RELATIVE OUTCOMES OF THE THREE DIFFERENT COMBINATION FUNCTIONS, FOR THE GEOLOGIC FACTORS ONLY. FM REFERS TO THE PLAY FAIRWAY METRIC. NOTE THAT FMAVG (PFMAVG) ALWAYS EXCEEDS FMGM (PFMGM), WHICH ARE GREATER THAN FMMIN (_PFMMIN), AND FOR ALL OF THE FAVORABILITY FACTORS AT SELECTED SITES. LINES REPRESENT APPROXIMATE 90% PROBABILITY INTERVALS (5TH TO 95TH PERCENTILE). PIS ARE BASED ON THE WEIBULL DISTRIBUTION FOR FMMIN, THE LOG-NORMAL DISTRIBUTION FOR FMGM, AND THE NORMAL DISTRIBUTION FOR FMAVG. NOTE THAT THE UNCERTAINTY IS OFTEN GREATEST FOR THE FUNCTION OF MINIMUM. THE REPORTED FM IS MARKED WITH AN 'X'. FROM WHEALTON (2016), BASED ON ANALYSIS OF THE NEAR-FINAL DATA SET.44

FIGURE 30: APPALACHIAN BASIN GEOTHERMAL PLAY FAIRWAY ANALYSIS PROCESS. EACH OF FOUR KEY RISK FACTORS STUDIED IN THE CONTEXT OF FAVORABILITY AND UNCERTAINTY WERE COMBINED USING PLAY FAIRWAY METRICS (PFM) TO CREATE FINAL PLAY MAPS AND OVERALL BASIN RISK.48

FIGURE 31: FLOW CHART FOR TASK 1 THERMAL RESOURCES RISK SHOWING PRIMARY DATA AND OVERVIEW OF STEPS.49

FIGURE 32: FLOW CHART FOR TASK 2 NATURAL RESERVOIRS RISK SHOWING PRIMARY DATA AND OVERVIEW OF STEPS.49

FIGURE 33: FLOW CHART FOR TASK 3 RISK OF SEISMICITY SHOWING PRIMARY DATA AND OVERVIEW OF STEPS.50

FIGURE 34: FLOW CHART FOR TASK 4 UTILIZATION ASSESSMENT SHOWING PRIMARY DATA AND OVERVIEW OF STEPS.50

FIGURE 35: FLOW CHART FOR TASK 5 COMBINING RISK METRICS SHOWING AN OVERVIEW OF MAIN STEPS AND METHODS FOR PRODUCING FAVORABILITY MAPS.51

FIGURE 36: FREQUENCY OF SURFACE LEVELIZED COST OF HEAT AMONG CENSUS PLACES IN THE APPALACHIAN BASIN THAT HAVE POPULATIONS >4000. OF THE TWO COLORED LINES AT BOTTOM, THE UPPER ONE SHOWS THE THRESHOLD SLCOH VALUES CORRESPONDING TO THE FIVE COLORS OF THE FIGURE 34 MAP.55

FIGURE 37: UTILIZATION RISK SEGMENT MAP (WITH 5-KM RADIUS BUFFERS AROUND PLACES). GREEN IS FAVORABLE (LOWER SLCOH) AND RED IS HIGHER SLCOH). SEE FIGURE 33 FOR THE THRESHOLD SLCOH VALUES BETWEEN COLORS.56

FIGURE 38: A) FAVORABILITY MAP FOR THE COMBINATION OF ALL FOUR RISK FACTORS USING AN AVERAGE, FOR THE RESERVOIR METRIC RPIW. GREEN-FAVORABLE, RED-UNFAVORABLE. B) UNCERTAINTY ON THE COMBINED RISK EXPRESSED AS STANDARD DEVIATION. DARKER TONES INDICATE LESS UNCERTAINTY.58

FIGURE 39: FAVORABILITY MAP FOR THE COMBINATION OF ALL FOUR RISK FACTORS USING THE GEOMETRIC MEAN, FOR THE RESERVOIR METRIC RPIW. GREEN-FAVORABLE, RED-UNFAVORABLE.59

FIGURE 40: FAVORABILITY MAP FOR THE COMBINATION OF ALL FOUR RISK FACTORS, FOR THE RESERVOIR METRIC RPIW, USING THE MINIMUM VALUE. GREEN-FAVORABLE, RED-UNFAVORABLE.60

FIGURE 41: FAVORABILITY MAP FOR THE COMBINATION OF THE THREE GEOLOGIC RISK FACTORS, FOR RFC AS THE RESERVOIR METRIC, USING AN AVERAGE. GREEN-FAVORABLE, RED-UNFAVORABLE.61

FIGURE 42: FAVORABILITY MAP FOR THE COMBINATION OF THE THREE GEOLOGIC RISK FACTORS, FOR RFC AS THE RESERVOIR METRIC, USING A GEOMETRIC MEAN. GREEN-FAVORABLE, RED-UNFAVORABLE.62

FIGURE 43: FAVORABILITY MAP FOR THE COMBINATION OF THE THREE GEOLOGIC RISK FACTORS, FOR RFC AS THE RESERVOIR METRIC, USING THE MINIMUM. GREEN-FAVORABLE, RED-UNFAVORABLE.63

FIGURE 44: COMPARISON OF THE FAVORABILITY MAP FOR THE COMBINATION OF THE FIRST THREE GEOLOGIC RISK FACTORS (FOR RPIW AS THE RESERVOIR METRIC) USING THE AVERAGE, TO THE LOCATIONS OF THE UTILIZATION INDIVIDUAL SITES. GREEN-FAVORABLE, RED-UNFAVORABLE.64

FIGURE 45. MAP OF THE TEMPERATURE PREDICTED AT A DEPTH OF 1.5 KM DEPTH BELOW THE LOCAL EARTH SURFACE THROUGHOUT THE STUDY AREA. SUPERIMPOSED ARE THE LOCATIONS OF RESERVOIR ROCKS IN THE RANGE OF DEPTH BELOW THE SURFACE OF 1000–2000 M, BASED ON OIL OR GAS PRODUCTION. FOR THOSE RESERVOIRS, THE RESERVOIR QUALITY METRIC BASED ON RPIW FOR A 5-POINT NON-DIMENSIONAL SCALE IS INDICATED BY THE COLOR OF THE SURROUNDING POLYGON: A BLACK LINE INDICATES A RESERVOIR RISK FACTOR OF 4 OR 5; A GRAY LINE INDICATES A RESERVOIR RISK FACTOR OF 3.65

FIGURE 46. MAP OF THE TEMPERATURE PREDICTED AT A DEPTH OF 2.5 KM DEPTH BELOW THE LOCAL EARTH SURFACE THROUGHOUT THE STUDY AREA. SUPERIMPOSED ARE THE LOCATIONS OF RESERVOIR ROCKS IN THE RANGE OF DEPTH BELOW THE SURFACE OF 2000–3000 M, BASED ON OIL OR GAS PRODUCTION. FOR THOSE RESERVOIRS, THE RESERVOIR QUALITY METRIC BASED ON RPIW FOR A 5-POINT NON-DIMENSIONAL SCALE IS INDICATED BY THE COLOR OF THE SURROUNDING POLYGON: A BLACK LINE INDICATES A RESERVOIR RISK FACTOR OF 4 OR 5; A GRAY LINE INDICATES A RESERVOIR RISK FACTOR OF 3.66

FIGURE 47. MAP OF THE TEMPERATURE PREDICTED AT A DEPTH OF 3.5 KM DEPTH BELOW THE LOCAL EARTH SURFACE THROUGHOUT THE STUDY AREA. SUPERIMPOSED ARE THE LOCATIONS OF RESERVOIR ROCKS IN THE RANGE OF DEPTH BELOW THE SURFACE OF 3000–4000 M, BASED ON OIL OR GAS PRODUCTION. FOR THOSE RESERVOIRS, THE RESERVOIR QUALITY METRIC BASED ON RPIW FOR A 5-POINT NON-DIMENSIONAL SCALE IS INDICATED BY THE COLOR OF THE SURROUNDING POLYGON: A BLACK LINE INDICATES A RESERVOIR RISK FACTOR OF 4 OR 5; A GRAY LINE INDICATES A RESERVOIR RISK FACTOR OF 3.67

FIGURE 48: COMPARISON OF THE GEOLOGY-ONLY RISK FACTORS, USING RFC AS THE RESERVOIR METRIC, A) COMBINED BY THE AVERAGE METHOD, AND B) COMBINED BY THE GEOMETRIC MEAN METHOD. GREEN-FAVORABLE; RED-UNFAVORABLE.68

TABLE 1: DISTRIBUTION OF SURFACE LEVELIZED COST OF HEAT (SLCOH) FOR CENSUS PLACES WITH POPULATION $\geq 4,000$ WITHIN THE APPALACHIAN BASIN FOR NY, PA AND WV. OF 248 SITES EVALUATED, 12 SITES ARE OMITTED FROM THIS TABLE BECAUSE THEIR SLCOH VALUES EXCEEDED 25 \$/MMBTU.37

TABLE 2: TOP TEN WEST VIRGINIA CENSUS PLACES WITH THE LOWEST SLCOH. ONLY PLACES WITH POPULATION OF 4,000 AND ABOVE ARE INCLUDED.37

TABLE 3: TOP TEN NEW YORK CENSUS PLACES WITH THE LOWEST SLCOH. ONLY PLACES WITH POPULATION OF 4,000 AND ABOVE ARE INCLUDED.38

TABLE 4: TOP TEN PENNSYLVANIA CENSUS PLACES WITH THE LOWEST SLCOH. ONLY PLACES WITH POPULATION OF 4,000 AND ABOVE ARE INCLUDED.38

TABLE 5: SUMMARY OF FIVE PLAY FAIRWAYS AND RECOMMENDATIONS FOR NEXT INVESTIGATION STEPS.73

LOW TEMPERATURE GEOTHERMAL PLAY FAIRWAY ANALYSIS FOR THE APPALACHIAN BASIN: PHASE 1 REVISED REPORT NOVEMBER 18, 2016

EXECUTIVE SUMMARY

Geothermal energy is an attractive sustainable energy source. Yet project developers need confirmation of the resource base to warrant their time and financial resources. The hydrocarbon industry has addressed exploration and development complexities through use of a technique referred to as Play Fairway Analysis (PFA). The PFA technique assigns risk metrics that communicate the favorability of potential hydrocarbon bearing reservoirs in order to enable prudent allocation of exploration and development resources.

The purpose of this Department of Energy funded effort is to apply the PFA approach to geothermal exploration and development, thus providing a technique for Geothermal Play Fairway Analysis (GPFA). This project focuses on four risk factors of concern for direct-use geothermal plays in the Appalachian Basin (AB) portions of New York, Pennsylvania, and West Virginia (Figure 1). These risk factors are 1) thermal resource quality, 2) natural reservoir quality, 3) induced seismicity, and 4) utilization opportunities (Figure 2). This research expands upon and updates methodologies used in previous assessments of the potential for geothermal fields and utilization in the Appalachian Basin, and also introduces novel approaches and metrics for quantification of geothermal reservoir productivity in sedimentary basins. Unique to this project are several methodologies for combining the risk factors into a single commensurate objective that communicates the estimated overall favorability of geothermal development. Uncertainty in the risk estimation is also quantified. Based on these metrics, geothermal plays in the Appalachian Basin were identified as potentially viable for a variety of direct-use-heat applications. The methodologies developed in this project may be applied in other sedimentary basins as a foundation for low temperature (50-150 °C), direct use geothermal resource, risk, and uncertainty assessment. Through our identification of plays, this project reveals the potential for widespread assessment of low-temperature geothermal energy from sedimentary basins as an alternative to current heating sources that are unsustainable.

There is an important distinction in this Geothermal Play Fairway Analysis project as compared to hydrothermal projects: this Appalachian Basin analysis is focused on the direct use of the heat, rather than on electricity production. Lindal (1973) illuminated numerous industrial and other low-temperature applications of geothermal energy for which this analysis can be useful. The major relationship to electricity is that direct-use applications reduce the electricity requirements for a region. Even though all of the geothermal resources in the Appalachian Basin are low grade, the high heating demand across New York, Pennsylvania, and West Virginia combined with the numerous populations centers translate into economic advantages if geothermal direct-use heating replaces electricity-based heating. The advantage is derived from the high efficiency of extracting heat from geothermal fluids rather than using the fluids to generate electricity (Tester et al., 2015).

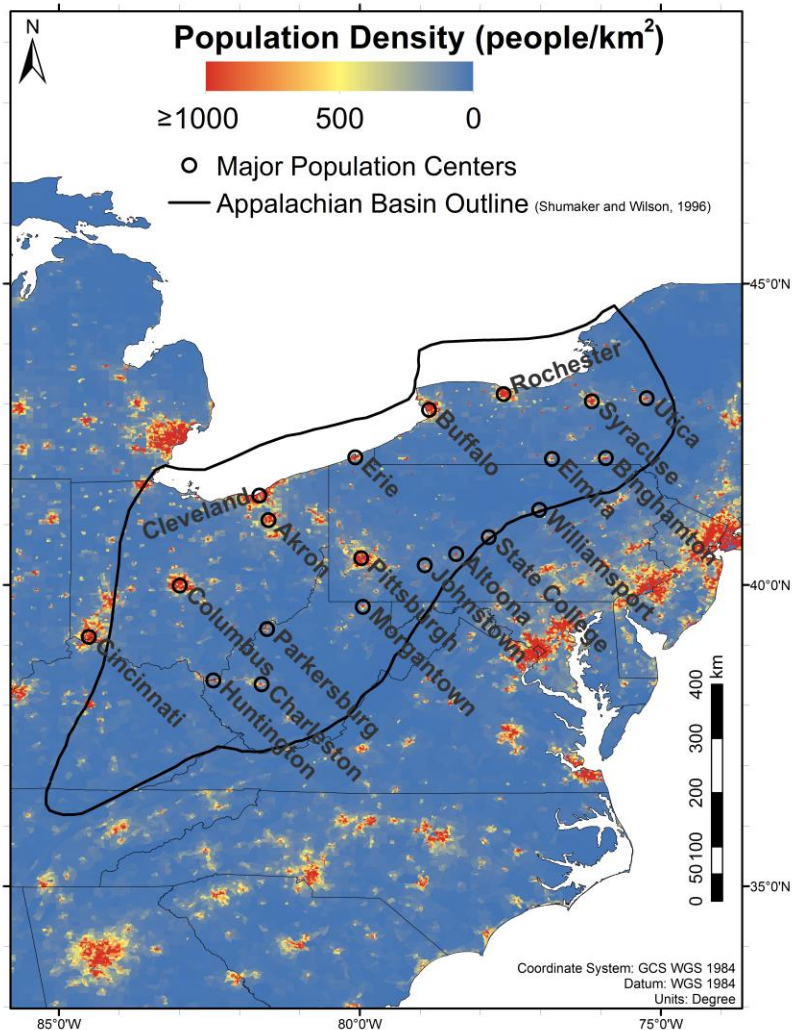


Figure 1: Population density (U.S. Census Bureau, 2010) within the Appalachian Basin region (Shumaker, 1996) highlighting the larger cities. The black polygon shows the boundary of the northern part of the Appalachian Basin.

The Geothermal Play Fairway Analysis of the Appalachian Basin is valuable for several reasons:

1. The fact that the Appalachian Basin is a sedimentary basin with a history of substantial hydrocarbon drilling activity increases the accessibility of knowledge about the subsurface thermal field and reservoirs. GPFA techniques developed here could be applied in other sedimentary basins with ample publicly available hydrocarbon drilling records around the U.S., such as the Williston Basin, Sacramento Basin, San Joaquin Basin, Gulf Coast Basin, Black Warrior Basin, Denver Basin, Anadarko Basin, Illinois Basin, Michigan Basin and others.
2. The Appalachian Basin, like most of the U.S. east of the Rocky Mountains, is considered a 'low temperature' geothermal area. Some low temperature geothermal areas are suitable for direct-use applications (e.g., district heating, greenhouses, aquaculture, and industrial processes, such as pasteurization) or coproduction, but not for electricity generation alone. Because low-temperature geothermal resources are more common than high grade in the U.S., this project is important

beyond its regional footprint for its development of analysis methods applicable to direct use low-temperature geothermal projects across the U.S.

3. Several major population centers located within the Appalachian Basin concentrate the demand for heat in small areas. These include Pittsburgh, PA; Williamsport, PA; State College, PA; Morgantown, WV; Charleston, WV; Buffalo, NY; Syracuse, NY; and Rochester, NY (Figure 1).
4. Space heating and cooling of homes is the #1 use of the residential consumption of produced electrical energy in the U.S. (U.S. Energy Information Administration, 2015). This project explores the possibility that communities in the Appalachian Basin may be able to employ geothermal district heating to relieve the growing stress on the electric power grid.

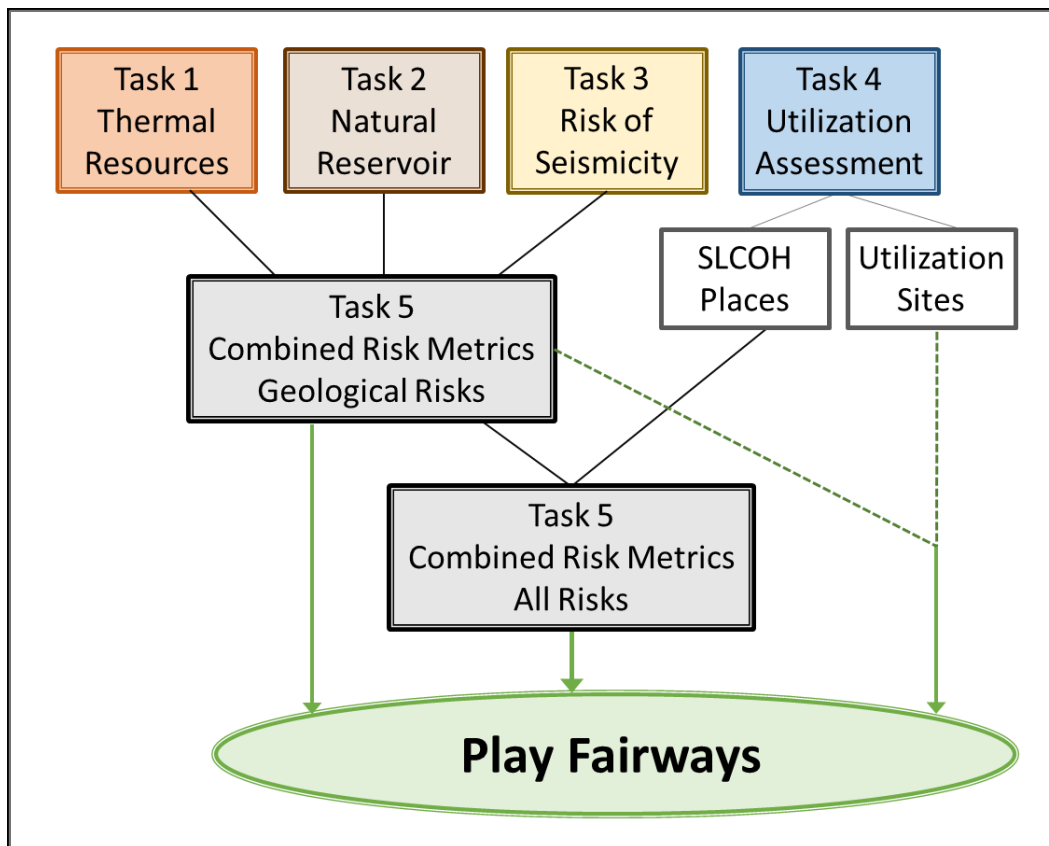


Figure 2: Appalachian Basin Geothermal Play Fairway Analysis Process. Each of four key risk factors studied in the context of favorability and uncertainty were combined using Play Fairway Metrics (PFM) to create final Play maps and evaluate the overall basin risk.

Data Sources and Project Flow

The team began by characterizing the constraints to developing a geothermal project that must be managed in an integrated fashion. These constraints were treated as four categories of risk: 1) Thermal Resource Quality, 2) Natural Reservoir Quality, 3) Risk of Seismic Activity, and 4) Utilization Viability. Each risk was quantified, as was the uncertainty associated with the resultant risk value. These four risk factors were then combined (Figure 2) into a single metric that was used to determine the most favorable fairways within the Appalachian Basin.

To conduct a quantitative analysis, we utilized data collected as part of previous national and state research efforts, as well as data from the National Geothermal Data System; the Midwest Regional

Carbon Sequestration Partnership; New York, Pennsylvania and West Virginia State geologic, oil and gas well data provided by the State Geological Surveys and by their oil and gas regulatory bodies; NOAA Climate data; NEIC and EarthScope (TA) seismicity data; regional-scale magnetic map; regional-scale gravity map; US Census Bureau population data; and Energy Information Agency power consumption data.

Thermal Resource Quality

Appalachian Basin temperature data from oil and gas bottom-hole temperatures (BHTs) are abundant (Figure 3) but of low quality. This project generated a new set of BHT corrections appropriate for this basin. At the location of each well, the corrected BHT was combined with generalized thermal conductivity stratigraphy to estimate the local geotherm using a 1-D heat conduction model. Analyses of local spatial outliers were performed on the geotherms, followed by a spatially stratified ordinary Kriging regression that predicted properties of the thermal field and its lateral variations. A sensitivity analysis on the input variables to the heat conduction model revealed that BHTs are the most critical input variable for quantifying properties of the thermal field. Overall, these methods resulted in higher quality results and a more robust evaluation of the uncertainty than previous studies.

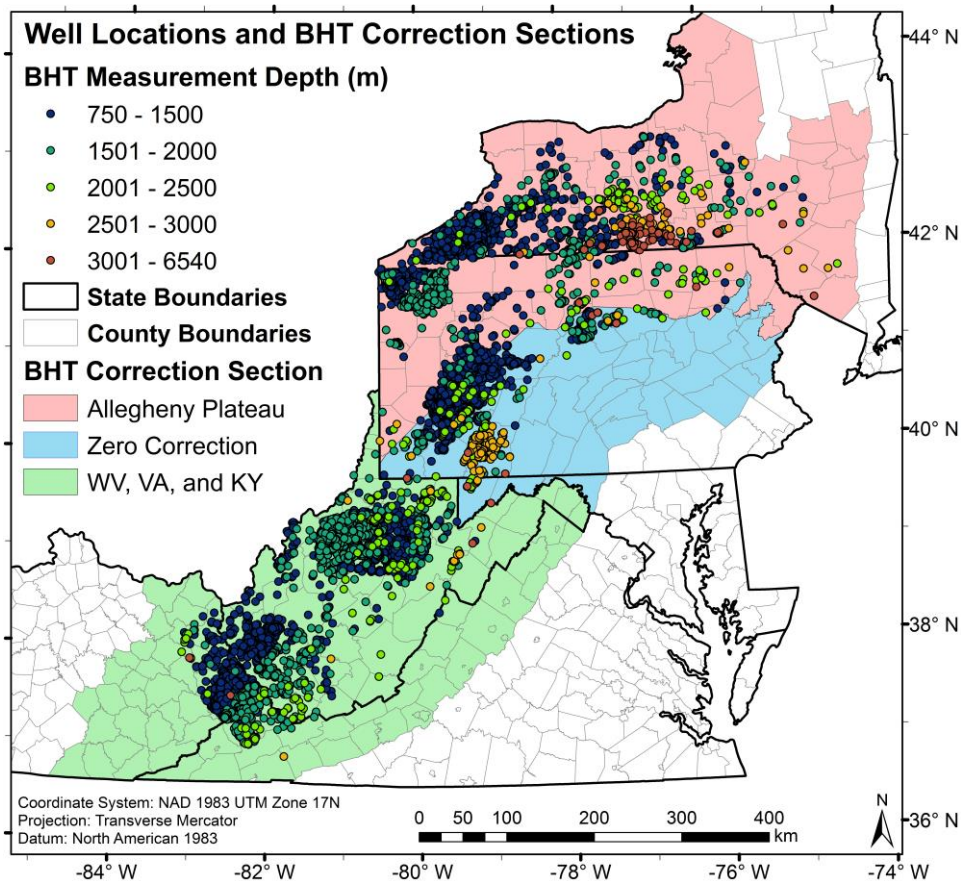


Figure 3: Well locations colored by depth of the BHT measurement, and BHT correction regions used in this project. County and state outlines are shown. For quality reasons, only those BHT measurements at depths greater than 1000 m were retained for analysis except for a small region in NW Pennsylvania where BHT's as shallow as 750 m were included.

Natural Reservoir Quality

The Appalachian Basin's conventional hydrocarbon fields and its unconventional shale reservoirs have been extensively studied (Engelder, Lash, & Uzcátegui, 2009; Nelson, 2009). In the second task, Natural Reservoir Quality analysis, we examined the suitability of rocks to function as natural reservoirs, which necessitate sufficient water flow rates between injection wells and production wells to harvest heat within the reservoir. This procedure included additional independent methods to predict permeability using information from carbon sequestration studies and porosity data, both overlapped with oil and gas exploration and production datasets. Some of the most vital data are very scarce in public records: permeability values, pressure data, and production data. The oil and gas reservoir property records are spatially biased toward those locations with profitable amounts of hydrocarbons in the rock pore spaces. This bias ought *not* be shared by this project's search for *water* in pore spaces, although the existing data cause persistence of this bias. The spatial bias and the lack of permeability and/or flow data impose a severe limit on the completeness of the reservoir assessment that was possible in Phase 1. The locations of the natural reservoirs and lateral variations in reservoir properties reported here must be considered with the understanding that there exist potential errors that are not quantified due to lack of data and because our data base focused on oil/gas rather than on formations with water. Indeed, more data could identify additional reservoirs.

Seismicity

With the extent of ongoing induced earthquake activity in several states (Oklahoma, Texas, Kansas, Ohio) and the potential for similar activity in portions of the Appalachian Basin, it is expected that the public will require an informed risk assessment in advance of undertaking a new type of energy extraction work in the subsurface. To anticipate this concern, we examined the options for a regional analysis to identify sub-regions that may be more or less at risk for slip along planes of weakness in the rocks. Acknowledging that data for such a task are insufficient, we utilized what was available: records of seismic activity, regional estimates of the orientations of principal stress directions, and locations and orientations of zones identified on gravity and magnetic data as sites of lateral change in rock properties at depths down to several kilometers below Earth's surface. Analysis of those data sets highlight areas within the basement that have higher or lower sensitivities to fluid pressure changes. With these data, we created a first approximation of spatially variable risks for induced earthquakes.

Utilization Opportunities

Economically viable projects for low-temperature direct-use geothermal heat must be located near the field where the hot water is extracted to limit thermal losses and excessive pumping costs. Therefore, for the Utilization risk factor we worked principally with population density as a regionally known variable. For this economic analysis, we employed a previously developed model by Beckers et al. (2014), GEOPHIRES (GEOthermal energy for Production of Heat and Electricity ["IR"] Economically Simulated), with variations to capture the surface costs associated with delivering heat from a wellhead to final consumers through a district heating system. The Utilization maps do not include the costs of producing the hot water at the well head, because the below-ground costs are directly coupled to the spatial variability of the heat resource and the reservoir properties, which are factors treated under the Thermal Resource risk and Natural Reservoir risks. The result of the district heating analysis is provided as a surface levelized cost of heat (SLCOH). Because we have now identified potential plays, the cost of heat delivery for individual locations within the plays, including all of the components needed to compute a true levelized cost of heat, should be calculated during a follow-up study. In addition to district heating, we located institutions and businesses that utilize large amounts of thermal energy at low temperatures across the three-state study area. These represent additional utilization opportunities for the region that should be investigated in more detail in future studies.

Combined Risk Metric

The final task developed and assigned a Combined Risk solution to incorporate each of the four project risk factors using a set of Play Fairway Metrics (PFMs). This task identified the most favorable locations within the study area to examine with additional scrutiny. The four individual risk factors were assigned favorability ratings from 0 – 5, with 0 unfavorable (red), 3 moderately favorable (yellow) and 5 favorable (green) (Figure 4) Several techniques were used to compute the combined risk metric at each location using a grid resolution of 1 km². These methods included using the average of individual risk factor favorability ratings, the geometric mean of individual favorability ratings, or the minimum (least favorable) value of the four risk favorability ratings. There is value in considering the outcomes of each of these methods:

1. The averaging approach highlights areas that appear favorable overall, but does not inform a decision maker if any given risk factor is unfavorable at a location.
2. The minimum value approach highlights the most unfavorable rating of the four risk factors, but does not inform a decision maker of how much more favorable are other risk factors.
3. The geometric mean approach highlights those few areas that are favorable in all four risk factors, but highly down-weights those areas that are even slightly less favorable.

Overall the average and geometric mean approaches rapidly identify areas for which additional study to reduce uncertainty related to any one of the risk factors is most warranted. The minimum value approach highlights the fact that there are some sites for which the minimum of the geologic risk factors (thermal, reservoir, seismic) is favorable, but no place where the existing results warrant immediate investment in commercialization

While it is almost impossible for analysts to say which method is best, the information conveyed by these methods is useful for the decision maker to consider in assessing their site, or when comparing sites for development. Where all three PFM methods are favorable, these sites are most robust as potential plays; however, uncertainty in each metric should also be considered while making a decision. Each individual risk is accompanied by a map of the uncertainty, which was then included as part of the final PFM.

Very Unfavorable	Unfavorable	Neutral		Favorable	Very Favorable				
0.0	1.0	1.0	2.0	2.0	3.0	3.0	4.0	4.0	5.0
Threshold 1		Threshold 2		Threshold 3		Threshold 4			

Figure 4: Individual Risk Factor maps and the combined Play Fairway Metric maps are expressed as a five-point scale (shown here) and a similar three-point scale. The thresholds are selected at values that correspond to differences in favorability of the risk factors.

The set of PFMs that combine all four risk factors highlight the spatial lay-out of existing population centers. Areas of low population density are matched by low favorability ratings, irrespective of their geological resources.

The geologic risk factors (thermal, reservoir, and seismic), when combined into a set of PFMs, emphasize the fixed natural-system properties that must be accommodated by engineering designs for well fields and for utilization scenarios. The advantage of the 3-factor geology-only PFMs is that they identify areas that a stakeholder group would find suitable for creation of a new industrial, commercial, or residential activity that utilizes the geothermal heat. These geology-only-PFMs express the fact that the Geothermal Play Fairway team cannot anticipate all possible thermal utilization scenarios that may interest a

particular future user group. This natural resource information can be combined in future studies with not only direct costs but also indirect benefits, such as reduced use of fossil fuels, regulatory considerations, or tax incentives, to develop more comprehensive descriptions of the spatial variation of costs and benefits.

There are five Play Fairways that we recommend be of highest priority for further investigation (Figure 5). The five designated Play Fairways are multi-county regions in which there are generally favorable combinations of some of the factors, but within each Play Fairway there is a high degree of spatial variability. Decision-makers should look at the detailed maps of the combined risk metrics that are most applicable to the type of geothermal system and type of use that most closely fit their criteria, and use that combined risk metric set as the basis for further investment. Technological progress in the extraction of geothermal heat from the rock reservoirs is one example in which future users of this report may find that the most favorable choices for their potential project differ from the reservoir attribute on which this research group focused in selecting the Fairways.

The Corning-Ithaca Play Fairway (mostly in New York) includes locations with especially favorable overall scores and small degrees of uncertainty, and warrants investigation to better determine the full costs of heat delivery as well as to determine the spatial extent of the high quality reservoirs. The Morgantown-Clarksburg Play Fairway (West Virginia), the Meadville–Jamestown Play Fairway (mostly in Pennsylvania) and the Charleston Play Fairway (West Virginia) also have favorable scores for most of the four risk factors, and deserve more in-depth analysis than was within the scope of this Phase 1 project. The Pittsburgh Play Fairway is a region of very few deep wells and therefore scant data for the subsurface depths at which the temperature exceeds 50 °C. Given the large utilization potential near the city of Pittsburgh, we recommend a more focused study of the deepest wells in order to better evaluate the potential for deep natural reservoirs.

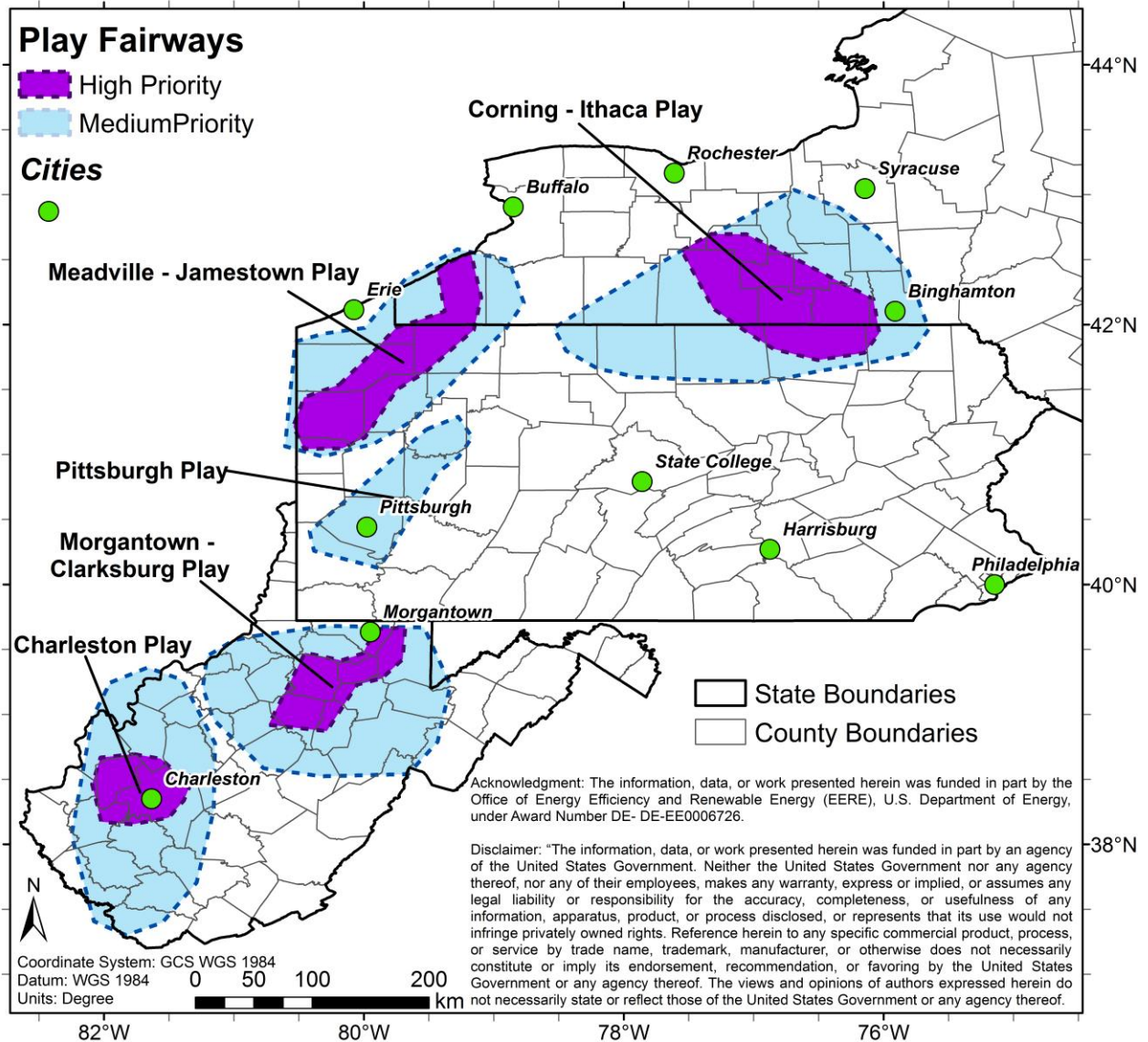


Figure 5: The most favorable Play Fairways within the Appalachian Basin based on this project synthesis of all Risk Factors as of Phase 1. Play fairways are named for one or more population centers within them. All but the Pittsburgh Play Fairway are subdivided into an inner fairway (high priority) and outer fairway (medium priority) regions, based on the combined risk analysis. Individual potential users should refer to the set of combined risk maps that best fits their criteria because the combined risk factors are highly heterogeneous within each Fairway.

SUMMARY OF PROJECT ACTIVITIES

Original Project Hypotheses

Given the characteristic stable-continent heat flows associated with the Appalachian Basin (Blackwell & Richards, Geothermal Map of North America; Explanation of Resources and Applications, 2004), the **resource is presumed to be suitable for lower temperature, direct-use geothermal applications**. The extensive hydrocarbon extraction in the vicinity affords prolific bottom-hole temperature (BHT) data with which to assess the thermal field, as well as oil and gas production data that are useful in determining other key geothermal reservoir characteristics, such as porosity and permeability. These **oil and gas industry data will be useful in modeling the sedimentary basin's suitability** for lower temperature, direct-use type geothermal applications, in terms of both heat resources and reservoir characteristics. Because project viability includes other factors, including risk of seismicity, population distribution, and demand for heat, these and other criteria will also be incorporated into an **economic viability model, used to inform the next step of project development**.

This report is organized into the following sections:

- Summary of Project Activities: original project hypotheses, approaches used, problems encountered, departure from planned methodology, and impact on project results.
- Methodology: underlying scientific theory and key assumptions, steps in the workflow, summary of the strengths and limitations of the process, mathematics used (including formulas and calculation methods), potential sources of error, software used, and results of tests to demonstrate satisfactory model performance.
- Discussion of Results: primary conclusions, comparison of actual accomplishments with original goals and objectives, risk factor and related error/uncertainty maps, and final favorability maps.
- Recommendations for Further Analysis Phase: objectives and outcomes, description of planned activities (SOPO tasks), partners identified and roles, timeline, preliminary budget information, and anticipated permitting requirements.
- Catalog of Supporting Files: a list of datasets used including the source(s), limitations on rights, and any operations performed on the data to prepare them for use), custom code/scripts/configuration files used to process data, GIS databases, risk factor maps and final favorability maps (as images and in georeferenced format). This section also includes a series of 'Project Memos' detailing major project tasks and methods, which will be useful for other researchers.
- References: Major works cited in this report. The Catalog of Supporting Files contains more detailed documents with additional references provided.

Approaches Used

The Statement of Project Objectives (SOPO) outlines the Phase 1 Project Plan as a series of seven Tasks, each with several subtasks, as summarized below. Tasks 1-5 comprise the primary research activities in Phase 1 and Tasks 6-7 are related to project management and outreach (Figure 2). Specific research details, equations, and methods are provided within the Catalog of Supporting Files section of this report. The plan was followed very closely, with only minor adjustments needed, as described in the next section, Accomplishments and Challenges. The following is the condensed list of our original major SOPO Tasks and a description of each one. For the full detailed list that includes all the subtasks, milestones, and deliverables, see the Catalog of Supporting Files document, SOPOTasksMilestones.pdf.

1. **Task 1.0 Thermal Resource Quality Assessment:** The purpose of this task and its several subtasks are to research and assemble the available thermal data in the published literature as well as thermal data available from non-published sources, to establish the data infrastructure for the project, and to carry out the assessment of the first of the proposed Risk Factors (RF1), Thermal Resource Quality.

Task 1 Deliverable: Deliver an improved region-wide map of depths to 80 °C isotherm and a county map for four counties per state, as well as a Green-Yellow-Red-ranked thermal resource map for the region and for the four counties per state, as derived from all the considerations described in Task 1, including lithologies, updated conductivity, and updated basement heat flux model, etc. as well as the supporting data according to the Data Management Plan and thermal models for the New York (NY), Pennsylvania (PA) and West Virginia (WV) region of the Appalachian Basin.

2. **Task 2.0 Natural Reservoir Quality:** The purpose of this task is to develop the supporting database to evaluate and map the distribution of potential geothermal reservoirs. The result will be Ranking Maps and supporting data for natural reservoirs in a majority of the Appalachian Basin of WV, NY and PA.

Task 2 Deliverable: Deliver reservoir quality maps, supporting data and related models for the NY, PA and WV region of the Appalachian Basin incorporating information such as reservoir quality and variability, porosity, permeability, and hydraulic conductivity.

3. **Task 3.0 Risk of Seismicity:** The purpose of this task is to review seismicity (excluding enhanced geothermal systems –EGS) as a Risk Factor and identify regions with enhanced likelihood for inducing unintended seismic activity during preparation of a reservoir, or during the course of geothermal heat production. The result of the task will be maps for the study area in the Appalachian Basin in NY, PA and WV of potential faults and of faults that are active.

Task 3 Deliverable: Deliver risk map, supporting data according to the Data Management Plan, and related models, for the NY, PA and WV region of the Appalachian Basin for induced or reactivated seismicity, incorporating fault positions and seismicity activity.

4. **Task 4.0 Utilization Variability:** The purpose of this task is to identify regions in the Appalachian Basin with the capacity to utilize low-grade geothermal heat and the related variability of demand. The result of the task will be utilization maps for the region of the Appalachian Basin in NY, PA and WV and estimates of Levelized Cost of Heat for a small set of communities.

Task 4 Deliverable: Deliver maps for spatial variability of population and heat demand, and a ranked map for utilization using supporting data according to the Data management Plan, for the NY, PA and WV region of the Appalachian Basin. Deliver estimated Levelized Cost of Heat (LCOH) for two communities in each state.

5. **Task 5.0 Risk Matrix Analysis:** The purpose of this task is to merge the risk segment maps described above to produce an overall risk map. This will be the compilation of factors and the most favorable combinations of multiple risk factors from the Risk Factors evaluated in Tasks 1-4. A risk matrix will be applied to combine the four sets of risk factors and will identify up to six “most promising Play Fairways” within the Appalachian Basin in NY, PA and WV.

Task 5 Deliverable: Deliver common risk assessment map, which delineates up to 6 Play Fairways within the NY, PA and WV region of the Appalachian Basin based upon the compilation of the spatial variability of the risk factors assessed in Tasks 1-4. The models and available supporting data, according to the Data Management Plan, will also be delivered.

- Task 6.0 Project Management and Reporting:** The three team leaders (Cornell, SMU, WVU) will interact bi-weekly to assure continued progress on the project. At each quarter's end, available team members will meet by conference call or in person to discuss project progress and needs. Quarterly project reviews will be held with DOE staff by phone or webinar to present project status and verify milestones. One quarterly review will be made in-person at the Geothermal Technology Office peer review (tentatively scheduled for spring 2015 in Denver).

Task 6 Deliverable A final report detailing all facets of the study and detailed suggestions for Phase II will be presented at the end of Phase 1. This report will be the basis for a competitive downselect process for Phase 2. The raw data collected and/or new data generated as part of the project will be uploaded to the NGDS at the end of the Phase I, following USGIN metadata guidelines.

- Task 7.0 Commercialization / Market Transformation:** Commercialization activities are to include 1) participation in a poster session at the Geothermal Resources Council (GRC) 2014 meeting, to lay out the project plans and objectives, and 2) a follow-up presentation summarizing project results (tentatively for GRC 2015).

Accomplishments and Challenges

The Geothermal Play Fairway Analysis - Appalachian Basin (GPFA-AB) project had few departures from the original SOPO. Southern Methodist University (SMU) and Cornell University team members are both experienced with large collections of data from oil and gas wells; Cornell and West Virginia University (WVU) are lead researchers for district heating models and wrote the code for GEOPHIRES (GEOthermal energy for Production of Heat and Electricity ["IR"] Economically Simulated (Beckers, 2015)); Cornell is experienced in analyzing datasets using statistical methodologies. The project accomplished all SOPO tasks and exceeded what was required. For instance, a set of BHT corrections specific to the Appalachian Basin region were developed, a set of three reservoir productivity metrics were created, the content model for Geologic Reservoirs was updated, innovative techniques were implemented for determining potential locations for induced seismicity that included stress orientations, a specialized list of site-specific industry locations of interest for utilization was created and Surface Levelized Cost of Heat was calculated for hundreds of Census Bureau Places, new methodologies for assigning and combining risk segment maps were developed, and detailed methodology 'memos' were written for future researchers to use in other Play Fairway Analysis projects (see Catalog of Supporting Files). Next, each of the Tasks are discussed to highlight changes from the planned methodology.

The Geothermal Play Fairway Analysis - Appalachian Basin (GPFA-AB) project is built from the foundation of previous work efforts by Cornell, SMU, and WVU (Blackwell et al., 2010; Aguirre et al., 2013; Stutz et al., 2015). In addition to the initial team members, we included other faculty, staff, and students who were able to provide valuable expertise to the project. The Catalog of Supporting Files in this Phase 1 report provides a full explanation of the methods, assumptions, formulas and references. The data uploads to the National Geothermal Data System (NGDS) via the Geothermal Data Repository include not only a wealth of detailed information drawn from thousands of oil and gas wells in the region,

but also provide summary maps indicating the risk factors evaluated in each of the Tasks undertaken and the composite of the four Task results.

Task 1 Thermal Resource Quality Assessment

Bottom-hole Temperatures

The foundation of our thermal resource assessment is bottom-hole temperature (BHT) data as control points of temperature at depth, and American Association of Petroleum Geologists (AAPG, 1994) Correlation of Stratigraphic Units of North America (COSUNA) lithology and thicknesses for subregions of the Appalachian Basin. BHT data were collected for New York, Pennsylvania, West Virginia, and a surrounding 50 km buffer into Maryland, Virginia, Kentucky, and Ohio. These BHTs, though prolific, are potentially subject to thermal disturbance from drilling activity and other errors that occurred when data were collected. Various BHT correction algorithms have been developed over the years to approximate equilibrium conditions (Harrison, Luza, Prater, & Chueng, 1983; Förster & Merriam, 1995; Blackwell & Richards, Geothermal Map of North America; Explanation of Resources and Applications, 2004). Through an extensive novel statistical evaluation of a small set of equilibrium well-log temperature measurements in the Appalachian Basin, a new set of BHT corrections appropriate for this basin were developed, which enables a rigorous treatment of the uncertainty related to application of the corrections. A set of equilibrium temperature wells (29) and 44 additional wells that were judged to be reliable temperature logs (Whealton, 2015, 2016; see also BHT Correction Memo) were used to devise correction functions. The focus on sub-regions increased the possibility to discover relationships between geological characteristics and the temperature corrections. Once the correction functions were defined, the depth-BHT data for over 13,000 wells were corrected.

Thermal Conductivity Stratigraphy

In order to determine properties of the thermal field, knowledge of lithology, thermal conductivity, radiogenic heat production, and formation thickness are needed. Each of these variables are unknown, and required assumptions backed by previous studies (Thermal Model Memo). Anadarko Basin thermal conductivity samples were used as representative of the Appalachian Basin because reliable data for Appalachian Basin rocks were not available, and because these basins reached similar burial depths. In order to capture the distribution of thermal conductivities that could be present, each formation in the Appalachian Basin was subject to a Monte Carlo analysis to determine the distribution of possible values in thermal conductivity (details are provided in the Catalog of Supporting Files within the memos). These formation values were used to determine the harmonic average thermal conductivity over the entire sedimentary column. Thermal conductivity measurements are associated with a 5-10% expected error (Gallardo & Blackwell, 1999), yet it is one aspect of the accuracy that can be readily improved, with reduced uncertainty, through collection in future studies of conductivity data specific to sites and formations of interest.

Thermal Model

The corrected BHTs were used along with the thermal conductivity stratigraphy to estimate the geotherm (i.e., temperatures at depth) at the location of each well using a 1-D heat conduction model developed for this project. This model improves upon and corrects equations previously published by Blackwell et al. (2007) and Stutz et al. (2012, 2015) (see Thermal Model Memo for details). These corrections are 1) the heat balance used to calculate the radiogenic heat production at the sediment-basement interface, 2) sediment thickness and sediment radiogenic heat production terms that were missing in the prior formulation for the temperature-at-depth for depths deeper than the well, 3) the calculation of surface heat flow relative to the radiogenic heat generation assumptions made, and 4) an explicit analytic solution to

the governing Ordinary Differential Equations, thus freeing ourselves from the need to evaluate the results of the thermal model via approximate numerical techniques. In other words, input BHT values are exactly reproduced using this method. Previous formulations did not reproduce the BHTs.

The model for steady state 1-D heat conduction was written in the open source language Python 2.7.9. This updated thermal model allows for a rapid computation of the surface heat flow and the geotherm on a site-by-site basis (>13,300 sites for this project). Input variables include the ground surface temperature, corrected BHT, depth of BHT measurement, radiogenic heat production, mantle heat flow, thermal conductivity for related COSUNA stratigraphy, and the total sediment thickness. A sensitivity analysis on the input variables to the heat conduction model was also performed, revealing that the quantification of properties of the thermal field is most sensitive to the BHTs and the sedimentary rock conductivities (Whealton, 2016). The Thermal Model Memo for this code has refined descriptions of the parameters, variables, and equations, thus making it easily adaptable. The code and full revision history are located on BitBucket (Horowitz et al., 2015).

Spatial Regression

Selected depths along the geotherms were subject to a spatial outlier analysis (see Outlier Memo). Points found not to be outliers acted as control points in a spatially stratified ordinary Kriging regression (e.g. Gaussian process regression) implemented in the 'gstat' package of R version 3.1.0 "Spring Dance". The justification for lateral stratification during Kriging is that laterally variable geological materials may cause lateral variability in the thermal field. The lateral boundaries were chosen based on gravity and magnetic potential field edges at depth (from the Seismic Risk Factor analysis). Smith (2016) and an Interpolation Memo provide details. This spatially stratified regression captured the structure of local spatial correlation in the predicted properties of the thermal field (e.g. depth to 80 °C) better than previously published regional approaches (Aguirre, 2014), thereby improving the accuracy and the uncertainty quantifications for the thermal resource assessment.

The results of this analysis are maps of the predicted mean and the standard error of the predicted mean for each thermal property. Figure 6 presents the depth to 80 °C resource map for the region.

Based on the map of depth to 80 °C (Figure 6), along with some consideration of the reservoir availability and population centers, at a mid-point in our project four of the most favorable counties in each state were selected and reviewed in greater detail (Figure 7). These twelve counties are shown in Figure 8 through Figure 17 as a set of 5 thermal resource maps paired with a cross section through each. The cross sections highlight the uncertainty and variability in the thermal resource through these counties.

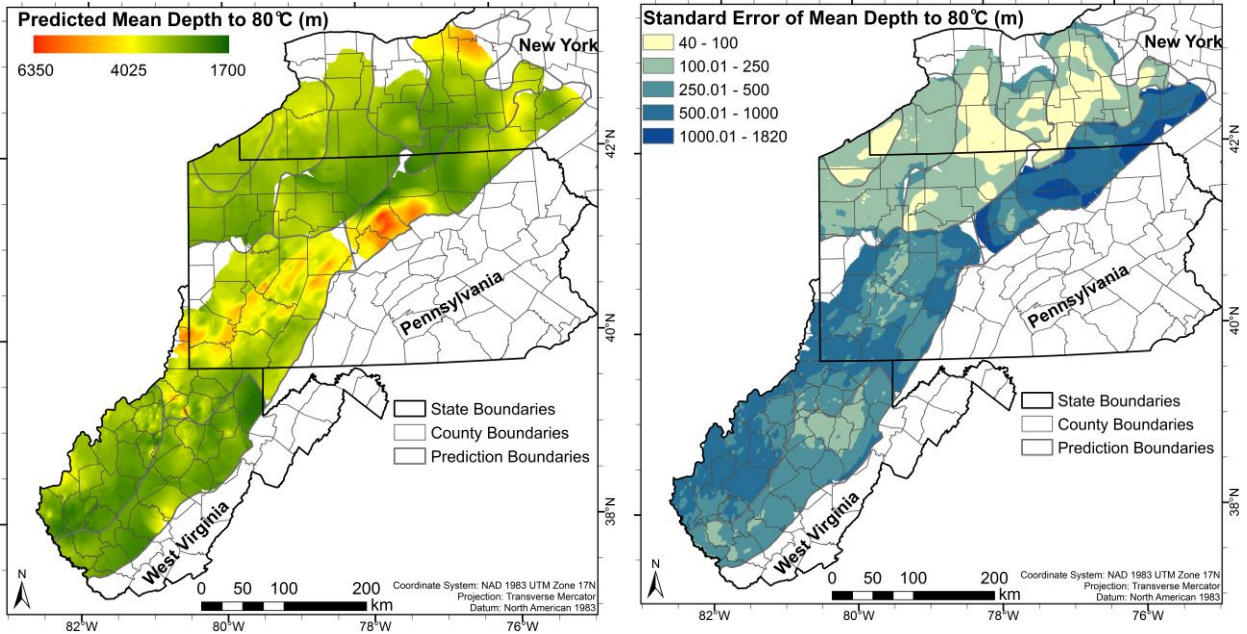


Figure 6: A) Predicted Mean Depth to 80 °C based upon thermal analysis. The sub-regions within the basin are boundaries for the spatially stratified Kriging interpolation of the thermal field properties. B) Uncertainty on the depth to 80 °C expressed as standard deviation.

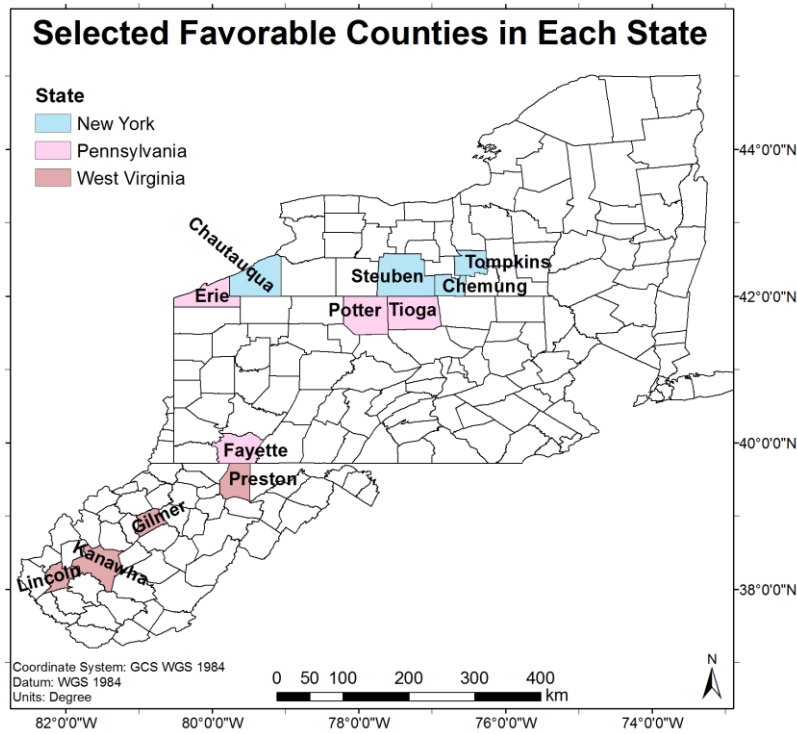


Figure 7: Counties selected for more detailed thermal maps based upon having favorable thermal properties, available reservoirs, and population centers.

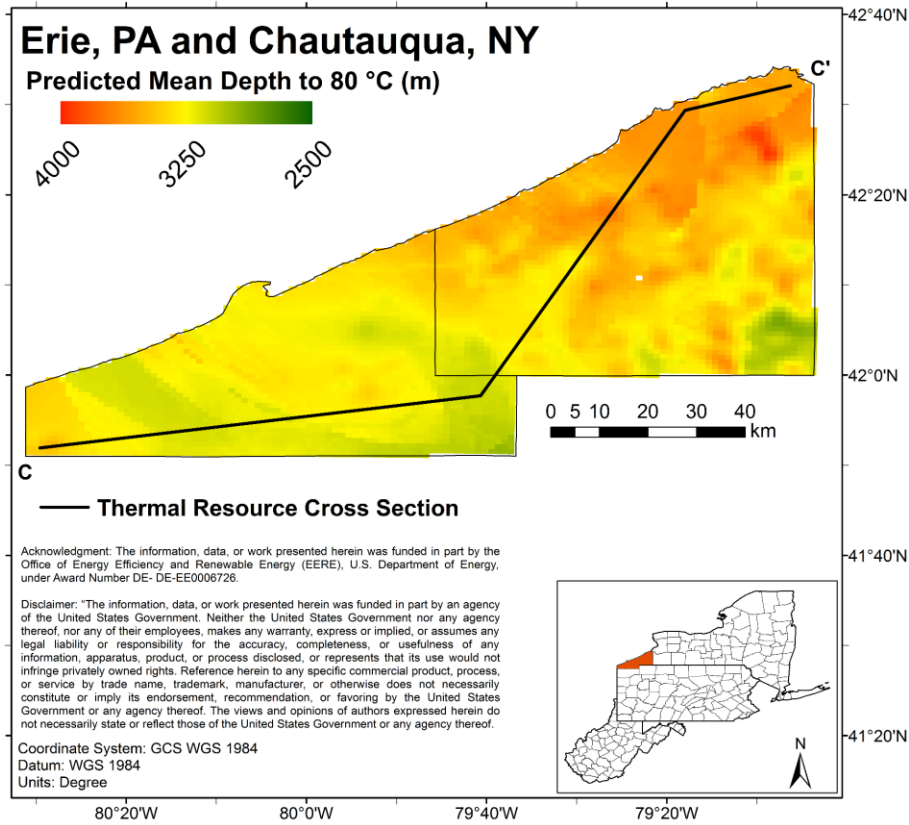


Figure 8: Erie, PA and Chautauqua, NY (Predicted Mean Depth to 80 °C [m]) with Cross Section.

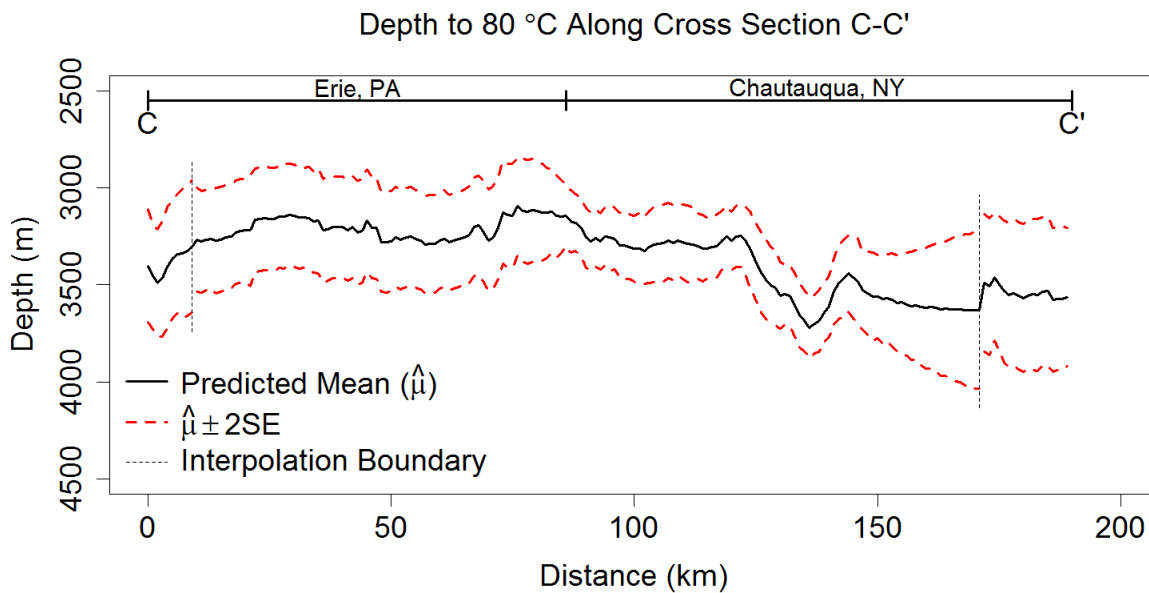


Figure 9: Variability and uncertainty in the predicted mean depth to 80 °C along cross section C-C'. Interpolation boundaries are marked by vertical dotted lines. Mean depths are significantly different when uncertainty bars do not overlap.

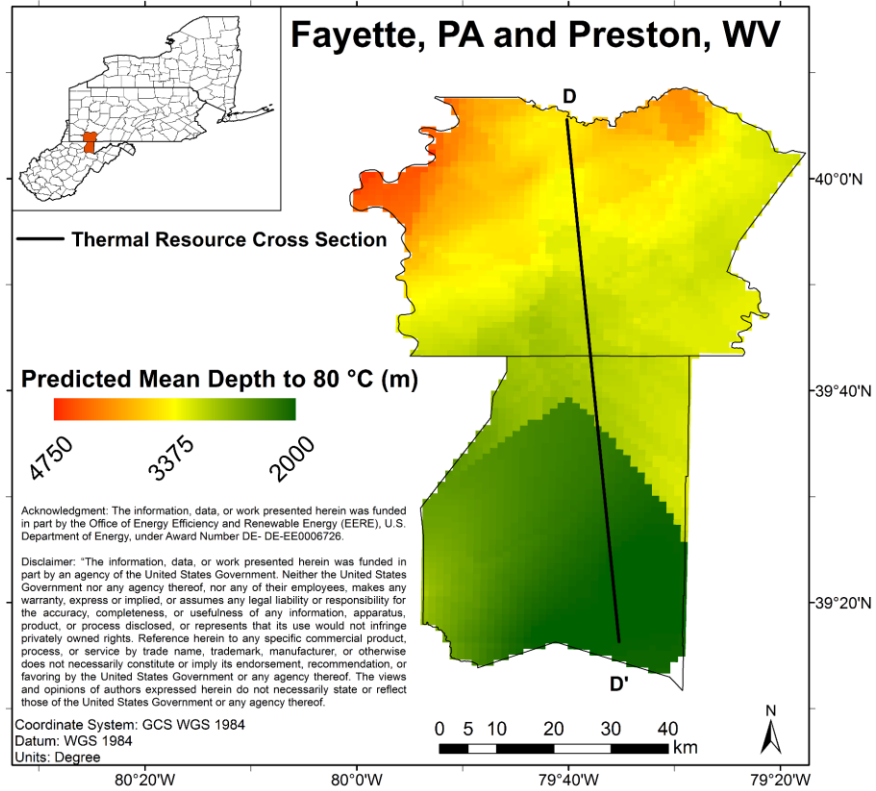


Figure 10: Fayette, PA and Preston, WV (Predicted Mean Depth to 80 °C [m]) With Cross Section.

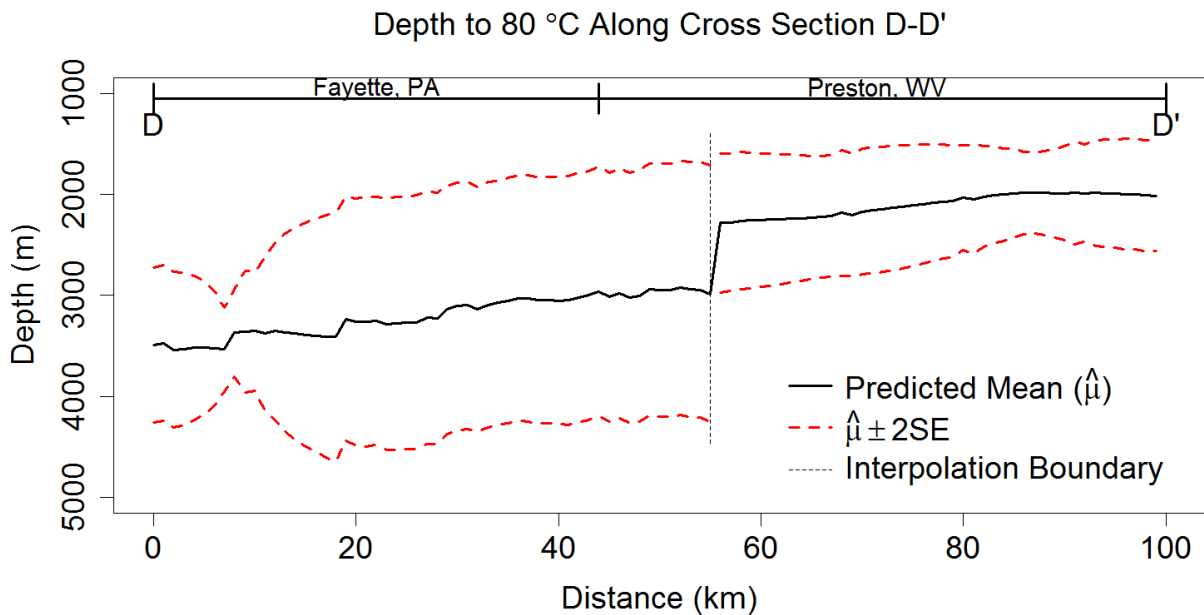


Figure 11: Variability and uncertainty in the predicted mean depth to 80 °C along cross section D-D'. Interpolation boundaries are marked by vertical dotted lines. Mean depths are significantly different when uncertainty bars do not overlap.

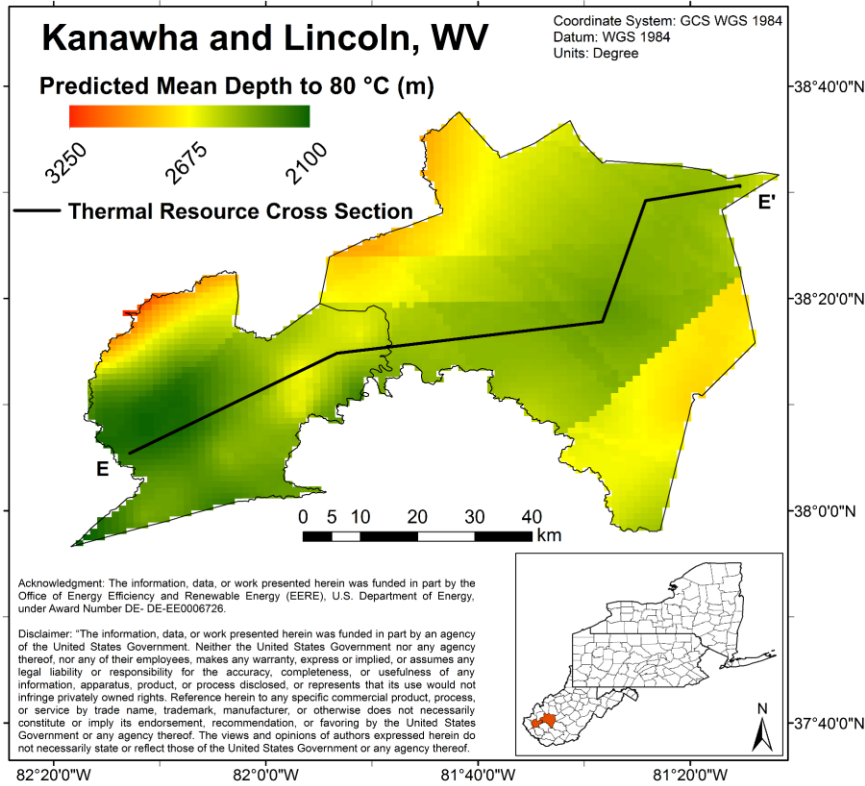


Figure 12: Kanawha and Lincoln, WV (Predicted Mean Depth to 80 °C [m]) With Cross Section.

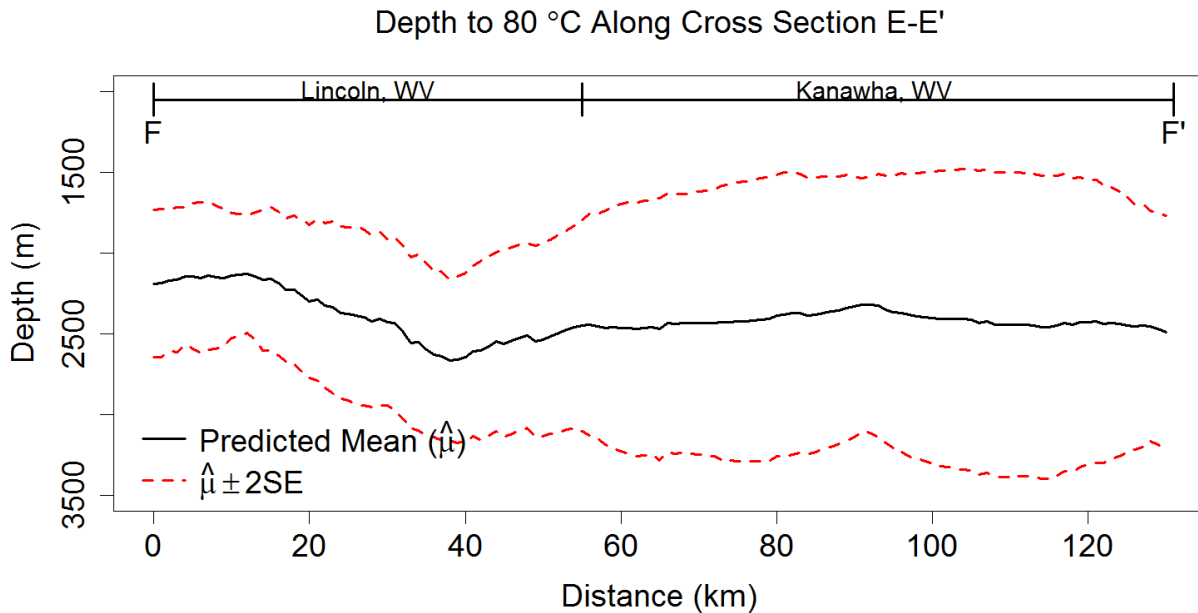


Figure 13: Variability and uncertainty in the predicted mean depth to 80 °C along cross section E-E'. Interpolation boundaries are marked by vertical dotted lines. Mean depths are significantly different when uncertainty bars do not overlap.

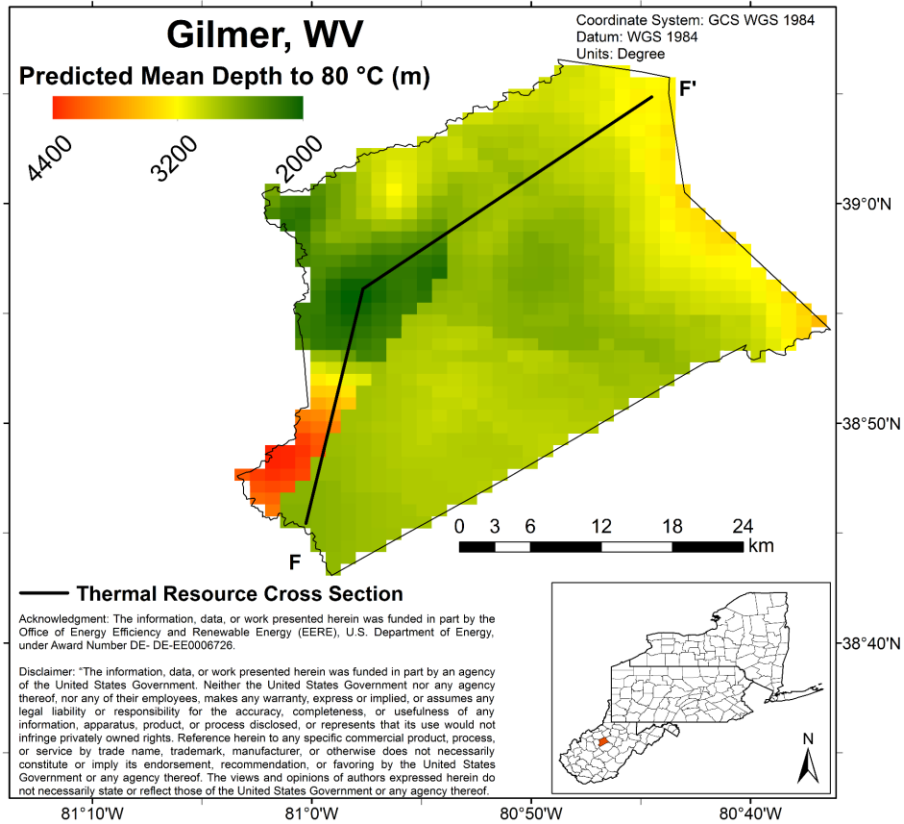


Figure 14: Gilmer, WV (Predicted Mean Depth to 80 °C [m]) With Cross Section.

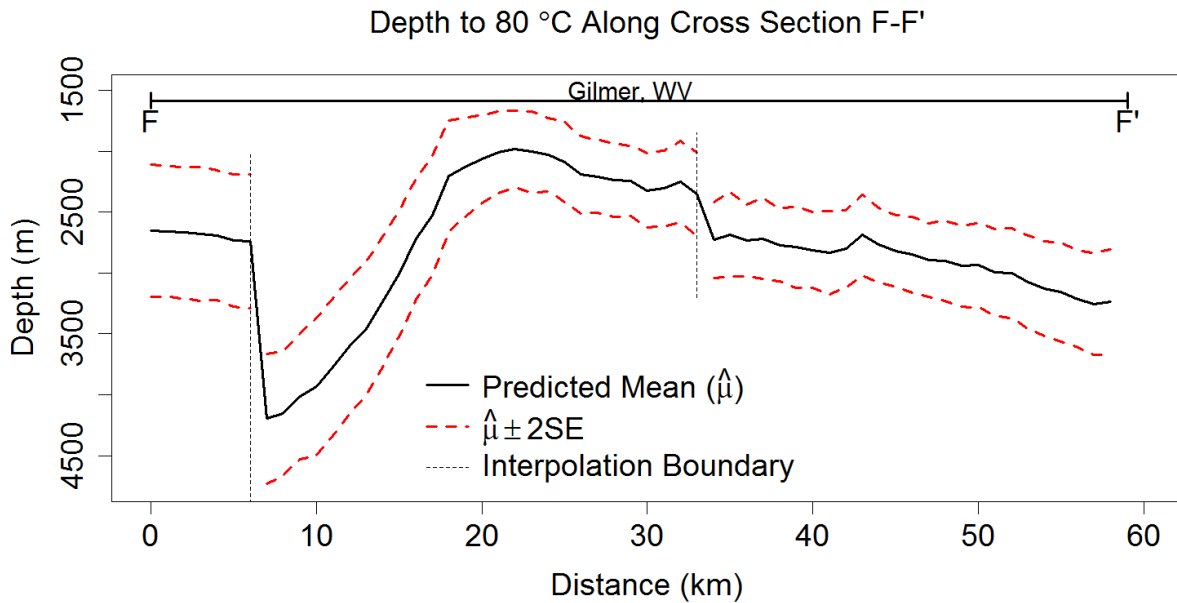


Figure 15: Variability and uncertainty in the predicted mean depth to 80 °C along cross section F-F'. Interpolation boundaries are marked by vertical dotted lines. Mean depths are significantly different when uncertainty bars do not overlap.

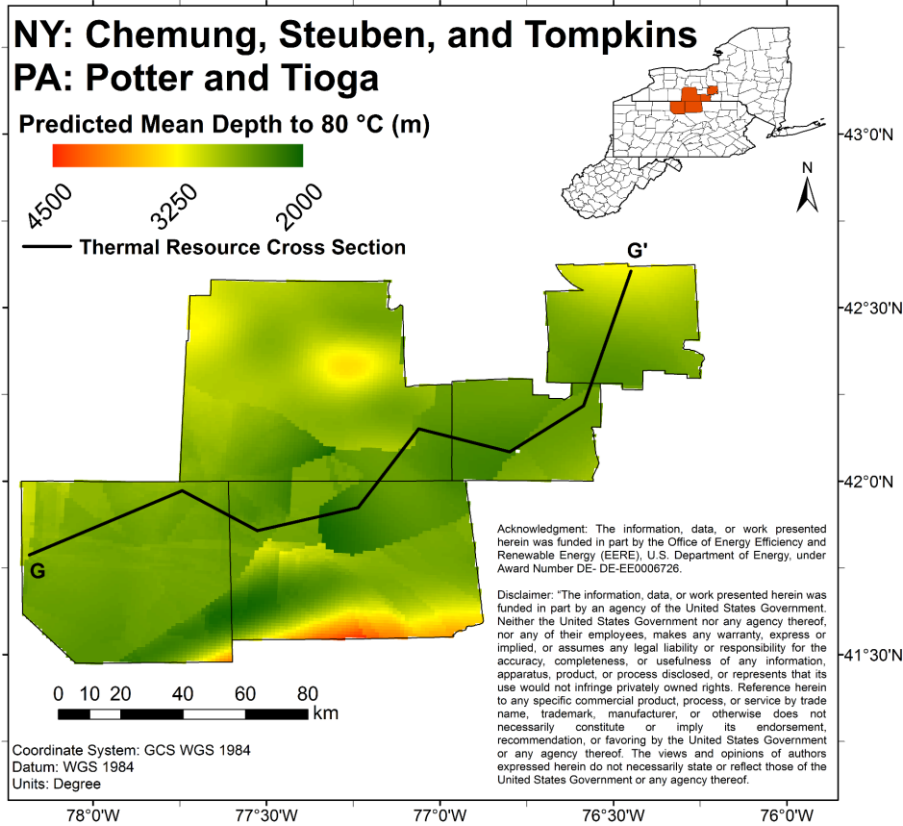


Figure 16: Predicted Mean Depth to 80 °C [m] With Cross Section for Chemung, Steuben, and Tompkins counties of NY and Potter and Tioga counties of PA.

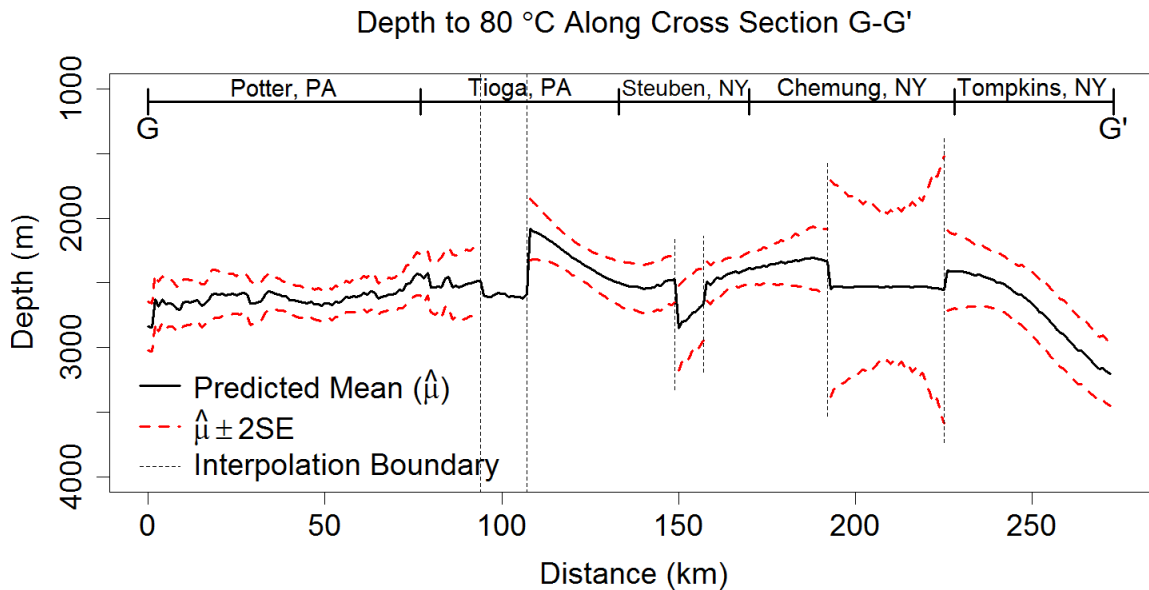


Figure 17: Variability and uncertainty in the predicted mean depth to 80 °C along cross section G-G'. Interpolation boundaries are marked by vertical dotted lines. Mean depths are significantly different when uncertainty bars do not overlap.

One approach to evaluate the confidence in the thermal analysis results is to compare the equilibrium temperature for the subset of 47 reliable wells with data as deep as 1.5 km to the predicted mean temperature at 1.5 km. Figure 18 reveals the number of standard errors difference between the recorded equilibrium temperature at or near 1.5 km and the predicted mean temperature at 1.5 km. Another approach was used to evaluate the results of the spatial regression. This approach was a “leave-one-out” cross validation. For the depth to 80 °C map in Figure 6, over 98% of the left-out wells had a calculated depth to 80 °C within 3 standard errors of the predicted mean at the location of the left-out point – a comforting result.

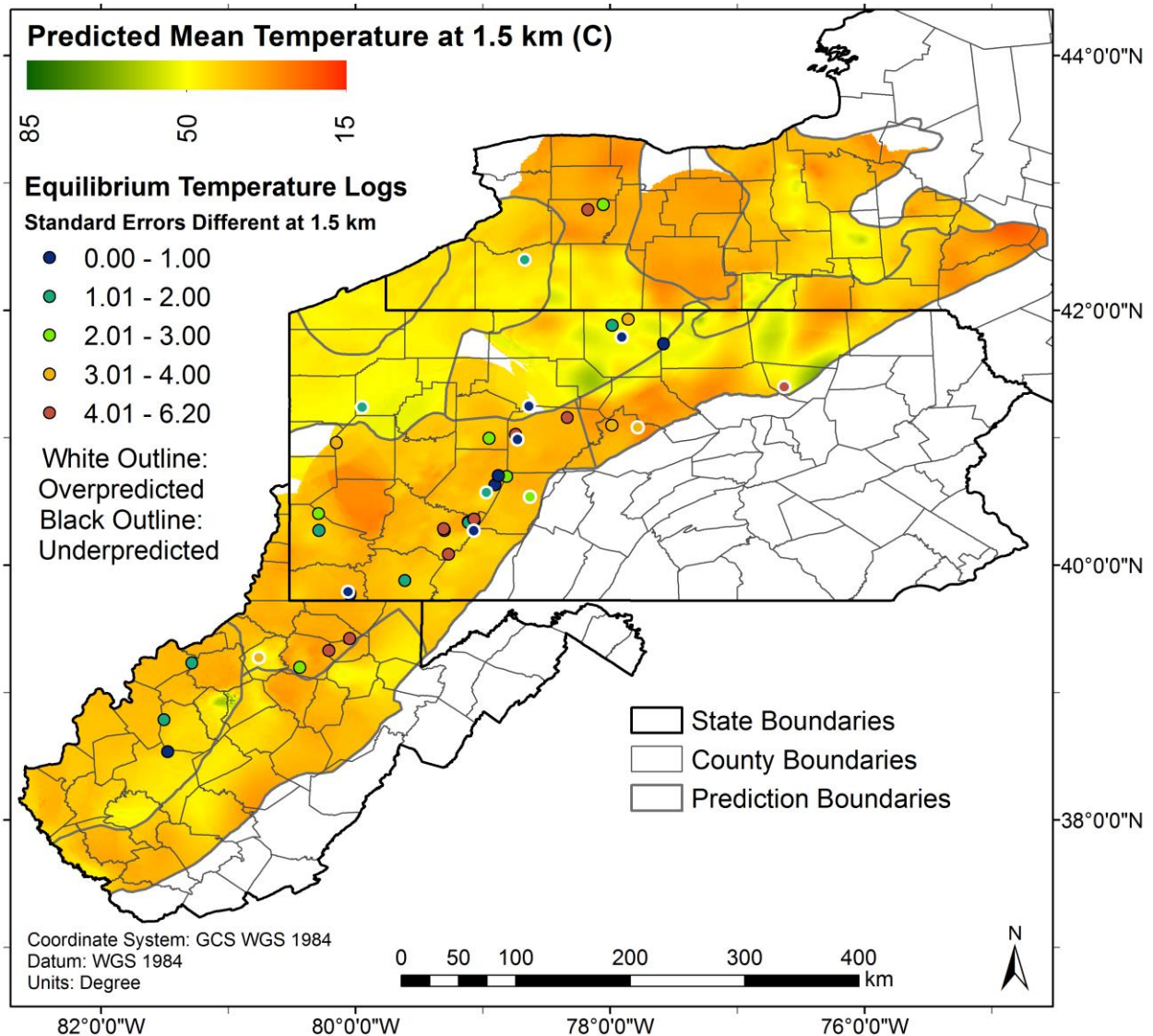


Figure 18: Wells considered equilibrium or having reliable temperature data are compared to predicted temperatures at 1.5 km depth. Colors of circles show differences in measured and predicted temperature at 1.5 km in terms of the number of standard errors that the equilibrium temperature was from the predicted mean.

The final product of the thermal analysis is a risk-factor map portrayed on a 3-color or 5-color scale (**Figure 19**). For this map, the depths of the modeled position of the 80 °C isotherm were converted to a non-dimensional measure of favorability that ranges from 0-3 or from 0-5, respectively, based on a set of threshold values. The thresholds are detailed in Memo 17 (Combining Risk Factors).

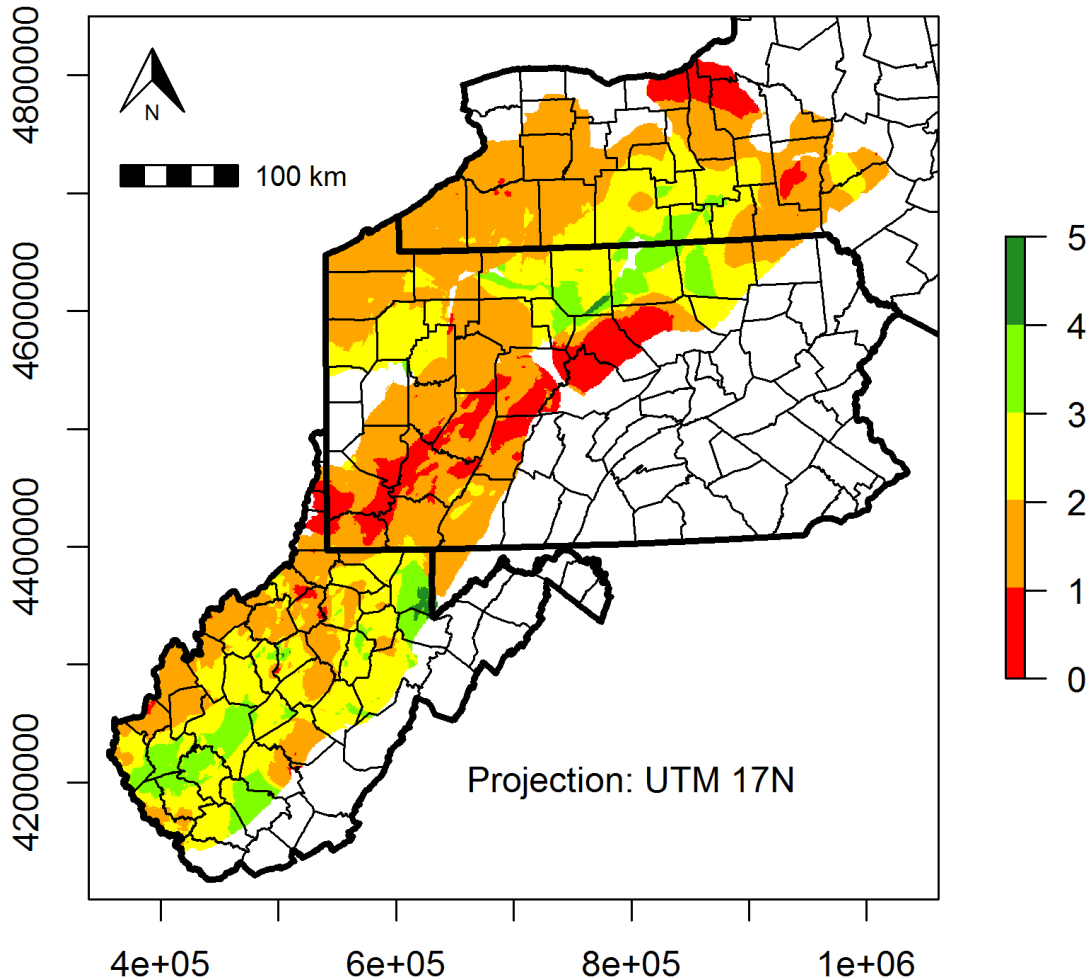


Figure 19: Play Fairway Metric risk segment map for the thermal resource with a five color scheme. Green-Favorable, Red-Unfavorable.

Challenges

We are aware that to select a site and have it be colder than predicted is much more costly than it being hotter than expected. Thus, as we complete Phase 1 there continues to be an emphasis on the thermal risk factor associated with the BHT correction used and the confidence related to the BHT values as a foundational parameter in the thermal resource assessment. To improve on past projects' efforts, we did not use the Harrison Correction (1983), which only uses a depth-dependent temperature change. Instead, we devoted significant effort to developing a set of sub-region-specific corrections for the Allegheny Plateau and the Rome Trough (the portion of the Rome Trough in Pennsylvania). A separate correction was also developed for West Virginia. Use of temperature data held by oil and gas companies would permit improved accuracy.

At the project outset we evaluated the possibility of running thermal conductivity measurements on core, but this could not be accomplished within the available resource constraints due to mechanical failure of the WVU divided bar. Further studies to obtain thermal conductivity data for samples of rocks collected at depths of project interest are recommended.

Task 2 Natural Reservoir Quality

The natural reservoirs task required a number of simplifying assumptions due to data availability limitations. Additional simplifying assumptions underpin the computation of reservoir productivity indices and reservoir fluid capacity. All assumptions made are listed within the Natural Reservoirs Methodology Memo in the Catalog of Supporting Files.

This project has incorporated the available reservoir parameters (permeability, thickness, and working fluid viscosity) in order to make a meaningful comparison of the potential flow rates from a total of 1,894 proven oil and gas reservoirs in this sedimentary basin. While not explicitly required in the SOPO, we developed three alternative metrics for quantifying reservoir favorability. The first metric, Reservoir Fluid Capacity (RFC), is based on the natural geologic qualities of the sedimentary aquifers. The RFC, expressed in units of mD-m, combines permeability and thickness. The second and third metrics, termed the Reservoir Productivity Indices (RPI), are sensitive to the design of a well field and to the pressure used to pump a well. The RPI metrics are built around Darcy's Law flow through porous media in a confined aquifer (Gringarten, 1978; Augustine, 2014). The RPI metrics report mass flow rate per pressure drop (Kilograms per Megapascal seconds; kg/MPa-s) for two different choices of working fluids in a reservoir: RPI_w considers the viscosity and permeability of water as the working fluid, whereas RPI_g considers the viscosity and permeability of supercritical carbon dioxide as the working fluid. A Monte Carlo simulation was used to calculate each reservoir's RFC, RPI_w and RPI_g, while taking into account the uncertainty on parameter values (e.g., reservoir permeability, thickness, and viscosity).

Because the distribution of RFC for the entire reservoir population is strongly skewed, we adopted reservoir quality rank thresholds based on a logarithmic scale (thresholds at 1000, 100, 10 and 1 md-m). A different approach to selecting thresholds was used for the RPI: in order to meet the required flow rates without any additional stimulation or enhancements, we estimate that >10 kg/MPa-s value for the reservoir productivity index is required for either RPI_w or RPI_g. The majority of the reservoirs we have identified are below this RPI value (Figure 20). On a map, areas with dark green color indicate locations with this most suitable value of reservoir productivity index (Figure 21). The spatial distribution of reservoirs of varying quality is partly expressed in Figure 21 although some regions have stacked reservoirs of differing qualities, and these are not well expressed on a single map.

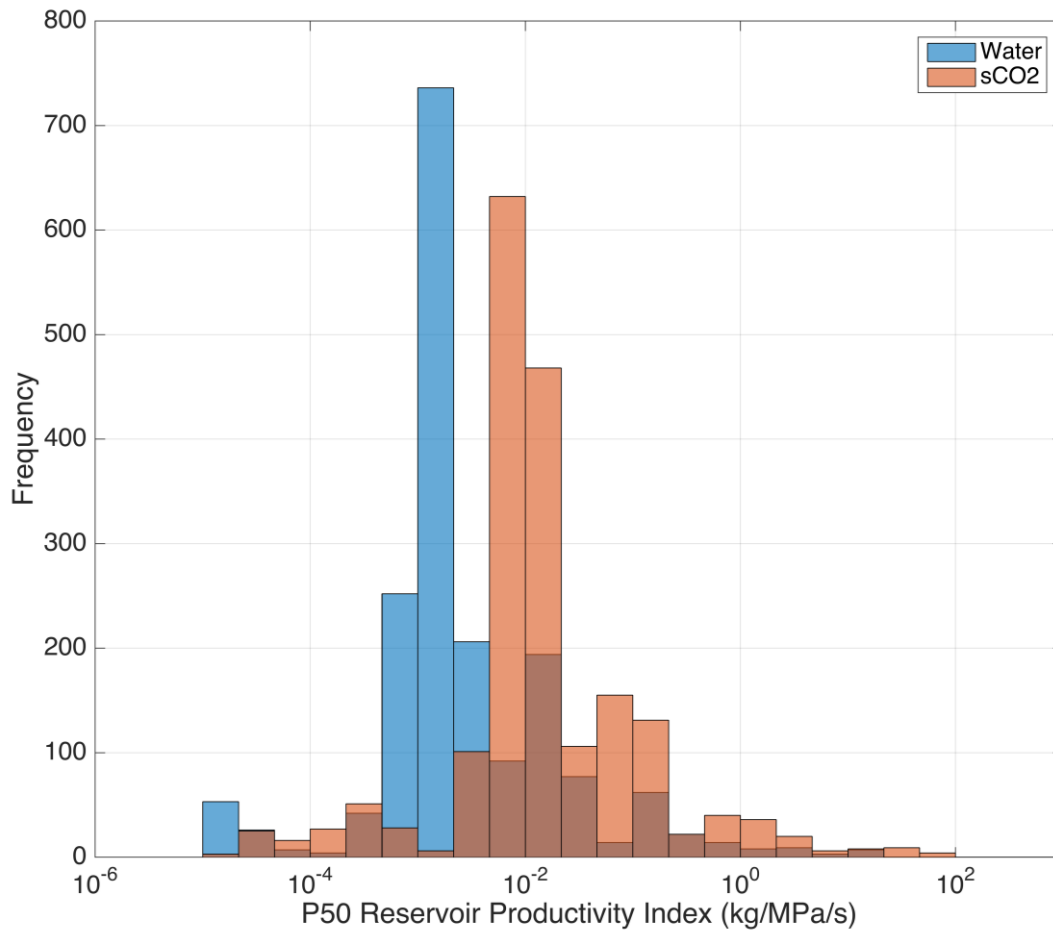


Figure 20: Histograms of the P50 RPIw (blue) and RPIg (brown) frequencies of reservoirs in the Appalachian Basin. Where RPIw data overlap with RPIg data, the values are displayed by a dark brown. The P50 expresses the most likely case given the set of 100,000 Monte Carlo realizations for each reservoir. The frequencies are ordered by the Reservoir Productivity Indices (kg/MPa-s).

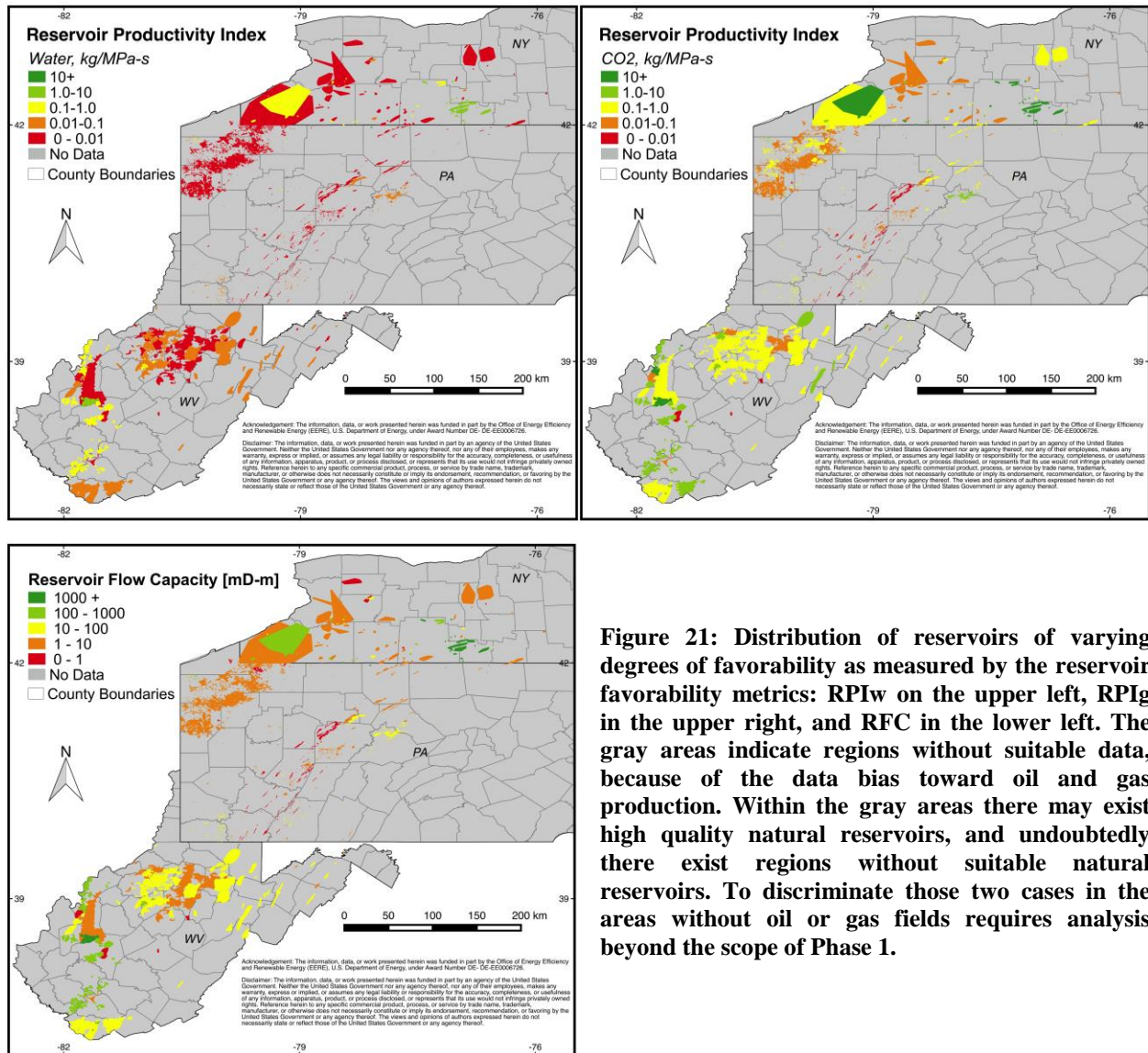


Figure 21: Distribution of reservoirs of varying degrees of favorability as measured by the reservoir favorability metrics: RPIw on the upper left, RPIg in the upper right, and RFC in the lower left. The gray areas indicate regions without suitable data, because of the data bias toward oil and gas production. Within the gray areas there may exist high quality natural reservoirs, and undoubtedly there exist regions without suitable natural reservoirs. To discriminate those two cases in the areas without oil or gas fields requires analysis beyond the scope of Phase 1.

The final product of the reservoir quality analysis is a set of maps portrayed on a 3-color or 5-color scale (**Figure 22** displays the result for RFC). For each of these maps, the estimated flow capacity at each location was converted to a non-dimensional measure of favorability that ranges from 0-3 or from 0-5, respectively, based on a set of threshold values. The thresholds are detailed in Memos 11 (Natural Reservoir Methodology) and 17 (Combining Risk Factors). The uncertainty corresponding to the Risk Factor map for RFC (**Figure 22**) and maps for RPIw and RPIg can be found in Memo 17 (Combining Risk Factors) and as individual files in the Geothermal Data Repository.

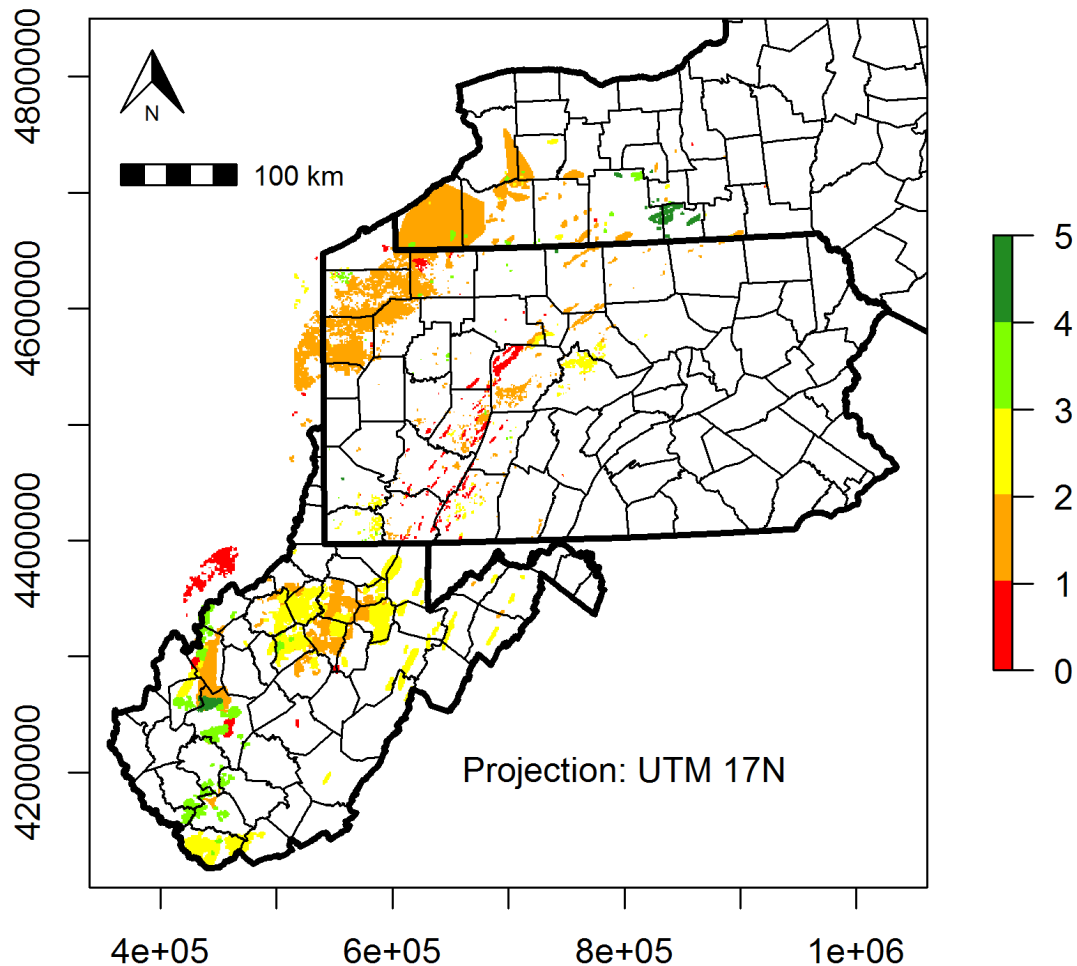


Figure 22: Play Fairway Metric risk segment map for the reservoir metric with a five color scheme. Green-Favorable, Red-Unfavorable. This map displays the result based on the metric Reservoir Fluid Capacity (RFC).

Challenges

The Natural Reservoir Analysis followed the SOPO tasks and methods as planned. Reliance on rock property information from the oil and gas industry imposed a location bias in the data sets. Suitable hot-water reservoirs may occur outside of the oil and gas fields, but to identify them will require time-intensive analyses of well production records and the development of geological models of the controls on matrix permeability and fracture permeability.

In working with low-temperature geothermal resources, the potential reservoir flow rate is of utmost importance (Bedre & Anderson, 2012). The project team concludes that the knowledge available falls significantly short of what would be needed to predict at any given location whether a high enough fluid

flux to support a district heating system can be extracted without stimulation. We recommend future studies to improve on the capacity to estimate flow potential by collecting data on production, injection, flow-back tests, and pressure tests in the most attractive prospective plays, to the extent that these data can be obtained from regulatory bodies, private companies, and data brokers.

This project analysis of natural reservoirs included more parameters than previously reported in the existing National Geothermal Data System (NGDS) content model for Geologic Reservoir Analysis, which had been developed by the Texas Bureau of Economic Geology. One new parameter is “Reservoir Productivity Index” (RPI), a metric adapted from the productivity index of a well, in units of kg/MPa-s. Instead of simply adding a field called RPI to the existing content model for Geologic Reservoirs, we updated the entire content model and added flexibility for numerous types of analysis projects to provide relevant reservoir data. Researchers can now use the content model to report “*Reservoir Favorability*” and describe the units and methods associated in their analysis – in our case RPI in kg/MPa-s. This is just one example of many such updates; the revised NGDS Geologic Reservoir Content Model is now available on USGIN (U.S. Geoscience Information Network, 2015) for others to use.

Task 3 Risk of Seismicity

The seismic risk factor analysis was initially aimed at determining whether a candidate location is near an active fault, and thereby potentially susceptible to induced seismicity from geothermal operations. Existing fault maps do not share the GPFA-AB boundaries or scale. Hence, their use leads to problems of uneven coverage, varying interpretation of faults vs. lineaments, and different mapping scales. For more uniformity across the GPFA-AB region, we use a Poisson wavelet analysis of gravity and magnetic fields, co-invented by Frank Horowitz (Hornby et al., 1999) and widely deployed in the mining industry since the late 1990s (e.g. GoldCorp, 2001).

Multiscale edge Poisson wavelet analyses of potential fields (“worms”) have a physical interpretation as the locations of lateral boundaries in a source distribution that exactly generates the observed field – see the Seismic Hazards memo for more discussion. Clearly, not all lateral boundaries (“worms”) are faults, and vice versa, thus only a subset might be active. As the basin is within an inter-plate region, deformation is very slow and return time for naturally occurring earthquakes is potentially >10,000 years. Also, only steeply dipping structures will be expressed by “worms”.

To identify seismically active structures, we plotted both the “worms” and the earthquakes from the National Earthquake Information Center (NEIC) and EarthScope Transportable Array (TA) catalogs. “Worms” within a small distance of epicenters are tracked spatially. To within errors in location, this identifies structures that might be seismically active faults - which we categorize with higher risk than other structures. We called this strategy the “proximity technique” (Figure 23, Proximity Earthquakes).

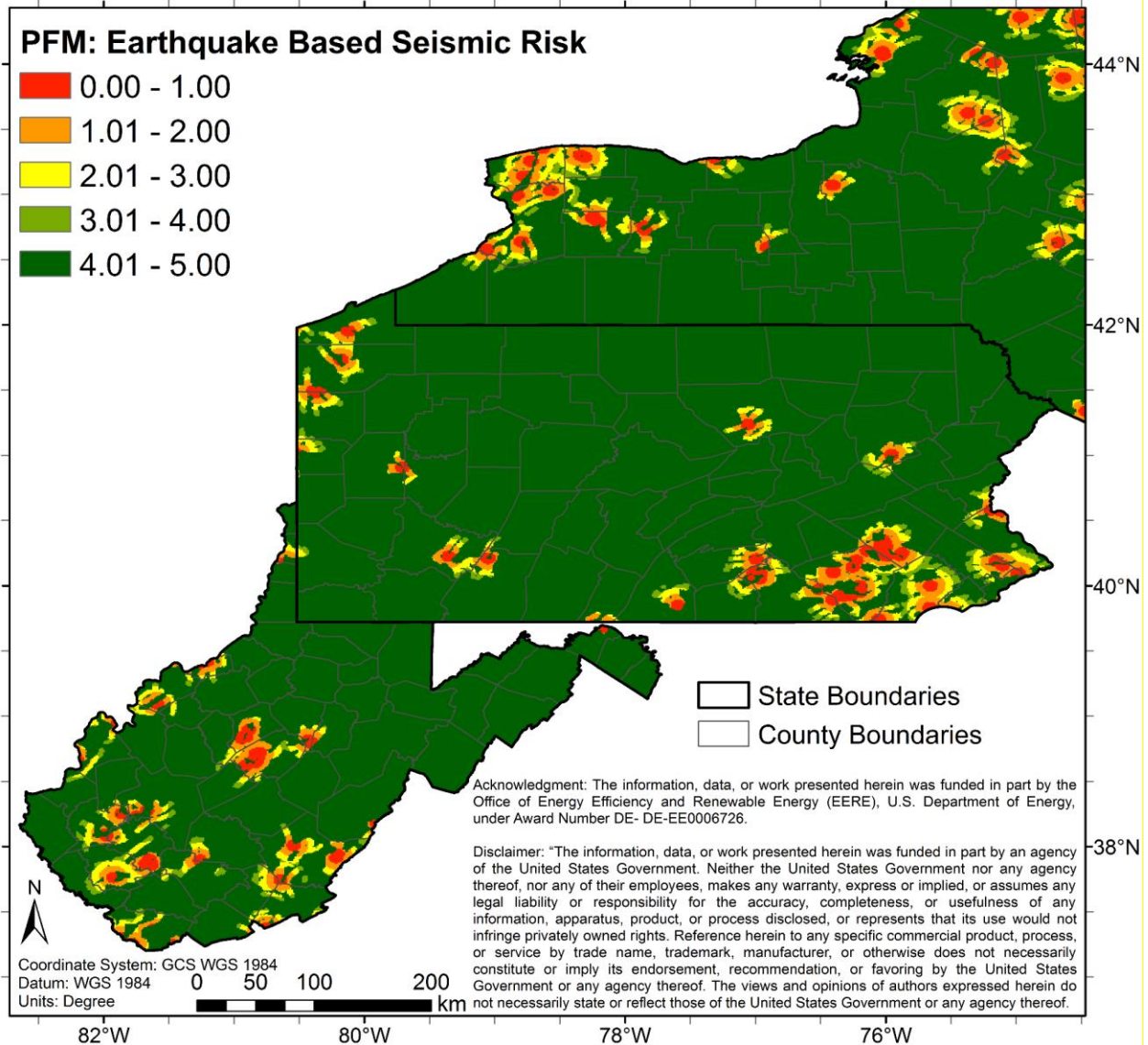


Figure 23: Map of spatial variability of the risk of induced seismicity based on the proximity of each location in the study area to a recorded seismic event and/or the co-occurrence of a “worm” and a nearby seismic event. Red indicates highest risk; green is lowest risk.

As the project progressed, after discussion with experts both within and outside of the team, we tried an additional approach, termed a slip-tendency estimate. Plotting multiscale edge Poisson wavelet analysis lateral boundaries within World Stress Map σ_1 directions (see Catalog of Supporting Files for more information in the Identifying Potentially Activatable Faults Memo) yields an alternative qualitative approach to identifying reactivatable geological structures. Here, we use “worms” to locate steeply-dipping structures with strikes favorably oriented for failure by Byerlee’s law (Figure 24, Stress Orientation Hazard). While this might be a necessary criterion for fault activation (under an assumption of the validity of Byerlee’s Law model) it is *not a sufficient criterion* because we lack detailed information about stress magnitudes throughout the GPFA-AB region.

Ultimately, we judged that the most useful representation of the total seismic risk resulted from the combined risk map formed by averaging the risk factor categories given by the proximity technique and the slip-tendency technique (Figure 25, Combined Seismic Risk).

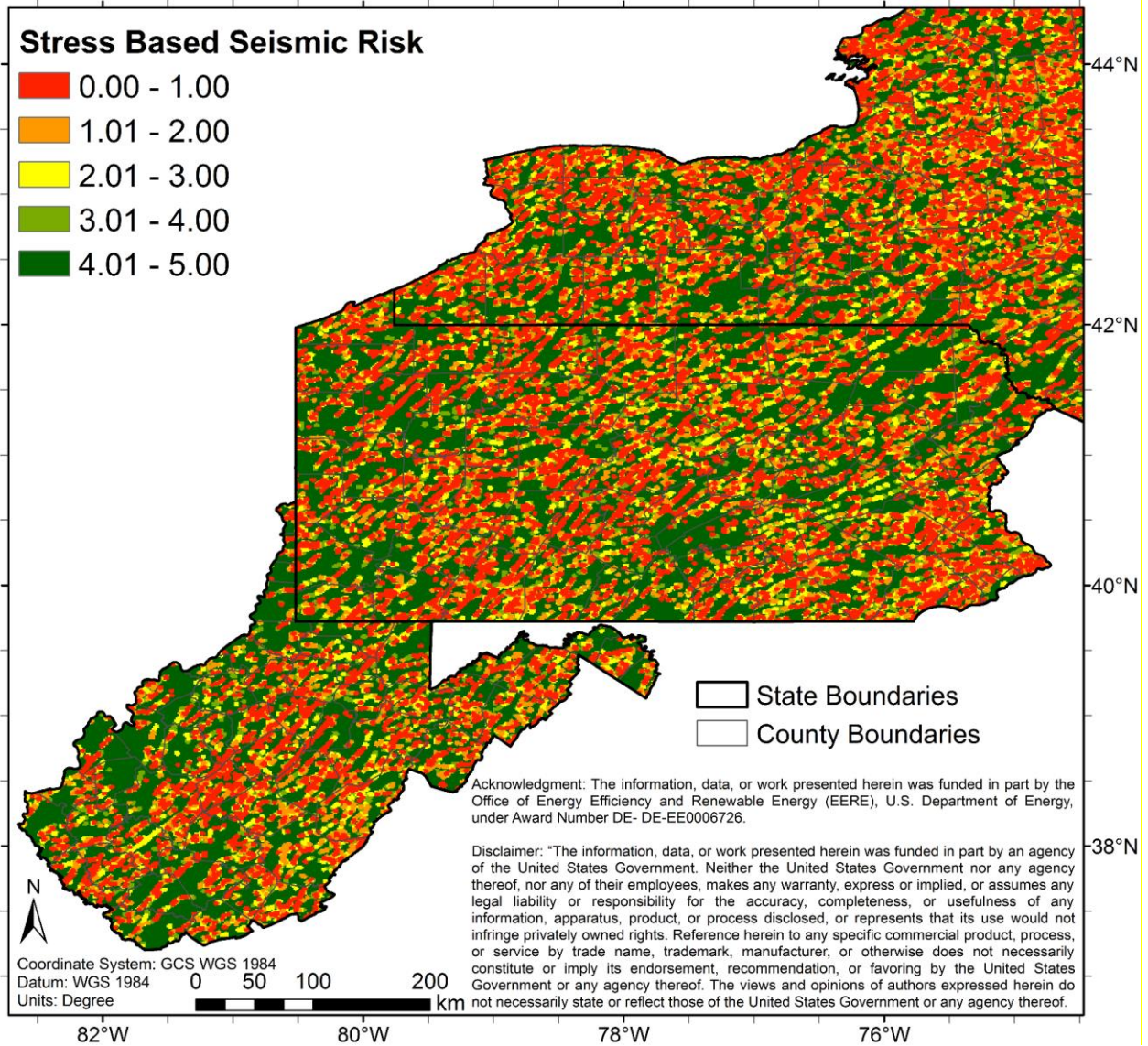


Figure 24: Map of the spatial variability of risk of induced seismicity estimated based on slip-tendency, as calculated by the premises of the locations of planes of weakness relative to the regional stress field. For this analysis, the “worms” are treated as if they are all planes of weakness, and Byerlee’s Law criteria used.

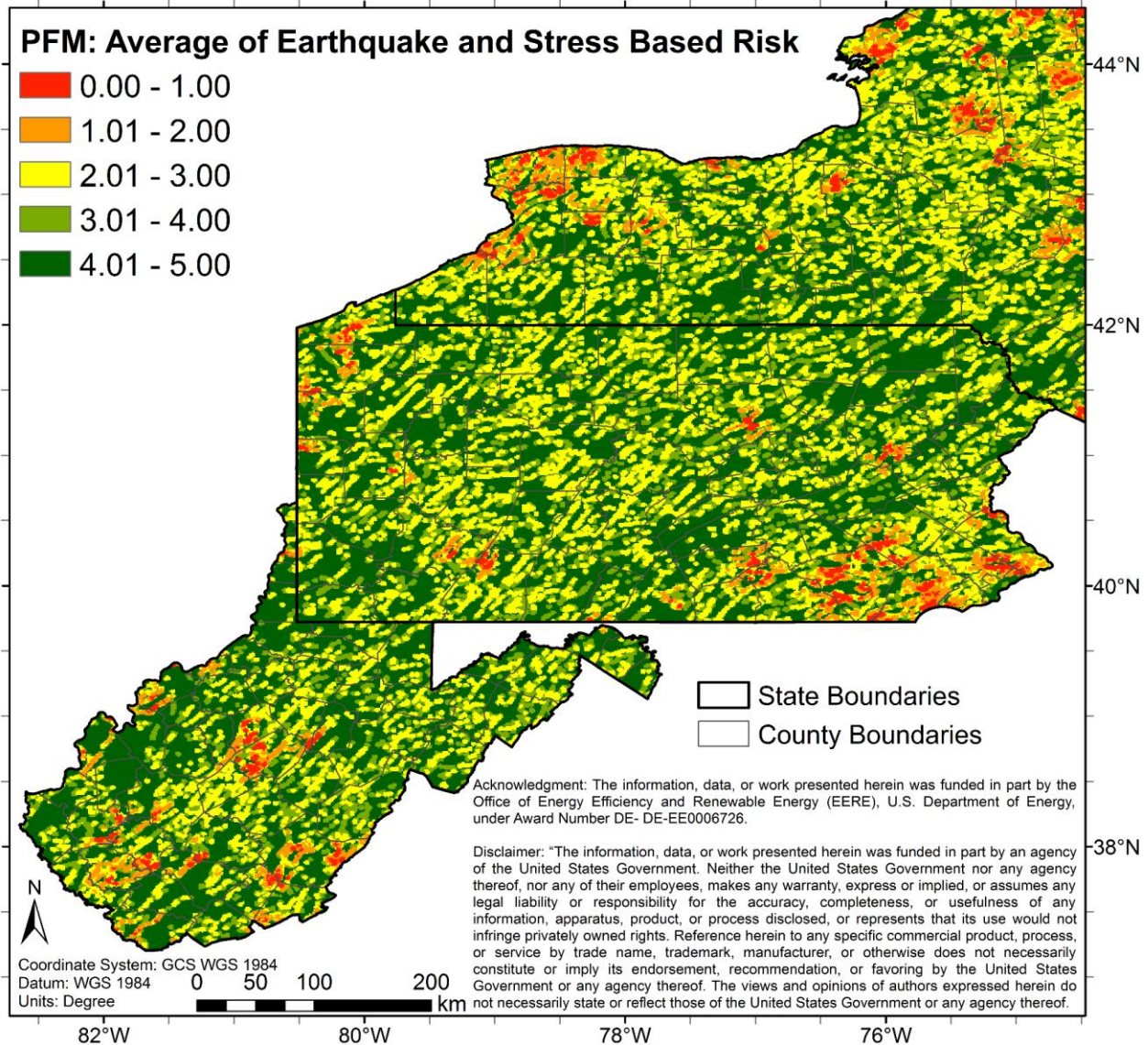


Figure 25: Preferred map of the spatial distribution of risk of induced seismicity, created by averaging the proximity and slip-tendency techniques.

In addition to the summary of the seismic risk method in the Catalog of Supporting Files, the reader should refer to (Seismic Risk Map Creation Methods Memo and the Identifying Potentially Activatable Faults Memo) for a complete discussion of these matters, including an overview of the wavelet theory, the earthquake catalog cleaning, and the computational techniques developed to estimate risks and their uncertainties at all points along the worms.

Challenges

The risk of induced seismic activity is now on many peoples' mind across the country. Those living in New York, Pennsylvania and West Virginia are no different. There is concern that the reinjection of water produced during oil and gas extraction will induce seismicity, and it is easy to imagine that a similar concern will be raised about the recirculation of water in a geothermal energy extraction project.

Initially the project had expected to use mapped faults that we anticipated would be available from the state agencies and the USGS. We found that there are extreme differences in the details and styles of surface fault maps within and between the states, making this dataset difficult to use for our basin-scale analysis. To make up for this data layer loss, we focused on generating a spatially consistent map of the gravity-field and magnetic-field variations (Hornby et al., 1999). This analysis located rock-property edges not only in the deeper levels of the sedimentary basin fill, but also in the basement beneath. In light of recent analyses that show that many of the induced earthquakes in Ohio, Oklahoma, Texas, and Kansas associated with oil and gas wells are related to deep basement faults, these new maps should be of value to the oil and gas industry and to geological carbon sequestration researchers and regulators, as well as to the geothermal industry.

The use of earthquake locations (from USGS/NEIC and the EarthScope TA) was chosen as the most direct indicator of areas of most concern. They are, except in areas of active mining (both surface and deep). The NEIC catalog explicitly categorizes earthquake events, while the TA event list includes everything recorded and located by a seismic array. The TA database added many more “apparent” earthquake locations, which we initially attributed to the higher sensitivity available from the TA’s closer station spacing than that found in the NEIC. Nevertheless, during our on-site visit to the State Geological Survey of West Virginia, they questioned the significance of numerous TA data located in areas of coal mining. Our experienced team members suggested filtering out TA events that occurred between 7 am and 6 pm, based on the fact that mine blasting is allowed only during daylight hours (Mining Safety and Health Administration, Title 30 CFR). The filtered results indeed nearly eliminated events located in the coal mining regions of West Virginia along with other suspicious locations (e.g., near quarries).

As evaluation of the potential for extraction of deep hot geothermal water advances in the Appalachian Basin, we recommend attention be given to experiences in the oil and gas industry. Lessons learned from their experience may inform successful approaches to avoid issues related to induced seismicity. Even within the single year duration of this project, induced seismicity emerged as a major hazard for the oil and gas industry and therefore the amount of research is escalating. It should be noted that the mapping of the Seismic Risk parameters presented here is at the regional scale. Nevertheless, it has been learned that the induced seismicity risk is highly dependent on the specific location. An early part of focused examination of any location-specific well field and utilization scenario should be to obtain relevant data with which to analyze the seismic background activity, fault locations and orientations, and state-of-stress.

Task 4 Utilization Assessment

The Utilization Assessment used US census data, Energy Information Agency (EIA) data and National Oceanic and Atmospheric Administration (NOAA) climate data to estimate the demand and surface costs associated with the delivering hot water to buildings via a single community district heating system, following methods detailed by Reber et al. (2014). The cost estimates include pipes, pumps and heat exchangers, and the annual demand expectations rely on place-specific climate conditions. The economic analysis was limited to the surface expenses, and therefore is termed the Surface Levelized Cost of Heat (SLCOH). The SLCOH was calculated using a software tool, GEOPHIRES (Beckers et al., 2014), which permitted repetition of the analysis for many communities.

The Utilization effort included two broad types of data in Phase 1: 1) residential – community ‘Places’, and 2) site-specific users with high heating demands such as universities, industrial users, government facilities, etc. Most analysis was focused on the first category of potential use, community district heating systems. Rather than using the 1500 population minimum as did Reber (2013), a population threshold of 4,000 residents per Place was applied for all three states, to focus on those Places with a sufficient number of users to justify the initial capital investment associated with a district heating system. This Census-

based analysis seemed to overlook the possible cases of individual commercial, industrial, or large private entities who seek sustainable, low-carbon, high capacity, heating or cooling systems. Therefore a second effort was completed that determined >165 site-specific plausible users whose work entails high heat loads, such as paper mills, wood drying kilns, dairy processing (includes yogurt and milk pasteurization products), college and university campuses, and select military locations. No economic analysis was conducted for those sites, but maps were generated to illustrate their locations relative to the favorability of the three geological risk factors.

The GEOPHIRES program was designed to output Levelized Cost of Heat (LCOH). For Phase 1 the team used only the above-ground portion of the GEOPHIRES program. Thus the output SLCOH (Table 1) cannot be compared to the usual LCOH of other projects as it does not include the site-specific below-ground costs of drilling and completion of wells. This division of the costs was done because the subsurface costs will depend on flow rates and temperatures, which for this project are analyzed as separate risk factors. Consequently, the full LCOH will be more expensive per MMBTU than what the Phase 1 products show. A 30-year lifetime for a geothermal field was assumed. For district heating systems already in place, they would not need most of the surface infrastructure. Additionally, using the surface components of GEOPHIRES enables those communities without installed district heating systems to consider the infrastructure costs of a system independent of the power supply (geothermal or natural gas).

Table 1: Distribution of Surface Levelized Cost of Heat (SLCOH) for Census Places with population ≥ 4, 000 within the Appalachian Basin for NY, PA and WV. A total of 236 sites are shown; an additional 19 sites had SLCOH values greater than 25 \$/MMBTU. Results given in US \$ are normalized to year 2012.

State	Best Case (Green) \$5 – \$13.5/ MMBTU SLCOH	Good (Yellow) \$13.5 - \$16/ MMBTU SLCOH	Unfavorable (Red) \$16 - \$25/ MMBTU SLCOH
New York	30	27	30
Pennsylvania	37	52	27
West Virginia	21	10	2

The top sites for each of the three states based on the Place analysis methodology described above are listed in Tables 2 - Table 4.

Table 2: Top ten West Virginia Census Places with the lowest SLCOH. Only Places and Cooperating Places with population of 4,000 and above are included.

County	Census Place Name	Place Population	SLCOH (\$/MMBTU)
Lewis County	Weston city	4110	7.0
Upshur County	Buckhannon city	5639	10.9
Wetzel County	New Martinsville city	5366	11.1
Randolph County	Elkins City-Beverly Town	7796	11.1
Wood County	Parkersburg city	31,492	11.2
Ohio County	Wheeling city	29,051	11.2
Kanawha County	Charleston city	53,031	11.4
Monongalia County	Morgantown-Westover City	36,249	11.6
Harrison County	Clarksburg City-Anmoore Town	19,154	11.6

Taylor County	Grafton City	5164	11.7
---------------	--------------	------	------

Table 3: Top ten New York Census Places with the lowest SLCOH. Only Places with population of 4,000 and above are included.

County	Census Place Name	Place Population	SLCOH (\$/MMBTU)
Erie	Kenmore Village	15,423	11.2
Erie	Lancaster Village	10,352	11.2
Erie	Buffalo City	340,149	11.3
Erie	Eggertsville CDP	15,019	11.3
Monroe	Rochester City	224,987	11.5
Ontario	Canandaigua City	10,545	11.7
Erie	Grandyle Village CDP	62,773	11.7
Niagara	Niagara Falls City	50,193	11.7
Erie	Tonawanda City	15,130	11.8
Onondaga	Syracuse City	147,414	11.8

Table 4: Top ten Pennsylvania Census Places with the lowest SLCOH. Only Places with population of 4,000 and above are included.

County	Census Place Name	Place Population	SLCOH (\$/MMBTU)
Luzerne	Kingston Borough	13,182	10.9
Allegheny	Dormont Borough	8593	11.1
Luzerne	Wilkes-Barre City	41,498	11.2
Clarion	Clarion Borough	5276	11.5
Allegheny	West View Borough	6771	11.7
Butler	Butler City	13,757	11.8
Washington	Paris CDP	20,478	11.8
Mercer	Greenville Borough	5919	11.8
Luzerne	Plymouth Borough	5951	11.9
Allegheny	Bellevue Borough	8370	12.0

One of the final products of the analysis of utilization for district heating systems is a map that portrays on a 3-color or 5-color scale (Figure 26). For these maps, the surface levelized cost of heat (SLCOH, \$/MMBTU) at each location was converted to a non-dimensional measure of favorability that ranges from 0-3 or from 0-5, respectively, based on a set of threshold values. The thresholds are detailed in Memo 17 (Combining Risk Factors). The map for a 3-color scale and for the uncertainty corresponding to the Risk Factor map (**Figure 26**) can be found in Memo 17 (Combining Risk Factors) and as individual files in the Geothermal Data Repository.

As noted below and described in Memo 17 (Combining Risk Factors), in the step of combining several risk factors to illumine their combined risk metrics we added a 5 km buffer around all of the Places and Collaborating Places. This represents the potential to transfer water in pipes from a well field to a community district heating system.

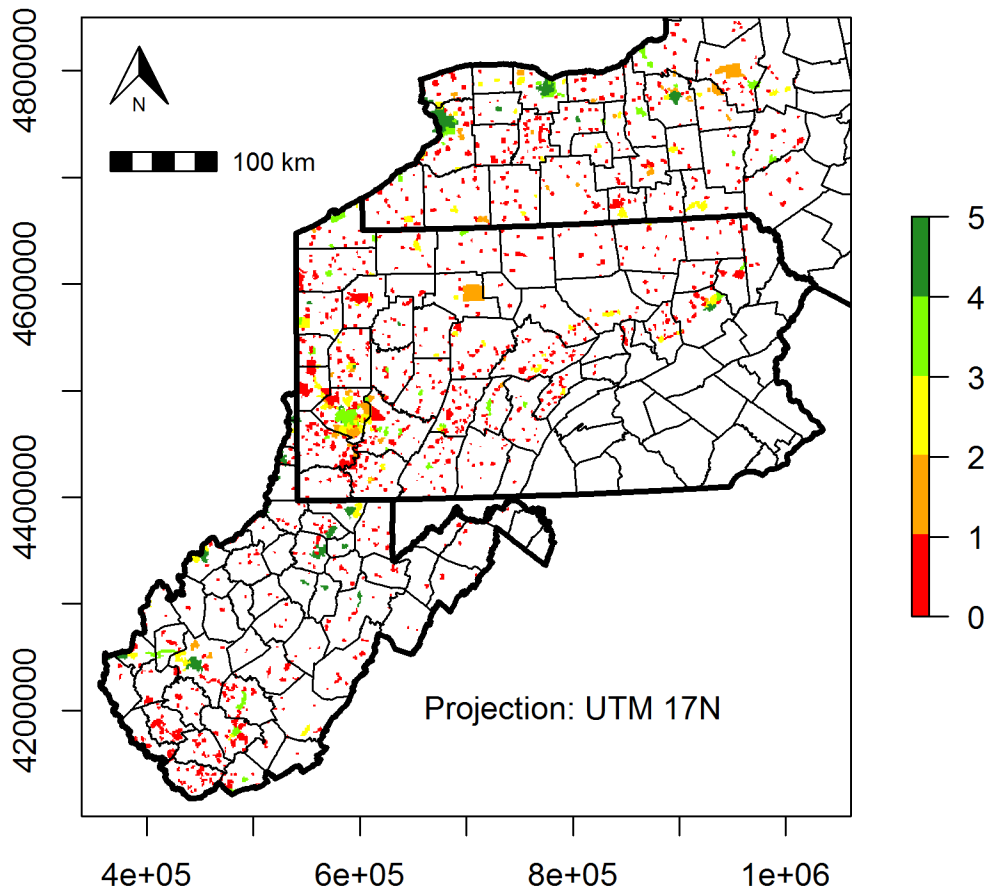


Figure 26: Play Fairway Metric risk segment map for the utilization of resource with a five color scheme. Green-Favorable, Red-Unfavorable. This illustrates the Places with no additional distance buffer; a buffer is added before combining this risk factor with others.

Challenges

For a utilization project focused on low-temperature geothermal applications, the temperatures are typically in the range of 50 to 120 °C. For these temperatures to be of value, utilization must occur close to the well field to avoid heat loss.

The Utilization Risk calculations followed the Reber et al. (2014) methodology; however only a subset of their methodology was most appropriate for the project and transferrable to other future phases of this project. The most significant challenge was to select between the slightly different methods to analyze the costs and benefits of utilization of geothermal fluids for district heating that had been developed in parallel by Cornell University and West Virginia University students. Both groups had worked on related projects that expanded the details within the GEOPHIRES program (Reber, 2013; He, 2015). It was determined that the addition of new variables and updates to the MATLAB code would be simpler if Reber's work scheme was applied uniformly across the three-state study area. Reber's files for the still-current 2010 US Census were used, along with the census data for WV. As a result of this work,

improvements to the methods and parameter names of Reber's code were made for ease of transferal to other users (see Catalog of Supporting Files for Utilization Analysis Memo).

Because the Utilization team removed the drilling expense component and the geotherm of a site from the analysis of costs of a direct-heating project, the value being mapped is not the Levelized Cost of Heat (LCOH) as originally planned as part of the SOPO, rather it is the Surface Levelized Cost of Heat (SLCOH). In the absence of drilling costs and their dependence on the site geotherm, the population density and climate-based heat demand became the variables of importance for the SLCOH. The impact on the Combined Risk of proximity of a community to a potential geothermal reservoir is expressed in the four-factor Combined Risk Maps.

For the compiled list of sites of commercial, industrial, or large private entities who plausibly might be interested in evaluating the potential to use deep direct geothermal heat, further analysis of potential utilization needs is recommended. We recommend that a full analysis of LCOH for several of those potential users be completed.

Task 5 Combined Risk Metric Analysis

The overall risk matrix analysis combined the four risk factors into an aggregate measure of the favorability of different locations, which we refer to as Play Fairway Metrics (PFMs). We explored several methods of combining the Task risk factors (discussed in more detail in Catalog of Supporting Files, Combining Risk Factors Memo). In the end we calculated the average, geometric mean, and minimum of the four scaled risk factors (SRF). The equations for calculating the average, geometric mean, and the minimum PFMs of the four SRFs are provided in EQ 1 to EQ 3.

Each of the risk factors are scaled to a non-dimensional measure of favorability from their original measure. One critical issue is that we require co-location of the resource with utilization locations; however in practice we expect that the resource can be a small distance (approximately 5 km) away from the utilization center. Therefore, each of the identified utilization places were buffered by 5 km. Many of the maps contained no data in some cells, for instance reservoirs are not known over the whole areal extent. Therefore only areas with all risk factors quantified at that cell (1 km² grid) were ranked in the final map.

$$PFM_{average} = 1/4(SRF_{seismic} + SRF_{thermal} + SRF_{reservoir} + SRF_{utilization}) \quad (1)$$

$$PFM_{geometric_mean} = \sqrt[4]{SRF_{seismic} * SRF_{thermal} * SRF_{reservoir} * SRF_{utilization}} \quad (2)$$

$$PFM_{minimum} = \min\{SRF_{seismic}, SRF_{thermal}, SRF_{reservoir}, SRF_{utilization}\} \quad (3)$$

In addition to simply calculating the PFMs, we also approximated the uncertainty of each using a first order Taylor series expansion. The Taylor series approximation is given in EQ 4, where m is the mean value of the SRF and the variance of each SRF_i is approximated by interpolating a table derived from Monte Carlo analysis, as described in the Methodology Overview document.

$$Var(PFM) \approx \sum_{i=1}^n \left[\frac{\partial PFM(m)}{\partial SRF_i} \right]^2 Var(\widehat{SRF}_i) \quad (4)$$

The Taylor series approximation is useful for the average and the geometric mean, but it is not a good representation of the minimum of several values unless 1 risk factor is always the minimum value. Because the distribution of each SRF is different, no general analytic results are provided for the uncertainty of the minimum. In order to obtain uncertainty in the minimum maps, we opted to run a Monte Carlo analysis with 10,000 replicates only for 5-color combined risk maps. These are provided in the text that follows.

Although the combined risk maps are useful, the ability to compare many locations at once on a site-by-site basis is also important. As an example of what is possible with the PFM analysis, we compared a small subset of potential sites to assess the individual Task Risk Factors that produced the final combined site PFM value for a site (**Figure 27**). At these same locations we computed more detailed measures of the uncertainty and generated boxplots that show the uncertainty in the mean of the combined risk for a site (**Figure 28**). This type of additional review will enable decision makers to understand if some projects are more or less appealing based on the uncertainty associated with different risk factors and the potential importance of that uncertainty. Multiple decisions makers may have different attitudes towards uncertainty, and uncertainty may be more or less important for varying types of projects.

For these sites we also compared the three methods of combining risk factors into PFMs. In general, the average value for a site (blue x in **Figure 29**) will always be greater than the geometric mean value (gray x in **Figure 29**), which will always be greater than the minimum value (black x in **Figure 29**). **Figure 29** also shows the Monte Carlo 90% probability interval (PI) for the mean value. In general, the uncertainty in the minimum is greater than the uncertainty in the geometric mean and the average.

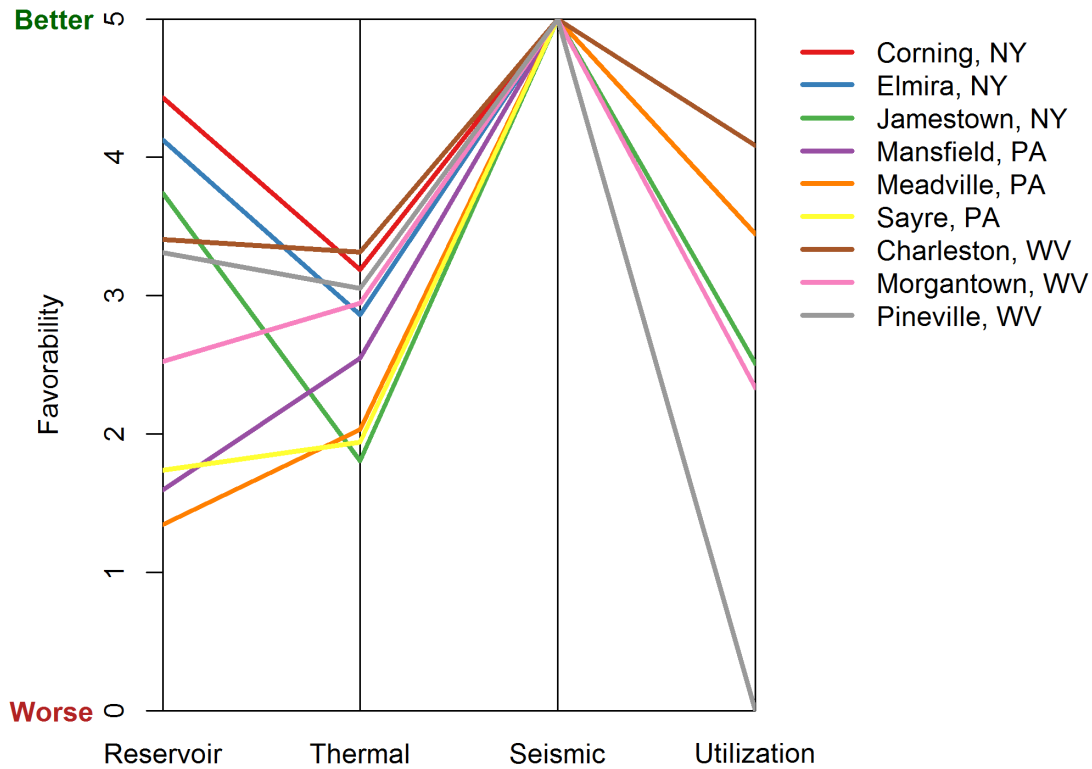
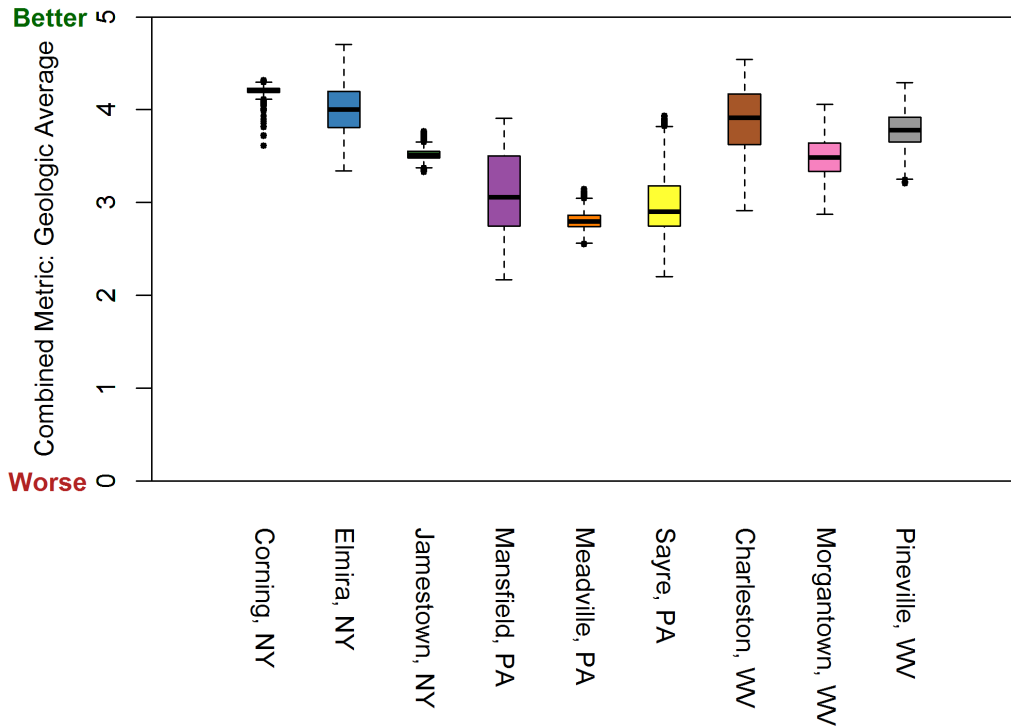


Figure 27: Example of a parallel axis plot for nine illustrative project locations. The reservoir metric illustrated is RFC and the risk factor combination method is the average. The plot emphasizes which sites tend to perform better on the metrics or if there are tradeoffs between objectives. This example illustrates the use of Reservoir Fluid Capacity as the reservoir metric.



Figure

Figure 28: Boxplots of the estimated empirical distribution of favorability for the three geologic variables for nine illustrative project locations, for combinations based on averaging the individual risk factors. The reservoir metric used is RFC. The distribution at each site reports the results of a Monte Carlo simulation. The box is defined as between the 25th and 75th percentiles with a line at the median. The whiskers extend to the most extreme observation that is within 1.5 times the interquartile range from the upper or lower quartile. Points outside the whiskers are plotted individually.

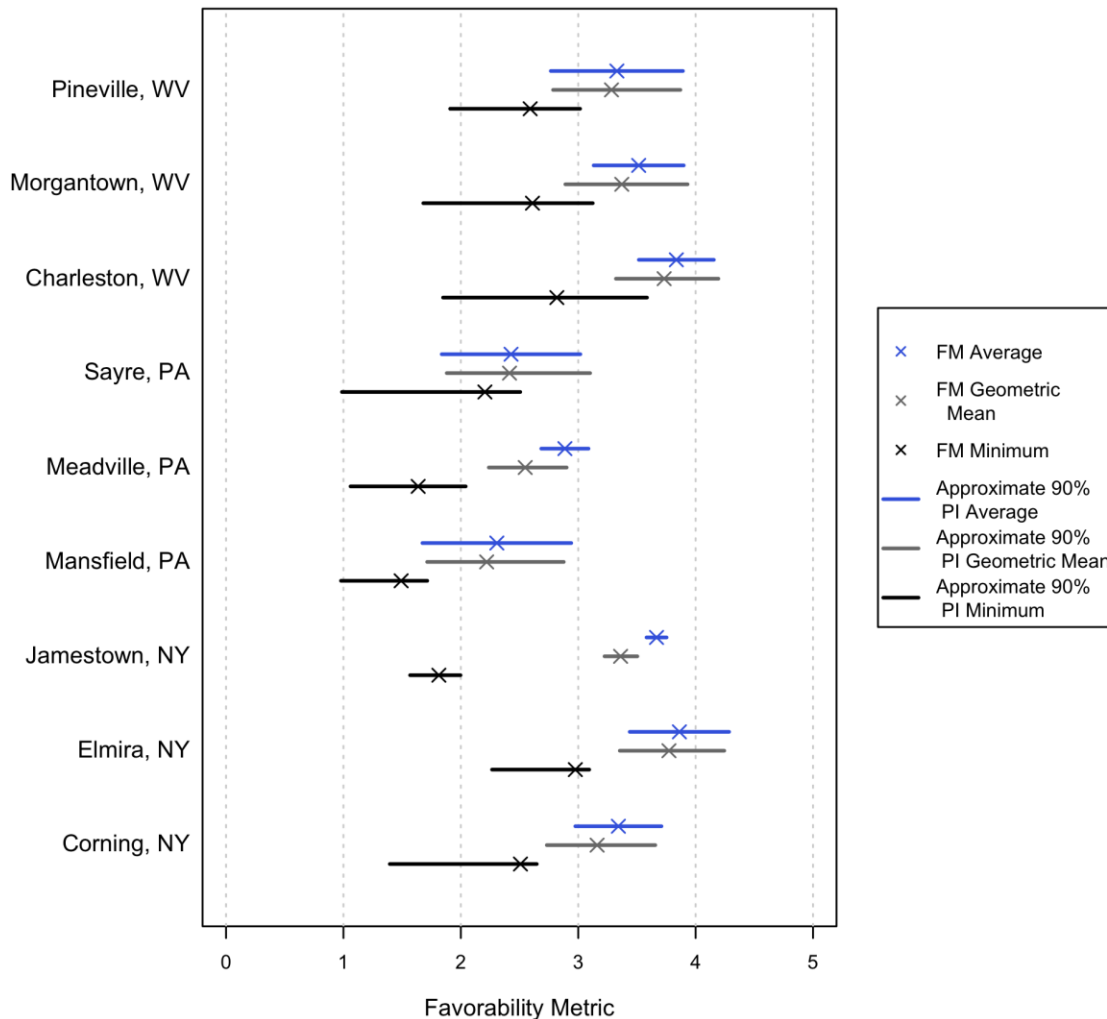


Figure 29: Graph showing the relative outcomes of the three different combination functions, for the geologic factors only. FM refers to the Play Fairway Metric. Note that FMavg (PFMavg) always exceeds FMgm (PFMgm), which are greater than FMmin (PFMmin) at selected sites. Lines represent approximate 90% probability intervals (5th to 95th percentile). PIs are based on the Weibull distribution for FMmin, the log-normal distribution for FMgm, and the normal distribution for FMavg. Note that the uncertainty is often greatest for the function of minimum. The reported FM is marked with an ‘x’. From Whealton (2016), based on analysis of the near-final data set for this project.

Challenges

Any attempt to combine different dimensions of a project, without a complete physical and economic analysis for a site, will involve critical approximations. A strength of the simple 4 risk factor analysis is that it provides several maps that could represent different ways a decision maker might consider combining the four risk factors. The values of each factor can also be represented spatially, which gives insight into where different factors are favorable. This allows identification of potentially favorable locations. Once a few especially attractive locations are identified, the decision maker can be presented

additional site-specific information including the uncertainty distribution of the four risk factors and of the combined metric.

This analysis is limited in several ways. First, there are no existing geothermal district heating systems in the Appalachian Basin study area, and therefore no test cases against which to compare our combined risk metric. Second, the combined PFMs are only relative representations of favorability because there is no unified economic model. If there were information on the economic costs of seismic insurance, for instance, then this could be incorporated into a single model; but this is not feasible in a preliminary screening analysis. We have implied equal weighting, but some risk factors might have disproportionate impacts on the economics of a project. Additionally, the thresholds are not uniformly specified across risk factors. For instance, a value of 2 in thermal does not imply the same level of favorability (likelihood of success) as a value of 2 for seismic. The thresholds used in scaling are relative rankings. Thresholds are reasonable measures of general favorability, but they will cause the result to only represent relative favorability in the combined PFMs.

The uncertainty values assigned to each risk factor were based on spatial prediction errors (thermal risk factor) and professional judgment of researchers who analyzed the other risk factors. Therefore, our estimates of the uncertainty of the combined metric also is dependent upon the assessment by the developers as to the relative precision of different factors. The intent of the uncertainty analysis is to honestly represent the precision of the analysis as understood by those who performed the calculations, and to improve the characterization of the uncertainty associated with the recommendations to direct additional investigations.

Utility of the Methods for Application at other Sites

From the onset, the Geothermal Play Fairway Analysis – Appalachian Basin (GPFA-AB) team emphasized a detailed regional study with a premium on developing methods that were transferable to other areas of interest (see Catalog of Supporting Files). Geological examples include widely available datasets and a detailed description of methods. The Utilization effort focused on two categories of direct use that are widely applicable, first to residential and community users and second to high heat-demands users such as universities, industrial processes, government facilities, etc. The methods and assumptions are extensively described in a series of memos (listed in the Catalog of Supporting Files). Numerous Tier 1, 2 and 3 data have been submitted to the National Geothermal Data System (NGDS) via the Geothermal Data Repository, as described in the Catalog of Supporting Files.

Commercial Viability of the Play

Phase 1 results for the best Play Fairways in the Appalachian Basin enhance commercial viability by reducing risk of development. Additional study is vital to address the economic viability of geothermal district heating of any given location in the study area. Recommendations for work to assure commercialization is laid out in the Catalog of Supporting Files.

The Phase 1 analyses clearly indicate the presence of a low temperature geothermal resource. The thermal analysis indicates useful temperatures can be accessed at reasonable drilling depths (e.g., 80 °C can be reached between 1000–3000 m depth in 30% of the Appalachian Basin (Figure 6). With some important local exceptions, the reservoir rocks are of low inherent porosity and, by inference, permeability, at these depths. The reservoirs that have high possibility for natural productivity should be targets for immediate follow-up research. Elsewhere that the thermal resource quality and utilization opportunities align, the reservoirs either lacked data for characterization, or stimulation would be needed, as it has been for many decades of hydrocarbon extraction in the basin. While the available flow rate at depths of interest is not

yet fully understood, the investment return analysis must consider the possibility of costs associated with both initial stimulation and ongoing circulation of fluids at relatively high flow rates to support a closed loop district heating system of sufficient scale to justify these costs.

While these costs are significant, the threshold for alternative energy sources in the study area is higher than the nation as a whole. The study area includes New York, with 2014 average retail price of electricity 156% of the national average. While Pennsylvania as a whole is just under the national average, both the residential and industrial sectors exceed the national average at 107% and 106% respectively. West Virginia actually pays less than the national average for electricity, but there are substantial environmental benefits associated with shifting a portion of West Virginia's electricity generation and consumption from coal (~80%) to cleaner alternatives. In this region, heating accounts for the primary electricity consumption. Because of this, district heating is proposed as the most economically justifiable use of the low temperature geothermal resources.

When analyzing the utilization risk factor, which is essentially the first stage of an economic analysis, the team considered scenarios that favor economic viability. For instance, because the up-front capital investment is significant, the utilization calculations intentionally excluded very small (population <4,000) municipalities that might otherwise be suitable in terms of the geological characteristics. Distance between resource (production wells) and consumers is also treated as an important economic factor, through both the impact on costs of piping and on heat loss. Many of the largest population centers within the study area are surrounded by suburban areas. Those suburbs have a large population and may be more suitable for siting a geothermal well field in a neighboring rural area within 10 km distance. Some potential consumers of the heat may have motivations beyond the cost of heat per BTU, such as independence from the utility grid, commitment to renewable energy, or atypical needs for heat such as an industrial or agricultural application. Our analysis does not quantify those benefits.

The primary environmental hurdle is believed to be seismic risk. This was addressed as one of the major factors in determining the viable plays. Other environmental factors, such as wetland protection, should be able to be addressed through proper engineering design, community education efforts, and permitting. The circulating geothermal fluids at the surface are presumed to be a closed loop system, with reinjection of all volumes produced, engineered to have casing in the upper portions of the wellbore within reach of fresh water aquifers and/or the water table. The target temperature of 80 °C would rarely be reached shallower than 1,000 m, which is likely deeper than drinking water aquifers. One environmental factor that has not been addressed during Phase 1 is the water needs associated with supplying necessary flow rates through the reservoir rock. Studies of water system risks related to high volume hydraulic fracturing have demonstrated that the availability of water in New York, Pennsylvania and West Virginia is not among the more important limiting environmental factors, though of course water supplies need to be planned and the extraction from certain streams avoided (Rahm and Riha, 2012; 2014).

An initial effort at understanding the permitting requirements was completed as shown in the Permitting Memo. There is a need for further review as part of the well site selection work. Geothermal energy extraction regulations are not established in NY, PA and WV, except for geothermal heat pumps, creating limited levels of legislative clarity concerning the deeper geothermal resource. For example, in Pennsylvania and West Virginia it has not been designated if geothermal energy is a mineral right or a surface right. In New York, it is not legislatively designated as a mineral, but it is at least listed as a type of drilling under the oil and gas permitting section. As a future effort, it is recommended that test scenarios be worked through the permitting process of the deep geothermal wells with the appropriate agencies to educate them and then assist them in expanding their forms and the permitting process. Further details are given in the Catalog of Supporting Files.

Possible heat resource users (>165 sites) in addition to Census-identified “places” have been identified in the three states. For three cases, explicit interest in extraction of geothermal heat in the temperature range investigated in this study has been brought to the team’s attention. For instance, the West Virginia National Guard is interested in pursuing alternative sources of onsite energy at military bases, motivated by the security associated with grid independence. The Cornell University community has adopted a Climate Action Plan, pledging to become carbon neutral by 2050, and there is interest in accelerating this to completion by 2035. West Virginia University is poised to upgrade an aged campus direct heating system, previously supplied by steam from a nearby coal-fired power plant under a contract that expires shortly, with a new heat source, and is considering geothermal energy among the options. More generally, the city of Pittsburgh, Pennsylvania participated in the DOE August Direct Use Workshop and has undertaken many energy efficiency initiatives with programs like Sustainable Pittsburgh and the 2030 District¹.

METHODOLOGY

The methodology applied to the Appalachian Basin Geothermal Play Fairway Analysis is described generally in this section, and more thoroughly in the Methodologies Overview found in the Catalog of Supporting Files. Additional details can be found in the 18 ‘Project Memos’ found in the Catalog of Supporting Files of this report.

The overarching process involved evaluation of each risk factor, resulting in 4 risk segment maps and 3 maps of uncertainty (the Utilization risk factor was assigned an uncertainty deviation equal to 5% of the computed value for the entire basin, and thus not mapped) (**Figure 19**, **Figure 22**, **Figure 25**, **Figure 26**). Following this, the 4 risk factors were combined into a single favorability map. The Catalog of Supporting Files discusses the methodology for computing each of the four risk factors as well as the combination effort, touching on: a summary of the strengths and limitations of the process, mathematics used, potential sources of error, software used, and the results of any testing used to demonstrate satisfactory model performance. Hyperlinks to specific Memos are inserted within the Catalog of Supporting Files text for more information on mathematical formulas and calculation methods, potential sources of error, details on the software used (such as version and hardware requirements), and code verification/validation, sensitivity analyses, history matching with lab or field data, as appropriate.

A key assumption central to the project is the understanding that this particular play fairway analysis is focused on low temperature and/or direct use applications. The Appalachian Basin, like much of the contiguous U.S., has relatively average continental heat flow (Blackwell and Richards, 2004). While not hot enough for traditional hydrothermal power generation, the basin is expected to be warm enough for a reduction of power load through direct use applications such as district heating (Reber, 2013). Despite the fact that these low-temperature systems can have a lower initial capital requirement than a large hydrothermal power plant, understanding where they will be most successful is critical.

The oil and gas industry has utilized Play Fairway Analysis as a means to site oil and gas well drilling in the most advantageous locale, within resource constraints. This project strives to use a similar approach. The four primary risk factors identified as critical to the success of a low-temperature geothermal project (e.g., quality of the thermal resource, potential for natural reservoir flow, induced seismic risk, and demand for the geothermal resource) are not considered to be a complete list of requirements. Indeed it is intended that a ‘down select’ based on these initial four criteria will allow later stages of the assessment

¹ <http://www.pittsburghpa.gov/green/energyefficiency.htm>

that may be more costly to focus on only the most advantageous locations. This Geothermal Play Fairway project proposes identifying sub-regions worthy of the next stage of activities (exploratory drilling and/or additional well logging, permitting due diligence, negotiation of project partnerships, funding avenues, etc.).

The project workflow consisted of a series of seven overlapping tasks, each with various subtasks, designed to identify the play fairways. The first four tasks were specific to the four risk factors (Figures 30-34). Task 5 evaluated the combined risk, to identify candidates for continued Phase II activities (Figure 35). Task 6 encompasses project management and Task 7 provides for sharing Phase I plans and results.

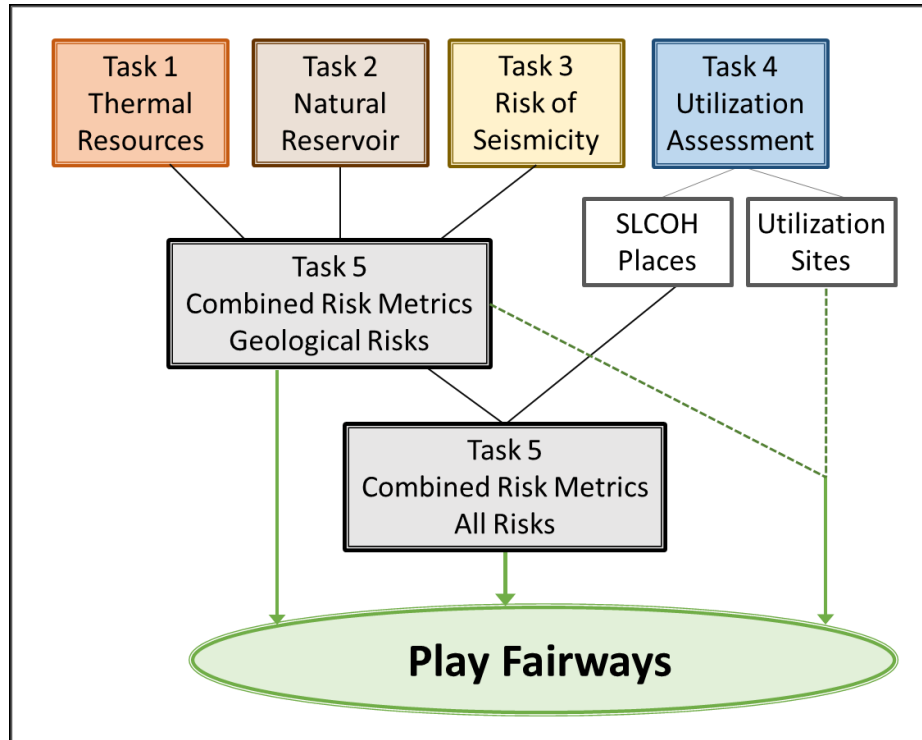


Figure 30: Appalachian Basin Geothermal Play Fairway Analysis Process. Each of four key risk factors studied in the context of favorability and uncertainty were combined using Play Fairway Metrics (PFM) to create final Play maps and overall basin risk.

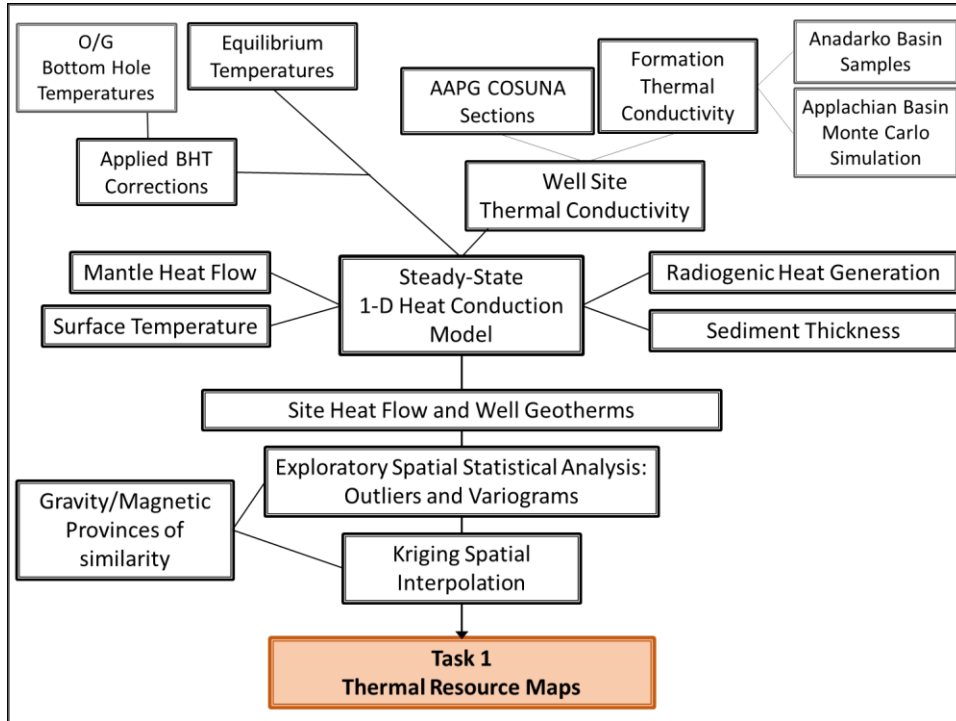


Figure 31: Flow chart for Task 1 Thermal Resources Risk showing primary data and overview of steps.

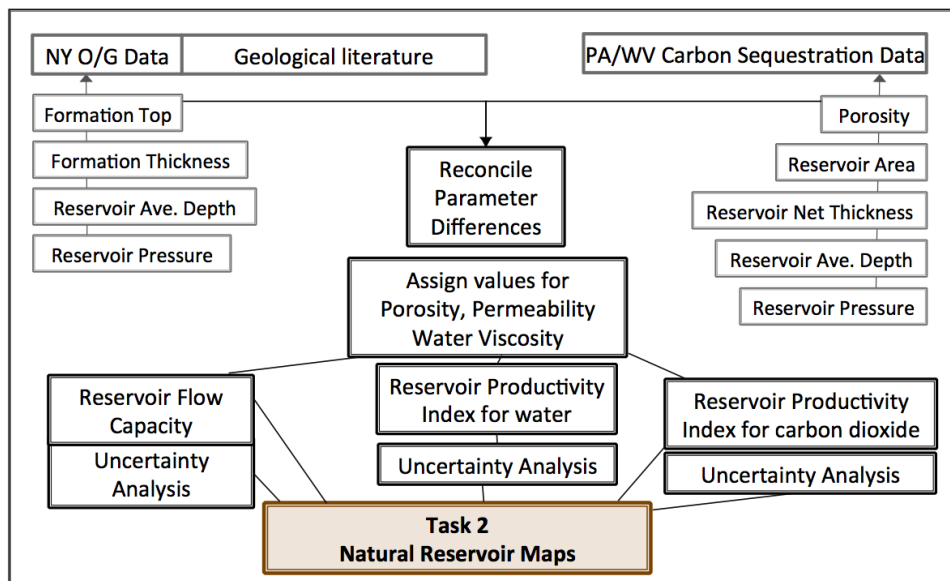


Figure 32: Flow chart for Task 2 Natural Reservoirs Risk showing primary data and overview of steps.

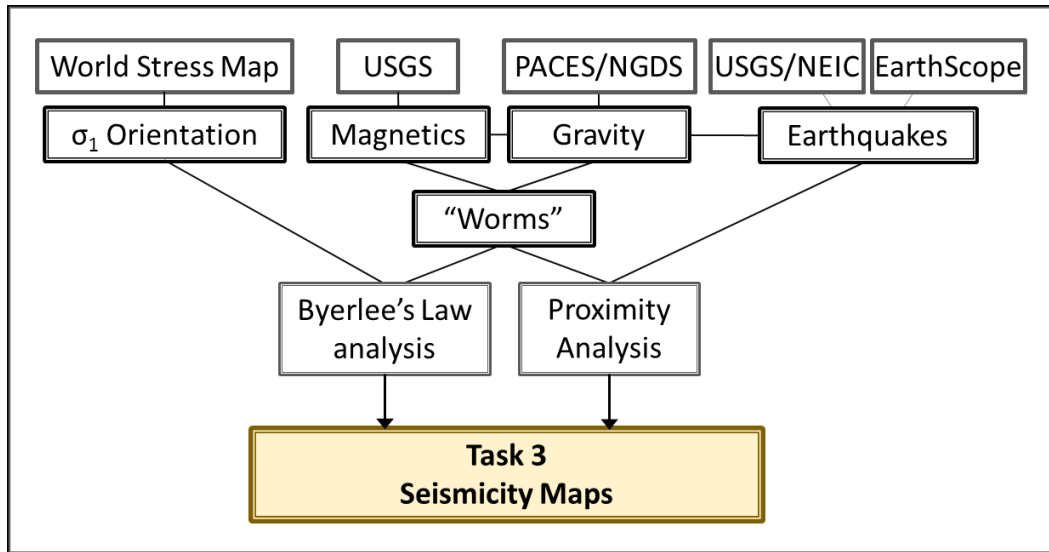


Figure 33: Flow chart for Task 3 Risk of Seismicity showing primary data and overview of steps.

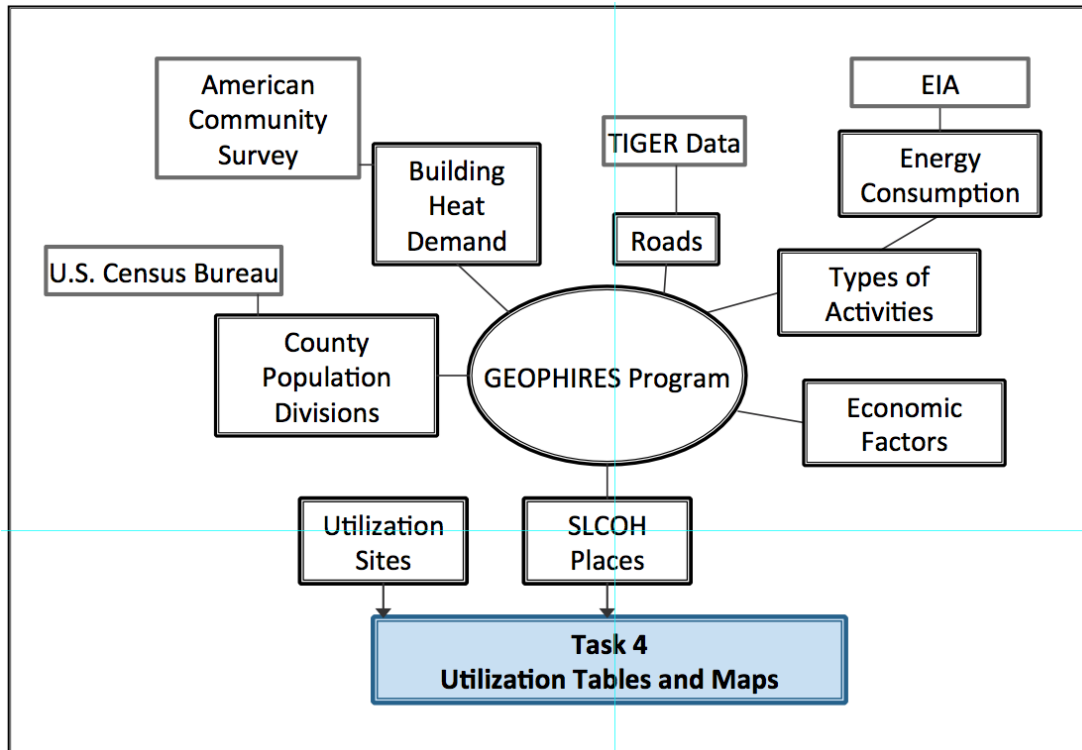


Figure 34: Flow chart for Task 4 Utilization Assessment showing primary data and overview of steps.

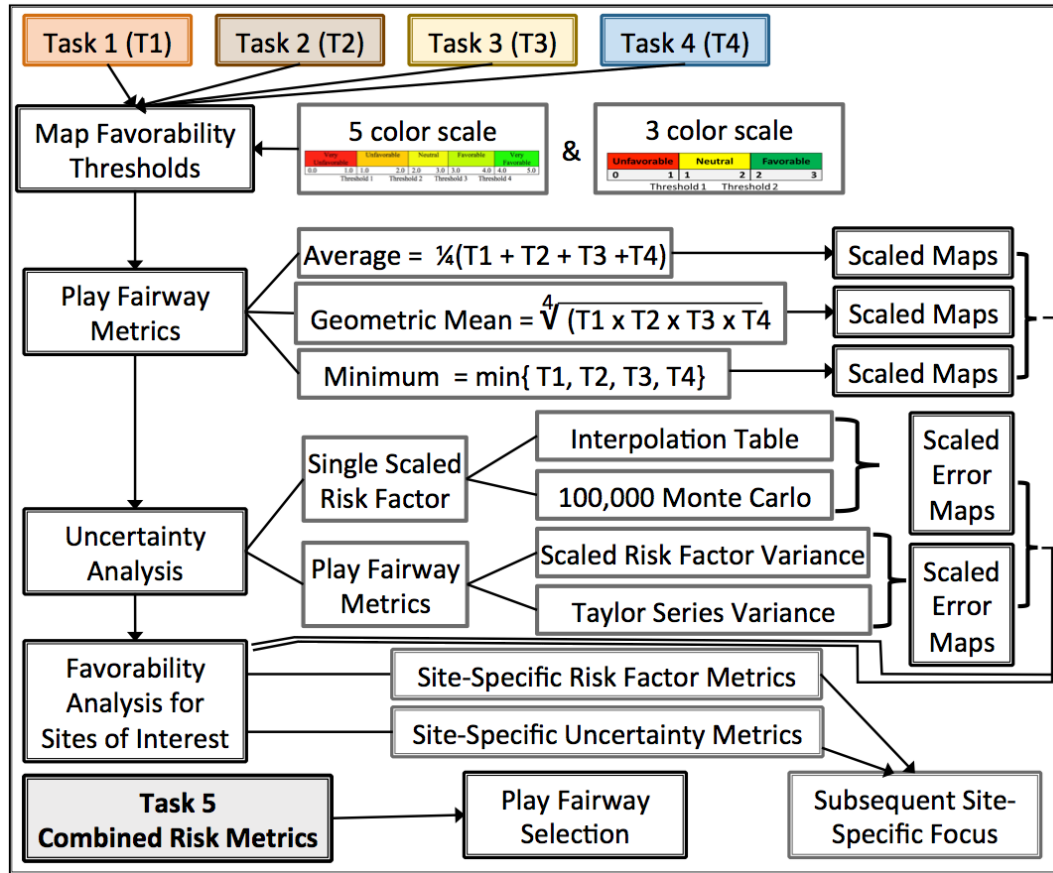


Figure 35: Flow chart for Task 5 Combining Risk Metrics showing an overview of main steps and methods for producing favorability maps.

The final step was designation of certain regions as Geothermal Play Fairways based on the computed common risk assessment maps. This step was both quantitative and qualitative. Quantitatively, the designations were informed by aggregated Play Fairway Metrics from a suite of models that combine all categories of risk and alternative models that combine subsets of the four major factors. Regions which had high potential in any 2 risk factor categories (e.g. good temperature and near a city; or near a city and a set of reservoirs of high quality) were considered to be candidates for designation as a play fairway of interest. Qualitatively, we consider the geological variability known to occur across the study area, the possibility for technological advancement in heat recovery from the rocks, and the possibility for uses of direct heat not described in our population-based analysis of the Surface Levelized Cost of Heat for district heating systems. Because the reservoir data set is highly discontinuous in space for a reason that is not pertinent to its potential to be used as a geothermal reservoir, namely the presence and absence of oil and gas, we selected Play Fairways that are much more spatially continuous than are the quantitative Play Fairway Metrics maps.

DISCUSSION OF RESULTS

Phase 1 of the Appalachian Basin Geothermal Play Fairway Analysis project was a success, with original goals and objectives accomplished.

Primary Conclusions

Thermal Analysis

The thermal resource maps created as intermediate products of this project improve upon some previously published Appalachian Basin thermal resource maps, including, but not limited to Blackwell & Richards (2004), Frone & Blackwell (2010), Shope et al. (2012), Aguirre (2014) and Stutz et al. (2015). Results of the Phase 1 thermal analyses show that geothermal resources in the Appalachian Basin are indeed almost exclusively low temperature, which is in agreement with previous analyses.

The results indicate that rocks of temperatures of 80 °C can be reached across approximately 30% of the coverage area at depths routinely accessed between 1000-3000 m (Figure 6), with varying levels of certainty. These depths are comparable to the average depth of oil development and natural gas development wells in the US, which were 1500 m and 2000 m, respectively, in 2008².

The costs of geothermal energy development projects will be strongly dependent on the depth to temperatures needed for a given project, thus we consider it paramount to better validate the regional thermal models, to reduce the uncertainty on temperature predictions and, in turn, the uncertainties on project costs. A priority for future work should be to validate or modify the BHT corrections. Additionally, uncertainties in the predicted depths to temperatures needed for projects also result from the use of inaccurate thermal conductivities (e.g., Crowell, 2015). Future studies should measure Appalachian Basin conductivities, thereby increasing the accuracy of the predicted temperature values relative to the use of Anadarko Basin thermal conductivities. Additionally, a future priority should include collecting detailed thermal logs from shut-in or about-to-be-abandoned wells. These logs will provide ground-truth for our thermal models and their assumption of conduction-only heat flow — as well as constraints on the distribution of thermal conductivities actually encountered in the rocks.

Reservoir Favorability/Productivity Analysis

A new methodology and set of metrics were developed to quantify the favorability of known hydrocarbon reservoirs to perform as low-temperature geothermal reservoirs. Either directly or indirectly, these productivity metrics take into account the depth, reservoir thickness, and permeability. A potential weakness of the method is that it uses an estimation of matrix permeability flow for all cases, including reservoirs dominated by fracture permeability. Nevertheless, in the validation of the methodology RPI performed well when compared to gas production volume data for both fractured and porous reservoirs.

The metrics RPIw and RFC predict similar distributions of the variability of reservoir quality across the study area, with RPIw generally one rank less favorable than RFC (Figure 21a,c). This similarity of pattern stems from the facts that both metrics depend direct on the permeability of water and permeability varies by several orders of magnitude whereas factors like thickness vary much less; a sensitivity analysis showed that permeability is the dominant factor in RPIw values (Methodology appendix). Future experience with direct-use geothermal energy systems, further analysis of the total leveled cost of heat for a family of possible end-use systems, and technological progress would lead to revisions of the

² http://www.eia.gov/dnav/ng/hist/e_ertwo_xwdd_nus_fwa.htm;
http://www.eia.gov/dnav/ng/hist/e_ertwg_xwdd_nus_fwa.htm

reservoir metric thresholds for ranking. Any such changes in the thresholds would alter the combined risk outcomes. Whereas the RPIg map appears much more favorable (Figure 21b) because the use of supercritical carbon dioxide increases the flux of working fluid through the reservoir pore system, the employment of supercritical carbon dioxide as a working fluid lies further into the future of technological advances and policy development than does the use of water as a working fluid.

With reference to the metric Reservoir Productivity Index for water as the working fluid (RPIw), the Phase 1 reservoir favorability analysis found that the reservoir productivity potential in the basin is highly variable (Figure 21), and the majority of the study area could not be ranked by reservoir productivity because of a lack of suitable data. While the great majority of reservoirs are of low natural quality (RPIw < 1 kg/[MPa-s]), a small subset has a productivity index >10 kg/(MPa-s) (Figure 21), which may be sufficient flow to produce without reservoir stimulation. The productivity index values in excess of 1 kg/MPa-s correspond to the following formations:

- Trenton-Black River dolomite fields in southern NY and northern PA
- Lockport dolomite in northern PA
- Galway (aka Theresa, or Rose Run) in northwestern PA and western NY
- Bass Islands Formation in NY and PA
- Newburg Sandstone in southwestern WV
- Onondaga Limestone Reefs in southern NY and northern PA
- The Elk Group Sandstones in various location in Pennsylvania
- Devonian Unconformity Play in southwestern PA.

A sensitivity analysis showed that the low productivity index for most reservoirs results from low permeability (see Catalog of Supporting Files: Methodology). Furthermore, the oil and gas industry has commonly employed stimulation for over 50 years in the study area, ranging from small degrees of stimulation in vertical wells up to high volume horizontal hydraulic fracturing. That history suggests that reservoir improvement by stimulation (hydraulic shearing of existing fractures to improve permeability and flow rate) should be given appropriate consideration in future studies.

We have drawn two major conclusions regarding the usefulness of the techniques employed for this risk factor. First, among the more than 1800 reservoirs analyzed, this technique successfully distinguished between low quality reservoirs and the best quality reservoirs. Second, reliance on data from oil and gas fields provides incomplete understanding of the regional distribution of and variations among natural reservoirs. There is a need for future evaluation of potential reservoirs that did not produce oil or gas (“saline water aquifers”) to increase reservoir coverage. In total, because there is such incomplete coverage of reservoirs in our study area (**Figure 22**), and also because our reservoir uncertainty index was based more heavily on data quality rather than on reservoir heterogeneity, we recommend that the calculated uncertainty map play a small role in reservoir decision-making. High uncertainty could be due to poor reservoir quality, or it could be due to a lack of data to make an accurate prediction of reservoir quality. Regardless, if natural reservoirs are to be exploited for geothermal energy in the Appalachian Basin, additional work is recommended to develop a better way to understand and estimate variability within the reservoirs themselves.

Part of the Phase 1 uncertainty exists because fractured reservoirs are common in the Appalachian Basin. Even though our sensitivity analysis of four reservoirs found a good match between the predicted RPI and gas production for a case of a fracture-dominated field, it is not known whether that success would hold for the majority of fracture-dominated reservoirs. Analysis of fracture-dominated reservoir systems could be improved by the integration of more well test and production data, and by further integration of

fracture-flow principles. A theoretical approach that considers the orientation of planes of weakness in the stress field predicts the orientations and locations of zones of dilatant strain, which should favor water flow through fracture systems. A regional prediction of the tendency toward dilation is straightforward to add to the analysis used to evaluate induced seismicity. If that theoretical analysis is completed, its results should be compared to the known locations of any of the fracture-dominated oil or gas reservoirs as a quality test.

Seismic Risk Analysis

Throughout the Appalachian Basin study region, based upon analysis of historical earthquake activity, of the locations of rock-property discontinuities that may be faults, and of the regional stress field, we highlighted areas at increased risk of induced seismicity (Figure 23 - Figure 25). Earthquake activity over the last 50 years occurred sparsely across the three states of interest, and no seismic events of magnitude exceeding approximately ML 4.7 occurred. Within the Appalachian Basin in New York, the natural faults with a known slip history are almost entirely limited to the northern half of the Basin region (Figure 23), where the insulating sedimentary basin rocks are thin and therefore the geothermal heat opportunities are not favorable. In Pennsylvania, most of the sparse natural earthquakes occurred in the northwestern extreme of the state, where the largest recorded event is of ML 4.5. This cluster of seismic events occurs in general proximity to good natural reservoirs but only modest quality thermal resources. In West Virginia, natural earthquakes are more widespread in the southwestern half of the state, including the ML 4.7 event in the southernmost county (McDowell), but no natural earthquake activity has been recorded in the northeastern half of the state in the last 50 years (Figure 23). Although the thermally favorable areas of southwestern West Virginia are in relatively close proximity to clusters of natural earthquakes, the thermally favorable areas of the north-central part of the state are distant from known earthquakes.

Acknowledging that a 50 year earthquake record is insufficient for characterizing risk, the incorporation of a second theoretical means of risk analysis suggests much more widespread occurrence of localized zones of enhanced risk (Figure 24). To acknowledge the theoretical slip-tendency solution while placing greater confidence on the proximity-based solution, we recommend considering the average risk index (Figure 25) as the working hypothesis for risk of induced seismicity. However, the accuracy of this prediction is likely low, because neither the orientation nor the magnitudes of the local stress field are known.

To make major improvements on the regional-scale analysis of risk of induced seismicity would require a very large research undertaking. The data collection effort needed to determine which “worms” are indeed zones of weakness, to determine the local stress orientations, and to measure stress magnitudes is large. We recommend that a collaboration among seismologists and potential-field geophysicists be undertaken as a step towards validation of the Phase 1 approach with detailed real-world microseismicity.

Utilization Analysis

The distribution of Surface Levelized Cost of Heat (SLCOH) is highly skewed (Figure 36): very few census locations provided an estimated cost of less than \$10/MMBTU. Our results show that roughly 9% of Census Place (and Cooperating Places) have a SLCOH in the range of \$10/MMBTU to \$15/MMBTU, 6% ranged from \$15/MMBTU to \$20/MMBTU, and for the remaining approximately 85% such a means of heat delivery by district heating system would cost much more.

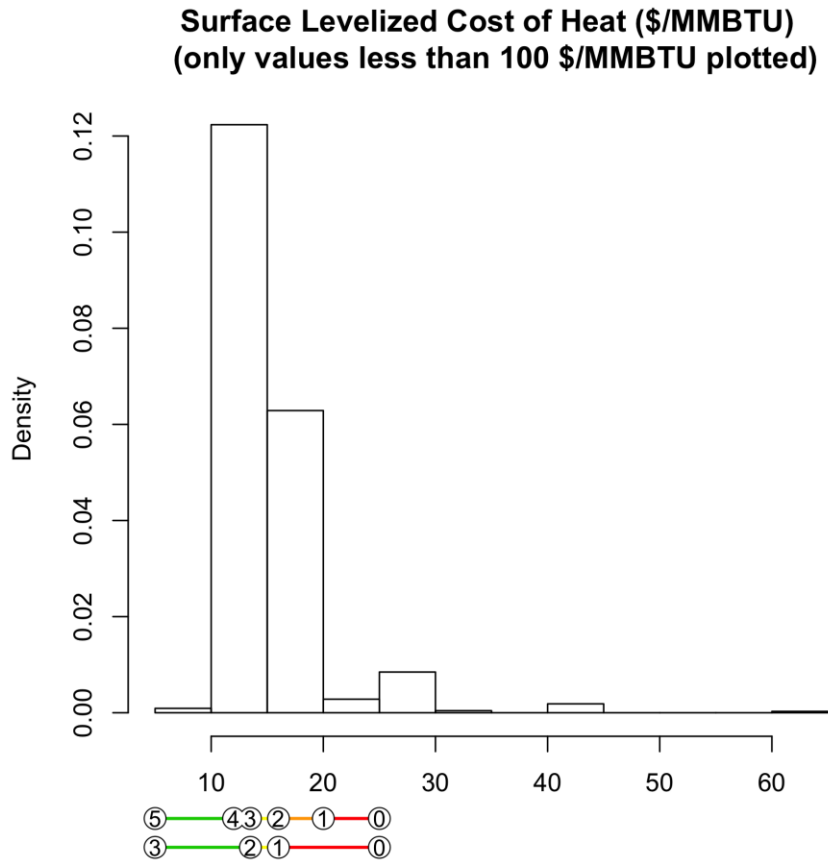


Figure 36: Density histogram of Surface Levelized Cost of Heat among Census Places in the Appalachian Basin that have populations >4000. Of the two colored lines at bottom, the upper one shows the threshold SLCOH values corresponding to the five colors of the Figure 37 map. The total area of the bars sums to 1.

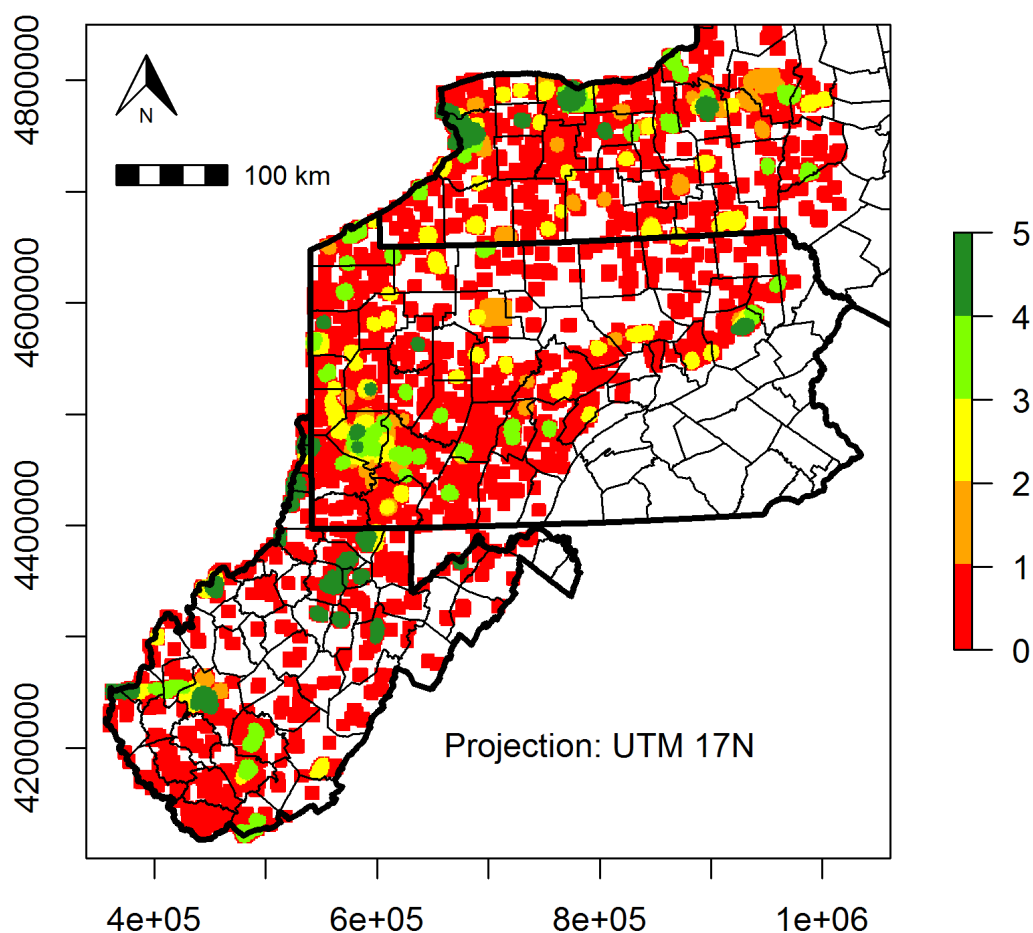


Figure 37: Utilization risk segment map (with 5-km radius buffers around Places). Green is favorable (lower SLCOH) and Red is higher SLCOH). See Figure 36 for the threshold SLCOH values between colors.

Some communities of favored low cost for such a system (Figure 37) occur in areas with moderate to favorable thermal resources, such as for the West Virginia cities of Buckhannon and Charleston (Table 2; Figure 6). In Pennsylvania, low SLCOH estimates overlap with moderate thermal resources for Greenville Borough in Mercer County and Clarion Borough in Clarion County (Table 4; Figure 6). In New York, the five high population areas with lowest SLCOH do not occur in thermally favored regions (Table 3; Figure 6), although some smaller cities in the southern tier of counties (i.e., Elmira in Chemung County) have reasonably favorable SLCOH (\$13.9/MMBTU), moderately good thermal opportunity, very good reservoir opportunities, and a minimum of seismic risk (Figure 56 of Memo 17, Combining Risk Factors: Detailed Calculations and Extended Results). Now that the distribution of resources in the subsurface has been newly established (temperature and reservoir resources), we recommend that a study be carried out to add the subsurface costs to the district heating surface costs for a few communities. The resultant LCOH for district heating systems will then be appropriate for discussion of alternative energy supply choices.

In addition to a risk factor analysis map based on census data, the team also identified more than 165 prospects for high value direct-use geothermal energy opportunities throughout the study area. These

include industrial sites, university campuses, and federal facilities, among others. We recommend also that some of these sites be selected for estimation of surface and subsurface costs and LCOH analysis.

Combination of Risk Analysis

The four individual analyses were combined into final favorability maps using several techniques (average, geometric mean, minimum values) (Figure 38 - **Figure 40**). The uncertainty associated with each combination of the four risk factors has been computed. We also computed the uncertainty for each of the methods. For the case of the combination achieved by averaging the four factors, a map of the spatial distribution of uncertainty is shown in Figure 35b. Similar uncertainty maps for all the other combinations can be found in the Methods Overview. The various techniques emphasize differing properties of the choices that an institution might make, and thus for now all are retained.

Using all 4 risk factors, the averaging of the individual risk factors (Figure 38) indicates the most favorable counties within the study area are the West Virginia counties of Monongalia, Harrison, Lewis (dubbed the Morgantown–Clarksburg play fairway), Putnam, and Kanawha (Charleston play fairway), the Pennsylvania counties of Mercer, Crawford, Erie, and Warren, and adjacent Chautauqua county in New York (together, the Meadville–Jamestown play fairway), and New York counties of Chemung and Steuben plus adjacent Bradford county in Pennsylvania (Corning–Ithaca play fairway). These areas are treated as the higher priority portions of four play fairways, surrounded by broader medium priority zones. Also treated as medium priority and worthy of additional exploration is a broad region near Pittsburgh Pennsylvania, for which the available geological data are insufficient to fully analyze the geological risks but yet the population is high. For uniformity, these five play fairways are illustrated on all of the following sets of Play Fairway Metric maps.

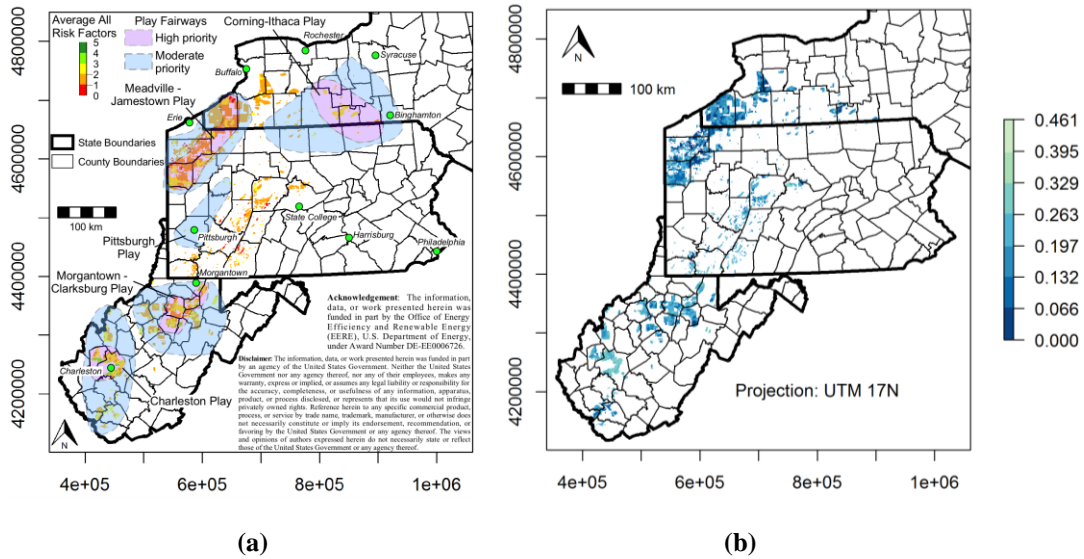


Figure 38: a) Favorability map for the combination of all four risk factors using an average, for the reservoir metric RPIw. Green-Favorable, Red-Unfavorable. b) Uncertainty on the combined risk expressed as standard deviation. Darker tones indicate less uncertainty.

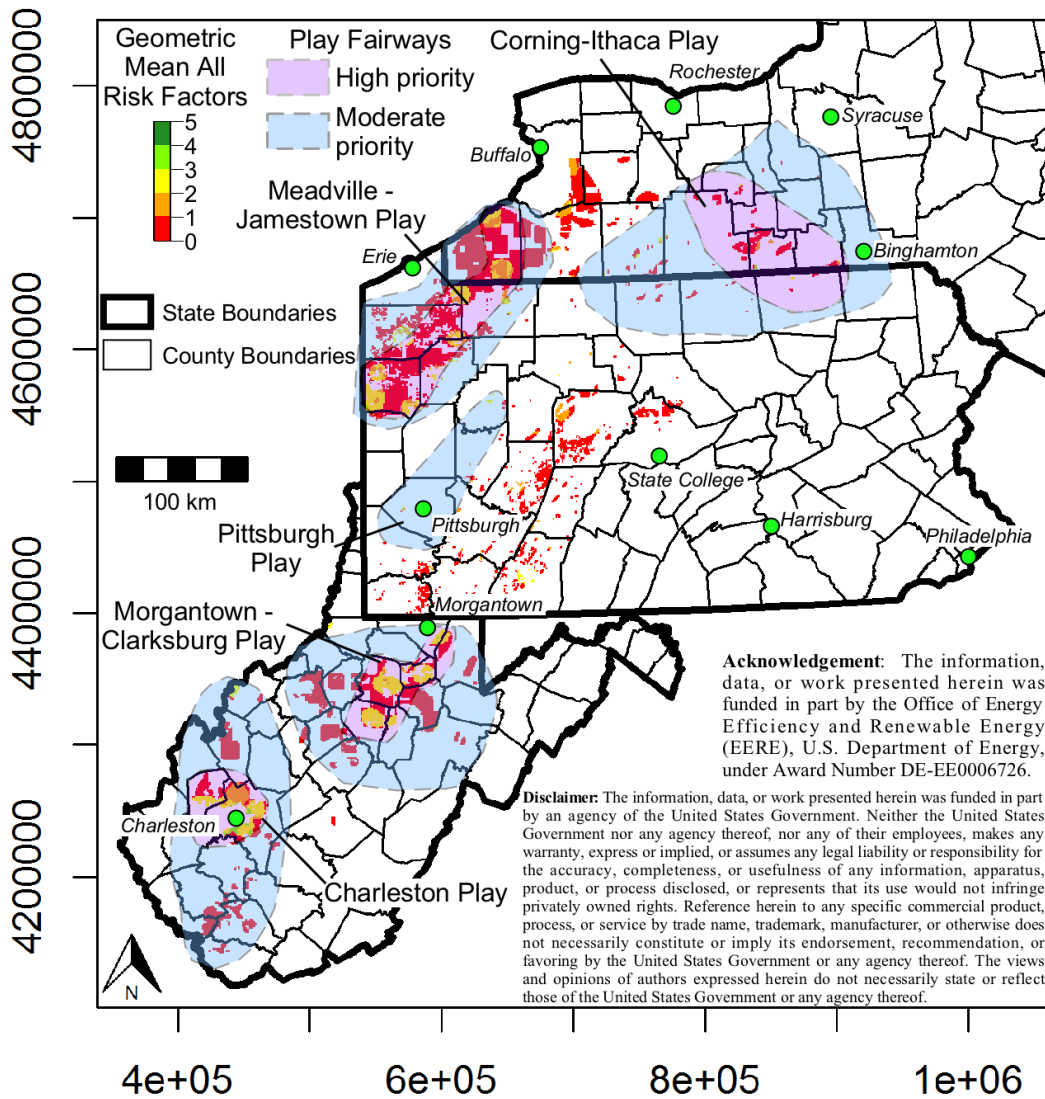


Figure 39: Favorability map for the combination of all four risk factors using the geometric mean, for the reservoir metric RPIw. Green-Favorable, Red-Unfavorable.

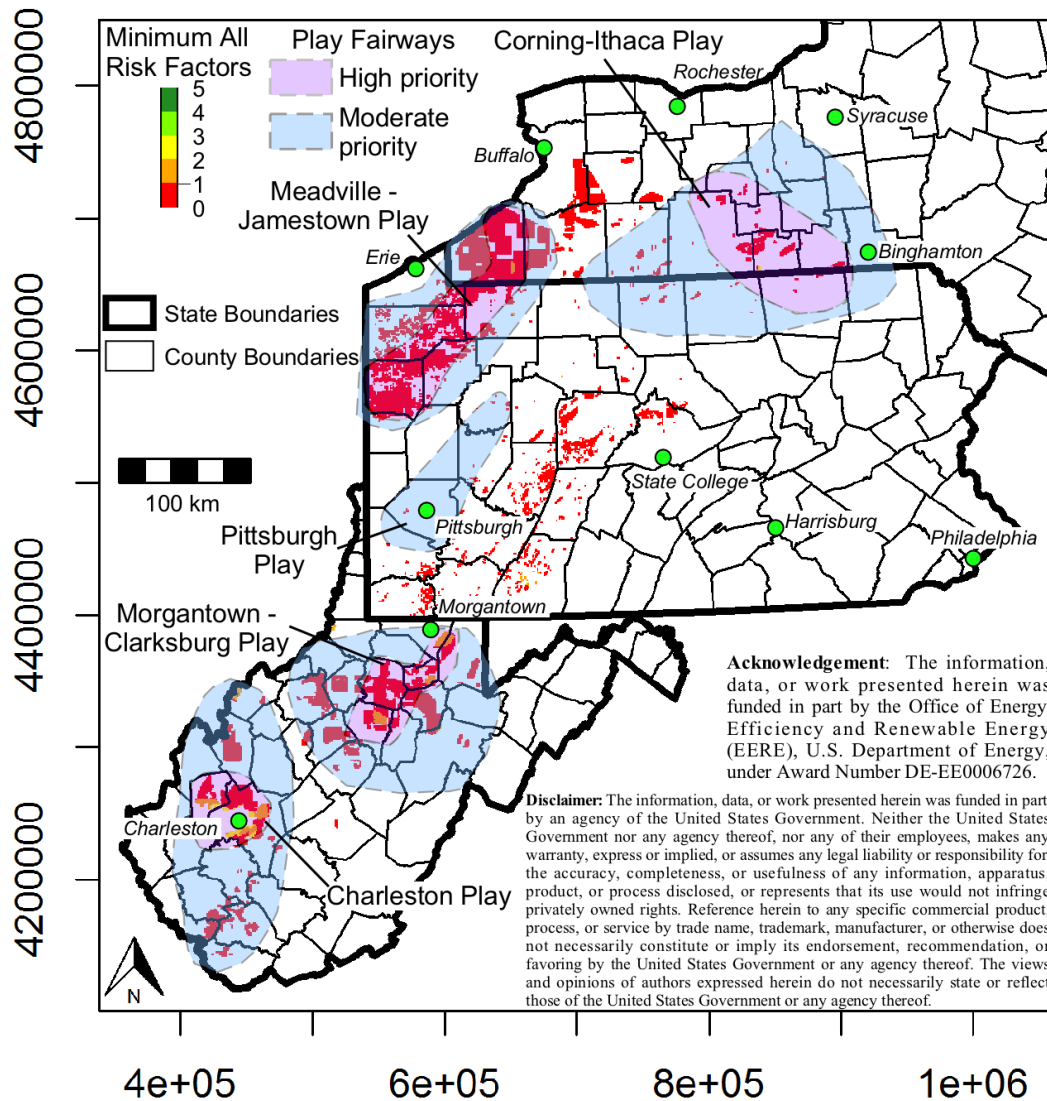


Figure 40: Favorability map for the combination of all four risk factors, for the reservoir metric RPIw, using the minimum value. Green-Favorable, Red-Unfavorable.

The maps presented above (Figure 38 - **Figure 40**) are designed to highlight utilization opportunities for communities and municipalities based on population clusters. However, the long list of other prospects for geothermal direct-use identified (over 165 across the 3 state area), independent of census data, points out that the utilization and the spatial variability in the cost of utilization are to a large degree functions of institutions. These factors contributing to the financial risk change through time and are spatially distributed. For example, a multi-year dynamic variability is true for regulations, carbon markets, community perceptions, and sites of employment or industry.

Therefore there is considerable value to examine the combined risks of the three geological characteristics only (**Figure 41** - Figure 43). This second combined risk map set represents the geologically fixed features, against which the dynamic human factors can be compared either qualitatively or quantitatively. Relative to the three geologic characteristics, the most favorable counties illuminated by the average combined risk are more widespread (**Figure 41**), especially in West Virginia. In West Virginia, these

occur in the central-northern region (Monongalia, Preston, Taylor, Barbour, and Upshur), various clusters of counties in the western part of the state (Ritchie, Doddridge, Gilmer Calhoun; Jackson, Putnam, Kanawha) and in the far south (Mingo, Wyoming; Raleigh). Pennsylvania shows little area with collectively favorable geological factors, with small areas within counties in the far west (Crawford, Venango, Warren), center (Elk, Cameron, southwestern Potter), and northern tier (Tioga, Bradford, Susquehanna). New York's coverage of favorable geological factors by the average method (**Figure 41**) is intermediate, revealing almost no strongly favorable areas in counties north of the southern tier. The certainty of that null result is diminished by the bias in the data, because there are few deep wells in that region of New York that could provide necessary BHT data. Along the southern tier, favorable areas are sparse in the west (Chautauqua County) and of increasing coverage from Allegany east through Chemung County.

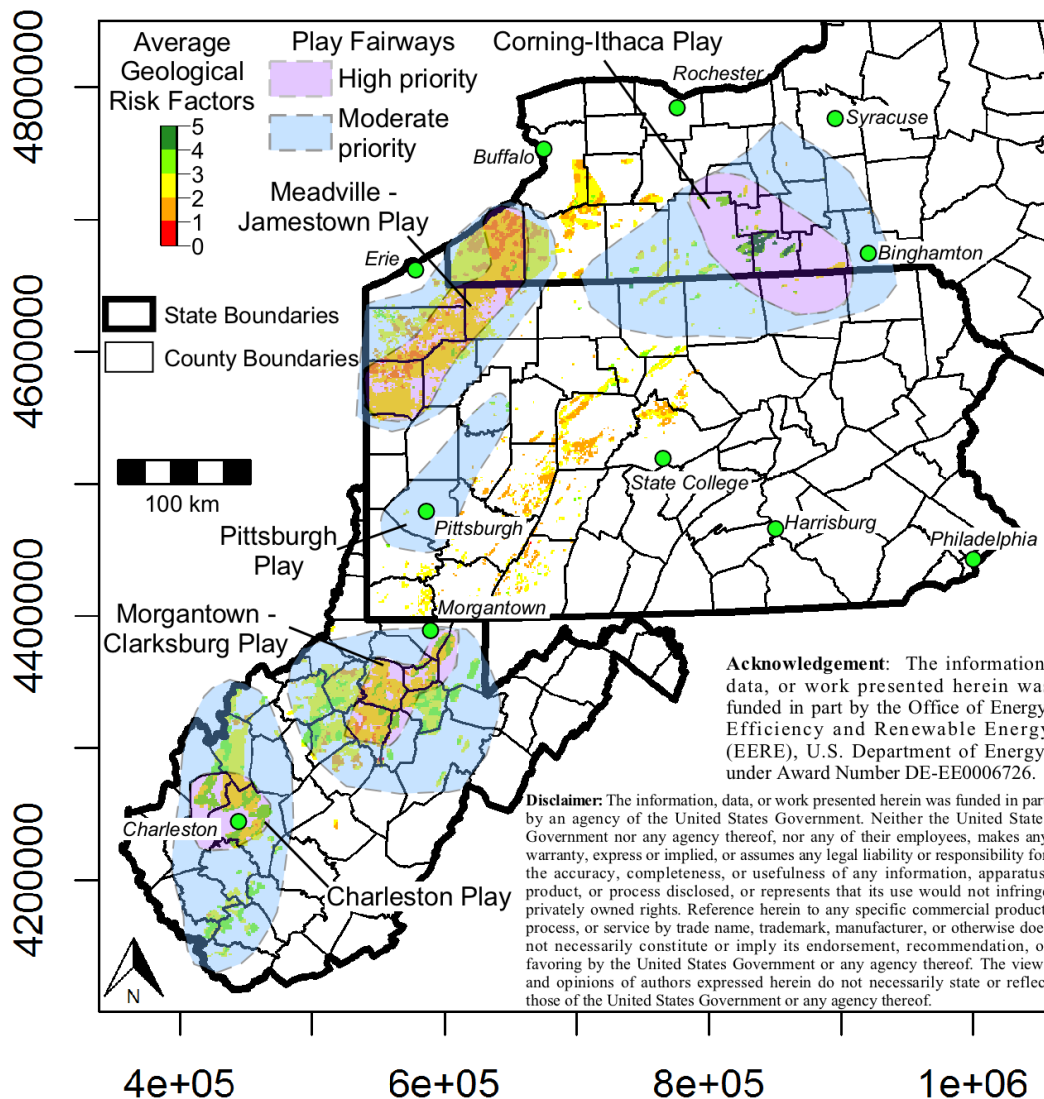


Figure 41: Favorability map for the combination of the three geologic risk factors, for RFC as the reservoir metric, using an average. Green-Favorable, Red-Unfavorable.

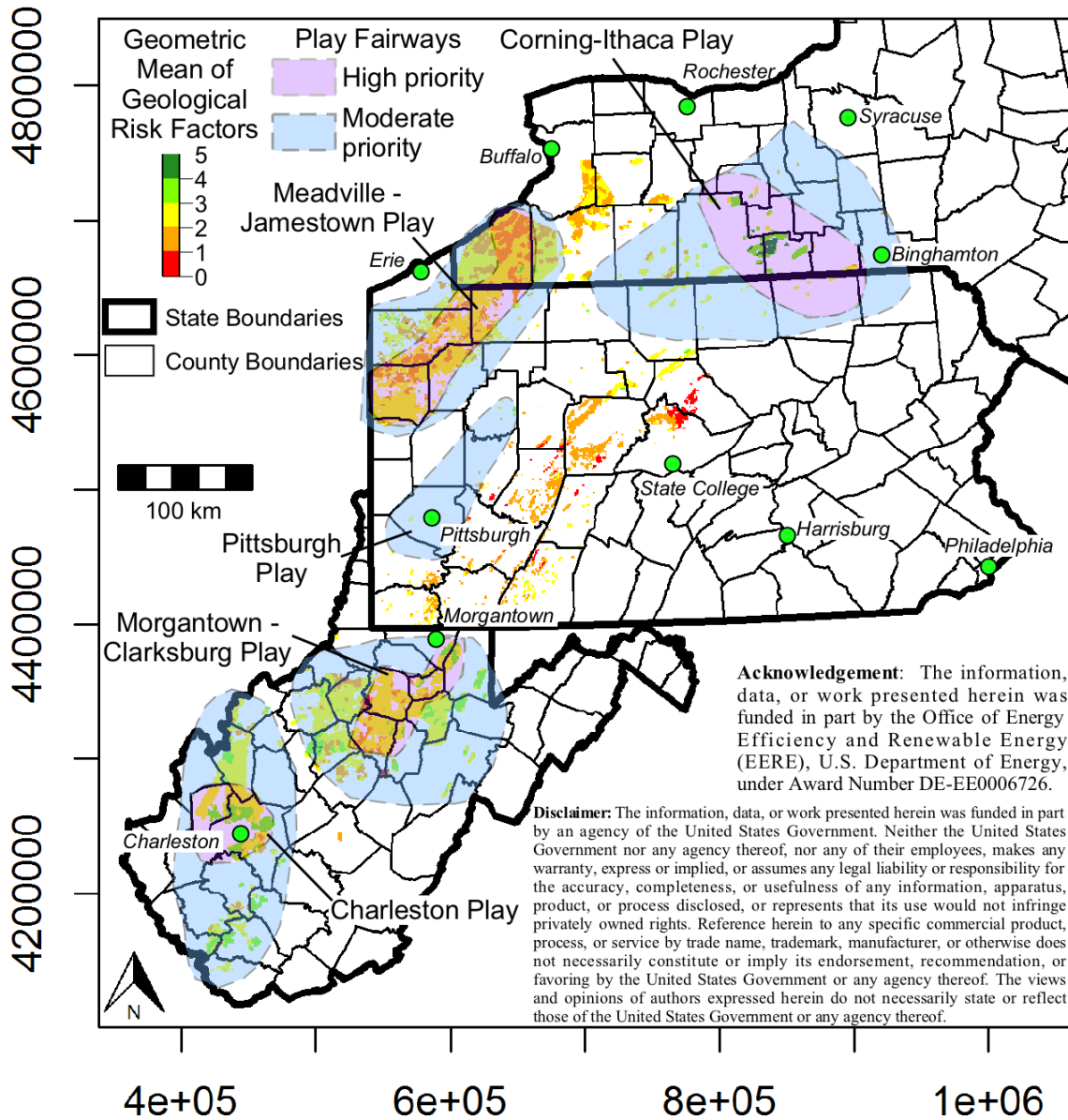


Figure 42: Favorability map for the combination of the three geologic risk factors, for RFC as the reservoir metric, using a geometric mean. Green-Favorable, Red-Unfavorable.

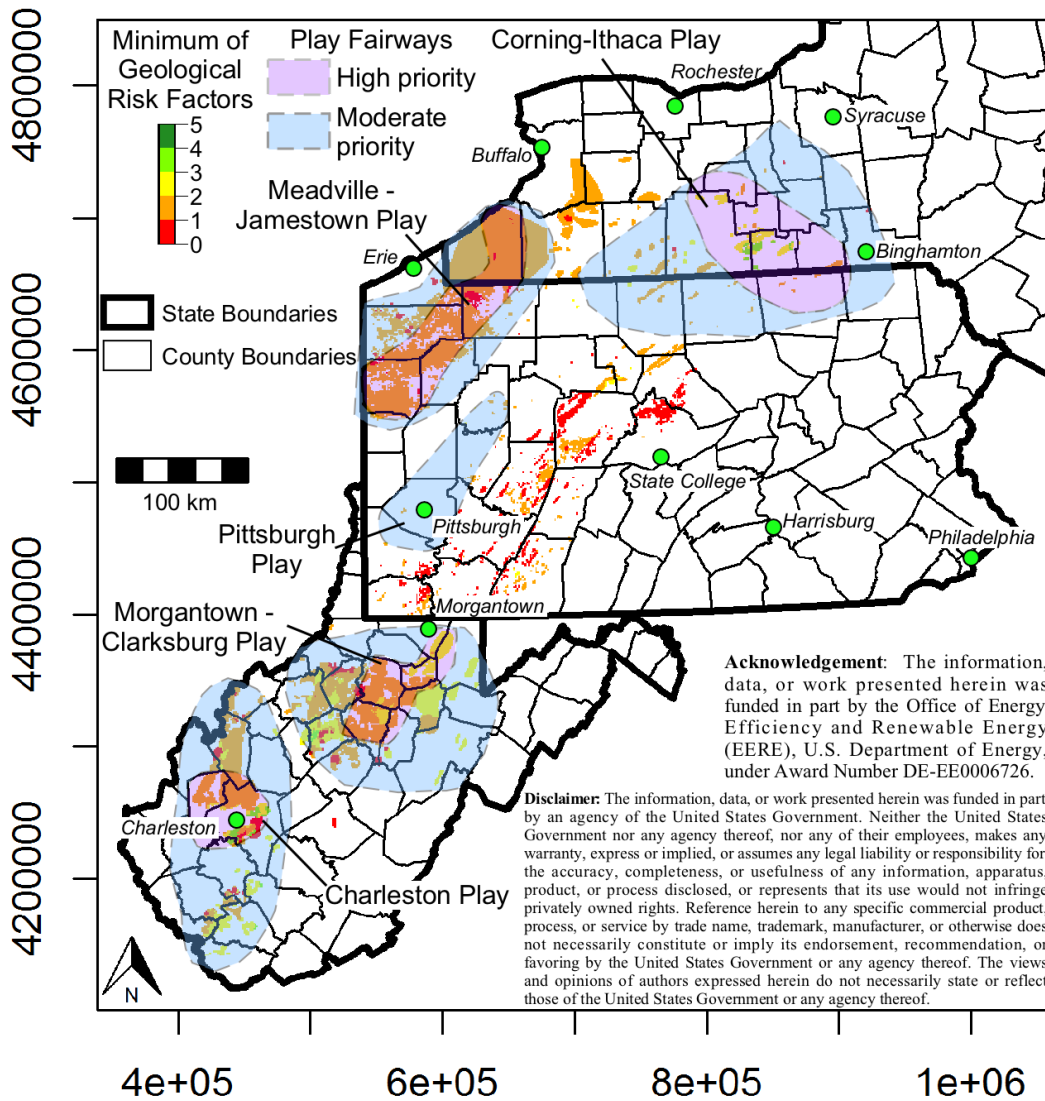


Figure 43: Favorability map for the combination of the three geologic risk factors, for RFC as the reservoir metric, using the minimum. Green-Favorable, Red-Unfavorable.

A focus on the three geological risk factors without the district-heating utilization factor facilitates consideration of the spatial variation of favorable conditions for end uses in industrial processing, military facilities, and institutions with a large capacity of temporary housing, like universities. Figure 44 illustrates the correspondence between the 165 identified potential industrial and special use sites and the geological favorability.

The success of a geothermal energy extraction project that is based on circulation of water through naturally existing pore spaces, on which this study has focused, requires the co-occurrence of favorable rock temperature and favorable reservoir conditions at the same depth. To illustrate the spatial variability of the intersection of those two properties, Figure 45,

Figure 46 and Figure 47 illustrate the temperature field at depths of 1.5 km, 2.5 km, and 3.5 km below the surface, respectively. On each of those maps, the documented oil and gas reservoirs are mapped that occur within vertical distances of 500 m above or below the reference depth of the temperature field.

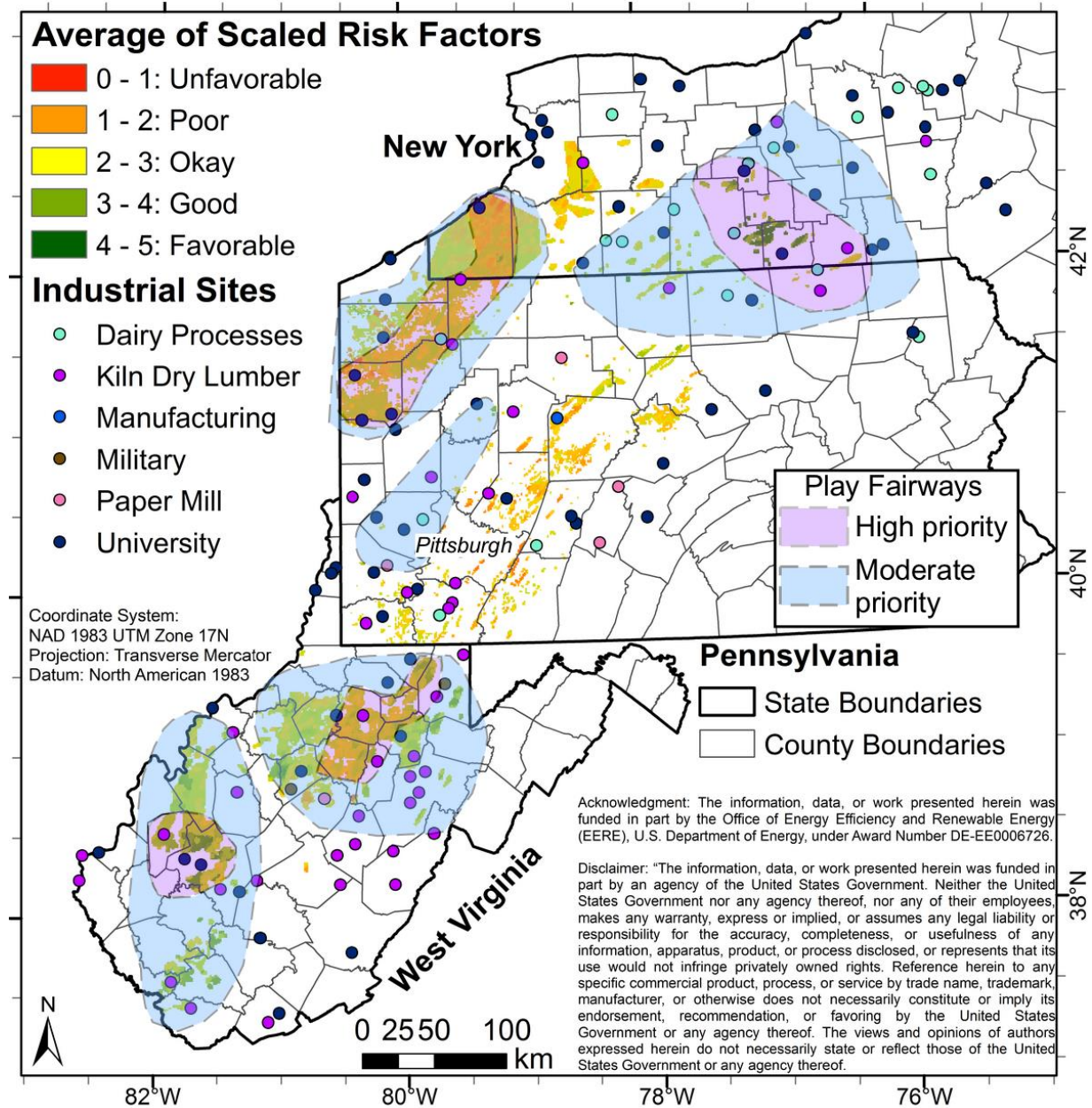


Figure 44: Comparison of the favorability map for the combination of the first three geologic risk factors (for RPIw as the reservoir metric) using the average, to the locations of the Utilization Individual Sites. Green-Favorable, Red-Unfavorable.

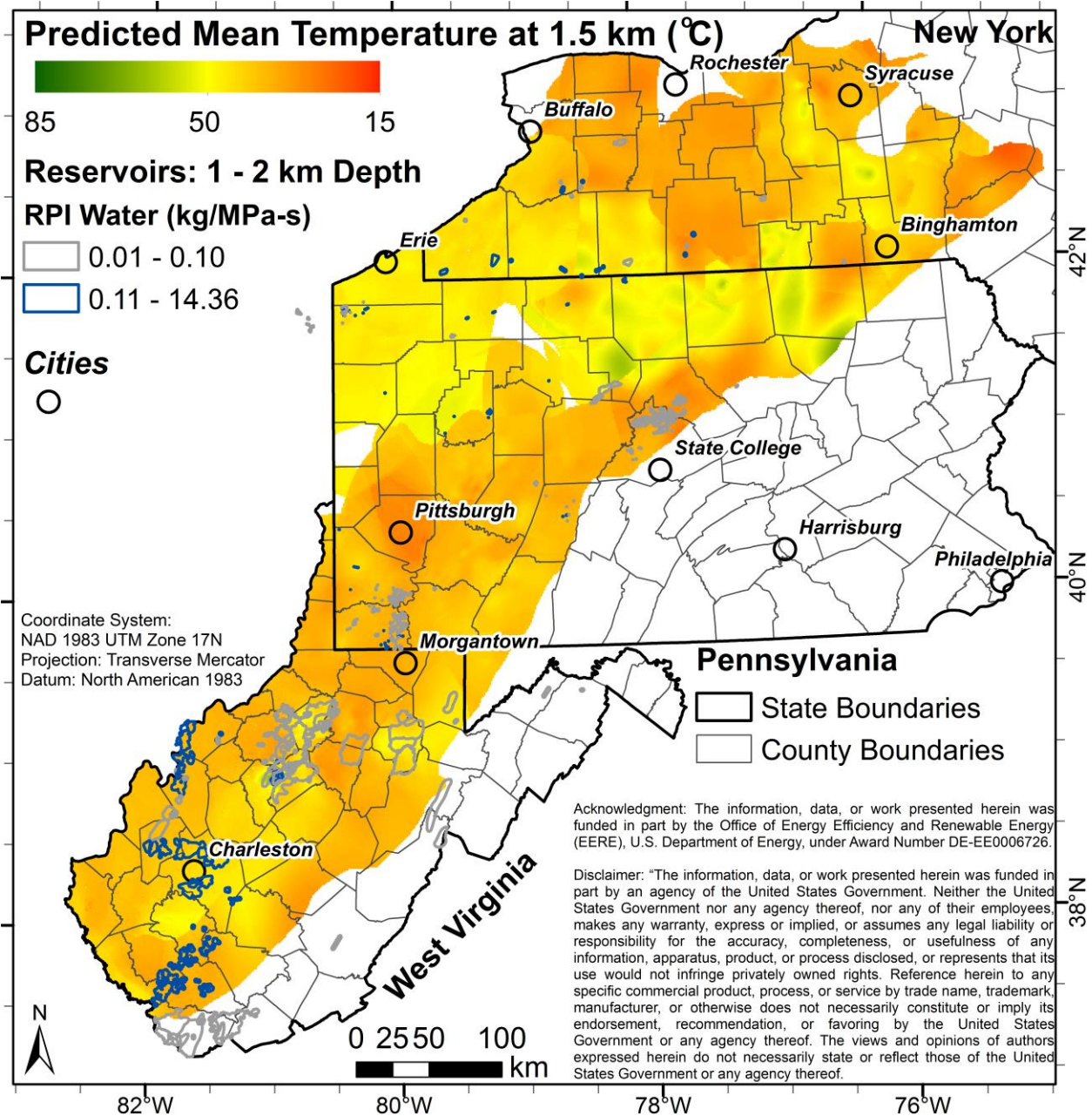


Figure 45. Map of the temperature predicted at a depth of 1.5 km depth below the local Earth surface throughout the study area. Superimposed are the locations of reservoir rocks in the range of depth below the surface of 1000–2000 m, based on oil or gas production. For those reservoirs, the reservoir quality metric based on RPIw for a 5-point non-dimensional scale is indicated by the color of the surrounding polygon: a black line indicates a reservoir risk factor of 4 or 5; a gray line indicates a reservoir risk factor of 3.

The resulting comparison of temperature and reservoirs at similar depths partially illuminates the qualitative aspects of the designation of regions as the five Play Fairways. For example, there is a region southeast of Buffalo (southeastern Erie County, NY) for which the four factor combined risk factor metric map illustrates a favorability score between 1 and 2 (on a 5-color scale, for which 5 is favorable). Examination of the maps of temperatures at 1.5 km and 2.5 km depths (Figure 45,

Figure 46) reveal that the favorable reservoirs occur almost entirely near 1.5 km depth where temperatures are <50 °C. At 2.5 km depth where the temperatures reach ~50 °C only a very small area is known to be underlain by good reservoirs. Consequently we did not designate this region as a play fairway.

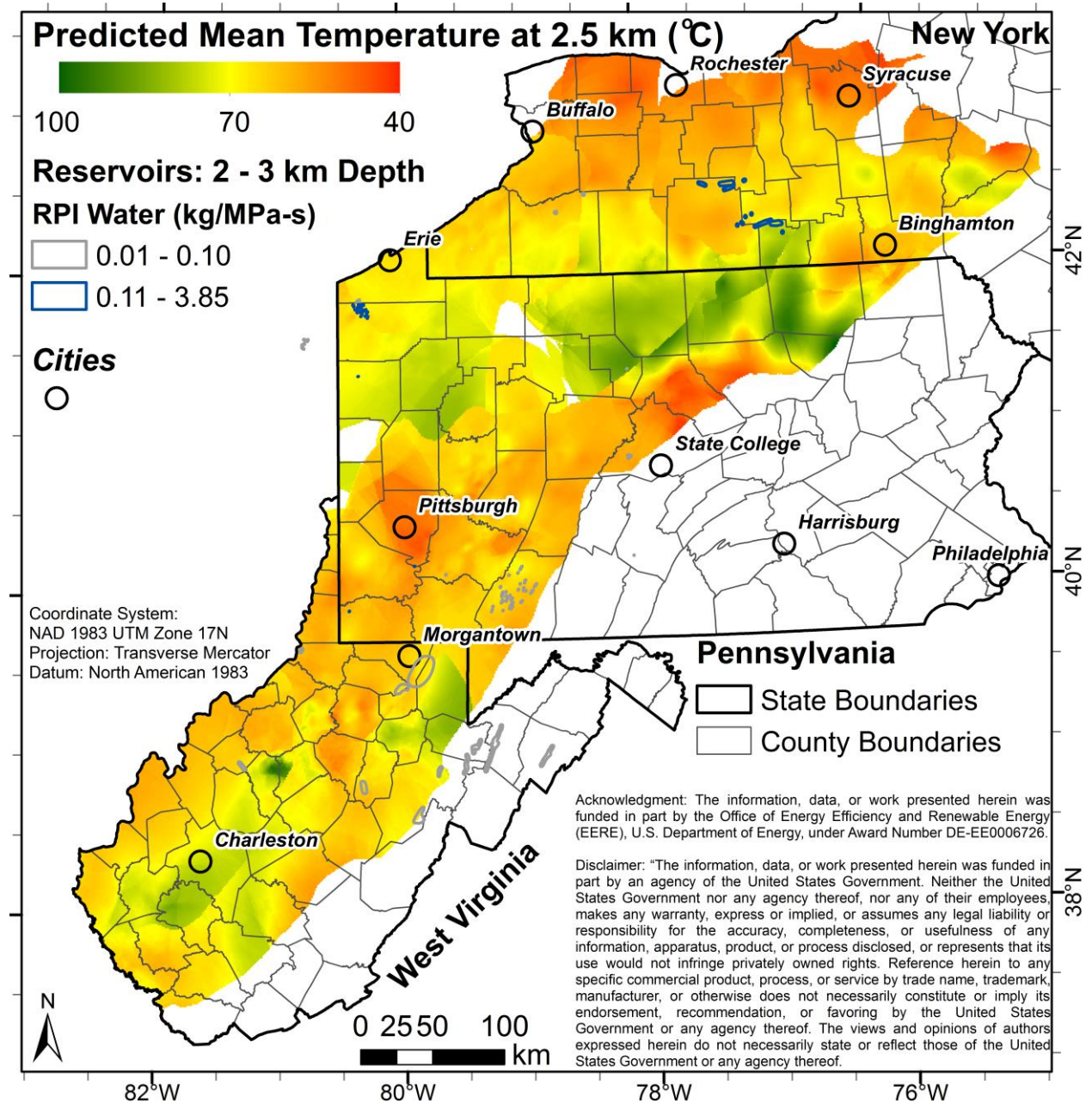


Figure 46. Map of the temperature predicted at a depth of 2.5 km depth below the local Earth surface throughout the study area. Superimposed are the locations of reservoir rocks in the range of depth below the surface of 2000–3000 m, based on oil or gas production. For those reservoirs, the reservoir quality metric based on RPIw for a 5-point non-dimensional scale is indicated by the color of the surrounding polygon: a black line indicates a reservoir risk factor of 4 or 5; a gray line indicates a reservoir risk factor of 3.

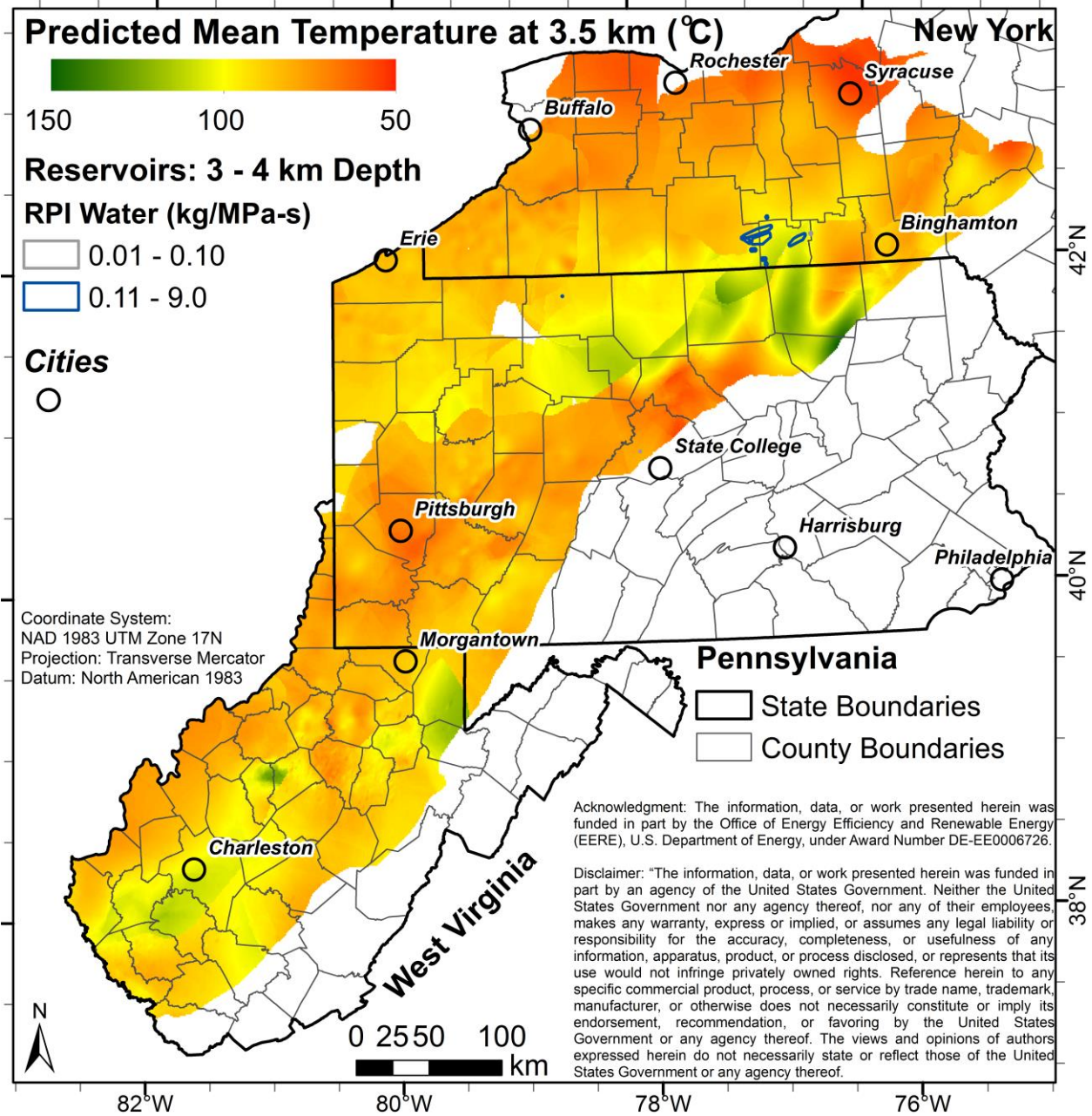


Figure 47. Map of the temperature predicted at a depth of 3.5 km depth below the local Earth surface throughout the study area. Superimposed are the locations of reservoir rocks in the range of depth below the surface of 3000–4000 m, based on oil or gas production. For those reservoirs, the reservoir quality metric based on RPIw for a 5-point non-dimensional scale is indicated by the color of the surrounding polygon: a black line indicates a reservoir risk factor of 4 or 5; a gray line indicates a reservoir risk factor of 3.

Consideration of a combined risk method that more strongly weights the geological weaknesses of the plays (Figure 42, geometric mean) reduces significantly the attractiveness of all but a handful of areas. The region favored by the averaging method which changed least when analyzed by the geometric mean method (Figure 48) is a three-county cluster in south-central New York (the border of Steuben with Yates and Schuyler counties, and Chemung County). There, favorable temperatures coincide with high potential from the Trenton-Black River reservoirs (Figure 47). These define a play fairway that is robust based on consistent PFM favorability (Corning–Ithaca Play Fairway; Figure 38, **Figure 41**), and should be a high priority for further analysis. In West Virginia the total number of possible sites increased dramatically when the utilization constraint was lifted (compare Figure 39 to Figure 42, geometric mean), identifying favorable plays primarily in eastern Monongalia, western Preston, Taylor and Harrison counties in the north (Morgantown–Clarksburg Play Fairway) and as patches in the southern counties of Kanawha, Putnam and Jackson (Charleston Play Fairway). The challenge for the Morgantown-Clarksburg Play Fairway will be to locate adequate natural reservoirs. In the Charleston Play Fairway the Oriskany stratigraphic reservoirs and Newburg Sandstone combine with favorable temperatures to create two types of play that warrant further investigation. A wide area in western Pennsylvania ((Mercer, Crawford, Venango and Warren counties) and southwestern New York (Chautauqua county) also has favorable scores for most of the four risk factors, garnering designation as the Meadville–Jamestown Play Fairway.

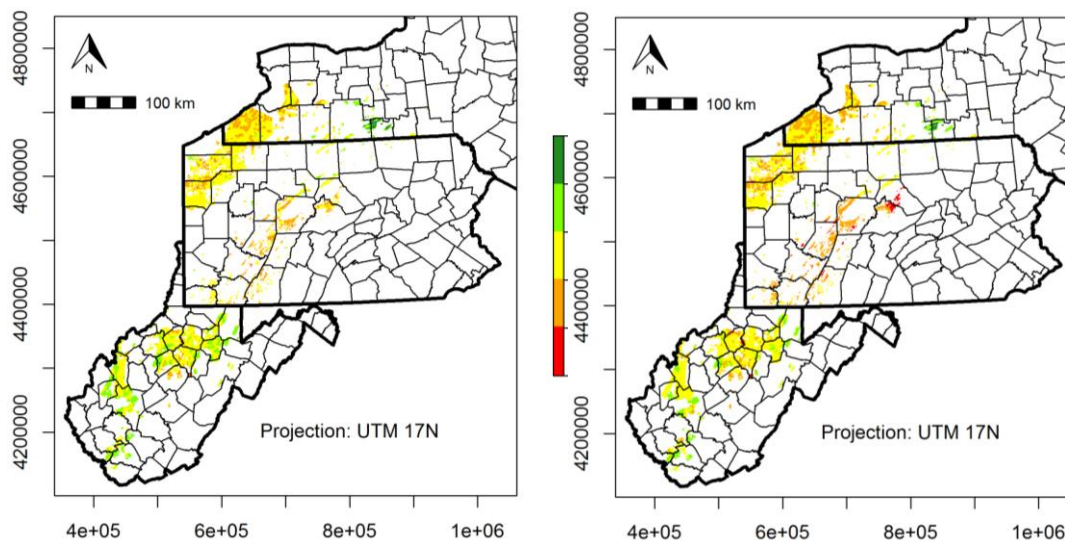


Figure 48: Comparison of the geology-only risk factors, using RFC as the reservoir metric, a) combined by the average method, and b) combined by the geometric mean method. Green-Favorable; Red-Unfavorable.

A region with a high population and thick insulating sedimentary rocks that is not highlighted by either combined risk analysis is the southwest Pennsylvania region around Pittsburgh. It is an example of a region with high use potential (Figure 37; Table 4's boroughs of West View, Brentwood, and Dormont are all near Pittsburgh) but there is little oil and gas well BHT data deeper than 1000 m and few documented reservoir rocks (Figure 21). Based on the sparse geological information near Pittsburgh on which to base this project and the high degree of utilization opportunity, Pittsburgh is designated as a region worthy of farther consideration (Pittsburgh Play Fairway), which we designate as medium priority (Figure 38 to **Figure 40**). The outlines of this play respect the variability of Risk Matrix values of the areas around Pittsburgh, but are mostly influenced by utilization opportunities (Figure 37).

Three of the institutions that we know are interested in investigating the feasibility of tapping deep sedimentary basin geothermal direct-use resources are located relatively near the better areas revealed by the combined geological risk analyses (Figure 38 - **Figure 40**). In south-central New York, Cornell University in Tompkins County is at the margin of the inner high priority region of the Corning–Ithaca Play Fairway. A lack of information about reservoirs is the primary shortcoming in Tompkins County. West Virginia University in Monongalia County and a West Virginia National Guard base in Preston County are within the Morgantown–Clarksburg Play Fairway.

The Geothermal Play Fairway – Appalachian Basin analysis has been conducted to provide guidance to individuals who are considering decisions about investing time or resources in further assessment. The products are both computed maps of the spatial distribution of combined risk factors that strictly reflect existing available data and analyses, and also generalized Play Fairway maps that draw upon additional qualitative judgments. The mixed quantitative-qualitative Play Fairway product includes the judgment that, if data were not strongly biased toward the geological distribution of oil and gas, the spatial distribution of reservoirs would be much more extensive and yet those additional hypothetical reservoirs would be of highly heterogeneous quality. Two additional qualitative judgments are that the current state of knowledge of a method by which to assess at a regional scale the risk of induced seismicity is immature, and that the data on which this project based its seismic risk analysis are insufficient. Because the selected play fairways cover much broader areas than the spatial variability of the seismic risk metric, users should recognize that some locations within each play fairway likely harbor a higher risk of induced seismicity than other locations. Therefore individuals using either the quantitative combined risk maps or the quantitative-qualitative play fairways should plan to analyze the site-specific seismic risk as part of a decision-making process.

The team recommends that users of these results focus their attention on the combinations of risk factors that best fit their potential projects and focus on the detailed maps rather than on the broad fairway designations. This is because the possible rank metrics and the spatial variability of favorable and unfavorable conditions depend upon which rank factors are included or excluded, and because the thresholds used for this assessment of district heating system utilization may differ from the thresholds that are appropriate to the user’s potential geothermal system. For example, a future user whose interest rests in off-the-grid heating of a military base may be willing to consider reservoir stimulation, whereas a user whose interest is to provide processing heat to a yogurt-making facility may only be interested if natural reservoir flow is sufficient at shallow depth. Both those users would be better served by use of the geology-only combined risk metrics without inclusion of our utilization metric than by the four-factor maps, and the first group might discount reservoir metrics entirely whereas the latter group would be keenly interested in the combined risk map that uses RPIw.

Furthermore, users should bear in mind that the play fairway designations do not take into consideration the full costs of a geothermal district heating system. Additional site-specific studies are needed to combine the subsurface risks and the above-surface expenses.

Comparison of Actual Accomplishments with Original Goals and Objectives

Referring to the project major tasks and deliverables described under Approaches Used in this report, all goals and objectives were achieved. Deliverables exceed those required, going beyond the risk segment maps and the final favorability maps, to also include a series of research Memos documenting the details of the analysis by topic and even some sub-topic areas. Maps and supporting documents can be found in the Geothermal Data Repository and the Memos can be found within the Catalog of Supporting Files.

Uncertainties Corresponding to the Final Favorability Maps

Accompanying the Final Favorability Map generated by averaging the four individual risk factors and using RPIw as the reservoir metric is a map depicting uncertainty (standard deviation) (Figure 38). A similar map of the uncertainty for each combination of the four risk factors and of the three different choices of reservoir metrics, as well as for most combinations of only the geologic metrics, exist in Memo 17 (Combining Risk Factors). These are among the Tier 2 files placed in the Geothermal Data Repository.

RECOMMENDATIONS FOR FURTHER ANALYSIS

Description of Objectives and Outcomes of Recommended Studies

At the closure of this regional-scale Geothermal Play Fairway Analysis of the northern Appalachian Basin, the most significant technical uncertainties, starting with the largest unknowns, are 1) reservoir distribution and capacities; 2) validity of thermal resource maps, and 3) the holistic estimation of Levelized Cost of Heat for favorable geological situations. Furthermore, in preparation for developing an operational geothermal heat supply and usage system at any location within the study area, additional groundwork is needed that pertains to permitting and public awareness.

Description of Recommended Activities

An overview of the recommended activities for each of the identified priority Play Fairways may be found in Table 5: Summary of five play fairways and recommendations for next investigation steps. We explain briefly here the nature of follow-on studies that we recommend in order to verify our Phase 1 analyses as well as to advance the analysis of geothermal energy potential for a few select “prospect scale” locations.

Broadly speaking, we recommend refinement, validation, and extension of the following aspects of our Phase 1 work:

- **Reservoir Productivity Maps.** We recommend three sets of study to improve the predictions of reservoir productivity. The first type of study focuses on improving the quality of results of the reservoir productivity index as presented in this report. More data on properties of known reservoirs exist in oil and gas production data sets (e.g., pump tests) and, if accessed, could be used to improve the analyses. The second and third types of study focus on identifying geothermal reservoirs outside of oil and gas fields and on better differentiating fracture-permeability reservoirs from matrix-permeability reservoirs. The second recommended type of study would use sedimentary facies and published structural geological knowledge to identify potential geothermal reservoirs. The third type of study would explore the possibility of locating dilational regions through one or two approaches based on geophysical data. An option is to combine the orientations of multiscale edges in magnetic and gravity field data (“worm analysis”) with stress field information, and calculate which of the potential fault zones (“worms”) are best oriented, in theory, for dilation. The other option is to identify locations of potential structural complexity by locating places that magnetic and/or gravity “worms” intersecting. Either of these approaches may identify zones with higher likelihood for fracture systems that can serve as a reservoir, yet the method should be validated against a few locations known from hydrocarbon production to be dominated by fracture permeability. Informed by the results of some or all of these three studies, the basin scale productivity indices could be reexamined and reservoir maps could be adjusted accordingly.
- **Thermal Resource Maps.** Because the accuracy of our Phase 1 result was limited by the availability of relatively few widely separated equilibrium temperature gradient determinations as well as by the need to assume thermal conductivity values that may or may not be appropriate, we recommend efforts to add more high quality data to the thermal analysis. First, we recommend acquisition of existing shut-in temperature data (as representative of an equilibrium value) from industrial partners. Second, we recommend that new equilibrium temperature profiles be logged in shut-in holes or those about to be abandoned. Those new equilibrium temperature data can

serve the dual purposes of testing the accuracy of this study's thermal model, as well as perhaps enabling refinement of the BHT correction analyses. Additionally, thermal conductivity of relevant core samples should be measured. Results from detailed thermal logs as well as statistics from conductivity measurements should then be jointly inverted to establish local heat fluxes and a conductivity stratigraphy at those locations. All of these aspects should be incorporated into enhancing the regional thermal model.

- **Seismicity Potential.** The validity of the seismicity risk factor maps should be tested against newly acquired seismic monitoring results in PA and NY. Also, to ground-truth the techniques we utilized against real-world situations, detailed analysis should be conducted of known induced seismicity (e.g., at the Dale brine mining site (Fletcher and Sykes [1977]) relative to our worm-based seismic risk estimates. Where higher resolution gravity and magnetic surveys may be acquired in the future, features within them that may be faults (e.g., the set of “worms”) should be subject to the “orientation in stress field” analysis described in this report and accompanying methods memo.
- **Structural Delineation at the Prospect Scale.** For specific project sites of interest for further examination of the geothermal development potential, geophysical studies are recommended to locate faults. These studies should include collection of high spatial resolution gravity and magnetics data, as well as purchase or acquisition of 2D seismic reflection lines along profiles that survey a variety of orientations. Where surface materials do not entirely obscure the sedimentary rocks, geological mapping of faults is equally recommended.
- **Utilization LCOH Methods.** Detailed scenarios for geothermal direct-use heating should be developed for interested communities or businesses. Alternatives for financing and potential tax benefits for the geothermal projects in these scenarios should be explored, and corresponding benefits and costs expressed by refinement of the GEOPHIRES computational model. GEOPHIRES should be used to estimate the Levelized Cost of Heat, inclusive of subsurface and surface parts, for those scenarios.
- **Potential Basement Reservoirs.** Our study focused on analyzing hot-sedimentary-type plays for the Appalachian Basin region. The analysis should be extended to the underlying basement rocks with an eye towards Enhanced Geothermal System (EGS) type projects. A recommended initial step is to describe expected basement lithologies, constrained by core/cuttings and outcrop where available. Additionally, basement fracture architectures (healed/open; spacing) should be estimated for these rocks.
- **Planning for pilot boreholes or full geothermal well fields.** Where a stakeholder group has significant interest in exploring the potential for geothermal direct-use heating, community education and efforts to secure necessary permits should be integral parts of their work. Outreach information must be developed and used within the communities surrounding prospect-scale locations. Additionally, permitting for well drilling and potential mitigation strategies must be planned. Other work should involve determining whether significant quantities of water – in addition to that naturally occurring in our reservoirs – will be required for a given prospect-scale location and, if so, how to secure the rights to that water. If so, the responsible agencies, costs, etc. for that location must be evaluated.

Table 5: Summary of five play fairways and recommendations for next investigation steps.

Summary of five play fairways and recommendations for the next investigation steps. The minimum “depth to 80 °C” values are for the best location in the inner high priority fairway, and the city values are the best location within 10 km from the city. Also given for those locations is the range of depths corresponding to 95% confidence². The reservoir units are the geological formations in or near the play fairway that are relatively deep (to access higher temperature rocks) and have a favorable reservoir productivity index. Blank boxes indicate no recommended immediate action, pending further reservoir analysis and improved assessment of probability of reservoir success

Play Fairway (Name of major community)	Conditions in inner high priority play fairways (2015 Phase 1 analysis results)			Recommendations		
	Depth (m) to 80 °C	Uncertainties (m): 95% Confidence Range of Combined Errors	Reservoir Target Unit and Depth(s) Below Local Surface (m)	Geophysical data & analysis	Borehole data & analysis	Utilization scenarios & analysis
Charleston	Location of Minimum: 2200 Charleston: 2500	Location of Minimum: 950-3500 Charleston: 950-4100	Newburg Limestone (~1700) Oriskany Sandstone (~1400-1500) (quality highly uncertainty)	Seismic for influence of the Rome Trough on thermal field and fracture networks	Use existing well logs to identify positions of deep formations that are known reservoirs in region, and evaluate by log data and models (facies, structure, and probability), the reservoir potential near Charleston. Log equilibrium temperature profile.	Define needs of a stakeholder district heating system and model the subsurface costs of delivering geothermal heat to meet their needs
Morgantown Clarksburg	Location of Minimum: 2300 Morgantown 2700 Clarksburg: 3380	Location of Minimum: 1000-3600 Morgantown: 1500-3900 Clarksburg: 2100-4700	Newburg Sandstone (~1500-2300)	Purchase or record gravity data & magnetics data and analyze for locations of faults	Log an existing well to obtain equilibrium temperature thermal profile and reservoir parameters	Define needs of WVU district heating system and model the subsurface costs of delivering geothermal heat to meet WVU needs; define needs of military base and model the subsurface costs of delivering geothermal heat to meet its needs
Pittsburgh	Location of Minimum:	Location of Minimum:	Formation associated with		For deep wells in neighboring counties, use existing well logs to	Define needs of a stakeholder district heating system and

	2400 Pittsburgh: 3800	1200-3600 Pittsburgh: 2100-5500	Devonian Unconformity (~1500) Elk Group (~1250-1430 m)		identify positions of deep formations that are known reservoirs in region, and evaluate by log data and models (facies, structure and probability) their potential near Pittsburgh	model the subsurface costs of delivering geothermal heat to meet their needs
Meadville – Jamestown	Location of Minimum: 2700 Meadville: 3000 Jamestown: 2900	Location of Minimum: 1500–3900 Meadville: 1800-4200 Jamestown: 1700–4100	Galway Formation (~2000) Onondaga Limestone (~1300)		Use existing well logs to identify positions of deep formations that are known reservoirs in region, and evaluate by log data and models (facies, structure and probability), their potential near Meadville and Jamestown. Log equilibrium temperature profile.	Define needs of a stakeholder district heating system and model the subsurface costs of delivering geothermal heat to meet their needs
Corning – Ithaca	Location of Minimum: 2300 Corning: 2500 Ithaca: 2600	Location of Minimum: 1500–3100 Corning: 2100–2900 Ithaca: 2100–3100	Trenton-Black River (2800-3100)	Purchase or record seismic reflection data, gravity data, magnetic data, and analyze for additional T-BR reservoir locations as well as for fault locations	Log an existing well to obtain equilibrium temperature thermal profile and reservoir parameters	Define needs of Cornell University district heating system and model the subsurface costs of delivering geothermal heat to meet CU needs; define needs of Corning area office campuses and model the subsurface costs of delivering geothermal heat to meet their needs

² The uncertainty is based on two components. The first uncertainty component is the standard error on the thermal model depth estimate, derived from relations between standard error vs. BHT depth in 77 wells with detailed stratigraphy, then applied to the area of interest based on the dominant BHT depths in counties near the named location. The second uncertainty component is the kriging standard error of predicted mean at the named location due to spatial extrapolation of the well-specific predicted values of depth to 80 °C. These two components are treated as independent, permitting derivation of the combined uncertainty as the square root of the sum of the squares. The upper and lower bounds of 95% confidence are expressed by the best estimate of depth minus and plus, respectively, the combined uncertainty.

REFERENCES

- Aguirre, G. A. (2014). *Geothermal Resource Assessment: A Case Study of Spatial Variability and Uncertainty Analysis for the State of New York and Pennsylvania*. Master's Thesis, Cornell University. Retrieved from <http://hdl.handle.net/1813/38982>.
- Aguirre, G. A., Stedinger, J. R., & Tester, J. W. (2013). Geothermal Resource Assessment: A Case Study of Spatial Variability and Uncertainty Analysis for the State of New York and Pennsylvania. *Proceedings, Thirty-Eighth Workshop on Geothermal Reservoir Engineering*. Stanford: Stanford University. Retrieved from <http://www.geothermal-energy.org/pdf/IGAstandard/SGW/2013/Aguirre.pdf>.
- American Association of Petroleum Geologists (AAPG). (1985). Correlation of Stratigraphic Units of North America (COSUNA).
- American Association of Petroleum Geologists (AAPG). (1994). CSDE, COSUNA, and Geothermal Survey Data_Rom.
- Augustine, C. (2014). Analysis of Sedimentary Geothermal Systems Using an Analytical Reservoir Model. *Geothermal Resources Council Transactions*. Portland: Geothermal Resources Council.
- Beckers, K. (2015). *GEOPHIRES Software Tool*. Retrieved from GEOthermal Energy for the Production of Heat and Electricity Economically Simulated: <http://koenraadbeckers.net/geophires/index.php>.
- Beckers, K. F., Lukawski, M. Z., Anderson, B. J., Moore, M. C., & Tester, J. W. (2014). Levelized costs of electricity and direct-use heat from Enhanced Geothermal Systems. *Journal of Renewable and Sustainable Energy, Vol. 6, No. 1*, 013141.
- Beckers, K. F., Lukawski, M. Z., Reber, T. J., Anderson, B. J., Moore, M. C., & Tester, J. W. (2013). Introducing GEOPHIRES V1.0: Software Package For Estimating Levelized Cost of Electricity and/or Heat from Enhanced Geothermal Systems. *Proceedings, Thirty-Eighth Workshop on Geothermal Reservoir Engineering*. Stanford: Stanford University. Retrieved from <http://www.geothermal-energy.org/pdf/IGAstandard/SGW/2013/Beckers.pdf>.
- Bedre, M., & Anderson, B. (2012). Sensitivity analysis of low-temperature geothermal reservoirs: effect of reservoir parameters on the direct use of geothermal energy. *Geothermal Resources Council Transactions*, 1255-1262. Geothermal Resources Council.
- Blackwell, D. D., & Richards, M. (2004). Geothermal Map of North America; Explanation of Resources and Applications. *Geothermal Resources Council Transactions, Vol. 28*, 317-320. Geothermal Resources Council.
- Blackwell, D. D., Negraru, P., & Richards, M. (2007). Assessment of the enhanced geothermal system resource base of the United States. *Natural Resources Research, Vol. 15, No. 4*. doi:10.1007/s11053-007-9028-7.
- Blackwell, D., & Richards, M. (Eds.). (2004). 2004 Geothermal Map of North America, Scale 1:6,500,000. American Association of Petroleum Geologists.
- Blackwell, D., Richards, M., Batir, J., Frone, Z., & Park, J. (2010). New Geothermal Resource Map of the Northeastern US and Technique for Mapping Temperature-at-depth. *Geothermal Resources Council Transactions, Vol. 34*, 313-318. Geothermal Resources Council.

- Blackwell, D., Richards, M., Frone, Z., Batir, J., Ruzo, A., Dingwall, R., & Williams, M. (2011). Temperature-At-Depth Maps for the Conterminous U.S. and Geothermal Resource Estimates. *Geothermal Resources Council Transactions, Vol. 35*, 1545-1550. Geothermal Resources Council.
- Boschetti, F., Hornby, P., & Horowitz, F. (2001). Wavelet Based Inversion of Gravity Data. *Exploration Geophysics, Vol. 32, No. 1*, 48-55. doi:10.1071/EG01048.
- Buescher, E. (. (2015). Green District Heating - Actual Developments of Deep Geothermal Energy in Germany. *Proceedings World Geothermal Conference 2015*. Melbourne, Australia: International Geothermal Association. Retrieved from <http://www.geothermal-energy.org/pdf/IGAstandard/WGC/2015/35000.pdf?>
- Camp Dawson West Virginia Army National Guard. (2015). *About Camp Dawson*. Retrieved from Camp Dawson West Virginia Army National Guard: <http://www.wv.ngb.army.mil/CampDawson/Form1.aspx?MP=MTc1&P=MTc1#Dawson>.
- Carter, L., Kelley, S., Blackwell, D., & Naeser, N. (1998). Heat flow and thermal history of the Anadarko basin, Oklahoma. *American Association of Petroleum Geologists Bulletin, Vol. 82*, 291-316.
- Cho, J., Augustine, C., & Zerpa, L. (2015). Validation of a Numerical Reservoir Model of Sedimentary Geothermal Systems Using Analytical Models. *Stanford Geothermal Workshop Proceedings*. Stanford University.
- Crowell, J., 2015, Quantifying How Errors in Thermal Conductivity Estimates Affect Geothermal Production Models: *Geothermal Resources Council Transactions, 39th Annual Meeting*, Reno, NV.
- Engelder, T., Lash, G., & Uzcátegui, R. (2009). Joint sets that enhance production from Middle and Upper Devonian gas shales of the Appalachian Basin. *AAPG Bulletin, Vol. 93, No. 7*, 857-889.
- Fletcher, J. B., & Sykes, L. R. (1977). Earthquakes related to hydraulic mining and natural seismic activity in western New York State. *Journal of Geophysical Research, Vol. 82, No. 26*, 3767-3780.
- Förster, A., & Merriam, D. F. (1995). A Bottom-Hole Temperature Analysis in the American Midcontinent (Kansas): Implications to the Applicability of BHTs in Geothermal Studies. (pp. 777-782). Potsdam: International Geothermal Association.
- Frone, Z. (2015). Heat Flow, Thermal Modeling and Whole Rock Geochemistry of Newberry Volcano, Oregon and Heat Flow Modeling of the Appalachian Basin, West Virginia. Southern Methodist University. ProQuest Dissertations Publishing.
- Frone, Z., & Blackwell, D. (2010). Geothermal Map of the Northeastern United States and the West Virginia Thermal Anomaly. *Geothermal Resources Council Transactions, Vol. 34*, 339-343. Geothermal Resources Council.
- Gallardo, J., & Blackwell, D. (1999). Thermal structure of the Anadarko Basin, Oklahoma. *American Association of Petroleum Geologists Bulletin, Vol. 83*, pp. 331-361.

- Gerard, A., Genter, A., Kohl, T., Lutz, P., Rose, P., & Rummel, F. (2006). The Deep EGS (Enhanced Geothermal System) Project at Soultz-sous-Forets (Alsace, France). *Geothermics, Volume 35*, 473-483.
- GoldCorp Inc. (2001, March 12). US\$575,000 Goldcorp Challenge Awards world's first 6 million ounce internet gold rush yields high grade results! Toronto. Retrieved from <http://www.infomine.com/index/pr/Pa065434.PDF>.
- Gringarten, A. (1978). Reservoir lifetime and heat recovery factor in geothermal aquifers used for urban heating. *Pure and Applied Geophysics, Vol. 117, No. 1-2*, 297-308.
- Harrison III, W., Grammer, G., & Barnes, D. (2009). Reservoir characteristics of the Bass Islands dolomite in Otsego County, Michigan: Results for a saline reservoir CO2 sequestration demonstration. *Environmental Geosciences, Vol. 16, No. 3*, 139-151.
- Harrison, W., Luza, K., Prater, M., & Chueng, P. (1983). Geothermal Resource Assessment of Oklahoma. *Special Publication 83-1, Oklahoma Geological Survey*.
- He, X. (2015). *Feasibility and Supply Analysis of U.S. Geothermal District Heating and Cooling Systems*. West Virginia University, Benjamin M. Statler College of Engineering and Mineral Resources. Morgantown: Proquest LLC, UMI Dissertation Publishing. Retrieved from <http://search.proquest.com/docview/1682034532>. Abstract Available at <http://gradworks.umi.com/37/01/3701975.html>.
- Hildenbrand, T. G., Briesacher, A., Flanagan, G., Hinze, W. J., Hittelman, A. M., Keller, G. R., Webring, M. (2002). *Rationale and Operational Plan to Upgrade the U.S. Gravity Database*. Retrieved from Gravity Database of the US: <http://research.utep.edu/default.aspx?tabid=37229>.
- Hornby, P., Boschetti, F., & Horowitz, F. (1999, April). Analysis of potential field data in the wavelet domain. *Geophysical Journal International, Vol. 137, No. 1*. 175-196. doi:10.1046/j.1365-246x.1999.00788.x.
- Hornby, P., Horowitz, F., & Boschetti, F. (2002). A Physical Interpretation of the Poisson Wavelet Transform of Potential Fields. *Proceedings, EGS XXV!! General Assembly*. Munich: European Geophysical Society. Retrieved from <http://www.cosis.net/abstracts/EGS02/05568/EGS02-A-05568.pdf>.
- Horowitz, F., Smith, J., & Whealton, C. (2015). *One dimensional conductive geothermal Python code*. Retrieved from Online Git Repository: <https://bitbucket.org/geothermalcode/jaredthermalconductivity>.
- Jordan, T., Camp, E., Smith, J., & Whealton, C., Horowitz, F., Stedinger, J., Tester, J., Richards, M., Hornbach, M., Frone, Z., Anderson, B., Xiaoning, H., Welcker, K., 2015, Low-Temperature Geothermal Energy Characterization by Play Fairway Analysis for the Appalachian Basin of New York, Pennsylvania and West Virginia: *Geothermal Resources Council Transactions*.
- Lewis, J., McDowell, R., Avary, K., & Carter, K. (2009). Characterization of the Helderberg Group as a geologic seal for CO2 sequestration. *Environmental Geosciences, Vol. 16, No. 4*, 201-210.
- Lienau, P., Lund, J., Rafferty, K., & Culver, G. (Augut 1994). *Reference Book on Geothermal Direct Use*. Klamath Falls, Oregon: GGeo-Heat Center, Oregon Institute of Technology. Retrieved from

- <http://www.oit.edu/docs/default-source/geoheat-center-documents/publications/direct-use/tp82.pdf?sfvrsn=2>.
- Lindal, B. (1973). Industrial and other applications of geothermal energy (except power production and district heating). Geothermal energy; review of research and development, (pp. 135-148). UNESCO.
- Lugert, C., Smith, L., Nyahay, R., Bauer, S., & Ehgartner, B. (2006). *Systematic Technical Innovations Initiative Brine Disposal in the Northeast*. Albany, NY: New York State Energy Research and Development Authority.
- Malinconico, L., & Moore, M. (2013). *Provisional Bouguer Gravity Map of Pennsylvania*. Retrieved from AASG Geothermal Data Repository:
<http://repository.stategeothermaldata.org/repository/resource/a748ce233a25e3e0dd00c9865d0af3e5/>.
- Midwest Regional Carbon Sequestration Partnership. (2009). *Phase II Report*. Midwest Regional Carbon Sequestration Partnership. Retrieved from
http://www.mrcsp.org/userdata/phase_II_reports/phase_ii_final_report_MRCSP.pdf.
- Nelson, P. H. (2009). Pore-throat sizes in sandstones, tight sandstones, and shales. *AAPG Bulletin*, Vol. 93, No. 3, 329-340.
- Obama, B.H. (2015). *Executive Order 13693 - Planning for Federal Sustainability in the Next Generation*. Washington, D.C.: U.S. Government Publishing Office. Retrieved 2015, from
<http://www.gpo.gov/fdsys/pkg/FR-2015-03-25/pdf/2015-07016.pdf>
- Rahm, B., & Riha, S. (2012). Toward strategic management of shale gas development: Regional, collective impacts on water resources. *Environmental Science & Policy*, Vol. 17, 12-23.
- Rahm, B., & Riha, S. (2014). Evolving shale gas management: water resource risks, impacts, and lessons learned. *Environmental Science Processes and Impacts*, Vol. 16, 1400-1412.
doi:10.1039/c4m00018h.
- Ravat, D., Finn, C., Hill, P., Kucks, R., Phillips, J., Blakely, R., Elawadi, E. (2009). *A Preliminary, Full Spectrum, Magnetic Anomaly Grid of the United States with Improved Long Wavelengths for Studying Continental Dynamics: A Website for Distribution of Data*. United States Geological Survey. Retrieved from <http://pubs.usgs.gov/of/2009/1258>.
- Reber, T. (2013). Evaluating Opportunities For Enhanced Geothermal System-Based District Heating In New York And Pennsylvania. Cornell University. Ithaca, NY: Cornell University. Retrieved from <http://hdl.handle.net/1813/34090> (restricted until 2018).
- Reber, T. J., Beckers, K. F., & Tester, J. W. (2014). The transformative potential of geothermal heating in the U.S. Energy market: a regional study of New York and Pennsylvania. *Energy Policy*, Vol. 70, 30-44.
- Roen, J., & Walker, B. (1996). The atlas of major Appalachian gas plays. *Publication V-25*.
- Sanyal, S., & Butler, S. (2009). Geothermal Power From Wells in Non-Convective Sedimentary Formations - An Engineering Economic Analysis. *Geothermal Resources Council Transactions*, Vol. 33, 865-870. Geothermal Resources Council.

- Shaalán, H. E. (2001). Generation of Electric Power. In *Handbook of Electric Power Calculations* (pp. 8.1-8.38). Retrieved from http://castlelab.princeton.edu/EnergyResources/GenerElectPower__Shalaan.pdf.
- Shope, E. (2012). *A Detailed Approach To Low-Grade Geothermal Resources In The Appalachian Basin Of New York And Pennsylvania: Heterogeneities Within The Geologic Model And Their Effect On Geothermal Resource Assessment*. Master's Thesis, Cornell University. Retrieved from <http://hdl.handle.net/1813/31206>.
- Shope, E. N., Reber, T., Stutz, G., Aguirre, G., Jordan, T., & Tester, J. (2012). Geothermal Resources Assessment: A Detailed Approach to Low-Grade Resources in the States of New York and Pennsylvania. *PROCEEDINGS, Thirty-Seventh Workshop on Geothermal Reservoir Engineering*. 37. Stanford: Stanford University. Retrieved from <https://pangea.stanford.edu/ERE/pdf/IGAstandard/SGW/2012/Shope.pdf>.
- Shumaker, R. (1996). Structural history of the Appalachian basin. In J. Roen, & B. Walker, *The Atlas of Major Appalachian Gas Plays: West Virginia Geological and Economic Survey Publication* (Vol. V-25, pp. 8-21).
- Smith, J.D. (2016). *Analytical And Geostatistical Heat Flow Modeling For Geothermal Resource Reconnaissance Applied in The Appalachian Basin*. Master's Thesis, Cornell University, Ithaca, NY, 236 p.
- Smith, L., Nyahay, R., & Slater, B. (2010). *Integrated Reservoir Characterization of the Subsurface Cambrian and Lower Ordovician Potsdam, Galway and Theresa Formations in New York*. New York State Energy Research and Development Authority (NYSERDA).
- Social Security Administration. (2015). *Cost-Of-Living Adjustment, Prior Cost-of-Living Adjustments*. Retrieved from Official Social Security Website: <http://www.ssa.gov/news/cola/facts>.
- Stutz, G. R. (2012). *Development, Analysis, and Application of a Well by Well Method for Estimating Surface Heat Flow for Regional Geothermal Resource Assessment*. Cornell Thesis, Cornell University. Retrieved from <http://hdl.handle.net/1813/31037>.
- Stutz, G. R., Shope, E., Aguirre, G. A., Batir, J., Richards, M. C., Blackwell, D. D., Tester, J. W., Stedinger, J. R., and Jordan, T. E. (2015). Geothermal energy characterization in the Appalachian Basin of New York and Pennsylvania. *Geosphere*, Vol 11, No. 5. 1291-1304. doi:10.1130/GES00499.1.
- Stutz, G., Williams, M., Frone, Z., Reber, T., Blackwell, D., Jordan, T., & Tester, J. (2012). A Well by Well Method for Estimating Surface Heat Flow for Regional Geothermal Resource Assessment. *Stanford Geothermal Workshop Proceedings*. Stanford University.
- Tester, J., Joyce, W., Brown, L., Bland, B., Clark, A., Jordan, T., Anderson, B. (2010). Co-generation Opportunities for Lower Grade Geothermal Resources in the Northeast - A Case Study of the Cornell Site in Ithaca, NY. *GRC Transactions*. Vol. 34, pp. 475-483. Geothermal Resources Council. Retrieved from <http://pubs.geothermal-library.org/lib/grc/1028690.pdf>.
- Tester, J., Reber, T., Beckers, K., Lukawski, M., Camp, E., Aguirre, G. A., Horowitz, F. (2015). Integrating Geothermal Energy Use into Re-building American Infrastructure. *Proceedings World*

- Geothermal Congress*. Melbourne, Australia: International Geothermal Association. Retrieved from <http://www.geothermal-energy.org/pdf/IGAstandard/WGC/2015/38000.pdf?>.
- The Coal Forum. (2015). *WV Leads SSEB in Rejecting 'Clean Power Plan'*. Retrieved from [wwwcoalforum.org: http://www.wvcoalforum.org/201510015019/recent-press/wv-leads-sseb-in-rejecting-clean-power-plan.html](http://www.wvcoalforum.org/201510015019/recent-press/wv-leads-sseb-in-rejecting-clean-power-plan.html).
- U.S. Census Bureau. (2000), Created 2003, Last Revised 2004, Accessed 2015). *U.S. Census Bureau*. Retrieved from Survey of Program Dynamics, Sampling Errors: <http://www.census.gov/spd/sampling.html>.
- U.S. Census Bureau. (2010). *2010 census population & housing unit counts – Blocks*. Retrieved from <https://www.census.gov/geo/maps-data/data/tiger-data.html>.
- U.S. Census Bureau. (2015). *U.S. Census Bureau*. Retrieved from State Quick Facts: <http://quickfacts.census.gov/qfd/states/>.
- U.S. Energy Information Administration . (2015, October 1). *Frequently Asked Questions, Estimated U.S. residential electricity consumption by end use, 2014*. Retrieved from U.S. Energy Information Administration: <http://www.eia.gov/tools/faqs/faq.cfm?id=96&t=3>.
- U.S. Environmental Protection Agency (EPA). (2015, October 1). *U.S. Environmental Protection Agency (EPA)*. Retrieved from Clean Power Plan for Existing Power Plants: <http://www2.epa.gov/cleanpowerplan/clean-power-plan-existing-power-plants>.
- U.S. Environmental Protection Agency (EPA). (2015, August 3). *U.S. Environmental Protection Agency (EPA)*. Retrieved from Clean Power Plan: State at a Glance, West Virginia: <http://www3.epa.gov/airquality/cpptoolbox/west-virginia.pdf>.
- U.S. Geoscience Information Network. (2015, August 27). *USGIN Content Model Schemas Geologic Reservoir 1.0*. Retrieved from <http://schemas.usgin.org/models/#geologicreservoir>.
- Walcott, C. (1896). *Cambrian Rock of Pennsylvania*. United States Geological Survey (USGS). Retrieved from <http://pubs.usgs.gov/bul/0134/report.pdf>.
- West Virginia Geological & Economic Survey. (2006). *Trenton Black River Project Appalachian Basin*. Retrieved from Trenton-Black River Project Website: <http://www.wvgs.wvnet.edu/www/tbr/>.
- Weston Solutions, Inc. (2014, June). *Engineering Evaluation/Cost Analysis Known Distance Range Munitions Response Site Berm Area*. Contract No. : W912DR-09-D-006, Delivery Order No.: 0008, West Chester, PA. Retrieved 9 2015, from West Virginia Army National Guard: http://www.wv.ngb.army.mil/CampDawson/Documents/kd_range_final.pdf.
- Wheaton, C. (2015). *Statistical Correction Of Temperature Data For New York And Pennsylvania Wells*. M.S. Thesis, Cornell University, Ithaca. Retrieved from <https://ecommons.cornell.edu/handle/1813/40609?show=full>.
- Wheaton, C. A., 2016, *Statistical Data Analysis, Global Sensitivity Analysis, and Uncertainty Propagation Applied to Evaluating Geothermal Energy in the Appalachian Basin*: Cornell University, Ithaca, NY, USA, Ph.D. dissertation, 250 pp.

Zoback, M. D., Barton, C. A., Brudy, M., Castillo, D. A., Finkbeiner, T., Grollmund, B. R., Wiprut, D. J. (2003). Determination of stress orientation and magnitude in deep wells. *International Journal of Rock Mechanics and Mining Sciences*, Vol. 40, No. 7, 1049-1076.

FINAL PHASE 1 RESEARCH REPORT

MEMO 1: CATALOG OF SUPPORTING FILES

Supporting documentation for GPFA-AB Phase 1 consists of Methodology overview, a series of Research Memos, numerous National Geothermal Data System Submissions, and project management documents correlating to the Phase 1 Statement of Project Objectives (SOPO). The text of the Methodology report, the research memos and the SOPO documents are included here, whereas the data submissions are a catalog listing.

Statement of Project Objective Task Milestones

The project tasks and milestones are available following this overview of methods.

Methodology Overview and Research Memos

This Methodology Overview (Memo 1) was generated at the conclusion of the project and provides a general description of the methods by which all the constituent tasks were completed. An extended and integrated description of research methods (Final Phase 1 Research Report – Methodologies for GPFA-AB) follows the overview and the Statement of Project Objective Task Milestones.

During the course of the Appalachian Basin Geothermal Play Fairway Analysis Phase I project, 17 written memos were developed and utilized. These served a dual purpose:

1. Solicitation of feedback and input in determination of assumptions, selection of methodology, etc. among the team members, particularly for project elements that required reflection and refinement, such as how best to correct Bottom Hole Temperatures (BHT) or what thermal conductivity values to assign to lithological strata.
2. Providing insight to other researchers wishing to expand on this research, in the Appalachian Basin or elsewhere, after the conclusion of the project.

Depending upon the subject, some memos are a brief description and justification of choices made, whereas others delve into more analysis and are the result of several authors editing over a period of weeks. For example, the Memo describing the BHT Corrections goes into detail about the statistical analysis of different approaches tried and why the formula selected was appropriate for this data set. In several cases, these memos also accompany a Tier 2 Data Submission as explanation of the data and methods utilized.

Memo 1: CATALOG OF SUPPORTING FILES.....	1
Statement of Project Objective Task Milestones	1
Methodology Overview and Research Memos	1
Methodologies for GPFA-AB.....	2
Memo 2: BHT Corrections in GPFA-AB	2
Memo 3: Anadarko Basin Thermal Conductivities in GPFA-AB.....	3
Memo 4: Assignment of Conductivity Stratigraphy for Individual Wells using COSUNA Methodology in GPFA-AB.....	3
Memo 5: Tests of Simplified Conductivity Stratigraphy by Monte Carlo Analysis in GPFA-AB	3

Memo 6: Thermal Outlier Assessment in GPFA-AB	4
Memo 7: Thermal Resource Thresholds in GPFA-AB.....	4
Memo 8: Thermal Model Methods and Well Database Organization in GPFA-AB.....	4
Memo 9: Exploratory Data Analysis and Interpolation Methodology for Thermal Field Estimation..	5
Memo 10: Selection of Four Counties in Each State with the Best Thermal Resources	5
Memo 11: Natural Reservoirs Methodology in GPFA-AB	5
Memo 12: Natural Reservoirs Database Inputs in GPFA-AB.....	5
Memo 13: Identifying Potentially Activatable Faults in GPFA-AB.....	5
Memo 14: Seismic Risk Map Creation Methods in GPFA-AB.....	6
Memo 15: Utilization Analysis in GPFA-AB.....	6
Memo 16: Risk Analysis in GPFA-AB.....	6
Memo 17: Combining Risk Factors in GPFA-AB.....	7
Memo 18: Permits for Geothermal District Heating Project in GPFA-AB	7
Available Data in Tier 1, 2 and 3 to GTDA:.....	7
Tier 1, Phase 1 Final Report and Associated Appendices	7
Tier 2, Thermal Quality Analysis Maps and Structured Data.....	8
Tier 2, Natural Reservoir Quality Analysis Maps and Structured Data.....	8
Tier 2, Risk of Seismicity Analysis Maps and Structured Data.....	8
Tier 2, Utilization Variability Maps and Structured Data.....	9
Tier 2, Combination of Risks Play Fairway Maps and Structured Data.....	9
Tier 3, Geologic Reservoir in New Revised Content Model Format.....	9
Tier 3, Heat Flow Updates in Content Model Format	10

File names listed in this Methodology Overview can be used in internet searches to go to the corresponding Memo in the Geothermal Data Repository.

[Methodologies for GPFA-AB](#)

Phase 1 of the project consisted of a series of 7 tasks, the first 5 of which justify detailed explanation of the methods. Tasks one through four evaluated 4 criteria in the context of risk: thermal resources, natural reservoir quality, seismicity, and utilization. The fifth task combined these risk elements into a series of combined risk maps in order to identify geothermal play fairways. This document describes the methodology for each of these five major tasks, making some references to additional research memos contained within this section.

Methodologies for GPFA-AB filename: GPFA-AB_Phase1Methodology.pdf

[Memo 2: BHT Corrections in GPFA-AB](#)

Determination of heat flow is a crucial element in estimating geothermal resource potential. Geothermal gradient is one of the key components in calculating heat flow. The oil and gas industry activity within

the Appalachian Basin is a wealth of temperature at depth data, as ‘raw’ or uncorrected Bottom Hole Temperature (BHT) values are routinely collected during the oil and gas drilling and/or extraction process. However, BHT can differ from true *in-situ* rock values due to drilling disturbances, circulation of fluids, and other human induced factors. Additionally, extreme terrain variations as seen in mountainous areas can impact accurate determination of geothermal gradient. For these reasons, BHT values are generally ‘corrected’ to approximate an equilibrium temperature-depth profile. Over the years, several approaches to BHT corrections have been used in heat flow determinations and geothermal resource estimations. This memo describes the BHT correction methodology used in this GPFA-AB project.

BHT Corrections in GPFA-AB filename: Memo2_GPFA-AB_BHTCorrections.pdf

[Memo 3: Anadarko Basin Thermal Conductivities in GPFA-AB](#)

One of the key components in calculating heat flow and temperatures at depth is the thermal conductivity of the rock layers. The thermal conductivity values of rocks within the Anadarko Basin have been studied in greater detail than many other sedimentary basins. While this GPFA is focused on the Appalachian Basin, values from the Anadarko Basin have been used as a proxy where measured values unavailable within the Appalachian Basin. This memo describes the results of a resampling of Anadarko Basin thermal conductivities from Carter et al. (1998). Methods for assigning specific thermal conductivity values to each Appalachian Basin formation are discussed in an appendix to the memo entitled Assignment of Conductivity Stratigraphy for Individual Wells using COSUNA Methodology in GPFA-AB. The thermal conductivity values for each formation will be provided as an NGDS data submission.

Anadarko Basin Thermal Conductivities in GPFA-AB filename:
Memo3_GPFA-AB_AnadarkoBasinThermalConductivity.pdf

[Memo 4: Assignment of Conductivity Stratigraphy for Individual Wells using COSUNA Methodology in GPFA-AB](#)

In order to determine properties of the thermal field at depth, the thermal conductivity stratigraphy of the basin must be known everywhere. In practice, it is infeasible to know the conductivity stratigraphy everywhere, so approximations are needed. For this project, the Correlation of Stratigraphic Units of North America (COSUNA) stratigraphic columns, available from the American Association of Petroleum Geologists were used as approximations of the stratigraphy because 1) well specific stratigraphy is not available for every well, and 2) the time constraints of Phase 1 would not be conducive to implementing specific geology to each well. COSUNA provides information on stratigraphy for ‘sections’ throughout the continent, including approximate thicknesses of different rock types. A weighted average of thermal conductivity for the entire wellbore can be approximated by consulting COSUNA charts for the various rock types and thicknesses encountered within the well. This memo documents the approach, assumptions, limitations, advantages, etc. of the COSUNA methodology for assignment of thermal conductivity and formation thicknesses to each well.

Assignment of Conductivity Stratigraphy for Individual Wells using COSUNA Methodology in GPFA-AB filename: Memo4_GPFA-AB_COSUNA_Documentation_NewConductivityMethod.pdf

[Memo 5: Tests of Simplified Conductivity Stratigraphy by Monte Carlo Analysis in GPFA-AB](#)

The simplification of well geology using the COSUNA approximation is tested by using Monte Carlo analysis to examine the potential differences of the thermal model outcomes for the COSUNA simplification compared to a full analysis of each well. For 77 wells, thermal model outcomes of the conductivity stratigraphy based on well details are compared to thermal model outcomes for the same

locations if the COSUNA approximation is used instead. This memo first describes the approach of selecting a smaller subset of wells from the large collection to better understand the Basin's characteristics. Criteria were established for well selection based on availability of better lithology detail, multiple temperature-depth readings at appropriate depths, spatial distribution throughout the region of interest, etc. against which to test the COSUNA-based thermal model. The memo then describes the Monte Carlo simulation parameters. The results of the analysis are that the differences between the COSUNA stratigraphy with Carter conductivities and the detailed stratigraphy are generally minor when compared over the whole region.

Tests of Simplified Conductivity Stratigraphy by Monte Carlo Analysis in GPFA-AB filename:
Memo5_GPFA-AB_ConductivityStratigraphyMonteCarloAnalysis.pdf

[Memo 6: Thermal Outlier Assessment in GPFA-AB](#)

The project team must determine which algorithm should be used to identify outliers in the geospatial datasets. Outliers pose a problem for non-robust regression schemes because they would have high squared residuals. Many regression techniques seek to minimize the squared residuals, so an outlier can have undue influence on the results of the analysis. This memo outlines the recommended outlier detection algorithm and contains several appendices within it. Appendix 1 outlines the previous work on outlier algorithms for the NY and PA geothermal dataset. Appendix 2 illustrates the sensitivity of the final results to algorithm parameters over a reasonable range of values. Appendix 3 provides Monte Carlo type I error rates for different distributions with known shape (e.g. normal, student t, uniform). The type I errors were derived empirically using Monte Carlo simulation for sample size of 25. In addition to references, appendices for this memo include:

1. Appendix 1: Summary of Outlier Algorithms Used at Cornell
2. Appendix 2: Sensitivity Analysis of Recommended Algorithm
3. Appendix 3: Type I Error Rates

Thermal Outlier Assessment in GPFA-AB filename: Memo6_GPFA-AB_ThermalOutlierAssessment.pdf

[Memo 7: Thermal Resource Thresholds in GPFA-AB](#)

The thermal risk factor needs to have thresholds assigned for visualizing the map in the discrete play-fairway color scheme. These thresholds should be objectively defined to reflect actual acceptability of the resource at that threshold level. Using this method, the resulting risk factor maps will reflect the favorability of the site. This memo discusses how the risk thresholds were determined for the Thermal Risk Factor, and the methods are transferrable to other risk factors.

Thermal Resource Thresholds in GPFA-AB filename: Memo7__GPFA-AB_ThermalResourceThresholds

[Memo 8: Thermal Model Methods and Well Database Organization in GPFA-AB](#)

This memo describes the reorganization of the GPFA well database into a format with additional data fields that are necessary to run the thermal model. It also describes the methods, assumptions, and equations used in the thermal model. These methods were used for creating the 3rd quarter and final thermal maps for this project. This memo will accompany the Tier 2 Data submission for the Thermal Analysis task, including a Derivation of 1-D Conduction Heat Balance. The Tier 2 Thermal Analysis data upload will contain several attached files with this memo:

- 1) Well Databases Folder
- 2) Trenton-Black River Sediment Thickness Map
- 3) Influence of Annual Temperature Fluctuation on Near-Surface Temperatures

- 4) Drilling Fluid Query in SQL
- 5) Probabilistic assignment of Drilling Fluid based on Nearest Neighbor Wells

Thermal Model Methods and Well Database Organization in GPFA-AB filename:
Memo8__GPFA-AB_ThermalModel

[Memo 9: Exploratory Data Analysis and Interpolation Methodology for Thermal Field Estimation](#)

This memo describes the methods, including formulas and assumptions, used to interpolate the geotherm data at each well to create the thermal risk factor and uncertainty maps for the project. Included in this memo is an exploratory data analysis on wells after processing in the thermal model.

Exploratory Data Analysis and Interpolation Methodology for Thermal Field Estimation filename:
Memo9__GPFA-AB_ExploratoryDataAnalysisAndInterpolationMethodologyForThermalFieldEstimation

[Selection of Four Counties in Each State with the Best Thermal Resources](#)

This memo describes the methods used to select the four “best” counties in each state according to the thermal resources. This analysis complements the Play Fairway maps that are based on the combination of the other three risk factors with the thermal resources. but this analysis is specific to thermal attributes.

Selection of Four Counties in Each State with the Best Thermal Resources filename:
Memo10__GPFA-AB_SelectionOfFourCountiesInEachStateWithBestThermalResources

[Memo 11: Natural Reservoirs Methodology in GPFA-AB](#)

Task 2 for this project involves the mapping and characterization of natural reservoirs within the Appalachian Basin region of New York (NY), Pennsylvania (PA), and West Virginia (WV). The intention of this memo is to present the methods that have been used for the completion of this task’s milestones. The reservoir data collection and compilation methods used for NY are different than those used for PA and WV, as will be described within. Reservoir analysis and uncertainty quantification methods are consistent across the tri-state region.

Natural Reservoirs Methodology in GPFA-AB filename:
Memo11__GPFA-AB_NaturalReservoirsMethods

[Memo 12: Natural Reservoirs Database Inputs in GPFA-AB](#)

This document is intended to augment the “Natural Reservoirs Methodology” document, by providing more details on the original and modified database inputs for New York, Pennsylvania and West Virginia. Additionally, all research and literature that affected decisions for the reservoir data input are recorded here. This especially includes data for geologic formations in the Appalachian Basin. This memo will accompany the Tier 2 Data submission for the Natural Reservoirs Quality Analysis task. The Tier 2 Thermal Analysis data upload will contain several attached files with this memo.

Natural Reservoirs Database Inputs in GPFA-AB filename:
Memo12__GPFA-AB_ReservoirsDataSelections

[Memo 13: Identifying Potentially Activatable Faults in GPFA-AB](#)

These analyses attempt to highlight the risk of induced seismicity related to a geothermal project. Absent a regionally complete map of deep faults, gravity and magnetic data are analyzed to extract a multi-scale-

edge Poisson wavelet representation of the locations of rocks of laterally contrasting physical properties. Among these lateral rock property boundaries are a subset that are candidates for future fault slip, if fluid pressures change and if a plane of weakness is properly oriented in space. To narrow the focus of this analysis onto rock property boundaries of greater concern (e.g., faults with demonstrated propensity to slip), a second step was to identify the co-occurrence of rock-property-boundaries at depths of 3-4 km and seismic activity registered in earthquake catalogs or by EarthScope. One approach to exploring the likelihood that some of the faults in the region might be reactivated if subsurface pressures change is an analysis of tendency to slip, which is based on determination of the spatial orientation of a structure (plane of weakness) relative to the direction of the regional principal compressive stress. This method will produce interesting results that foster further investigation although at this stage the results will be of low reliability as indicators of the risk of induced seismicity. Collection of pertinent data during follow-up investigation is vital to create more reliable risk results.

Identifying Potentially Activatable Faults in GPFA-AB filename:
Memo13_GPFA-AB_IdentifyingPotentiallyActivatableFaults

[Memo 14: Seismic Risk Map Creation Methods in GPFA-AB](#)

This memo describes the methods used to process the seismic data gathered and generated for this project into a Risk of Seismicity. Detailed methodology used to convert the seismic risk data (i.e. distance to nearest earthquake, and angle to critical stress) into a two independent seismic risk maps is presented. This memo accompanies the Tier 2 Data submission.

Seismic Risk Map Creation Methods in GPFA-AB filename:
Memo14__GPFA-AB_SeismicRiskMapCreationMethods

[Memo 15: Utilization Analysis in GPFA-AB](#)

Task four of Phase 1 of the project assesses the utilization demand for geothermal heat. This was done in two parallel efforts: 1) calculation of the Surface Levelized Cost of Heat (SLCOH) for Census Places exceeding a population threshold of 4,000 people and 2) identification of prospective users of geothermal heat, including larger commercial and/or industrial users. This memo is intended to accompany the Tier 2 data submission:

- 1) MATLAB code for interchange with GEOPHIRES
- 2) Result table for Census Places
- 3) Result table of Prospective Users
- 4) Shape file of Map showing Census Places and Prospective User locations

Utilization Analysis in GPFA-AB filename:
Memo15_GPFA-AB_Utililization_Analysis

[Memo 16: Risk Analysis in GPFA-AB](#)

This memo builds upon the 1 April 2015 memo entitled “Combining Risk Factors.” The relevant discussion from the previous memo is retained, when applicable. One difference here is an emphasis that map colors for 3-color or 5-color maps should be related to the *actual acceptability* of a location measured on that risk index at the scale of the analysis. They are not relative metrics providing just a comparison to other locations or projects, but absolute evaluations of project acceptability. This makes it reasonable to consider the minimum value across risk indices as a criterion for project acceptability. This memo outlines the required map data format for the individual risk factor maps, and the information that

will be required. That includes thresholds used for scaling. The memo also describes some of the ways to represent uncertainty in the analyses and visualization tools that may be used in our final analyses. This memo summarizes some methods that we thought would be applicable to combining risk factors, but it does not represent the final methods used in the analysis. The Memo 17 gives the final results and describes the methods used.

Risk Analysis in GPFA-AB filename: Memo16_GPFA-AB_RiskAnalysis

[Memo 17: Combining Risk Factors in GPFA-AB](#)

This memo provides details and extended results related to the play fairway computations. The results include values used in converting each risk factor into the play fairway scale (scaled risk factor) and extended results on different methods of combining risk factors. The robustness of the different combination methods is briefly discussed. Calculations of uncertainty are discussed, including methods used to approximate the uncertainty in a scaled risk factor and a combined map. Detailed graphics for project locations are provided. The general principles of the combinations were outlined in the previous memo, but this document gives details on the computations and actual results from the analysis.

Combining Risk Factors in GPFA-AB filename: Memo17_GPFA-AB_Combining_Risk_Factors

[Memo 18: Permits for Geothermal District Heating Project in GPFA-AB](#)

Permits will be required for any new drilling associated with a geothermal district heating project. This memo summarizes the anticipated permitting requirements and associated effort for subsequent phases of the project.

Permits for Geothermal District Heating Project in GPFA-AB filename:
Memo18_GPFA-AB_PermittingGeothermalDistrictHeating

[Available Data in Tier 1, 2 and 3 to GTDA:](#)

This project has resulted in data submissions to the National Geothermal Data System (NGDS) via the Geothermal Data Repository (GDR) in all three supported Tiers. The SOPO tasks addressed by these submissions appears below each explanation as well.

[Tier 1, Phase 1 Final Report and Associated Appendices](#)

A PDF of this Phase 1 Final Report including associated appendices and memos will be uploaded as a Tier 1 data submission.

Task 6.0 Project Management and Reporting: The three team leaders (Cornell, SMU, WVU) will interact bi-weekly to assure continued progress on the project. At each quarter's end, available team members will meet by conference call or in person to discuss project progress and needs. Quarterly project reviews will be held with DOE staff by phone or webinar to present project status and verify milestones. One quarterly review will be made in-person at the Geothermal Technology Office peer review (tentatively scheduled for spring 2015 in Denver).

Task 6 Deliverable A final report detailing all facets of the study and detailed suggestions for Phase II will be presented at the end of Phase 1. This report will be the basis for a competitive downselect process for Phase 2. The raw data collected and/or new data generated as part of the project will be uploaded to the NGDS at the end of the Phase I, following USGIN metadata guidelines.

Tier 2, Thermal Quality Analysis Maps and Structured Data

This zipped folder includes the raw data (bottom-hole temperature data retrieved from the NGDS and from the state geological surveys) and calculated data, such as corrected BHT values, formation thermal conductivity values, heat flow values, and depth-to-temperature values. The submission also includes the applicable memos, describing the BHT correction methodology, outlier detection, thermal conductivity assignment, and thermal model calculations. The folder includes shape file(s) of all points, georeferenced rasters, and image files of heat flow and depth-to-temperature maps, and a 'read me' file describing the contents of the zipped folder.

Task 1.0 Thermal Resource Quality Assessment: The purpose of this task and its several subtasks are to research and assemble the available thermal data in the published literature as well as that thermal data available from non-published sources, to establish the data infrastructure for the project, and to carry out the assessment of the first of the proposed Risk Factors (RF1), Thermal Resource Quality.

Task 1 Deliverable: Deliver an improved region-wide map of depths to 80 °C isotherm and a county map for four counties per state, as well as a Green-Yellow-Red-ranked thermal resource map for the region and for the four counties per state, as derived from all the considerations described in Task 1, including lithologies, updated conductivity, and updated basement heat flux model, etc. as well as the supporting data according to the Data Management Plan and thermal models for the New York (NY), Pennsylvania (PA) and West Virginia (WV) region of the Appalachian Basin.

Tier 2, Natural Reservoir Quality Analysis Maps and Structured Data

This zipped folder includes the raw data (reservoir thicknesses, depth, water viscosity, and area) and interpolated data, including the newly developed Reservoir Productivity Index (RPI). The submission also includes the applicable memo, describing the RPI formulas assumptions and methodology. The folder includes shape file(s) of all points, PDFs of the reservoir quality and reservoir quality uncertainty map images, and a 'read me' file describing the contents of the zipped folder.

Task 2.0 Natural Reservoir Quality: The purpose of this task is to develop the supporting database, to evaluate, and to map the distribution of potential geothermal reservoirs. The result will be Ranking Maps and supporting data for natural reservoirs in a majority of the Appalachian Basin of WV, NY and PA.

Task 2 Deliverable: Deliver reservoir quality maps, supporting data and related models for the NY, PA and WV region of the Appalachian Basin incorporating information such as reservoir quality and variability, porosity, permeability, and hydraulic conductivity.

Tier 2, Risk of Seismicity Analysis Maps and Structured Data

This zipped folder includes the raw data (historical record of earthquakes and fault data) and interpolated data, including the orientation as an indicator of fault reactivation. The submission also includes the applicable memo, describing the assumptions, equations, and the primary physics behind the analysis. The folder includes shape file(s) of all points, PDFs of the earthquake history and fault orientation seismicity map images, and a 'read me' file describing the contents of the zipped folder.

Task 3.0 Risk of Seismicity: The purpose of this task is to review seismicity (excluding enhanced geothermal systems –EGS) as a Risk Factor and identify regions with enhanced likelihood for inducing unintended seismic activity during preparation of a reservoir, or during the course of

geothermal heat production. The result of the task will be maps for the study area in the Appalachian Basin in NY, PA and WV of faults and of faults that are active.

Task 3 Deliverable: Deliver risk map, supporting data according to the Data Management Plan, and related models, for the NY, PA and WV region of the Appalachian Basin for induced or reactivated seismicity, incorporating fault positions and seismicity activity.

Tier 2, Utilization Variability Maps and Structured Data

This zipped folder includes the raw data (census bureau population data, EIA heat demand and power consumption, and the American Community Survey building size), and output sites with surface leveled cost of heat (SLCOH) for 248 Census Places. The submission also includes the applicable memo, describing the assumptions and modifications to the GEOPHIRES software. The MATLAB program used is included (executable as well as script). The folder includes shape file(s) of all points, PDFs of the SLCOH map image, and a 'read me' file describing the contents of the zipped folder.

Task 4.0 Utilization Variability: The purpose of this task is to identify regions in the Appalachian Basin with the capacity to utilize low-grade geothermal heat and the related variability of demand. The result of the task will be utilization maps for the region of the Appalachian Basin in NY, PA and WV and estimates of Levelized Cost of Heat for a small set of communities.

Task 4 Deliverable: Deliver maps for spatial variability of population and heat demand, and a ranked map for utilization using supporting data according to the Data management Plan, for the NY, PA and WV region of the Appalachian Basin. Deliver estimated Levelized Cost of Heat (SLCOH) for two communities in each state.

Tier 2, Combination of Risks Play Fairway Maps and Structured Data

This zipped folder includes the applicable memo, describing the methodology and assumptions and any modifications to the input data (such as combining the two seismicity risk elements into a single value). The folder includes a shape file of all points, georeferenced rasters, image files of combined risk maps using multiple approaches, and a 'read me' file describing the contents of the zipped folder.

Task 5.0 Risk Matrix Analysis: The purpose of this task is to merge the common risk segment maps described above, and to produce a common Risk segment map. This will be the compilation of factors and the most favorable combinations of multiple risk factors from the Risk Factors evaluated in Tasks 1-4. A risk matrix will be applied to combine the four sets of risk factors and will identify up to six "most promising Play Fairways" within the Appalachian Basin in NY, PA and WV.

Task 5 Deliverable: Deliver common risk assessment map, which delineates up to 6 Play Fairways within the NY, PA and WV region of the Appalachian Basin based upon the compilation of the spatial variability of the risk factors assessed in Tasks 1-4. The models and available supporting data, according to the Data Management Plan, will also be delivered.

Tier 3, Geologic Reservoir in New Revised Content Model Format

The results of our Natural Reservoir Quality analysis is also being submitted as Tier 3 data submission utilizing a significantly reworded Geologic Reservoir content model. The previous content model for describing Geologic Reservoirs, originally developed by the Texas Bureau of Economic Geology was adapted to accommodate not only this team's new project analysis and metrics, but project data from other geothermal play fairway analysis projects beyond oil and gas extraction geographies.

Tier 3, Heat Flow Updates in Content Model Format

The new heat flow calculated values are being made available as a Tier 3 standardized data formatted submission. (Note: These were submitted via the SMU Node of the NGDS at geothermal.smu.edu, rather than through the GDR).

Low Temperature Geothermal Play Fairway Analysis for the Appalachian Basin (GPFA-AB) Statement of Project Objectives

This document contains the Statement of Project Objectives for our project including the primary tasks, subtasks and milestones for DOE Contract Award Number: DE-EE0006726.

1. **Task 1.0: Project Organization, Data Review, and Thermal Resource Quality Assessment:** The purpose of this task and its several subtasks are to research and assemble the available data in the published literature as well as that data available from non-published sources, to establish the data infrastructure for the project, and to carry out the assessment of the first of the proposed Risk Factors (RF1), Thermal Resource Quality.

1.1 Subtask 1.1: Literature Review and Database Assembly

- 1.1.1 Assemble Data (thermal, well logs, etc.) from the National Geothermal Data System and other project files
- 1.1.2 Review literature, including porosity, permeability and reservoir information relevant to portions of the Appalachian Basin within New York, West Virginia and Pennsylvania
- 1.1.3 Work with State Geological Surveys to select wells for detailed analysis
- 1.1.4 Work with State Geological Surveys to compile the detailed analysis for the subset of wells

- 1.2 **Subtask 1.2: Data Management and Analysis Infrastructure.** Select and assemble required hardware, data infrastructure and software needed to assess, display, compile, spatially analyze, share back-up and otherwise manage the information collected and utilized throughout the project.

1.3 Subtask 1.3: Thermal Reservoir Modeling and Analysis

- 1.3.1 Combine the existing maps of the three states (NY, PA and WV) and use this as the baseline (note: “baseline” below refers to this current state of knowledge)
- 1.3.2 Subdivide basement provinces using potential field data
- 1.3.3 Compile thermal conductivity values for Appalachian basin lithologies
- 1.3.4 Combine in one dataset the many thousands of wells in all three states that were used in producing the existing maps, apply a uniform numerical approach, apply basement heat flow appropriate to the basement provinces, apply thermal conductivities appropriate to the Appalachian basin formations, kriging and analyze semi-variograms, and produce a set of region-wide temperature-at-depth maps that improve on the baseline.
- 1.3.5 Establish uncertainty levels for the regional thermal resource maps
 - 1.3.5.1 Select approximately 100 test wells based on criteria of data quality, of locations that span the full range of thermal quality predicted by the existing maps, and of proximity to the small set of existing wells for which there are thermally equilibrated temperature profiles
 - 1.3.5.2 Develop location-specific thermal models that utilize the full suite of geological properties of the approximately 100 individual wells

- 1.3.5.3 Validate the well-specific temperature estimates by comparison with existing equilibrated thermal profiles, where available; iterate thermal model methods if comparison is not judged adequate.
- 1.3.5.4 Compare the well-specific results to the combined pre-project baseline maps as well as to the newly improved three-state temperature maps.
- 1.3.5.5 Decide whether or not to continue using the compiled pre-project maps, or the then-current uniform maps, or to revise the model on which the maps are computed and repeat the prediction and uncertainty analysis. One of the decision criteria will be based upon the standard error of prediction expressed as a percentage of the predicted value, and its absolute magnitude relative to the required precision of the economic analysis.
- 1.3.5.6 If the uncertainty on the maps is judged to be unsatisfactory, team will create a new set of region-wide maps based on the test well set only, with corresponding analysis of spatial uncertainty.
- 1.3.5.7 Based on a map of the depth to 80 °C rock temperatures, for which the shallower depths designate the most favorable resources, select four counties per state with the most favorable thermal resource.
- 1.3.6 Evaluate thermal resources in four counties per state with most favorable thermal resource:
 - 1.3.6.1 Estimate temperature field based on thermal modeling of full geological data for approximately 10 wells per county.
 - 1.3.6.2 Use kriging and semi-variograms to analyze uncertainty associated with thermal field maps of most favorable counties.
- 1.3.7 Create maps of entire region ranking thermal quality
 - 1.3.7.1 As a project team, assign thresholds for depths to 80 °C corresponding to Green/Yellow/Red classes based on current knowledge of technical and economic thresholds.
 - 1.3.7.2 Create maps using these depth thresholds.

Task 1 Deliverable: Deliver an improved region-wide map of depths to 80 °C isotherm and a county map for four counties per state, as well as a Green-Yellow-Red-ranked thermal resource map for the region and for the four counties per state, as derived from all the considerations described in Task 1, including lithologies, updated conductivity, and updated basement heat flux model, etc. as well as the supporting data according to the Data Management Plan and thermal models for the NY, PA and WV region of the Appalachian Basin.

- 2. **Task 2.0: Natural Reservoir Quality:** The purpose of this task is to develop the supporting database, to evaluate, and to map the distribution of potential geothermal reservoirs. The result will be Ranking Maps and supporting data for natural reservoirs in a majority of the Appalachian Basin of West Virginia, New York and Pennsylvania.
 - 2.1. Collate from prior reports and NGDS and/or state databases the spatial and depth distribution of known hydrocarbon reservoirs and saline aquifers and record the information in GIS databases:
 - 2.1.1. Determine locations as well as rock and fluid properties of historical conventional reservoirs;

- 2.1.2. Compile, from carbon sequestration inventories and from prior studies conducted in support of analyses of the potential for injection wells, the locations, depths and properties of saline aquifers with high pore volume;
- 2.2. Characterize, based upon the collated information, case studies of each major category of natural reservoir
 - 2.2.1. Identify categories of natural reservoirs based on rock and fluid properties
 - 2.2.2. Extract data for reservoir quality and variability from databases
 - 2.2.3. Produce database tied to reservoir categories of porosity and, where reported in prior databases, the permeability, hydraulic conductivity and fluid pressure
- 2.3. Create ranking categories of reservoir as best, worst, and intermediate capacity for production
 - 2.3.1. Use the GIS 3D locations of potential natural reservoirs to identify reservoirs at < 4000 m. Restrict further analysis only to this depth range.
 - 2.3.2. Classify the potential reservoir categories by porosity, permeability and pressure criteria to identify the reservoirs with greatest potential for high flux of natural reservoir water during production and recirculation
 - 2.3.3. As a project team, assign weights to i) the values of thickness of each reservoir category at a specific location, as well as for b) the reservoir category itself. Select a combination of thickness and reservoir category weights that serves as a threshold, below which it is judged that an insufficient production rate of formation fluids is plausible. This decision will be informed by Task 4.
- 2.4. To create a regional map, first rank areas that fall below the threshold noted immediately above as Red. Then for all other depths and regions, combine the 3D distribution of thickness and category(ies) of the available reservoirs with their weighting factors to create a grid of the location-specific suitability of potential reservoirs. The project team will decide upon the most suitable algorithm for this combination of factors. Divide the gridded values into the upper half (to be designed green) and the lower half (to be designated yellow).
- 2.5. Produce maps of Green/Yellow/Red conditions for the three-state area.

Task 2 Deliverable: Deliver reservoir quality maps, supporting data and related models for the NY, PA and WV region of the Appalachian Basin incorporating information such as reservoir quality and variability, porosity, permeability, and hydraulic conductivity and other information as described in Task 2.

- 3. **Task 3.0: Risk of Seismicity:** The purpose of this task is to review seismicity (excluding enhanced geothermal systems –EGS) as a Risk Factor and identify regions with enhanced likelihood for inducing unintended seismic activity during preparation of a reservoir, or during the course of geothermal heat production. The result of the task will be maps for the study area in the Appalachian Basin in NY, PA and WV of faults and of faults that are active.

3.1. Compile fault maps

- 3.1.1. Extract fault locations from reports and literature, recording detection method used in original report;
- 3.1.2. Locate additional faults using potential field data
- 3.1.3. Accounting for scale differences in the data that underlie the methods, use differences among maps of faults identified by potential field methods and NYS existing detailed maps, to estimate the likelihood a fault is missed by the potential field methods.

- 3.1.4. Extract locations of faults detectable with similar criteria across the 3-state area
- 3.2. Determine distribution of active seismicity at shallow depths:**
 - 3.2.1. Based on earthquake catalogs compile hypocenters
 - 3.2.2. Create map of ongoing (2014-15) microseismicity shallower than 6 km based on, or extracted from data recorded by, EarthScope TA eastern US array.
- 3.3. Create maps of risk of activation or reactivation of faults**
 - 3.3.1. Create maps of distances to known faults, with uncertainties
 - 3.3.2. Create maps of distances to locations of seismically active faults, with uncertainties
 - 3.3.3. Review the rapidly evolving literature on the relationships between reactivation of faults, reservoir properties, distance to the well site, and categories of fluid management at the well site
 - 3.3.4. As a project team, adopt risk criteria for distances of a geothermal well from a fault with designations as unacceptable risk (Red), intermediate (Yellow), and acceptable risk (Green). The criteria will account for the length of the fault and for properties that are typical for the category of the closest reservoir
 - 3.3.5. Produce maps illustrating areas classified as Green/Yellow/Red

Task 3 Deliverable: Deliver risk map, supporting data according to the Data Management Plan, and related models, for the NY, PA and WV region of the Appalachian Basin for induced or reactivated seismicity, incorporating fault positions and seismicity activity and other information as described in Task 3.

- 4. **Task 4.0: Utilization Variability:** The purpose of this task is to identify regions in the Appalachian Basin with the capacity to utilize low-grade geothermal heat and the related variability of demand. The result of the task will be utilization maps for the region of the Appalachian Basin in NY, PA and WV and estimates of Levelized Cost of Heat for a small set of communities.

7.4 Develop maps of variable population density and demand for heat.

- 7.4.1 Review of US census data to extract population densities across 3 states;
- 7.4.2 Review of climate or surface temperature data to develop the spatial distribution of seasonal heat demand;
- 7.4.3 Combine population density, heat demand and seasonal demand to develop an index for annual heat demand.

7.5 Use the (GEOthermal energy for Production of Heat and Electricity (“IR”) Economically Simulated) model (GEOPHIRES) to conduct parametric analysis of the economics of developing integrated geothermal utilization systems as a function of reservoir performance, demand requirements, and financial factors such as capital costs, and debt and equity rates of return.

- 7.5.1 Update model for inflation and regional effects
- 7.5.2 Integrate current well drilling costs database and infrastructure capital costs
- 7.5.3 After a first draft of a CRS map is created, in anticipation of decision-making based on the finalized CRS map, select two communities in each state, one in a favorable (Green) and one in an unfavorable (Red) area, and for those communities estimate Levelized Cost of Heat (LCOH). The basis for selection of these few communities will depend on the availability of information about i) demand requirements in terms of temperatures, heat flux, and capacity factors, ii) the sub-surface geological features at

those locations, and iii) quality of existing infrastructure for implementing a district network as well as a number of social factors such as community interest.

7.6 Assign ranks to the proximity of a community or other heat consumer to a potential geothermal reservoir.

- 7.6.1 Use GEOPHIRES to test the sensitivity of the LCOH to the distance of a potential well field to a consumer end point
- 7.6.2 As a project team, decide upon the thresholds of distance and of heat demand to rank as Green/Yellow/Red
- 7.6.3 Create a map displaying the Green/Yellow/Red ranks

Task 4 Deliverable: Deliver maps for spatial variability of population and heat demand, and a ranked map for utilization, as described in Task 4, and supporting data according to the Data management Plan, for the NY, PA and WV region of the Appalachian Basin. Deliver estimated Levelized Cost of Heat (LCOH) for two communities in each state.

5. **Task 5.0: Risk Matrix Analysis:** The purpose of this task is to merge the common risk segment maps described above, and to produce a common Risk segment map. This will be the compilation of factors and the most favorable combinations of multiple risk factors from the Risk Factors evaluated in Tasks 1-4. A risk matrix will be applied to combine the four sets of risk factors and will identify up to six “most promising Play Fairways” within the Appalachian Basin in NY, PA and WV.

5.1 Adopt Common Risk Segment (CRS) calculation standard

- 5.1.1 Examine choices in available software or customize software
- 5.1.2 Run sensitivity analyses with GEOPHIRES to clarify the relative importance of the four risk factors in the viability of a low-temperature geothermal energy project, and the nature of threshold effects for those factors
- 5.1.3 As a project team, assign weighting factors for each risk category to develop a simple composite risk value, as well as considering an appropriate range of non-linear total risk functions (including the product of the individual risk factors or their compliments)

5.2 Create maps of individual risk values of each Risk Factor (RF)

- 5.2.1 Equalize spatial resolution of maps;
- 5.2.2 Create gridded fields of weighting factor for each of risk categories

5.3 Map spatial variability of geothermal resource from natural reservoirs

- 5.3.1 Run risk analysis for matrix of risk factors from Tasks 1-4.
- 5.3.2 Map spatial variability of combined and weighted information on resource, reservoirs, faults, and usage
- 5.3.3 As a project team, assign thresholds for Green/Yellow/Red ranks
- 5.3.4 Compare preliminary LCOH estimates for six communities to the current Green/Yellow/Red ranks for consistency.
- 5.3.5 Run risk analysis calculations for matrix utilizing alternative weightings as appropriate based on expert input.
- 5.3.6 Identify zones which are the most favorable identified play fairways.

Task 5 Deliverable: Deliver common risk assessment map which delineates more than 6 Play Fairways within the NY, PA and WV region of the Appalachian Basin based upon the compilation of the spatial variability of the risk factors assessed in Tasks 1-4. The models, and available supporting data according to the Data Management Plan, will also be delivered.

Task 6.0: Project Management and Reporting

Task 7.0: Commercialization / Market Transformations

FINAL PHASE 1 RESEARCH REPORT — METHODOLOGIES FOR GPFA-AB

The Phase 1 Final Report contains a discussion of the methodologies used for each of the major project tasks in GPFA-AB, including process flow charts. This document provides further details and references a series of research memos that were written throughout the course of the project. These memos provide the reader with a still deeper understanding still of the hypotheses, methods, analyses, etc. for various topics.

DISCLAIMER

The information, data, or work presented herein was funded in part by an agency of the United States Government. Neither the United States Government nor any agency thereof, nor any of their employees, makes any warranty, express or implied, or assumes any legal liability or responsibility for the accuracy, completeness, or usefulness of any information, apparatus, product, or process disclosed, or represents that its use would not infringe privately owned rights. Reference herein to any specific commercial product, process, or service by trade name, trademark, manufacturer, or otherwise does not necessarily constitute or imply its endorsement, recommendation, or favoring by the United States Government or any agency thereof. The views and opinions of authors expressed herein do not necessarily state or reflect those of the United States Government or any agency thereof.

Methodology Task 1, Thermal Analysis:

Analysis of abundant oil and gas bottom-hole temperatures (BHTs) and sparse equilibrium temperature data. **Methodologies:** . As of C item (NGDS) for New York, Pennsylvania, West Virginia, and a 50 km buffer into neighboring Appalachian Basin states. The NY, PA, and WV data were all cross checked with state oil and gas datasets for additional BHT information. Overall, state databases provided redundant temperature-depth information, so the NGDS data was used nearly exclusively for BHT data in this project. This temperature data was merged into a single database with common field headers (see [Thermal Model Memo](#) for details). After eliminating data for quality control reasons, selecting to analyze only wells deeper than 1000 m except in one area which lacked any, and ensuring that each spatial location had only one data point, the data set included approximately 13,300 temperature-at-depth points, prior to spatial outlier detection tests. Spatial outlier tests were performed on each thermal property for which a map was made, and on average removed about 1000 additional points (see [Outlier Memo for details](#)). Ultimately for one region in northwestern Pennsylvania the 1000 m minimum depth cutoff proved to create a thermal mapping data gap whose area exceeded 7000 km²; for that area, BHT data as shallow as 750 m were used (see [Interpolation Methodology Memo](#)).

BHT data are known to have many potential sources of error, including collection prior to the thermal field returning to equilibrium conditions post-drilling. A set of BHT correction equations were developed that reflect spatial variations in the observed data and the underlying geology; a detailed description is given in the [BHT Correction Memo](#) in the Catalog of Supporting Files and in Whealton (2016). Broadly speaking, a set of wells were identified with a thermal log that was interpreted as being of better quality (closer to equilibrium) than the surrounding BHT data. There were 48 equilibrium logs available; these

were grouped into 24 clusters, and neighboring BHTs were corrected to the estimated equilibrium temperature profile. Further analysis showed that the BHT corrections followed systematic patterns depending on geological province, and on that basis a small set of temperature correction functions were established and applied to all the remaining wells according to their geological province.

Estimations of heat flow and the temperature field at depth requires knowledge of the “conductivity stratigraphy” at the >13,300 boreholes whose BHT data were used. We assigned lithologic units, thicknesses of each unit, and corresponding thermal conductivities to each borehole from the surface to the basement. To accomplish this in the time available, we used the AAPG (1985a, 1985b) COSUNA lithology charts and regional maps published by the Trenton Black-River Project (West Virginia Geological & Economic Survey, 2006) of the depth to basement, above which the COSUNA information was applicable. Full details are given in the [COSUNA Methodology Memo](#) in the Catalog of Supporting Files and in Chapter 2 of Smith (2016). In the absence of detailed information regarding the thermal conductivity values of the Appalachian basin sedimentary rocks, values of conductivity for similar rock compositions from the geologically similar Anadarko Basin were used. Refer to both the [COSUNA Methodology](#) and [Anadarko Basin Thermal Conductivity Memos](#) for further details.

To transform the depth-specific and well-specific corrected BHT data into uniform thermal metrics, a computer program was developed to calculate the surface heat flow, and the geotherm (i.e. temperatures at depth) for all wells with BHTs and stratigraphic information. This program is a steady state, 1-D heat conduction model (Jaeger, 1965) that was developed and tested in the open source software program Python 2.7.9 (see the [Thermal Model Methods Memo](#) for details). This model updates and improves upon previous work by Cornell and SMU as part of the Google.org and NGDS projects (Blackwell D. D. et al., 2011; Stutz G. R. et al., 2012; Stutz G.R. et al., 2015). This model assumes that radiogenic heat production is constant and uniformly distributed in sedimentary rocks, and dies off exponentially in the basement crustal rocks as per Lachenbruch (1968). A constant mantle heat flow of 30 mW/m² is assumed to be present throughout the region based on the average mantle heat flow for the stable continents, including the Appalachian Basin (Roy, Blackwell, & Decker, 1972).

The inputs to the thermal model involve a variety of simplifications and assumptions. To evaluate the robustness of the output, Monte Carlo simulations were used to examine the variability of the predicted thermal properties as functions of the uncertainties of the input variables. One topic of broad uncertainty was the reliability of using the simplified conductivity stratigraphy based on the regional COSUNA lithologic simplification. To examine the consequences of this simplified method, we obtained well-specific conductivity stratigraphy data for 77 wells, distributed widely across the study area ([Tests of Simplified Conductivity Stratigraphy Memo](#)). These well data and the COSUNA-based simplified data for the same wells were each subjected to Monte Carlo simulations, and the thermal predictions were compared.

Using the results from the 1-D model, a local outlier analysis was run on each calculated thermal variable ([Thermal Outlier Assessment Memo](#)). The retained data were then subject to a spatial interpolation to generate the predicted mean and the standard error of the predicted mean for the resource, and create maps representing the thermal quality in a GeoTIFF format. Within the Appalachian Basin, wells are clustered where there are oil and gas reservoirs, and sparse in areas with little to no oil and gas exploration. Therefore, interpolation algorithms must be able to handle predictions for sparse and

clustered data. The spatial interpolation used in this analysis is so-called stratified¹ ordinary kriging implemented in the open source language R in the package `gstat` (Pebesma & Wesseling, 1998; [Interpolation Methodology Memo](#)). Lateral boundaries at depth within the region were defined based on natural geological boundaries, defined primarily by gravity potential field edges at depths from 7–15 km ([Interpolation Methodology Memo](#)). These geologic boundaries should enclose rocks with similar properties, and may represent small-scale “heat flow provinces” (Roy, Blackwell, & Birch, 1968). Statistically, lateral stratification/regionalization preserves this assumption by interpolating data separately for all provinces, which potentially have different data generating processes (e.g. differences in thermal conductivity, heat generation, mantle heat flow, etc.).

The kriging algorithm considers the spatial autocorrelation in the variable to be predicted, with the expectation that points closer to one another are more similar in value than points farther away. Semi-variograms corresponding to this structure of spatial (semi)variance illuminate differences in the structure of spatial autocorrelation with increasing separation distance on spatial scales smaller than the entire Appalachian basin. This result justifies the decision to model BHT corrections and the thermal map interpolations on local, smaller scales rather than on a global, regional scale. The stratified kriging interpolations capture this variability to provide the predicted mean and the spatial standard error of the predicted mean for each thermal variable calculated using the thermal model. For interpolations, the spatial correlation range (distance) was used as the maximum searching distance for nearest neighbor points – beyond this range there is no modeled spatial correlation. In addition to the searching distance restriction, a minimum of 5 points were required to make a prediction at any location within the basin. As a result of these interpolation restrictions and the 1000 m cutoff depth (or 750 m in one area), some areas on the thermal maps do not have predictions.

Maps were prepared that express the regional variations in the surface heat flow, the depths to an 80 °C surface and to a 100 °C surface, and the temperatures at depths of 1500 m, 2500 m, and 3500 m. The depth to 80 °C map and the surface heat flow maps have been updated to reflect changes in methodology that developed since the 2015 report was submitted. All other maps are products from the 2015 report.

A leave-one-out cross validation was performed for each of the interpolated thermal variables, with the result that about 98% of the values of left-out points were contained within 3 standard errors of the predicted mean for that thermal resource (see the [Tests of Simplified Conductivity Stratigraphy Memo](#) for the results of the cross validation in each of the 12 selected counties. These results are also from the 2015 data submission). Another evaluation of the interpolation performance was through comparison of equilibrium temperature logs at 1.5 km to the predicted mean at 1.5 km (Figure 18 in main body of the report).

The mapped heat resources were ranked by 3-level (Green/Yellow/Red) and 5-level (Green/Greenish-yellow/Yellow/Orange/Red) divisions. The thresholds could be selected based on either general economic considerations, in that costs for geothermal energy projects rise as the depth needed to reach the temperature of interest increases, or based on the temperature requirements of a given end-use technology ([Thermal Resource Thresholds Memo](#)). For a 5-division scheme for maps showing the depth to a selected temperature, the threshold to least favorable (red) conditions is set at a production depth that would cost approximately \$10 million to drill and complete a well, which for current estimates of drilling costs

¹ “Stratified” in this geostatistical context means an analysis regionalized by lateral boundaries. To other geoscientists, that terminology should not be confused with strata meaning vertical layering rather than lateral boundaries.

corresponds to an average depth of about 4000 m. The succession of thresholds for improved quality of the thermal resource were selected in approximately \$2 million cost increments. For a 5-division scheme for maps showing the temperature at selected depths, thresholds were selected based on the end-use temperatures, or favorable values of the geothermal gradient at the depth of interest (e.g. 1.5 km). Thresholds are different for each depth considered because the favorability in temperature changes with depth. The threshold to least favorable (red) conditions are set at or below 50 °C, the minimum useful temperature considered for this project. The most favorable (green) conditions are set between 90 °C (for 1.5 km depth) and 150 °C (for 3.5 km depth). Thresholds in between these depths are selected based on end use temperatures for certain projects.

Measurements of Thermal Conductivity

Specific to thermal conductivity, the Appalachian Basin did not have sufficient data available during Phase 1 to select representative values for each lithology encountered in the basin. The Anadarko Basin thermal conductivity samples were chosen as representative to the Appalachian Basin because of the similarities between the paleo-burial depth and age of the two basins. Thermal conductivity is strongly influenced by depth of burial (decrease in porosity), and these basins reached similar burial depths. During the past year, original samples from Carter et al. (1998) were rerun at SMU to confirm our understanding of certain formation values differing by more than 10% in the Carter et al. (1998) paper (see [Anadarko Basin Thermal Conductivities Memo](#)). The thermal conductivity of a formation, when measured on a divided bar, have had reported differences between samples of $\pm 5\%$ to $\pm 10\%$ depending on the formation (Gallardo & Blackwell, 1999; Carter et al., 1998). This reexamination of Carter et al (1998) data highlighted how the mineralogy of the rock sample can change even at the meter scale, thereby impacting the thermal conductivity on scales smaller than are of interest for this stage of the project. For this project, formation thermal conductivity on average is of interest, so the values from Carter et al. (1998) and available Appalachian Basin thermal conductivities were subject to a Monte Carlo simulation to obtain formation-specific average thermal conductivities and measures of uncertainty variance. These values were used to construct the COSUNA based thermal conductivity stratigraphy for use in the 1-D heat conduction model. In the thermal model, over the entire well the thermal conductivity is weighted by formation thickness and harmonically averaged as part of the heat flow and geotherm calculation. In an effort to move away from Anadarko Basin thermal conductivities, we recommend that during future assessment studies additional thermal conductivity measurements from core samples for the formations of interest in the Appalachian Basin be collected to confirm that our assigned values are appropriate, or to change them. The thermal conductivities of Appalachian basin samples can be analyzed at SMU or WVU.

Methodology Task 2, Natural Reservoir Quality:

Task 2 for this project involves the mapping and characterization of natural reservoirs within the Appalachian Basin region of New York (NY), Pennsylvania (PA), and West Virginia (WV). Phase 1 of this project was limited to the analysis of existing data. Because drilling for oil and gas in the Appalachian Basin has taken place for over a century, the petroleum industry has vast amounts of data for reservoirs. For the purpose of Phase 1, only proven hydrocarbon reservoirs were considered; future work may include the consideration of rocks with properties suitable to be reservoirs but that have not been used to produce oil or gas. Methods are detailed in a pair of companion memos, one focused on the principles of developing reservoir quality indices (see [Natural Reservoir Methods](#)), and the second on the selection of data needed to calculate the reservoir quality indices (see [Reservoir Data Section](#)).

The oil and gas industry uses the term “field” to describe a group of wells that all penetrate into the same formation to produce oil or gas; therefore, all sources of data for this project used the term field. However, in the geothermal industry, the term reservoir is more commonly used to mean a given volume of permeable rock from which heat can be extracted using circulation of fluids. A field and a reservoir are essentially the same thing, but the perspective is shifted from the wells to the entire body of rock. All cases where the term “field” was encountered in our original datasets were changed to reservoir for the remainder of the project.

After thermal quality, injection flow rate is most important factor affecting geothermal heat production (Bedre & Anderson, 2012). Given the purpose of this assessment, it was appropriate to select for ranking of reservoirs numerical thresholds of reservoir quality that measure the capacity to extract hot water from the reservoir. However, the production of fluid from a reservoir depends not only on the amount of *in situ* water in the reservoir but also on engineering and operational selections. Consequently, this evaluation of natural reservoirs sought to utilize one or more quality metrics that are firmly grounded to *in situ* geological capacity of the reservoirs and that also include the well-field design and field management to express the producible fluids from those reservoirs.

The natural geological properties encompass permeability, thickness (hydrocarbon pay thickness), temperature, depth, and area. Among the operational selections could be the use of a working fluid to transfer heat from rock to surface-based heat exchangers that is not water. For instance, supercritical carbon dioxide has been investigated as an alternative working fluid (Brown, 2000; Pruess, 2007). The chief well-field attributes and operational factors are the diameters of the well bores, the distance between production well and the injection well, and the pressure drop created by pumping a well.

We adopted three metrics (see details in Memo 11 Natural Reservoir Methodology):

- a Reservoir Fluid Capacity that is a geological quality description, which is the product of permeability and thickness of a reservoir
- a Reservoir Productivity Index which combines natural reservoir properties with well-field attributes, for the case that the working fluid has the viscosity of water or brine (RPI_w)
- a Reservoir Productivity Index which combines natural reservoir properties with well-field and operational attributes, if the working fluid has the viscosity of supercritical carbon dioxide or nitrogen (RPI_g).

A Monte Carlo simulation combines the reservoir parameters and their uncertainties to calculate a distribution, mean, and uncertainty for each reservoir's RFC, RPI_w and RPI_g .

The oil and gas industry, from which we collected the majority of our data, does not need to produce or inject fluids at an ongoing basis of geothermal magnitude (e.g., >300,000 gpd or 30 kg/s). Therefore the industry does not report maximum fluid flow rates from their wells. Nevertheless, some of the publicly available records include the initial production rate, which we treat as an approximation of a maximum potential fluid flow rate and, with these sparse data, we designed a validation test.

This project analysis of natural reservoirs included more parameters than previously reported in the existing National Geothermal Data System (NGDS) content model for Geologic Reservoir Analysis, developed by the Texas Bureau of Economic Geology. Instead of simply adding a field called RPI to the existing content model for Geologic Reservoirs, we updated the entire content model and added flexibility

for numerous types of analysis projects to provide relevant reservoir data. Researchers can now use the content model to report “*Reservoir Favorability*”² and describe the units and methods associated in their analysis – in our case RPI in kg/MPa-s. This is just one example of many such updates; the revised NGDS Geologic Reservoir Content Model is now available on USGIN (U.S. Geoscience Information Network, 2015) for others to use.

Key Assumptions, Reservoir Favorability:

- Horizontal homogenous porous media flow approximation for all reservoirs
- Hydrocarbon production thickness is a proxy for geothermal reservoir thickness
- Reservoirs in New York (which did not have porosity data associated with them) were assigned the same porosity value across similar geologic formations
- For each geologic formation, a single set of permeability data or porosity-permeability relationships were assumed to apply to all reservoirs within that formation

Primary Steps, Reservoir Favorability:

1. Compile all existing datasets from the oil and gas industry
2. Amalgamate the data across the three states, including reconciling differences in data collection styles/methods and inputting missing values where needed
3. Research porosity and permeability values for all reservoirs in NY; research porosity-permeability relationships, or average permeability values where relationships were unavailable, for reservoirs in PA/WV.
4. Create polygons in GIS for NY reservoirs using well locations.
5. Research geothermal reservoir metrics and develop a useful favorability index for this project’s reservoirs (RFC, RPIw, RPIg)
6. Develop an uncertainty index for reservoir data source and quality, and assign values to all reservoir’s parameters.
7. Determine best metric to illustrate reservoir uncertainty in map-view. Choice was Coefficient of Variation (standard deviation divided by mean)
8. Conduct a Monte Carlo Simulation to calculate the distribution, mean, and uncertainty of the RFC, RPIw, and RPIg for each reservoir.
9. Display results for the mean RFC, RPIg, RPIw, and uncertainty in a GIS.

Strengths of Reservoir Favorability Determination Process:

- The Reservoir Fluid Capacity (RFC) metric compares any and all reservoirs in a basin to each other using reservoir properties only.
- Compares reservoirs based on properties that are important to flow rate
- Temperature plays no role in determination of RFC and only enters into RPI through its influence on viscosity of the working fluid. Our strategy is to maintain independence of the reservoir and

2 The Content Model defines **ReservoirFavorability** as “Calculated expression of the reservoir's favorability for geothermal applications. Examples of suitable parameters include flow rate, productivity, etc. Chosen parameter description and units need to be provided in methodology field. Uncertainty and methodology are required if **ReservoirFavorability** is provided.” **ReservoirFavorabilityUncertainty** is defined as “An expression of the confidence in the **ReservoirFavorability** value. Best practice to include units and assumptions for calculating uncertainty within **ReservoirFavorabilityMethodology**.” **ReservoirFavorabilityMethodology** is defined as “The method for calculating **ReservoirFavorability** is stated here. Required if **ReservoirFavorability** is provided, to explain units and calculation of **ReservoirFavorability**. Also provide units and method for calculating **ReservoirFavorabilityUncertainty**.”

temperature maps, to be combined only at the end of the project when all risk factors are combined.

- The Uncertainty Index, constrained by typical variation in reservoir rocks (heterogeneity), acknowledges the differences in quality and source of data from state to state, formation to formation, and reservoir to reservoir.
- Coefficient of Variation compares the uncertainty of each reservoir to all other reservoirs, in a normalized manner.
- Monte Carlo Simulation provides a distribution of values for each reservoir quality metric, given the assigned Uncertainty Index of each reservoir parameter, thereby eliminating the ‘one-solution’ obstacle to a complex problem.

Limitations of Reservoir Favorability Determination Process:

- Many reservoirs overlap in map view, so maps were made at different depth intervals to better display results.
- The RPI equation applies to porous media formations only. A comparable equation for fractured reservoirs could not be derived. Nevertheless, the validation work of this project shows that the RPI equation performs well for both porous media and fractured reservoirs, when the RPI result is compared to natural gas production data from a small set of reservoirs. This validation is described below.
- Relative to NY and PA, it appears in the final maps that the typical reservoir in PA covers less area. This highlights the probability that some differences between states in the perceived coverage by reservoirs results from different practices by the PA and WV state agencies and our team for NY data for creation of polygons to express oil and gas field boundaries.

Mathematical components of Reservoir Favorability Determination:

The petroleum industry often uses a term called the well productivity index (PI) to quantify the productivity of a given oil or gas well producing from a reservoir that is dominated by matrix, or intergranular, flow. The PI is defined as the volumetric flow rate of a well divided by the pressure drop from the reservoir to the producing well, shown as follows:

$$PI = \frac{Q}{\Delta P} \left(\frac{m^3}{Pa-s} \right) = \frac{2\pi kH}{\mu \ln \frac{D}{r_w}} \quad \text{Equation 1}$$

where Q is flow rate (m³/s), ΔP is the pressure drop from the reservoir to the production well (Pa), k is permeability (m²), h is reservoir thickness (m), μ is the fluid viscosity (Pa-s), D is the distance between the injection and production well (m), and r_w is the wellbore radius (m) (Gringarten, 1978).

The PI has also been used to characterize the productivity of well doublet geothermal reservoirs, for both EGS reservoirs and sedimentary aquifer reservoirs (Gerard et al., 2006; Sanyal & Butler, 2009; Augustine, 2014; Cho et al., 2015; Hamm et al., 2016). The PI metric was adapted to this project by using it as an approximation of a reservoir’s productivity, rather than just a well pair. The metric is identical to Equation 1 but is called the Reservoir Productivity Index (RPI). Unlike a situation in an oil or gas field for which data specific to a given well would be used, in this study the parameters used are average reservoir values. Additionally, the final index value is expressed as a mass flow rate (kg/s) instead of a volumetric flow rate, so that RPI of an incompressible liquid working fluid can be compared fairly to the RPI of a compressible gas as the working fluid.

Equation 1 was applied to two different choices of possible working fluids: water RPI_w and supercritical carbon dioxide RPI_g . The differences between RPI_w and RPI_g are the respective inputs for viscosity and permeability.

The reservoir fluid capacity (RFC) was chosen as a favorability metric not only because it is comprised of only geologic parameters. This metric provides the opportunity to compare the quantitative favorability of each reservoir relative to the other reservoirs based on its natural reservoir qualities only. The RFC, shown as F below in units of mD-m, is a simple equation comprised of only permeability k in milliDarcies (mD), and thickness H in meters:

$$RFC = k * h \quad \text{Equation 2}$$

Equation 1 for RPI_w and RPI_g and Equation 2 for RFC are used as the model in a Monte Carlo Simulation to predict the uncertainty associated with each reservoir (see Natural Reservoir Memo).

At the conclusion of the analysis, the RPI model results were evaluated against volumetric gas production rate data for four reservoirs in New York. For each reservoir the RPI_w and RPI_g was compared to cumulative initial gas production flow rates from all wells in the reservoir based on gas production data in the New York ESOGIS database. The gas production data were converted to kilograms per second (kg/s) using the ideal gas law, the molecular weight of methane, and a conversion from days to seconds under the assumption that hydrocarbons flowed out of the reservoirs continuously over the course of the day. The final mass flow rates of methane were scaled for pressure drop that accounts for up to 1 MPa of parasitic pressure losses along the wellbore (see details in [Natural Reservoir Memo](#)). A Monte Carlo simulation was also run to predict the range of possible outcomes, using raw average permeability values and published natural gas viscosity values. Results from the gas volume productivity evaluation were compared to the stochastic RPI_w and RPI_g values for the same reservoirs (discussed below).

Potential Sources of Error in Reservoir Favorability Determination:

- RPI equation has many unrealistic assumptions: porous media, homogeneous rock, horizontal flow
- Average permeability values taken from literature not accurate
- Porosity-permeability relationships inaccurate

Software Used in Reservoir Favorability Determination:

- QGIS 2.6
- MatLab R2015a

Results of Sensitivity Analyses for Reservoir Favorability Determination:

Permeability is the primary variable affecting RPI; thickness is the second most important variable (Figure 1).

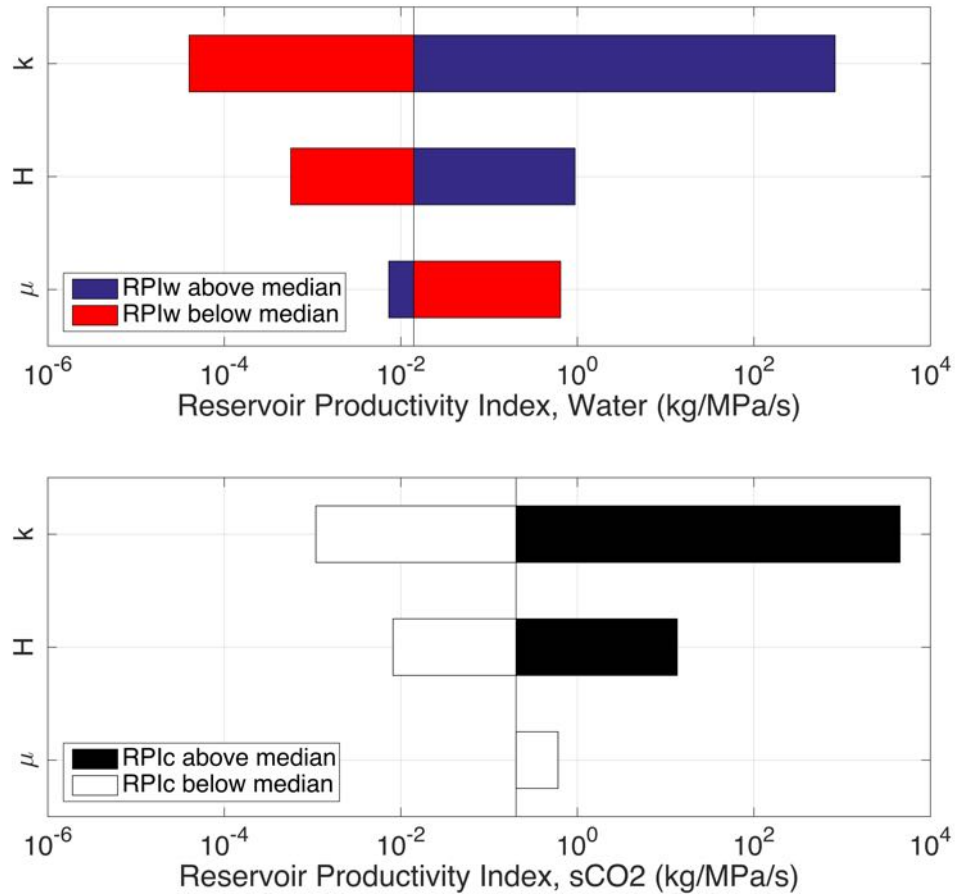


Figure 1: Sensitivity Analysis for Reservoir Productivity Index for water as the working fluid (RPI_w, above) and supercritical carbon dioxide (RPI_c, below). k refers to permeability; H refers to thickness of a reservoir; μ refers to fluid viscosity.

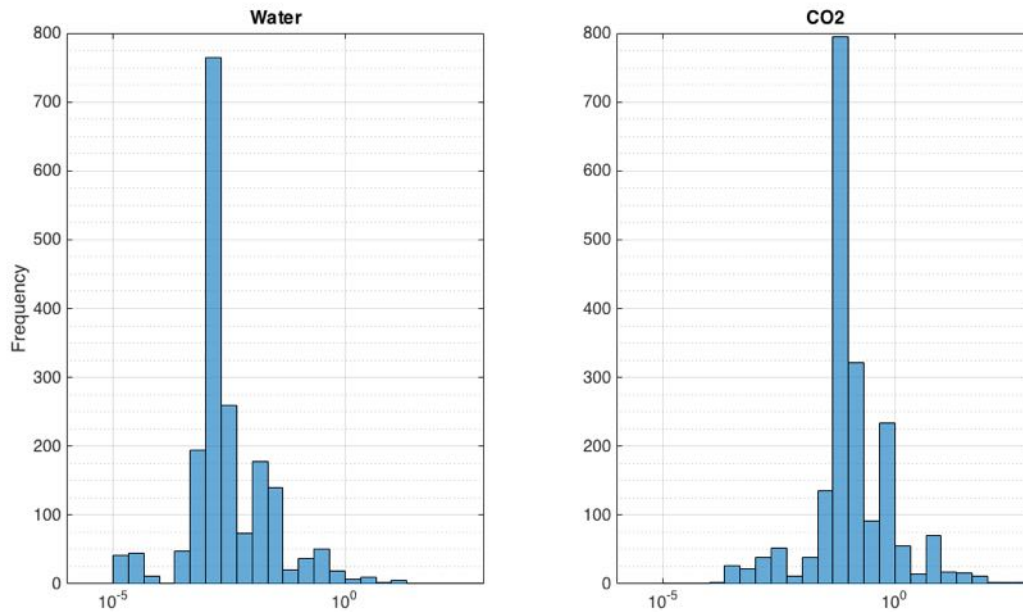


Figure 2: The distribution of reservoirs in the Appalachian Basin ranked by the Reservoir Productivity Index using water (left) or supercritical carbon dioxide (right) as the metric. Index values (horizontal axis, in kg/MPa-s) are the most like (P50) values of the 100,000 Monte Carlo realizations at each location.

Primary Conclusions of Reservoir Favorability Determination:

Most reservoirs in the Appalachian Basin have a low calculated RPI_w and RPI_g (Figure 2), likely due to low permeability in the geologic formations (see sensitivity analysis tornado plot above, Figure 1). Stimulation would likely be required to use low-permeability geologic formations.

There are several geologic formations that have good potential as geothermal reservoirs. These include: the Oriskany and Newburg Sandstones in WV; the Elk Group Formation, Devonian Unconformity Play, and Galway Sandstone in PA; the Trenton-Black River Dolomite and Onondaga Reef in NY.

When gas production data were compared to the stochastic RPI_g and RPI_w predictions, gas volume productivity matches closest with the stochastic RPI_g result, as expected (Figure 3). For the Quackenbush Hill (fractured dolostone in the Black River Formation), Wilson Hollow (fractured dolostone in the Black River Formation), and Bockhahn (porous sandstone in the Galway Formation) reservoirs, the gas volume productivity lies within one standard deviation of the predicted RPI_g . The gas production from Quinlan Reef reservoir (reef limestone in the Onondaga Formation), however, plots between the results for RPI_g and RPI_w . The gas production volumes lower than the RPI_g for the Quinlan Reef reservoir may be due to the fact that oil was also produced from the reservoir but initial production data for oil are unavailable. Alternatively, the original estimates of reservoir permeability or thickness for Quinlan Reef were overestimated.

Despite the fact that the RPI metric is derived from Darcy flow through porous media, the metric compares well against gas production data not only for porous reservoirs like the Bockhahn reservoir of the Galway Formation, but also for both naturally fractured reservoirs like the Quackenbush and Wilson Hollow reservoirs of the Black River Formation. However, the metric may not accurately predict the flow in a fossiliferous, vuggy porous media like the Onondaga Reef Limestone which is likely to be dominated by interparticle flow rather than typical intergranular flow (Jennings and Lucia, 2003); this may also explain the discrepancy between the RPI metric and gas production data in the Quinlan Reef reservoir.

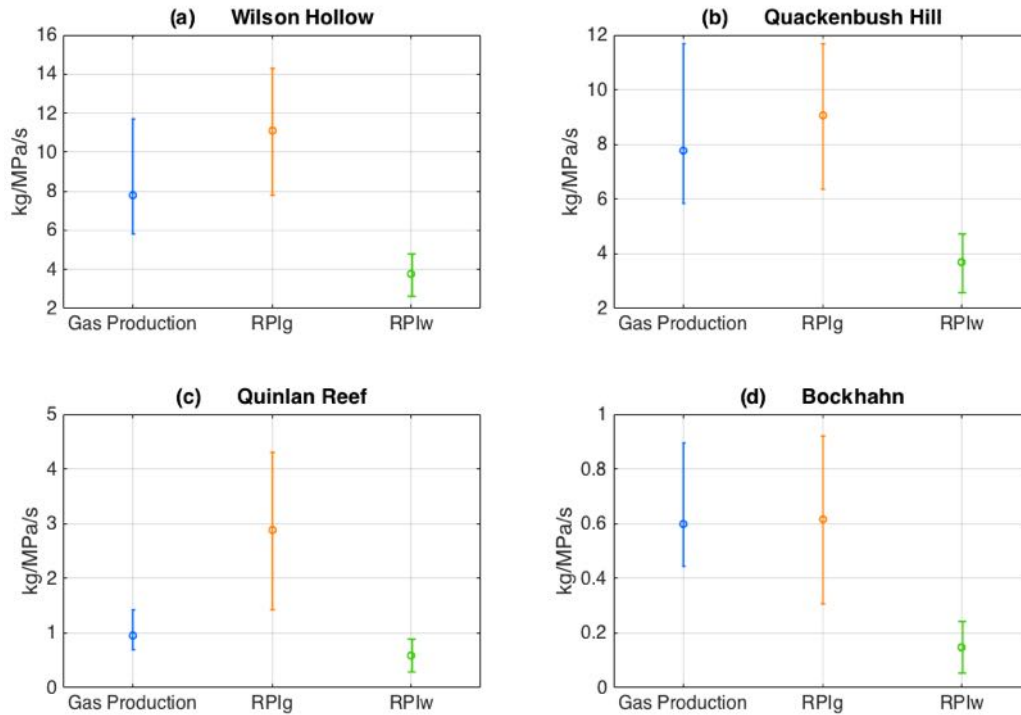


FIGURE 3. Results of RPI validation for the following reservoirs (a) Wilson Hollow and (b) Quackenbush Hill, which both currently produce gas from the Trenton–Black River hydrothermal dolomite; (c) Quinlan Reef, which produced gas from the Onondaga pinnacle reef limestone; and (d) Bockhahn, which currently produces gas from the Galway Sandstone Formation. In each panel, the gas production data are the blue open circle data point, which is the initial gas production (mcf/d) converted to kg/MPa/s using an average pressure drop of 3 MPa. Error bars represent drawdown of 2 MPa and 4 MPa. The orange and green open circle data points are the results for RPI_g and RPI_w respectively, with error bars representing one standard deviation from the Monte Carlo Simulation.

There are probably many potential reservoirs not displayed on the Reservoir maps (see main body of report) because they did not produce oil or gas, but instead are water-filled or dry porous formations. There is a need to map out and characterize dry reservoirs in a next phase, or perhaps to geologically extrapolate the possible existence of undrilled reservoirs.

Methodology Task 3, Seismic Analysis:

We considered recorded natural seismicity to be a primary indicator of the potential for inducing seismicity in any geothermal developments. To establish the locations and magnitudes of historical events, we combined all relevant data from two high quality seismic catalogs.

The first catalog, from the USGS National Earthquake Information Center (NEIC) provided hypocenter locations from 1965 to the present. A well-known weakness of this source of earthquake data stems from the relative scarcity of recording seismometers for the Appalachian Basin region of the country. This weakness appears as a relatively high “completeness magnitude” for this data source due to large distances (on average) from events to recorders – implying only larger earthquakes could be identified on enough stations to estimate locations and magnitude. Nevertheless, this catalog – due to its long time span – turned out to provide the majority of earthquakes actually used in our analysis. A major benefit of earthquake events included in this catalog stems from them having been analyzed by expert seismologists to classify the sources as actual earthquakes – as opposed to seismic energy generated from mine or quarry blasting. If an event from our region was categorized as an earthquake in the NEIC, we used it.

The second catalog, the Array Network Facility (ANF) Seismic Bulletin from the National Science Foundation’s EarthScope Transportable Array (TA) rolling deployment provided event locations in our region from approximately the beginning of 2011 through the end of May 2015. The array of broadband seismometers was deployed to temporary sites – with approximately 70 km spacing – and retrieved on a rolling schedule during this time period, so the regional event coverage varied with time. While we did find some events usable for our project from this source (red events in Figure 5 of the [Identifying Potentially Activatable Faults Memo](#)), the lower magnitude catalog completeness we had anticipated in the early stages of the project did not, in fact, play a large role. An unanticipated drawback of this source of earthquake data came from the fact that the ANF bulletin reports all events recorded by the TA, regardless of their source. As described in Astiz et al. (2014), this leads to the inclusion of blasting sources of energy in addition to the naturally occurring earthquakes in which we are interested. Indeed, this contamination led us to initially incorrectly identify seismic energy from the West Virginia coal mining regions and elsewhere as naturally occurring earthquakes. With the advice of Beatrice Magnani (SMU), we ameliorated this contamination problem by the rather crude means of simply eliminating TA events from 07:00 to 18:00 (local times) from our analysis – due to Federal mining regulations requiring blasting during daylight hours only. Clearly, this crude decontamination strategy might have eliminated some actual earthquakes. However, just due to raw probabilities from the daily timespans, the odds of keeping a true earthquake event from the TA are 13 in 24 – hence we might have lost a little under half of the true TA recorded earthquakes.

The resulting combined catalog retains all recorded earthquakes with epicenters in our region of interest -- regardless of depth, magnitude, or any other seismic attribute. For consistent quality control, no attempt was made to include either historical (pre-instrumental) seismicity or events from other catalogs such as the ISC. Events from the NEIC (green) and those not rejected by the decontamination procedure from the TA (red) are shown in Figure 7 of the [Identifying Potentially Activatable Faults Memo](#).

As described in great detail in the [Identifying Potentially Activatable Faults Memo](#), we used Poisson wavelet multiscale edge (“worm”) analysis of gravity and magnetic grids for a consistent mapping and identification of regional structures on which we anticipate seismicity could potentially occur. Briefly, worms are closely related to the traditional horizontal gradient analyses of potential fields, but a physical interpretation arising from the wavelet technique (e.g. Boschetti et al., 2001; Hornby et al., 2002) allows their classification at depth as candidate faults (see the [Identifying Potentially Activatable Faults Memo](#)

for more detail on the relevant mathematics). The Python based software to calculate worms is open sourced (Horowitz and Gaede, 2014).

We employed two different methods to estimate seismic risk for our region:

1. The first method focuses on proximity of potential fault zones, whether ancient or not, to known earthquake epicenters, and used both the gravity and magnetic worms as well as the located earthquakes. For this, the map distances between locations of earthquakes and the worms are the criteria with which to assign risk levels. The underlying principle is that geological structures in close proximity to earthquakes could unequivocally be classified as potentially active faults. This first method made no attempt at using orientations of the worms – only proximity. The result of this technique is plotted in Figure 7 in the [Identifying Potentially Activatable Faults Memo](#) where all worm points within 5 km of an earthquake location are classified as highest risk; from 5 to 10 km classified as moderately high risk; from 10 to 15 km classified as moderate risk; and from 15 to 20 km classified as moderately low risk. Those distance ranges were selected rather arbitrarily, but we judged them to provide a reasonable tradeoff between prudence and an overabundance of caution – not wanting to sterilize too large a region due to recorded earthquake activity. In the spirit of a play fairway analysis, we anticipate these risk categories to be used simply as a guide to more detailed analysis for any prospective regions. A clear drawback of this technique is that it can only identify active faults based on seismicity from approximately 50 years of instrumental records. This 50 year timespan is of insufficient length to be a representative sampling for earthquake cycles on the order of hundreds of years. However, the fact that these locations are unequivocally sites of active seismicity should play a significant role in determining prospectivity given that seismicity would impact the societal attitude toward acceptability of any candidate geothermal project site.
2. The second method performed in essence a “slip tendency” analysis for the orientations of worms in the regional stress field orientations. This method is an attempt to fill in some of the spatial and information gaps that diminish the utility of the first method. Regional stress field orientations were interpolated to each gravity and magnetic worm point using the technique described in Heidbach et al. (2010) – which modifies the directional statistics approach of Mardia (1972) to provide a weighted interpolation. Both the estimated orientation and an estimate of errors are available at every worm point via this method. Worm strike and error estimates were also calculated at every gravity and magnetic worm point according to Mardia’s (1972) techniques. From these two orientations and errors, we could then use the Byerlee’s (1978) law coefficient of friction (0.85) to derive the worm orientation in the regional stress field most favorably oriented for slip. Angular ranges in increments of 5 degrees around these favorable orientations were then used to classify worm points for seismic risk. Once again, this can only be a qualitative index of risk due to the fact that the actual magnitudes of the state of stress are unknown at our worm points – we only know the orientation with respect to σ_1 . See the [Identifying Potentially Activatable Faults Memo](#) for more details. We appreciate that this index is a “slip tendency” used in other GPFA projects to identify prospective areas, due to fault activity reworking fault gouge to create fresh porosity (and presumably permeability). However in our case, the very same mechanics represent a double-edged sword. Proximal to population centers, seismic risk due to this slip tendency might be considered by stakeholders to be unacceptable. Away from population centers, high slip tendency might indeed be a good attribute because of its relationship to permeability. Because we are operating under an assumption of direct use geothermal projects,

we anticipate any prospectivity in our region would be proximal to populations, and therefore on balance a work orientation that corresponds to a high tendency to slip presents more of a detriment to a candidate project than a benefit. Software to perform this analysis against World Stress Map and worm data stored in the GIS database PostGIS are available via a Git repository under <https://bitbucket.org/geothermalcode/>.

An additional attribute – possibly relevant to increasing the footprint of the reservoir analysis – can also be calculated from the same information used for slip tendency. If we define “dilation tendency” to be locations where worms are nearly normal to σ_3 (i.e. parallel to the σ_1 direction), we have an index for the potential locations of mode-I fracture openings. As used in several other GPFA projects, these may well be good locations to explore for fractured reservoirs. We leave further fleshing out and validation of this idea to future studies.

The two different methods described in the paragraphs above have quite different qualitative character. There is no consensus regarding to which of the two approaches offers more practical utility. Mathematically, the first “earthquake proximity” method represents a sufficient condition for seismic risk, while the second “slip tendency” method represents a necessary condition – at least under the assumptions inherent in applying a Byerlee’s law *model* to the real world. Neither method is simultaneously necessary and sufficient – which would be a logical prerequisite for a completely reliable seismic risk prediction. In the face of this dilemma, we combined the risk estimates from the two by averaging the risks– resulting in Figure 23 in the main report. In our judgment, this combined risk map is likely to be more reliable than either stand-alone method. This is because it emphasizes those worms proximal to earthquakes that also have high slip tendency. Those are sites near which it would be prudent to avoid perturbing the ambient effective stresses by injecting fluids. The additional improvement in the spatial footprint of seismic risk due to the slip tendency method in the combined map is also of benefit since it flags areas of concern where geothermal prospects would be wise to perform a detailed state-of-stress analysis from local data.

Methodology Task 4, Utilization Analysis:

The Utilization effort for the Geothermal Play Fairway Analysis of the Appalachian Basin (GPFA-AB) included two broad types of data: 1) residential – community ‘Places’ and 2) site specific users with high heating demands such as universities, industrial plants, government facilities, etc. to be considered as part of future studies. Below is a description of the data collected, the programs used, and the generalized results of the data processing for the residential – community Places. For the step-by-step descriptions of each parameter and the actual programs, see the Catalog of Supporting Files of this report for the [Utilization Analysis Memo](#).

Steps in Determining the Surface Levelized Cost of Heat

The foundation source code used for the utilization risk assessment is the program GEOPHIRES, (GEOthermal Energy for Production of Electricity and Heat Economically Simulated) (Beckers K. F. et al., 2013; Beckers et al, 2014; Beckers K. F., 2015). The software uses data about the subsurface characteristics and the surface characteristics as inputs to calculate Levelized Cost of Heat (LCOH). Because we have characterized the subsurface as part of other tasks (thermal resources and natural reservoir quality), we modified GEOPHIRES to focus strictly on the remaining elements: demand for heat as calculated from population and climate data, and surface costs associated with delivering that heat to those in demand. Thus, in our implementation, the final output is a Surface Levelized Cost of Heat (SLCOH). The SLCOH includes the surface piping, heat exchange equipment (residential and/or

commercial), operations, upfront capital cost, and maintenance costs over the lifetime of a 30 year project. A MATLAB³ program serves as an interface between the Microsoft Excel files of collected input data and the GEOPHIRES program. The GEOPHIRES program can also be used to include the below ground parameters, such as fluid temperature, flow rate, and drilling costs, but these were not included in this cost estimate because they were incorporated in the Natural Reservoir and Thermal Resources sections of the project.

1. The U.S. Census Bureau maintains a database of information that includes state, county, and county subdivision, under the broader term ‘Place.’ A Place is used to identify all individual cities, towns, villages, boroughs, universities, and other Census-Designated Places (CDP’s) defined as “settled concentrations of population that are identifiable by name but are not legally incorporated” (Census Bureau, 2012). The population and scope of a single Place may vary from the whole of New York City proper, with a population of over 8,000,000, to the smallest villages with populations as low as 10. In the New York, Pennsylvania, and West Virginia area we are using the 2010 Census data collection that includes 3,355 Places. These were downloaded via the census FactFinder website (<http://factfinder.census.gov>).
2. Starting from the 3,355 places in New York, Pennsylvania, and West Virginia using ESRI ArcGIS, the broader Place data were linked to their county and county subdivision. In order to complete this task, shapefiles of the Census Places and county subdivisions were loaded into ArcGIS. By using a spatial join and having the program find the Places within the county subdivision, this resulted in joining the attributes tables of the two files, allowing for the information for Places to have corresponding county subdivision data. Finally, all sites were checked and any places without a successful join had data manually added. This process was repeated to relate places with county information.
3. The place list was next limited to only those within this project’s Appalachian Basin outline. We used the Golden Software program Mapviewer and ArcGIS for a comparison to confirm accuracy of locations within the project boundary. This reduced the number of possible Places for the project to 1,697.
4. For this Play Fairway Analysis project, a minimum population threshold of 4,000 residents per Place was applied for all three states, to focus on those Places where a sufficient number of users more likely justifies the initial capital investment associated with a district heating system. There were 1,449 Places with populations of less than 4,000. Furthermore, to take into account the possibility that neighboring Places whose boundaries are located within 50 m distance of one another might develop jointly a district heating system, we merged such individual Places into composites, referred to informally as “Cooperating Places”. Together the Places and Cooperating Places totals 255; for these the SLCOH was analyzed. In order to have the Places with fewer than 4,000 people appear as red (unfavorable) on the final maps, each of them was assigned the same arbitrarily high SLCOH of \$100/MMBTU. The actual input data associated with these places

³ <http://www.mathworks.com/products/matlab/>

would lead to a different SLCOH and can still be calculated for future analyses as appropriate. The population threshold can be set as low as 1,500 residents per Place, and in doing so, makes the majority of the Places meet the criteria of good enough to consider. We determined the 4,000 resident level for population to be of value in focusing the attention to sites most likely to be first users of this regionally new energy concept.

5. The next parameter is the building density and heating demand per building (i.e. detached single-family, attached single-family, 2 unit buildings, 3-4 unit buildings, 5-9 unit buildings, 10-19 unit buildings, 20-49 unit buildings, and 50+ unit buildings). These detailed data are included within the Census Factfinder under “American Community Survey” using the 2010 5-year estimates and code B25024, representing the number and type of housing units per residential building category. The Energy Information Agency (EIA) performs a Residential Energy Consumption Survey (2009) that we used to determine average square footage of each designated unit and related heating load on a Census region basis.
6. Within many Places are commercial buildings, which can be put into 12 categories: 1) Accommodation, 2) Food, & Other Services, 3) Administrative and Waste Management and Remediation Services, 4) Arts, Entertainment, and Recreation, 5) Educational Services, 6) Health Care & Social Assistance, 7) Information Geographic Area Series, 7) Manufacturing, 8) Other Services, 9) Professional Scientific & Technical Services, 10) Real Estate & Rental and Leasing, 11) Retail Trade, and 12) Wholesale Trade.
 - a. In order to determine the heating loads for commercial sites within our Place dataset, we combined the energy consumption for building types, the square footage of a building, and the type of commercial application based on the 12 categories above. Three datasets were used: the EIA’s 2006 report of Commercial Buildings Energy Consumption Survey (CBECS) for the *floor space*, the US Factfinder 2007 ‘Economic Data’ for categories, and, the EIA manufacturing *energy consumption* database available at <http://www.eia.gov/consumption/manufacturing/>.
 - b. From these files, the number of establishments and number of employees were collected for each “economic place”. Unfortunately, the term “economic place” did not equate to that of the census definition of Place. The “economic place” can be related to the census classification of “county subdivision”, which we did have linked to each Place. Following the methodology of Reber (2013) and Tester et al. (2015), in the instance where a single “county subdivision” (i.e. “economic place”) contained multiple Places (typically around metropolitan areas) the data on commercial establishments for that county subdivision was divided amongst the Places within that county subdivision based on the relative population of each Place. In addition, due to the potentially identifiable nature of the reported economic data, some employment sizes were represented by a letter which stood for a range of values (ex. “A” meant an establishment had less than 20 employees, “B” meant an establishment may have between 20 to 99 employees, “C” means 100 to 249 employees, etc.). For these sites, the average of the range rounded up to

the next integer was used for the model (ex. “A” would have 10 employees, “B” would have 60 employees, “C” would have 175 employees, etc.). This allowed for the MATLAB/GEOPHIRES model to have a numerical value to perform the calculations.

7. Another dataset included was the location of roads (Road shapefiles from the Topologically Integrated Geographic Encoding and Referencing [TIGER] dataset). The total length of roads within each Place was used as a method to estimate the required piping length required to service a given location (Reber, 2013) and Tester et al. (2015). Based on Reber’s conclusions, the GEOPHIRES program uses 75% road coverage as a proxy for the length of pipes needed to provide adequate piping density to reach all buildings for geothermal district heating system.
8. The MATLAB script estimated the cost of a system for a lifetime of thirty years. The program uses a fixed annual charge rate (FACR), which allows the user to specify several factors, including discount rates. As reported by Shaalan (2001), this annual fixed-charge rate “represents the average or ‘levelized’ annual carrying charges including interest or return on the installed capital, depreciation or return of the capital, tax expense, and insurance expense associated with the installation of a particular generating unit.” A FACR of 6% was used for this Play Fairway Analysis effort. According to the U.S. Department of Commerce it calculated an effective discount rate of 3% in 2011 for Federal and Public energy projects. Therefore 1% was also added to this value, resulting in a discount rate of 4% applied to SLCOH.
9. The GEOPHIRES result output of SLCOH is a spreadsheet (.csv format). The output was grouped by state and then sorted based on the population size and the resulting SLCOH in the units of dollars per one million BTU (British Thermal Unit), \$/MMBTU. For all Places with a population of less than 4000 the SLCOH was assigned an arbitrary but high value of \$100/MMBTU. This allowed retention of smaller communities in the workflow in anticipation of assessments subsequent to the present study. Later improvements to these cost estimates for the entire Place list will be straightforward, since the GEOPHIRES and MATLAB programs allow updates for a few or many sites with the same amount of effort.

For the resulting 255 Places (and Cooperating Places) assessed, the best case (least expensive SLCOH) is 7 \$/MMBTU and the highest (most expensive SLCOH) is 59 \$/MMBTU. The Places were differentiated into three thresholds with the best case scenario for the SLCOH between \$5 and \$13.5, good between \$13.5 and \$16, and low or unlikely potential as \$16 to \$25 SLCOH. The distribution of the 255 Places is displayed in Table 1 of the main report, except for values of SLCOH over \$25 since it is considered not currently economically viable. In addition, there were 1,442 places assigned an arbitrary value for SLCOH of \$100 to separate out low populations.

A second set of values were assigned for the five-threshold combined layer risk assessment. Here the values were \$5 to \$12 (green - best), \$12 to \$13.5 (greenish yellow), \$13.5 to \$16 (yellow), \$16 to \$20 (orange) and \$20+ (red - worst). At the level of this Phase 1 project there is not enough site knowledge, even at the Place level, to assign increased levels of significance in the dollars amounts for the SLCOH. These were developed for the consistency of the combined risk task input files (see Catalog of Supporting Files for the [Combining Risk Factors Memo](#)).

For a comparison with current costs of energy, the FERC price of gas for New England states during the winter of 2014 was \$11.75/ MMBTU (DOE Federal Energy Regulatory Commission, 2013). This is only the price for the fuel, not all the additional infrastructure necessary for the heating/cooling of a building taken into consideration as it is within the SLCOH.

Error estimates for the Utilization risk factor were not calculated. Rather for the level of detail of Phase 1, the entire area is given a uniform uncertainty of 5% based on changes in population and cost. There are inherent uncertainties for Census tract data that are similar for all of the data, such as movement between tracts or building occupancy. The Census Bureau already includes within their Place data a correction, which takes into consideration the weights for nonresponse and the sampling error (U.S. Census Bureau, 2000). The state populations of NY and PA grew 1.9% and 0.7% respectively between 2010 and 2015 and WV decreased by -0.1% during the same time period (U.S. Census Bureau, 2015). The cost of surface infrastructure and equipment is based on the cost estimates used by Reber (2013), Reber et al. (2014) and Tester et al. (2015) that were best estimates at that time. Since 2013 the Social Security Administration has given a cost of living increase of 1.5% in 2014 and 1.7% in 2015 (Social Security Administration, 2015). Until we determine a site specific project and are able to include the below-ground information, the incompleteness of this economic analysis completely overshadows the impacts of these listed errors in the pricing. Utilization risk for the SLCOH can change, but at the Phase 1 level of this project the calculations for the overall high-density heat demand of an area will not significantly change.

In fact, the Utilization demand for the heat is potentially the best known risk factor of the GPFA Appalachian Basin project. During later projects a research team can work within one or more narrower areas of interest to differentially look at the sites under consideration. On a one-by-one basis an analysis of individual site uncertainty becomes necessary for prospective development locations. Items such as Government regulations (EPA), tax incentives (state, local), green awareness/desire of industry and/or community, areas of high economic growth, building codes, local competition of infrastructure materials, cost of electricity/fossil fuels, etc., must all to be considered during refined analysis stages for individual sites.

Methodology Changes and Improvements

An improvement on the Utilization programing included an updated shell interface for the MATLAB code to allow repeated iterations of the GEOPHIRES model with a single command. This MATLAB shell module is responsible for (1) reading all required inputs from an input *.csv spreadsheet; (2) performing preliminary calculations including estimating temperature and demand profiles, reinjection temperatures, required mass flow rates, surface infrastructure equipment sizes and costs, and pumping costs; (3) executing the GEOPHIRES software package with the appropriate inputs and rerunning it if need be to ensure accurate results; (4) storing pertinent variables, including the GEOPHIRES output LCOH, and writing them to an output spreadsheet; and (5) iterating the entire workflow for each town, community or other 'Place' of interest in the study group.

Results of the SLCOH Ranking

For the Surface Levelized Cost of Heat analysis, we started with 3,355 U.S. Census Places for the three states. Of these Places, 1,697 were located within the project area. Of those Places 1,449 had populations of less than 4,000, thus leaving 255 Places for the Utilization assessment. The lower the SLCOH of a project Place, the better will be overall project economics. The SLCOH is based on a 30 year system lifetime.

The top sites for each of the three states based on the Place analysis methodology described above are listed in Tables 2-4 of the main report. The results for West Virginia (Table 2, main report) include the smallest populations with lowest SLCOH. The low SLCOH combined with the fact that the region also has several wood drying sites appearing on the Prospect List of possible industrial users gives sites within West Virginia the best ranking for Utilization. Morgantown, with West Virginia University interested in converting its district heating system, has one of the higher rankings for the entire state (Table 2, Morgantown-Westover City, SCLOH of 11.2 \$/MMBTU). Another site of interest includes Kingwood (population 2,939 residents), site of Camp Dawson, ranked in the lower half of the WV results, yet it is still a good candidate because of the existing district heating system and interest of converting it to geothermal.

The top ten Places in New York have populations well above the 4000-person threshold (Table 3). The largest cities in the study region of New York are Buffalo in Erie County (261,000 pop) and Rochester in Monroe County (211,000 pop), and their dense housing led to an overall low SLCOH placing them among the top Places. The top counties for New York also include dairy processing sites as well as numerous colleges and universities such as Buffalo State College and University of Rochester (file within Geothermal Data Repository submission #623, GPFA-AB_Phase1ExamplesSitesByIndustryList.xlsx). Within the top locations for the state of Pennsylvania (Table 4 in the main report) are communities with a mixture of populations intermediate between those of New York and West Virginia. The counties with favorable SLCOH for Places also include many college campuses, e.g., Luzerne County Community College and King's College in Luzerne County; Seton Hill University in Washington County; Carnegie Mellon University and Slippery Rock University in Allegheny County (file within Geothermal Data Repository submission #623, GPFA-AB_Phase1ExamplesSitesByIndustryList.xlsx). Pennsylvania has two of the largest populations within the Appalachian Basin project with Pittsburgh in Allegheny County (305,000 pop) and Erie in Erie County (102,000 pop). The city of Pittsburgh has multiple green initiatives such as Sustainable Pittsburgh and District 2030. Although Pittsburgh itself did not rank among the top 10 communities with respect to SLCOH, three of its suburbs did: Dormont Borough, West View Borough, and Bellevue Borough.

Implications of SLCOH Results

All three states have numerous census Places with sufficient population to lead to initial estimates of surface infrastructure and operation costs that appear to be within reach of geothermal district heating resources. New York has some of the highest average prices for electricity in the country, particularly in the residential sector, as reported by the Energy Industry Association (EIA) (Table 1). New York has the highest residential and commercial rates of the three states and West Virginia has the lowest, and nationally is among the states with least expensive electricity. The comparative costs of electricity to the equivalent heating capacity from geothermal energy may change in the future as the states develop and execute policies to control carbon dioxide emissions that add to electricity prices. WV uses the coal mined in the state that is now going to be impacted by the new 2015 EPA Clean Power Plan (EPA, 2015). Whereas West Virginia has a stated goal to reduce their carbon dioxide emissions 29% by 2030 from their 2012 level (EPA – WV, 2015), the West Virginia coal industry is working actively against such federal and state plans (Coal Forum, 9.28.15). Pennsylvania plans to reduce their CO₂ by 23% and New York by 10% (EPA, 2015).

Table 1: Comparison of Retail Electricity Prices for New York, Pennsylvania, and West Virginia, and a comparison between these local costs and the National Average Rate, expressed as a percentage.

	2014 Average Retail Price of Electricity (cents per kilowatt-hour)				State Electricity Price as % of National Price		
	US	NY	PA	WV	NY	PA	WV
All Sectors	10.45	16.25	10.29	7.65	156	98	73
Residential	12.50	20.04	13.34	9.33	160	107	75
Commercial	10.75	16.11	9.72	7.99	150	90	74
Industrial	7.01	6.50	7.42	5.87	93	106	84
Transportation	10.27	13.70	7.70	9.11	133	75	89
Regional Cost Higher than National Average-More Favorable to Alternatives							
Regional Lower than National Average-Less Favorable to Alternatives Based on Cost							
Source: http://www.eia.gov/electricity/data/							
Note: West Virginia, while below the national average, sources nearly all of its electricity from coal.							

Limitations of LCOH Approach – A Case for ‘Manual Prospecting’

The purpose of the SLCOH analysis was to identify areas where efforts to inform residents, businesses, and governmental agencies would be most beneficial, due to the potential for utilization of geothermal district heating. However, relying on a single bulk data analysis to gauge demand for geothermal district heating within the study area would be inadequate. Indeed, an area may be completely missing from the ‘top five’ list and nevertheless be a viable candidate for a low temperature geothermal project. There are numerous situations where population distribution is not the only, or even the primary, predictor of demand for geothermal district heating. For instance, with less than 3,000 residents, the town of Kingwood in Prescott County, West Virginia is unlikely to justify a geothermal district heating system as a community – but just outside Kingwood is Camp Dawson, a state owned, federally funded Army Training Site. Camp Dawson is home to various West Virginia National Guard and Reserve units, as well as a Youth Challenge Program (WV-ANG, 2015). Spread over 4177 acres, Camp Dawson hosts active and reserve military training exercises, operates a conference center with auditorium and classroom facilities, provides a variety of lodging (hotel rooms and suites, multi person barracks, cottages, etc.) and dining options for large groups, and more. In addition to the recognition that Camp Dawson has economies of scale that may prove to make it economical to utilize a geothermal district heating system, their energy selection criteria are unique from many municipalities: they value any reduction in dependence on the local utility grid because of the national security benefit and they operate an environmental office charged in part with finding opportunities to preserve the environment. While not a federally owned facility, the federal funding certainly encourages implementation of Executive Order (EO) 13693, Planning for Federal Sustainability in the Next Decade (U.S. Executive Order, 2015). Further, a number of projects have previously studied the geology, hydrology, and ecology of Camp Dawson (Weston Solutions, 2014), which may expedite moving forward to the next stages of project preparation.

To address the likelihood of commercial businesses, industries, government agencies, and universities to be interested yet outside of the 255 Places assessed for their SLCOH, the team also identified over 165 prospective candidate locations, like Camp Dawson, which are included as one of the files uploaded to the Geothermal Data Repository (file within Geothermal Data Repository submission #623, GPFA-AB_Phase1ExamplesSitesByIndustryList.xlsx). The list of >165 include industrial applications for heat (wood drying, dairy processing), large commercial and/retail facilities, university campuses, resorts, etc. Additionally, federally owned or operated facilities and Native American Tribal lands were included in the compilation.

Steps for Inclusion of Site Specific Industrial Sites

Low temperature direct use geothermal energy has been used for numerous industries, including aquaculture, green houses, and food processing such as dehydration and dairy processing (Lienau et al., 1994). For the Appalachian Basin region and the anticipated temperatures at depths no more than 3 km below the surface, potential users of the geothermal heat occur in the following industry categories: paper mills, wood drying kilns, dairy processing (includes yogurt and milk pasteurization products), college and university campuses, and select military locations. Typical temperature ranges for these applications are listed in Table 2.

Table 2: Site-Specific industries of interest and required temperature ranges.

Industry	Temperature Range
Dairy	Butter/Yogurt production 80 – 90 °C Traditional pasteurization 72 – 75 °C
Wood Drying	43 – 82 °C
Paper/Pulp Mills	66 - 150 °C
University/College Campus	100 - 150 °C
Military Bases/Stations	100 - 150 °C

Each industrial site was located using a Google Map search for each category, except for the locations of the dairy processing sites found on the Dairy Plants USA website. All of these potential industrial users have a component of their process(es), which could benefit from incorporating a geothermal element into their system, either by preheating or reducing electrically heated steps. Similarly, sites of special use that include short-term housing for large numbers of people for which space heating of large buildings and residences would be suited potentially to a district heating system were considered, which led us to compile locations of military installations and colleges. The cumulative list for the three states of these industrial and special use sites has been submitted to the Geothermal Data Repository as the file “GPFA-AB_Phase1ExamplesSitesByIndustryList.xlsx” within data submission #623. The locations of the subset of these industrial and special use activities that occur within the Appalachian Basin regions of the three states, 165 compiled for this study, were then located relative to the combined favorability of the three risk factors of geological origin (thermal, reservoir, seismic risk) (see Figure 44 of Main report).

Permits

As part of the Phase 1 research, we looked into the Permitting process in order to understand the amount of time and expenses necessary for future studies of narrower regional location whose purpose would be preparation for a pilot study at a specific location. As a scenario for what would need to be permitted, we

assumed that a direct-use deep geothermal heat production system will involve drilling at least two boreholes. Geothermal energy extraction is not established in the study area, except for geothermal heat pumps, creating limited levels of legislative clarity concerning the deeper geothermal resource. For example, in Pennsylvania and West Virginia it has not been designated if geothermal energy is a mineral right or a surface right. In New York, it is not legislatively designated as a mineral, but it is at least listed as a type of drilling under the oil and gas permitting section. Future efforts are needed to engage in preparatory planning of the permitting process of deep geothermal wells with the appropriate agencies to educate them and then assist them in expanding their forms and the permitting process.

The permitting process includes Federal, State and Local laws to follow and / or permits to file. At the Federal level, all projects must comply with the National Environmental Policy Act (NEPA). If applicable, the Clean Air Act of 1970, Clean Water Act of 1987, Endangered Species Act and National Historic Preservation Act must also be followed.

Granting of permits to drill wells is a state function, except on federal land in which case it is a federal function carried out by the Bureau of Land Management. In New York, geothermal wells >500 feet are permitted in the same manner as oil and gas wells. There are no clear guidelines for geothermal wells in Pennsylvania and West Virginia. Whereas it is expected that permitting of deep (>1 km) geothermal wells in all three states will follow the permitting process for oil and gas wells, verification of any additional permitting needs to occur early in follow-on studies. The three state oil and gas permitting agencies include: the New York Department of Environmental Conservation Division of Mineral Resources, the Pennsylvania Department of Environmental Protection Office of Oil and Gas Management and the West Virginia Department of Environmental Quality Office of Oil and Gas.

State drilling permits involve many forms and documents including maps, spacing units, land permission, proposed drilling program, environmental assessment, nearby water users, nearby coal leases, reclamation plans, bond, fees and workers' compensation plans.

In addition to a drilling permit, permits for water removal and reinjection may also be required. States may regulate water removal, though much of the existing information concerns drinking water. The US EPA regulates re-injection of brine. Regulations such as building codes, local zoning and local roads must also be followed. Additional permits are required for stimulation procedures if needed to initiate production from wells.

During follow-on projects, early in the work it is recommended to begin meeting with the state permitting agencies to determine which of the permits referenced above will apply to one's project, determine the appropriate sequence of various forms that need to be submitted, the associated fees etc. This project team has already met with professionals in the U.S. Geological Survey, New York State Energy Research and Development Authority, and the geological surveys of each state. Yet many more contacts with agencies whose responsibility includes permitting will be needed during the permitting process.

Submission of drilling permits will occur at the stage that specific sites are targeted for pilot studies that include drilling. Permitting is a process that can take many months to years to accomplish. Groups interested in pursuing deep direct-use geothermal energy projects will need to begin this process as early as possible and with as much fore-knowledge as possible.

Methodology Task 5, Combination of Risk Analysis:

Once all of the risk factors were defined, they could be combined into a general measure of favorability, referred to as a play fairway metric (PFM). The method is fairly general in that risk factors are converted to the same scale using thresholds developed by each risk factor group, and then the scaled values are combined into an aggregate measure of favorability. We expanded the analysis to provide both three- and five-color maps; the five-color scheme was an attempt to include more resolution in the analysis. More discussion of the methods of combining the risk factors is given in the memo [Combining Risk Factors](#).

Steps in the Analysis

1. Scaled the risk factors (RFs) from the original values based on thresholds specified by each risk factor group, which resulted in scaled risk factors (SRFs) that are non-dimensional. The SRF had a lower bound of 0 and an upper bound of 3 or 5, depending on the number of thresholds. Points between thresholds were scaled linearly, so the SRF is continuous on the interval 0-3 or 0-5. Values outside of the acceptable range, for instance temperatures that are too low for direct-use heating, were assigned a value of 0. If a value was above the highest needed for use, for instance a high productivity reservoir, then it was given the highest value of 3 or 5, depending on the map. Reservoirs were scaled linearly in log-space because the thresholds were based on orders of magnitude.
2. Used several methods to calculate the aggregated play fairway metric (PFM). The methods of combining the risk factors included the following: average, geometric mean, and minimum. Combined risk maps based on these PFMs were produced for combinations of all four risk factors and for two special cases of three risk factors only. One of the three-risk factor cases illuminates the spatial variability of ‘geologic risk factors’ that include Thermal, Reservoir and Seismicity factors. The other three-risk factor case investigates a ‘no natural reservoirs’ set that includes Thermal, Seismicity and Utilization factors and illustrates the spatial variability of conditions that would be pertinent if considering the option of using EGS (enhance geothermal system) techniques to create a reservoir.
3. Employed uncertainty values estimated by the geologic risk factor groups, and a general estimate of uncertainty applied uniformly to the utilization risk factor. The range of the mean and the range of the uncertainty values for each risk factor were used to develop an interpolation table of the uncertainty in the SRF based on Monte Carlo simulation. The uncertainty in each SRF map was estimated based on interpolating within the tables that were specific to each risk factor. This method was used as an alternative to completing separate Monte Carlo simulations for each raster cell, which is computationally impractical for a region of this size at 1 km² resolution. The interpolation table method was reasonable for converting the uncertainty in the risk factor (RF) to the uncertainty in the scaled risk factor (SRF). The uncertainty in the PFM was then estimated using a first-order Taylor Series approximation of the PFM as a function of the individual SRFs. See equations below. More details are provided in the memo [Combining Risk Factors](#).
4. Illustrative project locations were selected for more in-depth analysis and graphical representation. The first step was to extract the values for a single cell associated with the project location. The values of cells were extracted and the distance to the nearest project location was calculated. The maximum average value of the four risk factors within 10 km of a project location was selected as the values for that project location. The analysis consisted of estimating the distribution of the PFM for each location based on

10,000 Monte Carlo replicates. This allows project locations to be compared, with their estimated uncertainty, which is informative for decision makers. The main report contains a parallel axis plot (Figure 27), which shows the SRFs for each of nine illustrative locations. This represents most of the information for a project location and can show tradeoffs from one location to another. Figure 28 in the main report shows the box plot of the same nine illustrative locations for the three geologic risk factors.

Summary of the Strengths and Limitations of the Process

Any attempt to combine different dimensions of a project, without a complete physical and economic analysis for a site, necessarily involves critical approximations. Strengths of the simple 4 risk factor analysis are that it provides several maps that could represent different ways a decision maker might consider combining the different factors. The values of each factor can also be represented spatially, which gives insight into where different factors are favorable. Thus potential users with a variety of perspectives on which risk factor is most important to themselves can readily identify potentially favorable locations. Once a few especially attractive locations are identified, the decision maker can use the files that accompany this report to obtain additional site-specific information including the uncertainty distribution of the four risk factors and of the combined metric, or they can commission additional studies to provide necessary data and further analysis.

This analysis is limited in several ways. First, the combined PFMs are only relative representations of favorability because there is no unified and comprehensive economic model. Second, the selection of thresholds between values that are here represented as favorable (green), intermediate (yellow) or poor (red) for the individual risk factor metrics as well as for the combined metric scores were in most cases not dictated by knowledge accrued through prior deep geothermal direct use projects, which is the goal of this play fairway analysis, but instead from reasoning based on other situations. If there were information on the economic costs of seismic insurance, for instance, then this could be incorporated into a single model, but this is not feasible in a preliminary screening analysis. Third, we have implied equal weighting to the four risk factors, but some risk factors might have disproportionate impact on the economics of a project.

Because experience-based values of thresholds are lacking, the thresholds likely signify differing degrees of risk from one risk factor to another. For instance, a value of 2 in thermal may not imply the same level of favorability as a value of 2 for seismic. The thresholds used in scaling are relative rankings and are reasonable measures of general favorability, but they will cause the resultant combined PFMs to only represent relative favorability.

The uncertainty of the many parameter values combined in the analysis is often not verifiable and, in those cases, uncertainty was assigned based on professional judgment of the people who developed the risk factor. Therefore, our estimates of the uncertainty of the combined metric is also uncertain and represents the assessment of the developers as to the relative precision of different factors. A goal for future research should be to improve the characterization of uncertainty.

Mathematics Used, Including Formulas and Calculation Methods

All of the calculations are for values of the scaled risk factors (SRFs) where 0 is the least favorable.

The methods of calculating the aggregated play fairway metric (PFM) were: Average, Geometric Mean, and Minimum. The equations are given below, where SRF is the scaled risk factor (scaled [0,3] or [0,5] depending on the resolution of the thresholds) and n is the number of risk factors. Generally, n=4 for the maps but in a few cases n = 3 when one risk factor is omitted.

$$PFM_{average} = \frac{1}{n} \sum_{i=1}^n SRF_i \quad \text{Equation 3}$$

$$PFM_{geometric_mean} = \sqrt[n]{\prod_{i=1}^n SRF_i} \quad \text{Equation 4}$$

$$PFM_{minimum} = \min\{SRF_1, SRF_2, \dots, SRF_n\} \quad \text{Equation 5}$$

The uncertainty for the combined maps can be approximated using a first-order Taylor series expansion along with the variance assigned to each risk factor RF_i , assuming that each risk factor is independent of all other risk factors considered. This method is only applicable for the average and geometric mean functions because these are “smooth” functions. The Taylor series approximation is not a good representation of the minimum of several values unless 1 factor is always the minimum value. Other closed-form solutions for the variance of the minimum of four values from different distributions are not readily available. Because the distribution of each SRF is different, no general analytic results are provided for the uncertainty of the minimum. In order to obtain uncertainty in the minimum maps, we opted to run a Monte Carlo analysis with 10,000 replicates only for 5-color combined risk maps. These are provided in the main report. These maps are computationally expensive to produce relative to the uncertainty maps for the geometric mean and the average.

The equation used in the Taylor series approximation is given below, where m is the mean value of the SRF and the variance of each SRF_i is approximated by interpolating a table derived from Monte Carlo analysis, as described above.

$$\text{Var}(PFM) = \sum_{i=1}^n \left[\frac{\partial PFM(m)}{\partial SRF_i} \right]^2 \text{Var}(SRF_i) \quad \text{Equation 6}$$

Note that the distributions of the PFM at the individual project locations were derived from Monte Carlo simulation for that specific site, rather than using the Taylor series approximation in Equation 6. The same Monte Carlo analysis methodology was used for these sites as was used for making a map of the uncertainty in the minimum of the risk factors.

Potential Sources of Error

There are several sources of error. First, the calculations of a PFM will not exactly represent the favorability of the location. Second, the calculated values are only as good as the input, so errors from the input risk factors will probably propagate through the SRF calculated and into the PFM calculations.

Software Used, Including Version and Hardware Requirements

- R: A Language and Environment for Statistical Computing, version 2.15.1 (2012-06-22, “Roasted Marshmallows”)
Packages: sp, raster, rgdal, rasterVis, maps, maptools, xlsx, rgeos, RcolorBrewer, pracma, rootSolve, Hmisc, maps, prettymapr
- ArcGIS, version 10.2.2 and 10.3.1

Robustness of Different PFMs

The memo [Combining Risk Factors](#) gives some results for the robustness of the different PFMs. We would like the results to provide generally the same ranking for each site, regardless of which PFM function was selected. The three PFM functions (average, geometric mean, minimum) were calculated and extracted for each of the census “Places” and “Cooperating Places” that had a population greater than 4,000, indicating a reasonable utilization target. Generally, the relative rankings for the functions are similar (see Figure 53 of memo 17, Combining Risk Factors). In particular, the average-to-geometric mean and geometric mean-to-minimum relationships reveal similar relative rankings at nearly all locations. This comparison reveals that the relative rankings of individual places could be the same even if the choices of color thresholds that express the favorability on the differing maps lead to map patterns that look different depending on the function.

METHODOLOGY REFERENCES

- AAPG. (1985). Northern Appalachian Region correlation chart. D.G. Patchen, K.L. Avary, and R.B. Erwin, regional coordinators.
- AAPG. (1985). Southern Appalachian Region correlation chart. D.G. Patchen, K.L. Avary, and R.B. Erwin, regional coordinators.
- Aguirre, G. A. (2014). *Geothermal Resource Assessment: A Case Study of Spatial Variability and Uncertainty Analysis for the State of New York and Pennsylvania*. Master's Thesis, Cornell University. Retrieved from <http://hdl.handle.net/1813/38982>
- Aguirre, G. A., Stedinger, J. R., & Tester, J. W. (2013). Geothermal Resource Assessment: A Case Study of Spatial Variability and Uncertainty Analysis for the State of New York and Pennsylvania. *Proceedings, Thirty-Eighth Workshop on Geothermal Reservoir Engineering*. Stanford: Stanford University. Retrieved from <http://www.geothermal-energy.org/pdf/IGAstandard/SGW/2013/Aguirre.pdf>
- Augustine, C. (2014). Analysis of Sedimentary Geothermal Systems Using an Analytical Reservoir Model. *Geothermal Resources Council Transactions*. Portland: Geothermal Resources Council.
- Beckers, K. F. (2015). *GEOPHIRES Software Tool*. Retrieved from GEOthermal Energy for the Production of Heat and Electricity Economically Simulated: <http://koenraadbeckers.net/geophires/index.php>

- Beckers, K. F., Lukawski, M. Z., Anderson, B. J., Moore, M. C., & Tester, J. W. (2014). Levelized costs of electricity and direct-use heat from Enhanced Geothermal Systems. *Journal of Renewable and Sustainable Energy, Vol. 6, No. 1*, 013141.
- Beckers, K. F., Lukawski, M. Z., Reber, T. J., Anderson, B. J., Moore, M. C., & Tester, J. W. (2013). Introducing GEOPHIRES V1.0: Software Package For Estimating Levelized Cost of Electricity and/or Heat from Enhanced Geothermal Systems. *Proceedings, Thirty-Eighth Workshop on Geothermal Reservoir Engineering*. Stanford: Stanford University. Retrieved from <http://www.geothermal-energy.org/pdf/IGAstandard/SGW/2013/Beckers.pdf>
- Bedre, M., & Anderson, B. (2012). Sensitivity analysis of low-temperature geothermal reservoirs: effect of reservoir parameters on the direct use of geothermal energy. *Geothermal Resources Council Transactions* (pp. 1255-1262). Geothermal Resources Council.
- Blackwell, D. (n.d.).
- Blackwell, D. D., & Richards, M. (Eds.). (2004). 2004 Geothermal Map of North America, Scale 1:6,500,000. American Association of Petroleum Geologists.
- Blackwell, D. D., & Richards, M. (2004). Geothermal Map of North America; Explanation of Resources and Applications. *Geothermal Resources Council Transactions, 28* (pp. 317-320). Geothermal Resources Council.
- Blackwell, D. D., Richards, M., Batir, J., Frone, Z., & Park, J. (2010). New Geothermal Resource Map of the Northeastern US and Technique for Mapping Temperature-at-depth. *Geothermal Resources Council Transactions, Vol. 34* (pp. 313-318). Geothermal Resources Council.
- Blackwell, D. D., Richards, M., Frone, Z., Batir, J., Ruzo, A., Dingwall, R., & Williams, M. (2011). Temperature-At-Depth Maps for the Conterminous U.S. and Geothermal Resource Estimates. *Geothermal Resources Council Transactions, Vol. 35* (pp. 1545-1550). Geothermal Resources Council.
- Blackwell, D., Richards, M., Frone, Z., Batir, J., Ruzo, A., Dingwall, R., & Williams, M. (2011). Temperature-At-Depth Maps for the Conterminous U.S. and Geothermal Resource Estimates. *Geothermal Resources Council Transactions, Vol. 35* (pp. 1545-1550). Geothermal Resources Council.
- Boschetti, F., Hornby, P., & Horowitz, F. (2001). Wavelet Based Inversion of Gravity Data. *Exploration Geophysics, 32*(1), 48-55. doi:10.1071/EG01048
- Brown, D.W. (2000). A hot dry rock geothermal energy concept utilizing supercritical CO₂ instead of water. *Proceedings, Proceedings of the twenty-fifth workshop on geothermal reservoir engineering*, Stanford University, 233-238.
- Buescher, E. (. (2015). Green District Heating - Actual Developments of Deep Geothermal Energy in Germany. *Proceedings World Geothermal Conference 2015*. Melbourne, Australia: International Geothermal Association. Retrieved from <http://www.geothermal-energy.org/pdf/IGAstandard/WGC/2015/35000.pdf>
- Byerlee, J. (1978). Friction of Rocks. *Pure and Applied Geophysics, 116*((4-5)), 615-626. doi:10.1007/bf00876528

- Camp Dawson West Virginia Army National Guard. (2015). *About Camp Dawson*. Retrieved from Camp Dawson West Virginia Army National Guard: <http://www.wv.ngb.army.mil/CampDawson/Form1.aspx?MP=MTc1&P=MTc1#Dawson>
- Carter, L., Kelley, S., Blackwell, D., & Naeser, N. (1998). Heat flow and thermal history of the Anadarko basin, Oklahoma. *American Association of Petroleum Geologists Bulletin*, 82, pp. 291-316.
- Cho, J., Augustine, C., & Zerpa, L. (2015). Validation of a Numerical Reservoir Model of Sedimentary Geothermal Systems Using Analytical Models. *Stanford Geothermal Workshop Proceedings*. Stanford University.
- DOE Federal Energy Regulatory Commission. (2013, October 17). *Winter 2013-14 Energy Market Assessment Report to the Commission, Item No. A-5*. Retrieved from <http://www.ferc.gov/CalendarFiles/20131017101835-2013-14-WinterReport.pdf>
- Engelder, T., Lash, G., & Uzcátegui, R. (2009). Joint sets that enhance production from Middle and Upper Devonian gas shales of the Appalachian Basin. *AAPG Bulletin*, 93(7), 857-889.
- Förster, A., & Memam, D. F. (1995). A Bottom-Hole Temperature Analysis in the American Midcontinent (Kansas): Implications to the Applicability of BHTs in Geothermal Studies. (pp. 777-782). Potsdam: International Geothermal Association.
- Frone, Z. (2015). *Heat Flow, Thermal Modeling and Whole Rock Geochemistry of Newberry Volcano, Oregon and Heat Flow Modeling of the Appalachian Basin, West Virginia*. Southern Methodist University. ProQuest Dissertations Publishing.
- Frone, Z., & Blackwell, D. (2010). Geothermal Map of the Northeastern United States and the West Virginia Thermal Anomaly. *Geothermal Resources Council Transactions*, V. 34 (pp. 339-343). Geothermal Resources Council.
- Gallardo, J., & Blackwell, D. (1999). Thermal structure of the Anadarko Basin, Oklahoma. *American Association of Petroleum Geologists Bulletin*, 83, pp. 331-361.
- Gerard, A., Genter, A., Kohl, T., Lutz, P., Rose, P., & Rummel, F. (2006). The Deep EGS (Enhanced Geothermal System) Project at Soultz-sous-Forets (Alsace, France). *Geothermics*, Volume 35, 473-483.
- GoldCorp Inc. (2001, March 12). US\$575,000 Goldcorp Challenge Awards world's first 6 million ounce internet gold rush yields high grade results! Toronto. Retrieved from <http://www.infomine.com/index/pr/Pa065434.PDF>
- Gringarten, A. (1978). Reservoir lifetime and heat recovery factor in geothermal aquifers used for urban heating. *Pure and Applied Geophysics*, 117 (1-2), 297-308.
- Hamm, V., Bouzit, M., and Lopez, S. (2016) Assessment of complex well architecture performance for geothermal exploitation of the Paris basin: A modeling and economic analysis: *Geothermics*, v. 64, p. 300-313.
- Harrison III, W., Grammer, G., & Barnes, D. (2009). Reservoir characteristics of the Bass Islands dolomite in Otsego County, Michigan: Results for a saline reservoir CO₂ sequestration demonstration. *Environmental Geosciences*, Vol. 16, No. 3, 139-151.

- Harrison, W., Luza, K., Prater, M., & Chueng, P. (1983). Geothermal Resource Assessment of Oklahoma. *Special Publication 83-1, Oklahoma Geological Survey.*
- He, X. (2015). *Feasibility and Supply Analysis of U.S. Geothermal District Heating and Cooling Systems.* West Virginia University, Benjamin M. Statler College of Engineering and Mineral Resources. Morgantown: Proquest LLC, UMI Dissertation Publishing. Retrieved from <http://search.proquest.com/docview/1682034532>. Abstract Available at <http://gradworks.umi.com/37/01/3701975.html>
- Hildenbrand, T. G., Briesacher, A., Flanagan, G., Hinze, W. J., Hittelman, A. M., Keller, G. R., . . . Webring, M. (2002). *Rationale and Operational Plan to Upgrade the U.S. Gravity Database.* Retrieved from Gravity Database of the US: <http://research.utep.edu/default.aspx?tabid=37229>
- Hornby, P., Boschetti, F., & Horowitz, F. (1999, April). Analysis of potential field data in the wavelet domain. *Geophysical Journal International*, 137(1), 175-196. doi:10.1046/j.1365-246x.1999.00788.x
- Hornby, P., Horowitz, F., & Boschetti, F. (2002). A Physical Interpretation of the Poisson Wavelet Transform of Potential Fields. *Proceedings, EGS XXV!! General Assembly.* Munich: European Geophysical Society. Retrieved from <http://www.cosis.net/abstracts/EGS02/05568/EGS02-A-05568.pdf>
- Jaeger, J. C. (1965). Application of the theory of heat conduction to geothermal measurements. In W. H. Lee (Ed.), *Terrestrial Heat Flow.* Washington, D.C.: American Geophysical Union. doi:10.1029/GM008p0007
- Lachenbruch, A. (1968). Preliminary geothermal model of the Sierra Nevada. *Journal of Geophysical Research*, 73(2), 6977-6989.
- Lewis, J., McDowell, R., Avary, K., & Carter, K. (2009). Characterization of the Helderberg Group as a geologic seal for CO2 sequestration. *Environmental Geosciences, Vol. 16, No. 4*, 201-210.
- Lienau, P., Lund, J., Rafferty, K., & Culver, G. (1994). *Reference Book on Geothermal Direct Use* (Vol. August). Klamath Falls, Oregon: GGeo-Heat Center, Oregon Institute of Technology. Retrieved from <http://www.oit.edu/docs/default-source/geoheat-center-documents/publications/direct-use/tp82.pdf?sfvrsn=2>
- Lindal, B. (1973). Industrial and other applications of geothermal energy (except power production and district heating). *Geothermal Energy; Review of Research and Development.*
- Lugert, C., Smith, L., Nyahay, R., Bauer, S., & Ehgartner, B. (2006). *Systematic Technical Innovations Initiative Brine Disposal in the Northeast.* Albany, NY: New York State Energy Research and Development Authority.
- Malinconico, L., & Moore, M. (2013). *Provisional Bouguer Gravity Map of Pennsylvania.* Retrieved from AASG Geothermal Data Repository: <http://repository.stategeothermaldata.org/repository/resource/a748ce233a25e3e0dd00c9865d0af3e5/>
- Mardia, K. (1972). *Statistics of Directional Data.* Academic Press. Retrieved from <http://www.worldcat.org/isbn/9780124711501>

- Midwest Regional Carbon Sequestration Partnership. (2009). *Phase II Report*. Midwest Regional Carbon Sequestration Partnership. Retrieved from http://www.mrcsp.org/userdata/phase_II_reports/phase_ii_final_report_MRCSP.pdf
- Nelson, P. H. (2009). Pore-throat sizes in sandstones, tight sandstones, and shales. *AAPG Bulletin*, v. 93, no. 3, 329-340.
- Obama, B.H. (2015). *Executive Order 13693 - Planning for Federal Sustainability in the Next Generation*. Washington, D.C.: U.S. Government Publishing Office. Retrieved 2015, from <http://www.gpo.gov/fdsys/pkg/FR-2015-03-25/pdf/2015-07016.pdf>
- Pebesma, E. J., & Wesseling, C. G. (1998). Gstat, a program for geostatistical modelling, prediction and simulation. *Computers & Geosciences*, 24 (1), 17-31.
- Pruess, K. (2007). Enhanced Geothermal Systems (EGS) comparing water with CO₂ as heat transmission fluids Proceedings, Lawrence Berkeley National Laboratory: Berkeley, California, 13 p.
- Ravat, D., Finn, C., Hill, P., Kucks, R., Phillips, J., Blakely, R., . . . Elawadi, E. (2009). *A Preliminary, Full Spectrum, Magnetic Anomaly Grid of the United States with Improved Long Wavelengths for Studying Continental Dynamics: A Website for Distribution of Data*. United States Geological Survey. Retrieved from <http://pubs.usgs.gov/of/2009/1258>
- Reber, T. J. (2013). *Evaluating Opportunities For Enhanced Geothermal System-Based District Heating In New York And Pennsylvania*. Cornell University. Ithaca, NY: Cornell University. Retrieved from <http://hdl.handle.net/1813/34090> (restricted until 2018)
- Reber, T. J., Beckers, K. F., & Tester, J. W. (2014). The transformative potential of geothermal heating in the U.S. Energy market: a regional study of New York and Pennsylvania. *Energy Policy*, Vol. 70, 30-44.
- Roen, J., & Walker, B. (1996). The atlas of major Appalachian gas plays. *Publication V-25*.
- Roy, R. F., Blackwell, D. D., & Birch, F. (1968). Heat generation of plutonic rocks and continental heat flow provinces. *Earth and Planetary Science Letters*, 5, 1 – 12.
- Roy, R. F., Blackwell, D. D., & Decker, E. R. (1972). Continental heat flow. In E. E.C. Robertson (Ed.), *The Nature of the Solid Earth* (pp. 506-44). New York: McGraw Hill.
- Sanyal, S., & Butler, S. (2009). Geothermal Power From Wells in Non-Convective Sedimentary Formations - An Engineering Economic Analysis. *Geothermal Resources Council Transactions*, Vol. 33 (pp. 865-870). Geothermal Resources Council.
- Shalan, H. E. (2001). Generation of Electric Power. In *Handbook of Electric Power Calculations* (pp. 8.1-8.38). Retrieved from http://castlelab.princeton.edu/EnergyResources/GenerElectPower__Shalaan.pdf
- Shope, E. N. (2012). *A Detailed Approach To Low-Grade Geothermal Resources In The Appalachian Basin Of New York And Pennsylvania: Heterogeneities Within The Geologic Model And Their Effect On Geothermal Resource Assessment*. Master's Thesis, Cornell University. Retrieved from <http://hdl.handle.net/1813/31206>

- Shope, E. N., Reber, T., Stutz, G., Aguirre, G., Jordan, T., & Tester, J. (2012). Geothermal Resources Assessment: A Detailed Approach to Low-Grade Resources in the States of New York and Pennsylvania. *PROCEEDINGS, Thirty-Seventh Workshop on Geothermal Reservoir Engineering*. 37. Stanford: Stanford University. Retrieved from <https://pangea.stanford.edu/ERE/pdf/IGAstandard/SGW/2012/Shope.pdf>
- Smith, L., Nyahay, R., & Slater, B. (2010). *Integrated Reservoir Characterization of the Subsurface Cambrian and Lower Ordovician Potsdam, Galway and Theresa Formations in New York*. New York State Energy Research and Development Authority (NYSERDA).
- Social Security Administration. (2015). *Cost-Of-Living Adjustment, Prior Cost-of-Living Adjustments*. Retrieved from Official Social Security Website: <http://www.ssa.gov/news/cola/facts>
- Spicer, H. C. (1964). A compilation of deep earth temperature data, U. S. A. 1910-1945. *Open-File Report 64-167, U.S Geological. Survey*.
- Stutz, G. R. (2012). *Development, Analysis, and Application of a Well by Well Method for Estimating Surface Heat Flow for Regional Geothermal Resource Assessment*. Cornell Thesis, Cornell University. Retrieved from <http://hdl.handle.net/1813/31037>
- Stutz, G. R., Shope, E., Aguirre, G. A., Batir, J., Richards, M. C., Blackwell, D. D., Tester, J. W., Stedinger, J. R. & Jordan, T. E. (2015). Geothermal energy characterization in the Appalachian Basin of New York and Pennsylvania: *Geosphere*, v. 11, no. 5, p. 1291-1304, doi: 10.1130/GES00499.1
- Stutz, G., Williams, M., Frone, Z., Reber, T., Blackwell, D., Jordan, T., & Tester, J. (2012). A Well by Well Method for Estimating Surface Heat Flow for Regional Geothermal Resource Assessment. *Stanford Geothermal Workshop Proceedings*. Stanford University.
- Tester, J., Joyce, W., Brown, L., Bland, B., Clark, A., Jordan, T., . . . Anderson, B. (2010). Co-generation Opportunities for Lower Grade Geothermal Resources in the Northeast - A Case Study of the Cornell Site in Ithaca, NY. *GRC Transactions*. 34, pp. 475-483. Geothermal Resources Council. Retrieved from <http://pubs.geothermal-library.org/lib/grc/1028690.pdf>
- Tester, J., Reber, T., Beckers, K., Lukawski, M., Camp, E., Aguirre, G. A., . . . Horowitz, F. (2015). Integrating Geothermal Energy Use into Re-building American Infrastructure. *Proceedings World Geothermal Congress*. Melbourne, Australia: International Geothermal Association. Retrieved from <http://www.geothermal-energy.org/pdf/IGAstandard/WGC/2015/38000.pdf?>
- The Coal Forum. (2015, 10 01). *WV Leads SSEB in Rejecting 'Clean Power Plan'*. Retrieved from [wvcoalforum.org](http://www.wvcoalforum.org): <http://www.wvcoalforum.org/201510015019/recent-press/wv-leads-sseb-in-rejecting-clean-power-plan.html>
- U.S. Census Bureau. (2000, Created 2003, Last Revised 2004, Accessed 2015). *U.S. Census Bureau*. Retrieved from Survey of Program Dynamics, Sampling Errors: <http://www.census.gov/spd/sampling.html>
- U.S. Census Bureau. (2015). *U.S. Census Bureau*. Retrieved from State Quick Facts: <http://quickfacts.census.gov/qfd/states/>

- U.S. Energy Information Administration . (2015, October 1). *Frequently Asked Questions, Estimated U.S. residential electricity consumption by end use, 2014*. Retrieved from U.S. Energy Information Administration: <http://www.eia.gov/tools/faqs/faq.cfm?id=96&t=3>
- U.S. Environmental Protection Agency (EPA). (2015, 8 3). *U.S. Environmental Protection Agency (EPA)*. Retrieved from Clean Power Plan: State at a Glance, West Virginia: <http://www3.epa.gov/airquality/cpptoolbox/west-virginia.pdf>
- U.S. Environmental Protection Agency (EPA). (2015, 10 01). *U.S. Environmental Protection Agency (EPA)*. Retrieved from Clean Power Plan for Existing Power Plants: <http://www2.epa.gov/cleanpowerplan/clean-power-plan-existing-power-plants>
- U.S. Geoscience Information Network. (2015, August 27). *USGIN Content Model Schemas Geologic Reservoir 1.0*. Retrieved from <http://schemas.usgin.org/models/#geologicreservoir>
- Walcott, C. (1896). *Cambrian Rock of Pennsylvania*. United States Geological Survey (USGS). Retrieved from <http://pubs.usgs.gov/bul/0134/report.pdf>
- West Virginia Geological & Economic Survey. (2006). *Trenton Black River Project Appalachian Basin*. Retrieved from Trenton-Black River Project Website: <http://www.wvgs.wvnet.edu/www/tbr/>
- Weston Solutions, Inc. (2014, June). *Engineering Evaluation/Cost Analysis Known Distance Range Munitions Response Site Berm Area*. Contract No. : W912DR-09-D-006, Delivery Order No.: 0008, West Chester, PA. Retrieved 9 2015, from West Virginia Army National Guard: http://www.wv.ngb.army.mil/CampDawson/Documents/kd_range_final.pdf
- Whealton, C. (2015). *Statistical Correction of Temperature Data for New York and Pennsylvania Wells*. M.S. Thesis, Cornell University, Ithaca. Retrieved from <http://hdl.handle.net/1813/40609>
- Whealton, C. A. (2016). Statistical Data Analysis, Global Sensitivity Analysis, and Uncertainty Propagation Applied to Evaluating Geothermal Energy in the Appalachian Basin, in Ithaca, NY, USA, Cornell University, Ph.D. dissertation, p. 250
- Zoback, M. D., Barton, C. A., Brudy, M., Castillo, D. A., Finkbeiner, T., Grollmund, B. R., . . . Wiprut, D. J. (2003). Determination of stress orientation and magnitude in deep wells. *International Journal of Rock Mechanics and Mining Sciences*, Vol. 40 No. 7, 1049-1076.

Application of Generalized Least Squares Regression in Bottom-Hole Temperature Corrections

Calvin A. Whealton, Jerry R. Stedinger, Franklin G. Horowitz

September 30, 2015

Abstract

Bottom-hole temperature (BHT) corrections are a subject of great interest to those interested in using non-equilibrium temperature data from well log headers. This article develops BHT corrections for New York, Pennsylvania, and West Virginia, using generalized least squares regression (GLS). It is shown that GLS regression can give more reasonable estimates of the BHT correction than traditional least squares when spatial clustering is present. Additionally, a nonlinear function for BHT corrections is proposed that explicitly avoids negative corrections at shallow depth and avoids the instabilities of extrapolated high-order polynomials.

1 Introduction

Bottom-hole temperature (BHT) corrections have been of continued interest for several decades because researchers want to use BHT datasets, which are often large and freely available; however, BHTs are notoriously problematic because they generally represent a temperature field that was disturbed by the drilling process (Deming, 1989). As a result, BHT corrections, both from theoretical models of the heat transfer in the well and from empirical comparison of data, have been developed.

This paper derives empirical BHT corrections for portions of New York, Pennsylvania, and West Virginia. The method of deriving the temperature correction dataset required spatial clustering of points, which meant that the alternatives to ordinary least squares fitting could be explored. Additionally, in part of the region there was available information on borehole fluid so separate models should be fit based on the expected drilling technology. Lastly,

we provide a functional form that avoids problems with the correction being negative at shallow depths or unstable in deeper data.

2 Literature Review

Empirical temperature corrections have generally been polynomials of depth. For instance, Kehle (1973) presents a quartic function of depth and the correction presented by Harrison et al. (1983) is often taken as a quadratic. Other examples include Förster et al. (1997) who report a linear function and Scott (1982) who presents linear to cubic polynomials.

Polynomials are typically well-behaved over the range of the data, but extrapolation of quadratic and higher-order models beyond the dataset can cause the BHT correction to become unstable: shallow trends can reverse. Another problem with polynomials is that the fitted equation is often negative at shallow depth, which is generally considered unreasonable because drilling should not substantially increase the temperature.

Several BHT corrections have been used in the area of interest (NY, PA, and WV). Hendry et al. (1982) did not correct BHTs in their study of West Virginia, Hodge et al. (1981) presented results for western NY with and without a BHT correction. Aguirre (2014) used the Harrison correction in her study of PA and western NY based on the work of Frone and Blackwell (2010), who evaluated the correction based on it generally moving the data closer to the Spicer (1964) wells. Frone and Blackwell (2010) recommended capping Harrison correction and using the peak value for deeper BHTs and Shope (2012) noticed that Harrison correction seemed less accurate than uncorrected BHTs for wells shallower than 1,000 m in NY and PA. No studies have tried to systematically look at the region to determine where the corrections are more or less accurate.

3 Regions, Data, and Clusters

The analysis uses data from New York, Pennsylvania, and West Virginia, mainly areas within the Appalachian Basin. Figure 1 shows the area and features discussed in this section. The region was partitioned into three areas based on data divisions and geologic features or the data sources. The first region was is the Rome Trough in PA, a rift (Shope, 2012), which curves from the south-west corner of PA towards northern PA (Repetski et al., 2008). The second region is the Allegheny Plateau, which is north of the Rome Trough and extends into western NY. West Virginia is considered as a

separate region because the data came from a separate source with different characteristics.

The data used for the Rome Trough and Allegheny Plateau are based on data collected for Whealton (2015). This dataset includes much of the information listed on well log headers including bottom-hole temperature (BHT), depth, and fluid recorded as in the borehole (Whealton, 2015). Data from West Virginia are from the National Geothermal Data System (NGDS) (Saucer, 2011).

All of the datasets contained raw BHTs, so the equilibrium temperature had to be estimated from “reliable” temperature logs. The Spicer (1964) temperature profiles are considered equilibrated because they are from wells drilled with older technology that does not disturb the temperature field as much (Frone and Blackwell, 2010). These were supplemented with temperature logs identified as close to equilibrium, mainly wells explicitly noted as air-drilled with at least several hundred meters of temperature log (Whealton, 2015). The Spicer wells were the only source of equilibrium profiles in West Virginia and were the majority of equilibrium profiles for the Allegheny Plateau. The equilibrium temperature profile was estimated for each “reliable” log by a linear gradient, which was estimated after removing temperature inversions and shallow portions of the log that did not appear to follow the same trends as the deeper well log.

The estimated equilibrium wells were used to define spatial clusters. In West Virginia, the clusters were defined by taking a 0.05° buffer around each of the Spicer wells, therefore a single BHT could be in multiple clusters. The West Virginia clusters are also almost exclusively defined in the Rome Trough portion of the state (see Figure 1). In the Rome Trough and Allegheny Plateau clusters are defined based on averaging two or more reliable temperature profiles and then taking BHTs close to the averaged wells, but without crossing the boundary of the regions. In this scheme a BHT can only belong to a single cluster.

The regression datasets are defined by taking all BHTs and correcting them to the estimated equilibrium temperature-at-depth for that cluster. This assumes that over small areal extents the equilibrium temperature at depth does not change significantly. The depth used in the Allegheny Plateau and Rome Trough was the minimum of the depth of the driller, depth of the logger, and bottom logged interval as reported on the well log header because the depth of the BHT measurement is generally not recorded. A few points were assigned a different depth because the BHT seemed consistent with much deeper data from that cluster and the unusual values could be attributed to incorrectly entered data for one of the depths. In West Virginia, the depth of the measurement was used, when possible, otherwise the true

vertical depth was used.

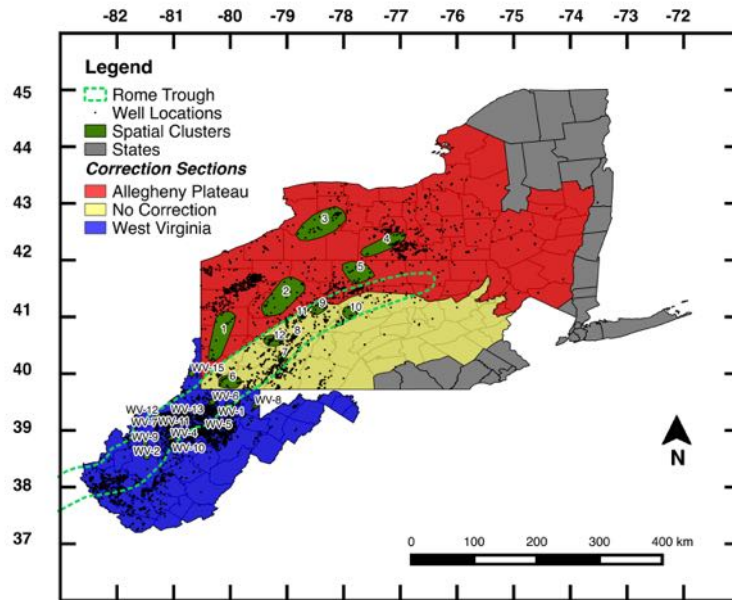


Figure 1: Map of NY, PA, and WV with the Rome Trough (Repetski et al., 2008) and spatial clusters used in analysis. Data sources: Bureau (2014), Saucer (2011); software: QGIS Development Team (2009)

4 Definition of Drilling Types

The data collected by Whealton (2015) included information on the fluid recorded in the borehole, which we used as a proxy for the well's drilling technology. The main categorization is into air-wells versus mud-wells. The classification scheme defined air-wells as those where the fluid listed on the well log header was air, gas, foam, soap, dusted, dry, or some combination of those. Mud-wells are classified as containing mud, gel, polymer, water (fresh, salt, brine), formation fluid, produced fluid, or some combination of those fluids. The categorization is defined to try and separate fluids that have mostly air in the borehole from those where water or other high heat capacity fluid is present. Additionally, some wells could not be categorized because no fluid was recorded or the fluid listed was empty or none.

The West Virginia dataset does not contain information on the type of fluid present in the borehole (Saucer, 2011).

5 Regression Statistical Models

Least squares regression assumes that the error (residual, difference in true and predicted BHT correction) are independent and identically distributed with zero mean. If the dataset contained paired data where each BHT is matched to an equilibrium temperature from the same well at the same depth, such as a drill-stem test, then this assumption might be valid. This assumption is also likely valid when all points are corrected to a region-wide estimate of the temperature-at-depth.

Because of spatial clustering, it is likely that all observations from a given cluster will be too high or too low relative to the region-wide average. Hence, observations in a cluster are “biased” on average. One possible reason for the differences is that drilling practices vary enough in the clusters so that there are systematic differences. Another potential cause is that the estimated equilibrium temperature for the clusters was imperfect, so errors in the estimation and extrapolation of equilibrium temperature could cause systematic tendencies for a cluster. Many of the well logs used to estimate equilibrium temperature were offset from each other but showed roughly the same gradient.

With clustering, the error between an observation and the region-wide model has two components: a cluster-specific “bias” and a random noise term. The cluster-specific “bias” represents how the points in a cluster are systematically different from the region-wide model. Several statistical models could be used to address the cluster-specific “biases” including using least-squares coefficient estimates with cluster-robust standard errors, least squares estimation of a model with cluster-specific constants and use of an average constant, and feasible generalized least squares. More details on these approaches can be found in an Econometrics text, such as Greene (2012, Ch. 11) or Kmenta (1986, Ch. 12), under methods used for panel data. The method used here is generalized least squares (GLS) which should increase efficiency for small datasets.

In GLS the goal is not to minimize the simple sum of squares errors, as in least squares regression, but to weight observations in a way that accounts for shared “bias” and their inherent noise. More details are provided in Appendix A. If the cluster “biases” are fairly small compared to the noise in the data, then the result will look very similar to a least squares fit and the fitting procedure will tend to treat the points as fairly independent; however, when the “biases” are large compared to the noise, each cluster is nearly treated as a separate point because additional points in a single cluster are highly discounted when fitting the model.

6 Regression Results

The regression results are reported for each of the three separate regions defined above. The fitted models for each region are summarized in Table 1. All depths are in meters and all BHT corrections are in °C.

6.1 West Virginia

West Virginia dataset included 187 points and did not have information on drilling fluid, so the comparison is between fitting a linear model (first-order function of depth) with least squares versus generalized least squares. Figure 2 shows the data and fitted lines and Table 1 shows the fitted coefficients. The models differ by minor amounts over the range of the data. Because the GLS model should be more efficient, it is recommended as the base model (Equation 1) but the temperature correction should be capped at 15°C (2,606 m). Although the regression dataset does not contain data to this depth, some alternative datasets that contained deeper observations did indicate corrections of about 15 °C. Generally, data used in studies is deeper than the depth at which the temperature correction becomes positive (305 m), so practically it is positive over the range of interest.

$$\Delta T_{West VA} = -1.99 + 0.00652z, \quad 305\text{m} < z < 2606\text{m} \quad (1)$$

6.2 Rome Trough of PA

The Pennsylvania Rome Trough dataset had 181 points. Regressions are plotted in Figure 3. The results do not conform to the expected model of BHT corrections, which is positive and increasing with depth. This behavior was regardless of the fitting procedure or whether the data was split based on fluid. Because of the lack of a credible model for this region the conservative approach is to apply no temperature correction. This recognizes that our knowledge of this region is not sufficient to justify any correction.

$$\Delta T_{Rome Tr.} = 0, \quad z > 0\text{m} \quad (2)$$

6.3 Allegheny Plateau

The Allegheny Plateau dataset of 121 points has some of the largest signal in all of the data analyzed, as can be seen in Figure 4. When a linear depth model was fit to the data the correction was negative until about 1,100 m.

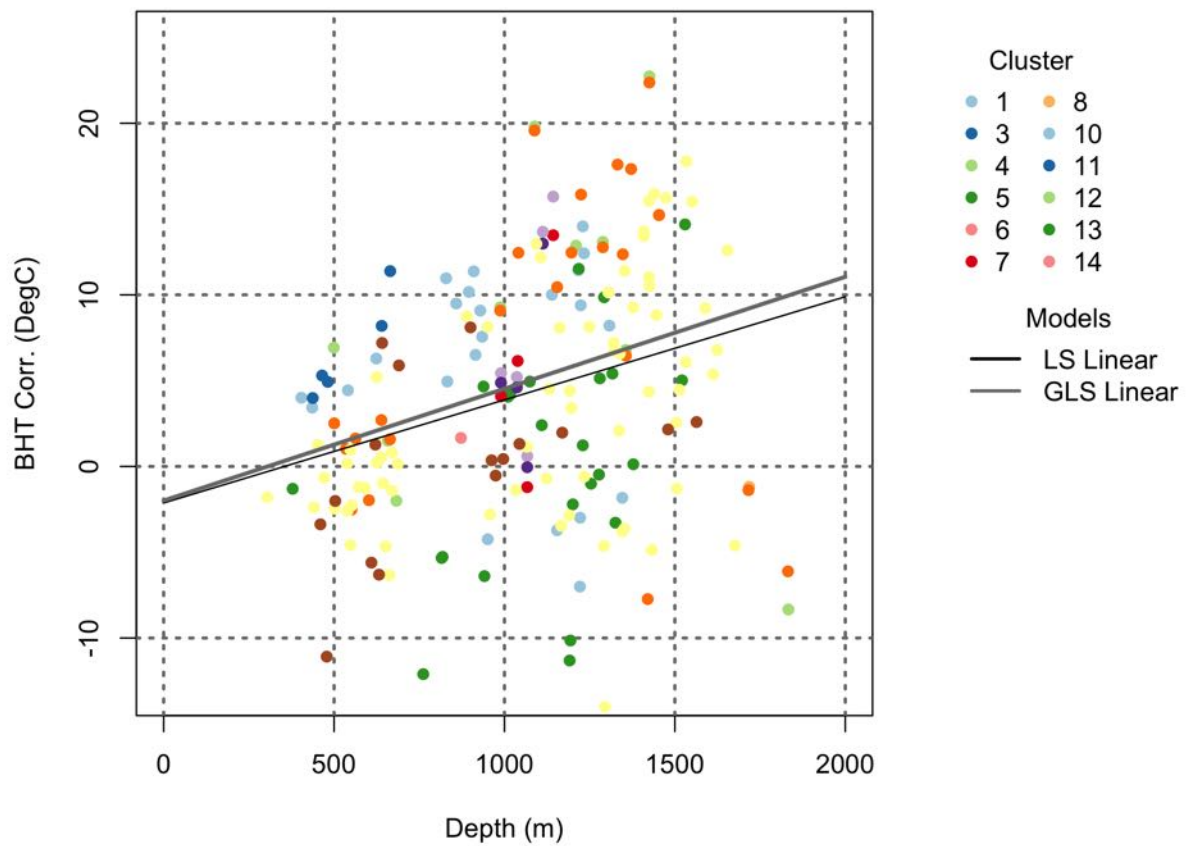


Figure 2: Plot of West Virginia data with ordinary least squares (OLS) and generalized least squares (GLS) fits for a linear model. Points are color-coded based on the cluster definition, which is based on spatial buffering of the Spicer wells. The Spicer well number is used as the identification of the cluster.

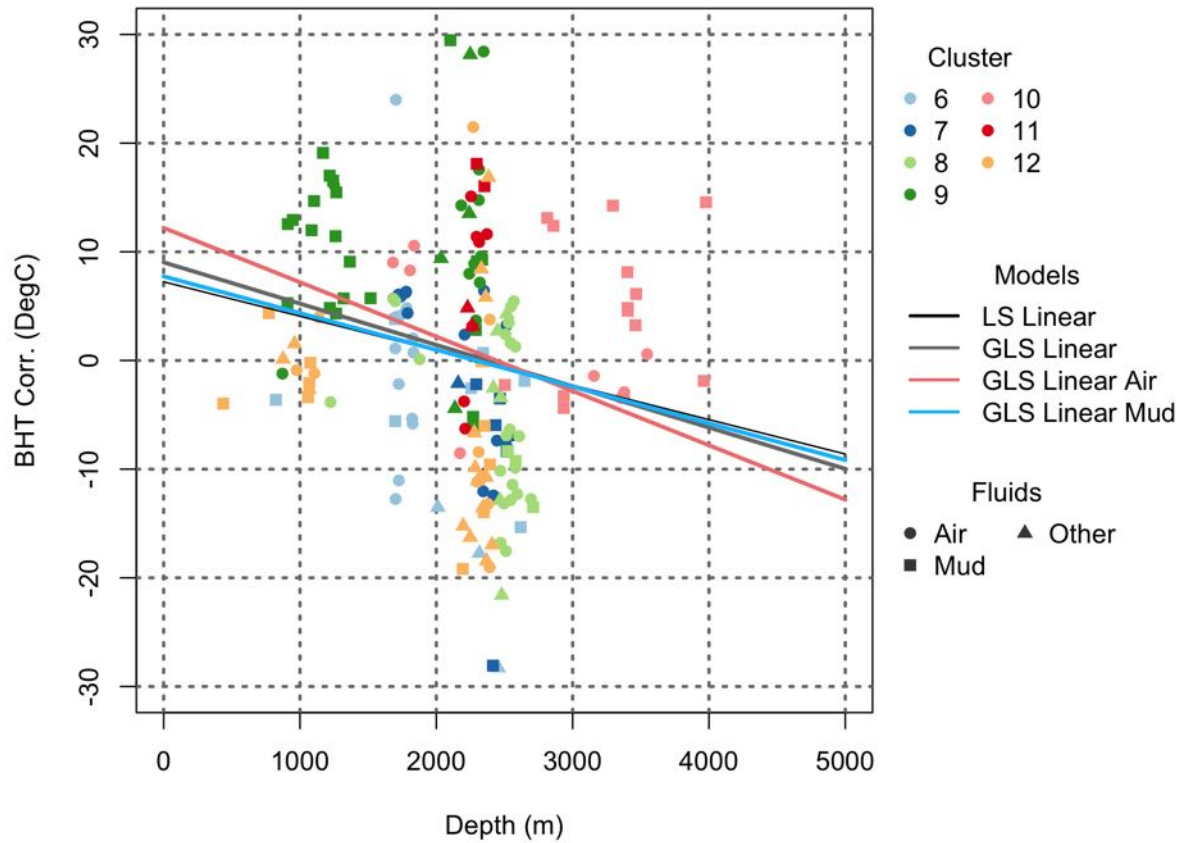


Figure 3: Plot of Rome Trough data with ordinary least squares (OLS) and generalized least squares (GLS) fits for a linear model and GLS fits for the air and mud wells. Points are color-coded based on the cluster definition in Figure 1.

There is little reason to believe in negative BHT corrections and it was more an artifact of the model, so a model of the form shown in Equation 3 was fit since it is always positive (if the initial coefficient is positive) and it behaves linearly for large depths. The curved transition zone is controlled by the exponent in the model. An exponent of 3 was used because it sufficiently matched the curvature of the data and it was conservative on the very shallow temperature corrections.

There are alternative models that could have been fit to the data. For example, the exponent parameter could be set to a different value. This was experimented with a little when fitting the mud model and the impact

was minor. The weighted sum of squares changes from 64.1 to 66.5 when changing the exponent from 2 to 5, and the predicted correction at 4000 m changes from 38.9 to 36.8 °C. Another possibility is to include an additive constant so that the correction will not cross at the origin. When this was included it was about 5 °C and this would likely cause arbitrary signals to appear in shallow counties, so it was not included. Lastly, a limiting case of the model is for the exponential parameter being infinite, which will be a model that is zero until it reaches a threshold depth and increases linearly after that. This form has a kink in the middle which causes problems with local minima when fitting the parameters and seems less physically plausible.

The nonlinear model showed that it was sensitive to the locations of points for the air-model. Inclusion or exclusion of points, especially in the curved portion of the function, could cause the fitted model to change from that shown in Figure 4 to one where the correction is nearly linear starting at a few hundred meters. We chose the dataset that had more points to help define the transition region because this was a larger sample and the results were more consistent with the physical intuition of the relationship between air and mud BHT corrections.

The models for different drilling fluids showed that there was no statistically significant difference (test statistic of 0.49 on χ^2 with two degrees of freedom, p-value of 0.78 \gg 0.05). One explanation for the lack of difference is that the air-model is not well controlled in the upper linear portion of the curve; the standard error of the slope parameter is over twice as large for the air model as it is for the mud-model. The air model is only supported for depth shallower than approximately 2,500 m whereas the mud model has data much deeper. Note: the highest air data (around 2700 m, 38 °C) was removed from fitting in all air-models because it was a rogue observation.

The recommended models for this area is the the air- or mud-model (Equations 3 and 4), as applicable when the drilling fluid is known, or a weighted sum of the air- and mud-models when the fluid is unknown. The air and mud corrections should be capped at 15.4 and 37.8 °C, respectively. For unknown wells, the weighting should represent the probability that the well is air or mud.

$$\Delta T_{Alle. Pt. Air} = 0.0104((1090^3 + z^3)^{1/3} - 1090), \quad z < 2500\text{m} \quad (3)$$

$$\Delta T_{Alle. Pt. Mud} = 0.0155((1660^3 + z^3)^{1/3} - 1660), \quad z < 4000\text{m} \quad (4)$$

Although the coefficients seem very similar, the standard errors using GLS are quite different. For instance, in the Allegheny Plateau fit using least

squares the standard error of the slope and shift parameter are 0.00412 and 340, respectively. The GLS estimates of the standard errors for the two parameters are 0.00324 and 1710. Generally, the least squares estimated of the coefficient standard errors are much smaller because the estimates are based on the data being independent and it does not discount observations from the same cluster.

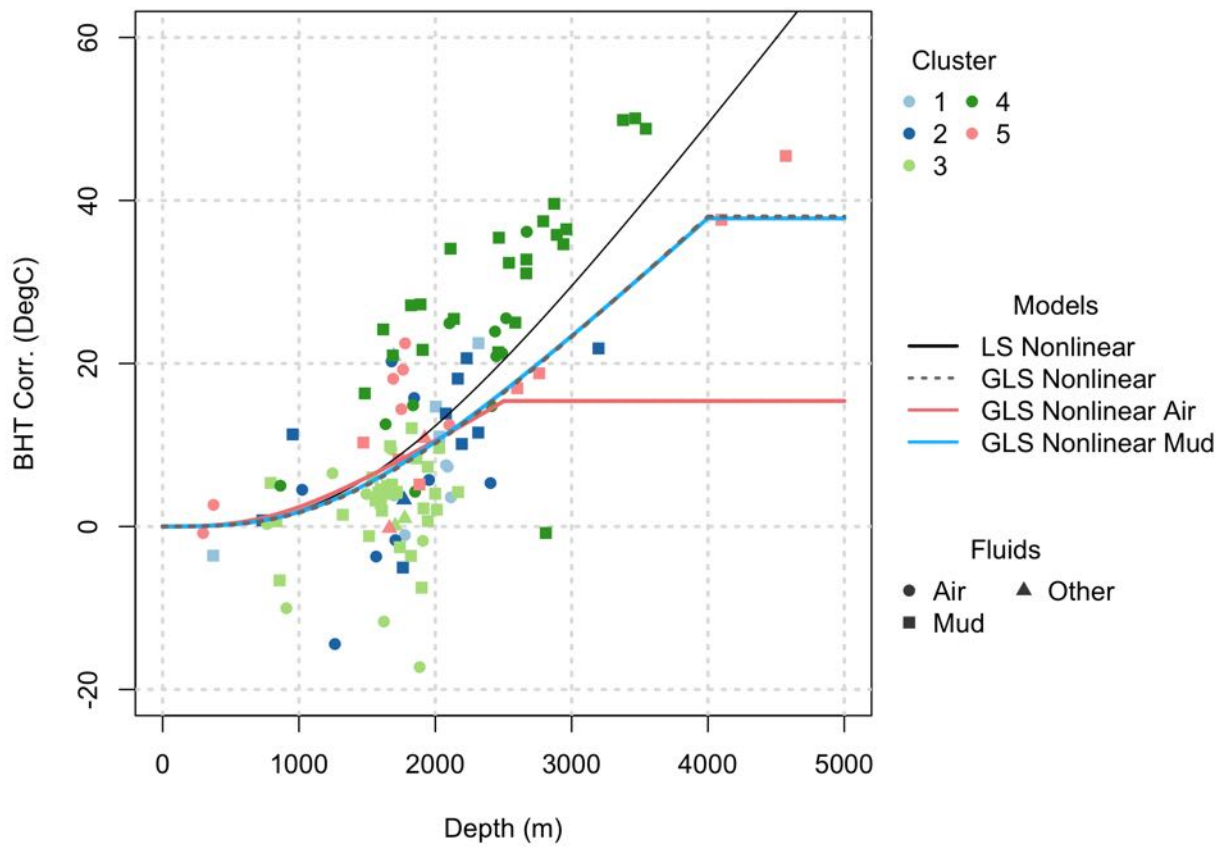


Figure 4: Plot of Allegheny Plateau data (121 points) with least squares (OLS) and generalized least squares (GLS) fits for a nonlinear model and GLS fits for the nonlinear air and mud wells. Points are color-coded based on the cluster definition in Figure 1. The GLS model is nearly hidden by the GLS mud model because their parameters are very close (see Table 1).

Table 1: Summary of fitted models. Selected models for each region are denoted with ‘*’. Statistically significant coefficients at the 5%-level based on two-sided tests are in bold. GLS, OLS, and LS stand for generalized least squares, ordinary least squares, and least squares respectively. The measure of fit, \widehat{R}^2 is defined in Equation 12. All depths, z , are in meters and all temperature corrections are in °C.

Model	ΔT Equation	\widehat{R}^2
West Virginia		
OLS Linear	$-2.13 + \mathbf{0.00601}z$	0.09
GLS Linear*	$-1.99 + \mathbf{0.00652}z$	0.08
Rome Trough		
OLS Linear	$\mathbf{7.24} - \mathbf{0.00317}z$	0.04
GLS Linear	$\mathbf{9.03} - \mathbf{0.00380}z$	0.03
GLS Linear Air	$\mathbf{12.2} - \mathbf{0.00500}z$	0.05
GLS Linear Mud	$\mathbf{7.74} - \mathbf{0.00338}z$	0.0
Used*	0	
Allegheny Plateau		
LS Nonlinear	$\mathbf{0.0221} \left((\mathbf{1900}^3 + z^3)^{1/3} - \mathbf{1900} \right)$	0.55
GLS Nonlinear	$\mathbf{0.0159} \left((\mathbf{1710}^3 + z^3)^{1/3} - \mathbf{1710} \right)$	0.50
GLS Nonlinear Air*	$0.0104 \left((1090^3 + z^3)^{1/3} - 1090 \right)$	0.25
GLS Nonlinear Mud*	$\mathbf{0.0155} \left((\mathbf{1660}^3 + z^3)^{1/3} - \mathbf{1660} \right)$	0.52

7 Conclusions

This paper derived BHT corrections for NY, PA, and WV using alternative methods to traditional least squares regression. The benefits of using GLS methods with spatial clusters are present were clearly shown in the Allegheny Plateau, where a traditional fitting technique would cause the estimated BHT corrections to be much higher because it did not recognize that the data were drawn from a few clusters and instead treated all observations equally. In the Rome Trough of PA there is not sufficient understanding of the system generate a BHT correction. In neither the Rome Trough of PA nor the Allegheny Plateau were the differences in drilling fluid statistically significant, but because the air data was over a much more limited interval in the Allegheny Plateau the air-model could not be extrapolated to the depth of the mud wells. In WV, the impact of clusters did not change the fitted model much and the data looks consistent with a linear model.

8 Acknowledgments

Cornell University’s Energy Institute and Southern Methodist University’s Geothermal Laboratory for providing data. Code used to estimate the models is available at <https://github.com/calvinwheaton/Bottom-HoleTemps>. Data used in the analysis is available from the corresponding author upon request.

A GLS Estimation and Definition of Statistics

The first step in generalized least squares is estimation of the data covariance matrix. This is done with a model where there was a constant for each cluster c , as shown in Equation 5, where ΔT is the temperature correction, $f(\cdot, \cdot)$ is a function of dependent variables \underline{x} and parameters $\underline{\beta}$, v_c is cluster-specific constant, ε is the error term, and subscript i is for the observation.

$$\Delta T_i = f(\underline{x}_i, \underline{\beta}) + v_c + \varepsilon_i \quad (5)$$

From this model the variance of the cluster-specific “bias” and the variance of the noise term must both be estimated, as shown in Equations 6 and 7, respectively. In these equations, the true parameters v and ε from Equation 5 were substituted with u and e , respectively, to show that the fitted model only gave estimates of the true parameters. These equations assume at all of the clusters will be equally noisy (homoscedastic) (Greene, 2012, Sec. 11.6.2). Although this assumption could be changed so that a separate value of s_e is estimated for each cluster, many clusters have 10 to 20 points and estimates of variances on such small samples are themselves quite variable.

$$s_u^2 = \frac{1}{C} \sum_{c=1}^C (u_c - \bar{u})^2 \quad (6)$$

$$s_e^2 = \frac{1}{n} \sum_{i=1}^n e_i^2 \quad (7)$$

Next, the data covariance matrix for an individual cluster c can be constructed as shown in Equation 8, which will have off-diagonal elements of s_u^2 and on-diagonal elements $s_e^2 + s_u^2$ (Greene, 2012, Sec. 11.5, Eq. 11-31).

$$\mathbf{S}_c = s_e^2 \mathbf{I} + s_u^2 \underline{\mathbf{1}} \underline{\mathbf{1}}' \quad (8)$$

Lastly, the data covariance matrix of the entire dataset can be constructed as shown in Equation 9 (Greene, 2012, Sec. 11.5, Eq. 11-32). This is essentially a matrix of matrices with the on-diagonal matrices being the estimated data covariance structure of a given cluster. The off-diagonal matrices are zero because these observations are from separate clusters and should be uncorrelated on average, hence there is no covariance structure to this portion of the dataset.

$$\mathbf{S} = \begin{bmatrix} \mathbf{S}_1 & \mathbf{0} & \cdots \\ \mathbf{0} & \mathbf{S}_2 & \\ \vdots & & \ddots \end{bmatrix} \quad (9)$$

Now that the covariance structure of the data is estimated, the model can be fit by minimizing the “weighted” sum of squared errors. Weighted is used loosely because it employs a diagonal data covariance matrix whereas this problem has a matrix with on- and off-diagonal elements that are non-zero. Therefore, this procedure is called generalized least squares to differentiate it from weighted least squares. The problem formulation is shown in Equation 10, where the estimated model parameters are \underline{b} and \underline{e} is an n -by-1 vector of estimated residuals. The result is a single value, which was minimized using an optimization software (R Core Team, 2012, 'optim').

$$\underline{b} = \min_{\underline{\hat{b}}} \underline{e}' \mathbf{S}^{-1} \underline{e} \quad (10)$$

When separate drilling fluids were considered, Equation 5 included separate predictors for each fluid but the cluster constants were the same for both fluids. The assumption is that the “bias” in a cluster is for the individual cluster and it should not depend on the type of fluid present. In the fitting of the final model the data covariance matrix was partitioned based on the drilling fluid and the model was fit to each fluid one at a time.

The model parameter covariance matrix is estimated using Equation 11. This is based on the second-order terms of a Taylor Series expansion of the objective function about the solution. The square root of the diagonal elements of this matrix represent the standard error of parameters.

$$\text{Var}(\underline{b}) = \left[\left(\frac{\partial f(\mathbf{X})}{\partial \underline{b}} \right)' \mathbf{S}^{-1} \left(\frac{\partial f(\mathbf{X})}{\partial \underline{b}} \right) \right]^{-1} \quad (11)$$

The measure of fit used in this analysis is a pseudo R^2 , referred to as \widehat{R}^2 and defined in Equation 12, where SSE and SST are the sum of squares error (sum of squared residuals from regression) and sum of squares total in the real, un-weighted space. The regression procedure will not maximize this

metric because least squares estimates minimize SSE, and for generalized least squares this value is not bounded on $[0,1]$ unlike traditional R^2 .

$$\widehat{R}^2 = 1 - \frac{\text{SSE}}{\text{SST}} \quad (12)$$

Throughout the analysis normal and χ^2 approximations, which are technically accurate only for large (asymptotic) samples, will be used when testing hypotheses and reporting p-values. The reason is that the simple degrees of freedom adjustments in linear ordinary least squares regression problem are not easily defined and the parameter covariance structure of the nonlinear models are only approximate.

References

- Aguirre, G. A. (2014). Geothermal Resource Assessment: A Case Study of Spatial Variability and Uncertainty Analysis for the States of New York and Pennsylvania. Master's Thesis, Cornell University, Environmental and Water Resources Systems Engineering.
- Bureau, U. S. C. (2014). Cartographic Boundary Shapefiles-Counties. cb.2014_us_county_rr.zip. https://www.census.gov/geo/maps-data/data/cbf/cbf_counties.html (Accessed 7 September 2015).
- Deming, D. (1989). Application of Bottom-Hole Temperature Corrections in Geothermal Studies. *Geothermics* 18(5/6), 775–786.
- Förster, A., D. Merriam, and J. Davis (1997). Spatial Analysis of Temperature (BHT/DST) Data and Consequences for Heat-Flow Determination in Sedimentary Basins. *Geologische Rundschau* 86(2), 252–261.
- Frone, Z. and D. Blackwell (2010). Geothermal Map of the Northeastern United States and the West Virginia Thermal Anomaly. *Geothermal Resources Council Transactions* 34, 339–344.
- Greene, W. H. (2012). *Econometric Analysis* (7 ed.). Prentice Hall.
- Harrison, W. E., K. V. Luza, M. L. Prater, and P. K. Cheung (1983). Geothermal Resource Assessment in Oklahoma. Oklahoma Geological Survey. Special Publication 83-1.
- Hendry, R., K. Hilfiker, D. S. Hodge, P. Morgan, C. A. Swanberg, and S. S. J. Shannon (1982). Geothermal Investigations in West Virginia. Los Alamos National Laboratory. LA-9558-HDR, UC-66a.

- Hodge, D. S., R. De Rito, K. Hifiker, P. Morgan, and C. A. Swanberg (1981). Investigations of Low-Temperature Geothermal Potential in New York State. Los Alamos National Laboratory.LA-8960-MS, UC-66b.
- Kehle, R. O. (1973). Geothermal Survey of North America: 1972 Annual Progress Report. American Association of Petroleum Geologists.
- Kmenta, J. (1986). *Elements of Econometrics* (2 ed.). Macmillan Publishing Company.
- QGIS Development Team (2009). *QGIS Geographic Information System*. Open Source Geospatial Foundation.
- R Core Team (2012). *R: A Language and Environment for Statistical Computing*. Vienna, Austria: R Foundation for Statistical Computing. ISBN 3-900051-07-0.
- Repetski, J. E., R. T. Ryder, D. J. Weary, A. G. Harris, and M. H. Trippi (2008). Thermal Maturity Patterns (CAI and %Ro) in Upper Ordovician and Devonian Rocks of the Appalachian Basin: A Major Revision of USGS Map I-917-E Using New Subsurface Collections: U.S. Geological Survey Scientific Investigations Map 3006.
- Saucer, J. (2011). AASG Geothermal Data: Borehole Temperature Observation Feature: West Virginia Geological and Economic Survey Borehole Temperature Observations. National Geothermal Data System <http://geothermaldata.org/dataset/west-virginia-borehole-temperatures> (Accessed 5 November 2014).
- Scott, G. N. (1982). Temperature Equilibration in Boreholes: A Statistical Approach. Master' Thesis, University of Michigan, Geology.
- Shope, E. N. (2012). A Detailed Approach to Low-Grade Geothermal Resources in the Appalachian Basin of New York and Pennsylvania: Heterogeneities within the Geologic Model and Their Effect on Geothermal Resource Assessment. Master's Thesis, Cornell University, Earth and Atmospheric Sciences.
- Spicer, H. C. (1964). A Compilation of Deep Earth Temperature Data, U. S. A. 1910-1945. United States Geological Survey.64-147.
- Whealton, C. A. (2015). Statistical Correction of Temperature Data for New York and Pennsylvania Wells. Master's Thesis, Cornell University, Environmental and Water Resources Systems Engineering.

Memo 3: Anadarko Basin Thermal Conductivities in GPFA-AB

To: Appalachian Basin Geothermal Play Fairway Analysis Group

From: Zachary Frone

Date: April 30, 2015

Subject: Anadarko Basin Thermal Conductivity Measurements

The Appalachian Basin Geothermal Play Fairway Analysis (AB-GPFA) team must determine which thermal conductivity values (K) to use for each formation in the thermal model. Data from Carter et al. (1998) from the Anadarko Basin (Oklahoma) is used due to the large number of measurements (n=275) and the similar ages and burial histories of the basins. The raw data from Carter shows large variations in K of sandstone, and generally smaller variations for other lithologies (Figure 1). Variations in sandstone samples do not show any systematic change with density or porosity (Figure 1).

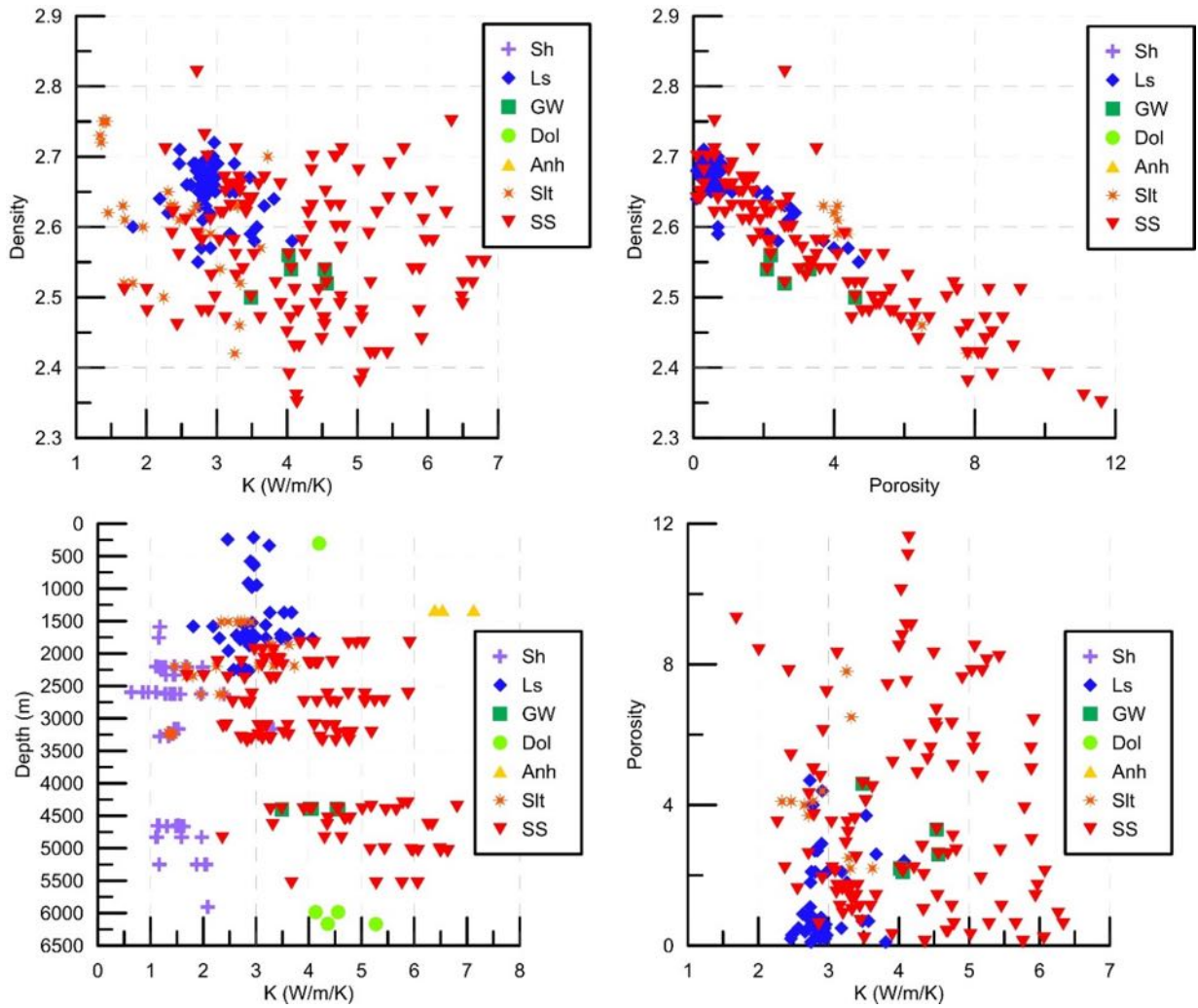


Figure 1: Original data from Carter et al. (1998). Sh: Shale, Ls: Limestone, GW: Greywacke, Dol: Dolomite, Anh: Anhydrite, Slt: Siltstone, SS: Sandstone.

Data from Carter et al. (1998) included measured K, density, and porosity values, along with core descriptions and grain size data. The original sampling methodology seems to have been to collect 3 samples over narrow 3-10 foot intervals. In order to see if the variability in the original K data is valid, a sub set of 18 samples were measured again. The 18 samples are from 6 wells, with 3 samples from each well. The 3 samples from each well are generally within 1-2 feet of each other, with two exceptions. All were selected to test whether the small scale variation in thermal conductivity that was measured was real. See table 1 for sample names, depth, lithology, and K.

All samples were prepared following the same procedure as Carter et al. (1998). The samples are weighed and measured dry, and a dry density is determined. The samples are then loaded into a vacuum/pressure cylinder where they are placed under vacuum for several hours to days to draw air out of the pores, followed by high pressure (~3000 psi) H₂O for up to 24 hours to saturate the cores. The samples are removed from the cylinder and then reweighted to determine a wet mass. The porosity, a parameter needed to calculate the thermal conductivity, is then calculated from the difference in the wet and dry masses and the volume of the core.

Once prepared, samples were run on a divided bar for 25 minutes each, with a temperature reading collected every 15 seconds. Each sample was run twice (once on each side of the bar) and the last 5 minutes of data were used. Thermal conductivity values are then calculated for the cores. 2 of the 18 cores were not run due to fractures and chipping of the cores. The results from the rest of the cores are shown on Table 1. All but two samples have values that are within $\pm 6\%$ of the values reported by Carter et al. (1998).

This data show that in general, the values from Carter et al. (1998) can be trusted and that there can be small scale (sub-meter) changes in thermal conductivity within a single lithology. Also, the range in values for sandstone appears to be real. The cause of this variation is unknown currently, but is likely caused by changes in mineralogy. Two methods to test this would be XRD or XRF analysis of the cores. XRD requires powdered samples so the cores would have to be destroyed. XRF analysis can be completed on cores and allows for multiple measurements along the length of the core. Changes in elemental composition measured by XRF could provide insight into why there are variations in thermal conductivity in cores from the same formation.

Table 1: Samples selected for re-measurement

Sample Name	Depth (ft)	Lithology	Carter K Value (W/m/K)	K1	K2	% difference
Dannehl 8609	8609	SH	1.38	1.46	1.43	4.71
Dannehl 8610	8610	SH	2.39	2.38	2.45	1.05
Dannehl 8611	8611	SH	1.46	1.53	1.51	4.11
Smallwood 8646	8646	SS	2.92	BROKEN		
Smallwood 8647	8647	SS	5.06	4.64	4.87	6.03
Smallwood 8648	8648	SS	4.35	3.9	3.72	12.41
Lloyd 5195	5195	LS	1.81	BROKEN		
Lloyd 5196	5196	LS	2.19	2.5	2.47	13.47
Lloyd 6157	6157	LS	2.88	2.84	2.9	0.35
Nightingale 10217	10217	SS	4.10	4.31	4.31	5.12
Nightingale 10219	10219	SS	2.43	2.54	2.45	2.67
Nightingale 10235	10235	SS	4.33	4.08	4.28	3.46
Brewer 7015	7015	SS	4.45	4.15	4.23	5.84
Brewer 7016	7016	SS	2.72	2.65	2.6	3.49
Brewer 7017	7017	SS	2.27	2.15	2.14	5.51
Scott 10834	10834	SS	2.71	2.56	2.57	5.35
Scott 10835	10835	SS	3.24	3.28	3.17	0.46
Scott 10836	10836	SS	4.21	4	4.13	3.44

Memo 4: Assignment of Conductivity Stratigraphy for Individual Wells

To: Appalachian Basin Geothermal Play Fairway Analysis Group
From: Jared Smith, Teresa Jordan, and Zachary Frone
Date: Original from July 31, 2015. Updated September 20, 2016
Subject: Assignment of thermal conductivity stratigraphy to individual wells using COSUNA columns

Applicability: The methods described in this memo were used to compute and assign thermal conductivities and thicknesses to stratigraphic units. The resulting thermal conductivity column is called the thermal conductivity stratigraphy. This stratigraphic information was assigned to individual wells in the 1-D heat conduction model to calculate the surface heat flow, temperatures at depth, and depths to temperatures of interest. Further details are provided in Smith (2016).

Definitions

COSUNA column Generalized representation of a vertical sequence of units in the subsurface, identified by general lithology and correlated to geologic age.

COSUNA section Geographic area in which the COSUNA column was defined by AAPG (1985a; 1985b).

Unit A member, formation, or group. These are nested ranks. In general, the uniformity of lithology is greatest at the rank of member and decreases progressively through formation and group.

Group (Gp.) A sequence of formations and/or members within a single named unit.

Formation (Fm.) A sequence of members in a single named unit.

Member (Mbr.) A layer, named or unnamed, in a group or formation.

Introduction

The Appalachian Basin Geothermal Play Fairway Analysis team needs to have a method for assigning lithologic unit thicknesses and corresponding thermal conductivities to locations of wells that have bottom-hole temperature (BHT) measurements. The resulting column of unit thicknesses and thermal conductivities is called the thermal conductivity stratigraphy. This information is needed in order to calculate the surface heat flow and temperatures at depth using the 1-D heat conduction model (see Memo 8: Well database organization and thermal model methods).

The American Association of Petroleum Geologists (AAPG 1985a; 1985b) Correlation of Stratigraphic Units of North America (COSUNA) columns have been used in previous studies in the Appalachian Basin (Aguirre, 2014; Shope, 2012; Stutz, 2012; Frone and Blackwell, 2010).

The COSUNA columns provide representative geology for broad sub-regions of the basin, within which the geology is fairly consistent (Fig. 1). Because a single COSUNA column applies to a broad area, yet the total thickness of the sedimentary rocks varies across any one of those areas, it is also necessary to scale the COSUNA column unit thicknesses to the specific location of the well whose thermal conductivity column is sought. A linear scaling of each unit was used to match the COSUNA column thickness to the sediment thickness (WVGES, 2006) at the location of each well. This approach allows for a rapid assignment of thermal conductivity stratigraphy to about 20,750 wells when a well-by-well geological analysis would be implausible to complete in the timeframe of this study. A well-by-well detailed geological analysis has been determined for 77 spatially distributed deep wells in the region. For these wells, the generalized COSUNA column approach is compared to their detailed stratigraphy (see Memo 5: Tests of simplified conductivity stratigraphy by Monte Carlo analysis).

COSUNA Column Data

The areas of the COSUNA sections vary greatly throughout the basin, with the 21 smallest sections (min ~970 km², mean ~ 1960 km², max ~3300 km²) concentrated in the eastern margin of the basin along the Appalachian Mountains, and the largest 25 sections (min ~4430 km², mean ~ 13900 km², max ~29300 km²) dispersed in the remaining portion of the basin (Fig. 1).

Each COSUNA column provides a vertical sequence of named units, unit age (Ma), unit thicknesses (m), and by color indicates the dominant lithology (Fig. 2). Additional, often more detailed lithologic information from the USGS mineral resources website (USGS, 2014) was coupled to the COSUNA units on a state-specific basis.

A range of unit thickness is reported for most units, and a single “normal” thickness is reported otherwise (Childs, 1985). The normal thickness is interpreted as an average thickness, but this may not be the case. Some columns are incomplete and do not include some Lower Paleozoic units. Other columns do not have reported thicknesses for some units. For COSUNA sections with missing data, if cross sections within the COSUNA section were available, the missing units and approximate thicknesses were added from the cross sections (Table 1). If cross sections were not available, the suspected missing information was documented (Table 2) and the columns were used as provided by AAPG (1985a; 1985b).

Summary of Desired Products

The goal of this analysis is to assign a thermal conductivity stratigraphy to each well in the dataset. To arrive at this product, the time-based COSUNA columns are transformed into thickness-based columns with lithologically distinct rock units for the assignment of conductivities. Therefore, unit lithology and thickness are the primary information to extract from COSUNA columns and organize into a useful format. The methodology for extracting this information is presented in the following sections.

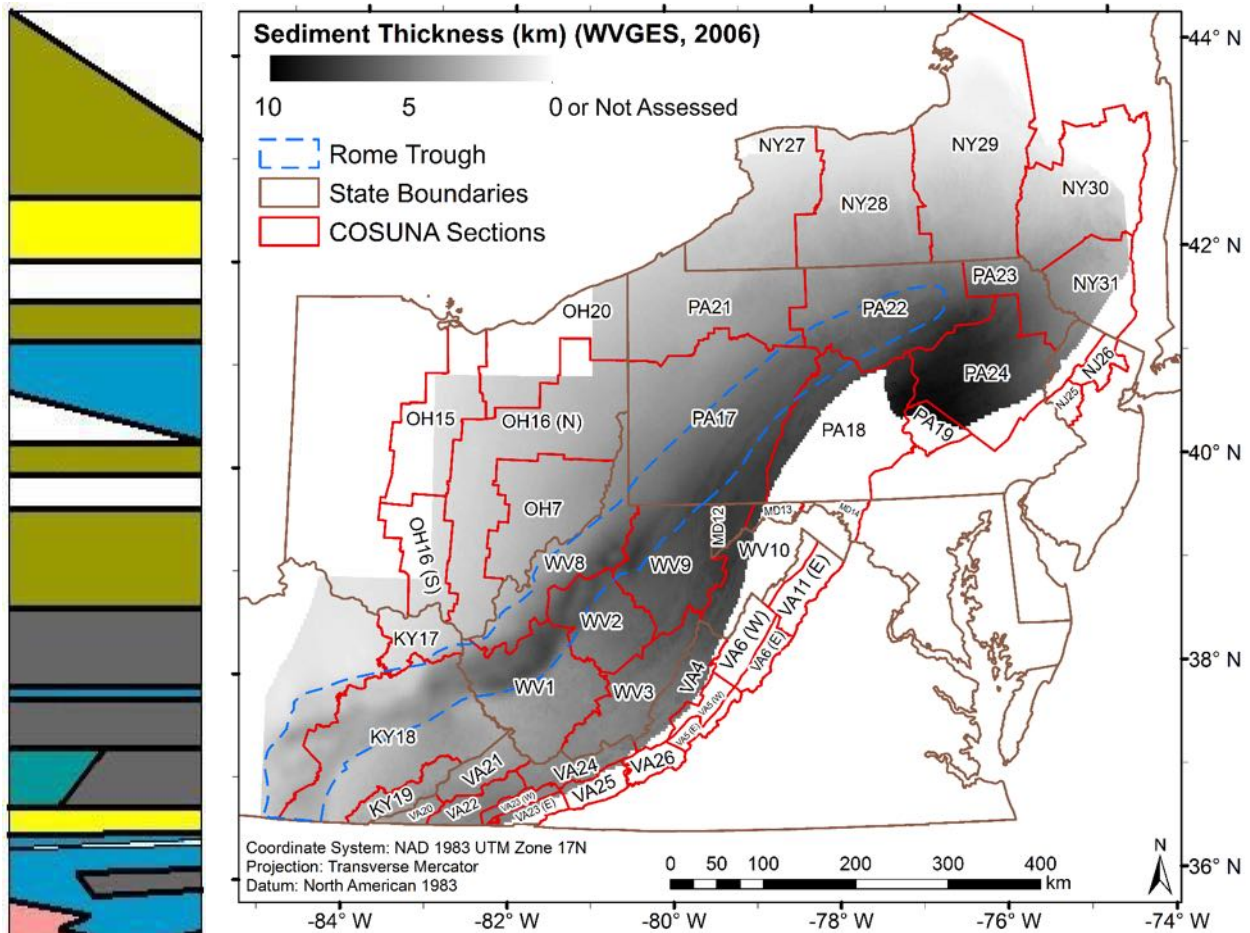


Figure 1: Map of the regions, referred to as sections, whose generalized sedimentary rocks are described by single COSUNA columns. The sections used in this study are labeled by state, followed by the number of the column and, where needed, the cardinal direction in parenthesis. For Virginia, cardinal directions indicate separate columns for the eastern and western side of the North Mountain Fault or the Pulaski Fault. For Ohio, the cardinal direction indicates on which COSUNA sheet (North [N] or South [S] Appalachian Basin) the column can be found. The sediment thickness derived from the Trenton-Black River Project (WVGES, 2006) is shown for reference. COSUNA sections that intersect the Rome Trough (Repetski et al., 2008) require adjustment and addition of some missing units (discussed below). Figure from Smith (2016).

Figure 2 (left): Digitized West Virginia 9 COSUNA Column (AAPG; 1985a) and geological ages from Smith (2016). Time progresses upward from the bottom. Colors: Blue – carbonate; Pink – evaporite; Grey – Shale, mudstone, siltstone; Tan – Interbedded sandstone, siltstone, shale; Teal – Chert; Yellow – Sandstone. Column shows examples of units occupying portions of the column (top), and of multiple units in the same time period (Shale\Chert in the middle of the column).

Method for Extracting Thickness from COSUNA Columns

The pictorial COSUNA column information is transformed into a spreadsheet that records as rows the individual named units of the COSUNA column. Spreadsheet columns are assigned subsidiary information about each rock unit. An effort was made to preserve as much detail as possible from the COSUNA columns. Groups and formations were split into the individual formations/members that comprised the group/formation, when possible. If a group/formation was all the same rock type (e.g. all limestone) then a single row in the spreadsheet was used to represent the group/formation, and all formations/members composing the group/formation were listed in the row, ordered from the geological top downward. Occasionally the minimum and maximum thicknesses of the formations/members did not sum up to the group/formation minimum and maximum thicknesses. In this case, the reported minimum and maximum thickness for each formation/member was listed in a separate row.

Rome Trough Units

The COSUNA columns reported knowledge that existed up to the date of publication in 1985, and they are spatially simplified such that lateral variability, which likely occurs across individual faults or folds, is not necessarily represented (Childs, 1985). In some cases, knowledge of structural features today known to be important, such as the Rome Trough, were not integrated into the early 1980's COSUNA data compilation. For the Rome Trough (Fig. 3), knowledge of the thicknesses of the deeply buried Appalachian basin sedimentary units evolved significantly as the spatial extent of very deep drilling increased and as deep penetration reflection seismic data progressively moved into the public domain. Thus, the COSUNA columns characterize well the Lower Paleozoic units of the Kentucky sector of the Rome Trough, but lack this information for parts of West Virginia and Pennsylvania. Therefore, an early step in this project's methods was to adjust several COSUNA columns to account for the Rome Trough units and associated thicknesses (Table 1). The Rome Trough was located within only a portion of each of the COSUNA sections listed in Table 1, so the addition of these units only applies to the portion of the COSUNA column located within the Rome Trough (Fig. 1). The thickness change represents the additional thickness of Lower Paleozoic strata present in the Rome Trough portion of the COSUNA column.

The COSUNA columns are as much as 1775 m thicker on average in the Rome Trough than outside of the Rome Trough (Table 1). This thickness change might occur: 1) over a horizontal distance of a kilometer if the trough at this location is bounded by a single major fault, 2) across a series of hundred-meter-scale steps spanning a width of 10-30 km via a series of minor faults, or 3) progressively across a wide ramp (Fig. 3). Ideally the style of the structural border zone would be known and dictate the thickness of strata assigned to each well. But that information is not known or not available, and a simplified strategy is needed for interpolation of thicknesses across the borders of the Rome Trough. Because the sediment thickness map governs the thickness transition across the Rome Trough boundary via scaling of the COSUNA columns, it is more important to capture the lithologic differences in and out of the Rome Trough with the COSUNA columns than it is to have a separate thickness scaling factor for columns of the Rome Trough based on, for example, distance to the Rome Trough boundary. Therefore the method adopted is to use a sharp division of column thickness across the Rome Trough boundaries, and allow the scaling of sediment thickness to account for the “true” thickness change.

Addition of Missing Rome Trough Units

The units added to each column are provided in Table 1. Column KY18 was unique in that it contained thicknesses of Rome Trough units, but a division for units in and out of the Rome Trough was not provided. For example, the thicknesses of units at the bottom of the column ranged from about 1700 m to 4700 m, which suggests that the KY18 section straddles one or more faults that comprise the borders of the Rome Trough (Fig. 1). Lacking information about the transition between these thicknesses, Equation 1 was used to assign the unit thicknesses in and out of the Rome Trough from the Brassfield Dolomite to the basal sandstone

$$Thick = \begin{cases} average + \frac{[max - average]}{2} , & \text{In Rome Trough} \\ average - \frac{[average - min]}{2} , & \text{Not in Rome Trough} \end{cases} \quad [1]$$

where *Thick* is the thickness assigned to the unit, *average* is the average thickness of the unit, *max* is the maximum thickness of the unit, and *min* is the minimum thickness of the unit. This equation is only used for Rome Trough units in column KY18.

Table 1: Rome Trough units and sources. Details for each unit are provided in the spreadsheet (COSUNA_Columns_NY-PA-WV-VA-OH-KY-MD.xlsm). Units to the left of forward slashes overlie units to the right of forward slashes. Units listed have been added to the bottom of the COSUNA columns, unless otherwise stated. The average thickness change is relative to the COSUNA columns without Rome Trough adjustment, unless otherwise stated.

COSUNA Section	Units Added to the Bottom of the Original COSUNA column	Average Thickness Change (m)	Sources
PA17	Pleasant Hill Fm. / Waynesboro Fm / Tomstown Dolomite / Basal Sandstone	+ 1635	Shope (2012) MS Thesis
PA18	Waynesboro Fm / Tomstown Dolomite	+ 404	USGS Cross Section B-B' (Ryder, 1992)
PA21	Unnamed shale between Gatesburg Fm. and Warrior Fm. Beekmantown Fm. thickness increased within the Rome Trough.	+ 577	USGS Cross Section B-B' (Ryder, 1992)
PA22	None added. Lacking further information, maximum thickness was used as the “assumed” thickness for Rome Trough units only.	+ 46.5	No cross sections found that pass through the Rome Trough portion of this COSUNA section.
WV1	Tomstown Dolomite (a.k.a. Shady Dolomite) between the Rome Fm. and basal sandstone. Adjusted thicknesses of the Conasauga Fm. and Rome Fm.	+ 1309	Plate 10A, Rome Trough Consortium Final Report (Harris et al., 2002)
WV2	Rome Fm. added between Conasauga Fm. and Tomstown Dolomite. Adjusted thicknesses of Conasauga Fm. and Tomstown Dolomite.	+ 976	Plate 12A, Rome Trough Consortium Final Report (Harris et al., 2002)
WV8	Waynesboro Fm. and basal sandstone. Adjusted the Conasauga Fm. Increased Dunkard Gp. thickness in the Rome Trough (Ryder et al., 2008).	+ 1775	USGS Cross Section E-E' (Ryder et al., 2008) and Plate 14A, Rome Trough Consortium Final Report (Harris et al., 2002)
WV9	Rose Run Sandstone / Copper Ridge Dolomite / Nollchucky Shale / Maryville Limestone / Rogersville Shale / Pumpkin Valley Shale / Waynesboro Fm. / Tomstown Dolomite / Chilhowee Gp. None of these units were on COSUNA. Few are exclusive to the Rome Trough.	+ 1700 to original column. + 1828 in the Rome Trough	USGS Cross Section E-E' (Ryder et al., 2008) and Plate 15A, Rome Trough Consortium Final Report (Harris et al., 2002)
KY18	None added. See Equation 1.	+ 1449	COSUNA column contains thickness ranges for each unit in the Rome Trough.

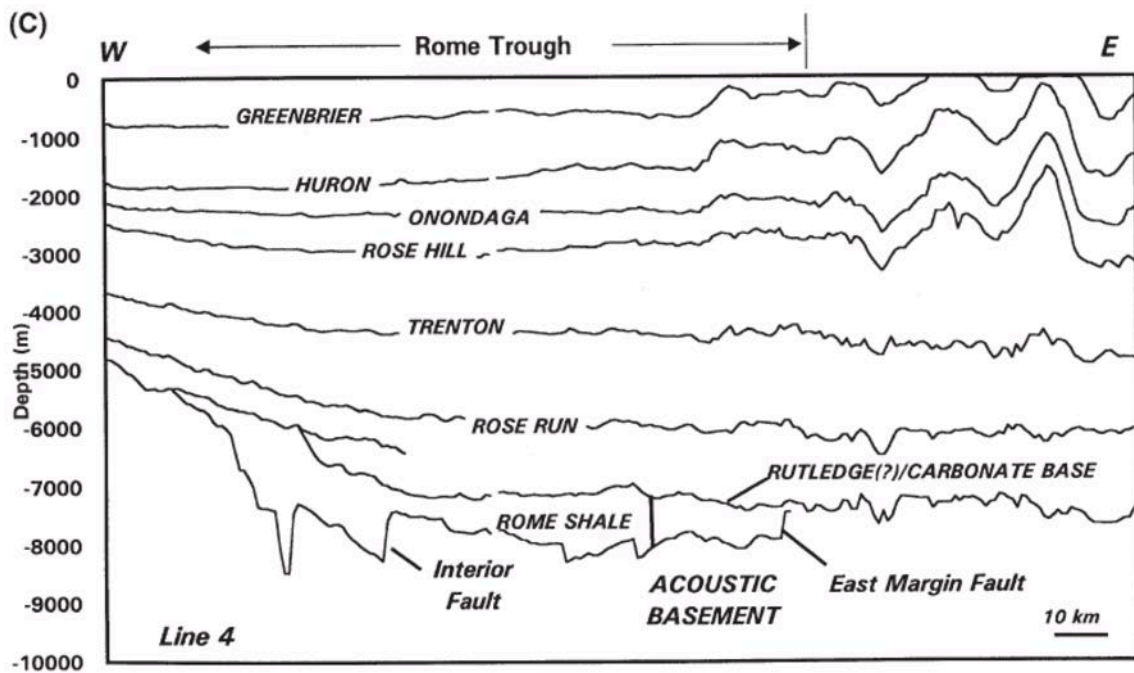
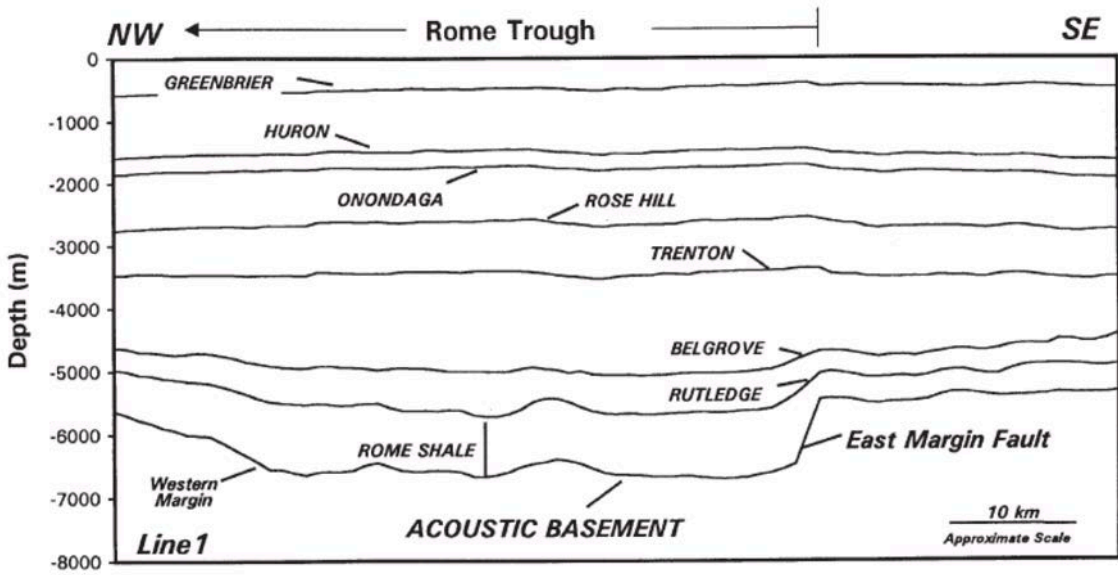


Figure 3: Depth sections of the Rome Trough in southwestern West Virginia (top) and northernmost West Virginia (bottom) that were constructed by Wilson (2000) based on seismic reflection data. Named units refer to ones that are readily recognized on seismic profiles; numerous intervening layers exist but are not labeled. Units deeper than roughly 4000 m are thicker within the Rome Trough than outside of it. The east side of the Rome Trough displays a change in thickness over a very short distance, from thin outside of the trough to thick within the trough, due to crossing the existence of a single fault zone. In contrast, the western margin displays changes across a gradual ramp (top) and a complex set of faults (bottom).

Unit Thickness Determination

Sorting information from COSUNA columns into useful unit thicknesses is not a trivial task because the primary organization unit for COSUNA columns is geologic age, not stratigraphic unit. The simplest units to assign thicknesses to are those that are found uniformly throughout a given COSUNA section. However, it is common for a geological unit to occur in only a portion of the section, and for another age-equivalent unit (or units) to occur elsewhere in the section. Physically, this means that for the same time of deposition, more than one unit formed within the COSUNA section; however there is no guarantee that the thickness of these units will be equal during that time period.

Multiple Units for the Same Time of Deposition

Unequal unit thickness within a section at a time of deposition results from variations in sediment supply, subsidence, or post-depositional erosion. The width of the unit on the COSUNA column chart (e.g., Fig. 2) represents the approximate proportion of area within the corresponding COSUNA section occupied by that unit. In the case of equal or roughly equal thicknesses for each unit during a time of deposition, a weighted average of the unit thicknesses was taken according to the proportion of the column width occupied by each unit. The weighted thickness of each unit is then calculated from Equation 2

$$\text{Weighted Thickness} = \sum_{i=1}^n \text{Thick}_i * w_i, \quad 0 < w \leq 1 \quad [2]$$

where w_i are the weights that are determined from the proportion of the column width for unit i , and Thick_i is the thickness of unit i . The weights in this equation must sum to the total extent of the unit(s) within the COSUNA section. For instance, for a single time period, if Gp. 1 was in 10% of the column, Gp. 2 was in 20% of the column, and Gp. 3 was in 50% of the column, the sum of the weights would be 0.8, indicating that for this time period, units were only present in 80% of the COSUNA section. If the lithology associated with these units was different, a note was made regarding the percentage of each rock type for this time period.

In the case of unequal unit thicknesses or complexities in the arrangement of units for a time period of deposition (Fig. 4), the best effort was made to aggregate a sequence of formations/units into cohorts of roughly equal thickness. Finding cohorts of equal thickness solves the problem of having thicknesses specified for a portion of the section and not in others (e.g. Hampshire compared to Ohio and Chemung in Fig. 4). Equation 2 was applied to determine the weighted thickness when suitable cohorts were found. Then, the percentage of each rock type within the cohort was determined according to the thickness of the units within the column. For example, in Figure 4, since each rock unit occupies a different portion of the section and a different amount of time, 4 cohorts were established that each occupy approximately 25% of the section. The average thickness is determined from the average of the cohort thicknesses: 1) 817.5 m Ohio/Java in 25% of the column, 780 m Chemung/lower Huron/Java in 25% of the column, 767.5 m Hampshire/Chemung/Java in 25% of the column, and 700 m Hampshire/Chemung in 25% of the column. The average thickness is 766.25 m, and the average lithology is 59%

interbedded sandstone, siltstone, and shale, 35% shale/shale, mudstone, siltstone, and 6% sandstone.

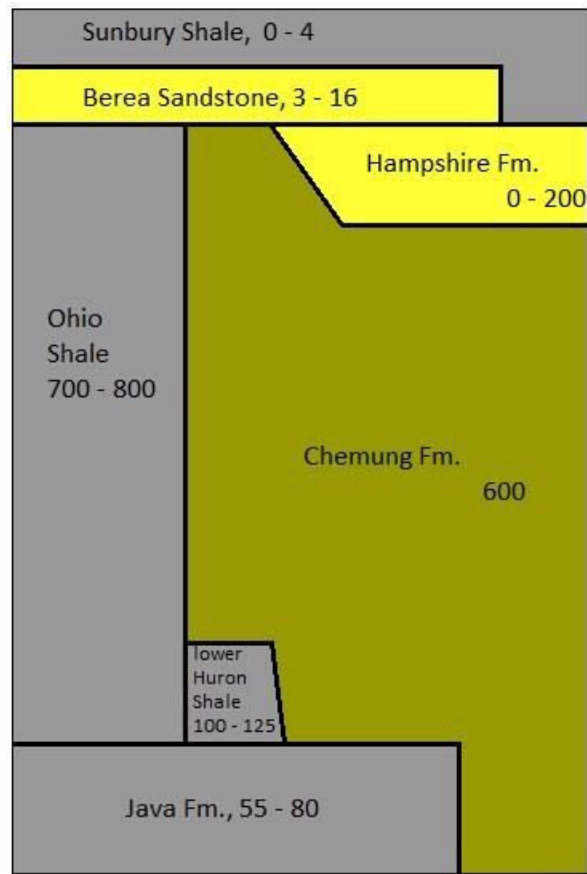


Figure 4: Example of cohorts from West Virginia 3 COSUNA column. Four cohorts were made from this section of the column: 1) Ohio/Java, 2) Chemung/lower Huron/Java, 3) Hampshire/Chemung/Java, and 4) Hampshire/Chemung. These are listed in a single cell in the spreadsheet. Figure from Smith (2016).

Incomplete COSUNA Columns

Some of the COSUNA columns state that older rocks are unknown, or it is clear that the columns do not include sedimentary rocks down to the basement rocks. These columns with missing information are listed in Table 2. Finding the thicknesses of the units that comprise the oldest sediment in these columns would be helpful to improve the accuracy of the COSUNA column approach.

Table 2: COSUNA columns with unknown or missing deep sedimentary rock information.

Column	Missing Sediment Information
PA22	Column does not reach basement rocks, but does have some Lower Paleozoic units present (e.g. Beekmantown Fm.).
PA23	Column goes to the Beekmantown Fm., undifferentiated, but states that older rocks are unknown. Even so, the minimum and maximum COSUNA thicknesses coincide well with the WVGES (2006) sediment thickness map.
PA24	There's a split in the column, with one side having thousands of meters thicker sedimentary rocks than the other. It would be great to determine where geographically this split occurs so that two columns can be made for this section. The assumed COSUNA thickness is near the maximum sediment thickness by WVGES (2006).
WV3	Cambrian and older rocks are unknown in the column. Beekmantown Fm. is the oldest formation. It is possible that no information is missing because the maximum sediment thickness according to WVGES (2006) is contained within the COSUNA column thickness range.
MD12 and MD13	Juniata is the oldest formation. Older rocks are unknown. These columns have the most time missing of all the columns. In terms of thickness, as much as 3 km are missing based on the WVGES (2006) map.
VA4	Possible formations missing based on sediment thickness map that ranges from 4.5 km - 7 km thickness (WVGES, 2006)
VA24	Possible formations missing based on sediment thickness map that ranges from 4.5 km – 5.5 km thickness (WVGES, 2006)

COSUNA Column Scaling to Basement

The COSUNA column thickness is at best an average of the sedimentary rock thickness within a section; however the actual sedimentary rock thickness within a section may vary greatly from the COSUNA derived thickness. Variations may occur due to missing units (Table 2), and due to variability in sediment thickness throughout the COSUNA section (Fig.1). To capture variations in the sediment thickness, the COSUNA unit thicknesses were scaled to the sediment thickness map developed by the West Virginia Geologic and Economic Survey (WVGES, 2006) according to Equation 3. Scaling is performed such that all units are adjusted linearly according to the fractional thickness between the assumed sediment thickness (WVGES, 2006) and the COSUNA column sediment thickness. For example, when the “true” depth to basement is less than the assumed COSUNA column depth to basement, the scaled unit thickness is less than the unscaled unit thickness, and vice versa. One problem with this approach is that, lacking further information about the missing units, the COSUNA column is (incorrectly) assumed to contain only those units reported by AAPG (1985a; 1985b). Another problem is that the scaled unit thickness can be less than the COSUNA-stated minimum possible unit thickness or greater than the COSUNA-stated maximum possible unit thickness. Correcting this problem would require a preferential scaling of units, such that some units would be adjusted first, and the remaining units scaled iteratively to match the “true” depth to basement. To avoid this complication, Equation 3 is used as written, and all units are equally scaled.

$$\text{ScaledUnitThickness} = \text{UnscaledUnitThickness} * \left(\frac{\text{TrueDepthToBasement}}{\text{COSUNADepthToBasement}} \right) \quad [3]$$

Thermal Conductivities

Selected Published Values

Carter et al. (1998) was the primary source used for thermal conductivity values because their samples were taken from the Anadarko Basin. The Anadarko Basin has a similar burial history as the Appalachian Basin, and thus would have comparable thermal conductivities due to an expected decrease in rock porosity as a result of prolonged burial. Carter et al. (1998) measured conductivity values on cores from the Anadarko Basin, and presented average values for the major lithologies in the basin. The average thermal conductivities from Carter et al. (1998) and the associated uncertainty about the average values are listed in Table 3. Thermal conductivity values for other lithologies not listed in Carter et al. (1998) are also provided in Table 3.

Table 3: Thermal conductivities, uncertainty, and sample size. The uncertainty is the standard deviation about the mean.

Lithology	Average Thermal Conductivity (W-m ⁻¹ -°C ⁻¹)	Uncertainty, 1 standard deviation (W-m ⁻¹ -°C ⁻¹)	Number of Samples	Reference and Notes
Sandstone	4.27	1.19	118	Carter et al. (1998)
Siltstone	2.34	0.768	31	Carter et al. (1998)
Shale / Mudstone	1.5	0.466	57	Carter et al. (1998)
Black Shale	0.9	0.06		From Cercone, Demming, and Pollock (1996)
Conglomerate	4.13	0.396	5	Used Granite Wash from Carter et al. (1998)
Chert	4.12	0.41		Average of Chert and Flint from Horai (1971)
Chemical	5.92	0.43		Hematite in Clinton Group. Conductivity is an average of temperature dependent values for the mineral Hematite from 0-200°C from Mølgaard and Smeltzer (1971)
Limestone	2.91	0.371	56	Carter et al. (1998)
Dolomite	4.5	0.412	5	Carter et al. (1998)
Anhydrite	6.68	0.319	3	Carter et al. (1998)
Salt / Evaporite	6	1		Value for Halite at ~25°C, Thermal conductivity of Halite is highly temperature dependent. From Birch & Clark (1940)
Gneiss	2.5	0.5		Clauser, 2011
Marble	3.0	0.5		Clauser, 2011
Quartzite	5.0	0.5		Clauser, 2011

Formation-Specific Thermal Conductivity

Each formation in the basin was assigned a thermal conductivity based on the average of the thermal conductivities listed in Carter et al. (1998) (Table 3) for the lithologies present within the formation. The approximate ranking of lithologies (e.g. primary, secondary, etc.) within each formation was determined from the USGS as listed on the USGS Mineral Resources website, specific to each state (e.g for West Virginia: <http://mrdata.usgs.gov/geology/state/fips-unit.php?state=WV>). Final thermal conductivity values for the formations were determined using a Monte Carlo analysis with 10^6 iterations, for which the percentage corresponding to ranks of the lithologies was varied.

For each lithology in a given formation, a truncated normal distribution of conductivity values and a random percentage were assigned. The normal distribution was truncated at two standard deviations from the mean thermal conductivity for the lithology in order to prevent 1) egregiously large or small values of thermal conductivity for any lithology, and 2) negative values for lithologies with large uncertainty. The random percentage assigned to each lithology for each Monte Carlo replicate represents the percent of the formation composed from each lithology. The sum of the percentages is 100 for each replicate. The highest percentage is assigned to the major (primary) lithology as determined from the USGS, the next highest percentage was assigned to the secondary lithology, and so on. All lithologies had to be assigned a percentage of at least 5% in each Monte Carlo iteration. The distribution of conductivity values and the random weighting for each lithology were used to calculate the harmonic mean thermal conductivity for each replicate, which assumes that the different lithologies are horizontal layers. The reported value of thermal conductivity for each formation is the mean of the thermal conductivities for the 10^6 replicates. The reported uncertainty is the standard deviation of the 10^6 values of the formation thermal conductivity. These are available in three files: NY_Conductivity_final.xlsx, PA_Conductivity_final.xlsx, and WV_Conductivity_final.xlsx.

COSUNA Unit-Specific Thermal Conductivity

The thermal conductivity for each unit in the COSUNA column was assigned based on the output of the Monte Carlo analysis if the formations composing the unit were available on the USGS website. If a formation was not listed on the USGS website, it was not subject to the Monte Carlo analysis and the COSUNA listed lithology was used instead, with the percentage of each rock type in the unit resulting from the COSUNA formation thicknesses (process described above in the Thickness Determination section). In this case, thermal conductivities from Carter et al. (1998) were used directly for each lithology. If only a group name was listed for the COSUNA unit, then the undifferentiated conductivity for the group was used, if available from the Monte Carlo analysis. If it was not available, then a simple average of the COSUNA lithologies was used.

There is room for improvement with this method of assigning thermal conductivities to units. For example, a literature review for published values of thermal conductivity for each formation on a state-by-state basis could be conducted for more accurate values. The data from the ongoing West Virginia University thermal conductivity study (B. Anderson, personal communication,

2015) can be used to inform values to use for the Appalachian Basin. Adjustments in the thermal conductivity can also be made according to the depth of the unit.

Related Files:

1. Name: COSUNA_Columns_NY-PA-WV-VA-OH-KY-MD.xlsm

Fields:

Unit: The group, formation, member, or cohort names.

ColumnMin: The minimum thickness of the group, formation, member, or cohort based on the extent in the section (m)

Min: The minimum thickness of the group, formation, member, or cohort as listed (m)

Max: The maximum thickness of the group, formation, member, or cohort as listed (m)

Min(avg): The weighted average minimum thickness of the group, formation, member, or cohort from Equation 2 (m)

Max(avg): The weighted average maximum thickness of the group, formation, member, or cohort from Equation 2 (m)

Assumed: The assumed thickness of the unit. This is the average of the “Min(avg)” and “Max(avg)” (m)

Rock Type: The COSUNA listed rock type for the group, formation, or unit.

Shope Conductivity: The conductivity assigned in Shope (2012). (W/[m °C]) Only applies to NY and PA columns.

Beardsmore and Cull Conductivity: The conductivity assigned by using the Beardsmore and Cull conductivities (W/[m °C])

USGS Lithology: The lithology of the unit as listed on the USGS Mineral Resources website, specific to each state (USGS, 2014).

Example:

The assumed thickness accounts for the presence of multiple units during the same time period, units being in a portion of the section, and the minimum and maximum possible thickness of the unit in the section. For example, if a unit was listed as 5-10 m thick, but was present in only 50% of the column, then the “Column Min” would be 0 m, the “Unit Min” would be 5 m, the “Unit Max” would be 10 m, the “Min(avg)” would be 2.5 m, and the “Max(avg)” would be 5 m, and the “assumed” thickness would be 3.75 m.

Color Scheme:

The rock types are color coded according to a key in the far right of each COSUNA column. The color red is reserved as meaning “questionable”. For instance, columns that do not have Lower Paleozoic rocks (Table 2) are highlighted in red at the bottom of the column.

Rock Types	Color
Sandstone	Yellow
Shale, Mudstone, Siltstone	Light Gray
Interbedded Sandstone, Siltstone, Shale	Light Brown
Carbonate	Light Blue
Conglomerate	Orange
Evaporite	Pink
Metamorphic	Dark Brown
Volcanic	Light Green

2. Name: CarterConductivities.xls

Fields: See Table 3.

3. Name: AllCosunaSections.shp

Attribute Metadata:

COSUNA_ID: A unique 6-digit ID code has been assigned to each COSUNA section within the shapefile. The first two digits are the column number, the second two digits (01 or 02) indicate whether the COSUNA column may be found in the Northern Appalachian Region (AAPG, 1985a) (01) or in the Southern Appalachian Region (AAPG, 1985b) (02), and the final two digits (00, 01, or 02) indicate whether the column is for the East column (01), West column (02), or not listed (00). Only Virginia COSUNA columns stated East and West because a geographic split in the geology occurred as a result of major faults.

Name: The COSUNA Section name.

4. Name: TBRsedimentThickness

Description:

This is a map of sediment thickness derived from contours of the Precambrian basement that were developed by the Trenton-Black River (TBR) Project (WVGES, 2006). The Precambrian contours were relative to sea level, so the elevation of the Appalachian Basin had to be added to arrive at a sediment thickness map. The resulting map was selected over the more recent map

developed by Mooney (2011) because of the inclusion of the Rome Trough. A simple comparison of the TBR sediment thickness map to the actual sediment thickness in the favorite wells is provided in Figure A1. Based on these results, we are comfortable with the choice of the TBR sediment thickness map.

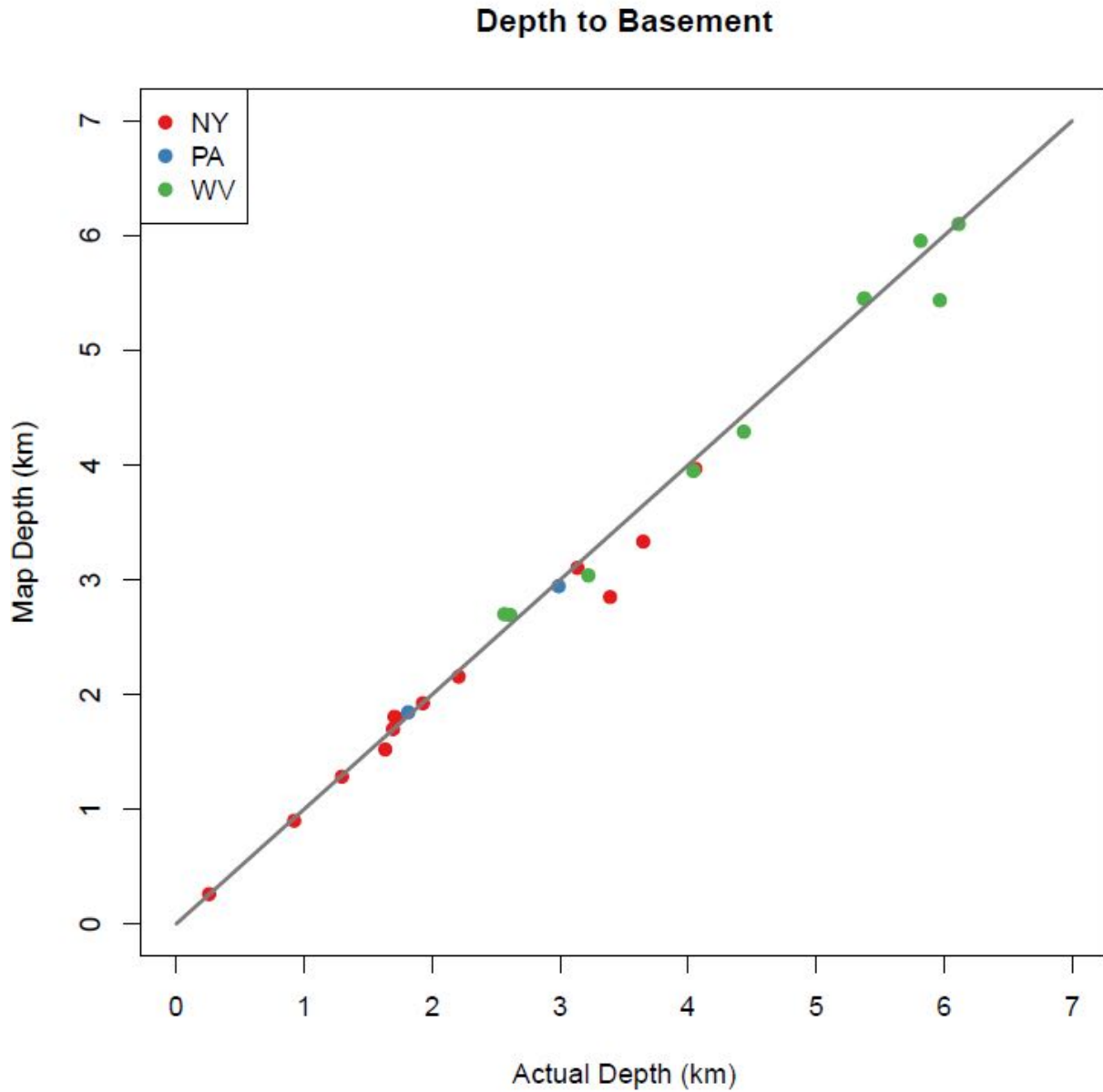


Figure A1. Comparison of TBR sediment thickness (Map Depth) to the actual sediment thickness from the subset of wells that reached basement rock. A 1:1 line is shown for reference. Depth to basement is the same as sediment thickness.

References:

- AAPG. (1985a). Northern Appalachian Region correlation chart. D.G. Patchen, K.L. Avary, and R.B. Erwin, regional coordinators.
- AAPG. (1985b). Southern Appalachian Region correlation chart. D.G. Patchen, K.L. Avary, and R.B. Erwin, regional coordinators.
- Aguirre, G.A., 2014. Geothermal resource assessment: A case study of spatial variability and uncertainty analysis for the states of New York and Pennsylvania. MS Thesis. Cornell University, Ithaca, NY.
- Beardsmore, G.R., and J.P. Cull. (2001). Crustal heat flow: A guide to measurement and modelling. Cambridge University Press.
- Birch, A. F., & Clark, H.: The Thermal Conductivity of Rocks and its Dependence Upon Temperature and Composition, *American Journal of Science*, 238(8), 529-558, (1940).
- Carter, L.S., Kelley, S.A., Blackwell, D.D., Naeser, N.D., 1998, Heat Flow and Thermal History of the Anadarko Basin, Oklahoma: AAPG Bulletin, v. 82, no. 2, p. 291-316.
- Cercone, K. R., D. Deming, & H.N. Pollack. (1996). Insulating effect of coals and black shales in the Appalachian Basin, Western Pennsylvania. *Organic Geochemistry*, 24(2), 243-249.
http://ac.els-cdn.com/0146638096000216/1-s2.0-0146638096000216-main.pdf?_tid=5d37a0e2-ea03-11e4-b2e4-00000aacb35d&acdnat=1429826269_52360d9754a8a01680ffc0885e5e06ab
- Childs, O.E.. (1985). Correlation of stratigraphic units of North America – COSUNA. *The American Association of Petroleum Geologists Bulletin*, V. 69, No. 2. P. 173-180
- Clauser, C. (2011). Thermal storage and transport properties of rocks, II: thermal conductivity and diffusivity. In *Encyclopedia of Solid Earth Geophysics* (pp. 1431-1448). Springer Netherlands.
- Frone and Blackwell, 2010. Geothermal Map of the Northeastern United States and the West Virginia Thermal Anomaly, *Geothermal Resources Council*, 34, 339-344.
- Harper, J.D., 2004, The Rome Trough in Pennsylvania. Speculation in the Absence of Non-Proprietary Seismic Data: AAPG Search and Discovery Article #90031, AAPG Eastern Section Meeting, Columbus, Ohio, October 3-5, 2004, downloaded from internet on 15 February 2015.
- Harris, D.C., J.A. Drahovzal, J.B. Hickman, B.C. Nuttall, M.T. Baranoski, and K.L. Avery. (2002). Rome Trough Consortium Final Report and Data Distribution.
- Horai, K. I. (1971). Thermal conductivity of rock-forming minerals. *Journal of Geophysical Research*, 76(5), 1278-1308.
<http://onlinelibrary.wiley.com/doi/10.1029/JB076i005p01278/epdf>
- Mølgaard, J. and W.W. Smeltzer. (1971). Thermal Conductivity of Magnetite and Hematite, *Journal of Applied Physics*, 42, 3644-3647. DOI:<http://dx.doi.org/10.1063/1.1660785>
- Mooney, J. (2011). Sediment thickness of North America and neighboring regions. *In Technical Report: Central and Eastern United States Seismic Source Characterization for Nuclear Facilities. Appendix A: Description of the CEUS SSC Project Database, Figure A-14, File: CEUS_sed_thickness_USGS_R0.tif.* EPRI, Pala Alto, CA, U.S. DOE, and U.S. NRC: 2012.
- Repetski, J.E., R.T. Ryder, D.J. Weary, A.G. Harris, and M.H. Trippi. (2008). Thermal Maturity Patterns (CAI and %Ro) in Upper Ordovician and Devonian Rocks of the Appalachian Basin: A Major Revision of USGS Map I-917-E Using New Subsurface Collections. USGS Scientific Investigations Map 3006. Reston, Virginia.

- Ryder, R.T.. (1992). Stratigraphic framework of Cambrian and Ordovician rocks in the Central Appalachian Basin from Lake County, Ohio, to Juniata County, Pennsylvania. IMAP 2200.
- Ryder, R.T., C.S. Swezey, R.D. Crangle Jr., and M.H. Trippi. (2008). Geologic Cross Section *E–E'* through the Appalachian Basin from the Findlay Arch, Wood County, Ohio, to the Valley and Ridge Province, Pendleton County, West Virginia. IMAP 2985.
- Shope, E.N.. (2012). A detailed approach to low-grade geothermal resources in the Appalachian Basin of New York and Pennsylvania: Heterogeneities within the geologic model and their effect on geothermal resource assessment. MS Thesis. Cornell University.
- Smith, J.D.. (2016). Assignment of thermal conductivity stratigraphy to individual wells using COSUNA columns. *Chapter 2 in Analytical and geostatistical heat flow modelling for geothermal resource reconnaissance applied in the Appalachian Basin*. MS Thesis. Cornell University, Ithaca, NY.
- Stutz, G.R., 2012. Development, analysis, and application of a well by well method for estimating surface heat flow for regional geothermal resource assessment: M.S. thesis, Ithaca, NY, USA, Cornell University, 161 p.
- United States Geological Survey (USGS). (2014). Geologic units in West Virginia (state in United States). Mineral Resources On-Line Spatial Data.
<http://mrdata.usgs.gov/geology/state/fips-unit.php?state=WV>
- West Virginia Geological and Economic Survey (WVGES). (2006). Trenton Black River Project. Data [Precambrian structure contours] available online
<http://www.wvgs.wvnet.edu/www/tbr/resources.asp>. Map viewer available online
http://ims.wvgs.wvnet.edu/TBR_ver3/viewer.htm.
- Wilson, T. H., 2000, Seismic evaluation of differential tectonic subsidence, compaction, and loading in an interior basin: AAPG Bulletin, v. 84, no. 3, p. 376-398

Memo'7: Tests of simplified conductivity stratigraphy by Monte Carlo analysis'p'I RHC/CD

Authors: Calvin Whealton, Teresa Jordan, Zach Frone

Executive Summary

Monte Carlo analysis was used to examine the implications of using the COSUNA approximations versus using more detailed information for a set of 77 wells chosen across the region. For each of the wells there were three cases for the stratigraphic columns: detailed stratigraphy with Carter conductivities, COSUNA stratigraphy with Carter et al. (1998) conductivities, and COSUNA stratigraphy with Beardsmore and Cull (2001) conductivities. All stratigraphic assumptions were tested with 50,000 Monte Carlo replicates with most parameters being modeled as triangular distributions.

The results of the analysis are that the differences between the COSUNA stratigraphy with Carter conductivities and the detailed stratigraphy are generally minor when compared over the whole region. When comparing surface heat flow, if there is a systematic difference it is probably around 2-5 mW/m², which is typically around 10% of the predicted value. The uncertainty of the two methods for a single well is also close on average, but the actual data shows more noise. When predicting temperature at 3 km, the two methods were typically within about 6 °C of each other when comparing their mean prediction, which illustrates the robustness of the COSUNA approximation with Carter et al. (1998) conductivities for this region.

Part 1: Acquisition of Detailed Well-Specific Conductivity Stratigraphy Columns

Criteria for inclusion of a given well:

- regional expert geologists (e.g., state geological survey staff or USGS geologists) have made available interpretation of formation tops for these wells
- deep wells (as close to basement as possible in a given county)
- widely and semi-uniformly distributed
- BHT available and judged to be relatively reliable

Data Sources

- state geological survey reports and publications
- Cornell, West Virginia University, and Southern Methodist University prior studies based on a given borehole
- USGS cross sections and specialty reports
- state well information sites (WV Pipeline, NY ESOGIS, PAIRIS-WIS)

Stages of selection work

- from lists of deep wells and county names, looked up which ones have geological reports of depths to formation tops.
- assembled list of >200 candidate wells
- compared the candidates list to wells in NGDS and other sources of BHTs, omitting from the “candidates” list those for which there are not BHT data
- after initially finding no matches of stratigraphically described deep wells and wells with reported BHTs for WV, went into WV Pipeline and well log headers, to add BHT information as another category of data for the WV candidates
- the subset with BHTs plus stratigraphic data available became the adopted well data set

State-specific information sources:

- New York State
 - ESOGIS well files
 - formation ID’s that needed de-coding, and their lithologies:

	James Leone, NYSGS suggestion for Rickard identification scheme	Rickard 1964 usage
Irondequoit		not used (seems inappropriate as this name used for a Silurian formation)
DK	Dunkirk shale	Dunkirk shale
PC	Pipe Creek shale	Pipe Creek shale
SB	Scraggy beds, marks Rhinestreet/Angola contact	not used
J	marker bed within Rhinestreet	not used
CO	marker bed within Rhinestreet	not used
BB	marker bed within Rhinestreet	not used
RG	Rhinestreet group?	Roricks Glen
DH	Devonian Hamilton (not sensible given stratigraphic order in which DH occurs)	Dunn Hill
CQ	Cashaqua shale	Cashaqua
SG	Sonyea Group	Sonyea Group (Cashaqua underlain by Middlesex)
M	Middlesex	Middlesex
GG	Genesee Group	Genesee Group
WR	West River shale (upper	West River

	formation in Genesee Group)	
PY	Penn Yan shale	Penn Yan
HP	a marker within the Genesee group	not used
G	Geneseo shale	Geneseo
TULLY-GILBOA		perhaps a lithologically mixed siliciclastic-limestone

- Sources consulted for lithologic information:
 - Hill, Lombardi, Martin, Fractured shale gas potential in New York: NYSERDA
 - Smith, G., 2002, Conneaut sequence, NYSERDA
 - Lugert et al., NYSERDA report
 - Young, W.H., Jr., and Krediler, W.L., 1957, NYSGA
 - Rickard, 1964, New York State Museum and Science Service Geological Survey, Map and Chart Series, no. 4
 - NY DEC SGEIS (http://www.dec.ny.gov/docs/materials_minerals_pdf/ogdsgeischap4.pdf)
- Pennsylvania wells
 - file of formation tops provided by Michele Cooney of PA geological survey
 - Sources of lithologies:
 - U.S. G.S. Mineral Resources On-Line Spatial Data (for example, <http://mrdata.usgs.gov/geology/state/fips-unit.php?code=f42115>)
- West Virginia wells
 - Pipeline (online data management system)
 - <http://www.wvgs.wvnet.edu/oginfo/pipeline/pipeline2.asp>
 - Sources of lithologies:
 - U.S. G.S. Mineral Resources On-Line Spatial Data (for example, <http://mrdata.usgs.gov/geology/state/fips-unit.php?code=f54015>)

Part 2: Analysis

Well Locations & Sediment Depth

The wells for this analysis are located as shown in Figure 1. In total 77 of the original 78 wells were used because there was not a bottom-hole temperature (BHTs) for one well. One of the wells in West Virginia had two BHTs so these were analyzed separately. Figure 2 compares the sediment depth from the sediment thickness map versus those from the detailed stratigraphy for wells that penetrated the basement. Figure 2 shows that the map sediment depth is generally very close to the true sediment depth.

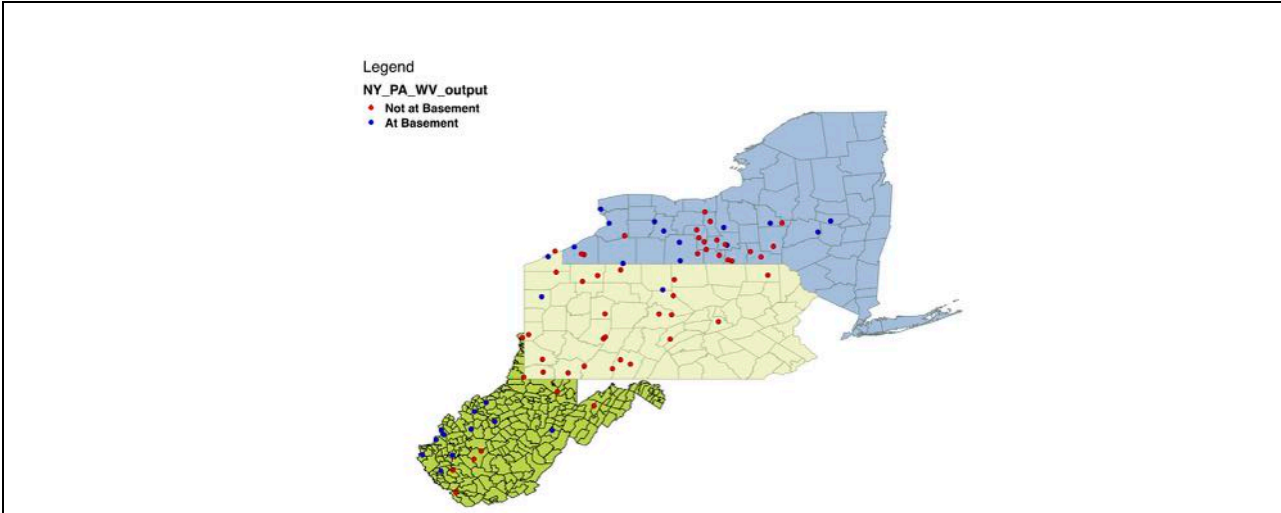


Figure 1: Map of well locations for the sensitivity analysis. The points are color-coded with blue being at basement and red not being at the basement.

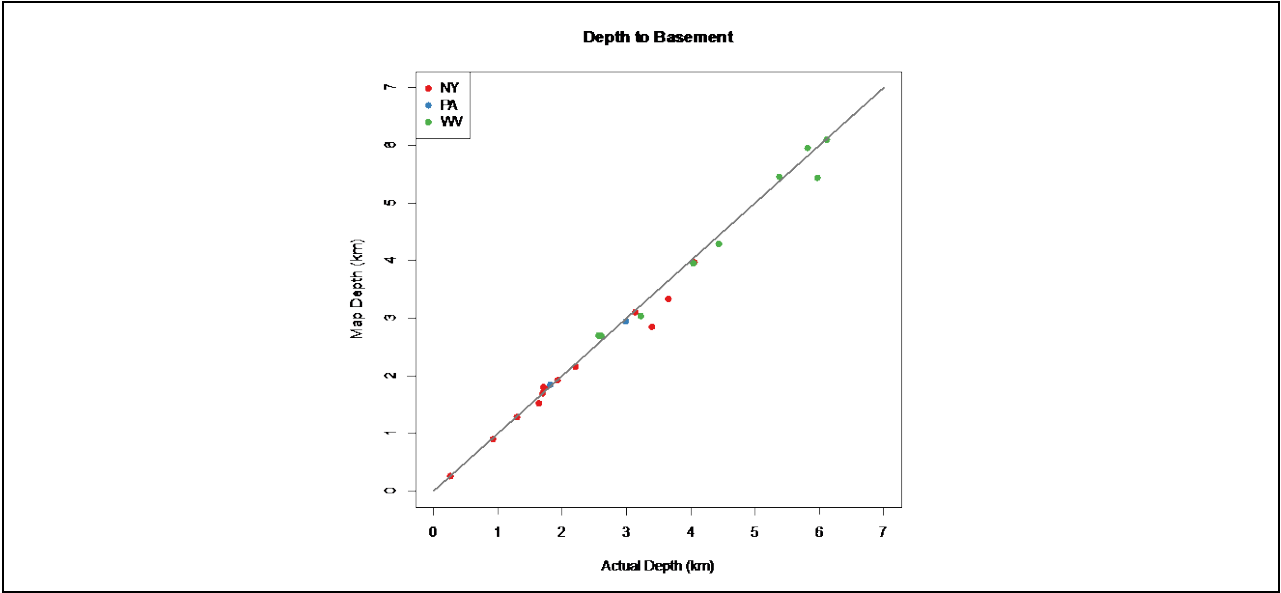


Figure 2: Plot of depth to basement from the sediment thickness map used versus from the depth to sediment for the detailed stratigraphy wells that reached basement. The black line is for perfect prediction (45°). New York wells are in thinner sediments and West Virginia wells are in thicker sediments.

Stratigraphy Sources

The stratigraphic columns can be divided into two types: detailed stratigraphy and COSUNA stratigraphy. More details are provided on both of these types are provided below.

COSUNA Stratigraphy

COSUNA (Correlation of Stratigraphic Units of North America) columns provide an approximate stratigraphy for generally multi-county areas. Jared Smith converted the original COSUNA documents into spreadsheets that contained information for each of the listed units (more details in cu.app-basin-gpfa.us/cu/GIS/COSUNA/COSUNA_Documentation_final.docx). The variables of interest are the thickness and the conductivity variables. The thicknesses used are the “Column Min”, “Max”, and “Assumed”, which are used to define the lower bound, upper bound, and most likely values of a triangular distribution, respectively.

There are multiple values of conductivities depending on which reference values one uses. In this analysis there are two values, the Beardsmore and Cull. and the Carter values. Carter values are for the Anadarko Basin, which is considered a sister basin to the Appalachian Basin. Beardsmore et al. values are essentially standard values for a given rock type, so they will not be as reflective of the burial history in the Appalachian Basin.

Detailed Stratigraphy

For the selected set of wells (part 1), the files contained depth to formation top, conductivity, and conductivity standard deviation. The conductivities are based on the values from Carter (see Memo on conductivities). The thickness of each unit was calculated as the difference of the depth to formation top of the unit below it and its own depth to formation top. In some cases the detailed stratigraphic information was not complete to the basement either because the well did not reach basement or because there were some intermediate layers that with unassigned depths.

When the well did not reach basement, the thickness of the last recorded formation (depth of the formation top recorded) was estimated and the remaining depth to basement was assigned as a single unit. To estimate the thickness of the last recorded formation the depth to the formation top was multiplied by the assumed thickness of the formation in the COSUNA column and divided by the depth to the formation top in the COSUNA column. For instance, if the depth to formation top in the detailed stratigraphy was 2,000 m and the depth to the formation top in the COSUNA column is 3,000 m and the thickness in the COSUNA column is 30 m, then the estimated thickness in the detailed stratigraphy would be $(2,000 * 30 / 3,000) = 20$ m. The remaining thickness between the filled-in thickness and the basement is assigned a single thickness unit. For instance, if there were 500 m of missing thickness between the last formation top and the basement (evaluated from sediment thickness map), and the last formation was filled-in with 20 m of thickness, then $500 - 20 = 480$ m was assigned as a single unit.

There were a few special cases for filling-in the depths. First, in some instances the thickness of the detailed stratigraphic column exceeds the thickness of the sediments from the map (depth to basement map layer). If the estimated thickness of the last formation layer caused the total thickness to be greater than the map sediment thickness, then the missing unit's thickness was set to the difference between the formation top and the map sediment thickness. Secondly, when only the last unit has unknown thickness (for instance the Potsdam in much of NY), then its thickness was set to the difference of the map sediment thickness and the formation top. Thirdly,

if the detailed stratigraphy divided individual groups (several units) into smaller units but the COSUNA column only listed only the group, then the thickness of the group was estimated and the missing unit thickness was the group thickness less the thickness of the other units in the group that were recorded. So if the estimated thickness of the group was 400 m and there were three units in that group, two with known thicknesses from the detailed stratigraphy of 100 m and 125 m, then the estimated thickness of the unknown unit would be $400 - 100 - 125 = 175$ m.

In a few cases there were missing thicknesses of intermediate units (defined formation tops above and below the units, but not of the unit or units in question). The first method of addressing the missing intermediate layers was to calculate the total missing thickness of the layers and then multiplying the total thickness by the percentage of thickness for each layer in the assumed COSUNA stratigraphy. When the COSUNA stratigraphy did not provide enough information detailed stratigraphy columns in the same COSUNA section were used to estimate the missing intermediate thicknesses based on the percentage of the thickness.

For each unit we assigned values for the conductivity and the standard deviation of the conductivity. These conductivities are based on the Carter conductivities from the Anadarko Basin, because those strata underwent similar extents of burial and are roughly as old as is the Appalachian Basin.

Distributional Assumptions

This section outlines the distributional assumptions for the parameters in the Monte Carlo experiment. UB, LB, and ML stand for upper bound, lower bound, and most likely (peak), respectively. Most distributions were chosen to be symmetric triangular distributions because they are bounded on reasonable ranges (no negative values) and they reasonably describe a peaked distribution. Most of the COSUNA thicknesses were also symmetric, but they were skewed when the column minimum thickness was not in the same range as the maximum thickness.

Note that the uncorrected bottom-hole temperature (BHT) was used because the BHT corrections are not finalized at the moment and the verification that the model can reproduce the BHT down the borehole does not depend on the BHT measurement.

Variable (units)	Distribution	Parameters	Notes
Bottom-Hole Temperature (°C) [uncorrected]	Triangular-Symmetric	UB = BHT + max(5, 0.1*BHT) LB = BHT - max(5, 0.1*BHT)	Shallow data often has large spread, hence the 5°C minimum; Uncertainty increases with depth because of BHT correction uncertainty
Surface Temperature (°C)	Triangular-Symmetric	UB = ST + 1 LB = ST - 1	Bounds set as +/- 1°C from the map value
Mantle Heat Flow (mW/m ²)	Triangular-Symmetric	UB = 30*1.2 LB = 30*0.8	Mantle heat flow bounds are approximately the expected range
Radiogenic Heat	Triangular-	UB = 1*1.2	Typical value is about 1, used

Production ($\mu\text{W}/\text{m}^3$)	Symmetric	LB = $1*0.8$	20% as the bounds
Detailed Stratigraphy Conductivity k ($\text{W}/\text{m}\cdot^\circ\text{C}$)	Triangular-Symmetric	UB = $k + 2*SD(k)$ LB = $k - 2*SD(k)$	Using +/- 2 standard deviations (SD) of the conductivity
COSUNA Stratigraphy Conductivity k ($\text{W}/\text{m}\cdot^\circ\text{C}$)	Triangular-Symmetric	UB = $1.4*k$ LB = $0.6*k$	Using +/- 40% of the conductivity for the bounds because for the Carter values the standard deviation is about 18% of the mean conductivity
COSUNA Thickness (m)	Triangular	UB = Max LB = Column Min ML = Assumed	Used column min and maximum values to defined bounds and the assumed value should be the most likely

Monte Carlo Experiment

The Monte Carlo experiment was designed to test whether there are any systematic differences in the COSUNA approximations and the detailed stratigraphy. This section outlines the generation of the replicates for all of the wells.

For a well the replicates of for the detailed stratigraphy, COSUNA Carter, and COSUNA Beardsmore and Cull were all generated at once. Figure 1 represents the generation of the data. When possible, all of the random inputs were kept the same across the different stratigraphy assumptions. For instance, all of the Monte Carlo replicates for a single well used the same set of BHTs and surface temperature inputs. Additionally, both of the COSUNA variations used the same thickness values. Holding as many parameters the same across the variables allows for a paired test, which should have higher power.

Replicate	BHT	Surface Temp	...	Detailed Conductivity			COSUNA Carter Conductivity			COSUNA Beardsmore and Cull Conductivity			COSUNA Thickness		
				1	...	n	1	...	m	1	...	m	1	...	m
1					
2					
...					
50000					

Figure 3: Representation of the generation of the replicates for the Monte Carlo experiment. The colors are for different blocks of data. There are n units in the detailed stratigraphy and m units in the COSUNA stratigraphy.

Standard uniform variables were generated for all of the variables. The standard uniform variables were then converted into the distribution (see section “Distributional Assumptions”)

using the inverse cumulative distribution function for the variable. The seed for each well is separate and based on the depth of the well, which allows reproducibility of the results without causing all of the random variables across the wells to be linked.

All of the output was calculated based on code developed by Jared Smith and Frank Horowitz (bitbucket.org/geothermalcode/jaredthermalconductivity, special functions for sensitivity analysis are in the branch 'calvinSA').

Individual Well Statistics

The statistics for an individual well are based on the 50,000 Monte Carlo replicates for the three stratigraphy assumptions of that well. The statistics calculated for the individual wells are:

- Mean (average, measure of location)
- Median (middle of the sorted values, robust measure of location, 50th percentile)
- Standard Deviation (measure of spread)
- Interquartile Range (IQR, robust measure of spread, difference of the 75th and 25th percentiles)

These statistics include both standard and robust measures of location and spread. The units of all of these statistics will be the same as the units of the original output variable.

For the analysis the surface heat flow and the temperature at 3 km are considered. The surface heat flow depends on the BHT, surface temperature, and the “average” conductivity between the BHT and the surface (the conductivity is calculated using a harmonic average accounting for thickness of formation). Temperature at 3 km represents a reasonable estimate of the depth range considered for development.

Figure 2 shows some sample boxplots of the output of the Monte Carlo experiment for different wells. The top two boxplots are for Surface Heat flow and the bottom two boxplots are for temperature at three kilometers.

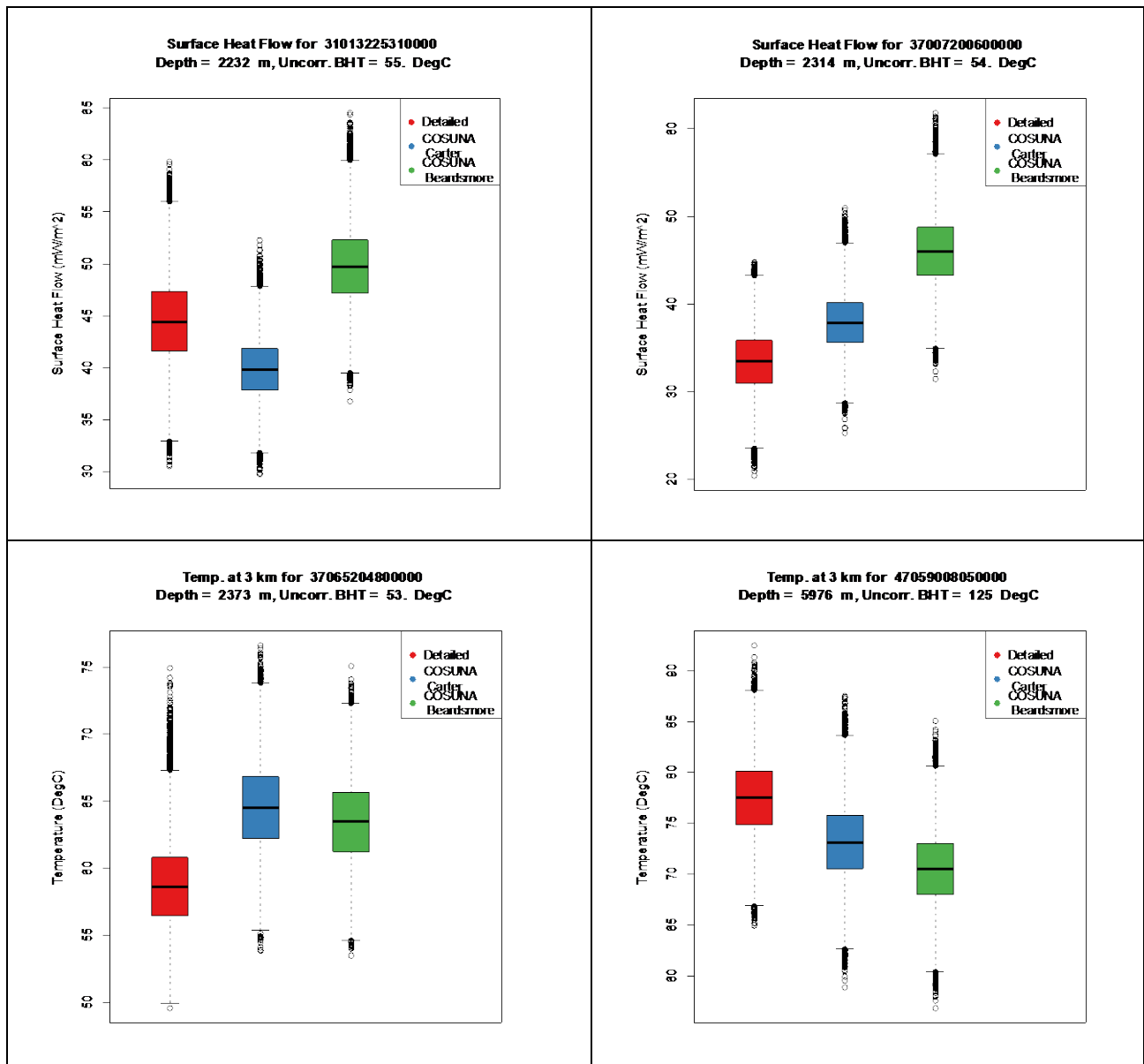


Figure 4: Examples of boxplots showing boxplots of the distribution of the results of 50,000 Monte Carlo replicates for each well stratigraphy/conductivity assumption (each boxplot is 50,000 points). Red is for the detailed stratigraphy, blue is for the COSUNA stratigraphy with Carter conductivities, and green is for the COSUNA stratigraphy with Beardsmore and Cull conductivities. The box is defined from the 25th to 75th percentiles with the middle line at the median (50th percentile). The whiskers extend up to 1.5 times the interquartile range.

Region-Wide Analysis

The goal of this section is to examine whether there were any systematic differences when using the stratigraphic assumptions for surface heat flow or temperature at 3 km. The main questions addressed are:

1. Are there any large systematic biases?
2. Are there any large differences in uncertainty and how does depth impact this?
3. Robustness in predicting temperature at depth?

Systematic Biases

Figure 5 shows plots of the mean and the median surface heat flow for the wells. The mean and the median for each point are calculated based on the Monte Carlo replicates for that point. Generally, the points seem to be clustered around the perfect prediction line (in black). If there is a systematic bias it is probably minor around 2-5 mW/m². Comparing the two plots in Figure 5 also shows that the distributions are fairly well behaved because the mean and median plots look very similar, indicating fairly symmetric distributions.

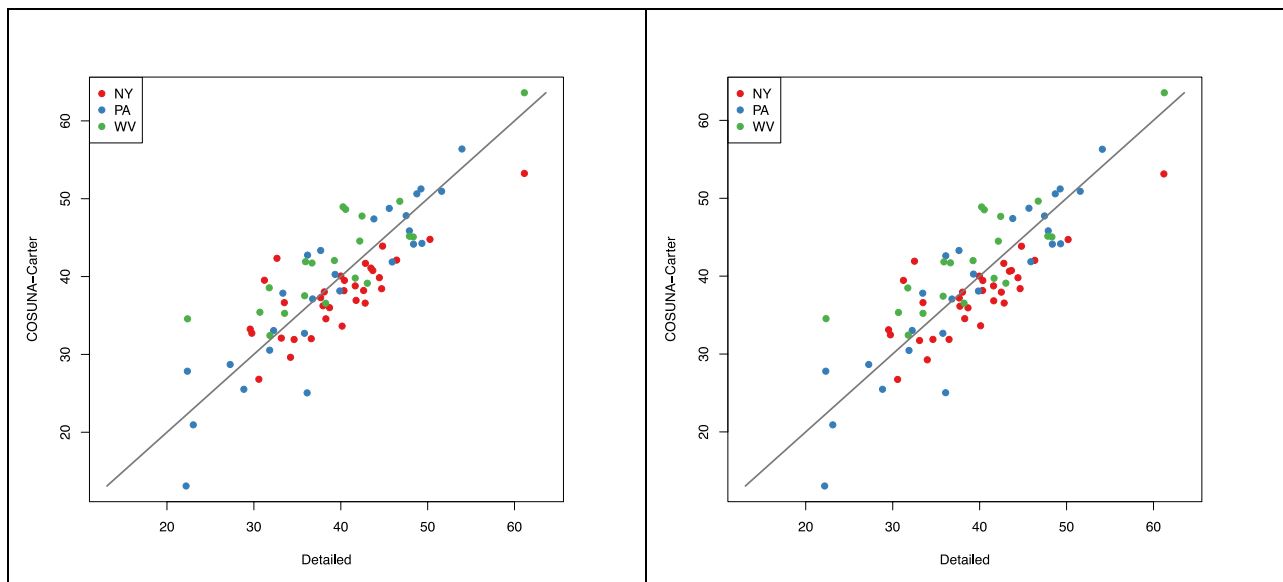


Figure 5: Plots of mean (left) and median (right) surface heat flow when using Detailed Stratigraphy and COSUNA Stratigraphy with Carter Conductivities. Points are color-coded by state (NY=red, PA=blue, WV=green). The black line is the 45° line for perfect matches.

Differences Uncertainty (Spread)

Figure 6 plots the uncertainty (spread) of the distributions of the Detailed Stratigraphy and COSUNA Stratigraphy with Carter conductivities against each other. Generally, the two plots look very similar, which is an indication that the distributions are well behaved and do not have very fat tails. If the distributions were perfectly normal, then the interquartile range would be about 1.35 times the median, which explains the difference in scale of the two figures. The measures of spread seem to be noisier around the prediction line than the mean or median results, but they still seem to be clustered around the line.

Figure 7 shows that as the depth of the bottom-hole temperature (BHT) increases, the uncertainty in the surface heat flow decreases until around 2000 m, at which point it stabilizes. Part of the reason for this behavior is probably due to the assumption of the BHT distribution, which was fairly wide even at shallow depths to reflect that shallow data is often very noisy. As the BHT becomes deeper, the bounds are specified as a percentage of the BHT value, which means the uncertainty is instant relative to the BHT value.

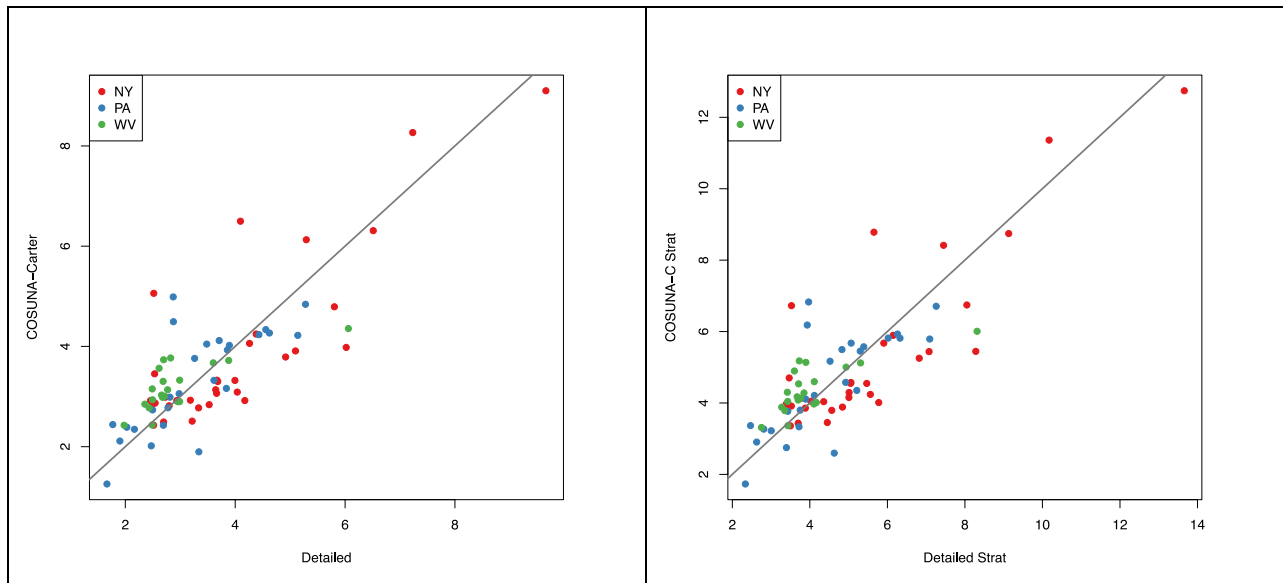


Figure 6: Plots of standard deviation (left) and interquartile range (right) surface heat flow when using Detailed Stratigraphy and COSUNA Stratigraphy with Carter Conductivities. Points are color-coded by state (NY=red, PA=blue, WV=green). The black line is the 45° line for perfect matches.

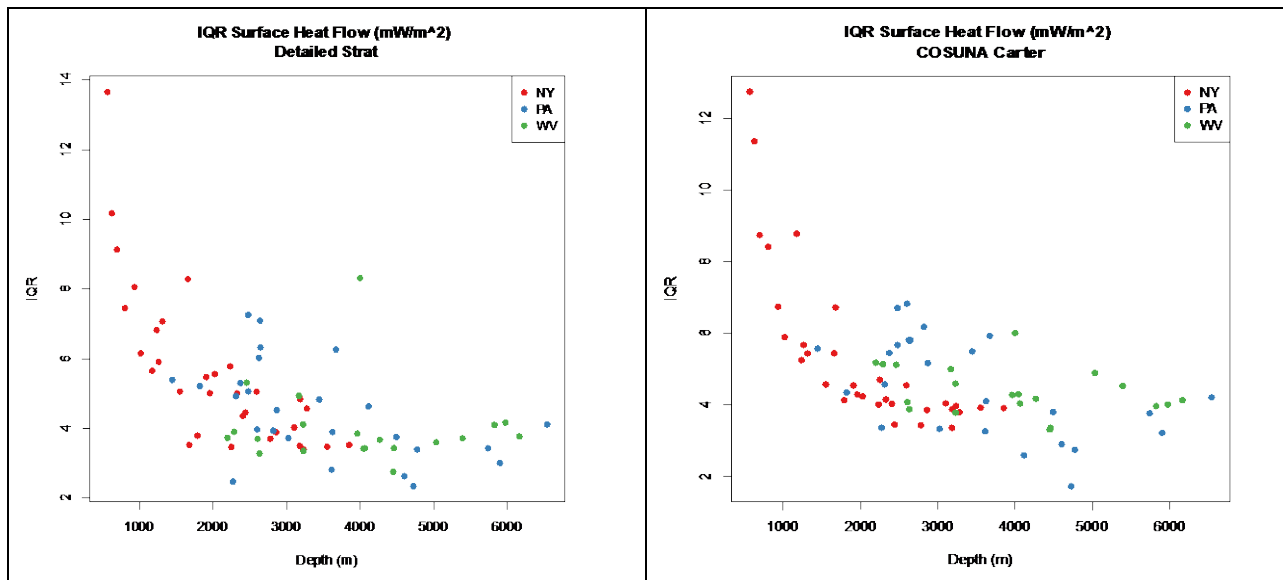


Figure 7: Plots of interquartile range (IQR) of surface heat flow for the Detailed Stratigraphy (left) and the COSUNA Stratigraphy with Carter conductivities (right). The horizontal axis is

the depth of the BHT measurement. Points are color-coded by state (NY=red, PA=blue, WV=green). The black line is the 45° line for perfect matches.

Robustness in predicting temperature at depth

Figure 8 shows the differences in the predicted mean temperature at 3 km for the wells in the Monte Carlo study (mean of 50,000 replicates) for the assumptions of Detailed Stratigraphy and COSUNA stratigraphy with Carter conductivities. Generally, the COSUNA-Carter approximation is very robust in the sense that the estimated temperature at depth is within 6 °C of the Detailed Stratigraphy estimation. It is difficult to determine if there is any difference in spread when the Detailed stratigraphy is known at the depth of estimation (BHTs deeper than 3 km) versus when only the upper portions of the detailed stratigraphy are known and missing units are appended to the detailed stratigraphy (BHTs less than 3 km).

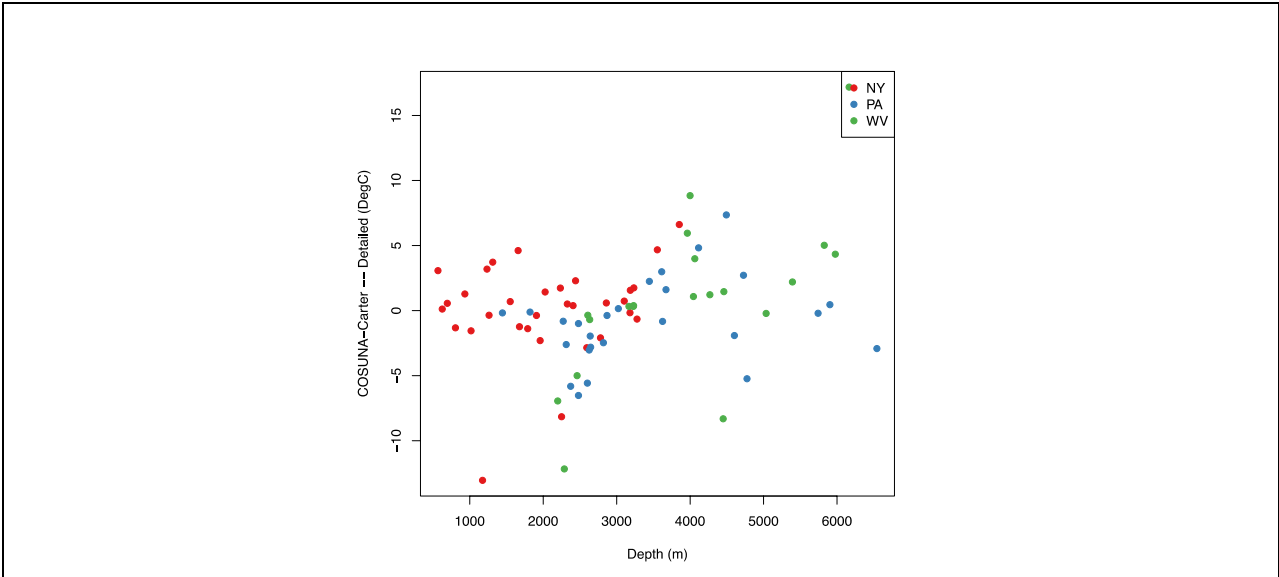


Figure 8: Plots of the difference in the predicted temperature at 3 km based on the depth of the BHT measurement. When BHT depth is greater than 3 km the detailed stratigraphy is know. When the BHT depth is less than 3 km only the upper portions of the detailed stratigraphy are known and the lower portions are assumed.

References

Beardsmore, G.R., and J.P. Cull. (2001). Crustal heat flow: A guide to measurement and modelling. Cambridge University Press.

Carter, L. S., Kelley, S. A., Blackwell, D. D., and Naeser, N. D., 1998, Heat flow and thermal history of the Anadarko Basin, Oklahoma: AAPG Bulletin, v. 82, no. 2, p. 291-316.

Memo 6: Thermal Outlier Assessment in GPFA-AB

To: Appalachian Basin Geothermal Play Fairway Analysis Group

From: Calvin Whealton and Jerry Stedinger

Date: February 19, 2015

Subject: Outlier Identification Procedure

The Appalachian Basin Geothermal Play Fairway Analysis (AB-GPFA) must determine which algorithm should be used to identify outliers in the geospatial datasets. Outliers pose a problem for non-robust regression schemes because they would have high squared residuals. Many regression techniques seek to minimize the squared residuals, so an outlier can have undue influence on the results of the analysis.

This memo outlines the recommended outlier detection algorithm. Appendix 1 outlines the previous work on outlier algorithms for the NY and PA geothermal dataset. Appendix 2 illustrates the sensitivity of the final results to algorithm parameters over a reasonable range of values. Appendix 3 provides Monte Carlo type I error rates for different distributions type I error rates when the distribution parameters are known.

Outliers can be defined as “an observation (or subset of observations) which appears to be inconsistent with the remainder of that set of data” (Barnett and Lewis, 1994, p. 7). The following terms are defined below for use in the memo:

- *Global*: relating to the whole dataset, irrespective of location
- *Local*: relating to a subset of the data defined by a spatial relationship (e.g. 25 closest observations to the nearest point, points within 16 km of a point, etc.)
- *Sparse*: areas where there's insufficient data to evaluate a point to see if it is an outlier (e.g. only 4 local points if criterion is at least 25 local points)

The asymmetric boxplot algorithm used by Aguirre (2014) calculates upper and lower bounds from the sample quartiles, as defined in equations 1 and 2.

$$B_{lower} = Q_{0.25} - k(Q_{0.5} - Q_{0.25}) \quad [1]$$

$$B_{upper} = Q_{0.75} + k(Q_{0.75} - Q_{0.5}) \quad [2]$$

where

- $Q_{0.25}$ is the lower quartile,
- $Q_{0.75}$ is the upper quartile,
- $Q_{0.5}$ is the median,
- B_{lower} is the lower bound,
- B_{upper} is the upper bound, and
- k is a constant (standard value of 3).

Points outside the bounds are considered outliers. Aguirre (2014) calculates bounds both globally and locally, and only removed points which were both local and global outliers. She performed the global outlier test first, given the calculated values of B_{lower} and B_{upper} computed for the entire region. This greatly reduced the number of times that the local outlier computation was required.

We recommend that GPFA-AB group apply this asymmetric boxplot rule *only locally* with a value of the constant, $k = 3$. Additionally, the definition of local should be changed to the nearest 25 points provided that the points are within 16 km of the point being tested. If there are not 25 points within 16 km, then no outlier test is performed. Requiring points to be both local and global outliers will bias cold areas to be warmer and warm areas to be colder. Also, using 25 points allows a reasonable comparison with expected identification rates for several null distributions (see appendix 3). Using the Cornell NY and PA dataset of 8919 observations (Cornell University 2014) with Harrison corrected gradient and the recommended algorithm parameters, 6.8% (607 observations) were in sparse areas (fewer than 25 points within 16 km); 7.1% of the total dataset (629 observations) were removed as outliers (see appendix 2).

Encl.:

Appendix 1: Summary of Outlier Algorithms Used at Cornell
Appendix 2: Sensitivity Analysis of Recommended Algorithm
Appendix 3: Type I Error Rates
References

Appendix 1: Summary of Outlier Algorithms Used at Cornell

Work at Cornell University has used outlier detection algorithms to remove potentially rogue observations before spatial regression. Rogue observations could have a high squared residual value, which can allow rogue observations to unduly influence the fit of non-robust spatial interpolation techniques.

Aguirre et al. (2013) broke the outlier analysis into global and local identification steps. For global analysis they considered a boxplot and asymmetric boxplot rules along with several other algorithms. Both of the boxplot-based algorithms use the quartiles of the data. The asymmetric boxplot rule was chosen because the global data seemed skewed and the asymmetric boxplot rule was robust to asymmetric data. They investigated several algorithms for local outlier analysis as well, but chose a method where the data was gridded in 16 km by 16 km blocks (other block sizes were also tested). In this early version of local outlier detection, local outliers were identified as more than three standard deviations from the block mean. The block standard deviation and the block mean were calculated for each block and only applied to points within that block. Although not explicitly mentioned, they do discuss that blocks with fewer than 20 points were not effective.

Aguirre (2014) continued to conduct global outlier analysis with the asymmetric boxplot rule. The final algorithm used the asymmetric boxplot rule for both local and global analysis. This allowed for a more robust local outlier detection algorithm because the standard deviation method used in her previous work was not robust. Only observations that were both local and global outliers and were in a box (32 km by 32 km) with 25 points were removed as outliers.

Aguirre's analyses are conservative because only points that are unusual both locally and globally are removed as outliers. If there is little signal (spatial trend) in the data then this is reasonable. Testing globally and then only testing global outliers to see if they are local outliers might reduce computation time, but the computational savings would be in the order of minutes. Given that the global outlier bounds differ by a factor of approximately 3, it seems that there could be signal of spatial variability in the data. If this were the case it would be best to use only a local analysis. Otherwise, "cold" areas will be biased warm because their coldest points will be both local and global outliers. Similarly, "warm" areas will be biased cold. Completing a local analysis would be robust to signal in the data, provided the local region is small enough. In the Cornell dataset about one quarter of the data comes from a single county in New York (Cornell University 2014). Given the large proportion of the data from a single county and the small variability within that one county, the global outlier test bounds could easily have been biased by this one county with Aguirre's methods. Choosing points that were spatially representative of the area in our dataset might have been more robust for determining global outlier bounds.

Appendix 2

Sensitivity Analysis of Recommended Algorithm

In the algorithm that we recommend there are essentially two parameters: the points used for a local test and the maximum radius one at which one can take points. To test the sensitivity of the algorithm to these two parameters we ran the algorithm on the Cornell dataset of 8,919 observations (Cornell University 2014). The variable tested was a gradient based on the Harrison correction (negative and past peak values used) and a uniform surface temperature of 9 °C. Figure 2.1 displays the results. Locations were projected from WGS84 into UTM 18N.

Figure 2.1 shows that for a large number of points and a small maximum radius, very little of the dataset can be evaluated as outliers (bottom right). As the radius increases and the points criterion decreases a greater fraction of the dataset can be tested as outliers. The increase in the percentage of data considered outliers grows from the bottom right because more of the dataset can be tested. However, eventually the increase will stop because 2.3% of the data is considered as outliers in a global test (when the local area is large the test converges to the global test). For instance, when the point's criterion was 1,000 and the radius criterion was 200 km, only 4.4% of the data was considered outliers. Note in the upper right hand portion of the graph the proportion of data removed as outliers is approximately twice what one would expect for normal data (6-8% versus 3% for normal, see table 3.1). The percentage of outliers identified is closer to what one would expect from a fairly fat-tailed kurtotic Student t distribution.

Based on these results it seems reasonable to choose the points criterion as 25 and the radius criterion as 16 km. This will be close to the parameters used by Aguirre (2014), except in her algorithm the grid spacing was 32 km. When the 25 points and 16 km radius were applied to the test dataset, this left 6.8% (607 observations) in sparse areas. In total, 7.1% of the whole dataset (629 observations) were removed as outliers. It is likely that some of the data in sparse areas would be omitted for other reasons, including not enough points in the county or the points are outside our area of interest.

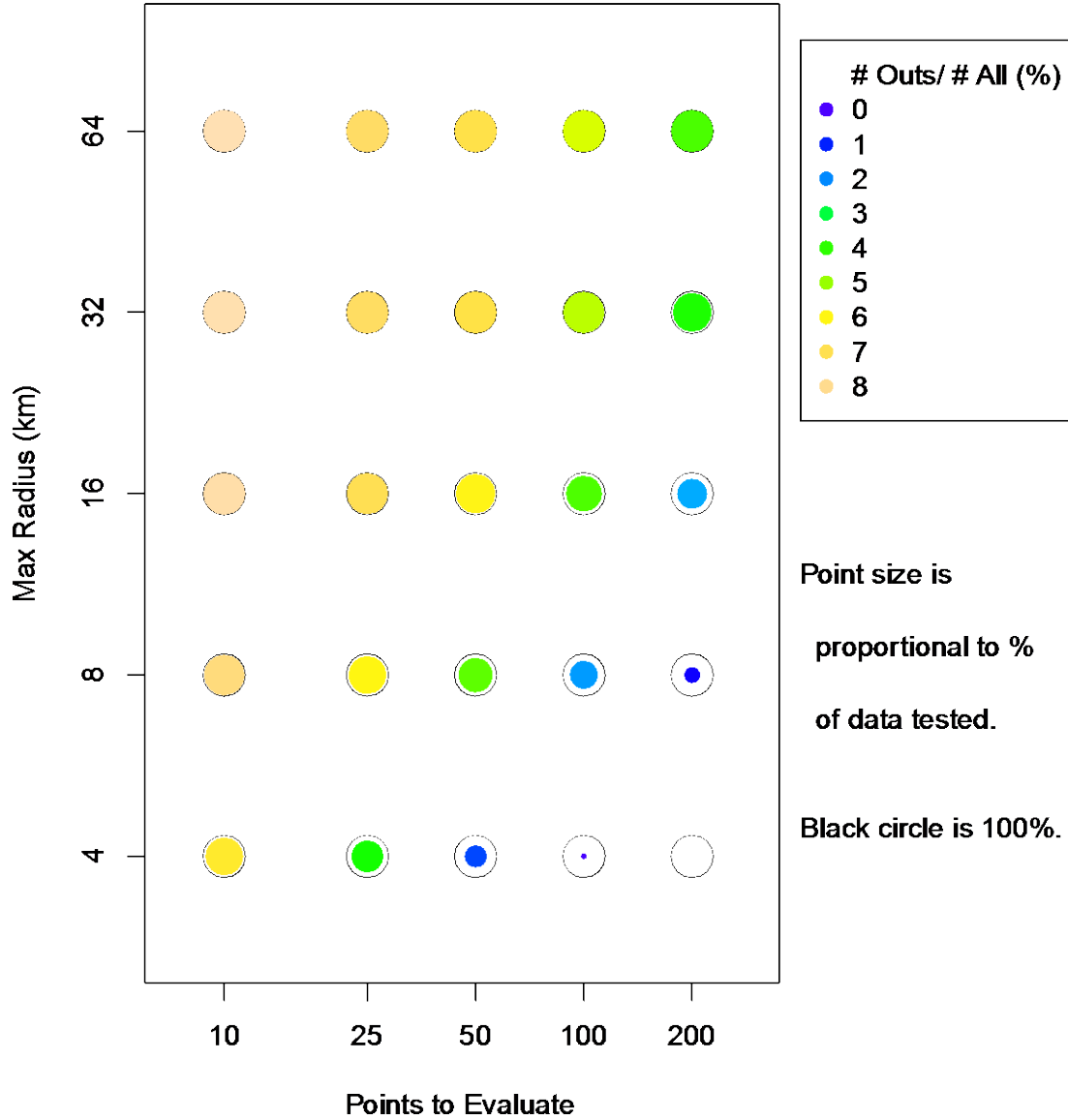


Figure 2.1: Plot showing the impact of the required number of points to evaluate a local outlier (horizontal axis) and the maximum radius at which points can be taken (vertical axis) on the percentage of the data set tested for local outliers (size of symbols) and the percentage of points considered outliers (color of symbol). The percentage of points considered outliers is relative to the number of points in the original dataset. The black circles represent 100% of the data being tested by the outlier algorithm. The recommended algorithm uses the 25 closest points within a maximum radius of 16 km.

Appendix 3 Type I Error Rates

The equations 1 and 2 given in the memo depend on k , which is a constant multiplied by the median-to-upper quartile or lower quartile-to-median range. Typically, one chooses an outlier criterion based on a specified type I error. Type I error is the probability that one incorrectly rejects the null hypothesis. In this example the null hypothesis is that the data is distributed according to the distribution listed. The type I error will be identifying a point as an outlier even though it is drawn from the specified distribution. Type I error rates in table 3.1 were calculated based on Monte Carlo calculation from 100,000 replicates of sample size 25.

For the recommended value of $k = 3$, if the data is normally distributed one would expect to identify about 3% (see table 3.1) of the data as outliers. Thicker tailed distributions, such as the Student t, will have higher identification rates. Thin-tailed Beta(1,1) (uniform distribution) and Beta(2,2) have high type I error rates in table 3.1 compared to the values in table 3.2. For example, in table 3.1 the type I error for Beta(2,2) with $k = 1.5$ is 8.29%, but if the distribution parameters were known exactly the type I error would be 2.49% as given in table 3.2. Beta(1,1) shows large differences between the two cases.

Table 3.1. Type I error (%) for asymmetric boxplot test based on 100,000 replicates of sample size 25. Beta(1,1) is the uniform distribution. The argument for the Student t distribution is the shape parameter (also referred to as the degrees-of-freedom), which controls the thickness of the tails. Student t (∞) is the normal distribution. Upper and lower bounds used to define outliers are based on equations 1 and 2 in the memo.

k	<u>Distribution</u>							
	Normal	Beta (1,1)	Beta (2,2)	Student t (2)	Student t (4)	Student t (6)	Student t (8)	Student t (10)
1.0	19.76	10.79	15.84	25.25	22.63	21.71	21.22	20.94
1.5	12.36	4.67	8.29	19.20	15.95	14.78	14.19	13.82
2.0	7.86	2.14	4.26	14.97	11.44	10.24	9.62	9.23
2.5	5.00	1.06	2.42	12.00	8.36	7.21	6.61	6.27
3.0	3.26	0.56	1.36	9.81	6.32	5.16	4.64	4.34
3.5	2.16	0.31	0.80	8.10	4.79	3.77	3.31	3.06
4.0	1.45	0.18	0.49	6.84	3.68	2.79	2.40	2.18
4.5	1.00	0.11	0.32	5.83	2.91	2.11	1.77	1.57
5.0	0.70	0.06	0.21	5.02	2.32	1.61	1.32	1.17

Table 3.2. Type I error (%) for asymmetric boxplot test based on perfect knowledge of parameters (large sample). Beta(1,1) is the uniform distribution. The argument for the Student t distribution is the shape parameter (also referred to as the degrees-of-freedom), which controls the thickness of the tails. Student t (∞) is the normal distribution. Upper and lower bounds used to define outliers are based on equations 1 and 2 in the memo and the quantiles are calculated from the population distribution.

<i>k</i>	<u>Distribution</u>							
	Normal	Beta (1,1)	Beta (2,2)	Student t (2)	Student t (4)	Student t (6)	Student t (8)	Student t (10)
1.0	17.73	0.00	12.57	24.41	21.26	20.13	19.54	19.19
1.5	9.18	0.00	2.49	17.80	13.77	12.30	11.54	11.08
2.0	4.30	0.00	0.00	13.40	9.04	7.48	6.69	6.21
2.5	1.82	0.00	0.00	10.37	6.05	4.58	3.86	3.43
3.0	0.70	0.00	0.00	8.23	4.14	2.84	2.23	1.88
3.5	0.24	0.00	0.00	6.67	2.90	1.79	1.30	1.03
4.0	0.07	0.00	0.00	5.51	2.08	1.15	0.77	0.57
4.5	0.02	0.00	0.00	4.62	1.52	0.76	0.46	0.32
5.0	0.01	0.00	0.00	3.92	1.13	0.51	0.28	0.18

References

- Aguirre, G. A., Stedinger, J. R. and Tester, J. W. (2013). Geothermal Resource Assessment: A Case Study of Spatial Variability and Uncertainty Analysis for the State of New York and Pennsylvania. *Proceedings: 38th Workshop on Geothermal Reservoir Engineering*. Stanford University.
- Aguirre, G. A. (2014). *Geothermal Resource Assessment: A Case Study of Spatial Variability and Uncertainty Analysis for the States of New York and Pennsylvania*. Master's Thesis. Environmental and Water Resources Systems Engineering, School of Civil and Environmental Engineering, Cornell University.
- Barnett, V. and Lewis, T. (1994). *Outliers in Statistical Data*. 3rd ed. John Wiley and Sons: New York.
- Cornell University (2014). Cornell University Heat Flow Database (NY and PA). Southern Methodist University Geothermal Laboratory. <http://geothermal.smu.edu/static/DownloadFilesButtonPage.htm> (Accessed 16 June 2014).

Memo 7: Thermal Resource Thresholds in GPFA-AB

To: Appalachian Basin Geothermal Play Fairway Analysis Group
From: Jared Smith
Date: Original from August 19, 2015. Updated August 25, 2016
Subject: Selection of Thresholds for Thermal Resource and Thermal Risk Factor Maps

Applicability: The methods described in this memo were used to develop the thermal resource and risk maps for this project. This memo discusses the steps to create thermal risk factor maps for the project. This memo also describes a method for objective selection of threshold values for any risk factor considered.

Definitions

Resource Map – Map representing a resource in the Appalachian basin. For example, these include depth-to-temperature maps, temperature-at-depth maps, reservoir productivity maps, etc. These may have continuous or discrete color scales.

Risk Factor Map – A discrete color map submitted as a representation of the risk for the end user considered. A risk factor map reflects actual acceptability (favorability) of the resource. The most general risk factor map would be a single color scheme for all end uses considered in the project. An example of a more specific map would be a single color scheme for all end uses between 50 °C and 80 °C. Separate thresholds would be defined for each of these maps.

Introduction

Thresholds must be assigned for visualizing the resource maps and risk factor maps in a play-fairway color scheme. A distinction must be made between thresholds for visualizing the thermal resource maps (e.g. temperature at depth and depth to temperature), and thresholds for visualizing the thermal risk factor maps. The resource maps may be viewed on any color scale desired that adequately displays the variability in the resource throughout the basin: the resource maps represent favorability relative to the predicted values of the resource in the assessed locations of the basin. The risk factor map must be placed on a color scale that represents the actual acceptability of developing the thermal field in an assessed location of the basin: the risk factor map represents favorability relative to the project(s) considered. For the thermal risk factor, the risk map represents the favorability of drilling to a depth and reaching a sufficient temperature for the project(s) considered. Therefore, the risk factor map thresholds should change based on the project considered. More detailed descriptions of Resource Maps versus Risk Factor Maps are provided in their respective sections.

To distinguish between resource maps and risk factor maps, the colors used to represent resource maps should not be exactly the same as colors used on risk factor maps (green/yellow/red) within reason. For example, it would be odd for temperature at depth to be on a purple/blue/pink color scale, so using green/yellow/red would be acceptable. Another distinction between resource maps and risk factor maps is that the resource map may be placed on a continuous color scale; whereas the risk factor must be on a discrete play-fairway color scale.

Selection of Maximum, Minimum, and Threshold Values

For a resource map the minimum and maximum values have little influence on the resulting map, other than bounding the color scale. On a risk factor map the minimum and maximum values define 0.0 and 3.0 or 0.0 and 5.0, and therefore are of great importance when calculating the commensurate risk metrics. For example, if the maximum value on a resource map is 100 and 100 is advantageous, but threshold 2 (2.0) is a value of 1, and the maximum (3.0 on 3-color scale) is assigned (arbitrarily) a value of 1000, then 100 would be scaled to a value of 2.1 for the commensurate metric calculation. Thus, the minimum and maximum values on a risk factor map must be selected with care, and represent what is truly a minimum acceptable and maximum acceptable value, within reason.

One way to assign the maximum and minimum risk factor values is to treat them as thresholds, for which any value below the selected minimum would be assigned a value of 0.0, and any value above the selected maximum would be assigned a 3.0 or a 5.0 depending on the color scheme. This formulation allows for an objective selection by asking “what is a value above which we could do any project?” and “what is a value below which we could accomplish nothing?” This formulation is more flexible than assigning a single value to 0.0 and 3.0 or 5.0.

The threshold values determine the color divisions on all maps. The thresholds should be selected objectively, at least to a point of being defensible. As such, resource map thresholds could be determined based on the expected cost of drilling and completing a geothermal well (for depth-to-temperature maps) and potential end use temperatures (for temperature-at-depth maps). Risk factor map thresholds are to be defined based on the expected cost of drilling to depths for the project(s) considered. The most general risk factor map would consider all possible projects. An example of a more specific risk factor map would be a single color scheme for all end uses between 50 °C and 80 °C. Separate thresholds would be defined for each risk factor map. The thresholds used for the final risk factor maps are provided in the final section of this memo.

Threshold Selection for Resource Maps

In determining the threshold values for the resource maps, some consideration was given to how much of the map area appeared a certain color. The main concern is that the resource map must display a variety of colors to maximize its utility. For example (using green/yellow/red) this does not mean that areas that are green are favorable to develop, and areas that are red are unfavorable: it only means that green areas are better than red areas.

To ensure that visual comparison is simple between potentially many maps, only one set of thresholds could be used per resource, no matter the selected depth or temperature. For instance, the temperature at 1 km could use the same color scheme as the temperature at 4 km. Likewise, the Depth to 80 °C could use the same color scheme as Depth to 100 °C.

For resource maps, no consideration was given to the use of different thresholds for different end uses. For example, one may be interested in a district heating project, and therefore sites would likely require temperatures above 80 °C to be considered. These end-use specifications are potentially important for risk factor maps (below), but are not reflected in the resource maps.

The following section discusses how thresholds could be assigned to resource maps using a single set of thresholds. This approach was not adopted for final products, but it could be useful for other projects, or future phases of this project.

Depth to Temperature Maps

Threshold values for depth to temperature maps are selected based on the current state of knowledge about the average cost of drilling and completing geothermal wells (Beckers et al., 2014). The main consideration was that the rate of change in the cost for drilling and completing a well is less for shallow depths. For instance, drilling a well 2 km instead of 4 km causes the average cost to increase by about \$7 million; whereas drilling a well 4 km instead of 6 km, or 6 km instead of 8 km causes an average cost increase of about \$10 million.

Other factors affecting the economics of geothermal operations including the price of competing heating fluids (e.g. natural gas), the natural permeability of the reservoirs at depth, the expected fluid production rate, and the expected temperature of the produced fluid were not taken into account to determine the threshold values; however each factor may aid in an economics-based objective selection of threshold values.

Minimum and Maximum Depth

The minimum depth is 500 m, which is approximately the minimum depth to a corrected BHT of 50 °C in the region – the minimum useful temperature considered. This hot spot is located in Gilmer and Calhoun counties in West Virginia. Additionally, 500 m is the depth of the shallowest reservoir identified in this study. The maximum depth is 8750 m, which is the maximum predicted mean depth to 80 °C in the region considered, plus two times the standard error of the predicted mean. Again, these values may be adjusted with little effect on the resource maps, other than shifting the color scale values.

Thresholds for 5-color Scheme for All Temperatures

Threshold 1 is set at an average cost of approximately \$12 million to drill and complete each well. This corresponds to a depth of 4500 m. Clearly drilling to a depth of 4500 m would be too costly for low temperatures, and only in the very few hottest areas would it be beneficial to drill to deeper depths.

Thresholds 2 through 4 were all selected in approximately \$2 million increments, starting with threshold 2 at \$8.2 million and 3500 m, to threshold 3 at \$6.0 million and 2900 m, and finally threshold 4 at \$3.9 million and 2200 m. To place the 2200 m threshold into a thermal perspective, the 50 °C minimum temperature considered in this project would correspond to an average gradient of about 18 °C/km. Therefore, even at the coolest temperature considered there would be a distinction between green, yellow-green, yellow, orange, and red areas on the map (though most of the area would appear green).

Thresholds for 3-color Scheme for All Temperatures

Threshold 2 on the 3-color scale is located between thresholds 3 and 4 on the 5-color scale. Threshold 1 on the 3-color scale is a \$5 million increment from threshold 2.

Temperature at Depth Maps

Temperature at depth thresholds are selected based on the end-use temperatures considered in this project. The minimum temperature is 15 °C, which is the average annual ground temperature throughout the region (Gass, 1982), rounded up to the nearest multiple of 5. The maximum temperature is 250 °C, which is the maximum calculated temperature at 4 km depth for wells in the database, rounded up to the nearest multiple of 10. A depth of 4 km was selected because maps for temperature at depth were created up to 4 km depth.

Thresholds for 5-color Scheme for All Depths

Threshold 1 is 50 °C, which is the minimum useful temperature considered in this project.

Threshold 2 is 75 °C, which is desirable to meet the legal minimum temperature of 72 °C needed for Grade A milk pasteurization by the High Temperature Short Time (HTST) method (USHHS, 2011). HTST is typically used for high volume production of milk because of the short 15 second heating time. Lower temperatures of 63 °C are acceptable for pasteurization if milk is heated for 30 minutes (USHHS, 2011), but this is more typical for at-home projects than large scale production. Other processes related to large scale milk pasteurization are possible at temperatures between 60 °C and 70 °C.

Threshold 3 is 90 °C, which is a desirable temperature for direct-use of hot water for district heating.

Threshold 4 is 150 °C, which is considered a minimum temperature for electricity generation in an Organic Rankine Cycle (ORC) geothermal power plant.

Thresholds for 3-color Scheme for All Depths

Threshold 1 is 50 °C, which is the minimum useful temperature considered in this project. Again, threshold 2 on the 3-color scale is located between threshold 3 and 4 on the 5-color scale.

Table 1a: Thresholds for 3-color scheme for depth-to-temperature thermal resource maps.

3 – Color Scale Divisions	Depth to Temperature Maps (m)
Minimum	8750 (too costly)
Bad, unacceptable [8750, 4000]	
Threshold 1	4000 (~\$10.1 Million/well)
Okay, acceptable [4000, 2500]	
Threshold 2	2500 (~\$4.8 Million/well)
Great, advantageous [2500, 500]	
Maximum	500 (shallowest reservoir)

Table 1b: Thresholds for 3-color scheme for temperature-at-depth thermal resource maps.

3 – Color Scale Divisions	Temperature at Depth Maps (°C)
Minimum	15 (no need to drill)
Bad, unacceptable [15, 50]	
Threshold 1	50 (min useful temperature)
Okay, acceptable [50, 120]	
Threshold 2	120
Great, advantageous [120, 250]	
Maximum	250

Table 1c: Thresholds for 5-color scheme for depth-to-temperature thermal resource maps.

5 – Color Scale Divisions	Depth to Temperature Maps (m)
Minimum	8750 (too costly)
Bad, unacceptable [8750, 4500]	
Threshold 1	4500 (~\$12.2 Million/well)
Marginally acceptable [4500, 3500]	
Threshold 2	3500 (~\$8.2 Million/well)
Okay, acceptable [3500, 2900]	
Threshold 3	2900 (~\$6.0 Million/well)
Favorable [2900, 2200]	
Threshold 4	2200 (~\$3.9 Million/well)
Advantageous [2200, 500]	
Maximum	500 (shallowest reservoir)

Table 1d: Thresholds for 5-color scheme for temperature-at-depth thermal resource maps.

5 – Color Scale Divisions	Temperature at Depth Maps (°C)
Minimum	15 (no need to drill)
Bad, unacceptable [15, 50]	
Threshold 1	50 (min useful temperature)
Marginally acceptable [50, 75]	
Threshold 2	75 (milk pasteurization)
Okay, acceptable [75, 90]	
Threshold 3	90 (district heating)
Favorable [90, 150]	
Threshold 4	150 (ORC power plant)
Advantageous [150, 250]	
Maximum	250

Thresholds for Risk Factor Maps

The risk factor maps must combine temperature and depth in a meaningful way. These risk factor maps may be defined based on the overall risk of developing any project, or be more specific to selected end uses, such as technologies that require temperatures from 50 °C to 80 °C.

The thresholds selected for risk factor maps give no consideration to the percentage of map area assigned to each color because the thresholds are objectively defined for acceptability. It is therefore possible for a risk factor map to omit some of the colors because that level of acceptability is not reached in the assessed area.

Definition of risk factor thresholds can be determined from two methods (M1 or M2) by asking:

- M1) “What temperatures are being considered for this use map?” Thresholds for a thermal risk map would be assigned based on unfavorable, okay, and advantageous depths to reach those temperatures considered.
- M2) “At what depth are the interesting reservoirs that are being considered for this map area?” Thresholds describing thermal risk would be based on unfavorable, okay, and advantageous temperatures to be reached at those reservoir depths.

Examples of thresholds for the thermal risk factor using each of these methods (M1 and M2) are provided in Table 2. Thresholds selected for use in the project are provided in the following section. In Table 2, the thermal gradient is used as a simple method of assigning thresholds, but using the thermal gradient does not account for complexities in thermal conductivity or heat generation with depth, or any economic factors that may want to be considered.

Alternatively to M1) and M2), a map depicting overall thermal risk may be made from the combination of maps created at depth intervals. For example, taking the average of the 3-point or 5-point scaled values for depths ranging from 1.5 km to 3.5 km in 1.0 km increments. The threshold values would be defined in temperature units and would be different for each depth considered because of a change in favorability of a temperature with depth. For example, 80 °C at 1000 m is great, but 80 °C at 5000 m is awful. These thermal maps could be combined with the reservoirs, which are defined on 0.5 km intervals, to create combined thermal and reservoir risk maps. This is an option for further communicating risk in Phase 2.

Table 2a: Example thresholds for 3-color scheme and point scale for thermal risk factor maps in Method 1 (above). M1 considers a single map for end use temperatures from 60 °C – 80 °C.

3 – Color Scale Divisions and Point Value (0 = Worst, 3 = Best)	M1) Depth to End Use Temperatures from 60 – 80 °C (m)
All Values Above 0.0: Unacceptable	4000 (~15 °C/km for 70 °C)
Bad, unacceptable [0.0, 1.0]	
Threshold 1 1.0	3000
Okay, acceptable [1.0, 2.0]	
Threshold 2 2.0	2000
Great, advantageous [2.0, 3.0]	
All Values Below 3.0: Very favorable	1000

Table 2b: Example thresholds for 3-color scheme and point scale for thermal risk factor maps in Method 2 (above). M2 considers a single map for reservoirs between 2000 m and 3000 m.

3 – Color Scale Divisions and Point Value (0 = Worst, 3 = Best)	M2) Temperature at Reservoirs Depths from 2000 m– 3000 m (°C)
All Values Below 0.0: Unacceptable	50 (~15 °C/km for 2.5 km)
Bad, unacceptable [0.0, 1.0]	
Threshold 1 1.0	80 (~28 °C/km for 2.5 km)
Okay, acceptable [1.0, 2.0]	
Threshold 2 2.0	120 (~45 °C/km for 2.5 km)
Great, advantageous [2.0, 3.0]	
All Values Above 3.0: Very favorable	180 (~68 °C/km for 2.5 km)

Table 2c: Example thresholds for 5-color scheme and point scale for thermal risk factor maps in Method 1 (above). M1 considers a single map for end use temperatures from 60 °C – 80 °C.

5 – Color Scale Divisions and Point Value (0 = Worst, 5 = Best)	M1) Depth to End Use Temperatures from 60 – 80 °C (m)
All Values Above 0.0: Unacceptable	5000 (~\$14.5 Million/well)
Bad, unacceptable [0.0, 1.0)	
Threshold 1 1.0	4000 (~\$10 Million/well)
Marginally acceptable [1.0, 2.0)	
Threshold 2 2.0	3000 (~\$6.4 Million/well)
Okay, acceptable [2.0, 3.0)	
Threshold 3 3.0	2500 (~\$4.8 Million/well)
Favorable [3.0, 4.0)	
Threshold 4 4.0	2000 (~\$3.3 Million/well)
Advantageous [4.0, 5.0)	
All Values Below 5.0: Very favorable	1000 (~\$1 Million/well)

Table 2d: Example thresholds for 5-color scheme and point scale for thermal risk factor maps in Method 2 (above). M2 considers a single map for reservoirs between 2000 m and 3000 m.

5 – Color Scale Divisions and Point Value (0 = Worst, 5 = Best)	M2) Temperature at Reservoir Depths from 2000 m– 3000 m (°C)
All Values Below 0.0: Unacceptable	50 (minimum useful temp.)
Bad, unacceptable [0.0, 1.0)	
Threshold 1 1.0	70 (~25 °C/km at 2.5 km)
Marginally acceptable [1.0, 2.0)	
Threshold 2 2.0	100 (~35 °C/km at 2.5 km)
Okay, acceptable [2.0, 3.0)	
Threshold 3 3.0	130 (~48 °C/km at 2.5 km)
Favorable [3.0, 4.0)	
Threshold 4 4.0	150 (~56 °C/km at 2.5 km)
Advantageous [4.0, 5.0)	
All Values Above 5.0: Very favorable	180

Thresholds Used for Final Thermal Resource and Risk Factor Maps

The resource maps made as products for this project did not use the method of resource threshold assignment described in this memo. Instead, resource maps were made by simply stretching the colorbar from the minimum to the maximum value recorded for the resource in the basin.

Risk factor maps did follow the procedure outlined here for assignment of favorability thresholds. Lists of thresholds for each thermal risk factor map in 3 and 5 color scheme are provided below. Thresholds for the 3-color scheme are all located between thresholds in the 5-color scheme. The risk factor maps for this project included Depth to 80 °C, Depth to 100 °C, Temperature at 1.5 km, Temperature at 2.5 km, and Temperature at 3.5 km. The Play Fairway Metrics that combined thermal, reservoir, seismic, and utilization risk factors were created using only the Depth to 80 °C risk factor map, as stated in the SOPO. Other Play Fairway Metric maps could be created using the other thermal risk factors, but time did not permit to perform these calculations in Phase 1. With additional time, Play Fairway Metrics could be computed using all of these thermal risk factors, and the most robust areas would be favorable in all renditions of the Play Fairway Metric. Heat flow is not considered to be a risk factor because heat flow alone is not of great value to those interested in drilling a geothermal well.

Dollar values for depth to temperature thresholds are from Beckers et al. (2014) and represent the average cost in 2012 US dollars needed to drill a single geothermal well. Dollar values are rounded. A value of \$15 million/well is used as the worst value, corresponding to a depth of 5000 m. Approximate \$2 million/well increments are used to select thresholds 1 through 4 on a 5-color scheme. Temperature thresholds for temperature at depth maps are selected based on typical utilization temperatures, or favorability of thermal gradients from the temperature-at-depth to the annual average ground surface temperature of 15 °C, as discussed above. All values greater than the maximum are assigned a value of 3 or 5, and all values less than the minimum are assigned a value of 0.

Depth to 80 °C

5-color scheme

- 0: 5000 m (\$14.5M/well)
- 1: 4000 m (\$10M/well)
- 2: 3000 m (\$6.5M/well)
- 3: 2500 m (\$4.8M/well)
- 4: 2000 m (\$3.3M/well)
- 5: 1000 m (< \$2M/well)

3-color scheme

- 0: 5000 m (\$14.5M/well)
- 1: 3750 m (\$9.2M/well)
- 2: 2350 m (\$4.2M/well)
- 3: 1000 m (< \$2M/well)

Depth to 100 °C

5-color scheme

- 0: 5000 m (\$14.5M/well)
- 1: 4200 m (\$11M/well)
- 2: 3700 m (\$9M/well)
- 3: 3200 m (\$7M/well)
- 4: 2600 m (\$5M/well)
- 5: 1900 m (\$3M/well)

3-color scheme

- 0: 5000 m (\$14.5M/well)
- 1: 4000 m (\$10M/well)
- 2: 3000 m (\$6.5M/well)
- 3: 1900 m (\$3M/well)

Temperature at 1.5 km

5-color scheme

- 0: 30 °C (~10 °C/km)
- 1: 50 °C (Minimum useful temperature)
- 2: 60 °C (~30 °C/km)
- 3: 70 °C (~37 °C/km)
- 4: 80 °C (~43 °C/km)
- 5: 90 °C (~50 °C/km)

3-color scheme

- 0: 30 °C (~10 °C/km)
- 1: 50 °C (Minimum useful temperature)
- 2: 75 °C (~40 °C/km)
- 3: 90 °C (~50 °C/km)

Temperature at 2.5 km

5-color scheme

- 0: 40 °C (~10 °C/km)
- 1: 60 °C (~18 °C/km)
- 2: 75 °C (~25 °C/km)
- 3: 90 °C (~30 °C/km)
- 4: 100 °C (~35 °C/km)
- 5: 110 °C (~40 °C/km)

3-color scheme

- 0: 40 °C (~10 °C/km)
- 1: 70 °C (~22 °C/km)
- 2: 95 °C (~32 °C/km)
- 3: 110 °C (~40 °C/km)

Temperature at 3.5 km

5-color scheme

- 0: 50 °C (Minimum Useful Temperature)
- 1: 75 °C (Milk Pasteurization)
- 2: 90 °C (Small-Scale District Heating)
- 3: 100 °C (25 °C/km)
- 4: 120 °C (Large-Scale District Heating)
- 5: 150 °C (ORC Power Generation)

3-color scheme

- 0: 50 °C (Minimum useful temperature)
- 1: 80 °C (~19 °C/km)
- 2: 110 °C (~28 °C/km)
- 3: 150 °C (ORC Power Generation)

References

- Beckers, K.F., M.Z. Lukawski, B.J. Anderson, M.C. Moore, and J.W. Tester. (2014). Levelized Costs of Electricity and Direct-Use Heat from Enhanced Geothermal Systems - Supplemental Material. GEOPHIRES.
- Gass, T. E., 1982, The geothermal heat pump: Geothermal Resources Council Bulletin, v. 11, p. 3–8.
- United States Department of Health and Human Services (USHHS), Public Health Service, and Food and Drug Administration. (2011). Grade ‘A’ Pasteurized Milk Ordinance 2011 Revision. National Conference on Interstate Milk Shipments Model Documents. Retrieved 7/23/2015 from <http://www.fda.gov/Food/GuidanceRegulation/GuidanceDocumentsRegulatoryInformation/Milk/ucm2007966.htm>

Memo 8: Thermal Model Methods and Well Database Organization in GPFA-AB

To: Appalachian Basin Geothermal Play Fairway Analysis Group

From: Jared D. Smith and Franklin G. Horowitz

Date: Original from August 11, 2015. Updated September 21, 2016.

Subject: Well database organization and heat conduction model methods

Applicability: This memo describes the assumptions, methods, and equations for the one-dimensional heat conduction model that was used in this project. The heat conduction model was used to calculate the temperatures at depths, depths to temperatures, and the surface heat flow at individual well locations. This memo also describes the organization of the well database used in this project into a format that is more useful for heat conduction modeling. Portions of this memo are taken from Smith (2016) with permission of the author. More details are provided in Smith (2016).

Nomenclature:

A_B	Radiogenic heat generation within the rocks at the top of the basement (W/m^3)
A_s	Radiogenic heat generation within sedimentary rocks (W/m^3)
a_T	Amplitude of the annual surface temperature fluctuation ($^{\circ}\text{C}$)
B	Thickness corresponding to one log decrement (i.e. e-folding thickness) in radiogenic heat generation in basement rocks (m)
BHT_{corr}	Corrected BHT ($^{\circ}\text{C}$)
$G(x, y, z)$	Straight line geothermal gradient at surface location (x, y) to depth z . z may also be specified as an interval ($z = Z_2 - Z_1$). ($^{\circ}\text{C}/\text{km}$)
\bar{k}	Harmonic average thermal conductivity for rocks ($\text{W}/[\text{m } ^{\circ}\text{C}]$)
k_B	Thermal conductivity of basement rocks ($\text{W}/[\text{m } ^{\circ}\text{C}]$)
\bar{k}_w	Harmonic average thermal conductivity for rocks from the ground surface to the depth of the well ($\text{W}/[\text{m } ^{\circ}\text{C}]$)
\bar{k}_s	Harmonic average thermal conductivity for rocks from the ground surface to the top of the basement ($\text{W}/[\text{m } ^{\circ}\text{C}]$)
$\bar{k}_{z_2-z_1}$	Harmonic average thermal conductivity for rocks between depth Z_1 and depth Z_2 ($\text{W}/[\text{m } ^{\circ}\text{C}]$)
N	Total number of geologic layers referred to in the text

P	Period of the annual surface temperature fluctuation (s)
$Q(z)$	Heat flow upwards through depth, z (W/m^2)
Q_B	Heat flow contributed to Q_s from basement rocks (W/m^2)
Q_m	Mantle heat flow (W/m^2)
Q_s	Surface heat flow (W/m^2)
Q_{sb}	Heat flow through the top of the basement rocks (W/m^2)
Q_{sed}	Heat flow contributed to Q_s from sedimentary rocks (W/m^2)
T_B	Temperature in basement rocks ($^{\circ}\text{C}$)
T_{Sed}	Temperature in sedimentary rocks ($^{\circ}\text{C}$)
T_s	Average annual surface temperature ($^{\circ}\text{C}$)
T_z	Temperature at depth z ($^{\circ}\text{C}$)
t	Time (s)
t_a	Time elapsed since the mean annual surface temperature (s)
Z_s	Thickness of the sedimentary rock column (i.e. depth to basement) (m)
Z_w	Depth of the well (m)
z	Depth below the surface (m)
z_{bottom}	Depth from the surface to the bottom of a rock formation (m)
z_{calc}	Calculation depth (m)
z_{top}	Depth from the surface to the top of a rock formation (m)
α	Thermal diffusivity (m^2/s)

List of Tables

Table 1: Information added to the AASG combined well database..... 6

List of Figures (Figure 2 and Figure 4 are from Smith [2016])

Figure 1: Schematic of the 1-D conduction heat balance. 7
Figure 2: Spatial distribution of calculated values of B using the thermal model. 10
Figure 3: Histogram of A_B values calculated using the thermal model. 14
Figure 4: Spatial distribution of calculated A_B values in wells..... 15

Appendices from Smith (2016)

- 1) Derivation of the One-dimensional Conduction Heat Balance

Attachments from Smith (2016)

- 1) Well Databases Folder
- 2) Trenton-Black River Sediment Thickness Map
- 3) Influence of Annual Temperature Fluctuation on Near-Surface Temperatures
- 4) Drilling Fluid Query in SQL
- 5) Probabilistic assignment of Drilling Fluid based on Nearest Neighbor Wells

Introduction

The Appalachian Basin Geothermal Play Fairway Analysis (GPFA-AB) team needs to have a method for calculating the surface heat flow and temperatures at depth from corrected bottom-hole¹ temperature (BHT) measurements. The method used in this project calculates these variables based on a vertical (1-D), steady-state, N-layer heat conduction model with two layers of radiogenic heat generation. This model was developed in Python 2.7.9. A 1-D model is used rather than a 3-D model because published cross sections available for the basin are sparse in New York and Pennsylvania, and constructing a volume of basin stratigraphy based on individual wells would be infeasible for the time constraints of this project. Steady state conditions are assumed so that the thermal field in the rock can be modeled without regard to surface temperature fluctuations (Attachment 3): other transient variables, such as radioelement decay and mantle heat flow, would not affect calculations because the time scale of impact for these variables is much greater than the time scale over which the BHTs were sampled. Advection and convection of heat via moving fluid are not considered because the rock is essentially stationary, and information about groundwater transport is not available for the entire basin and would be infeasible to collect and/or model within the timeframe this project. Additionally, Frone et al. (2015) showed via a 2-D model along a cross section in West Virginia that heat conduction modeling alone is sufficient for reproducing BHTs at depth, within reasonable error. Therefore, it is likely that neglecting advection in this analysis provides an adequate representation of the thermal field for regional thermal resource assessment. Further details about the heat conduction model are provided below.

A primary necessity for running any model is preparation of the input data and specification of model parameters. The well database described in this memo and the generalized stratigraphic columns from the American Association of Petroleum Geologists (AAPG) (1985a; 1985b) Correlation of Stratigraphic Units in North America (COSUNA) project are the inputs to the thermal model. This memo discusses the organization of the well data into a useful format for the thermal model. Processing of the COSUNA data is described in another memo (see Memo 4: Assignment of thermal conductivity stratigraphy to individual wells using COSUNA columns).

The parameters in the thermal model are the heat flow upward through the base of the crust (referred to as mantle heat flow), the radiogenic heat generation in sedimentary rocks, the thermal conductivity of basement rocks, and the log decrement (e-folding length) of radiogenic heat generation in basement rocks. These parameters are selected from published studies.

Following these sections, the memo describes the methods, assumptions, and equations used for calculating properties of the thermal field at each well using the heat conduction model. Appendices provide derivations of equations that have not been documented in previous studies. Attachments provide references to databases and additional methodological details. The appendices and attachments are from Smith (2016).

¹ Some temperature measurements do not correspond to the bottom of the well, but BHT is used as an abbreviation, as per traditional use.

Selecting and Processing Wells for Analysis

Wells were gathered from the Association of American State Geologists (AASG) Geothermal Data Repository for the states of New York (Slater, 2012), Pennsylvania (Shank et al., 2012), West Virginia (WVGES, 2011), Maryland (Brezinski, 2011), Virginia (VDGMR, 2011), Kentucky (Curl, 2011), and Ohio (Leftwich, 2011). All of the available wells were combined into a single spreadsheet with common field headers (Attachment 1, “AASG_Combined.xlsx”). There were a total of 41,099 records from approximately² 39,000 wells in this database. Some processing steps were needed to make this dataset useful for the assessment of the thermal field.

Additional data fields beyond those provided by AASG were needed to use these wells in the thermal model. Table 1 lists the additional fields and respective sources of the data. All information was joined to the well data based on spatial location (ArcGIS Spatial Join tool) or added from the output of an R function written for this project (Table 1).

To limit edging effects that would occur from using interpolations near state lines, only those wells within New York, Pennsylvania, West Virginia, and a 50 km buffer zone into surrounding states were retained in the database for analysis (32,385 total records remained). Further, only those wells with a depth of BHT measurement were retained for quality purposes, as opposed to a total/true vertical depth or driller/log depth (arc length) that may or may not correspond to the depth of the BHT measurement (21,104 total records remained). Then, records lacking any of the information in Table 1 as a result of spatial coverage of the map layer were removed (29 records were not in a COSUNA section and an additional 324 records did not have a basement depth, so 20,751 total records remained). One record was removed because the depth of measurement was less than 10 m (minimum depth to run the thermal model) so the final record count is 20,750. These processed records were sent to the thermal model (Attachment 1, AASG_Processed.xlsx). An exploratory data analysis (EDA) that included local spatial outlier detection was conducted on these well data after processing in the thermal model (see Memo 9: Exploratory Data Analysis and Interpolation Methodology for Thermal Field Estimation).

² This number is approximate because the number of unique API numbers was used as a proxy for the number of unique wells. Some wells do not have an API number, so the well name was used instead of the API number for these records. Other wells do not have either, so these 1,500 records were not counted. Therefore, the actual number of unique wells is likely greater than reported.

Table 1: Information added to the AASG well database. Attachment 1 (AASG_Processed.xlsx) contains field names for these data types.

Data Type	Source
COSUNA section	“All_COSUNA_Sections_Final.shp”, created for this project.
Sediment thickness	Derived from the Trenton-Black River (TBR) Project (WVGES, 2006) Precambrian basement contours. Map created for this project (Attachment 2).
Rome Trough identifier	Traced from a georeferenced figure in Repetski et al. (2008) (see Memo 4 for an image). “Rome trough final.shp”, created for this project.
Average annual ground surface temperature	Derived from Gass (1982) shallow (15 m – 46 m) groundwater temperature measurements. These measurement depths are considered resistant to annual surface temperature fluctuations, as shown by Lovering and Goode (1963) (Attachment 3).
BHT correction section	“BHTCorrectionSections.shp”. See Memo 2: BHT Corrections.
Corrected BHT	Output from BHT correction code. See Memo 2: BHT Corrections.
Drilling Fluid	Whealton (2015) well database for NY and PA (1755 records), modified with generalized drilling fluid groups (air and mud) in this project. A PostgreSQL query in PgAdmin III was used to select all wells in this database that matched with wells in the AASG database. 687 records (245 wells) matched. Attachment 4 contains the query used and a more detailed description.
Proportion Air or Mud Drilled Neighbor Wells	Proportion of nearest neighbor wells that are air or mud drilled. Nearest neighbor wells are from the Whealton (2015) database. Attachment 5 describes how this proportion was calculated.
Mantle Heat Flow	Parameter in the thermal model. Discussed below.
Sediment Heat Generation	Parameter in the thermal model. Discussed below.

One Dimensional Heat Conduction Model Assumptions and Equations

A vertical (1-D) steady state heat conduction model with two heat generation layers was developed in Python 2.7.9 (Horowitz, Smith, and Whealton, 2015). A schematic of this model is provided in Figure 1. This model calculates the geothermal gradient at the surface, heat flow at the surface, and the geotherm temperature at depth profile for wells in the input database. This model assumes the traditional approach to subsurface 1-D heat conduction modeling (Jaeger, 1965) that at some depth there is a constant value of heat flowing upward from the mantle, Q_m , and that all variations in the surface heat flow, Q_s , are a result of differences in the radiogenic heat production, A_s or A_B , in sedimentary and basement rocks, respectively. Frone et al. (2015) showed that these assumptions of radiogenic heat contribution to the surface heat flow are appropriate to estimate the BHTs using a 2-D heat conduction model along a cross section in West Virginia. Another approach to 1-D heat conduction modeling is described by Lachenbruch (1980), who shows that one could assume that the radiogenic contribution is constant and that all variations in surface heat flow are a result of changes in the mantle heat flow. This approach is more relevant for locations that have recently experienced rifting, not for the stable continent settings, like the Appalachian Basin.

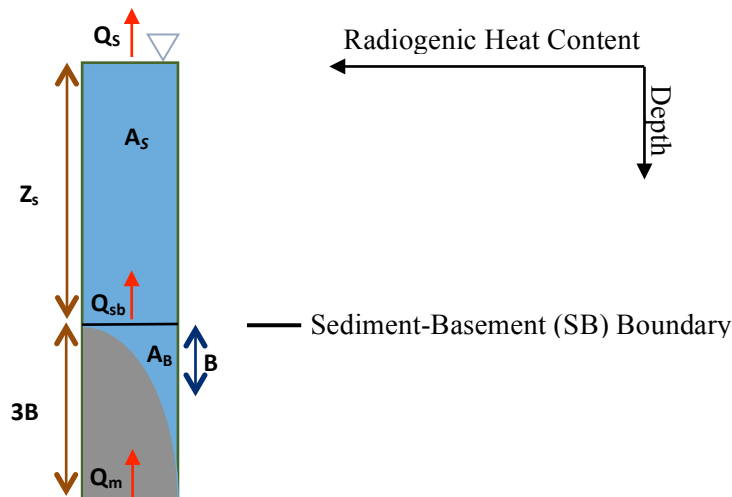


Figure 1: Schematic of the 1-D conduction heat balance. There is a sediment heat generation layer and a basement heat generation layer, which follows an exponential decrease with increasing depth. Figure from Smith (2016).

A 1-D model is an appropriate first-order estimation of the surface heat flow and temperatures at depth (Lachenbruch, 1970; Jaupart, 1986). Additionally, Lachenbruch (1970) states that the consistency in the relationship between heat flow and heat production across a variety of geologic settings indicates that lateral heat flow must be much less important than vertical heat flow (e. g. $\frac{\partial T}{\partial x}, \frac{\partial T}{\partial y} \ll \frac{\partial T}{\partial z}$) in cases for which advection of heat may be neglected. Therefore, a 1-D model is adequate for a basin scale evaluation of the thermal field: higher dimensions may be assessed for smaller scale analyses in Phase 2, if data are available.

Using a 1-D model, there is an implicit assumption that strata are perfectly horizontal, or that the input formation thicknesses have been adjusted for folds, because heat preferentially flows normal to the bedding plane. Reliable folding information is available on published cross sections, but these cross sections are not available throughout the extent of the basin (Ryder, 1992; Ryder et al., 2008; Ryder et al., 2009; Ryder et al., 2012; Harris et al., 2002). Based on available cross sections, areas west of the eastern margin of the Rome Trough have minimal folding, and areas east of the eastern margin of the Rome Trough (e.g. Valley and Ridge) have folds that may violate the assumption of perfectly horizontal strata. Even so, based on the location of available wells, only small portions of West Virginia and Pennsylvania would be affected by this assumption. The expected effects of 2-D heat conduction are higher temperatures on anticlinal crests, and lower temperatures on synclinal troughs as compared to horizontal strata (Frone et al., 2015). Additional effects may happen where abrupt changes in lithology occur (e.g. the eastern margin of the Rome Trough).

Input Variables

The inputs to the model are the processed AASG well database described above, and the COSUNA-based conductivity stratigraphy for each COSUNA section, described in the COSUNA memo.

Parameter Selection

Radiogenic Heat Generation: Sedimentary Rocks

This model assumes that radiogenic heat generation is constant and uniformly distributed in sedimentary rocks, and decreases exponentially in the basement rocks, as per Lachenbruch (1968; 1970). Uniformly distributed radiogenic heat generation in sedimentary rocks is not accurate; however the range of radiogenic heat generation in sedimentary rocks is small, typically between $0.5 \mu\text{W}\cdot\text{m}^{-3}$ (for non-clastic rocks) to $2.0 \mu\text{W}\cdot\text{m}^{-3}$ (for radiogenic clastic rocks) (Waples, 2002). One exception is organic rich shale, which tends to have higher concentrations of uranium. These shales may have radiogenic heat generation values as great as $5.5 \mu\text{W}\cdot\text{m}^{-3}$ (Waples, 2002). Even so, a greater value was not assigned to black shales because so few formations in the basin consist of only black shales, and those that are black shale are not a great enough thickness to significantly deviate from thermal model calculations assuming $1 \mu\text{W}\cdot\text{m}^{-3}$ (difference in heat flow of $0.45 \text{ mW}\cdot\text{m}^{-2}$ per 100 m thickness). Therefore, for this project, a value of $1 \mu\text{W}\cdot\text{m}^{-3}$ was assigned to all sedimentary rocks within the basin.

As an alternative to assuming a single heat generation value, formation specific values may be calculated from ordinary (Bücker and Rybach, 1996) or spectral (Rybach, 1973) gamma ray logs. The availability of spatially well distributed and interpreted gamma ray logs, and time to process them resulted in lithologic complexity in radiogenic heat generation to be undetermined for the basin. Waples (2002) suggests that published values should be used for each lithology in lieu of gamma log measurements for more accurate surface heat flow calculations. Despite this claim, formation specific values were not added into the thermal model because it is unlikely that the heat flow or temperatures at depth will deviate significantly from small changes to sediment heat generation relative to the assumed value. Phase 2 models on the project scale can include these

formation specific values, along with appropriate uncertainty analysis, in order to improve the accuracy of the model.

Radiogenic Heat Generation: Basement Rocks

Heat generation in basement rocks is mainly a result of potassium-bearing felsic rocks. These rocks may exist as plutons (thick mass of intrusive igneous rock), or as part of the matrix rock. The basement rocks of the Appalachian Basin are Grenville age, consisting from east to west of a granulite terrane, a metasedimentary belt, and a gneiss belt, all separated by shear zones (DeWolf and Mezger, 1994). The Grenville basement is exposed nearest the Appalachian Basin in the Canadian Shield, the Adirondack Highlands in New York, and the Blue Ridge of Maryland, Virginia, and further south. Based on the lithology of these rocks surrounding the basin, it is likely that the Appalachian Basin basement does contain plutons (charnockitic suites and other granitoids (Bartholomew and Lewis, 1984)); however the plutons may not be the same thickness or composition throughout the basin. Without detailed knowledge of the composition and thickness of plutons, the basement rocks are assumed to be similar composition (e.g. granitic gneisses and schists, (Saylor, 1999)), with any variation in heat production estimated by the radiogenic heat production at the sediment-basement interface calculated in this model. It is possible that the multiscale potential field edges (see seismic risk memo) identify locations of plutons and/or locations where the composition of the crust is different on either side of the boundary. Therefore, revisions to the assumption of similar basement rocks throughout the basin can be made in future model iterations based on these edges.

From a geochemical perspective, radiogenic heat generation decreases with depth in basement rocks as a result of a decrease in felsic rocks with increasing depth in the crust, and radioelement decay with time. An exponential decay modelling the decrease in radiogenic heat generation with depth has been the traditional assumption since the relationship was first discovered (e.g. Birch et al., 1968; Lachenbruch, 1968, 1970). More recent studies (Sandiford and McLaren, 2002; Vendanti et al., 2011) have shown that the exponential model does not provide the best fit for all basement rocks. For example, Vendanti et al. (2011) demonstrate that power law decay models fit well for six deep boreholes around the world; however the power decay selected for most of these boreholes does not deviate far from the exponential fit. The exponential model is likely a low-end estimate of the heat produced in the crust because it decays faster than the power law fits in Vendanti et al. (2011). Therefore, the exponential model is assumed for this project as a conservative model of heat generation in the basement.

For the exponential model, the scale parameter is the crustal thickness corresponding to a one log decrease in heat generation. Previous studies that have assessed Grenville basement found a variety of estimates for the scale parameter. Variation in the scale parameter is generally thought to represent differences in the geochemical composition of the continental crust (Lachenbruch, 1970). Jaupart (1986) reports 10 km, Jaupart and Mareschal (1999) suggest 9 km, Frone et al. (2015) suggest 7.5 km for West Virginia, Artemieva and Mooney (2001) report a range of 4.6 km – 13.6 km for North American cratons, and Blackwell et al. (2007) suggest using a varying value based on the thickness of sedimentary rock overlying the basement. The logic behind the varying value is that thick sedimentary basins would form only over attenuated (post-rifting) or eroded continental crust; thus the radioactive contribution from the basement would be reduced

due to the reduced crustal thickness. This approach is also used in this model, and will capture the wide variety of reported values for this region. The variable thickness used in this model is provided in Equation 1

$$B = \begin{cases} 10 \text{ km}, & Z_s \leq 3 \text{ km} \\ 13 \text{ km} - Z_s, & Z_s > 3 \text{ km} \end{cases} \quad [1]$$

where B is the value of B as a function of Z_s , and Z_s is the sediment thickness. The maximum value of B is taken to be 10 km for Grenville basement, and areas that have more than 3 km of sediment have a reduced B value. This is the same approach used in Blackwell et al. (2007) and Stutz et al. (2012). The spatial distribution of the calculated values of B using this approach are provided in Figure 2.

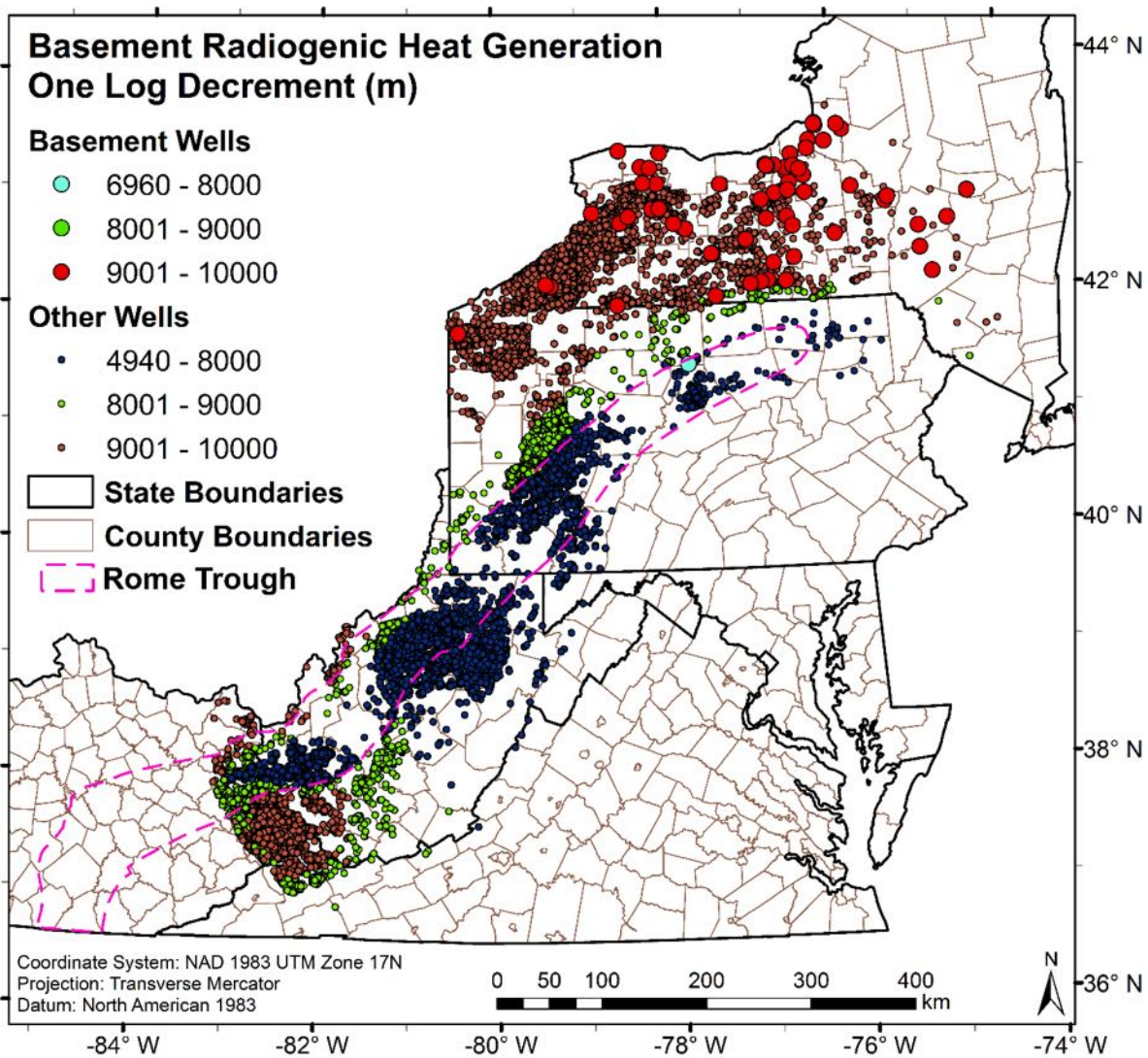


Figure 2: Spatial distribution of calculated values of B using the thermal model. Wells drilled into the basement are shown as larger circles with lighter colors. Figure from Smith (2016).

Thermal Conductivity of Basement Rocks

A value of $2.7 \text{ W}\cdot\text{m}^{-1}\cdot\text{°C}^{-1}$ was selected as the thermal conductivity for basement rocks. This is the mean value of the basement rocks in the regional heat flow database for the United States (Blackwell et al., 2007). This value could be changed in future models and made variable based on location within the basin based on the multiscale potential field analysis. As part of this project, a value of $2.83 \text{ W}\cdot\text{m}^{-1}\cdot\text{°C}^{-1}$ was determined for basement rocks consisting of gneiss, marble, and quartzite. The COSUNA memo outlines the approach taken to arrive at this value. Even so, $2.7 \text{ W}\cdot\text{m}^{-1}\cdot\text{°C}^{-1}$ was used for calculations in this project.

Mantle Heat Flow

The final parameter is the heat flow at the base of the basement rocks. A mantle heat flow of $30 \text{ mW}\cdot\text{m}^{-2}$ is assumed for the Appalachian Basin region of interest in New York, Pennsylvania, West Virginia, and surrounding 50 km buffer zone. This is a lower than average value of the mantle heat flow for the Central Stable Region of the continents as reported by Roy, Blackwell, and Birch (1968), a higher than average value for stable continents as reported by Sclater, Jaupart, and Galson (1980), and about average as reported by Artemieva and Mooney (2001) and Jaupart and Mareschal (1999). This value could be changed based on spatial location in future models based on the multiscale potential field analysis.

Model Output

The properties of the thermal field determined from this model include the thermal gradient, the surface heat flow, temperatures at depths of interest, depths to temperatures of interest, the average thermal conductivity from the surface to the depth of BHT measurement, and the average thermal conductivity for the entire sedimentary rock section at the location of the well. The output thermal variables are stored in a spreadsheet (Attachment 1, “AASG_Thermed.xlsx”).

Equations

The general equations used in the thermal model and their assumptions are discussed in this section. This model updates and corrects three equations previously published by Blackwell et al. (2007), Stutz et al. (2012), and Stutz et al. (2015). These corrections are:

- 1) the heat balance used to estimate the value of radiogenic heat generation at the sediment-basement interface,
- 2) the calculation of surface heat flow relative to the assumptions made, and
- 3) a sediment radiogenic heat generation term in the calculation for the temperature-at-depth for depths deeper than the well.

This model also provides an analytical solution to the Ordinary Differential Equation (ODE) that results from a two-layer model of heat conduction; thus eliminating the need for numerical approximations to the solutions of temperatures at depth, and surface heat flow.

Geothermal Gradient

The geothermal gradient from the surface to the BHT depth is computed using Equation 2

$$G(x, y, Z_w) = \frac{\partial T}{\partial z} = \frac{BHT_{corr} - T_s}{Z_w} \quad [2]$$

where $G(x, y, Z_w)$ is the geothermal gradient at spatial location (x, y) between the surface and Z_w , BHT_{corr} is the corrected BHT, T_s is the average annual surface temperature, and Z_w is the depth of the BHT measurement in the well. This is a linear approximation of the geothermal gradient at location (x, y) from $z = 0$ to $z = Z_w$. Under the assumptions made, the temperature gradient is curved with depth because heat is generated at all locations in the crust. The temperature gradient is also different for each lithology as a result of differences in thermal conductivity.

Some interest may lie in knowing what the geothermal gradient is for a depth range of interest (e.g. from the top of a reservoir to the bottom of a reservoir). This equation is not currently provided in the model, but can be implemented in future versions in Phase 2.

Average Thermal Conductivity

The average thermal conductivity for a column of rock with N perfectly horizontal strata is calculated using Equation 3

$$\bar{k} = \frac{z_{calc}}{\left(\sum_{i=1}^{N-1} \frac{z_{bottom,i} - z_{top,i}}{k_i} \right) + \frac{z_{calc} - z_{top,N}}{k_N}} \quad [3]$$

where \bar{k} is the average thermal conductivity to calculation depth z_{calc} , k_i is the thermal conductivity for lithologic unit i , $z_{bottom,i}$ is the distance from the ground surface to the bottom of unit i , $z_{top,i}$ is the distance from the ground surface to the top of unit i , and n is the number of lithologic units to z_{calc} . The denominator is a summation of thermal resistance in the vertical column. All thicknesses of units would have been scaled to the sediment thickness at the location of the well prior to this calculation, as described in Equation 3 of the COSUNA documentation (Memo 4 of this project). Calculation of thermal conductivity values for sedimentary rock formations (k_i) is also described in the COSUNA documentation. The conductivity of basement rocks is a parameter in the model, described above.

Surface Heat Flow

Using the calculated gradient at the surface and the average thermal conductivity to the depth of the BHT allows for the computation of the surface heat flow. Equation 4 is a rearrangement of Equation 6 solved for surface heat flow

$$Q_s = \begin{cases} G(x, y, Z_w) * \bar{k}_w + \frac{A_s Z_w}{2} & , \quad Z_w \leq Z_s \\ \left[\begin{aligned} & (BHT_{corr} - T_s) + \frac{A_s Z_s^2}{2k_s} + \frac{A_s Z_s (Z_w - Z_s)}{k_B} \\ & + \frac{(Q_m + A_s Z_s)}{k_B (1 - e^{-3})} \left[B \left(1 - e^{-\frac{Z_w - Z_s}{B}} \right) - (Z_w - Z_s) \right] \end{aligned} \right] \\ \frac{Z_w}{\bar{k}_w} + \frac{B \left(1 - e^{-\frac{Z_w - Z_s}{B}} \right) - (Z_w - Z_s)}{k_B (1 - e^{-3})} & , \quad Z_w > Z_s \end{cases}$$

[4]

where Q_s is the surface heat flow, Q_m is the mantle heat flow, $G(x, y, Z_w)$ is the geothermal gradient from the surface to the BHT measurement as computed in Equation 2, T_s is the surface temperature, \bar{k}_w is the average thermal conductivity to the depth of the well, \bar{k}_s is the average thermal conductivity of the sedimentary rocks, k_B is the thermal conductivity in basement rocks, A_s is the radiogenic heat generation in the sediment, Z_w is the depth of the well, Z_s is the thickness of the sedimentary rocks, and B is the log decrement in radiogenic heat production in the basement rocks. This equation is the exact solution to the heat flow present under the assumptions of heat generation in this model from the depth of the BHT to the surface. Not including heat generation would cause a $1 \text{ mW}\cdot\text{m}^{-2}$ difference in surface heat flow for every kilometer of sediment above the well measurement. Differences in basement rocks would vary depending on the value of B .

Heat Generation in Basement Rocks

The heat generation at the sediment-basement interface is determined from the 1-D heat balance (Appendix 1), which leads to Equation 5

$$A_B = \frac{Q_s - Q_m - A_s Z_s}{B * (1 - e^{-3})}$$

[5]

where A_B is the value of radiogenic heat generation at the sediment basement interface and all other terms are described above. It is assumed that no radiogenic heat generation exists at depths greater than $3B$, such that mantle heat flow is present at $3B$. Mathematically, the exponential decay in heat generation would only reach a value of zero at a depth of infinity. This depth is unrealistic because the crust is not infinitely thick. Three times B is selected as a representative thickness of radiogenic heat generation in the crust (Lachenbruch, 1968); however the total thickness of the crust may be greater than $3B$. The variation in the value of B across the basin introduces variability in pluton thickness throughout the basin as a function of sediment thickness.

For wells drilled into basement rocks, Equation 4 is derived using Equation 5 as the second equation needed to solve for the two unknowns of Q_s and A_B . Therefore, the most reasonable estimates of the value for A_B within the basin come from these deep wells, but rely on the assumptions of mantle heat flow, the exponential decay model, the BHT correction equation, and accurate well log information. Even so, the values can inform what reasonable values of A_B for the region would be under these assumptions. Values of A_B generated from the thermal model are provided in Figure 3 and a spatial distribution is provided in Figure 4.

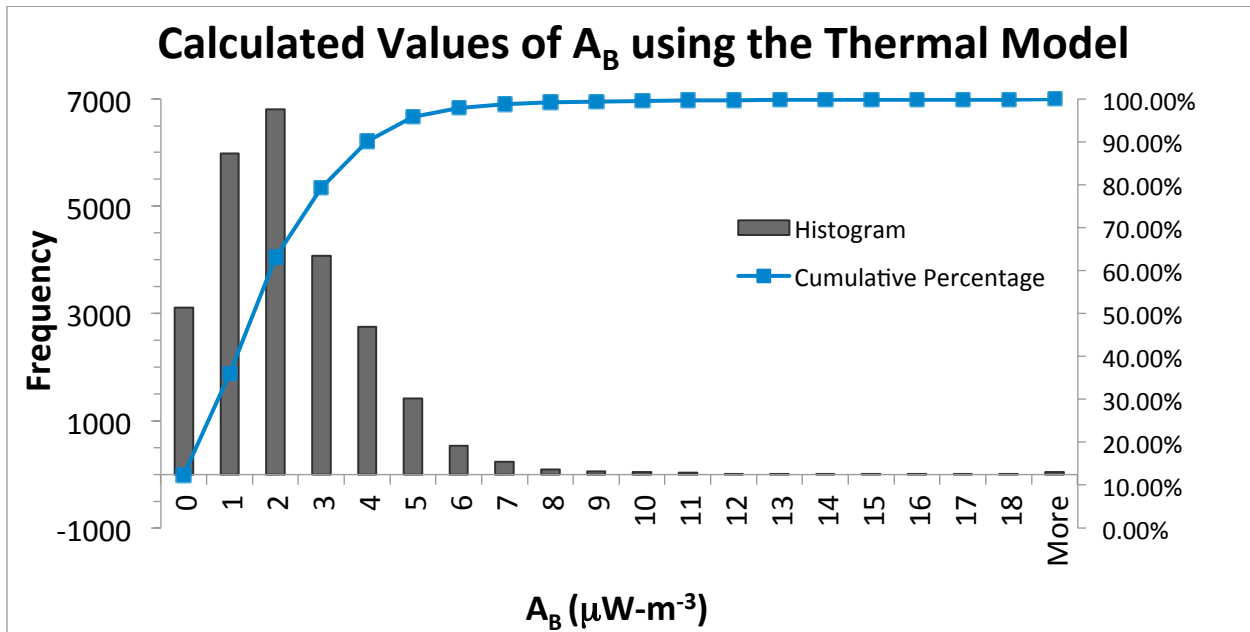


Figure 3: Histogram of A_B values calculated using the thermal model. All 0s are from wells that had negative A_B values (see below for discussion on negative values).

The average value of radiogenic heat generation throughout the entire crustal thickness for Grenville basement is reported as ranging between $0.39 \mu\text{W}\cdot\text{m}^{-3}$ and $0.95 \mu\text{W}\cdot\text{m}^{-3}$ (Artemieva and Mooney, 2001). Adjusting these values to an equivalent exponential decay model corresponds to A_B values between $1.4 \mu\text{W}\cdot\text{m}^{-3}$ and $3.6 \mu\text{W}\cdot\text{m}^{-3}$. Approximately 90% of the calculated A_B values are less than $4.0 \mu\text{W}\cdot\text{m}^{-3}$. All wells deeper than the basement have A_B values less than $5 \mu\text{W}\cdot\text{m}^{-3}$ (Figure 4), and approximately 95% of the records used in the thermal model have values less than or equal to $5.0 \mu\text{W}\cdot\text{m}^{-3}$. Those wells with A_B values greater than $10 \mu\text{W}\cdot\text{m}^{-3}$ all have very high heat flow values ($> 100 \text{ mW}\cdot\text{m}^{-2}$). Some of these may be identified as outliers (see EDA discussion in Memo 9: Exploratory Data Analysis and Interpolation Methodology for Thermal Field Estimation).

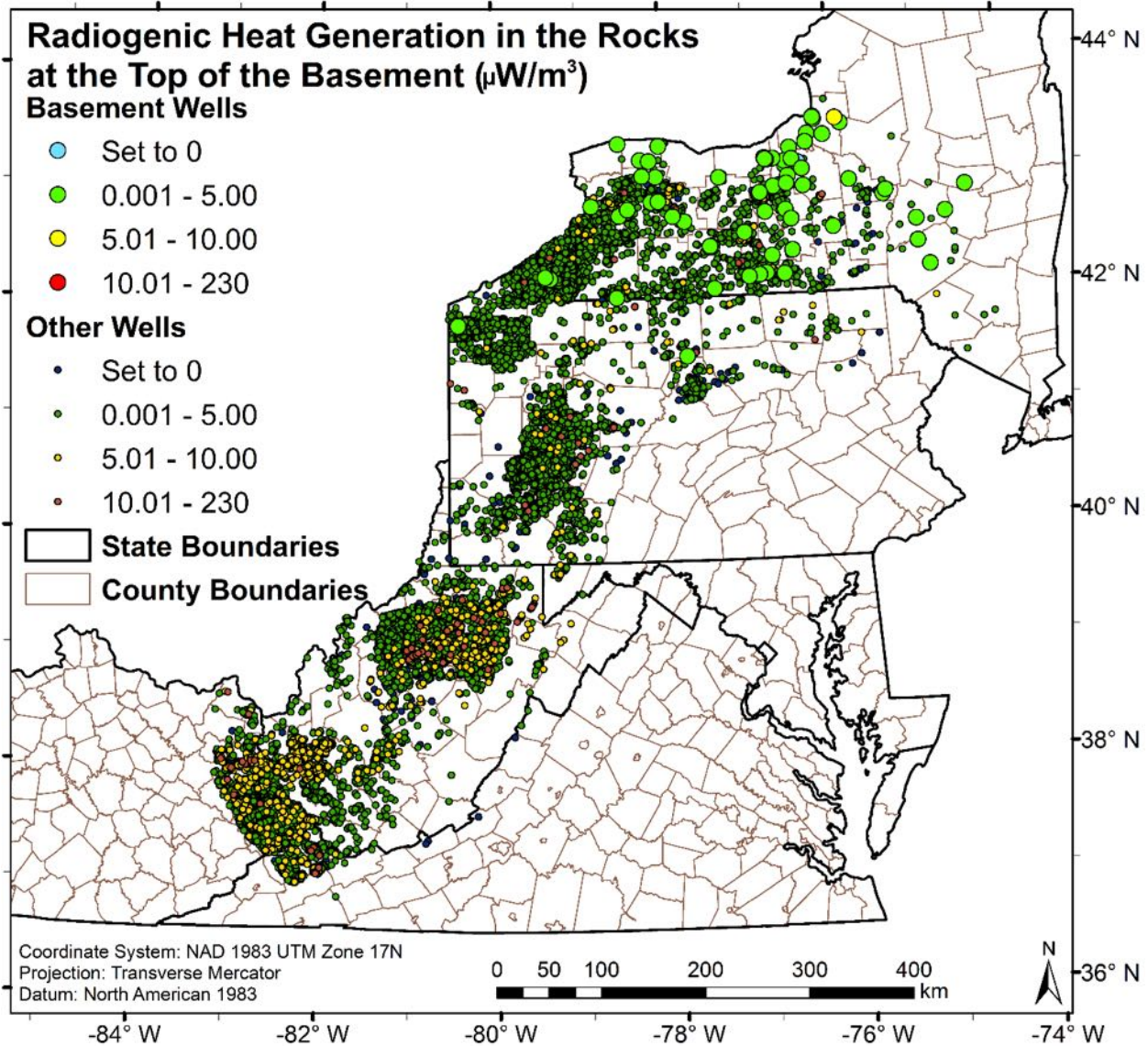


Figure 4: Spatial distribution of calculated A_B values in wells. Wells that are deeper than the basement are shown in larger circles and lighter colors. Figure from Smith (2016).

Negative values of A_B and very high values of A_B may result from this method, which indicates that any input parameter (Q_m , A_s , and/or B) may be incorrect. For negative values, the mantle heat flow or A_s is likely too high. For very high values, the mantle heat flow is likely too low. Because none of the inputs are well constrained, it is not possible to adjust one parameter to make A_B a reasonable value. Additionally, Jaupart (1986) observes that it is not possible to vary the mantle heat flow and the basement radiogenic heat production independently. Even so, A_B and Q_m are treated as independent values in this model because when A_B is negative, the value of A_B is set to 0 without adjusting another parameter (e.g. decreasing mantle heat flow). This means that the estimates of temperature at depth and surface heat flow are greater for these wells than they should be.

Temperature at Depth

The general equations used for calculating temperature at depth are provided in Equation 6 (e.g. Jaeger, 1965). The thermal conductivity subscripts indicate over what depth range the thermal conductivity ought to be calculated.

$$T_{Z_{calc}} = \begin{cases} T_s + \frac{Q_s Z_{calc}}{\bar{k}_{Z_{calc}-0}} - \frac{A_s Z_{calc}^2}{2\bar{k}_{Z_{calc}-0}} & , Z_{calc} \leq Z_w < Z_s \\ T_{Z_w} + \frac{(Q_s - A_s Z_w)(Z_{calc} - Z_w)}{\bar{k}_{Z_{calc}-Z_w}} - \frac{A_s (Z_{calc} - Z_w)^2}{2\bar{k}_{Z_{calc}-Z_w}} & , Z_w < Z_{calc} \leq Z_s \\ T_{Z_s} + \frac{(Q_m - A_B B e^{-3})(Z_{calc} - Z_s)}{k_B} + \frac{A_B B^2 \left(1 - e^{-\left(\frac{Z_{calc} - Z_s}{B}\right)}\right)}{k_B} & , Z_{calc} > Z_s \end{cases} \quad [6]$$

Using this equation, BHT values are calculated exactly for all wells except the 3 basement wells that had negative values of A_B . The BHT in these 3 wells are not perfectly predicted because the A_B value was set to 0; it would need to be negative for it to perfectly reproduce the BHT, which is geologically implausible. The temperature difference from the BHTs in all 3 wells is about 0.1 °C. This difference is not worrisome.

Improvements for Phase 2

The methods presented in this memo were sufficient for Phase 1 time constraints, but can be improved with more time and resources in Phase 2. Accuracy of the thermal model results may be improved by using Appalachian Basin specific thermal conductivities (see Memo 4 for a discussion of potential sources of basin-specific data). Another improvement in accuracy may be accomplished by 1) calculating the surface heat flow at all wells, 2) performing a spatial interpolation of the surface heat flow using the methods presented in Phase 1 to obtain a 1 km² grid of surface heat flow, then 3) using the thermal model on each grid cell to calculate temperatures at depth throughout the basin. This would be an improvement over the current methods because this method will include information about the sediment thickness at all locations of prediction.

On the small-scale of a single play or reservoir for which a detailed economic analysis is to be performed in Phase 2, inclusion of formation specific radiogenic heat generation may become important for estimating the lifetime of the reservoir, and the necessary operating conditions and expenses. Values of heat generation may be obtained from gamma ray logs, if available. The current formulation of the model is not written to handle formation specific radiogenic heat producing elements. From a mathematical perspective, using a different value of radiogenic heat generation in each formation would mean that each formation represents a new layer within the thermal model (as opposed to the 2-layer sediment-basement model used in this analysis). This generalization of the model will prove useful for this project, and possibly to other researchers, but will be computationally more time consuming. Appendix A of Smith (2016) contains the equations needed for an N-layer model of heat generation.

Other potential improvements are listed throughout this memo. Generally speaking, these improvements are related to understanding of the basement rocks via interpretation of the potential field analysis, and assigning appropriate values according to the types identified.

References

- AAPG. (1985a). Northern Appalachian Region correlation chart. D.G. Patchen, K.L. Avary, and R.B. Erwin, regional coordinators.
- AAPG. (1985b). Southern Appalachian Region correlation chart. D.G. Patchen, K.L. Avary, and R.B. Erwin, regional coordinators.
- Artemieva, I.M., and W.D. Mooney. (2001). Thermal thickness and evolution of Precambrian lithosphere: A global study. *J. Geophys. Res.* 106(B8). Pp. 16,387 – 414.
- Bartholomew, M.J., and S.E. Lewis. (1984). Evolution of Grenville massifs in the Blue Ridge geologic province, southern and central Appalachians in M.J. Bartholomew, ed., *The Grenville Event in the Appalachians and Related Topics. Geological Society of America, Special Paper 194.* P. 287
- Beltrami, H., G.S. Matheroo, and J.E. Smerdon. (2015). Impact of borehole depths on reconstructed estimates of ground surface temperature histories and energy storage. *J. Geophys. Res.: Earth Surf.*, 120. doi:10.1002/2014JF003382.
- Birch, F., R.F. Roy, and E.R. Decker. (1968). Heat flow and thermal history of New England and New York, in E. Zen, W.S. White, J.B. Hadley, J.B. Thompson, eds., *Studies of Appalachian Geology: Northern and Maritime.* Interscience. New York. pp. 437-51
- Blackwell, D.D., P.T. Negraru, and M.C. Richards. (2007). Assessment of the enhanced geothermal system resource base of the United States. *Nat. Res. Research.* DOI: 10.1007/s11053-007-9028-7
- Brezinski, D.K.. (2011). Maryland borehole temperatures [Data file]. AASG Geothermal Data Repository. Last modified December 29th, 2011. Retrieved from <http://repository.stategeothermaldata.org/repository/resource/cc54f15894222c91e71e4530dc088fec/>
- Bücker, C., and L. Rybach. (1996). A simple method to determine heat production from gamma-ray logs. *Mar. Pet. Geol.*, 13(4). Pp. 373–5.
- Curl, D.. (2011). Kentucky borehole temperatures [Data file]. AASG Geothermal Data Repository. Last modified July 26th, 2011. Retrieved from <http://repository.stategeothermaldata.org/repository/resource/168566464e3d5f8f3cde3b9fc004bd38/>
- DeWolf, C.P., and K. Mezger. (1994). Lead isotope analyses of leached feldspars: Constraints on the early crustal history of the Grenville Orogen. *Geochemica et Cosmochimica Acta.* 58(24). Pp. 5537-50.
- Frone, Z.S., D.D. Blackwell, M.C. Richards, and M.J. Hornbach. Heat flow and thermal modeling of the Appalachian Basin, West Virginia. *Geosphere.* V. 11(5). Pp. 1279-90. doi: 10.1130/GES01155.1
- Gass, T.E.. (1982). The geothermal heat pump. *Geothermal Resources Council Bulletin*, 11. Pp. 3-8.
- Harris, D.C., J.A. Drahovzal, J.B. Hickman, B.C. Nuttall, M.T. Baranoski, and K.L. Avery. (2002). Rome Trough Consortium Final Report and Data Distribution.

- Horowitz, F.G., J.D. Smith, and C.A. Whealton. (2015). JaredThermalConductivity [Data repository]. GeothermalCode. Available online <https://bitbucket.org/geothermalcode/jaredthermalconductivity>
- Ingersoll, L.R., O.J. Zobel, and A.C. Ingersoll. (1948). Heat conduction; with engineering and geological applications. New York, McGraw-Hill Book Co.. p. 278
- Jaeger, J. C. (1965). Application of the theory of heat conduction to geothermal measurements, *in* W. H. K. Lee, ed., *Terrestrial Heat Flow*. American Geophysical Union. Washington, D.C.. doi: 10.1029/GM008p0007
- Jaupart, C.. (1986). On the average amount and vertical distribution of radioactivity in the continental crust, *in* Burrus, J., ed., *Thermal Modeling in Sedimentary Basins: Éditions Technip*. Paris. pp. 33–47.
- Jaupart, C., and J.C. Mareschal. (1999). The thermal structure and thickness of continental roots. *Lithos*, 48. Pp. 93-114.
- Lachenbruch, A.H. (1968). Preliminary geothermal model of the Sierra Nevada. *J. of Geophys. Res.*, 73(2). Pp. 6977-89.
- Lachenbruch, A.H. (1970). Crustal temperature and heat production: Implications of the linear heat-flow relation. *J. of Geophys. Res.*, 75(17). Pp. 3291-300.
- Lachenbruch, A.H. (1980). Comment on ‘A reinterpretation of the linear heat flow and heat production relationship for the exponential model of heat production in the crust’ by R.N. Singh and J.G. Negi. *Journal of the Royal Astronomical Society*, 63. Pp. 791-95.
- Leftwich, T.. (2011). Ohio borehole temperatures [Data file]. AASG Geothermal Data Repository. Last modified June 30th, 2011. Retrieved from <http://repository.stategeothermaldata.org/repository/resource/ba2f0b9d21f71acfe10609f76e2699e6/>
- Lovering, T.S., and H.D. Goode. (1963). Measuring geothermal gradients in drill holes less than 60 feet deep, East Tintic District, Utah. *Geological Survey Bulletin*, 1172. United States Government Printing Office, Washington.
- Mooney, J. (2011). Sediment thickness of North America and neighboring regions *in* Technical Report: Central and Eastern United States Seismic Source Characterization for Nuclear Facilities. Appendix A: Description of the CEUS SSC Project Database, Figure A-14, File: CEUS_sed_thickness_USGS_R0.tif. EPRI, Pala Alto, CA, U.S. DOE, and U.S. NRC: 2012.
- Repetski, J.E., R.T. Ryder, D.J. Weary, A.G. Harris, and M.H. Trippi. (2008). Thermal maturity patterns (CAI and %Ro) in upper Ordovician and Devonian rocks of the Appalachian Basin: A major revision of USGS Map I–917–E using new subsurface collections. USGS Scientific Investigations Map 3006. Reston, Virginia.
- Roy, R.F., D.D. Blackwell and F. Birch. (1968). Heat generation of plutonic rocks and continental heat flow provinces. *Earth and Planetary Science Letters*, 5. Pp. 1 – 12. North Holland Publishing Comp. Amsterdam.
- Roy, R.F., D.D. Blackwell and E.R. Decker. (1972). Continental heat flow, chapter 19 *in* E.C. Robertson, ed., *The Nature of the Solid Earth*. McGraw Hill. New York. Pp. 506-44.
- Rybach, L.. (1973). Determinations of heat production in rocks of the Swiss Alps. Beiträge zur Geologie der Schweiz. *Geotechnische Serie*, 51. Kümmerly & Frei. Bern. 43 p.
- Ryder, R.T.. (1992). Stratigraphic framework of Cambrian and Ordovician rocks in the Central Appalachian Basin from Lake County, Ohio, to Juniata County, Pennsylvania. IMAP 2200.

- Ryder, R.T., C.S. Swezey, R.D. Crangle Jr., and M.H. Trippi. (2008). Geologic cross section E-E' through the Appalachian Basin from the Findley Arch, Wood County, Ohio, to the Valley and Ridge province, Pendleton County, West Virginia. USGS SIM-2985.
- Ryder, R.T., R.D. Crangle Jr., M.H. Trippi, C.S. Swezey, E.E. Lentz, E.L. Rowan, and R.S. Hope. (2009) Geologic cross section D-D' through the Appalachian Basin from the Findley Arch, Sandusky County, Ohio, to the Valley and Ridge province, Hardy County, West Virginia. USGS SIM-3067.
- Ryder, R.T., M.H. Trippi, C.S. Swezey, R.D. Crangle Jr., R.S. Hope, E.L. Rowan, and, E.E. Lentz. (2012) Geologic cross section C-C' through the Appalachian Basin from Erie County, North-Central Ohio, to the Valley and Ridge Province, Bedford County, South-Central Pennsylvania. USGS SIM-3172.
- Saylor, T.E.. 1999. Precambrian and Lower Paleozoic metamorphic and igneous rocks - in the subsurface. Chap. 3C in C. H. Shultz, ed., *The Geology of Pennsylvania*. Pennsylvania Geological Survey/Pittsburgh Geological Society. *Special Publication 1*. Pp. 51-58.
- Sclater, J.G., C. Jaupart, and D. Galson. (1980). The heat flow through oceanic and continental crust and the heat loss of the Earth. *Reviews of Geophysics and Space Physics*, 18(1). Pp. 269 – 311.
- Shank, S., R. Kaiser, M. Sullivan, M. Deemer, K. Stuckert, E. Macklin, & T. Suskie. (2012). Pennsylvania Borehole Temperatures [Data file]. AASG Geothermal Data Repository. Last modified December 11th, 2012. Retrieved from <http://repository.stategeothermaldata.org/repository/resource/9e15e1a59b768b330d029e86dc0d6512/>
- Singh, R.N., and J.G. Negi. (1979). A reinterpretation of the linear heat flow and heat production relationship for the exponential model of heat production in the crust. *Geophysical Journal of the Royal Astronomical Society*, 57. Pp. 741-4.
- Slater, B.. (2012). New York Borehole Temperatures [Data file]. AASG Geothermal Data Repository. Last modified October 4th, 2012. Retrieved from <http://repository.stategeothermaldata.org/repository/resource/9e15e1a59b768b330d029e86dc00481f/>
- Smith (2016). Analytical and geostatistical heat flow modeling for geothermal resource reconnaissance applied in the Appalachian Basin. MS Thesis. Cornell University, Ithaca, NY.
- Southern Methodist University (SMU) Geothermal Lab. (2016). Near ground surface temperature map [dataset]. Data and Maps / Temperature Maps. Available online <http://www.smu.edu/Dedman/Academics/Programs/GeothermalLab/DataMaps/TemperatureMaps>. Accessed 22 June 2016.
- Stutz, G. R. (2012). Development, analysis, and application of a well by well method for estimating surface heat flow for regional geothermal resource assessment. MS Thesis. Cornell University, Ithaca, NY.
- United States Geologic Survey (USGS) National Map. (2015). DEM Product Index 1/3rd arc-second. <http://viewer.nationalmap.gov/viewer/>
- Vendanti, N., R.P. Srivastava, O.P. Pandey, and V.P. Dimri. (2011). Fractal behavior in continental crustal heat production. *Nonlin. Processes Geophys.*, 18. Pp. 119-24. doi:10.5194/npg-18-119-2011
- Virginia Division of Geology and Mineral Resources (VDGMR). (2011). Virginia borehole temperatures [Data file]. AASG Geothermal Data Repository. Last modified December

- 28th, 2011. Retrieved from
<http://repository.stategeothermaldata.org/repository/resource/b99f8f8e3a7d798d77d4c343bd16b987/>
- Waples, D.W.. (2002). A new model for heat flow in extensional basins: Estimating radiogenic heat production. *Nat. Res. Res.*, 11(2). Pp. 125 – 33.
- West Virginia Geologic and Economic Survey (WVGES). (2011). West Virginia borehole temperatures [Data file]. AASG Geothermal Data Repository. Last modified June 30th, 2011. Retrieved from
<http://repository.stategeothermaldata.org/repository/resource/168566464e3d5f8f3cde3b9fc0052329/>
- West Virginia Geological and Economic Survey (WVGES). (2006). PCMB_Contours.zip [Data file]. Trenton Black River Project. Data available online
<http://www.wvgs.wvnet.edu/www/tbr/resources.asp>.
- Whealton, C.A.. (2015). Statistical correction of temperature data for New York and Pennsylvania Wells. M.S. Thesis, Cornell University, Ithaca, NY, May 2015. Pp. 1-289
- Whealton, C.A. and J.D. Smith (2015). [geothermal_pfa] code repository. Available Online
https://github.com/calvinwhealton/geothermal_pfa. Accessed 22 June 2016.

Appendix 1: Derivation of the One-Dimensional Conduction Heat Balance

The content presented in this appendix is taken from portions of Appendix A and Appendix B of Smith (2016) with permission of the author. Minor changes to text have been made, including equation numbers, and references to the body of the thesis.

Assumptions

Steady state, one dimensional (vertical) heat conduction is assumed. There are two layers of radiogenic heat generation: 1) a constant value of heat generation in sedimentary rocks, and 2) an exponential decrease in heat generation with increasing depth in the basement rocks. Deeper than 3 e-folding lengths in the basement ($3B$) there is no longer any heat generation (e.g. Lachenbruch, 1968; 1970). Thermal convection and advection are not considered. The thermal conductivity stratigraphy (derived from the COSUNA rock columns, see Memo 4 of this project) consists of N-1 layers of sedimentary rock, and 1 layer of basement rock. The thermal conductivity remains constant within each layer. This derivation proceeds from the bottom to the top of the column in Figure A1. A constant value of heat generation is assumed for sedimentary rocks.

Heat Flow deeper than $3B$

At depths deeper than $3B$ it is assumed that there are no longer any radiogenic elements in the crust that contribute to the surface heat flow. In effect, a depth of $3B$ in the basement rocks is the depth to the mantle heat flow value, even if the depth does not correspond to the boundary associated with Q_m (e.g. the crustal thickness, or the asthenosphere). Therefore, the heat flow, $Q(z)$, at depths greater than or equal to $3B$ is the mantle heat flow, Q_m .

$$Q(z) = Q_m, \quad z \geq 3B \quad [A1]$$

Heat Flow through the Top of the Basement

Let $Z = Z_{calc} - Z_s$.

At depths from $Z = 0$ (the surface of the basement) to $3B$, A_B decays exponentially according to Equation A2.

$$\begin{aligned} Q_B &= A_B \int_0^{3B} e^{\left(-\frac{z}{B}\right)} dz \\ Q_B &= -A_B B \left[e^{\left(-\frac{z}{B}\right)} \right]_0^{3B} \\ Q_B &= -A_B B * \left[e^{\left(-\frac{3B}{B}\right)} - 1 \right] = A_B B [1 - e^{-3}] \end{aligned} \quad [A2]$$

Generally, the heat flow at any location within the basement rocks is the sum of the mantle heat flow and the generated heat from $3B$ to a location z in the basement.

$$Q(z) = Q_m + A_B B \left[e^{\left(-\frac{z-Z_s}{B}\right)} - e^{-3} \right] \quad , \quad Z_s \leq z \leq 3B + Z_s \quad [A3]$$

Note that when $z = 3B + Z_s$ the radiogenic heat generation term goes to 0, and $Q(Z_s+3B) = Q_m$. When $z = Z_s$, the heat flow through the top of the basement rocks is:

$$Q_{sb} = Q_m + Q_B \quad [A4]$$

Surface Heat Flow

Radiogenic heat generation in sedimentary rocks is assumed to be constant. Under this assumption, the total heat produced in the sedimentary rocks from decaying radioactive material is given by Equation A5.

$$Q_{sed} = A_s Z_s \quad [A5]$$

The heat flow at any depth, z , within the sedimentary rocks is the summation of the heat from the mantle, basement rocks, and sedimentary rocks below z , as shown in Equation A6.

$$Q(z) = Q_m + Q_B + A_s(Z_s - z), \quad 0 \leq z \leq Z_s \quad [A6]$$

At $z = Z_s$, $Q(Z_s) = Q_{sb}$. The heat flow at the ground surface ($z = 0$) is provided in Equation A7.

$$Q_s = Q_m + Q_B + Q_{sed} \quad [A7]$$

In this heat conduction model, the value of radiogenic heat generation in the volume of rock at the top of the basement is unknown. The heat balance in Equation A7 may be rearranged to solve for this variable for each well based on the known or assumed variables and parameters.

$$A_B = \frac{Q_s - Q_m - A_s Z_s}{B * [1 - e^{-3}]} \quad [A8]$$

If there are N-1 layers of heat generation from sedimentary rocks, $A_s Z_s$ in Equation A8 could be replaced with a summation: $A_1 Z_1 + \sum_{i=2}^{N-1} A_i (Z_i - Z_{i-1})$.

Attachments

These attachments provide references to databases (Attachments 1 and 2) and additional methodological details (Attachments 3 through 5). The files referenced in this memo are available on the Geothermal Data Repository (Cornell University, 2015). These attachments and data files are copied verbatim from portions of Chapter 3, Section 3.7; Chapter 2, Section 2.7; and Appendix C of Smith (2016) with permission of the author. Minor changes to text have been made, including equation and figure numbers, and references to the body of the thesis.

List of attachments

- 1) Well Databases Folder
- 2) Trenton-Black River Sediment Thickness Map
- 3) Influence of Annual Temperature Fluctuation on Near-Surface Temperatures
- 4) Drilling Fluid Query in SQL
- 5) Probabilistic assignment of Drilling Fluid based on Nearest Neighbor Wells

1. Well Database Files

File 1: All_States_BHT_HeatFlow_Raw_Combined.xlsx

Description:

This file contains all of the raw well data gathered for this project. These state databases do not necessarily have BHT measurements for all wells, and may contain duplicate records within-database and between databases.

For quality purposes, only those records that were submitted to the AASG State Geothermal Data Repository were selected for use in this project because all of these records had BHT data. Additional data sources collected include 1) Pennsylvania records from American Association of Petroleum Geologists (AAPG), 2) New York records from Empire State Oil and Gas Information System (ESOGIS) 4) West Virginia records from the National Geothermal Data System (NGDS had 1000 fewer records than AASG), and 5) Ohio heat flow wells. Many of the wells with BHT measurements available in these databases are likely recorded within AASG wells, though this was not checked for all databases.

File 2: AASG_Combined.xlsx

Description:

The data contained within this database are taken from the AASG Geothermal Data Repository (all references in body of memo for each state). This database has 41,099 records. Duplicate records have not been removed. The spreadsheets for each state did not have the same field names, or the same fields. When combining the data, only those fields needed for analysis (listed below) were placed into the AASG_Combined file. All of the original data may be joined to this database using the StateID field, if further information is desired*.

This database was screened for obvious data entry errors in fields important to the project. These fields included the latitude, longitude, depth of measurement, and the BHT. Latitude and longitude were checked by ensuring that all wells were located in the county specified. All but one well (RowID 11604) passed this test. Depth of measurement and BHT were screened for abnormally high or low values. Several obvious instances were found and corrected as described below. As part of this screening, an additional record was found and added for API number 31003042480000 at 7560 ft and 140 °F based on the log data for the well.

* StateID is used as a unique identifier because some wells do not have an APINo. A StateID field was added into the original state databases for joining purposes.

Corrections to Records:

RowID numbers 19375 and 35927 had a very high depth of measurement. RowID 19375 had 2 leading 3s but one 3 was deleted to match the driller depth. RowID 35927 had a depth of measurement of 36,885, but it seemed like the 6 was a typo because by deleting the 6 the depth was the same as the TVD. RowID 35939 depth of measurement was about 10 times deeper than the TVD and driller depth with no apparent typo, so the depth of measurement for this well was deleted. RowID 37534 has a depth of measurement that is about 10,000 ft more than the TVD, with a BHT that did not match that depth, so the depth of measurement was deleted. RowID 22772 had a -9999 as the depth of measurement, so this value was deleted.

Database Fields

RowID	Unique identifier for the wells, starting at 1.
StateID	Unique identifier that matches the original state database. Labels have the state postal code followed by a number, starting at 1.
WellName	Name of the well as listed by the state datasets (blank if not available).
APINo	API number for the well, if one exists (blank if not available).
County	County where the well is located.
State	State where the well is located.
LatDegree	Decimal degree latitude for the well.
LongDegree	Decimal degree longitude for the well.
SRS	Coordinate reference system as listed by the state database.
DrillerTotalDepth	Total depth as logged by the driller. This may include any horizontal, non-vertical component of the drilling (m or ft).
TrueVerticalDepth	The vertical depth of the well (m or ft).

DepthOfMeasurement The depth of temperature measurement as listed by the state database (m or ft).

ElevationGL Ground level elevation (m or ft)

LengthUnits Units used for the depth fields (m or ft).

MeasuredTemperature Temperature measured at the depth of measurement (°C or °F).

TemperatureUnits Unit of the temperature measurement (°C or °F).

DrillingFluid Fluid used to drill the well, if provided. Blank otherwise.

File 3: AASG_Processed.xlsx

Description:

This file has all of the above fields, and the following additional fields. Before running through the heat conduction model, all wells were checked for depth of measurement being greater than the first increment of calculation in the heat conduction model (10 m). It was found that RowID 35925 had a depth of measurement shallower than 10 m, so this record was removed from the database before using the heat conduction model.

Additional Fields Added Before Heat Conduction Model Calculations

BHT_C The MeasuredTemperature in Celsius.

CalcDepth_m The well depth corresponding to temperature measurement based on quality hierarchy of 1) DepthOfMeasurement, 2) TrueVerticalDepth, and 3) DrillerTotalDepth. If no depth is available, NA is listed. (This field was not used for this project, but it is provided for reference).

MeasureDepth_m The DepthOfMeasurement in meters. If no depth is available, NA is listed.

ReportedElevation_m The ElevationGL in meters.

CRS Coordinate reference system rewritten as WGS84 and NAD83 for database consistency.

API_14Dig 14 digit API number for each state, when available. If no API number exists, NA is listed. This is intended to be a well identifier, but values may be truncated in some programs.

Fluid_Type	Generalized fluid type based on Whealton (2015). (all_agfs, all_mgpw for air and mud, respectively; blank if not available).
Pct_Air	Proportion of nearest neighbor wells that are air drilled. 1 if the well is known to be air drilled, 0 if the well is known to be mud drilled. All values are between 0 and 1, inclusive.
Pct_Mud	Proportion of nearest neighbor wells that are mud drilled. 1 if the well is known to be mud drilled, 0 if the well is known to be air drilled. All values are between 0 and 1, inclusive.
BHTReg	BHT correction region.
CorrBHT	Corrected BHT. (°C)
Corr_error	Error code for corrected BHT. 0 if there's not an error.
UTM_Long	Universal Transverse Mercator (UTM) Zone 17N longitude. (m)
UTM_Lat	Universal Transverse Mercator (UTM) Zone 17N latitude. (m)
BasementDepth	Depth to the basement (i.e. sedimentary rock thickness). (m)
SurfTemp	Average annual surface temperature derived from Gass (1982).
COSUNA_ID	The ID number assigned to the COSUNA section for the well.
COSUNA_NAME	COSUNA column name corresponding to the COSUNA_ID.
ROME_ID	Binary. 1 if a well is in the Rome Trough, 0 if it is not.
SedRadHeat	Radiogenic heat generation in sedimentary rocks ($\mu\text{W}/\text{m}^3$)
QMantle	Mantle heat flow (mW/m^2)

File 4: AASG_Thermed.xlsx

Description:

This is the data after processing in the heat conduction model. This file has all of the above fields and the following additional fields calculated in the model. Enough information is reported in this database such that calculations may be made using the heat flow equations in the text. The temperature at depth equations (Eq. 6) require knowledge of the thermal conductivity and thickness of each rock layer, scaled to the sedimentary rock thickness. This information is not provided here, but is provided in the Cornell University (2015) data submission.

Additional Fields Added After Heat Conduction Model Calculations

BaseRadHeat	Calculated radiogenic heat generation in the volume of rock at the top of the basement ($\mu\text{W}/\text{m}^3$)
Gradient	The geothermal gradient calculated from CorrBHT at the MeasureDepth_m ($^{\circ}\text{C}/\text{km}$)
HeatFlow	Heat Flow calculated using the thermal model (mW/m^2)
Depth50C	Depth to 50 $^{\circ}\text{C}$ calculated using the thermal model (m)
Depth80C	Depth to 80 $^{\circ}\text{C}$ calculated using the thermal model (m)
Depth100C	Depth to 100 $^{\circ}\text{C}$ calculated using the thermal model (m)
Temp2km	Temperature at 2 km calculated using the thermal model ($^{\circ}\text{C}$)
Temp3km	Temperature at 3 km calculated using the thermal model ($^{\circ}\text{C}$)
Temp4km	Temperature at 4 km calculated using the thermal model ($^{\circ}\text{C}$)
Temp5km	Temperature at 5 km calculated using the thermal model ($^{\circ}\text{C}$)
Kw	Harmonic average thermal conductivity to the MeasureDepth_m ($\text{W}/[\text{m } ^{\circ}\text{C}]$)
Kc	Harmonic average thermal conductivity to the BasementDepth ($\text{W}/[\text{m } ^{\circ}\text{C}]$)
BHT_diff	Difference between the calculated BHT at the MeasureDepth_m and the CorrBHT. ($^{\circ}\text{C}$)

2. Trenton-Black River Sediment Thickness Map

Description:

The map of sedimentary rock thickness was created from the Trenton-Black River (TBR) project structural contours of the Precambrian basement, relative to mean sea level (WVGES, 2006). These structural contours were converted to a raster file in ArcMap 10.2 (ESRI, 2015; Contour to Raster tool). The raster represents the depth to the Precambrian basement from mean sea level. The raster was processed to represent the sedimentary rock thickness by adding the elevation using 30 m resolution DEMs from the USGS National Map (2015) that were mosaicked together into a single DEM for the region using ArcGIS (Mosaic tool). Finally, the resulting TBR raster was manually clipped to an approximate 10 km distance from the extent of the Precambrian contour lines to avoid extrapolation of the sedimentary rock thickness beyond the data support. This clip did not greatly impact the number of wells capable of being used in the assessment of the thermal field for the basin.

The accuracy of this map of sedimentary rock thickness was in question for West Virginia because of thickness differences on the order of kilometers compared to the more recent map of sedimentary rock thickness by Mooney (2011). Upon inspection, the map created by Mooney (2011) was derived from 1985 data, which is before detailed knowledge of structural features of importance, such as the Rome Trough in West Virginia, were established in portions of the Appalachian Basin. To check the accuracy of the TBR derived sedimentary rock thickness map, a set of wells, with detailed stratigraphic information that were drilled into the Martinsburg formation or deeper in West Virginia, were used. First, the well-reported depth to the touchdown formation top was compared to the depth to the formation top in the COSUNA columns. If the well depth-to-formation was within the minimum and maximum depth-to-formation as listed on the COSUNA column, the true thickness of sedimentary rocks at the well location was assumed to be within the minimum and maximum sedimentary rock thickness as listed on the COSUNA column. Using this method, the TBR sedimentary rock thicknesses were all within the COSUNA sedimentary rock thickness ranges. Therefore, the TBR sedimentary rock thickness map is reasonably accurate within West Virginia. As another check for West Virginia, the depth to basement for Ryder et al. (2008) cross section E-E' is ~7.5 km in the southeast region of WV; whereas the TBR map is 7 km and the Mooney (2011) map is nearly 12 km.

A simple comparison of the TBR sedimentary rock thickness map to the actual sedimentary rock thickness in a set of wells that reached the basement is provided in Figure B1. The choice of the TBR sedimentary rock thickness map seems appropriate for the region.

Depth to Basement

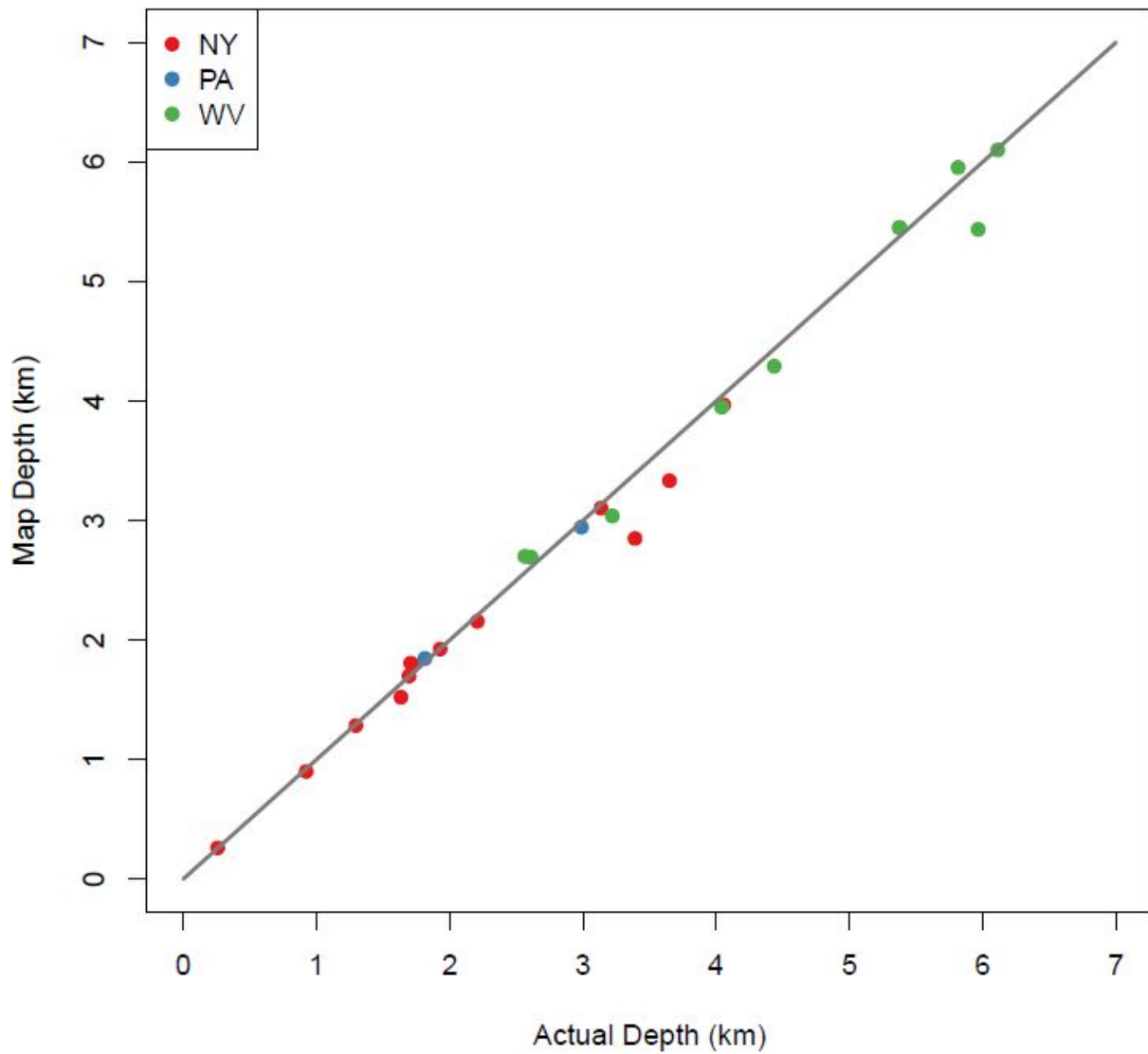


Figure B1: Comparison of the sedimentary rock thickness derived from the Trenton-Black River Project (Map Depth) to the actual sedimentary rock thickness from a subset of wells that reached basement rock. A 1:1 line is shown for reference. Depth to basement is the same as sedimentary rock thickness.

3. Influence of Annual Temperature Fluctuation on Near-Surface Temperatures

Surface temperature fluctuations on time scales ranging from annual to millennial have been shown to affect near-surface temperatures at depths from 15 m to 600 m (e.g. Beltrami, Matheroo, and Smerdon, 2015). Millennial and centennial scale variations are not of concern in this project because the BHT data used for calculations are deeper than 1000 m, which is deeper than the 600 m potential penetration depth for these time scales. However, it is worthwhile to assess the potential impact of the annual temperature fluctuation on the shallow groundwater temperatures taken by Gass (1982) at depths between 15 m and 46 m. This assessment only considers heat conduction. Advection of heat via groundwater could also impact the measurements taken by Gass (1982). Additionally, disturbances to the thermal field as a result of surface landscape alteration (Roy, Blackwell, and Decker, 1972) are not considered here, but may have had an effect on the temperature measurements taken by Gass (1982).

Under these assumptions, the depth of disturbance in the thermal field as a result of the annual surface temperature fluctuation varies according to the thermal diffusivity of the subsurface medium; the more thermally diffuse, the deeper the propagation. Sandstone has the greatest thermal diffusivity of the rocks located at the surface of the Appalachian Basin. A high-end thermal diffusivity of sandstone ($0.014 \text{ cm}^2/\text{s}$) was used to approximate a worst-case impact on Gass' (1982) measurements. The dampening of the annual surface temperature fluctuation with depth follows an exponentially decaying sine curve given in Equation B1 (Ingersoll, Zobel, and Ingersoll, 1946)

$$T(z) = a_T \left(\left(e^{-z\sqrt{\frac{\pi}{\alpha P}}} \right) * \sin \left(\frac{2\pi t_a}{P} - z\sqrt{\frac{\pi}{\alpha P}} \right) \right)$$

[B1]

where a_T is the amplitude of the surface temperature fluctuation ($^{\circ}\text{C}$), α is the thermal diffusivity (cm^2/s), z is the depth below the surface (cm), P is the period of the annual temperature fluctuation (1 year, in seconds), and t_a is time since the annual average surface temperature (s). The bounds of the annual near-surface temperature with depth are provided by Equation B2.

$$T(z) = a \left(e^{-z\sqrt{\frac{\pi}{\alpha P}}} \right)$$

[B2]

From Figure B2 it is clear that the shallow groundwater temperature measurements taken by Gass (1982) would have been relatively stable with regard to the annual temperature fluctuation, which is less than $\pm 0.5 \text{ }^{\circ}\text{C}$ at the depths measured. Because the depths of measurement were taken between 15 m and 46 m, the heat conduction model calculations implicitly assume that the map of surface temperature that was created by the Gass (1982) measurements is also the average annual temperature at the surface (0 m). This is a reasonable assumption based on this analysis. The uncertainty in the value of Gass (1982) measurements may be assumed to be $0.5 \text{ }^{\circ}\text{C}$ based on the temperature fluctuation with depth. Additional uncertainty in the derived map results from creation of the contour map, and interpolating between the contours; however this

uncertainty is not provided by Gass (1982) or the map provider, Southern Methodist University (2016).

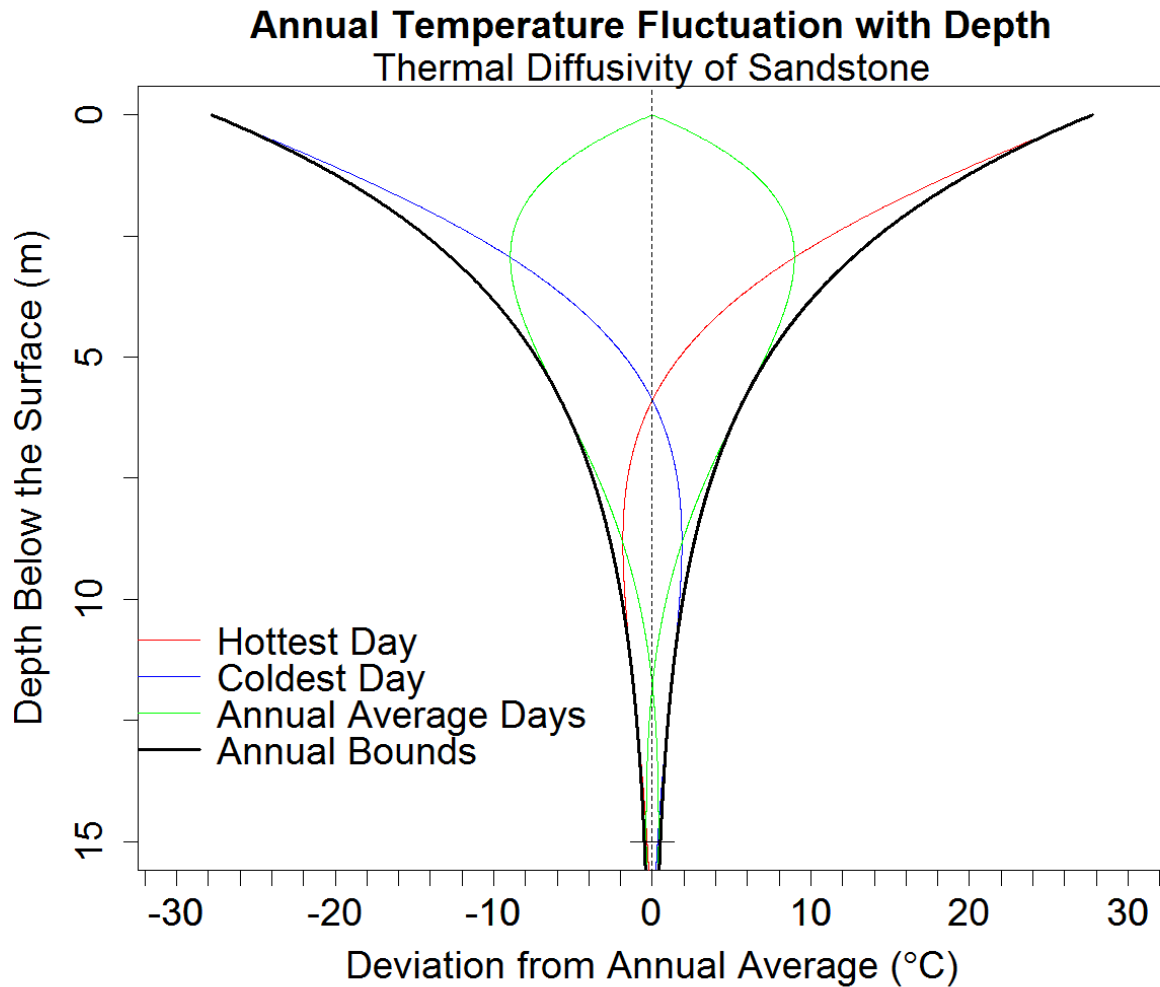


Figure B2: Annual temperature fluctuation with depth for a sandstone with higher than average thermal diffusivity ($0.014 \text{ cm}^2/\text{s}$). The surface temperature is assumed to fluctuate $\pm 28 \text{ }^\circ\text{C}$ from the annual average surface temperature. Hottest day, coldest day, and average days refer to the surface temperature. Figure modified from Ingersol, Zobel, and Ingersol (1946).

4. DrillingFluidQuery_ALL.SQL

Query:

```
SELECT * FROM ("Whealton_Wells_GDB"  
              JOIN "aasg_whealton"  
                ON "aasg_whealton".whealton_pk = "Whealton_Wells_GDB".id)  
JOIN "AASG_Wells_GDB"  
ON "aasg_whealton".aasg_pk = "AASG_Wells_GDB".id
```

Description:

Because the API number is not a unique identifier (e.g. a well with 2 BHT measurements creates 2 records with the same API number) a method for joining many wells with the same API numbers in the Whealton (2015) database to many wells with the same API numbers in the AASG database was needed. This is called a many-to-many join.

First, a link table called [aasg_whealton] was created by combining the [AASG_Wells_GDB] and [Whealton_Wells_GDB]. This table consists of five fields: 1) a primary key (unique identifier) for the Whealton database [whealton_pk] 2) primary key for the AASG database [aasg_pk], 3) API number for AASG database [aasg_api], 4) API number for the Whealton (2015) database, and 5) spatial geometry of the data.

This code selects all [*] information from the wells in the Whealton (2015) database for which the API number [id] equals the Whealton primary key in [aasg_whealton]. Then, the AASG wells for which the API number [id] equals the AASG primary key in [aasg_whealton] are joined to the previous table. This resulted in 687 matching records for 245 unique wells in NY and PA before processing of the data, as described in Selecting and Processing Wells for Analysis. Post processing, only 137 records matched.

5. Drilling Fluid Nearest Neighbors [WhealtonWells_NAD_FinalProcessing.xlsx and whealtonAir&Mud_NAD3_RemovedNoLongLatPts_Reg_Unique.shp]

Description:

All wells in the Allegheny Plateau BHT section in New York and Pennsylvania needed to have drilling fluid information in order to use the BHT adjustment equation, as defined in Memo 2 of this project. For the 137 records in the processed AASG database that matched the Whealton (2015) drilling fluid database, the use of the BHT equation for air or mud drilled wells is not a problem. For all other wells, no drilling fluid information is available.

When a well did not have drilling fluid information, a weighted average of the BHT corrections for air and mud drilled wells was used based on the drilling fluid used to drill nearest neighbor wells. The nearest neighbor wells were the Whealton (2015) wells. The logic behind using a probabilistic assignment of nearest neighbors is that the wells close to each other are more likely to be drilling for the same resource and drilled by the same company, and therefore use a similar drilling fluid.

An important step prior to running the nearest neighbor function was to check the Whealton (2015) database for wells with the same API number. Multiple records for the same well would count that well's drilling fluid multiple times, thus assigning an inappropriate proportion of air and mud to a well with unknown drilling fluid. Of the 2233 records in the Whealton (2015) database, there were 1755 unique wells.

A function was written to determine the proportion of air and mud drilled wells (see Whealton and Smith [2015] code repository). This function uses the nearest 25 points within 50 km to compute the proportion of air and mud for an unknown well. The algorithm is defined such that the distance to the 25th nearest neighbor is the distance cutoff for the inclusion of wells in the calculation of the proportion. If the 25th nearest point happens to have another point the same distance away (same location or different location), then there may be more than 25 points used to compute the proportion of air and mud. If 25 points did not exist within 50 km, then that well was assigned the regional average proportion of air and mud drilled wells of 0.194 air drilled and 0.806 mud drilled.

Memo 9: Exploratory Data Analysis and Interpolation Methodology for Thermal Field Estimation
To: Appalachian Basin Geothermal Play Fairway Analysis Group
From: Jared Smith
Date: Original from October 16, 2015. Updated on September 27, 2016.
Subject: Exploratory Data Analysis and Interpolation Methodology for Thermal Field Estimation.

Applicability: This memo describes an exploratory spatial data analysis on the temperature-at-depth well data. This memo also presents the methods used to interpolate the temperature-at-depth data to create the thermal risk factor and uncertainty maps for this project. Smith (2016) Chapter 4 contains further methodological details and results, specifically for the Appalachian Basin surface heat flow.

Introduction

The Appalachian Basin Geothermal Play Fairway Analysis team needs to have a method for creating the thermal resource and risk factor maps, and to quantify associated uncertainties of the spatial predictions. The data available for these spatial predictions are the tens of thousands of well bottom-hole temperature (BHT) measurements, which are primarily from regional oil and gas drilling. These data are known to have errors and are considered low quality temperature information (e.g. Demming, 1989). Some of the data processing steps for these BHT data are described in Memo 4 of this project. Memo 4 also describes the heat conduction model that was used to calculate the surface heat flow and the geotherm temperature at depth profiles at the surface location corresponding to each well's BHT-depth measurement.

As a result of using lower quality BHT data, an exploratory data analysis (EDA) is employed on the calculated thermal variables (e.g. the temperature at 1.5 km depth) to scan for potentially anomalous observations, and retain only those observations that are deemed to be of sufficient quality. The EDA involved an assessment of each variable according to the depth of the BHT measurement, followed by the identification and removal of spatial outliers. The details of the outlier analysis algorithm developed for this project are provided in Memo 6. This memo presents general results from the outlier analysis for each thermal variable of interest. The EDA also included an evaluation of the spatial autocorrelation for each thermal variable of interest. The results of the spatial autocorrelation analysis are provided for the Depth to 80 °C, which is the selected thermal risk factor in this project. All other thermal resource variables were subject to the same EDA methodology. Detailed EDA methods for the surface heat flow are presented in Smith (2016).

The thermal information obtained at the spatial location of each well may be viewed as control points in a basin-scale spatial prediction of temperatures at a specified depth and depths to a specified temperature. Many interpolation algorithms may be suitable for prediction of these thermal variables of interest in the Appalachian Basin. The results of the EDA were used to inform which interpolation algorithm to use for this project. Recent work by Smith (2016) showed that the Appalachian Basin surface heat flow does not have a stationary spatial correlation structure (i.e. the semi-variogram is nonstationary). As a result, Smith (2016) used

stratified ordinary kriging interpolation to laterally stratify the basin into sub-regions, many of which have statistically significantly different spatial correlation structures for the surface heat flow. Lateral stratification boundaries are defined by the gravity and magnetic potential field edges at depths from 7 km – 15 km (see Memo 13 of this project for details on these potential field data). The interpolation regions used in Smith (2016) have also been used in this project. This memo briefly discusses the creation of the interpolation boundaries based on the gravity and magnetic potential field edges. Smith (2016) Appendix D provides further geological interpretation of these edges and their use as interpolation boundaries.

The performance of the stratified ordinary kriging algorithm was tested using two cross validation techniques. The first was a leave one out cross validation (LOOCV). Results and details of the LOOCV are provided at the county level in Memo 10. The second was an evaluation of the kriging predicted mean temperature at 1.5 km depth. This evaluation compared the set of 47 equilibrium well BHT measurements near 1.5 km depth with the kriging predicted mean temperature at 1.5 km depth, and the uncertainty standard error in the predicted mean. The results from this evaluation are presented at the end of this memo.

Well Data Processing and Exploratory Data Analysis

After each thermal variable of interest was calculated using the heat conduction model (see Memo 4), a few additional data processing steps were required before employing the exploratory data analysis (EDA). These processing steps are presented in the sections that follow.

Negative Thermal Gradients

Out of the 20,750 wells that were used in the heat conduction model, 39 of them had negative values of the geothermal gradient calculated between the surface and the depth of the BHT measurement. Calculated values of the geothermal gradient are negative if the assumed annual average surface temperature is greater than the BHT measurement. A negative geothermal gradient is not physically reasonable. Thus, for these wells a calculated negative gradient may indicate that 1) the annual average surface temperature is too high, 2) the BHT was cooled as a result of advection of heat via groundwater, or 3) the BHT or depth of measurement was not properly recorded. Case 1) would affect shallower wells more than deeper wells, whereas case 2) and 3) could affect any well.

Figure 1 shows the spatial locations of the 39 wells with negative surface to BHT depth thermal gradients. Some clustering of wells with negative geothermal gradients exists, which may indicate local advection of heat. However, clustering could also be a result of improper recording of data from a local drilling company. Given that many more wells surrounding the wells with negative geothermal gradients have positive geothermal gradients, and further information is not available to quality control these data, the wells with negative geothermal gradients were removed from the dataset.

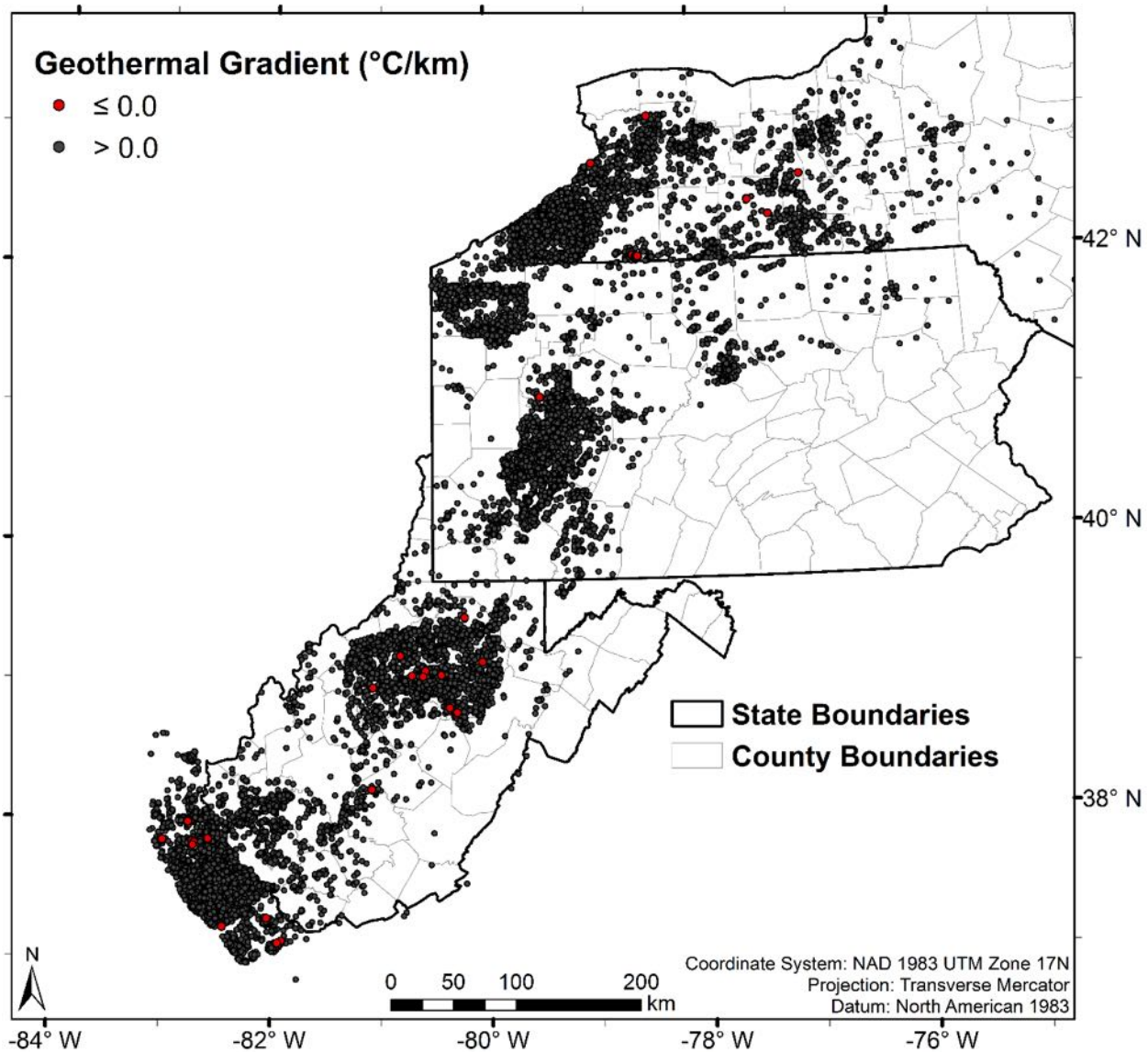


Figure 1: Locations of all 20,750 wells (black) and the 39 wells with negative surface-to-BHT depth geothermal gradients (red). Figure from Smith (2016).

Minimum BHT Depth for Data Quality Purposes

Each of the thermal variables were plotted against the depth of measurement to determine if there were any biases based on depth. The plot for the surface heat flow (Q_s) is provided in Figure 2. Based on previous studies of the Appalachian Basin geothermal field (Stutz et al., 2015; Frone and Blackwell, 2010), values of the surface heat flow greater than 100 mW/m^2 are likely too high, but may be real if the data are spatially clustered. Based on Figure 2 and similar analyses for the other thermal variables, it was decided that many wells with BHT measurements shallower than 1,000 m were likely unreliable. These wells were removed from the database for

quality control. Aside from a few likely high outliers for West Virginia, the heat flow values for wells with a depth of BHT measurement greater than 1000 m appear to be in agreement.

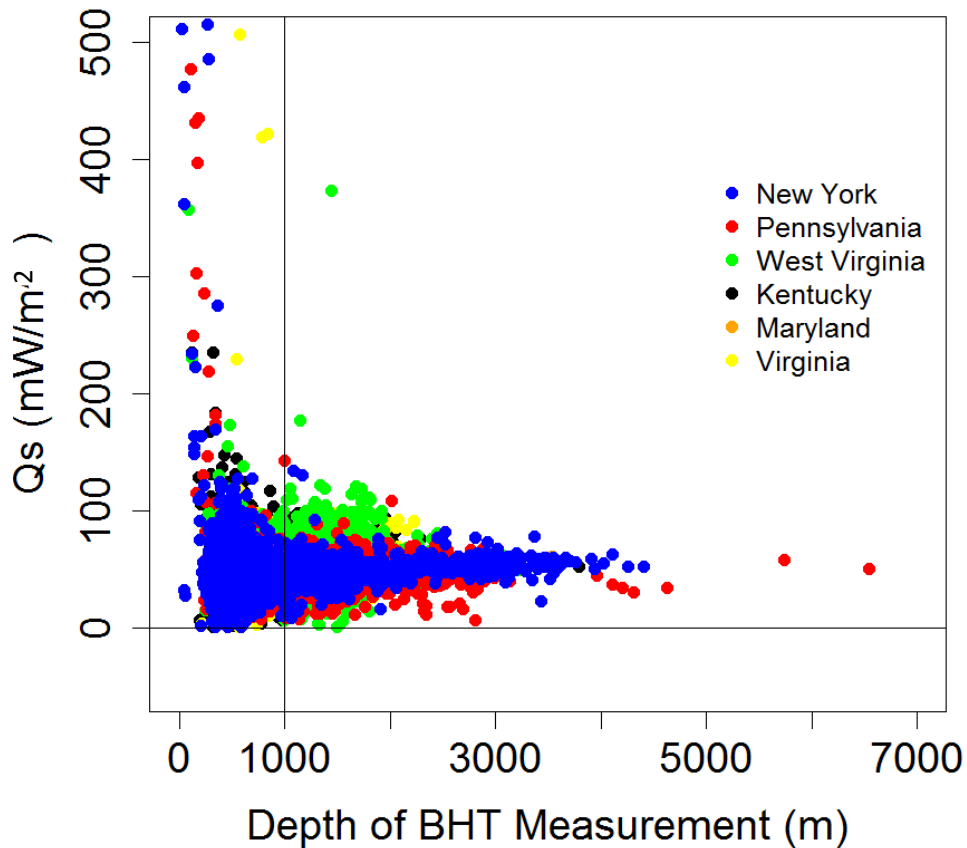


Figure 2: Surface heat flow versus the depth of BHT measurement for the 20,711 wells with positive geothermal gradients. Only wells deeper than the 1000 m cutoff (vertical black line) were retained for further analysis.

For the large majority of the region, a 1000 m minimum BHT depth cutoff did not cause major data gaps to appear on the map (Figure 3). Generally, northern New York wells are removed because of a shallow depth to basement, and the oil and gas resource of interest was shallower than 1000 m. In northwestern Pennsylvania near the Allegheny National Forest there is insufficient deep well data, which would cause gaps in spatial predictions of the temperature at depth. Therefore, this region was examined closely in Smith (2016) for data agreement at shallower depths. As a result, the minimum BHT depth for this region was selected as 750 m (Smith, 2016).

In summary, using these minimum BHT depths resulted in 13,818 records for further analysis.

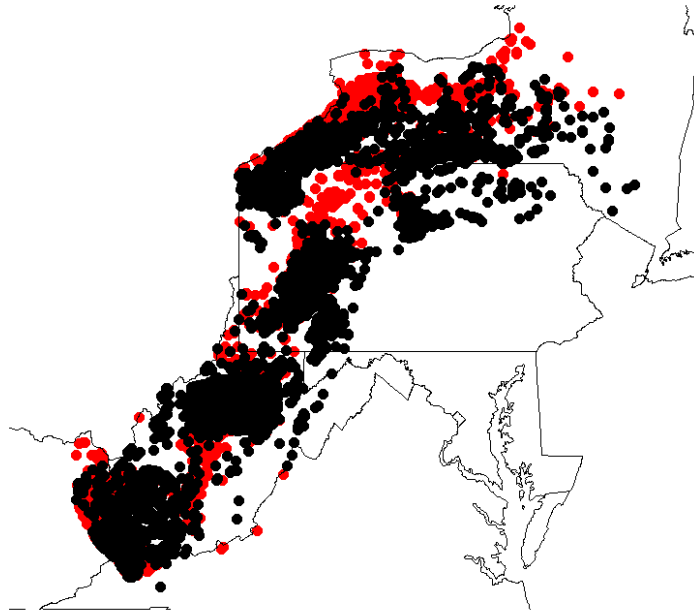


Figure 3: Wells remaining for outlier analysis (black) and wells removed based on the 1000 m cutoff depth (red). Note that some wells were added back to the data gap in northwestern Pennsylvania.

Wells in the Same Spatial Location

Several records in the database had the exact duplicate coordinates as another record. Observations in the same spatial location could interfere with spatial exploratory data analyses. For example, in a spatial outlier analysis a location should only be counted once, assuming that the information about the thermal field provided by the multiple BHT measurements is the same. Exact duplicate locations in the database may result from a well having more than one measurement at different depths (same API number), from multiple wells starting at the same offshoot but branching off from each other (different API numbers), from wells being located on the same drill pad and assigned the average coordinates of the pad (different API numbers), or from a duplicate of a record in the database. In all of these cases, only the deepest measurement for a location was retained for analysis. The deepest measurement was used as a method of rapid quality control. Other methods that include all of the temperature measurements at different depths may be more accurate to the true geotherm temperature at depth profile.

In a few locations the deepest depth had two or more different BHTs. The measurement date and time were not available for these wells, so it was not possible to tell if these temperature

differences were spread out in time, and thereby indicative of temporal variations in the thermal field. For these data, only the wells with BHTs at the same depth that were within 2 °C of each other were retained – the remainder were dropped from the dataset for quality concerns. The retained wells were checked for potential errors in recording the depth of measurement that could explain the difference in BHTs at same depth. Each well in the database has up to three depths: a driller depth (arc length), a true vertical depth, and a depth of temperature measurement. The depth of temperature measurement is used for wells in this project; however the database could contain errors. Therefore, the quality control was that the smaller of the multiple BHTs should correspond to the lesser of the depth of measurement and the true vertical depth or the driller depth. For wells that had sufficient information to make this assignment, the BHT corresponding to the depth of measurement was retained. For all other wells, the average of the multiple BHTs at the same depth were taken, and the geotherm was recomputed using the thermal model described in Memo 4 to reflect the average BHT. Only 1 well (2 records) needed to be rerun in the thermal model, so an adjustment of uncertainty in the BHT measurement was not made to reflect that 2 measurements were taken at the same depth for this well, rather than 1.

After taking only the deepest wells in each spatial location, 13,381 BHT measurements remained for the spatial outlier analysis.

Spatial Outlier Analysis

Each thermal variable of interest in this project was subject to a spatial outlier analysis prior to the spatial correlation analysis and the spatial interpolation. Memo 6 of this project contains the details of the spatial outlier analysis algorithms developed for this project. The selected algorithm used the nearest 25 points within a 32 km radius for outlier analysis. For the roughly 200 points that did not have 25 points within 32 km, the outlier analysis was not conducted by the algorithm. Instead, these points were inspected manually by looking at the values of the available nearest neighbor points. Only two wells were removed based on manual inspection. Table 1 summarizes the number of outliers removed for each thermal variable. It is interesting that points that are outliers for one thermal variable may not be outliers for another variable. This result suggests that a multivariate spatial outlier analysis would be worth evaluating.

Table 1: Outliers identified and removed for each thermal variable of interest in this project.

Variable	Number of Outliers	Percentage of Data Removed
Surface Heat Flow *	1014	7.6%
Depth to 80 °C ⁺	1184	8.8%
Depth to 100 °C [†]	1117	8.4%
Temperature at 1.5 km [†]	979	7.3%
Temperature at 2.5 km [†]	944	7.1%
Temperature at 3.5 km [†]	970	7.3%

* From Smith (2016).

⁺ Updated using the 750 m minimum BHT depth in northwestern Pennsylvania.

[†] Original results, which use a 1000 m minimum BHT depth everywhere. These numbers may change if they are rerun using the 750 m minimum BHT depth in northwestern PA.

Spatial Autocorrelation

Previous studies of the Appalachian Basin geothermal field have shown that there is significant spatial autocorrelation that ought to be captured in spatial predictions (Smith, 2016; Aguirre, 2014). Smith (2016) showed that the structure of surface heat flow spatial autocorrelation (the semi-variogram) is nonstationary on the scale of the Appalachian Basin. In order to capture more local spatial correlation structure, Smith (2016) used a different model of spatial autocorrelation for several sub-regions of the Appalachian Basin. These sub-regions were defined by the gravity and magnetic potential field edges described in Memo 13 of this project. The physical and statistical justification for using sub-regions is that rocks with different physical properties (e.g. concentration of radiogenic heat producing elements) may contribute different amounts of heat to the surface, thereby acting as different data generating processes that must be modeled separately in prediction of the thermal field.

We believe that the use of potential field edges to define sub-regions reflects physical differences in rock properties (density and magnetite) better than do physiographic provinces, which do not necessarily define regions of similar rock composition. The following section briefly describes how these sub-regions were created from the potential field edges. Smith (2016) Appendix D provides more detailed information.

Creating Interpolation Boundaries

The concept of a heat flow province was first discussed in Roy, Blackwell, and Birch (1968) and referred to the apparent transition zone in heat flow originating from the mantle across a major continental structural divide on the order of about 100 km width. The Appalachian Basin is expected to be within a single heat flow province because it is within a stable continent setting. However, several studies (e.g. Rao, Rao, and Narain, 1976) have identified heat flow sub-provinces (Roy, Blackwell, and Decker, 1972) in basement rock, related to spatial differences in the contribution of heat production to the surface heat flow. This concept of a heat flow sub-province is applied to the interpolation boundaries defined in this project. A geostatistical argument for heat flow sub-provinces in the Appalachian Basin is presented in Smith (2016).

The interpolation boundaries used in this project are provided in Figure 4 (from Smith [2016]). The gravity edges were the primary source for selecting the interpolation boundaries. The magnetic edges were used to refine the interpolation boundaries when large anomalies appeared within any section. Only the SWPA interpolation region was defined by the magnetic potential field edges.

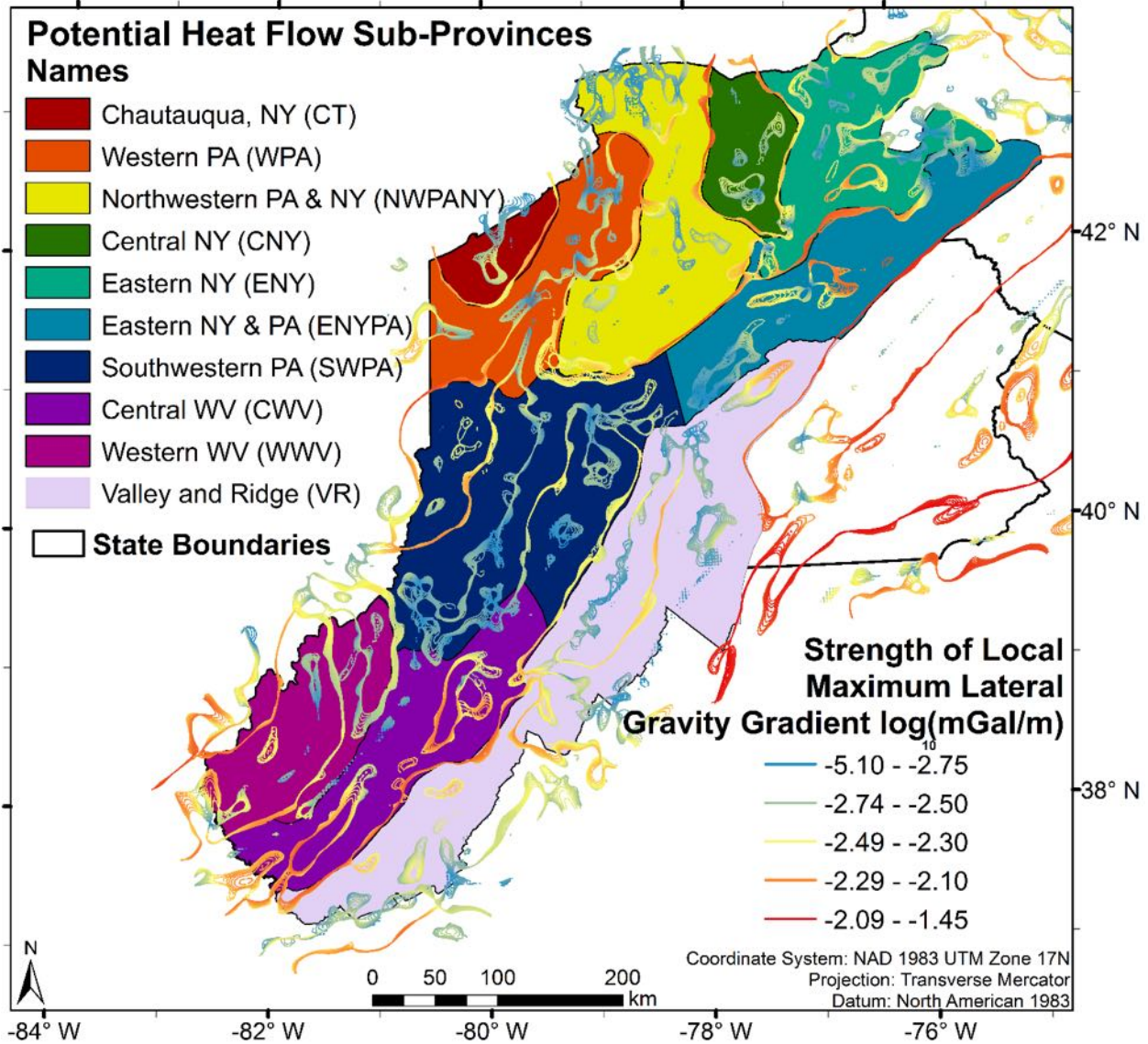


Figure 4: Interpolation boundaries (potential heat flow sub-provinces) used in this project and the gravity potential field edges at depths from 7 km – 15 km from Memo 13. This figure is from Smith (2016) Appendix D. The sub-regions are colored starting in the top left, proceeding clockwise. The gravity edges are colored by the strength of the lateral gravity gradient, with red having higher contrast in rock density on either side of the boundary.

Stratified Ordinary Kriging Interpolation

The potential heat flow sub-provinces in Figure 4 are laterally defined strata (regions) in a stratified ordinary kriging interpolation. Ordinary kriging (e.g. Cressie, 1988) assumes that the mean is unknown within the estimation window. In this study, the radius of the estimation window is selected based on the distance of spatial correlation on the semi-variogram. Ordinary kriging also assumes that the error may be modeled as a stationary stochastic field within the region for which the field is defined. Each of the strata are assumed to have their own stationary stochastic field, which is modeled for each thermal variable using semi-variograms. Semi-variograms are models of spatial autocorrelation. All sub-regions in Figure 4 except for the Valley and Ridge were used. The Valley and Ridge sub-region was not used because too few well data points were available to construct a reliable semi-variogram.

Stratified ordinary kriging was implemented in the `gstat` package of R (Pebesma, 1998).

Semi-variogram Analysis

In expectation, the difference in the geothermal field for observations that are closer to one another should be smaller than the difference in the geothermal field for observations that are more distant from each other. One metric that describes this relationship is the semi-variogram: the semi-variance as a function of distance between all $(n*(n-1))/2$ point pairs in the dataset. There are five key parameters that must be fit in order to empirically model the semi-variogram. These are the nugget, range, sill, anisotropy, and shape of the semi-variogram. The nugget refers to the apparent discontinuity in semi-variance at infinitesimal distances between two wells. If we had perfect measuring devices, and properties of the thermal field remained constant through time, and the assumptions used to model the thermal field were perfectly accurate, the nugget would be essentially zero. Because the nugget is not zero, it represents the measurement, positioning, and modelling errors present within the dataset. The range is the distance to which spatial correlation is modeled, and the sill is the value of semi-variance at the range. The shape of the semi-variogram may be selected from a collection of nearly 20 classic functional forms that provide positive definite and non-singular matrices for spatial prediction (Pebesma, 2014). Of these options, the Gaussian, Exponential, and Spherical shapes were used in this project to model and fit semi-variograms.

Semi-variograms were fit using a weighted regression. The weights were determined by the number of point-pairs, n , divided by the distance, h , to the bin squared: n/h^2 . This is a common approach, which ensures that more weight is placed on points closer to one another rather than farther away. For complex (nested) semi-variograms, ordinary least squares regression was used instead of weighted regression. A further explanation of the ordinary kriging methods used in this analysis is provided in the Appendix of Stutz et al. (2015) under the subheading Kriging Interpolation. Smith (2016) also provides further details.

Anisotropy

Anisotropy refers to directional dependence in the structure of spatial autocorrelation. Figure 5 shows the anisotropy within each of the nine sub-regions identified in Figure 4. As expected,

each sub-region does not exhibit the same degree of anisotropy, and some do not appear to exhibit anisotropy at all. This result supports the use of stratified kriging that can capture these differences in prediction and uncertainty analysis of the thermal field. Figure 6 shows the sample (points) and fitted (black lines) semi-variograms along the major and minor axes of the anisotropy ellipse for each of these interpolation regions.

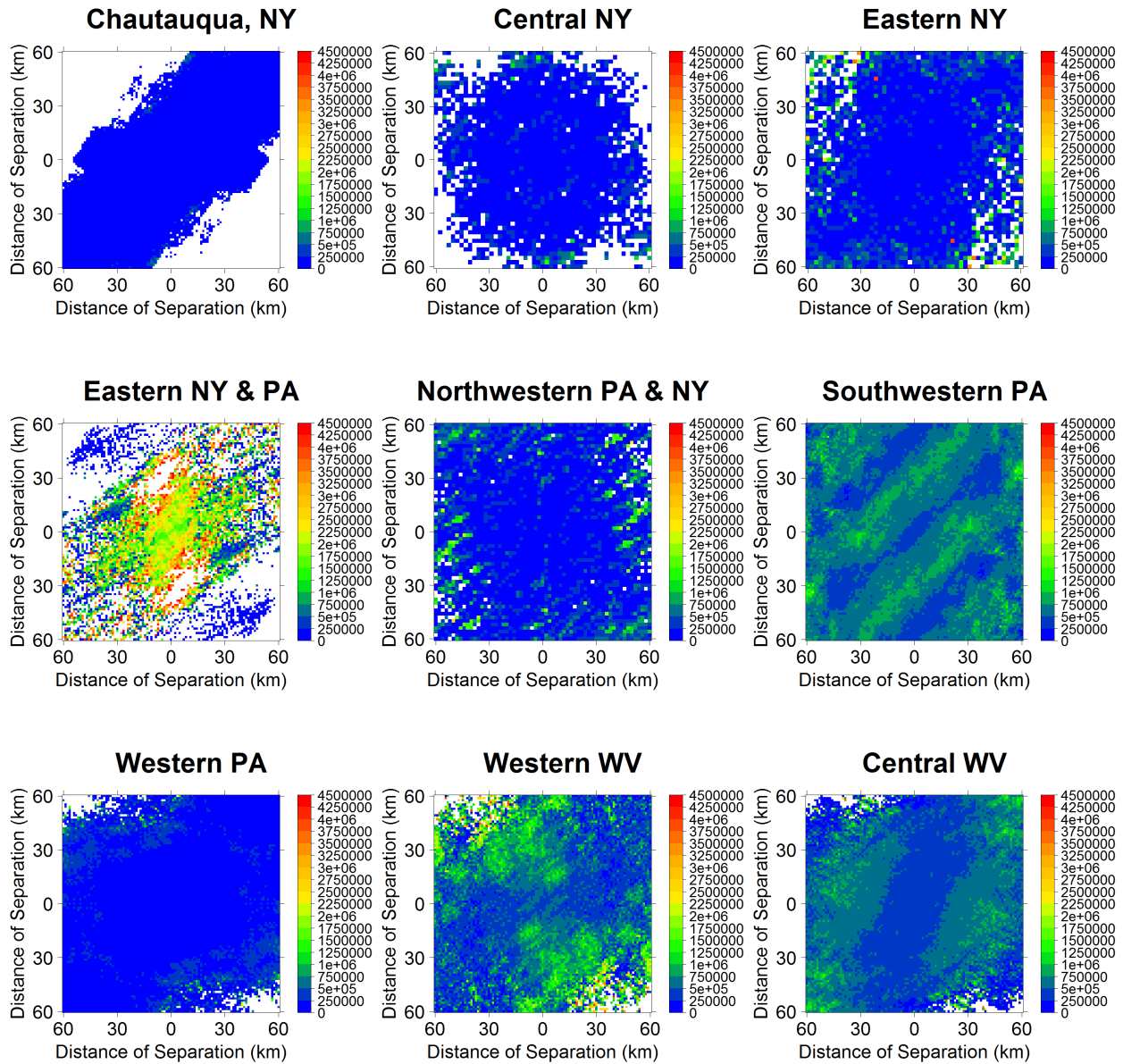


Figure 5: Directional semi-variance plots for the Depth to 80 °C. All plots have the same distance on the x and y axes, and the same semi-variance color bar. White areas are where insufficient data exist to calculate a value of the semi-variance. Where the plots appear elliptical, there is anisotropy (directional preference) in the structure of spatial correlation.

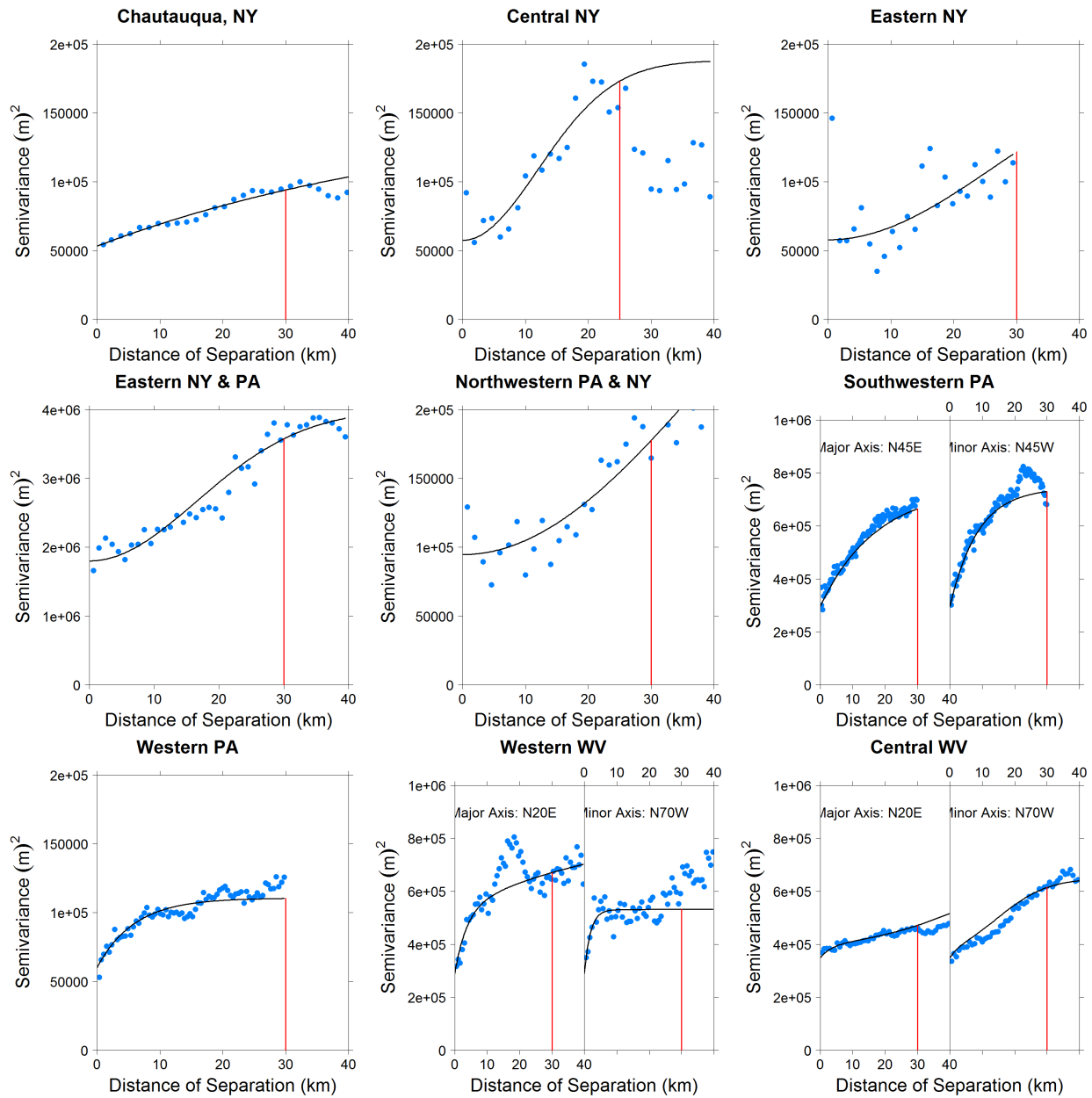


Figure 6: Fitted semi-variograms used for the interpolation of the Depth to 80° C within each of the nine sub-provinces. Sub-provinces that showed anisotropy in Figure 5 have semi-variograms defined along the major and minor axes of the anisotropy ellipse. Note that all plots have the same x-axis, but the y-axis is not the same on all plots. The vertical red line indicates the maximum interpolation distance of 30 km. In Central NY the maximum interpolation distance was 25 km because the semi-variogram only fit well to a 25 km distance.

Using these fitted semi-variogram models, the ordinary kriging interpolation was run within each of the sub-provinces. Only those wells located within a sub-province were used to predict in the sub-province. Additionally, a minimum of 5 points within 30 km of a location were needed to make a prediction. A maximum of 50 points were used for computational efficiency.

Results

The predicted mean and the standard error of the predicted mean Depth to 80 °C are provided in Figure 7. Generally, south-central New York, north-central Pennsylvania, and several areas in West Virginia appear to have the shallowest mean depth to 80 °C. The uncertainty in the predicted mean is quite different spatially as a result of differences in the semi-variogram structure in each of the sub-provinces. Uncertainty in the mean value should be a great interest to decision makers who aim for investigating in more detail those locations that have the smallest uncertainty and the shallowest depth to 80 °C.

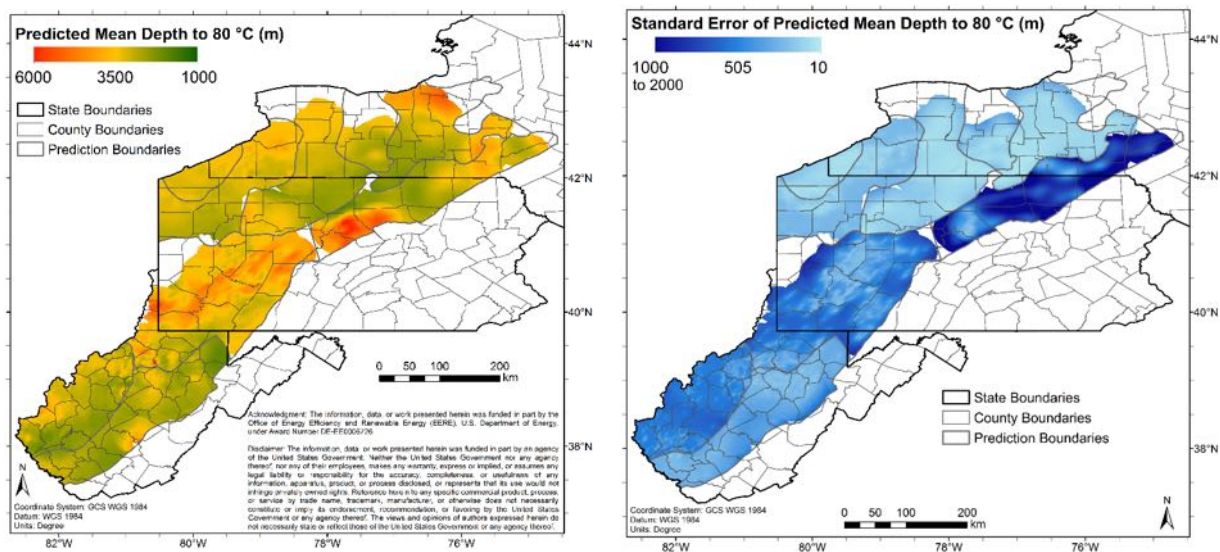


Figure 7: Predicted mean (left) and standard error of the predicted mean (right) depth to 80 °C. The interpolation boundaries (Figure 4) are shown in light gray lines. Note that red (deeper) is bad and green (shallower) is good on the predicted mean map. The upper end of the standard error map has a range because nearly all error between 1000 – 2000 m is contained within one section – Eastern New York and Pennsylvania.

Cross Validation

The results of the leave one out cross validation (LOOCV) are provided at the county level in Memo 10. The cross validation using equilibrium temperature data at 1.5 km is presented in Figure 8. The goal is to have kriging predicted mean temperatures at 1.5 km depth that match the recorded equilibrium well temperature at 1.5 km depth. Where red and blue points are nearly co-located there may be very small scale variability in the thermal field, which would be smoothed over in the kriging interpolation. This exercise provides insight into regions of the map that may have been over predicted or under predicted by the kriging interpolation. Generally, the cooler temperatures in south-central Pennsylvania are under predictions.

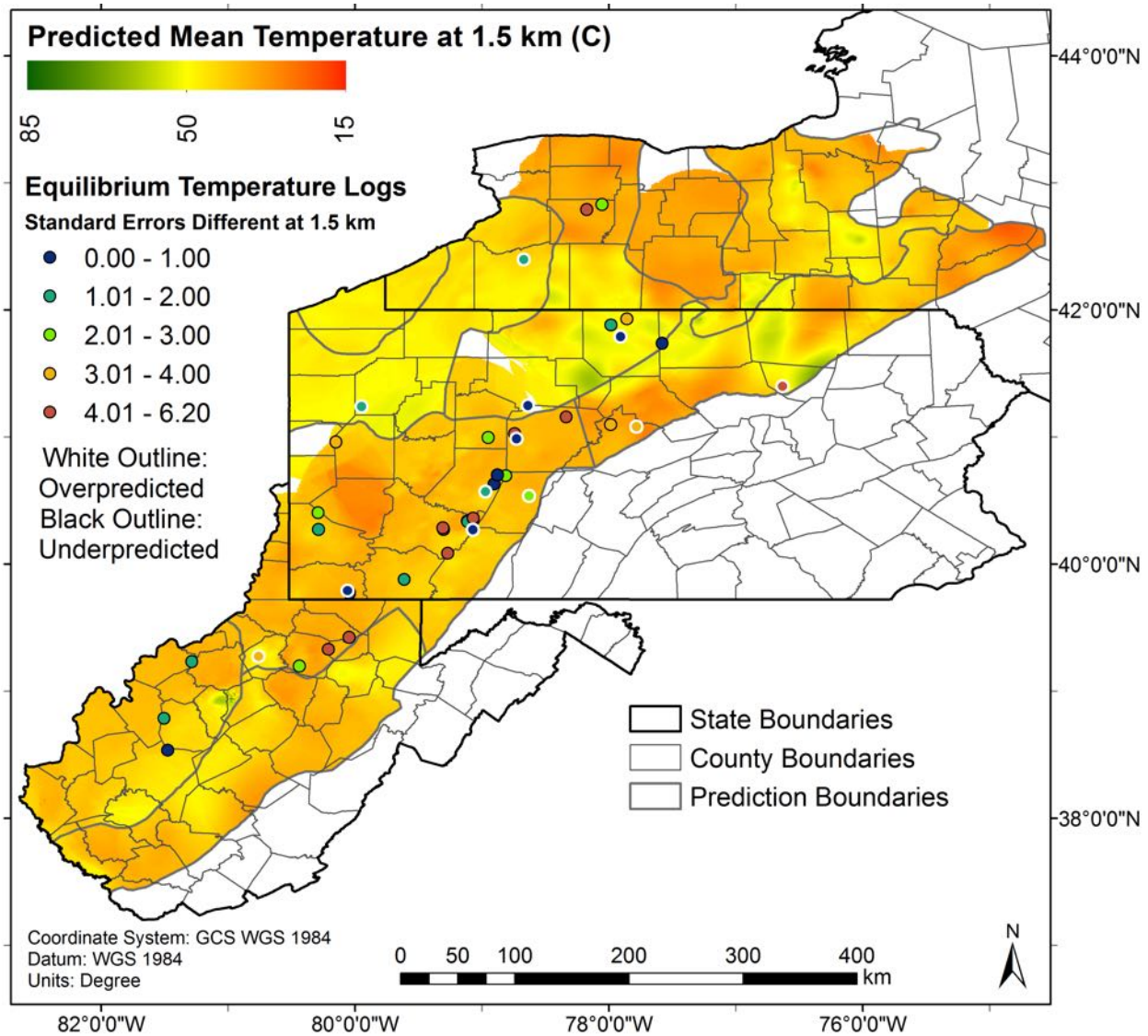


Figure 8: Wells (points) with equilibrium or reliable temperature data at 1.5 km depth are compared to the kriging predicted mean temperatures at 1.5 km depth (map). The colors of the circles show differences from measured and predicted temperature at 1.5 km. The outline color indicates if the map over predicts (white) or under predicts (black) the equilibrium temperature.

References:

- Aguirre, G.A.. (2014). Geothermal resource assessment: A case study of spatial variability and uncertainty analysis for the states of New York and Pennsylvania. MS Thesis. Cornell University, Ithaca, New York.
- Cressie, N.. (1988). Spatial prediction and ordinary kriging. *Mathematical Geology*, 20(4). Pp. 405 – 421.
- Demming, D.. (1989). Application of bottom-hole temperature corrections in geothermal studies. *Geothermics*, 18(5/6). Pp. 775 - 786.
- Pebesma, E.. (2014). gstat user's manual. Available online <http://www.gstat.org/gstat.pdf>. Accessed 20 July 2016.
- Pebesma, E.J. and C.G. Wesseling. (1998). Gstat, a program for geostatistical modelling, prediction and simulation. *Computers & Geosciences*, 24(1). Pp. 17-31.
- Rao, R.U.M., G.V. Rao, and H. Narain. (1976). Radioactive heat generation and heat flow in the Indian Shield. *Earth and Planetary Science Letters*, 30. Pp. 57-64.
- Roy, R.F., D.D. Blackwell and F. Birch. (1968). Heat generation of plutonic rocks and continental heat flow provinces. *Earth and Planetary Science Letters*, 5. Pp. 1 – 12. North Holland Publishing Comp. Amsterdam.
- Roy, R.F., D.D. Blackwell and E.R. Decker. (1972). Continental heat flow. Chapter 19 In E.C. Robertson (ed.). *The Nature of the Solid Earth*. McGraw Hill. New York. Pp. 506 - 544.
- Smith, J.D.. (2016). Analytical and geostatistical heat flow modeling for geothermal resource reconnaissance applied in the Appalachian Basin. MS Thesis. Cornell University, Ithaca, NY.
- Stutz, G.R., E. Shope, G.A. Aguirre, J. Batir, Z. Frone, M. Williams, T.J. Reber, C.A. Whealton, J.D. Smith, M.C. Richards, D.D. Blackwell, J.W. Tester, J.R. Stedinger, and T.E. Jordan. (2015). Geothermal energy characterization in the Appalachian Basin of New York and Pennsylvania. *Geosphere*, 11(5). Pp. 1291–304. doi: 10.1130 /GES00499.1.

Memo 10: Selection of Four Counties in Each State with the Best Thermal Resources

To: Appalachian Basin Geothermal Play Fairway Analysis Group

From: Jared Smith

Date: 15 October, 2015

Subject: Selection of Four Counties in Each State with “Best” Thermal Resources

Applicability: The methods described here were used to select the four “best” counties in each state according to the thermal resource. This analysis complements the Play Fairway maps that are based on the combination of the other three risk factors with the thermal resource, but this analysis is specific to thermal attributes. Note that the maps and cross sections in this memo reflect 2015 results, and do not reflect the 2016 results from the final report.

Introduction

At the conclusion of Phase 1 of this Geothermal Play Fairway Analysis project, the four most favorable or attractive counties in each of New York, Pennsylvania, and West Virginia must be selected for further inspection of the commensurate favorability of geothermal development. Favorability is primarily determined by high thermal resource quality, specifically the depth to 80 °C as defined in the Statement of Project Objectives [SOPO]. Anticipating that the thermal resource quality will be a core factor in decisions regarding development of geothermal direct-use projects at specific locations, in this memo we investigate the values and uncertainty of the thermal resource in the counties that currently appear to be of best thermal quality and of high interest to potential users.

The following analysis could be applied to any county or site of interest to a potential user. To select counties for which to illustrate the insight that is gained from the analysis, additional factors we have taken into consideration are:

- i) Whether or not reservoirs and population/utilization centers are available to use the resource in the county
- ii) The number of wells within the county from which additional detailed lithology may be obtained to cross-examine the predicted thermal values, and from which to collect additional data in Phase 2
- iii) The location of all selected counties within the region of study. Spatial variety was desired such that the selected counties did not all occupy the same hot spots.

High thermal resource quality was interpreted as a location having both a shallow predicted mean depth to 80 °C, and relatively high certainty in the predicted mean depth. No value was assigned to the certainty that was considered to be high; however in all but three counties the average uncertainty in the predicted mean throughout the county has a two-standard-error spread within ± 500 m.

The selected counties are presented in Figure 1. Each of the counties are represented below in a series of cutout maps of the predicted mean depth to 80 °C within the counties. The color scale

on each map is different, tuned to the local temperature-depth relations in order to show variability within the counties of interest. A cross section through each county is provided, which depicts the uncertainty in the predicted mean as

$$\hat{\mu} \pm (2 * SE) \tag{1}$$

where $\hat{\mu}$ is the predicted mean and SE is the standard error of the predicted mean. These bounds can be thought of as 95% confidence bands about the predicted mean. A second cross section of the Thermal Play Fairway Metric (0-5 point scale, see ThermalResourceThresholds_final.doc memo for discussion) is also provided for each county.

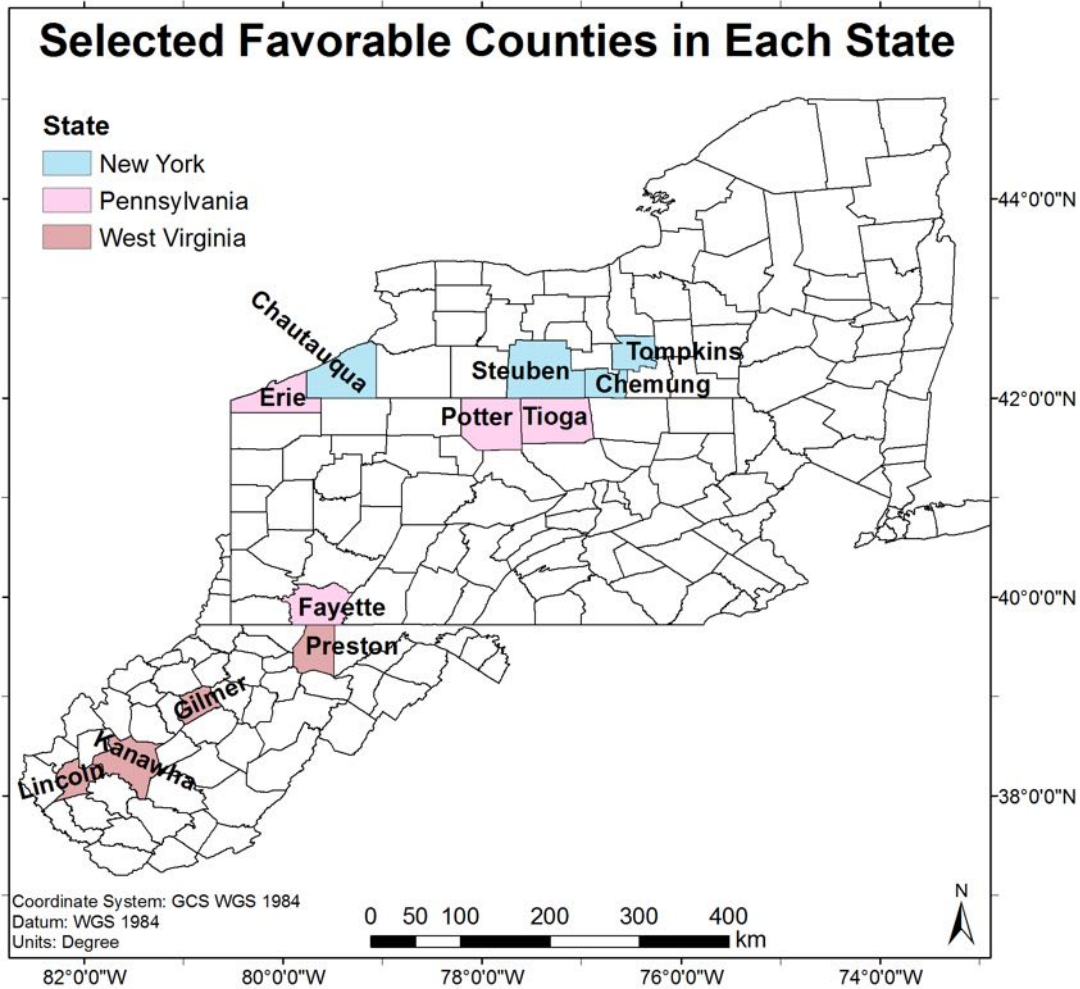


Figure 1. Selected four best counties in New York, Pennsylvania, and West Virginia based on thermal resource, presence of reservoirs, population centers, and variety of location within the Appalachian Basin.

Results and Discussion

The most promising counties have predicted mean depths to 80 °C that are shallower than 2500 m. These include Preston, Gilmer, Lincoln, and Kanawha counties in West Virginia; Chemung, Steuben, and Tompkins counties in New York, and Tioga and Potter counties in Pennsylvania.

Chautauqua, NY, is a great example of where there is high certainty in the prediction as a result of many wells (Figure 2). The highly clustered well data provides insight to the spatial variability of the thermal field on a small scale. For example, the variation in the predicted mean depth to 80 °C is in some locations on the order of a hundred meters on a horizontal scale of about 10 km in map distance (Figure 3). This provides insight to the spatial scale of thermal resource variability that may be expected everywhere in the basin, but is not captured on the maps as a result of fewer data available to support the predictions.

Many of the counties have prediction boundaries (e.g., interpolation zone boundaries) that cut through the county (prediction boundaries are not shown on the individual county maps, but are provided on the cross sections, and the regional thermal resource maps for the basin). As a result, predictions on one side of the boundary may be discontinuous compared to those on the other side of the boundary; however not all boundaries show a meaningful statistically significant difference (e.g. at the $\alpha \approx 5\%$ level) in the predicted mean on either side. The meaningful statistically significant differences are potentially indicative of real boundaries in the thermal field. An example of one meaningful statistically significant difference is in Gilmer County, WV (Figure 8, Figure 9). This boundary is thought to represent the Rome Trough – a feature of known structural importance in the basin. It is not clear if the concurrence of a statistically significant difference and the Rome Trough is a result of poor well sampling, or if this is a real boundary in the thermal field. One argument against poor well sampling is that a two-sample t test in the difference of the mean depth to 80 °C calculated for each well rejected the null hypothesis:

$$\mu_1 - \mu_2 = 0$$

with a p-value of 1.2×10^{-4} and 314 degrees of freedom. Assuming unequal variance, the p-value is 8.9×10^{-5} with 313.6 degrees of freedom. Even so, the wells included in this test are located predominantly in northern Gilmer County, so the test reflects the difference in two means across this northern boundary rather than the sharper difference in southwestern portion of the county. More sampling in southern Gilmer County may change the significance of this test.

At this time, it is also not clear if all statistically significant differences across interpolation boundaries coincide with features of similar importance to the basin, and further influence the thermal field. Even so, the gravity and magnetic potential field edges were used to define prediction boundaries in an attempt to capture differences in the subsurface that may correspond to variations in the thermal field (e.g. changes in the data generating process). Having one statistically significant difference appear along a feature of importance is encouraging support of this assumption.

Evaluation of the predicted mean depth to 80 °C was conducted for the region using a “leave one out” cross validation. For N points, this cross validation runs the kriging interpolation algorithm N times, with one point left out of the prediction in each of the N repetitions. The results of the cross validation are provided for each county below in Figure 2, Figure 4, Figure 6, Figure 8, and Figure 10 as ‘bubble plots’ that display the Z-Score: $Z = \frac{x - \mu}{SE}$, where x is the geothermal variable for the well point, μ is the predicted mean for the grid cell, and SE is the standard error of the

predicted mean for the grid cell. Results indicate that on a regional scale about 98% of the data for the left-out points lie within 3 standard errors of the predicted mean.

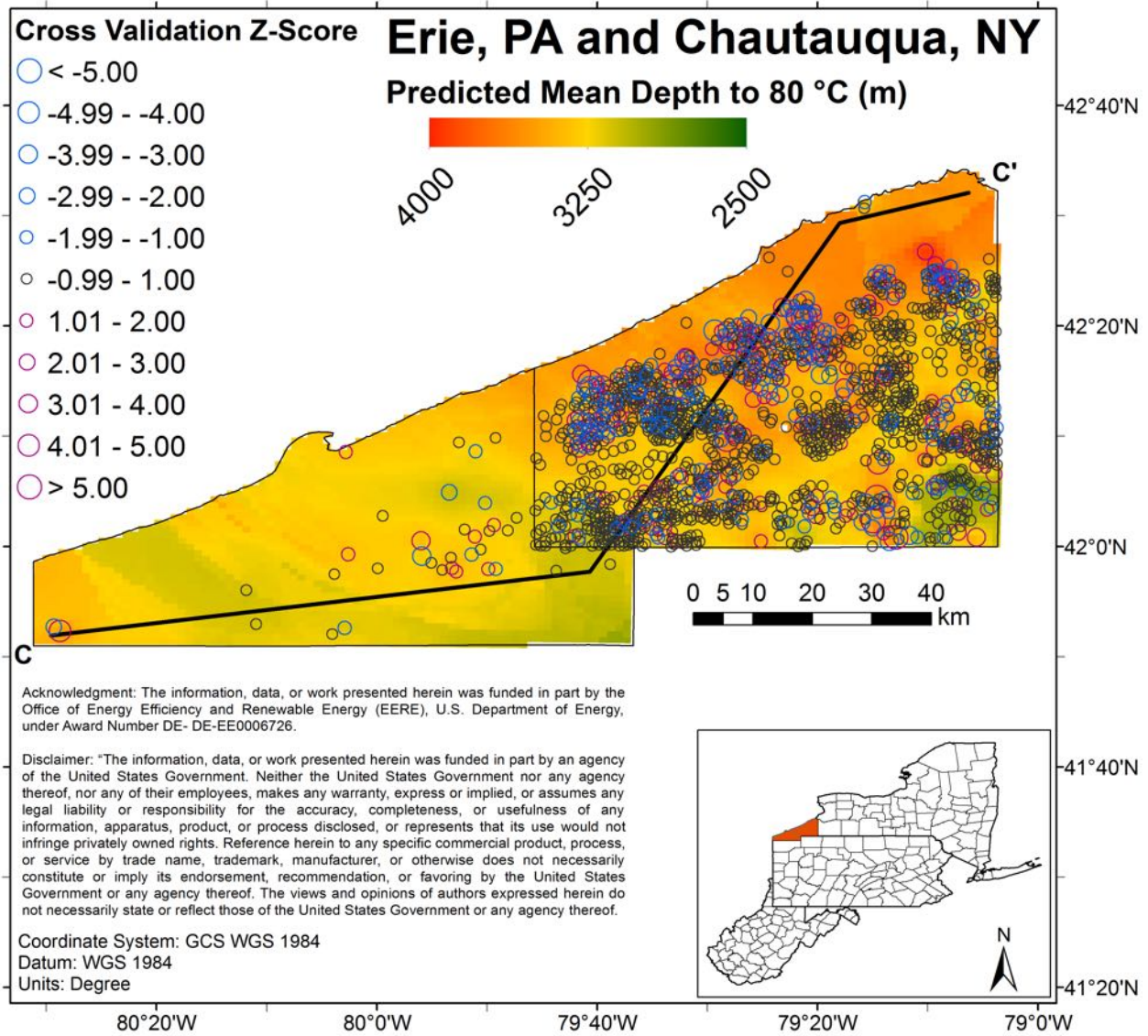


Figure 2. Depth to 80 °C in Erie County Pennsylvania, and Chautauqua County New York. Leave one out cross validation results are shown as ‘bubbles’ that increase in size as the error, measured as a Z-Score, increases in magnitude. Red indicates that the value of the point was greater than the predicted mean at the location (grid cell) of the left-out point. Larger circles may indicate that the point had more influence in the spatial prediction.

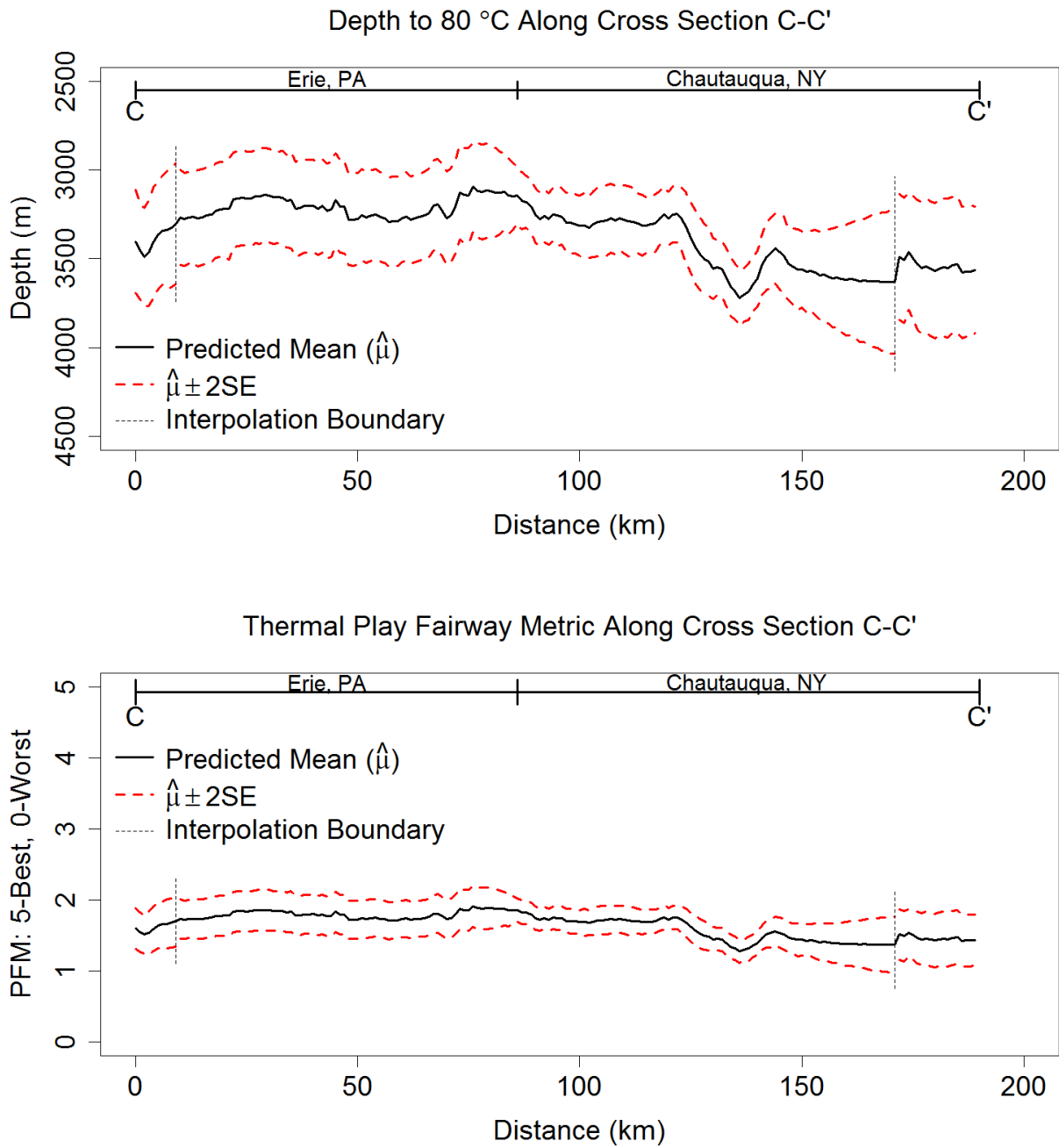


Figure 3. Variation in depth to 80 °C and the thermal Play Fairway Metric along cross section C-C' in Figure 2. These two counties display moderate depths with relatively high certainty compared with other locations ($\hat{\mu} \pm 2SE$ spans approximately 500 m in most locations).

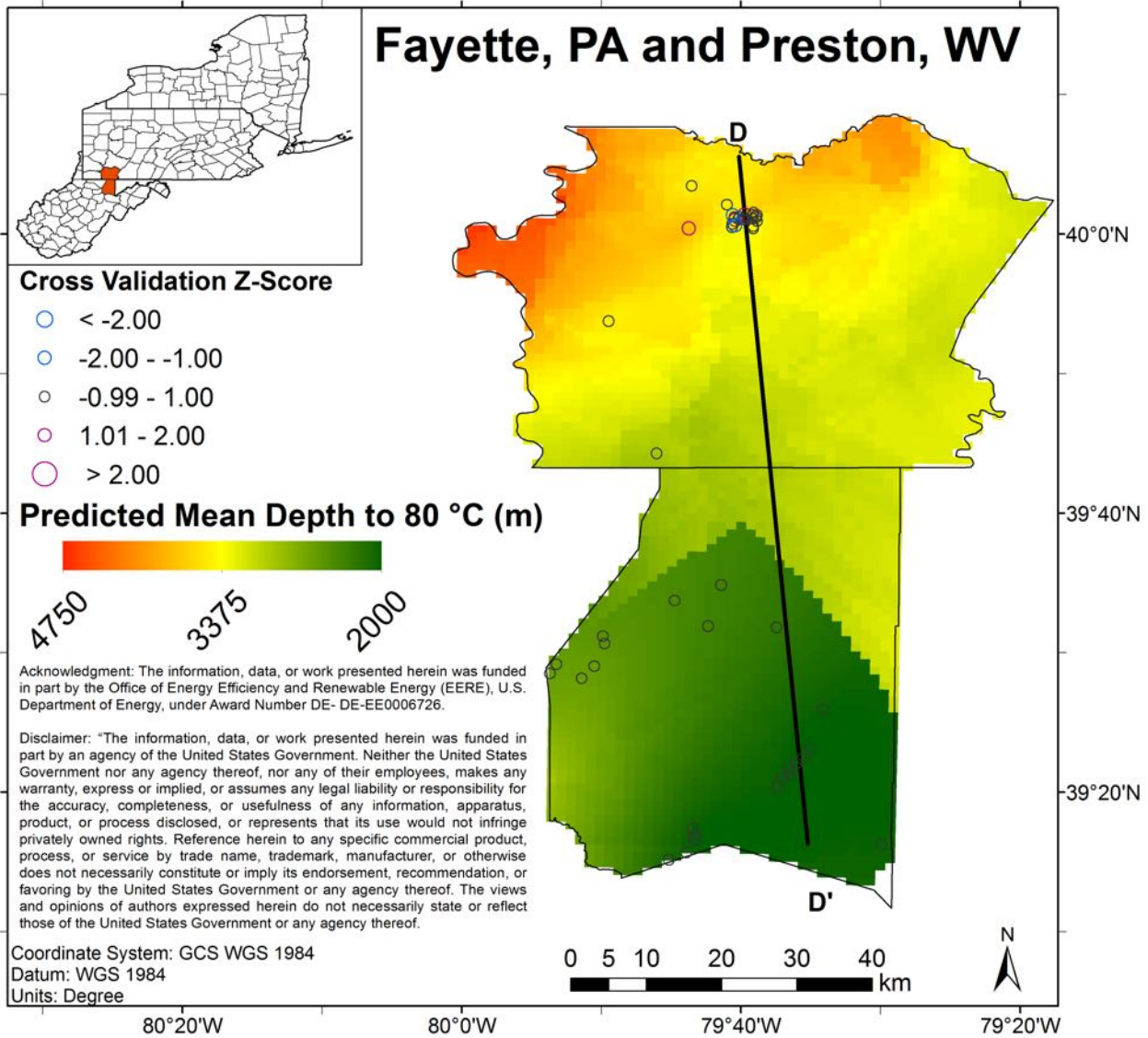


Figure 4. Depth to 80 °C in Fayette County Pennsylvania, and Preston County West Virginia. Leave one out cross validation results are shown as 'bubbles' that increase in size as the error, measured as a Z-Score, increases in magnitude. Red indicates that the value of the point was greater than the predicted mean at the location (grid cell) of the left-out point. Larger circles may indicate that the point had more influence in the spatial prediction.

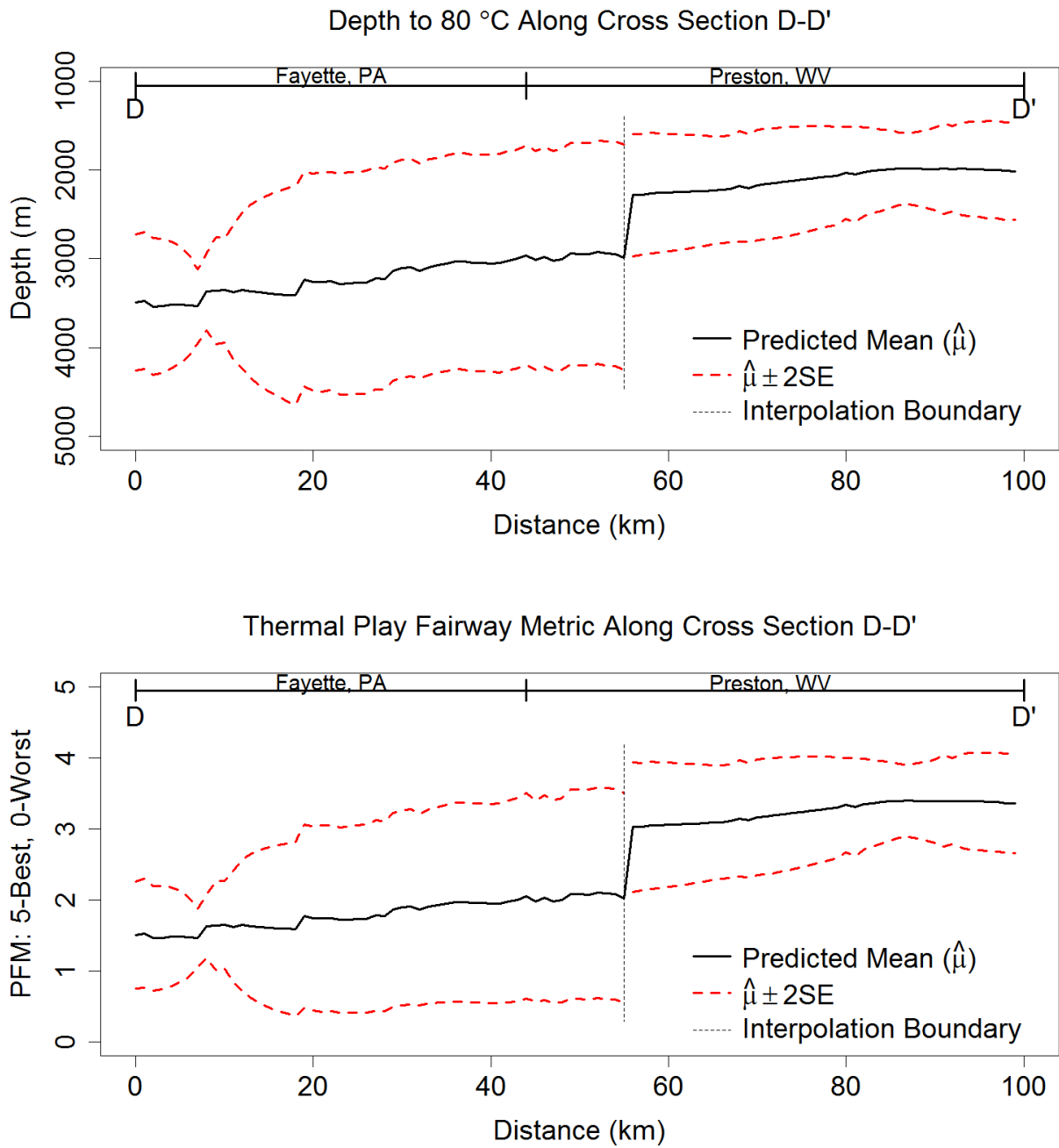


Figure 5. Variation in depth to 80 °C and the thermal Play Fairway Metric along cross section D-D' in Figure 4. While Preston County has a higher predicted mean, it is not statistically different than the mean in Fayette County.

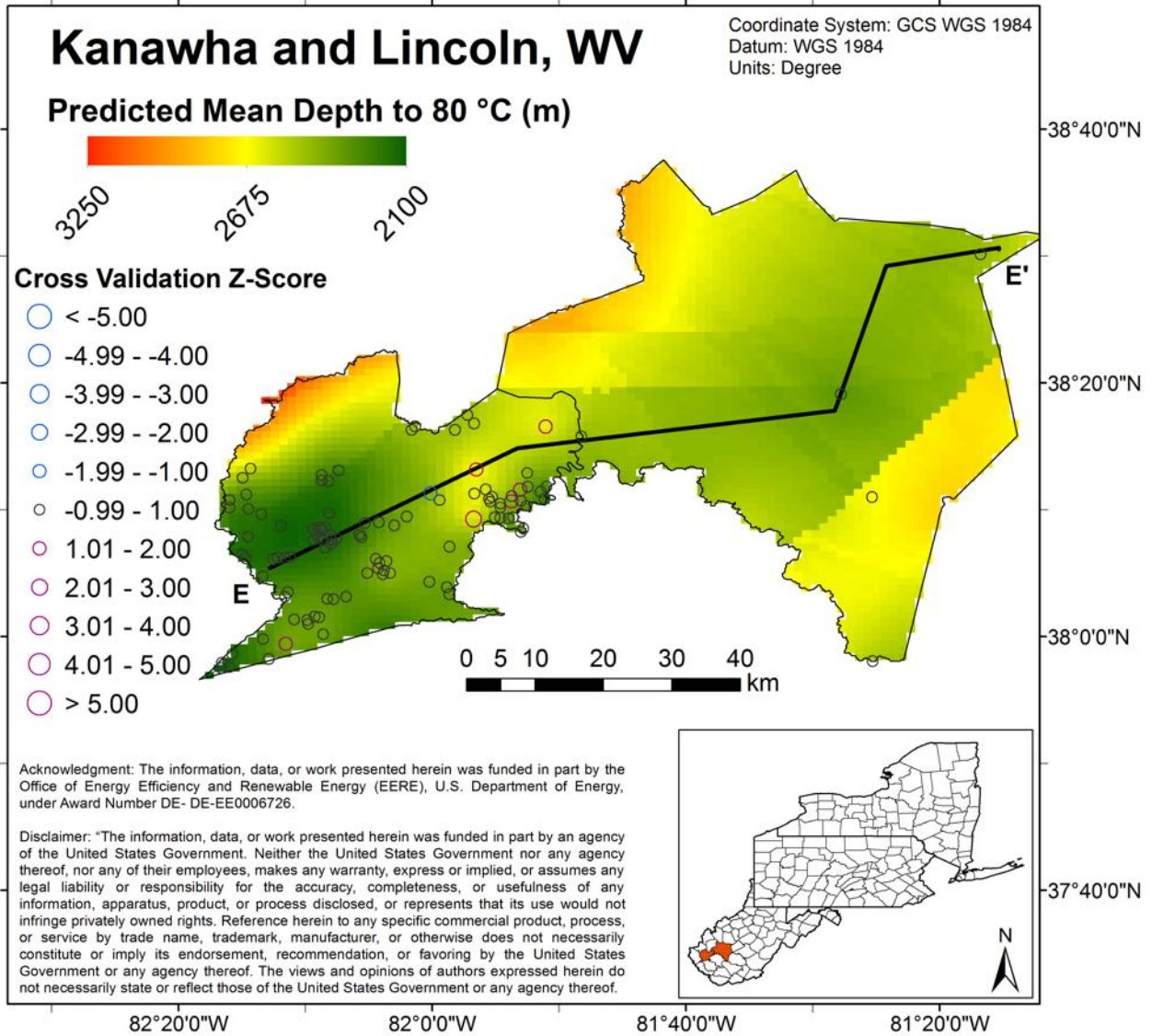


Figure 6. Depth to 80 °C in Lincoln and Kanawha counties in West Virginia. Leave one out cross validation results are shown as 'bubbles' that increase in size as the error, measured as a Z-Score, increases in magnitude. Red indicates that the value of the point was greater than the predicted mean at the location (grid cell) of the left-out point. Larger circles may indicate that the point had more influence in the spatial prediction.

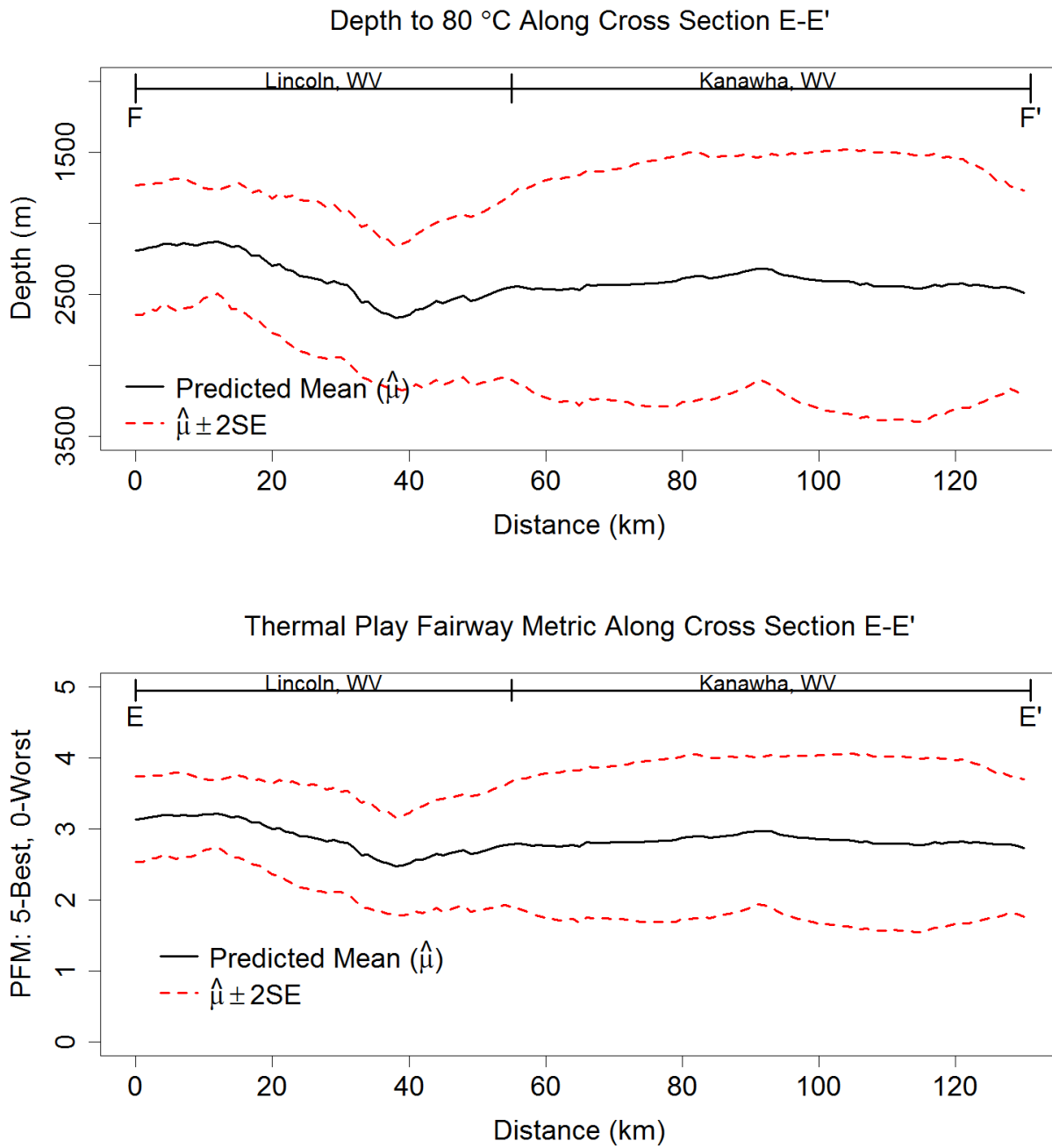


Figure 7. Variation in depth to 80 °C and the thermal Play Fairway Metric along cross section E-E' in Figure 6. The uncertainty in the predicted mean increases along the cross section as a result of decreasing well density.

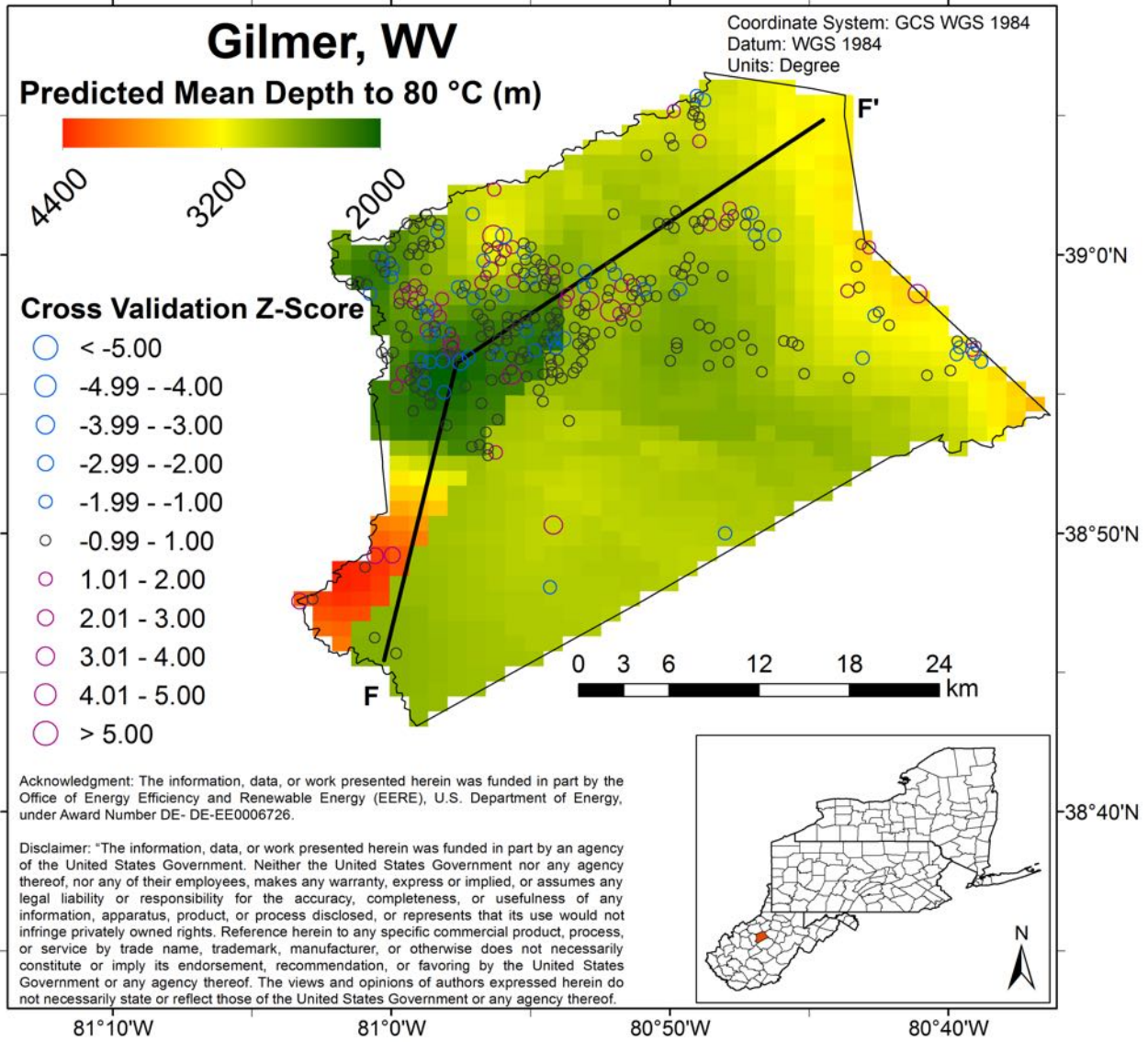


Figure 8. Depth to 80 °C in Gilmer County West Virginia. Leave one out cross validation results are shown as 'bubbles' that increase in size as the error, measured as a Z-Score, increases in magnitude. Red indicates that the value of the point was greater than the predicted mean at the location (grid cell) of the left-out point. Larger circles may indicate that the point had more influence in the spatial prediction.

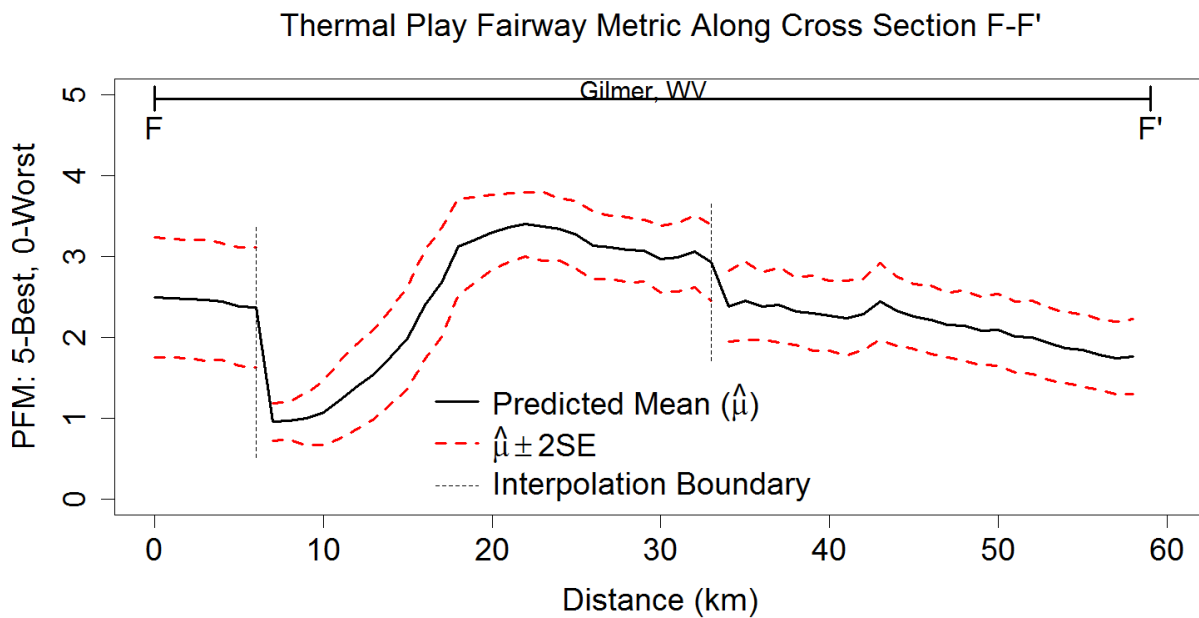
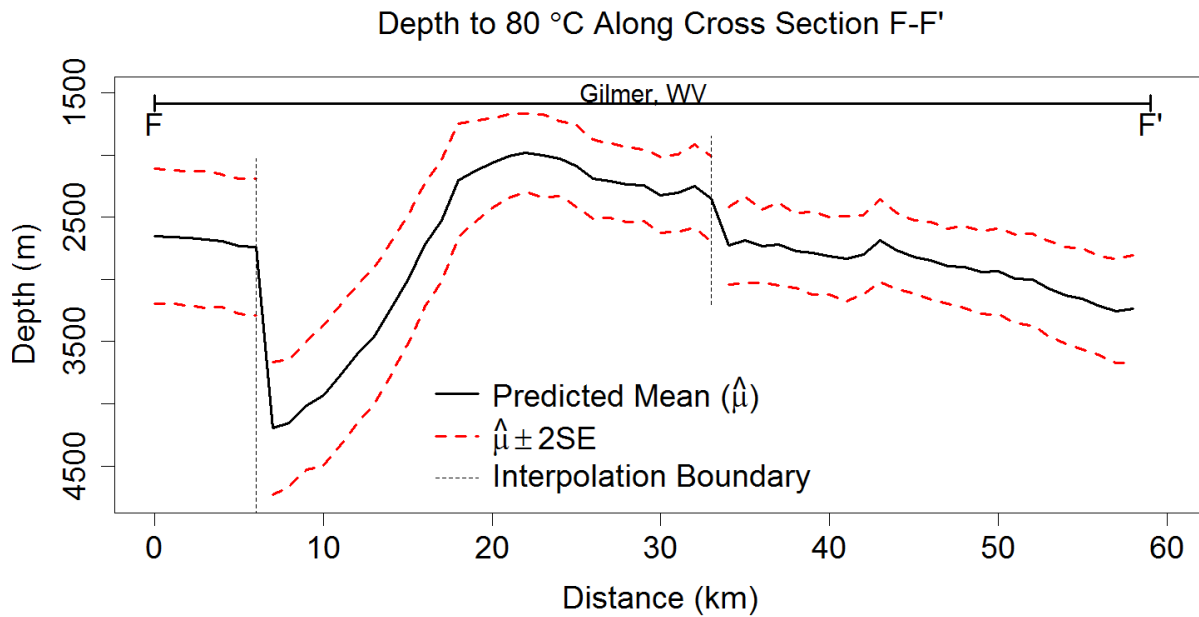


Figure 9. Variation in depth to 80 °C and the thermal Play Fairway Metric along cross section F-F' in **Error! Reference source not found.** The most certain shallowest location is about 2300 m.

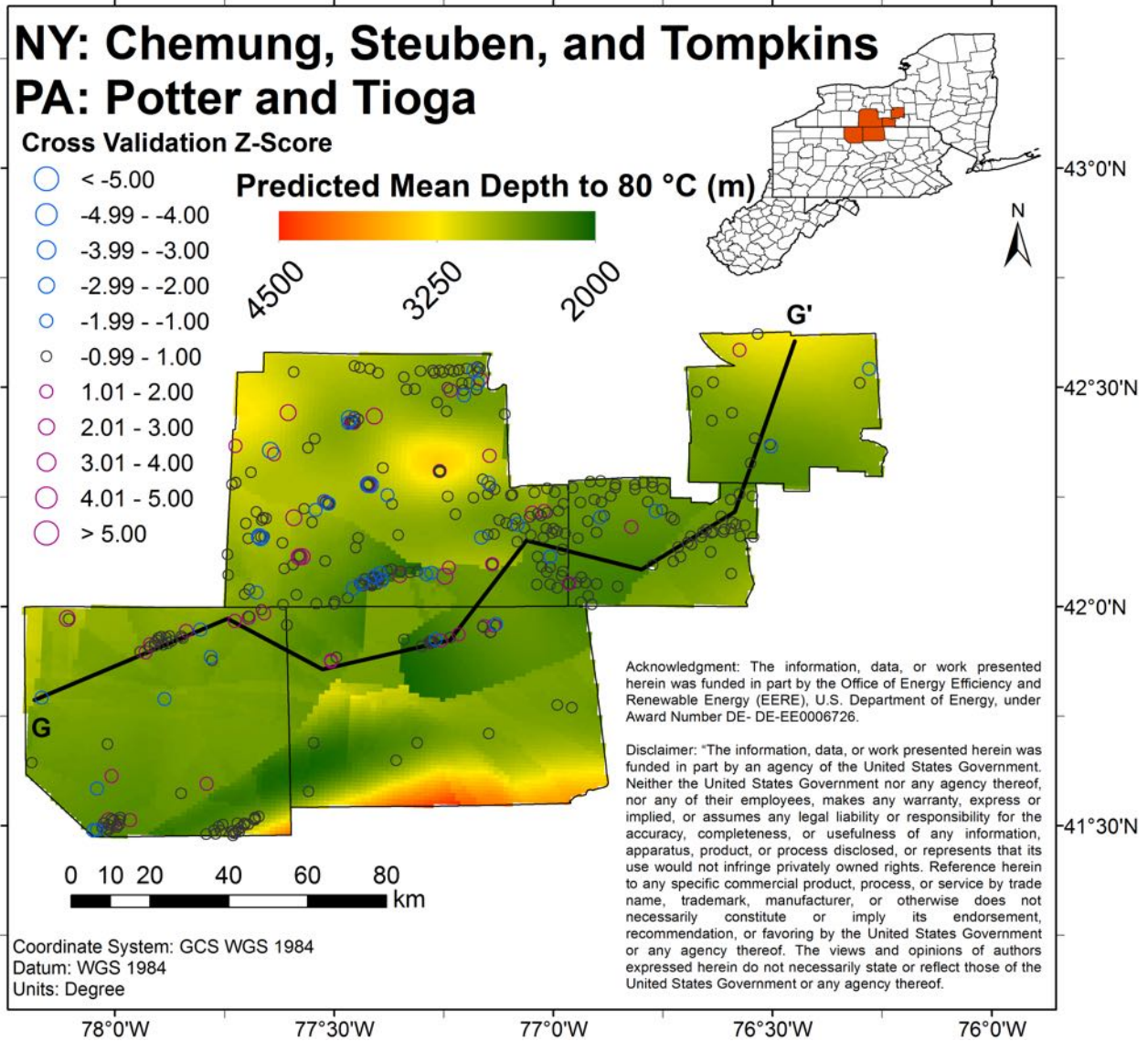


Figure 10. Depth to 80 °C in Chemung, Steuben, and Tompkins counties in New York, and Potter and Tioga counties in Pennsylvania. Leave one out cross validation results are shown as ‘bubbles’ that increase in size as the error, measured as a Z-Score, increases in magnitude. Red indicates that the value of the point was greater than the predicted mean at the location (grid cell) of the left-out point. Larger circles may indicate that the point had more influence in the spatial prediction.

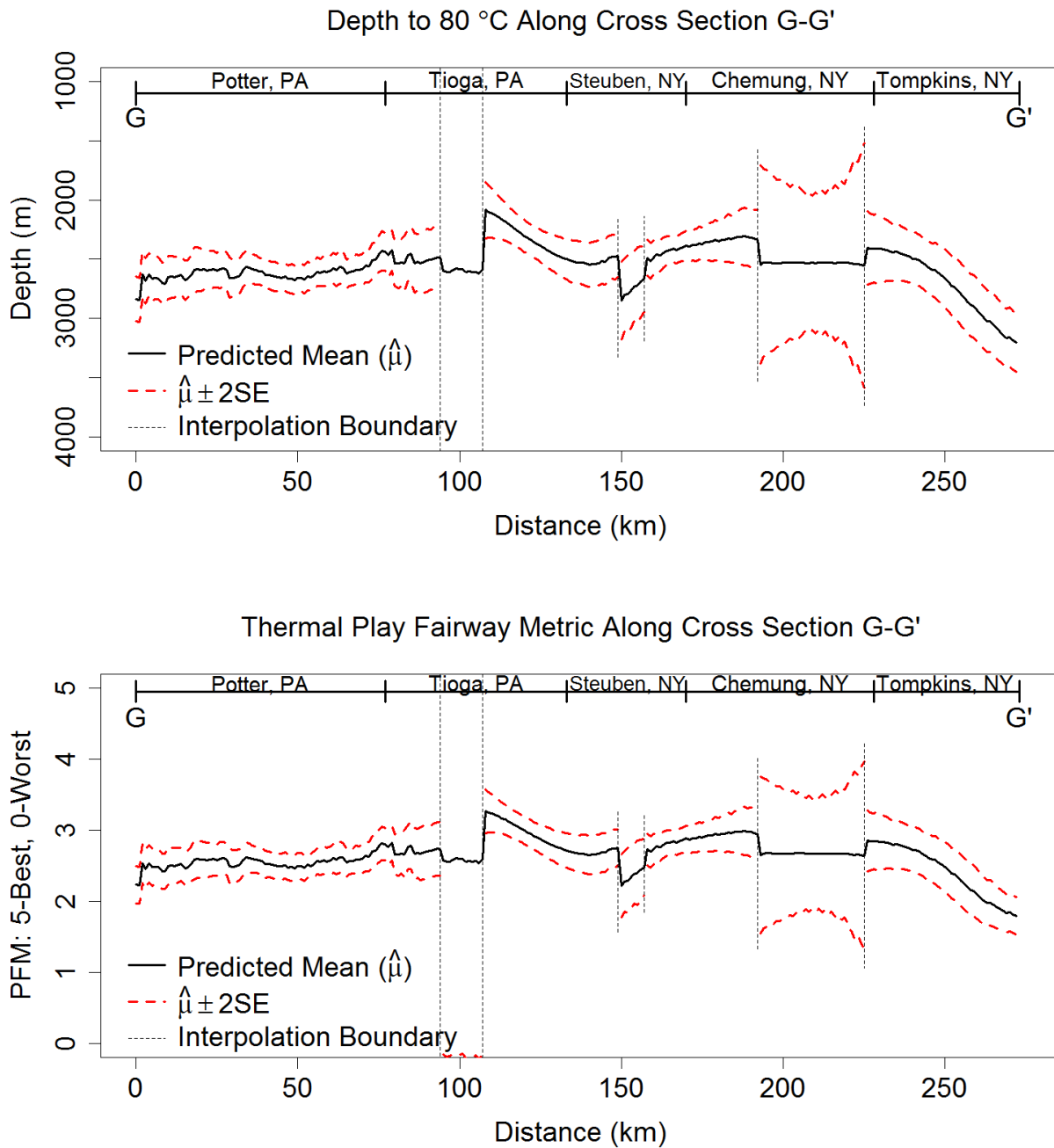


Figure 11. Variation in depth to 80 °C and the thermal Play Fairway Metric along cross section G-G' in Figure 10. The most certain shallowest location is between Tioga through Chemung counties, which contain reservoirs and two population centers (Elmira, NY and Corning, NY).

Memo 11: Natural Reservoirs Task Methodology in GPFA-AB

Erin Camp
Erc85@cornell.edu

Last modified: August 10, 2016

The Natural Reservoirs Task of the Appalachian Basin Geothermal Play Fairway Analysis project involves mapping and characterizing the proven natural reservoirs, which have the potential to be utilized for geothermal energy production within the Appalachian Basin region of New York (NY), Pennsylvania (PA), and West Virginia (WV). The results of this task are intended to accompany the analyses of the Thermal Resource, Seismic Risk, and Utilization tasks, for the purpose of a Combined Risk Map (CRM) to determine the most optimal locations in the basin for future geothermal investment. The goals of the Natural Reservoirs task were:

- i. Collect data on known natural reservoirs in the Appalachian Basin, and integrate data sources for consistency,
- ii. Research geologic formations in the basin to populate empty fields in the database,
- iii. Choose or develop a metric for quantifying reservoir favorability,
- iv. Predict the likely range of outcomes for all natural reservoirs in the basin, and
- v. Map the reservoir results in a Geographic Information System (GIS)

Reservoir data collection and compilation methods differed state by state; however, reservoir analysis and uncertainty quantification methods are consistent across the tristate region. This memo and its accompanying Memo 12 (Reservoir data selections) presents a detailed description of all methods that were used for the completion of this task's milestones.

1. The Desired Resource: Natural Reservoirs

For the purposes of this project, a geothermal reservoir is defined as a volume of rock in the subsurface that has sufficient permeability to allow fluids to flow through it. Fluids are pumped into one well, heated by contact with the rock, and pumped back to the Earth's surface via a second well. This scope of this project was limited to consideration of naturally-occurring reservoirs, or those in which sufficient permeability already exists. Enhanced or Engineered Geothermal Systems (EGS)—the process by which permeability is artificially created in a rock using high pressure fluids—was excluded from the analysis as described in the Statement of Project Objectives (SOPO).

Because this project was limited to the analysis of existing data, our proposal hinges on the application of subsurface data that has already been collected by the petroleum industry via drilling for oil and gas. Such non-proprietary datasets of proven conventional hydrocarbon reservoirs generally include depth, thickness, location, spatial extent, porosity, and less frequently permeability, though publicly available data vary from state to state and from basin to basin. Analyzing petroleum reservoirs for geothermal exploration may lower geothermal project risk because:

- i. Non-proprietary hydrocarbon reservoir data is already collected and access to those data is low- or no-cost
- ii. Hydrocarbon reservoirs have some degree of inherent porosity and permeability given that large amounts of hydrocarbons existed within and flowed out of those reservoirs.
- iii. Sedimentary units generally have higher permeability values than crystalline igneous or metamorphic units, in which hydrothermal or EGS projects generally occur.

2. Data Collection

The reservoir dataset available for New York differed from that of Pennsylvania and West Virginia. This section describes the differences between the two datasets.

2.1. Pennsylvania and West Virginia

Extensive data collection and reservoir mapping was completed in the early 2000s for the purpose of carbon sequestration research through the Midwest Regional Carbon Sequestration Partnership (MRCSP). A GIS database from the MRCSP was available for use as a starting point for this project, courtesy of the West Virginia Geological and Economic Survey (WVGES). The dataset is not open-source, but it can be purchased from the WVGES. The dataset includes oil and gas reservoirs located in PA and WV, but does not include reservoirs in NY. The MRCSP calculated potential storage volume for the reservoirs by using a volumetric analysis (total volume of rock corrected by reservoir porosity); therefore, the following reservoir parameters were included in the dataset: average reservoir production depth, reservoir name, formation code (geologic code for the producing formation, see Memo 12 (Reservoir data selections)), state, reservoir pressure, porosity, net thickness, and shapefiles (polygons).

Due to the large size of the PA and WV database and narrow time constraints of the Phase One GPFA, reservoirs shallower than our chosen threshold were trimmed from the database to reduce the workload. To pick the depth threshold, a temperature threshold of 40°C was first selected using the Lindal Diagram of temperatures and potential end-uses (Lindal, 1973). An average geothermal gradient and surface temperature for the region (calculated from the Thermal Resource Task) resulted in a threshold of 1250 meters (4100 feet).

2.2. New York

The dataset from carbon sequestration research conducted in NY was available to us through the New York State Geological Survey (NYSGS); however, it did not prove useful to our project because it does not contain any information about potential reservoirs except for their depth. Because New York joined the MRCSP years later than the other states in the Consortium, their efforts did not produce the same final data products or use the same volumetric analysis method as for WV and PA. NYSGS instead approximated the storage potential for carbon dioxide sequestration using oil and gas production volumes to estimate storage capacity of each reservoir. Because porosity and thickness values were not required to conduct their analyses those parameters are not included in the database.

Instead, we used the Empire State Organized Geologic Information System (ESOGIS) online database to access the information that was required for this project. This dataset holds data by well rather than by reservoir. Well locations (latitude and longitude) were downloaded from ESOGIS and uploaded into a GIS. To create reservoir area polygons similar to those in the database for PA and WV, we used a GIS tool to create “buffer zones” around wells that pertain to a given reservoir. For details on the process of calculating the reservoir well buffer, see the accompanying Memo 12 (Reservoir data selections).

The available digital well data from ESOGIS included well Total Vertical Depth (TVD), producing formation, reservoir name, latitude, and longitude. Reservoir thickness was not available in the digital database, and was extracted manually from downloaded PDFs of Well Completion Reports.

The ESOGIS database does not report either formation or reservoir porosity as a separate data field. Porosity data for each reservoir in NY had to be extracted from the published

literature. In the interest of time, the reservoirs were categorized by producing formation, and an average reservoir porosity was assigned to each formation based on values reported in literature. Details on porosity value choices can be found in the Memo 12 (Reservoir data selections).

No minimum temperature threshold for reservoir analysis was necessary for NY, as the database was small enough to be evaluated by the available personnel in a short time. This decision was made knowing that any shallow reservoirs in NY would be eliminated once the thermal map was integrated with the reservoir map.

2.3. Permeability

Neither the MRCSP database nor ESOGIS contains information about reservoir permeability, which is the most important parameter for estimating reservoir favorability. Reservoirs across the basin were again grouped by producing formation, and a permeability value was assigned to each reservoir based on published values for its formation, or an empirical relationship with porosity. For more details on the process of estimating permeability for each formation, see Memo 12 (Reservoir data selections).

3. Reservoir Favorability Metrics

Following the compilation of the three-state reservoir database, reservoir favorability metrics were chosen using the available parameter constraints: permeability, thickness (hydrocarbon pay thickness), temperature, depth, and area. Three metrics were ultimately chosen to express reservoir favorability: one is a geologic quality metric that serves mostly as a reservoir ranking tool and relies only on the geologic properties detailed above; the other two include engineering inputs to predict production-stage performance of the reservoirs. The Reservoir Flow Capacity (RFC) is the metric that is used as a comparator for the geologic parameters in each reservoir.

The latter metrics are the Reservoir Productivity Index for supercritical CO₂ (RPI_c) and for water (RPI_w), used to quantify potential productivity, or fluid flow rate, in each reservoir during production. The following sections describe each metric and their purposes.

3.1. Reservoir Flow Capacity

The reservoir flow capacity (RFC) was chosen as a favorability metric not only because it is comprised of only geologic parameters, but also because the levelized cost of energy is sensitive to this metric (Sanyal and Butler, 2009). This metric provides the opportunity to compare the quantitative favorability of each reservoir relative to the other reservoirs based on its natural reservoir qualities only. The RFC, shown as F below in units of mD-m, is a simple equation comprised of only permeability k in millidarcies (mD), and thickness H in meters:

$$F = kH \quad (1)$$

3.2. Reservoir Productivity Index

A separate metric was chosen for this project as a means of quantifying the favorability of the reservoirs in the basin during energy production. After thermal quality, flow rate is the second-most important factor affecting geothermal heat production (Bedre and Anderson, 2012). The petroleum industry often uses a term called the well productivity index (PI) to quantify the flow of a given oil or gas well producing from a hydrocarbon reservoir. The PI is defined as the volumetric flow rate of a well divided by the pressure drop from the reservoir to the producing well:

$$PI = \frac{Q}{\Delta P} = \frac{2\pi kH}{\mu \ln \frac{D}{r_w}} \quad (2)$$

where Q is flow rate (m³/s), ΔP is the pressure drop from the reservoir to the production well (Pa), k is permeability (m²), H is reservoir thickness (m), μ is the fluid viscosity (Pa-s), D is

the distance between the injection and production well (m), and r_w is the wellbore radius (m) (Gringarten, 1978). Equation 2 assumes that the reservoir is a homogeneous porous medium with horizontal intergranular flow.

PI has also been used to characterize the productivity of a well doublet for geothermal reservoirs, for both EGS reservoirs and sedimentary aquifer reservoirs (Gérard et al., 2006; Sanyal and Butler, 2009; Augustine, 2014; Cho et al., 2015; Hamm et al., 2016). The PI metric was adapted to this project by using it as an approximation of a reservoir's productivity, rather than just a well pair. The metric is identical to Equation 2, but is called the Reservoir Productivity Index (RPI) and the parameters used are average reservoir values. Additionally, mass flow rate (kg/s) was used instead of volumetric flow rate, so that RPI can be compared fairly for an incompressible liquid and a compressible gas as the working fluid. RPI is used as the model in a Monte Carlo Simulation to predict the uncertainty associated with each reservoir, which is described below.

The RPI was subdivided by the type of working fluid that could be used in the geothermal system. Water (RPI_w) and supercritical carbon dioxide (sCO_2 , RPI_c) were chosen as the two working fluid options for this project. For each reservoir, RPI_w and RPI_c were modeled. The differences between RPI_w and RPI_c are the respective inputs for viscosity and permeability.

3.2.1. Viscosity

The viscosity of water varies with temperature, therefore the temperature at the depth of each reservoir was calculated. Because the thermal and reservoir tasks were being completed simultaneously, reservoir-specific temperatures at depth were not available. Therefore, state-wide averaged thermal gradients and surface temperatures were used for

this work. Uncertainty can be reduced in future work by applying reservoir-specific estimates of temperature at depth for a more accurate estimate of fluid viscosity. The following values in Table 1 are averages taken from work done by Smith (2015). Those geothermal gradients and surface temperatures were used to calculate the temperature at the depth of each reservoir using the following equation modified from Tester et al. (2012):

$$T(z) = z_r \frac{dT}{dz} + T_s \quad (3)$$

where z_r is the depth of the reservoir in meters, $\frac{dT}{dz}$ is the temperature gradient in °C/km, and T_s is the temperature at the surface in °C (Table 1). The dynamic viscosity of water as it varies with temperature (Engineering Toolbox, 2015) is presented in

Table 2. The effects of salinity on viscosity were assumed to be negligible.

Table 1. Average temperature gradient and surface temperatures for New York, Pennsylvania, and West Virginia. Values averaged from work done by Smith (2015).

	Gradient (°C/km)	Average Surface Temperature (°C)
New York	22.19	9.66
Pennsylvania	21.19	11.33
West Virginia	23.19	13.87

Table 2. Dynamic viscosity of water as a function of temperature. Temperatures are categorized in 10° increments (Engineering Toolbox, 2015).

Temperature (°C)	Viscosity, water (Pa-s)
< 30	0.000900
30-39.99	0.000726
40-49.99	0.000600
50-59.99	0.000507
60-69.99	0.000436
70-79.99	0.000380
80-89.99	0.000335
90+	0.000299

Data for dynamic viscosity of sCO₂ come from Ouyang (2011). The viscosity of sCO₂ varies as a function of both temperature and pressure. The assumed pressure of the injected sCO₂ was 10 MPa (100 bar; 1500 psi). At all temperature ranges at a pressure of 10 MPa, the estimated viscosity of sCO₂ is 0.00002 Pa-s.

3.2.2. Permeability

Most permeability values are derived from direct measurement of cored rock samples using a gas as the fluid. Use of the raw permeability measurements (k_g) is acceptable when estimating the flow of a gas through a reservoir rock, but not when trying to estimate the flow of water through the rock, which is the typical fluid used in geothermal systems. In the case of RPI_c , the gas permeability was retained because the viscosity of sCO_2 is much like that of a gas (Brown, 2000; Pruess, 2007); however, for RPI_w the gas permeability was corrected for the Klinkenberg effect. This correction is more important for low permeability rocks than high permeability rocks (Tanikawa and Shimamoto, 2006). Since most reservoirs in the Appalachian Basin are of low permeability, this is an important step for the RPI_w calculations.

Corrections were applied to all reservoirs based on the reservoir's primary lithology. For carbonate reservoirs, the following correlation from Al-Jabri et al. (2015) was applied,

$$k_w = 0.578k_g^{1.097} \quad (4)$$

where k_w is the permeability of the rock with water, and k_g is the permeability of the rock with gas, both in units of mD. For all other lithologies, the following correlation from Jones (1987) was used:

$$k_w = \frac{k_g}{1 + \frac{b}{p}}; \quad (5)$$

$$b = 15.61 \left(\frac{k_g}{\phi} \right)^{-0.447} \quad (6)$$

where p is the mean flowing pressure in psi, and ϕ is the porosity as a decimal fraction.

3.2.3. Thickness

The MRCSP dataset holds values for each reservoir's net pay thickness, or the vertical column from where oil and gas was produced. The New York ESOGIS database does not contain information on reservoir thickness, so pay thickness was extracted manually from well production reports downloaded from ESOGIS. If the producing interval was not reported, then the perforated interval was used as an approximation. The pay thicknesses from all wells in each reservoir were averaged to calculate the mean reservoir pay thickness.

3.2.4. Well Distance and Wellbore Radius

These geothermal field design parameters were held as constants in the RPI_w and RPI_g equations. D , or distance between wells, was assumed to be 1000 m, while r , or wellbore radius, assumed to be 0.1 m. These parameters were not used in the RFC equation.

3.3. Reservoir Architecture and Flow Considerations

During the database compilation phase of this project, our reservoirs were categorized as either stratigraphically-controlled (porous medium) or structurally-controlled (fractured medium), based on what is known about the reservoirs from literature (i.e. Roen and Walker, 1996). The original intention was to calculate the RFC and RPI of each reservoir using an appropriate equation based on the flow type; however, in the allotted time of the project, a comparable equation for fracture-dominated reservoirs was not identified. Therefore, the equation for RPI in porous medium reservoirs was applied to all reservoirs as a first-order approximation, regardless of reservoir architecture.

4. Uncertainty

An important piece of this project is the quantification of uncertainty in reservoir data, and therefore, also in the uncertainty of the calculated RFC, RPI_c and RPI_w for each reservoir in the basin. In order to calculate the range of possible outcomes (RFC, RPI_c and RPI_w) for each reservoir, we performed a Monte Carlo Simulation on each metric. To do this, the required inputs for each variable were the average value, the standard deviation, and probability distribution type (normal, log-normal, etc.).

4.1. Reservoir Parametric Uncertainty Index

Each average parameter value (i.e. k , H , μ) from the database has inherent uncertainty associated with it, both in terms of the variation in data quality and in terms of the natural variation, or heterogeneity, of each reservoir. Though average parameter values were available in the database for each reservoir, standard deviations and probability distributions were not, and therefore had to be selected. To maintain consistency during the assignment of standard deviations and distribution types to each parameter for all the reservoirs, we created an uncertainty index that ranges from 0 (no uncertainty) to 5 (most uncertain).

Each uncertainty index value (0-5) corresponds to the likely standard deviation from the parameter input, shown in Table 3. The standard deviation increments for each parameter were chosen based on reports in reservoir literature of typical variations in reservoir thickness, permeability, and temperature (which affects the fluid viscosity) due to heterogeneity (i.e., Murtha, 1994; Society of Petroleum Engineers, 2001; Satter et al., 2008; Peters, 2012).

Because the sources of data for the average parameter value were not equally reliable for all reservoirs, data quality guided the selection of the uncertainty index value for each

reservoir’s parameters, as shown in the example in Table 4. For example, permeability data that was calculated from a published empirical porosity-permeability relationship for the respective geologic formation and region would be assigned an uncertainty factor of 2. That reservoir’s average permeability value would therefore be assigned a standard deviation of 25% with a log-normal distribution. Additionally, each parameter was assigned a probability distribution type for a Monte Carlo Simulation. Distribution types were determined based on reservoir engineering and modeling best practices and literature. More details on how the uncertainty indices were assigned can be found in the Memo 12 (Reservoir data selections).

Table 3. Uncertainty Index reference chart for each parameter in the Monte Carlo Simulation model.

Uncertainty Index	Permeability	Thickness	Viscosity
	<i>k</i>	<i>H</i>	μ
0	0%	0%	0%
1	12.5%	10%	10%
2	25%	20%	20%
3	50%	30%	30%
4	100%	40%	40%
5	200%	50%	50%
Probability Distribution	log-normal	triangular	normal
References	Murtha, 1994; Satter, 2008	Peters, 2012; SPE, 2001	Based on temperature distribution from Smith (2015)

Table 4. Example of Uncertainty Index assignment criteria for reservoir permeability data.

1	<ul style="list-style-type: none"> Data from a published empirical porosity-permeability relationship, applicable to the respective geologic formation and reservoir.
2	<ul style="list-style-type: none"> Data from a published empirical porosity-permeability relationship, applicable to the respective region and formation but not the respective reservoir.
3	<ul style="list-style-type: none"> Data from unpublished empirical porosity-permeability relationship, applicable to the respective geologic formation but not the respective reservoir. Data are a published or unpublished range of values or average value for the respective geologic formation and region.
4	<ul style="list-style-type: none"> Data come from unpublished empirical porosity-permeability relationship An average value can be applied from a similar formation or the same formation located in another region Data are a published or unpublished range of values or average value for a similar geologic formation in the respective region
5	<ul style="list-style-type: none"> Generic low value ($\leq 1\text{mD}$) assigned due to lack of available data

4.2. Monte Carlo Simulation

A Monte Carlo Simulation with 100,000 repetitions was coded in MatLab and performed on the RFC, RPI_c , and RPI_w for each reservoir, with inputs for parametric mean, standard deviation, and distribution. The simulation generated stochastic results for each reservoir, using the assigned uncertainty indices and parameter probability distributions in Tables 3 and 4. From those data outputs, the 10th, 25th, 50th, 75th, and 90th percentile results were calculated. The 50th percentile is the median, or the most likely, result.

4.3. Uncertainty Metric

The metric deemed most useful for illustrating the uncertainty of each reservoir was the Coefficient of Variation (CV), which is the ratio of the standard deviation of the sample to the mean of the sample (Jensen et al., 2000). Using the CV allowed us to normalize the result (RFC , RPI_c , and RPI_w) of each reservoir by its uncertainty. For example, a reservoir with a

low CV has a smaller standard deviation relative to its mean, and therefore there is less uncertainty about its predicted RFC, RPI_c or RPI_w .

5. Quality Thresholds for Mapping

Thresholds for the reservoir favorability metrics are required to segregate the reservoirs into favorability ‘grades’ for mapping. A five-grade threshold map was required by the project SOPO. Threshold choices based on conversations with experts and the results of the Monte Carlo Simulation are listed below.

5.1. Reservoir Flow Capacity Thresholds

Because RFC was used primarily to rank reservoir favorability, the RFC thresholds were chosen based on the distribution of RFC for the entire reservoir population. The distribution of RFC across the entire basin is strongly left-skewed, and therefore is better illustrated on a semi-log plot (Figure 1). The RFC thresholds were chosen based on a logarithmic scale, base ten. RFC values range from 0.003–15500 mD-m, and thresholds were placed at 1000, 100, 10, and 1. Reservoirs with RFC greater than 1000 mD-m are deemed most favorable.

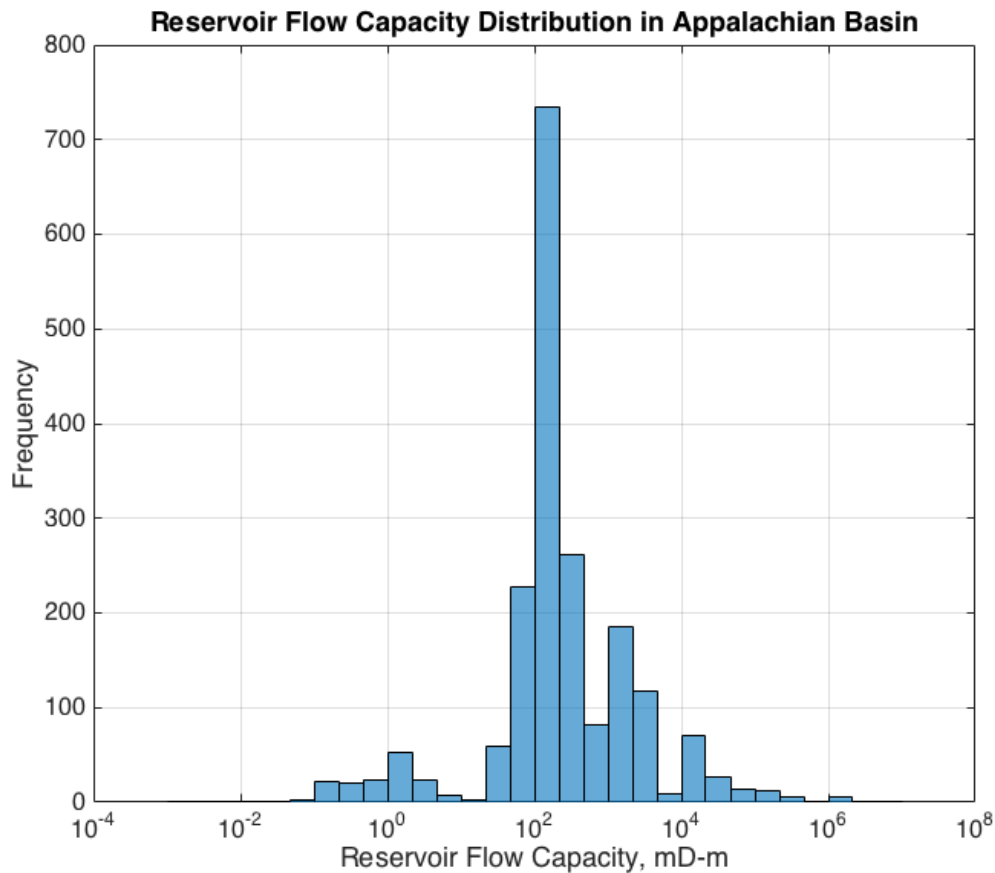


Figure 1. Distribution of average Reservoir Flow Capacity for all natural reservoirs in the Appalachian Basin.

5.2. Reservoir Productivity Index Thresholds

RPI_c and RPI_w metrics thresholds were chosen based on information regarding economic productivity rates published in the geothermal literature.

5.2.1. RPI_w Thresholds

Agemar et al. (2014) report that pressure drawdown for sedimentary geothermal systems typically range between 1-3 MPa. If we assume the greatest pressure drop of 3 MPa, and assume that 30 kg/s is the minimum mass flow rate acceptable for the water-based system, our RPI_w threshold for the reservoir which would not require stimulation (i.e. no EGS) is approximately 10 kg/MPa-s. Because the distribution of RPI_w in the basin is

strongly left-skewed, the remaining thresholds are logarithmic: 10, 1, 0.1, 0.01. Reservoir enhancement techniques can improve productivity by six to nine times (Cladouhos et al., 2014; Cho et al., 2015), so reservoirs in the 10–1 kg/MPa-s may be suitable with EGS.

5.2.2. RPI_c Thresholds

The thresholds for RPI with sCO₂ as the working fluid were determined using the thresholds for RPI_w as a baseline, which needed to be adjusted to normalize for the amount of heat extracted. For direct use heat applications, the difference in required mass flow rate of sCO₂ instead of water should only be related to the difference in heat capacity. According to Chen and Lundqvist (2006), the heat capacity of sCO₂ is about 4 kJ/kg-K, assuming the CO₂ is maintained at a constant pressure of 10 MPa and an average reservoir temperature of 60 °C. At equivalent temperatures, the heat capacity of water is 4.2 kJ/kg-K. These values are very close, therefore the same thresholds were applied to RPI_c.

5.3. Thresholds for the Coefficient of Variation

The Coefficient of Variation of the RPI ranges from 0.08-0.39. The thresholds were selected using equal interval groups, in order to best illustrate relative uncertainty across the reservoir population in the basin. The thresholds selected are: 0.14, 0.20, 0.27, and 0.33.

6. Selection of Most Favorable Reservoirs

In order to isolate the reservoirs that have the highest potential productivity with the least risk, the RPI or RFC can be combined with the CV results, depending on the desired outcome. If the interest is reservoirs that have a high predicted productivity, RPI can be used; whereas if the interest is in highlighting reservoirs with the most ideal geologic properties, RFC can be used. For the RPI_c and RPI_w maps, reservoirs with an RPI greater than 10 kg/MPa-s and with a CV

lower than 0.25 (25% uncertainty) were selected as the most favorable reservoirs. For the RFC map, reservoirs with an RFC greater than 100 mD-d and with a CV lower than 0.25 were selected as the most favorable reservoirs. The selected reservoirs with the highest potential but a greater risk can also be isolated for further research to better constrain and quantify the risk.

References Cited

- Agemar, T., Weber, J., and Schulz, R., 2014, Deep geothermal energy production in Germany: *Energies*, v. 7, no. 7, p. 4397-4416.
- Al-Jabri, R.A., Al-Maamari, R.S., and Wilson, O.B., 2015, Klinkenberg-corrected gas permeability correlation for Shuaiba carbonate formation: *Journal of Petroleum Science and Engineering*, v. 131, p. 172-176.
- Augustine, C., 2014, Analysis of Sedimentary Geothermal Systems Using an Analytical Reservoir Model, *in Proceedings, Geothermal: A Global Solution*: Davis, CA, 641-647.
- Bedre, M.G., Anderson, B.J., 2012, Sensitivity analysis of low-temperature geothermal reservoirs: effect of reservoir parameters on the direct use of geothermal energy: *Geothermal Resources Council Transactions, in Proceedings, Geothermal Resources Council 2012 Annual Meeting*, 1255-1262.
- Brown, D.W., 2000, A hot dry rock geothermal energy concept utilizing supercritical CO₂ instead of water, *in Proceedings, Proceedings of the twenty-fifth workshop on geothermal reservoir engineering*, Stanford University, 233-238.
- Chen, Y., and Lundqvist, P., 2006, Analysis of supercritical carbon dioxide heat exchangers in cooling process.
- Cho, J., Augustine, C., Zerpa, L.E., 2015, Validation of a Numerical Reservoir Model of Sedimentary Geothermal Systems Using Analytical Models, *in Proceedings, Fortieth Workshop on Geothermal Reservoir Engineering*, Stanford University.
- Cladouhos, T.T., Petty, S., Nordin, Y., Moore, M., Grasso, K., Uddenberg, M., and Swyer, M.W., 2014, Reservoir construction from the Newberry Volcano EGS Demonstration: *Journal of Groundwater Science and Engineering*, v. 2, no. 3, p. 1-7.
- Gérard, A., Genter, A., Kohl, T., Lutz, P., Rose, P., and Rummel, F., 2006, The deep EGS (enhanced geothermal system) project at Soultz-sous-Forêts (Alsace, France): *Geothermics*, v. 35, no. 5, p. 473-483.

- Gringarten, A.C., ed., 1978, *Geothermics and Geothermal Energy*: Springer, p. 297-308.
- Hamm, V., Bouzit, M., and Lopez, S., 2016, Assessment of complex well architecture performance for geothermal exploitation of the Paris basin: A modeling and economic analysis: *Geothermics*, v. 64, p. 300-313.
- Jensen, J.L., Corbett, P.W., Lake, L.W., and Goggin, D.J., 2000, *Statistics for petroleum engineers and geoscientists*: Amsterdam, The Netherlands, Elsevier.
- Jones, S.C., 1987, Using the inertial coefficient, b , to characterize heterogeneity in reservoir rock, *in* Proceedings, SPE Annual Technical Conference and Exhibition.
- Lindal, B., 1973, Industrial and other applications of geothermal energy , *in* Armstead, C., ed., *Geothermal Energy: Review of Research and Development*, UNESCO, p. 135-148.
- Murtha, J.A., 1994, Incorporating Historical Data Into Monte Carlo Simulation: *SPE Computer Applications*, v. 6, no. 02, p. 11-17.
- Ouyang, L.-B., 2011, New correlations for predicting the density and viscosity of supercritical carbon dioxide under conditions expected in carbon capture and sequestration operations: *Open Petroleum Engineering Journal*, v. 5, no. 1, p. 13-21.
- Peters, E.J., 2012, *Advanced Petrophysics: Volume 1: Geology, Porosity, Absolute Permeability, Heterogeneity, and Geostatistics*: Live Oak Book Company, Palo Alto, CA, 238 p.
- Pruess, K., 2007, *Enhanced Geothermal Systems (EGS) comparing water with CO₂ as heat transmission fluids*.
- Roen, J.B., and Walker, B.J., 1996, *The atlas of major Appalachian gas plays*, West Virginia Geological and Economic Survey, Publication V-25.
- Sanyal, S.K., and Butler, S.J., 2009, *Geothermal Power from Wells in Non-Convective Sedimentary Formations--An Engineering Economic Analysis*: Transactions Geothermal Resources Council, v. 33, p. 865-870.
- Satter, A., Iqbal, G.M., and Buchwalter, J.L., 2008, *Practical enhanced reservoir engineering : assisted with simulation software*: Tulsa, Okla., PennWell Corp.
- Smith, J., Horowitz, F., and Whealton, C., 2015, *Thermal Model Methods*, in *Appalachian Basin Play Fairway Analysis: Thermal Quality Analysis in Low-Temperature Geothermal Play Fairway Analysis*, Geothermal Data Repository, <https://gdr.openei.org/submissions/638>.
- Society of Petroleum Engineers, 2001, *Guidelines for the evaluation of petroleum reserves and resources: a supplement to the SPE*: Richardson, TX, Society of Petroleum Engineers.

Tanikawa, W., and Shimamoto, T., 2006, Klinkenberg effect for gas permeability and its comparison to water permeability for porous sedimentary rocks: Hydrology and Earth System Sciences Discussions, v. 3, no. 4, p. 1315-1338.

Tester, J.W., Drake, E.M., Driscoll, M.J., Golay, M.W., and Peters, W.A., 2012, Sustainable energy: Choosing among options: Cambridge, MA, MIT Press.

Engineering Toolbox, Water Dynamic and Kinematic Viscosity,
http://www.engineeringtoolbox.com/water-dynamic-kinematic-viscosity-d_596.html (March 2015).

Memo 12: Natural Reservoirs Data Selection in GPFA-AB

Erin Camp

Last modified: August 31, 2016

This memo is intended to augment the Natural Reservoirs Methodology memo, by providing additional details about the original databases and modified inputs for the Appalachian Basin Geothermal Play Fairway Analysis project. All research and literature that affected decisions for the reservoir data inputs are recorded here, including data for geologic formations in the Appalachian Basin.

DATABASE INTEGRATION

Two disparate databases were integrated for this project: 1) the Empire State Organized Geologic Information System (ESOGIS; data for reservoirs in New York), and 2) the Midwest Regional Carbon Sequestration Partnership (MRCSP; data for reservoirs in Pennsylvania and West Virginia). When the two databases were merged, there were discrepancies between the available data and the terminology used in each database.

1. Geologic Formation Name: The following formation codes were listed in the MRCSP database. The decrypted formation name for each is listed next to the code. Very often, the name of a formation in Pennsylvania and West Virginia is different than the given name of the same formation in New York. For those formations, the New York formation name was used. If a reservoir is listed as having produced from a smaller unit within a larger formation, the formation name was used. Any formation name changes are listed in parentheses next to the original formation name, shown below.

- a. BLDG: Bald Eagle
- b. BILDF: Bass Islands Formation
- c. BKMN: Beekmantown
- d. BNSN: Benson
- e. BERE: Berea
- f. BRRL: Brallier (Elk Group)
- g. CHZY: Chazy (Black River)
- h. CLNN: Clinton (Medina)
- i. DVSHL: Devonian Shale
- j. DVNNU: Devonian Unconformity Play
- k. ELKG: Elk Group
- l. GBRG: Gatesburg (Rose Run)
- m. GRDN: Gordon
- n. HDBG: Helderberg
- o. HRVL: Huntersville
- p. HVOK: Huntersville/Oriskany
- q. KEFR: Keefer
- r. LCKP: Lockport
- s. MDIN: Medina
- t. MLTI: "Multi"
- u. NWBG: Newburg
- v. ONDG: Onondaga
- w. ORSK: Oriskany
- x. RSRN: Rose Run
- y. SCHR: Scherr (Elk Group)
- z. SDCI: Silurian Devonian Carbonate Interval (Lockport)
- aa. TRNN: Trenton
- bb. TLLY: Tully
- cc. TCRR: Tuscarora
- dd. WEIR: Weir

2. Average Reservoir Depth

The MRCSP database holds values for each reservoir's "Average Production Depth", which is interpreted as the top of the reservoir production zone. The ESOGIS database does not have production depth data reported; therefore, reservoir depth was extracted manually from well completion reports downloaded from the ESOGIS website. To calculate an average production depth for the NY reservoirs, the reported reservoir tops from each well in a given reservoir were averaged.

3. NY Reservoir Polygons

The MRCSP database includes shapefiles of the reservoir polygons, which is an estimate of the aerial extent of each reservoir. The ESOGIS database does not contain shapefiles, so they were created manually in a GIS. The buffer distance around producing wells in each reservoir in NY was chosen as 900 meters. This choice was made by comparing the only available polygons for NY reservoirs, which were the Trenton-Black River reservoirs (Patchen et al., 2006). Inputting those shapefiles into a GIS and comparing them to the locations of the wells showed that an average distance of 900 meters around all wells in a reservoir would create polygons compatible with Patchen et al.'s approach (Figure 1).

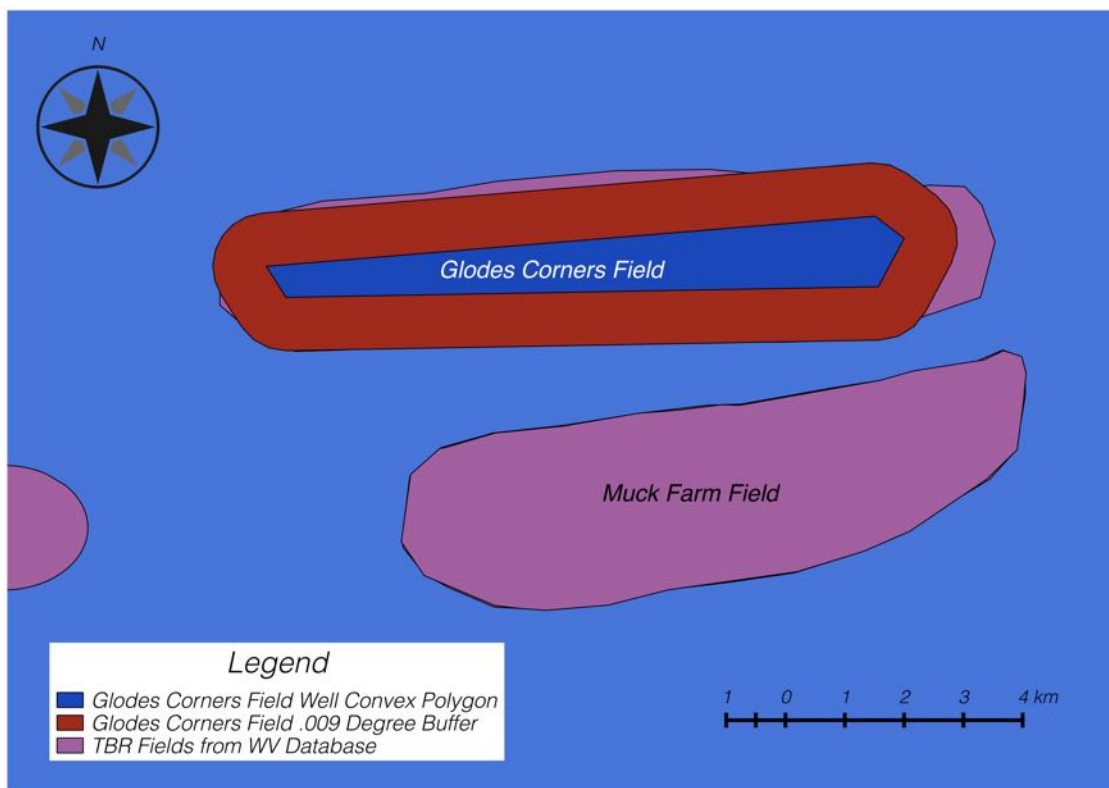


Figure 1. Example of Trenton-Black River polygons in GIS, which aided in creating a systematic buffer zone for NY reservoirs. 0.009 degrees is equivalent to 900 meters. The West Virginia Database comes from Patchen et al. (2006).

4. Porosity and Permeability

Porosity and permeability values were assigned based on the producing geologic formation in which the reservoir is located. New York reservoirs derivation required derivation of both porosity and permeability values from sources other than ESOGIS. The MRCSP database provided porosity data for reservoirs in Pennsylvania and West Virginia, so only permeability had to be input based on other sources. For all three states, empirical porosity-permeability relationships (if available) were applied to the porosity values for each formation. Otherwise, average permeability values were applied to all reservoirs of a given geologic formation.

If empirical relationships were used, the calculated permeability values are not reported below because the data vary from reservoir to reservoir. However, if an average permeability value was applied to all reservoirs of a given formation, that value is listed below. The first section describes formations that are host to reservoirs in New York, and therefore require porosity inputs; however, these formations may also be host to reservoirs in Pennsylvania and West Virginia. In such cases, any differences in average values across the three states are noted below. The last section describes formations that are host to reservoirs only in Pennsylvania and West Virginia, and therefore only require permeability inputs.

Formations located in New York:

- a. Queenston: Data chosen for the Queenston were taken from Lugert et al. (2006). Eighty-three samples from the Delany Core were analyzed by H.J. Gruy and Associates, which gave the following results:

- i. Average porosity of core: 10.8%
- ii. Porosity-permeability fit from core data, where k is permeability in units of mD and ϕ is porosity in porosity units (p.u.):

$$k = 0.0005 \exp(0.5478\phi)$$

- iii. Average core permeability for a porosity of 10.8% is 0.185 mD
- iv. Lithology: Sandstone

- b. Black River: Data chosen for the Black River Formation (also known as the Trenton-Black River in New York State) were taken from Lugert et al. (2006). Samples from the Whiteman #1 Core were analyzed by CoreLab, Inc.

- i. Average porosity of core: 7%
- ii. Porosity-permeability fit from core data, where k is permeability in units of mD and ϕ is porosity in porosity units (p.u.):

$$k = 1.8716 \exp(0.4967\phi)$$

- iii. Average Permeability for a porosity of 7% is 60.56 mD.
- iv. Lithology: Limestone/Dolomite

- c. Galway/Theresa/Rose Run:

- i. New York: The Galway Formation has long been called the Theresa Sandstone play in the subsurface, but that name is inaccurate when compared to the outcrop stratigraphy. Smith et al. (2010) show that the Galway Formation is Upper Cambrian in age and occurs above the Potsdam Sandstone (earliest Upper Cambrian in age) and below the Little Falls Formation (uppermost Cambrian in age). The Theresa is Ordovician in age and is actually younger than even the Tribes Hill

Formation. The Theresa can only be found in northernmost New York in the Ottawa Graben. The producing formation in Western New York is the Galway Formation. Smith et al. (2010) confirm that Bockhahn, Cascade Brook, and Northwoods fields all produced from the Rose Run, in the Galway Formation. Those are 3 of the 10 Galway fields in the New York database, and those 10 fields are all in the same region. It is believed that the Rose Run is the unit within the Galway which produced gas (B. Slater, pers. comm.). The following porosity and permeability core data are from the Hooker Chemical #1 Well, which include measurements from the Potsdam Sandstone. For this work, the Potsdam data were removed, as they are not stratigraphically part of the Galway Formation.

1. Average porosity: 6.5% for the Galway/Theresa/Rose Run reservoirs. (Smith et al., 2010)
2. Porosity perm relationship fit from core data, where k is permeability in units of mD and ϕ is porosity in porosity units (p.u.):

$$k = 0.6621\phi - 1.7261$$

3. Average permeability is 2.6 mD for a porosity of 6.5%, according to the above equation
- ii. Galway in Pennsylvania and West Virginia: Data taken from reports of producing fields in Pennsylvania and West Virginia, in Roen and Walker (1996).

1. Porosity ranges from 2-25% and averages 10%.
2. Permeability ranges from 0.01 to 198 mD and averages 5 mD.
3. The MRCSP database reports porosities between 8-10 for the Galway/Rose Run fields, so an average of 5 mD was applied for all the PA and WV Rose Run reservoirs.

iii. Lithology: Sandstone

d. Medina: Data chosen for the Medina were taken from Lugert et al. (2006). No core data were available, so average values from a high-volume producing field—the Lakeshore Field—were applied. The following values were applied to Medina reservoirs in all three states.

i. Average porosity: The report states that porosity ranges between 6-8%, so an average porosity of 7% was chosen.

ii. Average permeability: 0.1 mD.

iii. Lithology: Sandstone

e. Onondaga: Data for Onondaga reservoirs come from Roen and Walker (1996). Average porosity and permeability values were derived from plugs taken from a productive Onondaga field in Steuben County, NY. The following values were used for reservoirs in all three states, due to a lack of permeability data available for Onondaga reservoirs in Pennsylvania and West Virginia. Because reported porosity values from Onondaga reservoirs in Pennsylvania and West Virginia were similar to the average porosity of Onondaga reservoirs in New York, the average permeability value from Onondaga reservoirs in New York was applied to those in Pennsylvania and West Virginia as well.

- i. Average porosity: 5.2%.
 - ii. Average permeability: 22.4 mD.
 - iii. Lithology: Limestone
- f. Oriskany: Data for the Oriskany reservoirs come from Appendix D of Riley et al. (2010). All the data presented there come from cores in Pennsylvania and Ohio, but were applied to reservoirs in New York and West Virginia as well.
 - i. Average porosity: 5%.
 - ii. Average permeability: 1 mD
 - iii. Lithology: Sandstone
- g. Helderberg: There is one producing field from the Helderberg Formation in the database: the Stagecoach field. According to Lugert et al. (2006), geologists reclassified the producing formation of the Stagecoach to the Oriskany Formation (page 23).
- h. Bass Islands: There is no available porosity or permeability data for the Bass Islands Formation in the Appalachian Basin; however, there are data from the Bass Islands Formation in the Michigan Basin (Harrison III et al., 2009). The following value were used for Bass Islands reservoirs in all three states.
 - i. Average porosity: 12.5%. This value from Harrison et al. (2009) agrees with the range of porosity values listed for Bass Islands reservoirs in the PA/WV database, which is 10–14% porosity.
 - ii. Average permeability: 22.4 mD
 - iii. Lithology: Dolomite

Formations found only in Pennsylvania and/or West Virginia regions of the Basin:

i. Lockport: Data for the Lockport reservoirs come from Appendix A of Riley et al. (2010).

i. Porosity-permeability relationship fit from core data, where k is permeability in units of mD and ϕ is porosity in porosity units (p.u.):

$$k = 3.0 \times 10^{-5} \exp(1.1716\phi)$$

ii. Lithology: Dolomite

j. Elk Group: For simplicity, the Brallier, Gordon, and Benson were combined into the Elk Group, based on formation grouping. Data for the Elk Group were taken from Roen and Walker (1996).

i. Porosity of the Elk Group ranges from 5–10%

ii. Permeability ranges from 0.1–2.0 mD.

iii. Validation: The MRCSP database reports an average porosity of 11% for all the Elk Group reservoirs; therefore, the upper end of average permeability (2 mD) was used.

iv. Lithology: Sandstone; clay-rich turbidite slope apron deposit (Roen and Walker, 1996).

k. Lockhaven: Lockhaven was given the same permeability values as Elk Group, but not renamed.

i. Lithology: Mudstone

l. Bald Eagle: There is only one Bald Eagle reservoir in the MRCSP database: the Grugan field, located in Pennsylvania.

- i. Permeability: 0.07 mD was reported in Roen and Walker (1996). Most permeability is from fractures.
 - ii. Lithology: Sandstone
- m. Beekmantown: Lugert et al. (2006) state that there are no major distinctions between the reservoir properties of the Queenston and the Beekmantown, so they were not evaluated separately.
 - i. Permeability: 0.185 mD
 - ii. Lithology: Limestone/Dolomite
- n. Berea:
 - i. Porosity: 12% (Roen and Walker, 1996)
 - ii. Permeability: 3.84 mD (Roen and Walker, 1996)
 - iii. Validation: The Berea reservoirs in the MRCSP database report 10% porosity, which is consistent with the Roen and Walker (1996).
 - iv. Lithology: Sandstone
- o. Chazy: According to Walcott (1896), the Chazy is another term for the Black River limestone. These fields are listed as having porosity of 8% in the MRCSP database. Their formation name was therefore changed to Black River, and the empirical porosity-permeability relationship from the Black River reservoirs in New York was applied. This results in a permeability of 99.5 mD for all four reservoirs in Pennsylvania.
- p. Helderberg: According to Lewis et al. (2009), the permeability of the Helderberg Formation is very low, approximately 0.001 mD.
 - i. Lithology: Limestone

q. Huntersville and Huntersville/Oriskany play: Riley et al. (2010) provides a maximum permeability of 0.003 mD for the Huntersville/Oriskany play. This value was used for the Huntersville reservoirs as well, due to a lack of data unique to the Huntersville.

i. Lithology: Chert and Sandstone

r. Loysburg: Applied values from Beekmantown Dolomite. No other data available.

s. Newburg: The accompanying database to Roen and Walker (1996) contains two sets of core porosity and permeability data points. Because the other fields without permeability data had very similar porosity values, those data were fit to get an exponential relationship where permeability is in mD and porosity is in porosity units:

$$k = 2.1591 \exp(0.1699\phi)$$

i. Lithology: Limestone

t. Weir: There are two Weir reservoirs with porosity data in the MRCSP database, and one of those reservoirs is listed in Roen and Walker (1996) and has average porosity and permeability values. Because the porosity values aligned with what was already reported in the MRCSP database, the following permeability value was applied to both reservoirs.

i. Permeability: 8 mD

ii. Lithology: Sandstone

- u. Keefer:
 - i. Permeability: Roen and Walker (1996) report an average permeability for the Keefer Formation of 7.06 mD. That value was applied to the single Keefer reservoir in the MRCSP database.
 - ii. Lithology: Sandstone
- v. Devonian Unconformity Play:
 - i. Permeability: Roen and Walker (1996) report an average permeability of 15.3 mD for this formation.
 - ii. Lithology: Limestone

Formations with Very Limited Data:

- w. Tuscarora: Roen and Walker (1996) report one Tuscarora field with permeability ranging from 0 to 10.7 mD. Many reports note similarities between Tuscarora, Medina, and Clinton. Due to a lack of specific data, a value of 0.1 mD was used for the Tuscarora, consistent with the Medina Formation.
 - i. Lithology: Sandstone
- x. “Multi”: These are reservoirs that produced hydrocarbons from a wide variety of undetermined formations. With no data to use, a high uncertainty and low permeability value of 0.1 mD was used.
- y. Trenton: This play is found only in West Virginia, where permeability is associated primarily with fractures. Just like similar play types, a permeability of 0.1 mD was applied because more precise data cannot be found.
 - i. Lithology: Limestone

- z. Tully: There is only one Tully reservoir in the MRCSP database. There is no permeability data available, so it was assigned a low permeability value of 0.1 mD with a high uncertainty.
 - i. Lithology: Limestone
- aa. Mahantango: There is only one Mahantango reservoir in the MRCSP database. There are no permeability data available, so it was assigned a low permeability value of 0.1 mD with a high uncertainty.
 - i. Lithology: Mudstone

UNCERTAINTY INDEX ASSIGNMENTS

Permeability

The following list describes how the uncertainty index was assigned to each reservoir's permeability value, and the respective assignment of standard deviation from the mean:

- 0: Data is site-specific (pertains to that *exact* reservoir). This assignment was very uncommon. 0% SD
- 1: Published porosity-perm equation available from local/nearby reservoirs of same formation. Standard deviation: 12.5% SD
- 2: Data come from use of a published equation from data that is region specific. Standard deviation: 25% SD
- 3: Computed equation from available data; Range or average value for the formation is available, or state/region specific data are available. Standard deviation: 50% SD
- 4: Porosity-permeability relationship (or average value) can be applied from a similar formation or same formation from another state/region. Standard deviation: 100% SD
- 5: Generic low value assigned due to lack of data or understanding. Standard deviation: 200% SD

Reservoir Thickness

The following list describes how the uncertainty index was assigned to each reservoir's thickness value:

- 0 Not used for reservoir thickness. 0% SD
- 1 Not used for reservoir thickness. 10% SD
- 2 Assigned to all reservoirs in the project, because all reservoir thickness data are derived from the producing thickness of the hydrocarbon reservoir. 20% SD
- 3 Not used for reservoir thickness. 30% SD
- 4 Not used for reservoir thickness. 40%
- 5 Not used for reservoir thickness. 50%

Fluid Viscosity

Because fluid viscosity is a function of the reservoir temperature, the uncertainty of the assigned viscosity values was dependent on the uncertainty underlying the calculation of the temperature of the reservoir. The following list describes how the uncertainty index was assigned to each reservoir's fluid viscosity value:

- 0 Not used for fluid viscosity. 0% SD
- 1 Assigned to all reservoirs in the project. One standard deviation of the reservoir temperatures is 10°C, which equates to a viscosity standard deviation of approximately 10% from the mean value. 10% SD
- 2 Not used for fluid viscosity. 20% SD
- 3 Not used for fluid viscosity. 30% SD
- 4 Not used for fluid viscosity. 40% SD
- 5 Not used for fluid viscosity. 50% SD

References Cited

- Harrison III, W.B., Grammer, G.M., and Barnes, D.A., 2009, Reservoir characteristics of the Bass Islands dolomite in Otsego County, Michigan: Results for a saline reservoir CO₂ sequestration demonstration: *Environmental Geosciences*, v. 16, no. 3, p. 139-151.
- Lewis, J.E., McDowell, R.R., Avary, K.L., and Carter, K.M., 2009, Characterization of the Helderberg Group as a geologic seal for CO₂ sequestration: *Environmental Geosciences*, v. 16, no. 4, p. 201-210.
- Lugert, C., Smith, L., Nyahay, R., Bauer, S., and Ehgartner, B., 2006, Systematic Technical Innovations Initiative Brine Disposal in the Northeast: Albany, NY, New York State Energy Research and Development Authority.
- Patchen, D.G., Hickman, J.B., Harris, D.C., Drahovzal, J.A., Lake, P.D., Smith, L.B., Nyahay, R., Schulze, R., Riley, R.A., and Baranoski, M.T., 2006, A geologic play book for Trenton-Black River Appalachian basin exploration: U.S. Department of Energy Report: Morgantown, West Virginia, U.S. Department of Energy.
- Riley, R., Harper, J., Harrison III, W., Barnes, D., Nuttall, B., Avary, K.L., Wahr, A., Baranoski, M., Slater, B., and Harris, D., 2010, Evaluation of CO₂-Enhanced Oil Recovery and Sequestration Opportunities in Oil and Gas Fields in the MRCSP Region MRCSP Phase II Topical Report October 2005 October 2010. DOE Cooperative Agreement No.
- Roen, J.B., and Walker, B.J., 1996, The atlas of major Appalachian gas plays, West Virginia Geological and Economic Survey, Publication V-25.
- Slater, B., March 2015, pers. comm.
- Smith, L., Nyahay, R., and Slater, B., 2010, Integrated Reservoir Characterization of the Subsurface Cambrian and Lower Ordovician Potsdam, Galway and Theresa Formations

in New York: Albany, NY, New York State Energy Research and Development
Authority.

Walcott, C., 1896, Cambrian Rock of Pennsylvania, United States Geological Survey,
<http://pubs.usgs.gov/bul/0134/report.pdf>.

Memo 13: Identifying Potentially Activatable Faults in GPFA-AB

Identifying Potentially Activatable Faults for the Appalachian Basin
Geothermal Play Fairway Analysis

Frank Horowitz

18-September-2015

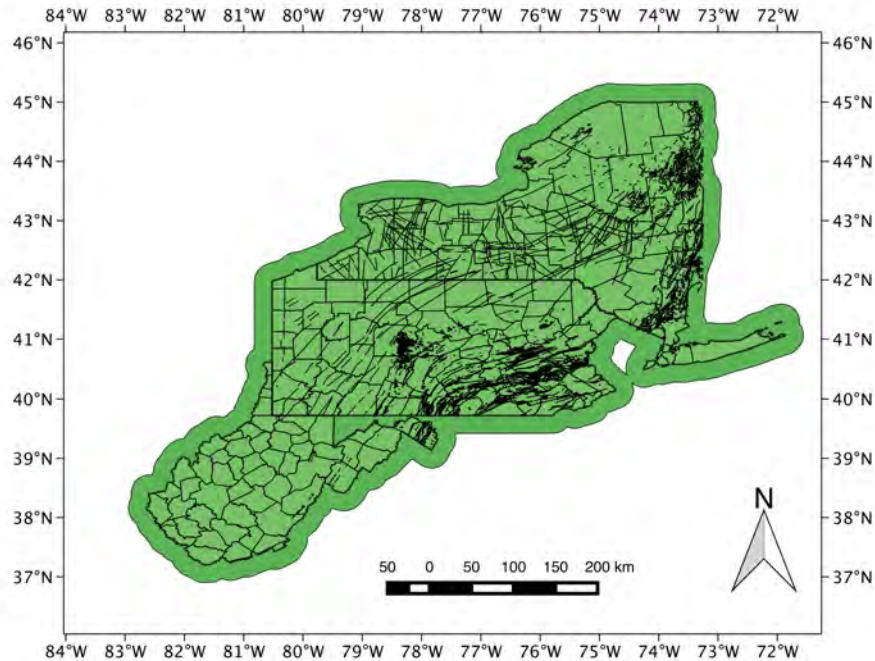


Figure 1: Mapped faults and other lineaments available in GIS form on the GPFA-AB server. Note the uneven regional coverage and un-geological artifacts such as state-boundary truncations of structures.

Existing fault maps (Figure 1) do not share the Appalachian Basin Geothermal Play Fairway Analysis (GPFA-AB) boundaries or scale. Hence, their use leads to problems of uneven coverage, varying interpretation of faults vs. lineaments, and different mapping scales. For more uniformity across the GPFA-AB region, we use an analysis of gravity and magnetic fields discussed next.

In order to provide a spatially uniform coverage of candidate faults, I turned to the Poisson wavelet multi-scale edge analysis of potential fields – informally known for brevity as the ‘worm’ technique – my co-workers and I developed starting nearly 20 years ago: Hornby et al. (1999) (independently derived by Moreau et al., 1997). This technique, widely deployed in the mining community in Australia and elsewhere (e.g. GoldCorp, 2001), uses gravity and magnetic fields to detect lateral contrasts in mass density or magnetization strength respectively. Figure 2 displays a cartoon summary of the technique.

Some theoretical advantages of the technique include:

- Marrying wavelet theory and potential field physics by building a wavelet from the Green’s function of the Poisson equation (Laplace’s equation with sources).
- The inverse wavelet transform has a physical interpretation as an *induced* inversion to a dipole source distribution (Boschetti et al., 2001; Hornby et al., 2002) that produces a field that is exactly the starting field. The regularizing assumption is that ‘Rocks Have Edges’.
- The field values at the locations of the multiscale edges (worms) alone, when combined with the inverse wavelet transform above, produce a field that is a close approximation of the starting field via

Physical Interpretation of the Worms (Induced Inversion)

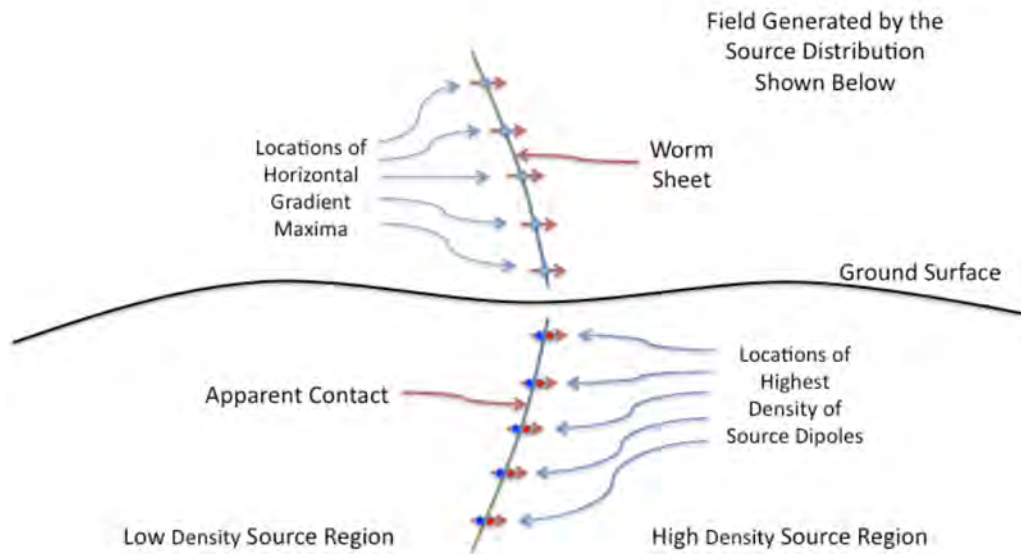


Figure 2: A vertical cross-section cartoon of the worm technique. The gravity or magnetic field is notionally known completely at the ground surface. The field is upward continued to a suite of heights. Hornby et al. (1999) show that each level of upward continuation corresponds to a (continuous) wavelet scale. The locations of maxima in the horizontal gradient of the field at each height become an edge (or a 'worm') for the corresponding scale (the intersection of these 1D features with the plane of section are shown as blue dots above ground), the collection of edges at all scales are 'multiscale edges'. A suite of worms arising from connected locations on the ground is a 'worm sheet'. As explained in the text, an underground inversion is induced via a physical interpretation of the inverse wavelet transform as a distribution of dipole sources. Draping the worm sheets underground (blue and red dots) results in a visualization of the locations of highest density of dipole sources. These are interpreted as the locations of apparent lateral contacts.

the result from Mallat and Zhong (1992).

Hornby et al. (1999) show that the magnitude of the horizontal gradient – normalized appropriately to correspond with wavelet theory – changes amplitude with upward continuation/scale-change in such a fashion as to identify the Lipschitz exponent (related to the fractal dimension) of the underlying singularity in the source distribution. That is, if we define

$$M \equiv (z/z_0) \|\overrightarrow{\partial f / \partial x} + \overrightarrow{\partial f / \partial y}\| \quad (1)$$

where f is our potential field (e.g. $f = \|g_z\|$ for gravity surveys, or $f =$ pseudogravity for magnetic surveys) then $\partial M / \partial z$ is the quantity of interest in determining the Lipschitz exponent. M is usually displayed as the worm color, and one can visually assess $\partial M / \partial z$ from the graphical representation. The Lipschitz exponent concept is closely related to the geophysically-more-widely-known ‘structural index’ from Euler deconvolution (e.g. Reid et al., 1990). An in-prep. masters thesis (Navarrete, 2015) has shown that the locations of worms and Euler solution routinely coincide, but that the worm technique offers significantly enhanced lateral coverage over the Euler deconvolution solutions.

Some practical advantages of the worm method include:

- When draped underground as in Figure 2, the worms resemble lateral contacts and reproduce (at least near the surface) the sense of dip of the contact. This provides an immediate cue towards a sensible geologic interpretation. Unfortunately – once getting beyond ‘shallow’ and ‘steep’ – the magnitude of dip is more problematic, since the field is due to more than one body and interactions between sources cause complexities. Jessell (2001) summarizes a large number of cases of worm behavior for different structural geologic settings.
- The worms commonly extend information about lateral discontinuities over large regions. This offers the geological interpreter a chance to connect structures that might not be recognized as being related.
- Deep worms tend to represent (smoothed) major lateral boundaries. By following the worm sheets upwards, the connected shallow expressions can be identified. At the scale of the GPFA, those major lateral boundaries are commonly associated with terrane boundaries or other major tectonic sources.

The worms are best visualized in 3 dimensions in order to see their interrelations. In previous efforts, that has led to working with them primarily in graphical visualization packages such as VTK (Schroeder et al., 2004) and VisIt (Childs et al., 2005) or commercial mining industry visualization packages such as FracSIS (RungePincockMinarco, 2015). For the GPFA-AB project, we need to incorporate the worms with other GIS information, but few GIS packages deal fluidly with 3D visualization. ArcScene – a component of ArcGIS – can in fact display 3D GIS information, but worms present a serious performance problem for ArcScene due to the large number of individual items that must be displayed. For the GPFA-AB project, we work around this problem by displaying worms from a restricted series of depths in 2D map view in ArcMap or QGIS, but the results are less useful than a wished-for performant 3D GIS could produce.

The worm results for the GPFA-AB project are calculated by open-source code described in Horowitz and Gaede (2014). A git repository of that code may be found at <https://bitbucket.org/fghorow/bsdwormer> with its complete revision history. Figure 3 shows worms calculated using that software from a 2.5 km resolution interpolation of the gravity Bouguer anomaly calculated from the GPFA-AB study region. The gravity station measurements were drawn both from the PACES database (Hildenbrand et al., 2002) and from a preliminary compilation filling in gravity stations in Pennsylvania (Malinconico and Moore,

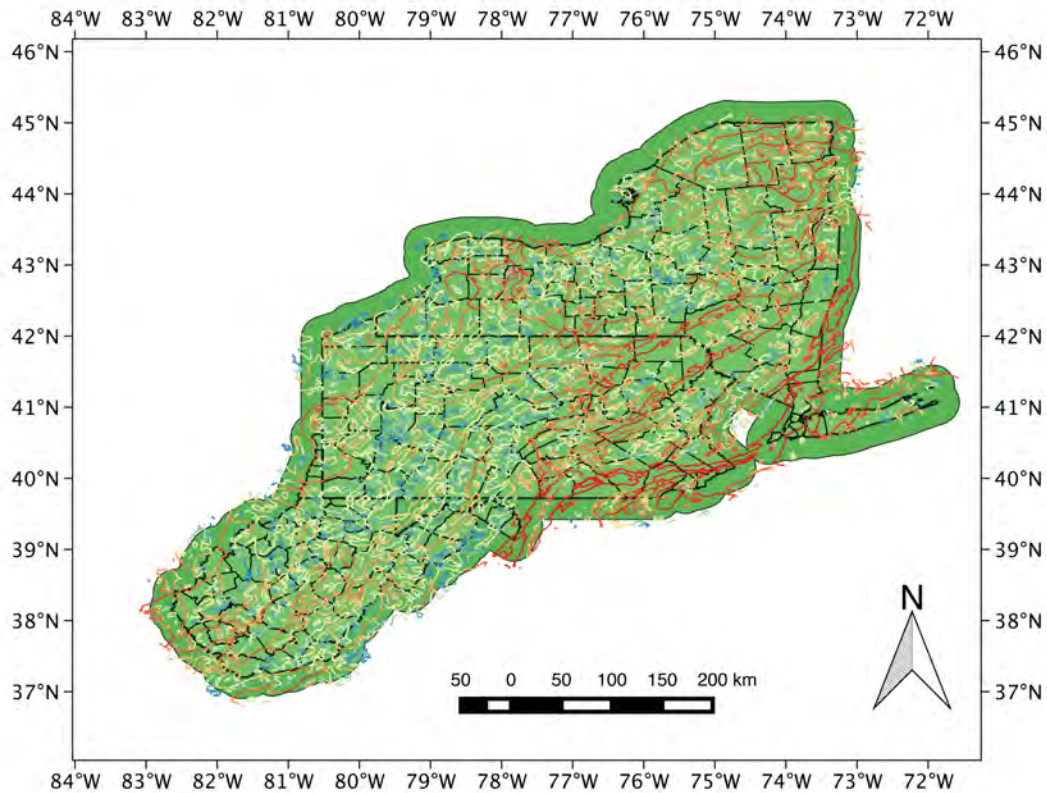


Figure 3: Displayed are gravity worms from the GPFA-AB region. The worms are from upward-continued heights (corresponding to depths as discussed above) ranging from 1 to 3 km inclusive. Each worm segment is colored according to \log_{10} of the M defined in equation (1) above. The worm color scale ranges from violet for low values of M to red for high values of M . See text for a more complete description.

2013). The preprocessing for those data – performed in the commercial software Oasis/Montaj – included selected removal of outliers and interpolation using a minimum curvature algorithm. Figure 4 shows worms calculated using that software from a 1.25 km resolution interpolation (Ravat et al., 2009) of the magnetic pseudogravity anomaly (e.g. Blakely, 1996) from the GPFA-AB study region. The pseudogravity calculation from the underlying magnetic grid was also performed in Oasis/Montaj.

Displayed in Figure 5 are locations of all earthquakes in the region retrieved from two catalogs: the US National Earthquake Information Center’s (NEIC) catalog – from 1 January 1965 through 31 May 2015, and EarthScope’s Transportable Array (TA) catalog of events from the Array Network Facility recorded during the TA’s deployment in the region (currently being removed). The date range for events from the TA are 16 March 2011 through 31 May 2015.

Importantly, the NEIC catalog, drawing on USGS seismologists’ manual efforts, identifies events that are categorized as earthquakes – as opposed to (e.g.) blasting events associated with mining or quarrying – enabling a simple database query to retrieve only earthquake events. Unfortunately, the TA catalog has no such categorization underpinning it (Astiz et al., 2014) – which resulted in my initially including events that

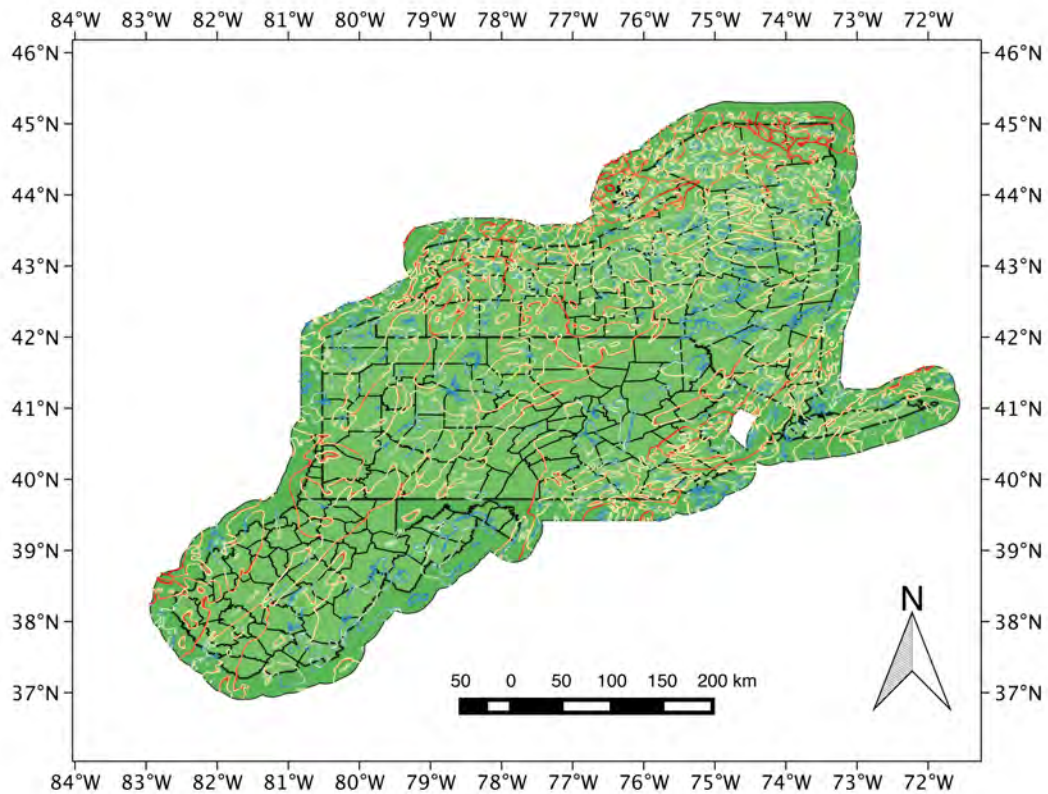


Figure 4: Displayed are magnetic worms from the GPFA-AB region. The worms are from upward-continued heights (corresponding to depths as discussed above) ranging from 1 to 3 km inclusive. Each worm segment is colored according to \log_{10} of the M defined in equation (1) above. The worm color scale ranges from violet for low values of M to red for high values of M . See text for a more complete description.

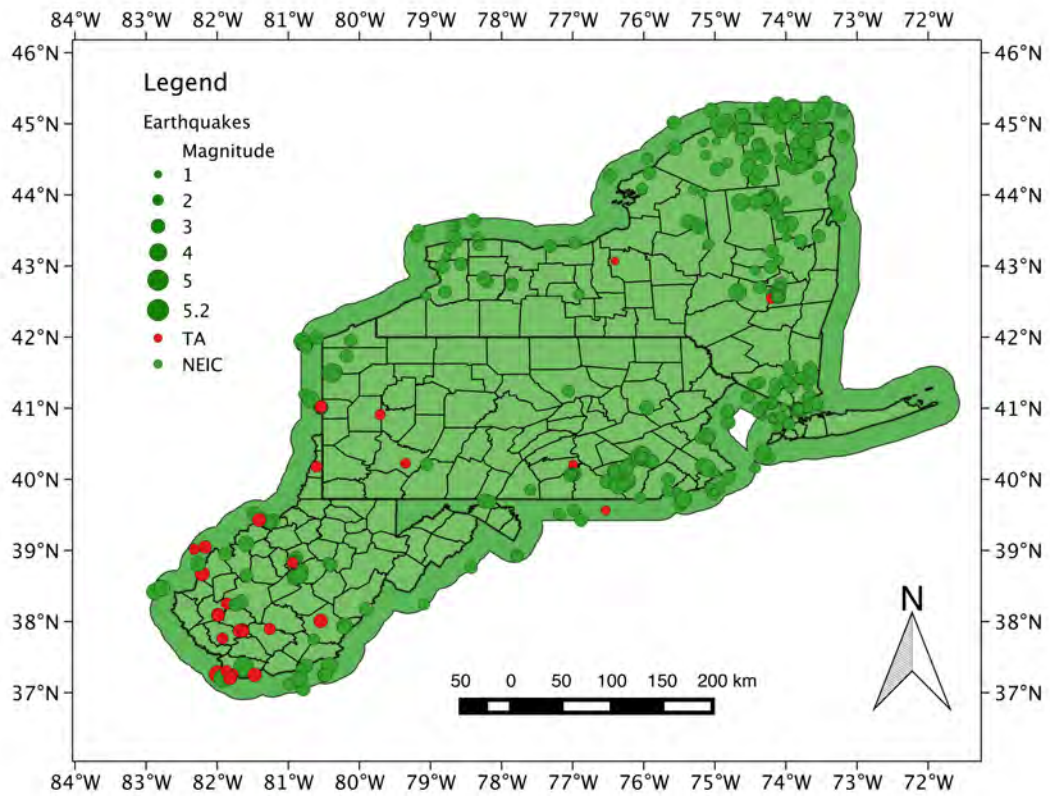


Figure 5: Displayed are earthquake epicenters from the GPFA-AB region. Shown in green are earthquake events drawn from the NEIC catalog. Shown in red are events not identified as potential blasts drawn from the TA catalog after application of the approximate de-contamination algorithm described in the text. Earthquake magnitudes M_L are displayed proportional to the radius of each event.

were almost certainly artificial blasts in the combined catalog. This was most discernible in the coal mining areas of southwest West Virginia, which appeared to have a large and active region of seismicity when plotting the raw TA data. After consultation with colleagues at the West Virginia Geological and Economic Survey drew our attention to this error, GPFA-AB investigator Beatrice Magnani of SMU suggested implementing an approximate de-contamination algorithm based on a time-of-day attribute of anthropogenic mining blasts. Quoting Astiz et al. (2014), "...mine blasting in the United States is allowed only between sunrise and sunset (Mining Safety and Health Administration, Title 30 CFR, MSHA, U.S. Department of Labor)." This led me to remove all TA events in the GPFA-AB region occurring between 07:00 and 18:00 local times. While those are only approximate local hours for sunrise and sunset, that simple algorithm removed the vast majority of TA events in the coal mining region of southwestern West Virginia – as well as some suspicious events from quarries located near to the New York State Thruway corridor and others possibly associated with shale gas hydraulic fracturing activities in regions of Pennsylvania associated with Marcellus shale development (Figure 6). Clearly, however, some natural earthquakes might also have been removed by this approximate algorithm. The odds of retaining detected natural seismicity in the TA results are only 13 in 24 because 11 hours each day were rejected. This unfortunate feature of our analysis must remain until seismologists can evaluate seismograms for the characteristics of blasts (e.g. emergent P arrivals, low amplitude S arrivals) from all 1647 TA events flagged as "daylight" in our region – deemed well beyond the scope of this study.

One method for identifying active faults was to simply find (via GIS methods) those worms which are physically close to a recorded earthquake. Under the assumption that any earthquake epicenters from sparse seismometer locations and poorly known velocity structures would yield mislocations of some distance, I felt this was an appropriate 'objective' way of identifying activated faults. Figure 7 displays a subset of those worms from figures 3 and 4 that are near to earthquakes. These structures are deemed to have an elevated risk factor for seismicity. The example distance ranges in 5 km increments shown in Figure 7 are not the actual values chosen in the combined risk factor assessment map – see that memo for details. Also, for error estimates, all earthquake locations were assumed to have 2.5 km standard deviation circles, while gravity and magnetic worm point location errors were assumed to have 500m and 250m standard deviations respectively. A clear drawback of the technique is that it only identifies structures active recently enough to have instrumentally recorded earthquakes.

After discussions with several people both inside the project and outside (including David Castillo, a former director of the oilfield borehole stability consultants Geomechanics International – now part of Baker-Hughes), it became clear that a potentially more relevant approach to estimating the risk factor for seismicity would be to determine the angle of a structure to the regional direction of the principal compressive stress (σ_1). This is supported by examination of figure 8, which shows some relevant Mohr's circles along with both Byerlee's Law (Byerlee, 1978) and Griffith-Coulomb failure envelopes. In those Mohr-space figures, two planes best oriented for failure by Byerlee's Law are marked with red dots. (There are two additional symmetrical orientations in the lower half of the Mohr diagram not shown for visual simplicity.) Those planes with normals not parallel to the principal stress directions would plot in the interstitial crescents between the circles. This leads to the conclusion that the angle a candidate plane normal makes from σ_1 is a sensitive parameter for proximity to failure under a Mohr-Coulomb failure model (Rick Allmendinger, pers. comm., 2015).

One major caveat: that orientation-in-a-regional-stress-field conclusion holds true wherever the actual state of stress is known (i.e. where the radii of the Mohr's Circles in figure 8 are established). In our situation however, we have very little information about the magnitudes of the principal stresses – other than the trivial vertical lithostatic case due to burial depth and ρgh . An unavoidable consequence of that fact is that

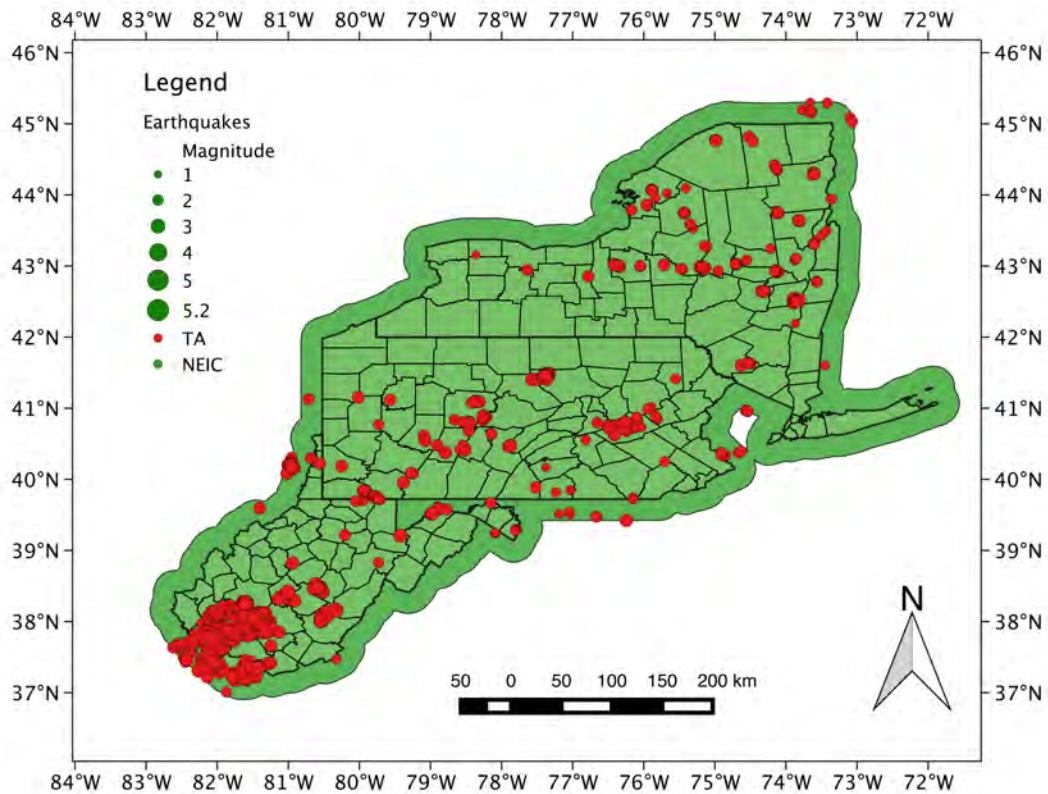


Figure 6: Displayed are suspected mining and quarry blasts from the GPFA-AB region. Shown in red are events identified as suspected mining and quarrying blasts drawn from the TA catalog after application of the approximate de-contamination algorithm described in the text. Earthquake magnitudes M_L are displayed proportional to the radius of each event.

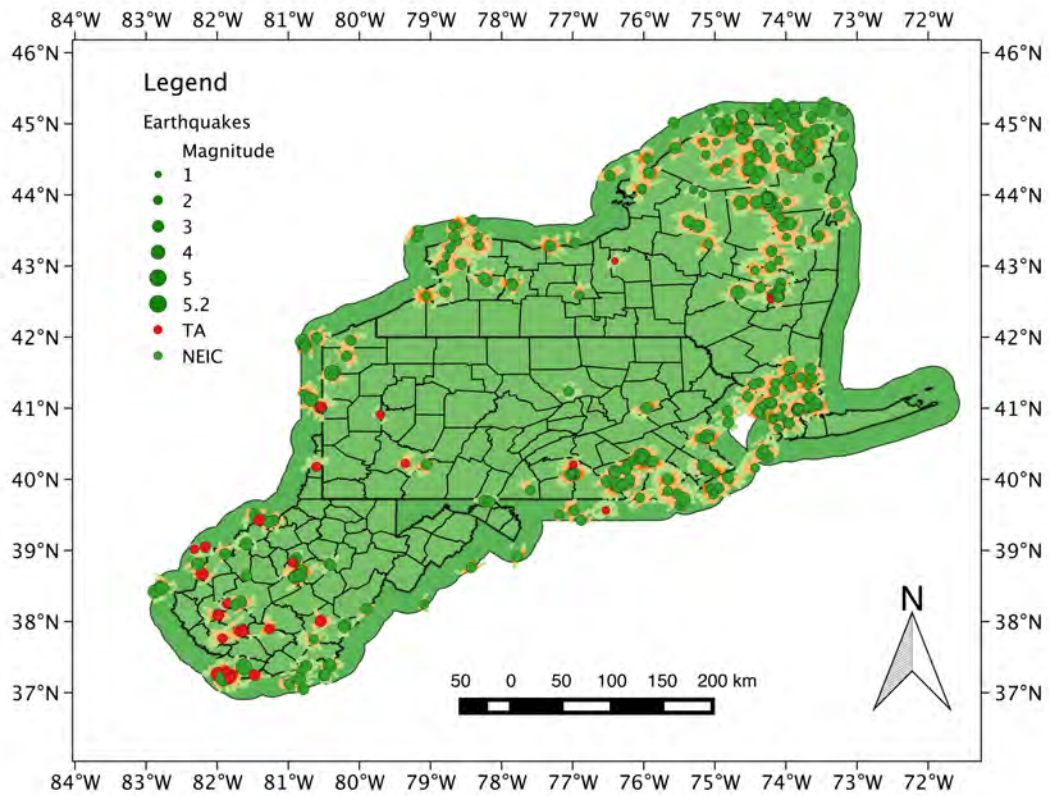
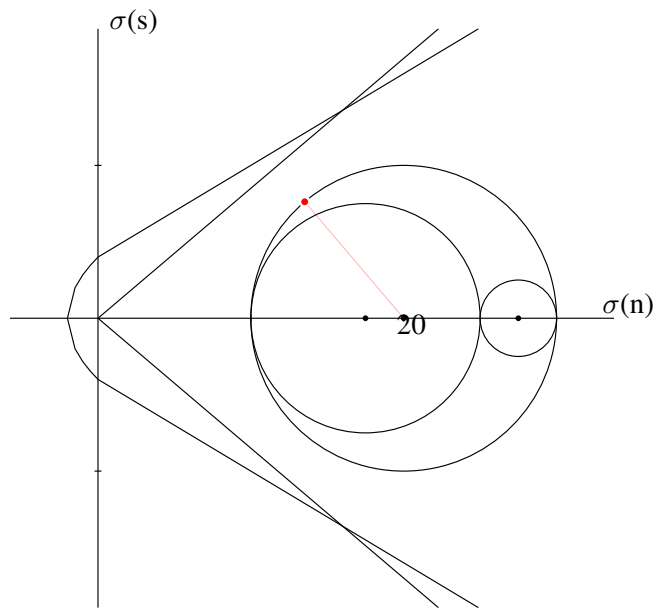
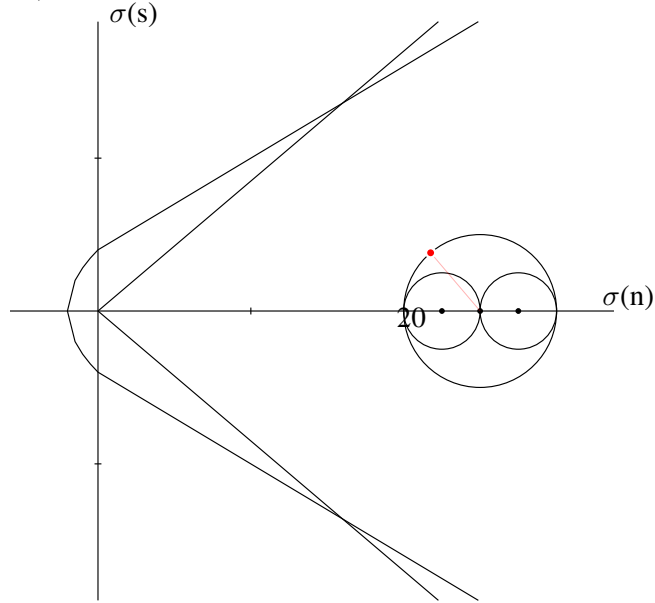


Figure 7: The subset of worms from both figures 3 and 4 that are found within specified ranges of the recorded earthquakes described in Figure 5. Shown in red are worm points within 5km of an earthquake; in orange are points between 5 and 10km; in yellow are points between 10 and 15km; and in light green are points from 15 to 20km.



(a) 3D Mohr's circles for notional principal stresses of 30, 25, and 10 MPa.



(b) 3D Mohr's circles for notional principal stresses of 30, 25, and 20 MPa.

Figure 8: Shown in (a) are 3D Mohr's circles, along with failure envelopes for both pre-existing fractures (Byerlee's Law – straight line envelope; coefficient of friction $\mu = 0.85$) and failure of intact rock (Griffith-Coulomb criterion – curved envelope). Similarly for (b), but with a different value of σ_3 resulting in a significantly further from failure situation. In both plots, the poles of the closest-to-failure planes are plotted as a red dot on the circumference of the outer (σ_1 - σ_3 plane) circle. The angles of poles to the closest-to-failure plane are identical in the two situations even though (b) is less risky than (a) because its red dot is further away from a failure envelope. Plotted using Rick Allmendinger's MohrPlotter software.

any risk estimates we make using this technique are *local only*. Local changes in risk nearby along worm segments should be qualitatively captured – assuming locally smooth changes in stress magnitudes. However, quantitatively comparing the seismic risk factor from one location to another location at some distance removed is not feasible because the unknown stress magnitudes also play a role not captured by orientation. Hence, segments identified as possessing the same ‘risk factor’ using this technique will unavoidably have different quantitative risks of seismicity. Another way of saying the same thing is that planes with poles nearly normal to the Byerlee’s Law envelope in both figures 8a and 8b, will be estimated to have the same risk using this technique, even though the situation in figure 8a is significantly closer to failure.

An alternative take on these drawbacks focusing more on *induced* seismicity in a geothermal field – and due originally to Katie Keranen and Terry Jordan – is as follows:

...It is unavoidable that the products of the Phase 1 analysis at the regional scale are of low reliability as indicators of the risk of induced seismicity for two reasons. First, some of the critical information used to predict rock failure is only available by use of long distance extrapolation of sparse data points. Second, the local details of rocks, fluids, and stresses are not merely down-scaled samples of the regional tendencies. Instead, local details produce field-specific conditions of stress and of failure even in the unlikely situation that the population of fault orientations happens to be alike in two different fields, and even if the production/injection fluid pressure design is equal in two different fields.

I turn the orientation-in-a-regional-stress-field sensitivity conclusion into a practical method for determining a quantitative index of seismic risk (and its error) via the the following procedures. Figure 9 shows the relevant geometry for estimating worm orientation and error at each worm point. The worm azimuth at node n_i is estimated as α_i^s , and the normal to that direction is the unit vector ν_i . The circular error variance of both α_i^s and ν_i is computed as follows. Briefly, if one half of the magnitude of the vector sum of unit vectors in the α_i and α_{i+1} directions is defined as \bar{R} , the circular variance (S_0) is defined as $1 - \bar{R}$ (Mardia, 1972, Eq. 2.3.5). That procedure establishes the local worm orientation, its normal unit vector (under an approximation of vertical dip), and provides an estimate of error for those quantities. Hence, via that procedure all required quantities are assigned to nodes rather than edges.

Next, I turn to estimating the orientation of the regional stress field from the World Stress Map (WSM) project (Heidbach et al., 2010). Figure 10 shows the locations of both the primary observations of σ_1 orientations (in red), and the result of a smoothing algorithm that plots the orientations on a 0.5 degree of arc grid (in black). Briefly, the WSM smoothing algorithm weights observed stress orientations by quality, then at each candidate point where an interpolation is to be estimated it collects all observations within a 1000 km radius. If there are more than 5 observations included, it continues, otherwise it stops, “censors” that point from the interpolation, and moves on to the next candidate interpolation point. If a candidate interpolation point is still valid, the algorithm additionally weights those observations by the inverse of the distance between an observation and the interpolation point (to a minimum allowed distance of 20 km), takes those exact quantities, and performs a Mardia (1972) style average direction and error estimate. If the standard deviation is less than 25° , the procedure stops and those average orientations and error estimates are used. If, however, the standard deviation is greater than 25° , the algorithm reduces the search radius by 100 km, and repeats itself down to a minimum search radius of 100 km. Thus, there are 2 separate ways in which a point can be “censored” from an interpolation: by having fewer than 5 observations within a search radius, or never finding a standard deviation of less than 25° for all search radii down to 100 km.

Heidbach et al. (2010) cite Mardia (1972) as the origination of the quality and inverse-distance weighted spatial interpolation algorithm they use. I believe that is inaccurate – because one of Mardia’s

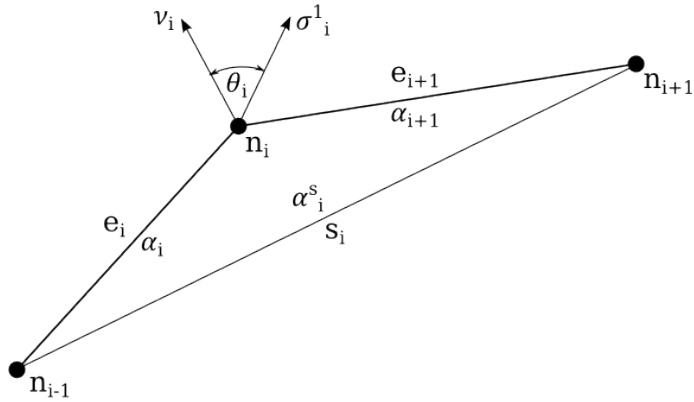


Figure 9: Map view of the relevant geometry of worm segments in a regional stress field. Displayed with labels n and e are nodes and edges (respectively) of the worm segments computed by the code described by Horowitz and Gaede (2014). All subscripts in this figure denote indices for consecutive elements of worm geometry components. The angles α_i denote the azimuthal (strike) angles for the corresponding segments e_i . The so-called secant line between nodes n_{i+1} and n_{i-1} is labeled s_i , and its azimuthal strike angle is labeled α_i^s . That azimuth α_i^s is assigned to node n_i , as is the orientation of a unit vector normal to s_i denoted here as ν_i . Also shown at node n_i is a unit vector in the direction of the maximum principal compressive stress σ_i^1 . The angle θ_i between ν_i and σ_i^1 is the primary risk index for point n_i under this approach. The analysis described here and in the text is repeated for all worm nodes except for those at the ends of individual worm segments – where angle variances are ill-defined. See the text for more discussion on why these quantities were selected.

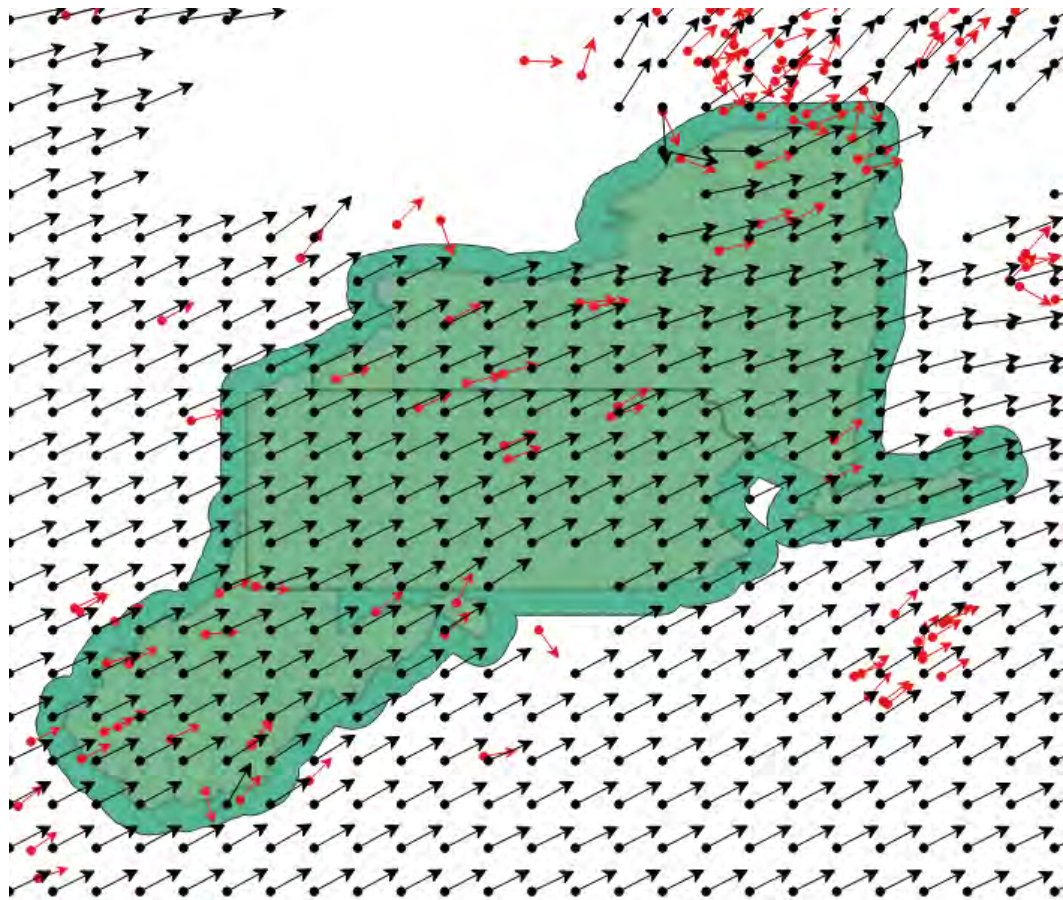


Figure 10: Principal compressive stress (σ_1) directions from the World Stress Map (WSM: Heidbach et al., 2010). Plotted in red are all regional primary observations from the WSM drawn from their quality ratings of A,B, or C. Plotted in black are their smoothed results. The smoothed directional field is evaluated on gridpoints of spacing 0.5 degrees of arc, using a censoring procedure also described in their paper. Gaps in the smoothed (black) field result from that decimation.

key concepts is to always work on the unit circle, which is violated by weighting the vector lengths as described above. Additionally, Mardia (1972) does not contain any mention of spatial interpolations – that I was able to find at least. Hence, for better or worse, I attribute that algorithm to Heidbach et al. (2010). I perform the algorithm just described to estimate the regional stress orientation and the associated angular error at the position of each worm point.

The final component of the orientation-in-stress-field risk estimation procedure is to calculate the angle between the σ_1 direction and the worm segment normal direction, and to compare that angle with the angular values most favored for failure in Figure 8. For the depth ranges appropriate for this work, the normal stresses are likely to be below 200 MPa and thus Byerlee's Law (Byerlee, 1978) claims a coefficient of friction of $\mu = 0.85$ as appropriate for a broad range of rock types. I adopt that value here.

For reference, converting that coefficient of friction value to the angular orientation of the normals ideally oriented for failure by Byerlee's law (the red lines in Figure 8) proceeds as follows. Denoting θ_B as the Mohr space angle between the Byerlee failure envelope and the σ_1 direction, examination of the relevant geometry implies that $\theta_B = \tan^{-1}(\mu) \approx 40.4^\circ$. Hence, the complement of θ_B is about 49.6° , and the supplement of that ($\approx 130.4^\circ$) is the Mohr-space angular deviation from the σ_1 direction of the highest-risk orientation. Accordingly, by the properties of the Mohr diagram construction, the critical angle in real-space is $\theta_{crit} \approx 130.4^\circ/2 = 65.2^\circ$. There is another critical orientation with the opposite sense (not plotted for visual simplicity) in Figure 8. The end result is that there are two critical angular deviations from the σ_1 direction, $\theta_{crit} = \pm 65.2^\circ$.

Thus, I establish angular risk categorization for this orientation-in-stress-field analysis by identifying arcs of orientations of \pm a specified angular range around both sides of both critical orientations. Figure 11 illustrates that technique for ranges increasing by 5° between risk categories.

Once again, the specific break values in risk categorization discussed here may not be the final categorization used in the overall risk-factor merging process. Please consult that separate memo for details.

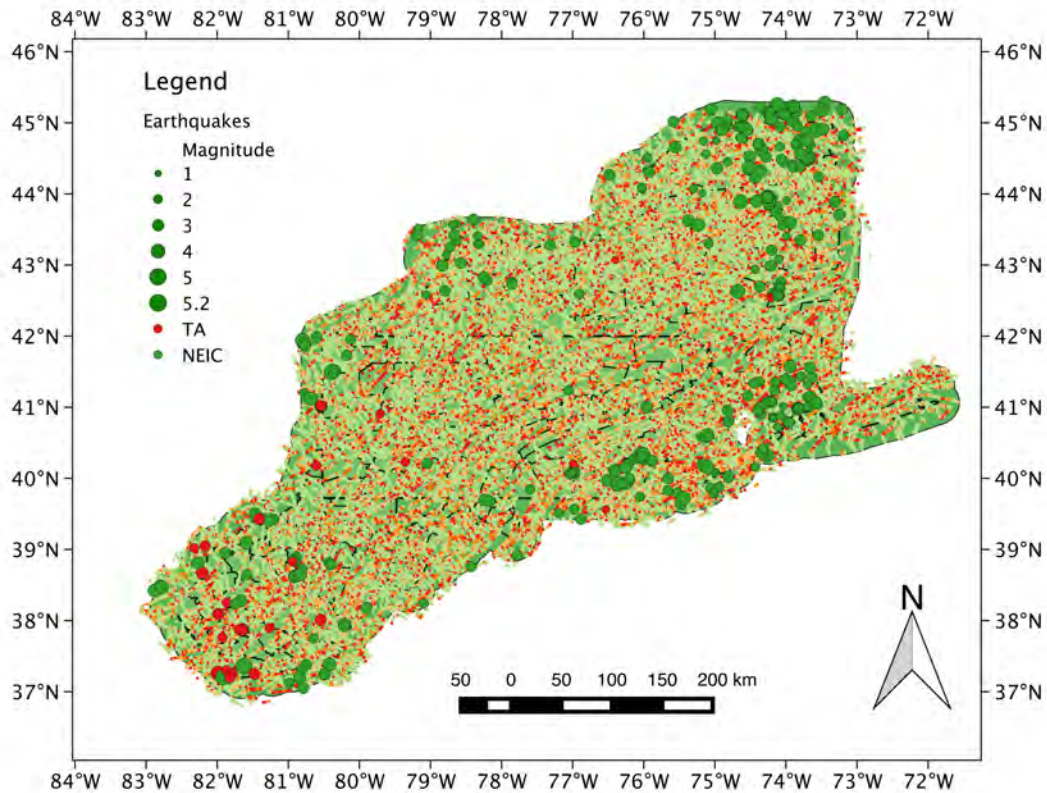


Figure 11: Worms combined from both figures 3 and 4 showing relative risks due to orientation in the estimated regional stress field. Points are colored red for the case where worm segments are within 5° on both sides of the θ_{crit} values; orange for an additional 5° arc outside the red range; yellow for an additional 5° arc outside the orange range; and light green for all positions on structures oriented outside the yellow range. In this classification, all points on structures identified by worms have slightly elevated (“moderately low”/light green) risks of seismicity simply due to the fact that they are on identified geological structures – which are heterogeneities that might localize stresses. Points not on worms are assigned to the “low-risk” category, and are not explicitly plotted in this figure. Also not shown in this figure are the error estimates calculated from the procedure discussed in the text – although both the relative orientation and error values were incorporated into the combined risk estimate phase of the GPFA-AB project.

References

- Astiz, L., Eakins, J. A., Martynov, V. G., Cox, T. A., Tytell, J., Reyes, J. C., Newman, R. L., Karasu, G. H., Mulder, T., White, M., Davis, G. A., Busby, R. W., Hafner, K., Meyer, J. C., and Vernon, F. L. (2014). The Array Network Facility Seismic Bulletin: Products and an Unbiased View of United States Seismicity. *Seismological Research Letters*, 85(3):576–593. Available from: <http://dx.doi.org/10.1785/0220130141>.
- Blakely, R. J. (1996). *Potential Theory in Gravity and Magnetic Applications*. Cambridge University Press, Cambridge. Available from: <http://dx.doi.org/10.1017/CBO9780511549816>.
- Boschetti, F., Hornby, P., and Horowitz, F. G. (2001). Wavelet Based Inversion of Gravity Data. *Exploration Geophysics*, 32,(1):48–55. Available from: <http://dx.doi.org/10.1071/EG01048>.
- Byerlee, J. (1978). Friction of rocks. *Pure and Applied Geophysics*, 116(4-5):615–626. Available from: <http://dx.doi.org/10.1007/bf00876528>.
- Childs, H., Brugger, E. S., Bonnell, K. S., Meredith, J. S., Miller, M., Whitlock, B. J., and Max, N. (2005). A Contract-Based system for large data visualization. In *Proceedings of IEEE Visualization 2005*, pages 190–198. Available from: <http://visit.llnl.gov/>.
- GoldCorp (2001). US\$575,000 Goldcorp Challenge Awards world's first 6 million ounce internet gold rush yields high grade results! Press Release. Available from: <http://www.infomine.com/index/pr/Pa065434.PDF>.
- Heidbach, O., Tingay, M., Barth, A., Reinecker, J., Kurfeß, D., and Müller, B. (2010). Global crustal stress pattern based on the World Stress Map database release 2008. *Tectonophysics*, 482(1-4):3–15. Available from: <http://dx.doi.org/10.1016/j.tecto.2009.07.023>.
- Hildenbrand, T. G., Briesacher, A., Flanagan, G., Hinze, W. J., Hittelman, A. M., Keller, G. R., Kucks, R. P., Plouff, D., Roest, W., Seeley, J., Smith, D. A., and Webring, M. (2002). *Rationale and Operational Plan to Upgrade the U.S. Gravity Database*. Number 02-463 in USGS Open File Report. Available from: <http://research.utep.edu/default.aspx?tabid=37229>.
- Hornby, P., Boschetti, F., and Horowitz, F. G. (1999). Analysis of potential field data in the wavelet domain. *Geophysical Journal International*, 137(1):175–196. Available from: <http://dx.doi.org/10.1046/j.1365-246x.1999.00788.x>.
- Hornby, P., Horowitz, F. G., and Boschetti, F. (2002). A physical interpretation of the Poisson wavelet transform of potential fields. In *Proceedings, EGS XXVII General Assembly, Munich*. European Geophysical

- Society, European Geophysical Society. Available from: <http://www.cosis.net/abstracts/EGS02/05568/EGS02-A-05568.pdf>.
- Horowitz, F. G. and Gaede, O. (2014). BSDWormer; an open source implementation of a Poisson wavelet multiscale analysis for potential fields. In *2014 Fall Meeting*, number T43C-4743. American Geophysical Union. Available from: <https://agu.confex.com/agu/fm14/meetingapp.cgi\#Paper/26847>.
- Jessell, M. (2001). An atlas of structural geophysics II. *Journal of the Virtual Explorer*, 05. Available from: <http://virtualexplorer.com.au/journal/2001/05>.
- Malinconico, L. and Moore, M. (2013). Provisional Bouguer gravity map of Pennsylvania. AASG Geothermal Data Repository. Available from: <http://repository.stategeothermaldata.org/repository/resource/a748ce233a25e3e0dd00c9865d0af3e5/>.
- Mallat, S. and Zhong, S. (1992). Characterization of signals from multiscale edges. *Pattern Analysis and Machine Intelligence, IEEE Transactions on*, 14(7):710–732. Available from: <http://dx.doi.org/10.1109/34.142909>.
- Mardia, K. V. (1972). *Statistics of directional data*. Academic Press. Available from: <http://www.worldcat.org/isbn/9780124711501>.
- Moreau, F., Gibert, D., Holschneider, M., and Saracco, G. (1997). Wavelet Analysis of Potential Fields. *Inverse Problems*, 13:165–178. Available from: <http://dx.doi.org/10.1088/0266-5611/13/1/013>.
- Navarrete, L. (2015). Crustal structure of NE N America from constrained models of potential field data. Master's thesis, University of Rochester.
- Ravat, D., Finn, C., Hill, P., Kucks, R., Phillips, J., Blakely, R., Bouligand, C., Sabaka, T., Elshayat, A., Aref, A., and Elawadi, E. (2009). *A Preliminary, Full Spectrum, Magnetic Anomaly Grid of the United States with Improved Long Wavelengths for Studying Continental Dynamics: A Website for Distribution of Data*. Number Open-File Report 20091258. USGS. Available from: <http://pubs.usgs.gov/of/2009/1258/>.
- Reid, A. B., Allsop, J. M., Granser, H., Millett, A. J., and Somerton, I. W. (1990). Magnetic interpretation in three dimensions using Euler deconvolution. *GEOPHYSICS*, 55(1):80–91. Available from: <http://dx.doi.org/10.1190/1.1442774>.
- RungePincockMinarco (2015). Data Integration and 3d Visualisation Software - FRACIS. webpage retrieved 23 June 2015. Available from: <http://www.rpmglobal.com/mining-software/data-visualisation-fracsis>.
- Schroeder, W., Martin, K., and Lorensen, B. (2004). *The Visualization Toolkit*. Kitware Inc., third edition. Available from: <http://www.worldcat.org/isbn/1930934122>.

Acknowledgements

I thank David Castillo, Katie Keranen, Rick Allmendinger, and Geoff Abers for suggesting that I use orientation in a regional stress field as a method of determining the risk of seismicity on a structure. I thank Ronald McDowell and others from the West Virginian Geological and Economic Survey for calling to our attention that we had mine blasts contaminating our TA seismic catalog information, and I thank Beatrice Magnani of SMU for suggesting the statistically viable decontamination method of removing daylight events. I also thank Jerry Stedinger for keeping me honest about determining quantitative errors in my risk estimates.

Memo 14: Seismic Risk Map Creation Methods in GPFA-AB

To: Appalachian Basin GPFA
From: Jared Smith and Franklin Horowitz
Date: Original from September 15, 2015. Updated August 11, 2016
Subject: Conversion of Seismic Risk Data to Risk Maps

Applicability: This memo presents detailed methodology that was used to convert the seismic risk data into two seismic risk maps. These data are the distance to the nearest earthquake, and the angular deviation from the two critical orientations for failure under Byerlee's Law for pre-existing fractures.

Earthquake Based Risk Map

The goal of this analysis is to arrive at a map of the risk of an earthquake occurring based on nearby earthquakes and the gravity and magnetic potential field edges ("worms"). Refer to Memo 13 of this project by Horowitz for a detailed description of the worms. The worms trace contrasts in subsurface density and magnetic content, respectively, and may be indicative of faults at depth. Earthquakes would be more likely to occur on a fault than away from a fault. The distance to the nearest earthquake is described first, followed by a description of how the worms were used to identify higher risk areas near previous earthquakes.

Note: each risk map in this project is placed on the same standardized 1 km² raster grid. This is sometimes called a fishnet. The grid cell centers are stored as a points file (*Fishnet2_label.shp*).

Distance to the Nearest Earthquake

The distance from the grid cell centers to the nearest earthquake was determined in several steps. Voronoi tessellation was used on the epicenters in the earthquake database. This resulted in one Voronoi polygon per epicenter. The earthquake information was joined to the attribute table of each polygon. The epicenter nearest to all grid cell centers within a Voronoi polygon is the nearest epicenter for the grid cells located in that polygon.

A spatial join was used to add the earthquake information for each polygon to the attribute table of the grid cell centers. The resulting attribute table contained the location (lat., long.) of the grid centers and the location (lat., long.) of the earthquake nearest to each grid cell center. The distance from a grid cell center to the nearest earthquake was determined using a simple spatial Postgres query. Any tool capable of calculating ellipsoidal distances using (lat., long.) or Euclidian distances for (easting, northing) would suffice. The grid cell centers were converted into a raster of the distance to the nearest earthquake for all locations in the basin using the Points to Raster tool in ArcGIS.

Worm Proximity to Earthquakes

The distance to the nearest earthquake information was combined with the gravity and magnetic potential field analyses to create the earthquake-based seismic risk factor map. First, the gravity and magnetic potential field edge points ("worm" points) that were within 20 km of an earthquake epicenter were selected. These points were buffered by 2 km. The buffers for gravity

and magnetic worms were dissolved independently, resulting in polygons for the gravity and magnetic buffered worms. A buffer around worm points is used because of potential hydrologic connectivity of the subsurface that may allow for fluid migration to the worm point within some distance of the point. The use of 2 km as the buffer is arbitrary. More detailed knowledge about the subsurface hydrology could better inform the buffer that would be most beneficial to limit the migration of fluids to activate faults at the location of each worm point.

After buffering, the raster of distance to the nearest earthquake was clipped to the buffered worm polygons. This resulted in two clipped rasters (one for gravity worms and one for magnetic worms). These clipped rasters represent the distance to the nearest earthquake for all grid points within 2 km of a worm point that is within 20 km of an earthquake. The ArcGIS Extract Multi Values to Points tool was used to add the clipped raster information to the grid cell centers. This information was assigned the field names GravDist and MagDist, representing the distance to the nearest earthquake for gravity worms and magnetic worms, respectively.

The GravDist and MagDist fields cannot be used directly to determine the most risky value (smallest distance to an earthquake) for each grid cell center. The gravity and magnetic worm points did not cover the same areas, so some gravity and magnetic points were co-located (within the same 1 km² pixel) and others were not co-located. Points that were co-located have the same value for GravDist and MagDist, so the distance value for both is the risk value. The risk distance field is called the RiskDist. In areas without co-located gravity and magnetic worms, one of GravDist or MagDist will be the RiskDist. The other field will have the value that is assigned to a grid cell center that does not have nearby gravity or magnetic worms within the buffered state boundaries (see Processing Notes section below). This value was arbitrarily selected as 1,234,567 m. This value is greater than the distance to any earthquake. So, the minimum distance to an earthquake for each grid cell was determined using a query for the minimum of the GravDist and MagDist. The result of the query was written to the RiskDist field.

The standard deviation (see *Uncertainty* section below) corresponding to the minimum distance (GravDist or MagDist) was placed in a new field called RiskVar. For collocated points (GravDist = MagDist), the smaller standard deviation was selected. Finally, the RiskDist and RiskVar grid points were converted into a raster (Point to Raster tool in ArcGIS) to create the earthquake-based seismic risk factor map and uncertainty map.

Uncertainty

Simply put, the uncertainty in the distance to the nearest earthquake is the sum of the uncertainty in the earthquake location and the potential field point location (one of magnetic or gravity). These measurements are independent. Uncertainties in this case are taken as standard deviations of distance, so the overall uncertainty of earthquake and worm point positioning error is

$$RiskVar = \begin{cases} \sqrt{s_{EQ}^2 + GravVar^2}, & GravDist < MagDist \\ \sqrt{s_{EQ}^2 + MagVar^2}, & MagDist < GravDist \end{cases}$$

where *RiskVar* is the standard deviation of the earthquake-based risk, s_{EQ} is the standard deviation of the earthquake position, *GravVar* is the standard deviation of the gravity worm position, and *MagVar* is the standard deviation of the magnetic worm position.

The uncertainty in earthquake locations is not available for all earthquakes in the database. As a result, a conservative estimate of the uncertainty is selected as 2.5 km in any lateral direction from the epicenter, regardless of the magnitude of the earthquake. Earthquakes with greater magnitudes likely have smaller uncertainty in their epicenter location.

The uncertainty in the potential field point locations is difficult to quantify as a result of the many processing steps involved. Lacking the time to quantify the uncertainty in the potential field points via a Monte Carlo analysis, 20% of the distance between potential field points is assumed as the uncertainty for all points. Therefore, gravity points have an assumed uncertainty of 500 m (2500 m spacing between points), and magnetic points have an assumed uncertainty of 250 m (1250 m between points).

The uncertainty values in the earthquake locations and worm point locations are treated as standard deviations. Therefore, the RiskDist standard deviation, RiskVar, under these assumptions is 2550 m for gravity points and 2515 m for magnetic points. For both gravity and magnetic points, the standard deviation corresponds to 3 pixels at the resolution of the risk factor maps.

Stress Field Based Risk Map

The goal of this analysis is to arrive at a map of the risk of an earthquake occurring based on the orientation of the gravity and magnetic worm segments relative to the critical orientations for failure of pre-existing fractures in the region (Byerlee's Law; see Memo 13 of this project by Horowitz for a description of how the critical orientations were found).

The gravity and magnetic worm points calculated by Horowitz contain information about the angle normal to the principal compressive stress (values ranging from 0° to 180°), and the uncertainty (standard deviation) in that angle. The critical failure orientations are located at 65.2° and 114.8° on [0°, 180°] relative to σ_1 . The angles of interest for calculating risk are the angles between the normal angle and each of the critical orientations. These are referred to as the GravAng and MagAng.

The GravAng and MagAng fields are calculated as the minimum of the absolute value of the angle needed to arrive at each of the critical orientations, in degrees. The minimum is selected because this represents the greatest risk (closer to one of the critical angles). Note that the following equation is only valid if the normal angle is on [0°, 180°]. If the normal angle ranges from 0° to 360°, then 180° may be subtracted from all angles greater than 180° to convert to [0°, 180°].

$$\text{GravAng} = \min(\text{abs}[\text{normal_angle} - 65.2^\circ], \quad \text{abs}[\text{normal_angle} - 114.8^\circ])$$

Next, the gravity and magnetic worm points were buffered by 2 km, for the reasons described above. These buffers were dissolved independently, and converted into 4 rasters: angle for gravity (GravAng), uncertainty for gravity (GravVar), angle for magnetic (MagAng), and uncertainty for magnetic (MagVar). The values in each of these rasters were added to the standardized grid cell centers using the Extract Multi Values to Points tool in ArcGIS.

For each grid cell center, the minimum of the GravAng and MagAng was assigned as the RiskAng. The assigned uncertainty (standard deviation) was the uncertainty corresponding to the minimum of GravAng and MagAng (either GravVar or MagVar) and was called the RiskVar. Note that the RiskVar in this case assumes that errors in the positioning of the worm points are captured in the error of the angle, because the same positioning error is assumed for all points along a worm segment (see above discussion for earthquake-based uncertainty). Therefore, positioning errors in the worms are assumed to be implicitly captured. A Monte Carlo analysis that includes positioning errors could be used to verify this assumption.

Because many points overlap a single grid cell center, a raster plotting priority field called Weight was added to the worm data. This field was equal to $65.2^\circ - \text{RiskAng}$, where 65.2° is the maximum number of degrees that an angle could be from one of the critical angles on [0°, 180°]. This field is used to determine plotting preference when converting this data into a raster dataset – higher values have higher preference. This ensures that a RiskAng value of 0° has the highest plotting preference, and therefore will be selected as the raster value over larger RiskAng values.

Finally, the stress field based seismic risk factor maps were created by converting the RiskAng and RiskVar grid cell centers into rasters using Point to Raster conversion in ArcGIS.

A Note on Uncertainty

The standard deviation in some angles is large enough that the nearest critical failure orientation is not the one used to calculate the RiskAng. For example, if an angle has a mean of 20° and a standard deviation of 40°, then it is possible that the true angle is closer to 114.8° than to 65.2° on [0°, 180°]. This is accounted for in the Monte Carlo analysis that is used to create the scaled risk factor maps, and the uncertainty in the scaled risk factor maps. The R code used to do this is in “make_interp_tables.R”. An excerpt of this code is provided below. In this code, “rand” is 10⁵ Monte Carlo replicates. The first while loop converts all negative angles to positive angles by adding 360 degrees. The second while loop converts all angles to [0°, 180°]. Variables a1 and a2 are the angles to each of the two critical angles. The final value assigned to rand is the minimum of a1 and a2 (most risky angle).

```
# Find the randomly generated values that are negative and add 360 degrees to them until they are all positive.
while (length(rand[which(rand < 0)]) != 0){
  rand[which(rand < 0)] = rand[which(rand < 0)] + 360
}
# Now convert all values to [0,180]
while (length(rand[which(rand > 180)]) != 0){
  rand[which(rand > 180)] = rand[which(rand > 180)] - 180
}
# Now take all angles and convert them to a risk angle
a1 = abs(rand - critical_ang1)
a2 = abs(rand - critical_ang2)
# Bind them
b = rbind(a1, a2)
# Assign the minimum value (most risky) to those points
rand = apply(b, 2, min)
```

Memo 17 in this project describes how the scaled risk factor maps and their scaled uncertainty were created from each individual unscaled risk factor.

Processing Notes:

Before each seismic risk factor map was converted to a final map, information about whether or not a standardized grid cell center was located within the 50 km buffered states region was added to the point features (binary variable, in [1] or out [0] of the region). The grid cell centers that are not located within the state boundaries are assigned a value of -9999 to indicate that these areas were not assessed for seismic risk. The grid points within the state boundaries that did not intersect buffered worm points are assigned a value of 100° for stress-based risk maps and a value of 1,234,567 m for earthquake-based risk maps. These areas have low seismic risk. These arbitrary high values were selected because they are numbers greater than the maximum RiskAng and RiskDist, respectively, and are easily identified by data processing programs. In contrast, 1,000,000 m was not used because it is converted to 1E+6 in some programs, which is further converted to text in some programs. Text fields are not numbers, and cannot be displayed on rasters.

Memo 15: Utilization Analysis in GPFA-AB

Memo for Utilization Assessment

Original from October 2015. Updated October 2016

Projected included members from Cornell University, Southern Methodist University, and West Virginia University.

Memo Written by: Maria Richards SMU, mrichard@smu.edu; Revised 2016 by Calvin Whealton and Teresa Jordan

Project Effort Overseen by: Brian Anderson WVU, Brian.Anderson@mail.wvu.edu and Jeff Tester Cornell University, (jwt54@cornell.edu)

Work completed by the following students: Xiaoning He (WVU), Zachary Frone (SMU), Kelydra Welker (WVU), Calvin Whealton (CU)

DISCLAIMER

The information, data, or work presented herein was funded in part by an agency of the United States Government. Neither the United States Government nor any agency thereof, nor any of their employees, makes any warranty, express or implied, or assumes any legal liability or responsibility for the accuracy, completeness, or usefulness of any information, apparatus, product, or process disclosed, or represents that its use would not infringe privately owned rights. Reference herein to any specific commercial product, process, or service by trade name, trademark, manufacturer, or otherwise does not necessarily constitute or imply its endorsement, recommendation, or favoring by the United States Government or any agency thereof. The views and opinions of authors expressed herein do not necessarily state or reflect those of the United States Government or any agency thereof.

The Utilization effort for the Geothermal Play Fairway Analysis of the Appalachian Basin (GPFA-AB) included two broad types of data: 1) residential – community ‘Places’ and 2) site specific users with high heating demands such as universities, industrial users, government facilities, etc. to be considered as part of Phase 2. Below is a description of the data collected, and the programs used. For results and a discussion of the effort, see the Final Report for Phase 1 of the Low Temperature Geothermal Play Fairway Analysis for the Appalachian Basin, DOE Contract Award Number: DE-EE0006726.

The process for the GPFA-AB was primarily based on the previous research by students at Cornell University and West Virginia University. Below are main steps from this project and the last section includes the Chapter 3 details submitted by Tim Reber (2013) for his MS degree with every parameter described.

Steps in Determining the Surface Levelized Cost of Heat

The foundation source code used for the utilization risk assessment is the program GEOPHIRES, (GEOthermal Energy for Production of Electricity and Heat Economically Simulated). The software uses key data as input to calculate Levelized Cost of Heat (LCOH). Because we have characterized the subsurface as part of other tasks (thermal resources and natural reservoir quality), we modified GEOPHIRES to only focus on those remaining elements, which includes demand for heat as calculated

from population and climate data, and the surface costs associated with delivering that heat to those in demand. Thus, in our implementation, the final output is a Surface Levelized Cost of Heat (SLCOH). The SLCOH includes the surface piping, heat exchange equipment (residential and/or commercial), operations, upfront capital cost, and maintenance costs over the lifetime of a 30 year project. A MATLAB¹ program serves as an interface between the Microsoft Excel files of collected input data and the GEOPHIRES program. The MATLAB code and Microsoft Excel files are included with the resulting data as part of the Catalog submission to the National Geothermal Data System (NGDS).

1. The U.S. Census Bureau maintains a database of information that includes state, county, and county subdivision, under the broader term ‘Place.’ A Place is used to identify all individual cities, towns, villages, boroughs, universities, and other Census-Designated Places (CDP’s) defined as “settled concentrations of population that are identifiable by name but are not legally incorporated” (Census Bureau, 2012). The population and scope of a single Place may vary from the whole of New York City proper, with a population of over 8,000,000, to the smallest villages with populations as low as 10. In the New York, Pennsylvania, and West Virginia area we are using the 2010 Census data collection that includes 3,355 Places. These were downloaded via the FactFinder website (<http://factfinder.census.gov>).
2. Starting from the 3,355 places in New York, Pennsylvania, and West Virginia, using ESRI ArcGIS, the broader Place data were linked to their county and county subdivision. In order to complete this task, shapefiles of the Census Places and county subdivisions were loaded into ArcGIS. By using a spatial join and having the program find the Places within the county subdivision, this resulted in joining the attributes tables of the two files, allowing for the information for Places to have corresponding county subdivision data. Finally, all sites were checked and any places without a successful join had data manually added. This process was repeated to relate places with county information.
3. The place list was next limited to only those within this project’s Appalachian Basin outline. We used the Golden Software program Mapviewer and ArcGIS for a comparison to confirm accuracy of locations within the project boundary. This reduced the number of possible Places for the project to 1,697.
4. To represent cooperation and coordination among smaller U.S. Census Places, which are generally townships or villages, we merged small places with their neighbors. Neighbors were determined by buffering around all of the U.S. Census Places polygons a distance of 50 m. Buffered polygons that intersected were neighbors. The small buffer was used because many of the places were quite close, but did not exactly share a border and this made neighbors for places that were within 100 m of each other. The U.S Census Places were sorted by population. Starting with the lowest population Place, it was checked to

¹ <http://www.mathworks.com/products/matlab/>

see if it had already been merged. If it had been merged, then no further action was taken for that place and the analysis moved to the next smallest Place. If the Place had not been merged, then we checked for neighbors. If there were neighbors, the Place was merged with all of its neighboring places. The analysis began again. If the Place had no neighbors, then the analysis continued to the next place. The merging stopped when all places below 10,000 population had already been merged or had no neighbors. Note that a Place was not merged multiple times. Below, these are referred to as “Cooperating Places” or, when the context is generic, simply as “places.”

5. For this Play Fairway Analysis project, a minimum population threshold of 4,000 residents per Place or Cooperating Place was applied for all three states, to focus on those communities with a sufficient number of users to justify the initial capital investment associated with a district heating system. There were 1,442 Places with populations of less than 4,000, leaving the final number of Places for the SLCOH analysis to be 255. Thereafter, in order to have those Places and Cooperating Places with fewer than 4,000 people appear as red (unfavorable) on the final maps, they were assigned the same arbitrarily high SLCOH of \$100/MMBTU. The actual input data associated with these places would lead to a different SLCOH and can still be calculated for future analyses as appropriate. The population threshold can be set as low as 1,500 residents per Place, and in doing so, makes the majority of the Places meet the criteria of good enough to consider. Although a positive outcome, we determined the 4,000 resident level for population of increased value in focusing the attention to sites most likely to be first users of this regionally new energy concept.
6. The next parameter is the building density and heating demand per building (i.e. detached single-family, attached single-family, 2 unit buildings, 3-4 unit buildings, 5-9 unit buildings, 10-19 unit buildings, 20-49 unit buildings, and 50+ unit buildings). These detailed data are included within the Census Factfinder under “American Community Survey” using the 2010 5-year estimates and code B25024, representing the number and type of housing units per residential building category. The Energy Information Agency (EIA) performs a Residential Energy Consumption Survey (2009) that we used to determine average square footage of each designated unit and related heating load on a Census region basis.
7. Within many Places are commercial buildings, which can be put into 12 categories: 1) Accommodation, 2) Food, & Other Services, 3) Administrative and Waste Management and Remediation Services, 4) Arts, Entertainment, and Recreation, 5) Educational Services, 6) Health Care & Social Assistance, 7) Information Geographic Area Series, 7) Manufacturing, 8) Other Services, 9) Professional Scientific & Technical Services, 10) Real Estate & Rental and Leasing, 11) Retail Trade, and 12) Wholesale Trade.

- a. In order to determine the heating loads for commercial sites within our Place dataset, we combined the energy consumption for building types, the square footage of a building, and the type of commercial application based on the 12 categories above. Three datasets were used: the EIA manufacturing *energy consumption* data (<http://www.eia.gov/consumption/manufacturing/>), the EIA's 2006 report of Commercial Buildings Energy Consumption Survey (CBECS) for the *floor space*, and the US Factfinder 2007 'Economic Data' for categories.
 - b. From these files, the number of establishments and number of employees were collected for each "economic place". Unfortunately, the term "economic place" did not equate to that of the census definition of Place. The "economic place" can be related to the census classification of "county subdivision", which we did have linked to each Place. Following the methodology of (Reber, 2013) and Tester et al. (2015), in the instance where a single "county subdivision" (i.e. "economic place") contained multiple Places (typically around metropolitan areas) the data on commercial establishments for that county subdivision was divided amongst the Places within that county subdivision based on the relative population of each Place. In addition, due to the potentially identifiable nature of the reported economic data, some employment sizes were represented by a letter which stood for a range of values (ex. "A" meant an establishment had less than 20 employees, "B" meant an establishment may have between 20 to 99 employees, "C" means 100 to 249 employees, etc.). For these sites, the average of the range rounded up to the next integer was used for the model (ex. "A" would have 10 employees, "B" would have 60 employees, "C" would have 175 employees, etc.). This allowed for the MATLAB/GEOPHIRES model to have a numerical value to perform the calculations.
8. Another dataset included was the location of roads (Road shapefiles from the TIGER dataset). The total length of roads within each Place was used as a method to estimate the required piping length required to service a given location (Reber, 2013) and Tester et al. (2015). Based on Reber's conclusions, the GEOPHIRES program uses 75% road coverage to provide adequate piping density required to reach all buildings for geothermal district heating system.
 9. The MATLAB script estimated the cost of a system for a lifetime of thirty years. The program uses a fixed annual charge rate (FACR), which allows the user to specify several factors, including discount rates. As reported by Shaalan (2001), this annual fixed-charge rate "represents the average or 'levelized' annual carrying charges including interest or return on the installed capital, depreciation or return of the capital, tax expense, and insurance expense associated with the installation of a particular generating unit"

(Shalan, 2001). A FACR of 6% was used for this Play Fairway Analysis effort. According to the U.S. Department of Commerce it calculated an effective discount rate of 3% in 2011 for Federal and Public energy projects. Therefore 1% was also added to this value, resulting in a discount rate of 4% applied to SLCOH.

10. The GEOPHIRES result output of SLCOH is a spreadsheet (.csv format). The output was grouped by state and then sorted based on the population size and the resulting SLCOH in the units of dollars per one million BTU (British Thermal Unit). \$/MMBTU. For all Places with a population of less than 4000 the SLCOH was assigned an arbitrary but high value of \$100/MMBTU. This allows us to continue to keep smaller communities in the workflow as we get ready for Phase 2. We will be able to improve our cost estimates for the entire Place list, since the GEOPHIRES and MATLAB programs allow updates for a few or many sites with the same amount of effort.

For the resulting 255 Places assessed, the best case (least expensive SLCOH) is 7 \$/MMBTU and the highest (most expensive SLCOH) is 65 \$/MMBTU. The Places were differentiated into three thresholds with the best case scenario for the SLCOH between \$7 and \$13.5, good between \$13.5 and \$16, and low or unlikely potential as \$16 to \$25 SLCOH. Among the 255 Places, Table 1 shows the distribution of the 236 Places whose SLCOH is less than or equal to \$25. In addition, there were 1,449 places assigned an SLCOH of \$100 because of low population (< 4000 people).

Table 1: Distribution of 255 Census Places and Cooperating Places over 4,000 in population within the Appalachian Basin for NY, PA, and WV based on a three color ranking of the calculated Surface Levelized Cost of Heat (SLCOH).

State	Best Case (Green) \$5 – \$13.5/ MMBTU SLCOH	Good (Yellow) \$13.5 - \$16/ MMBTU SLCOH	Unlikely (Red) \$16 - \$25/ MMBTU SLCOH
New York	30	27	30
Pennsylvania	37	52	27
West Virginia	21	10	2

A second set of values were assigned for the five-threshold risk assessment. Here the values were \$5 to \$12 (green - best), \$12 to \$13.5 (greenish yellow), \$13.5 to \$16 (yellow), \$16 to \$20 (orange) and \$20+ (red - worst). The level of detail in this Phase 1 project does not provide enough site knowledge, even at the Place level, to assign increased levels of significance in the dollar amounts for the SLCOH. These were developed for the consistency of the combined risk task input files (see Catalog for the Combining Risk Factors Memo).

Error estimates for the Utilization risk factor were not calculated. Rather for the level of detail of Phase 1, the entire area is given a uniform uncertainty of approximately 5% based on changes in population and cost.

Steps for Inclusion of Site Specific Industrial Sites

In addition to the US Census 'Place' areas, this project researched low-temperature direct use geothermal energy applications for numerous industries, including aquaculture, green houses, and food processing such as dehydration and dairy processing (Lienau, et al., 1994). For the Appalachian Basin region and the anticipated temperatures at depths shallower than 3 km, potential users of the geothermal heat occur in the following industry categories: paper mills, wood drying kilns, dairy processing (includes yogurt and milk pasteurization products), college and university campuses, and select military locations. Typical temperature ranges for these applications are listed in Table 2.

Table 2: Site-Specific industries of interest and required temperature ranges.

Industry	Temperature Range
Dairy	Butter/Yogurt production 80 – 90 °C Traditional pasteurization 72 – 75 °C
Wood Drying	43 – 82 °C
Paper/Pulp Mills	66 - 150 °C
University/College Campus	100 - 150 °C
Military Bases/Stations	100 - 150 °C

Each industrial site was located using a Google Map search for each category, except for the locations of the dairy processing sites found on the Dairy Plants USA website. All of these potential industrial users have a component of their process(es), which could benefit from incorporating a geothermal element into their system, either by preheating or reducing electrically heated steps.

References

- DOE Federal Energy Regulatory Commission. (2013, October 17). Winter 2013-14 Energy Market Assessment Report to the Commission, Item No. A-5. Retrieved from <http://www.ferc.gov/CalendarFiles/20131017101835-2013-14-WinterReport.pdf>.
- Lienau, P., Lund, J., Rafferty, K., & Culver, G. (1994). Reference Book on Geothermal Direct Use (Vol. August). Klamath Falls, Oregon: GEO-Heat Center, Oregon Institute of Technology. Retrieved from <http://www.oit.edu/docs/default-source/geoheat-center-documents/publications/direct-use/tp82.pdf?sfvrsn=2>.
- Reber, T. J. (2013). Evaluating Opportunities for Enhanced Geothermal System-Based District Heating In New York and Pennsylvania. Cornell University. Ithaca, NY: Cornell University. Retrieved from <http://hdl.handle.net/1813/34090> (restricted until 2018).
- Reber, T. J., Beckers, K. F., & Tester, J. W. (2014). The transformative potential of geothermal heating in the U.S. Energy market: a regional study of New York and Pennsylvania. *Energy Policy*, Vol. 70, 30-44.
- Shalan, H. E. (2001). Generation of Electric Power. In *Handbook of Electric Power Calculations* (pp. 8.1-8.38). Retrieved from http://castlelab.princeton.edu/EnergyResources/GenerElectPower__Shalaan.pdf.
- Social Security Administration. (2015). Cost-Of-Living Adjustment, Prior Cost-of-Living Adjustments. Retrieved from Official Social Security Website: <http://www.ssa.gov/news/cola/facts>.
- Tester, J., Reber, T., Beckers, K., Lukawski, M., Camp, E., Aguirre, G. A., . . . Horowitz, F. (2015). Integrating Geothermal Energy Use into Re-building American Infrastructure. *Proceedings World Geothermal Congress*. Melbourne, Australia: International Geothermal Association. Retrieved from <http://www.geothermal-energy.org/pdf/IGAstandard/WGC/2015/38000.pdf?>.

Detailed documentation of the MATLAB implementation of this model is available from:

Reber, T. J. (2013). Evaluating Opportunities for Enhanced Geothermal System-Based District Heating in New York and Pennsylvania. Cornell University. Ithaca, NY: Cornell University. Retrieved from <http://hdl.handle.net/1813/34090> (restricted until 2018).

Memo 16: Risk Analysis in GPFA-AB

To: Appalachian Basin Geothermal Play Fairway Analysis Group

From: Calvin Whealton, Jerry Stedinger, Frank Horowitz, and Jared Smith

Date: September 17, 2015 (Revised October 2016 by T.E. Jordan)

Subject: Risk Analysis and Required Risk Factor Descriptions

In preparation for the analysis of the combined risk factors, it is wise to resolve what information will be needed to construct the final 4 risk-factor maps and the resultant summaries, and to conduct appropriate sensitivity and uncertainty analyses. Having this discussion now will allow more time for implementation later, and for those generating critical results to include in their analysis the ability to generate the needed information.

This memo focuses on required map data and formats, including methodologies for uncertainty analysis and sensitivity analysis of the final risk matrix. Methods of scaling each risk factor to a 3-point or 5-point scale are also described. Two critical issues are addressed: (i) completing the risk-matrix tasks as they are described in the SOPO, and (ii) being creative and innovative in methodologies for the analysis of the risk matrix information, and visualization of the results.

We emphasize that, when possible, map colors for 3-color or 5-color maps should be related to the *actual acceptability* of a location measured on that risk index at the scale of the analysis. Using this point of view, they are not relative metrics providing just a comparison to other locations or projects, but absolute evaluations of project acceptability. If color ranking represents the scale of project acceptability, then it is reasonable, for example, to consider the minimum value across the four risk factors as a criterion for project acceptability. Other options for representing the combined risk maps are presented below.

We claim that it is critical for groups who are contributing to a combined risk product submit correctly formatted component maps to 1) construct the risk matrices, 2) efficiently complete the effort which requires analysis of alternative projects, and 3) conduct uncertainty analysis and visualization of results.

List of Appendices:

1: Methods for creating the standardized raster grid for all risk factors, and converting vectors to the standardized raster grid.

Map Data and Formats

This section outlines the required data for each risk factor map. There should be two or three raster maps submitted for each risk factor:

- 1) the value of a continuous risk variable (one raster), and
- 2) the uncertainty, described by either the standard deviation or coefficient of variation (1 raster), or 5-95% CI (2 rasters), of the estimated risk value at each point.

The raster should include a value for “no information,” which is equivalent to stating that we do not have data to estimate the risk. The selected value for “no information” is “-9999” for this project (a numerical value is used because raster formatting does not allow text).

“No information” should be distinguished from areas that have information, but are not suitable for a geothermal project. One may wish to consider development in regions for which no data exists; however we would not consider development where a risk factor has an infeasible value. When mapping, no information (-9999) may be represented as white pixels for individual risk factors. These pixels would remain white when combining risk factors into a summary statistic. For example, if no information about reservoirs exists, but data regarding seismic, thermal, and utilization risk factors are available, then a summary statistic considering all risk factors would receive a white pixel; whereas a map that considers only seismic, thermal, and utilization risk factors would be colored according to the selected color scheme.

Groups must also submit *thresholds* for a 3-color map (2 thresholds) or 5-color map (4 thresholds). When possible, threshold values should be based on previous studies of what is considered high, medium, and low risk (or performance levels) for each risk factor. Level 3 for a 3-color map and level 5 for a 5-color map are considered to be excellent conditions. Level 1 in both color schemes represents unsatisfactory levels, indicating a project would not be successful, regardless of the values of the other risk factors.

Finally, for the purpose of scaling or transforming the continuous risk variables into composite or summary values, we request for each risk factor a *maximum* and a *minimum* value be specified. We do not anticipate that these are the maximum and minimum values within this dataset across the map, but rather the maximum and minimum values that might be generated (or values we wish to employ for scaling to a 3-point or 5-point scale). The maximum and minimum values may also be viewed as extreme thresholds. For example, all values below the minimum useful temperature of 50 °C (scaled to a value of 0.0) also receive a scaled value of 0.0 because the temperature below 50 °C is not useful for this project’s consideration.

Required deliverables:

1. Raster map* of the continuous risk factor (in original units) on the grid developed for the project (Raster grid name: GridNAD.tif).
 2. Raster map(s)* representing the uncertainty of the continuous risk factor.
 3. A set or sets of 2-thresholds for defining a 3-color map, including a third value for no information.
 4. A set or sets of 4-thresholds for defining a 5-color map, including a fifth value for no information.
 5. Maximum and minimum values for each risk factor.
- * See Appendix 1 for a description of how the project grid was developed, and how vector files (e.g. reservoirs) were converted into rasters.

It may be unclear how to adequately represent one or more of the risk factors as a single raster set (risk metric and uncertainty rasters). In this case, we recommend that the risk factor be submitted in a manner that captures the complexity. The values of the ranking thresholds do not have to change between submitted sets of rasters. For example, a single depth at which the thermal risk factor should be represented is unclear because many depths could be selected and justified as reasonable (maximum economical drilling depth, minimum depth to reach the minimum use temperature, average depth between these two extremes, etc.). It is plausible that each of these depths could be evaluated using the same thresholds to arrive at a composite thermal risk. Alternatively, because the temperature corresponding to, for instance, “unfavorable” will change depending on the depth, temperatures in depth slices can be evaluated separately in the risk matrix analysis to provide depth-specific thermal risk factor contributions to the composite project risk. Therefore, when complexities exist with depth, we recommend that raster sets be submitted in incremental depth slices of the risk factor to allow for flexibility in computing the composite project risk. Thermal and reservoir risk factors have been submitted in this manner.

Proposed Simple Risk Standardization

A first computational task is to convert the continuous variable for each risk factor into the play fairway color scheme. The conversion into the play fairway ranking system (e.g. 0 to 3) will be accomplished using the thresholds, unique to each risk factor. For example, for a 3-color scheme with thresholds at 15 and 25, a risk metric value ≤ 15 would be plotted as red, a value between 15 and 25 would be yellow, and a value > 25 would be plotted as green. The map will not be colored using a continuous color bar; however values of the risk variable will be continuous.

Using the continuous values of each risk variable with its specified thresholds allows plotting the 3- or 5-levels of each variable across the map. But, how to combine these variables when they have completely different units, and perhaps very different scales is unclear. We propose to use the thresholds and min/max values with linear interpolation to generate standardized values for each risk variable.

For a 3-color system, one expects that 1 and 2 represent the thresholds. Zero is appropriate to represent a score for the minimum value of the variable, and three is appropriate to represent the best value of the variable. (This may require reversing the scale of some variables so that 3 is good and 0 is bad.)

Thus the ranges are:

- 0 – 1 Red = Bad, unacceptable
- 1 – 2 Yellow = okay, marginally acceptable
- 2 – 3 Green = good, advantageous

For a 5-color scheme, thresholds are located at 1, 2, 3, and 4, with 0 representing the minimum, and 5 representing the maximum value.

Very Unfavorable	Unfavorable	Neutral		Favorable		Very Favorable			
0.0	1.0	1.0	2.0	2.0	3.0	3.0	4.0	4.0	5.0
	Threshold 1		Threshold 2		Threshold 3		Threshold 4		

After linear interpolation of continuous risk variables to this standardized scheme, all of the variables will be on a 0-3 score for 3-colors, and a 0-5 score for 5-colors. Using these scores it would be reasonable to compute the minimum value of the standardized scores, their geometrical mean, or a weighted average (functional forms, below). Perhaps of special interest would be the average score, \bar{s} , for all pixels whose minimum score exceeds s_{\min} for each risk factor, where one might take s_{\min} to be any of the thresholds (e.g. 1 or 2, or an intermediate value such as 1.6). Thus one would consider among all of the acceptable projects, those that appeared to do best overall.

Uncertainty Analysis and Visualization

A final step will be to select a few interesting locations for visualization of the four individual project risk factors, and consideration of uncertainty in the computed values.

Map-level

The SOPO deliverable is to combine all of the risk factors using a single objective function (risk matrix) to calculate the combined risk. The combined risk factor (CRF) for pixel (i,j) may be calculated using one of these suggested functions in Table 1.

Table 1: Functional forms for the combined risk factor calculation, along with advantages and disadvantages of each function.

Functional Form	Advantages and/or Disadvantages
Average of Risk Factors	Equal weighting. Not dependent on the scale (min/max values to represent color)
Geometric Mean of Risk Factors	Penalizes areas where there is one especially low value. Highlights areas with one especially high value. Therefore the min/max values representing 0 and 3 (or 5) become very important.
Minimum of Risk Factors	Focuses on the most unfavorable risk factor at a location because all of the other risk factors are at least as good as the minimum. Unclear how much better a location is in other risk factors.

Combinations of the approaches listed in Table 1 are also feasible. For example, one might first compute the minimum risk factor, and accept only those location above a selected threshold (say 2.0), and then plot the average risk factor for acceptable locations.

Examples of the functional forms listed in Table 1 are provided in the equations below. The utilization risk factor has a tilde accent because it will be calculated as the maximum of the utilization values within a certain distance d of the pixel of interest. The distance d can be thought of as a pumping distance to reach the utilization target. In this calculation of the CRF map, each pixel is where to develop the resource, not necessarily where surface utilization is present. Using a utilization distance avoids potential problems with sharp edges to reservoirs. Areas without reservoir information would be “whited out” in the risk factor maps and also in the CRF map because of no information, which might lead to abrupt transitions from high CRF areas to no information CRF areas. The utilization distance would alleviate this problem because areas on the no information side of such a boundary would be able to utilize the resource a few pixels away.

$$\left. \begin{aligned}
 \text{CRF}(i, j) = \begin{cases}
 \frac{\text{RF}_{\text{thermal}}(i, j) + \text{RF}_{\text{reservoir}}(i, j) + \text{RF}_{\text{seismic}}(i, j) + \widetilde{\text{RF}}_{\text{utilization}}(i, j, d)}{4}, & \text{Average} \\
 \sqrt[4]{\text{RF}_{\text{thermal}}(i, j) * \text{RF}_{\text{reservoir}}(i, j) * \text{RF}_{\text{seismic}}(i, j) * \widetilde{\text{RF}}_{\text{utilization}}(i, j, d)}, & \text{Geometric Mean} \\
 \min\{\text{RF}_{\text{thermal}}(i, j), \text{RF}_{\text{reservoir}}(i, j), \text{RF}_{\text{seismic}}(i, j), \widetilde{\text{RF}}_{\text{utilization}}(i, j, d)\}, & \text{Minimum}
 \end{cases}
 \end{aligned}
 \right.$$

For the commensurate function calculated using any of the above equations, a combined play fairway map is defined. The advantage of using a continuous variable on the play fairway scheme is that it allows for more precision in numerical values used to compute the final map, and the uncertainty analyses as compared to a discretized metric (e.g. 3.2 vs. 3). The risk factor map coloring should only be discrete 3- or 5- colors as opposed to a continuous coloring scheme that could cause slight color differences in areas to appear meaningful.

Project-level

Once the final combined risk map is generated, a few project sites should be selected for more detailed presentation of results. For these individual sites, and with the uncertainty for each risk factor map, a Monte Carlo or first-order Taylor Series analysis can be used to arrive at the distribution of the commensurate risk statistic for that site. An example of such a plot is given in Figure 1. Using such methods will allow for:

1. Evaluation of whether a project might really be unsatisfactory
2. Test of statistically significant differences in the play fairway metric among project sites
3. Easy visualization of sites that seem to be more or less certain
4. Overall comparison of play fairway metrics across the most promising sites

Technically, we have a four-objective problem that was commensurated into the single play fairway metric. Once a group of a few potential project sites is selected, the problem can be represented again as a four-objective problem. One method of comparing sites is with a parallel axis plot, such as shown in Figure 2. Once the initial map has shown some likely good areas for development, a parallel axis plot will show four objectives for the same resource and will convey more information to a decision maker. It could be that there are large tradeoffs in the objectives, for instance the highest utilization might be near seismically active areas. Conveying more information for a few cases can be informative for a decision maker.



Figure 1: Example of plots comparing uncertainty in the computed commensurate play fairway objective for selected project locations. The circle would represent the combined risk factor map value and the bars could be the 5 and 95% limits based on Monte Carlo or first-order Taylor series analysis.

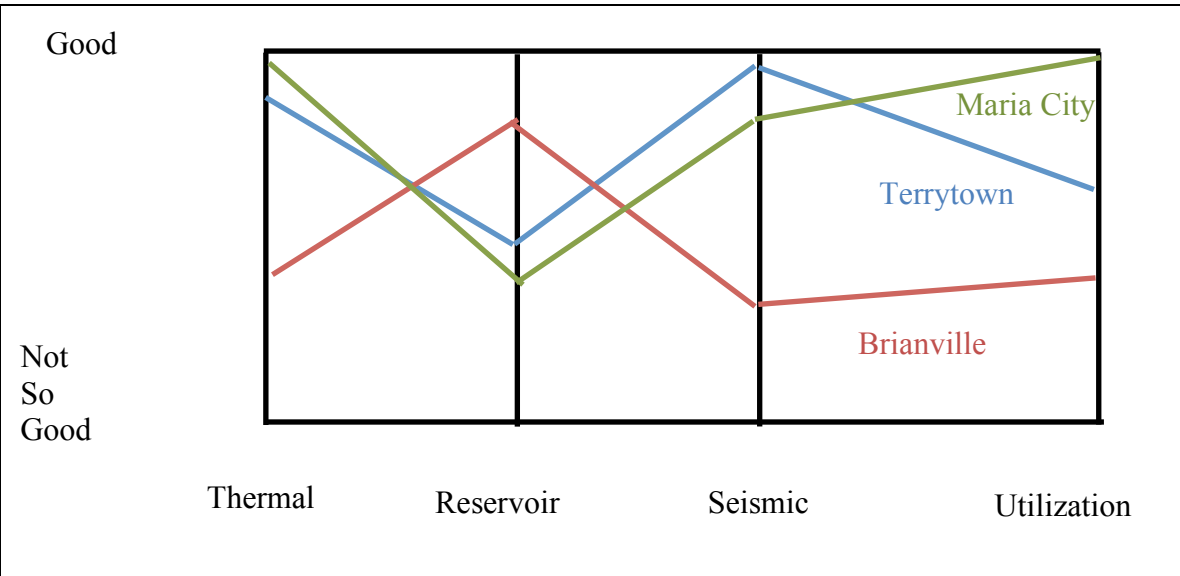


Figure 2: Example of a parallel axis plot where the objectives are plotted separately for each site. Such a plot would allow a decision-maker to look at the various objectives for a few sites and select places for further study.

Sensitivity Analyses

Sensitivity analysis of any CRF map will proceed by considering the impact of:

- (i) Varying the thresholds for the individual risk factor maps, and
- (ii) Varying the pumping distance d used to represent distance to utilization.

Other variables may also be explored.

This sensitivity analysis of the map does not address the uncertainty of inputs or of the economic model. The analysis in (i) addresses the thresholds used for green/yellow/red classification on the output summary. If we changed our thresholds, would the output map be very similar or drastically different? (ii) This set of results looks at the impact of the selected value of d describing feasible pumping distance.

Discussion of Weighting

It was the original intent for this Geothermal Play Fairway analysis of the Appalachian Basin to introduce weighting when combining the risk maps. One can assign weights, but if one does not have a justification for the weighting scheme, then it is arbitrary and could be (unknowingly) manipulated to favor certain sites or general conclusions. Also, weights can easily be manipulated by specifying special cases for certain geographic areas.

One justifiable method of weighting would be based on an economic model of the system for each pixel. In this case the weights would be derived economically because the cost of the project could be divided into portions associated with each risk factor. For instance, the levelized cost of heat (LCOH) would reflect the thermal quality of the reservoir, the natural quality of the reservoir, and the utilization infrastructure and pricing. Seismic hazard could be reflected by insurance premiums.

A problem with the use of an economic model is that, although it might be related to the cost of the project, it does not model the preferences of different agents. It is possible that willingness-to-pay for geothermal heat will be different across the agents, and this would be difficult to capture accurately in a model without clear agent preference data. Additionally, accurately specifying all inputs, or input distributions, would be very time consuming.

After consideration of these factors and the preliminary exploratory nature of this project, we determined that weights initially be assigned equally to all risk factors in calculating the commensurate play fairway metric. Time permitting in follow-on projects, other options can be explored.

Closing Thoughts

Using simple metrics will provide easy to interpret results for decision makers. The map itself should not be considered a complete analysis of whether developing a geothermal resource at that site is appropriate because a much more detailed analysis should be done before a major decision is made. Completing a holistic analysis is outside the scope of this initial portion of the project. Realistic economic and risk analyses would include a range of factors and considerations, which would be unique for each developer. The individual risk factor (RF) maps and composite risk factor (CRF) maps described here support and allow an initial or exploratory analysis of the development of geothermal resources in the Appalachian Basin.

Appendix 1: Methods for creating the risk factor grid, and converting vectors to rasters

Creating the raster grid

From a computational perspective, there is a need to have a single grid on which to plot all risk factors so that calculations of the combined risk factor metric may be easily performed without manipulation of the original data to a different grid via resampling of the risk factor products. Two main considerations are needed for the grid: 1) what should the spatial extent be, and 2) what should the resolution of the grid be?

The spatial extent of the grid was determined based on the rectangular area enclosing the 50 km buffered states of New York, Pennsylvania, and West Virginia (State_NADBuff.shp). Much of the grid area will not have data for most risk factors, but rasters must be rectangular, so this is the smallest possible extent of the grid.

In this project, a 1 km² pixel size is selected for the grid. This size was selected based on the minimum expected size of a single risk factor output. In this case, seismic risk and reservoir risk are determined based on buffered points. The minimum reservoir extent is slightly greater than 1 km², so the pixel size needed to capture these reservoirs is 1 km².

Using this information, the project grid was created in three formats: points (cell centers) and polygons using the Create Fishnet tool in ArcGIS. The resulting files are Fishnet2_label.shp and Fishnet2.shp, respectively. It is important to note that this grid was created in coordinate system NAD83 UTM Zone 17N so that cells were all of equal size (1 km on each side). The input cell size in UTM coordinates is 1000 m x 1000 m, with a “template” plotting extent of the buffered states. The polygons were converted into a raster called GridNAD.tif using the Polygon to Raster tool in ArcGIS. A combination of points, polygons, and the raster grid were used in extracting individual risk factor data to this standardized grid format.

For final maps, this grid was projected into WGS84, so the cell sizes may warp, but they will occupy a 1km² area.

Converting vector files to rasters

The thermal risk factor is computed directly on the grid and does not require any conversion from vector to raster; however some processing is required (see Thermal section below). All other risk factors are computed as vector files that must be converted to rasters on this standardized grid. A simple tool called PolygonToRaster_wPolygons was developed in ArcGIS Model Builder for this conversion process. The steps of the tool are outlined here.

- 1) Spatial Join of the risk factor polygons to the standard grid polygons, ensuring that many risk factor attributes can be joined to a single grid cell. This is important when overlapping occurs within a single risk factor (for example, reservoirs at different depths in the same surface location).
- 2) Convert the specified field in the joined data files to a raster using the Polygon to Raster tool. The cell size of the resulting raster should be specified as the cell size of the GridNAD.tif raster. The result is a raster of the risk factor.

This tool was sufficient for converting the utilization vectors to rasters. Reservoir and seismic risks required additional processing.

Reservoirs:

Specific to reservoirs, a model was built to deal with overlapping reservoirs in the same spatial location. This model was called ReservoirConversion_FINAL. The steps of this model are summarized below.

Prior to processing, reservoirs must be sorted into depth slices from 1000 m to 4000 m in 500 m increments, plus one file for reservoirs shallower than 1000 m, for a total of 7 vector files.

- 1) Call the PolygonToRaster_wPolygon tool, with inputs as the depth slice of interest and the standardized grid polygons. This resulted in a raster of the risk factor and an intermediate file.
- 2) The intermediate file from this tool is the polygons containing the joined risk factor data. The uncertainty of the risk factor is a field in the attribute table of this file, so this field is converted to a raster using Polygon to Raster tool in ArcGIS. This resulted in a raster of the uncertainty in the risk factor.
- 3) These files contain data in the spatial extent of the reservoir polygons and ArcGIS default NoData elsewhere. NoData values are not desirable for calculations, so all of these NoData points are converted to -9999 to indicate no information using the Raster Calculator tool. This processing takes place in a separate model developed for this project, called FullRegionGrid, described below.

The FullRegionGrid model takes an input raster and converts NoData locations to -9999. The steps are as follow:

- 1) Use the Extract Values to Points tool to extract the raster with NoData values to the cell centers of the standardized grid (Fishnet2_label.shp). This field will be named the Arc default RASTERVALU
- 2) Use the Add Field tool to add a field name to the attribute table. This will be the field for the resulting raster.
- 3) Use the Calculate Field tool to populate the values in the added field with the RASTERVALU.
- 4) Convert the points to a raster using the Point to Raster tool.
- 5) Use Raster Calculator to convert all NoData (IsNull) fields to -9999.

Seismic:

Earthquake-Based Maps

A tool called SeismicEQ_ToRaster was created to convert the distance to the nearest earthquake information to a raster of distance to nearest earthquake.

- 1) Use the Spatial Join tool to join the distance to nearest earthquake attribute table to the standardized grid points.
- 2) Use the Point to Raster tool to convert these points into a raster.

A tool called New_EQJoin was created to make rasters of the

- 1) Clip the raster of distance to nearest earthquake to the buffered gravity worm points (buffering is described in Memo 14, “Seismic Risk Map Creation Methods”).
- 2) Clip the raster of distance to nearest earthquake to the buffered magnetic worm points.
- 3) Use Extract Multi Values to Points tool to add this clipped raster information to the standardized grid points.

This results in a point file that has distance to the nearest earthquake for the buffered gravity and magnetic worm locations. These are processed to obtain the risk metric, as described in Memo 14, “Seismic Risk Map Creation Methods”. Post processing, the risk metric and the uncertainty are converted into rasters on the standardized grid using the Polygon to Raster tool.

Stress Field-Based Maps

A tool called SeisStressMagGrav was developed to convert the information about angle to normal into a raster.

- 1) Buffer and dissolve the magnetic or gravity points by a selected amount (2 km in this project).

- 2) Use the Polygon to Raster twice: once to convert the prediction angle, and once to convert the uncertainty. The priority field should be set to the Weight field.
- 3) Use the Extract Multi Values to Points tool to add the prediction and uncertainty information to the standardized grid points.

This results in a point file that has the angle to the critical stress and the uncertainty in that angle. These points are processed to obtain the risk metric as described in the memo “Conversion of Seismic Risk Data to Risk Maps”. Post processing, the risk metric and the uncertainty are converted into rasters on the standardized grid using the Polygon to Raster tool.

Thermal:

Converting separate raster files to a single raster

The thermal risk factor maps are created using laterally stratified boundaries. This means that the resulting rasters do not occupy the original extent of the standardized grid. In order to convert these files into a single raster in standardized grid format, two tools were developed.

The Final_MosaicPred tool takes all of the resulting rasters for the thermal risk factors and combines them into a single raster.

- 1) Make a copy of one of the rasters to be combined, save it in a different directory, and rename it. This will be the combined raster file.
- 2) Use the Mosaic tool in ArcGIS to combine the individual rasters. The target raster is the raster that was copied.

The resulting raster is on the standardized grid, but it does not occupy the full extent of the grid. The ThermalFiles_Final tool converts the mosaicked raster onto the full extent of the standardized grid.

- 1) Use the Extract Multi Values to Points tool to extract the prediction map and the uncertainty map raster information to the standardized grid cell centers.
- 2) Convert these points to 2 rasters: one for the prediction map, and the other for the uncertainty map.
- 3) Use Raster Calculator to convert all of the locations with values less than 0 to the no information value of -9999.

Memo 17: Combining Risk Factors in GPFA-AB Combining Risk Factors: Detailed Calculations and Extended Results

Calvin A. Whealton, Jared D. Smith, Teresa Jordan
Original from September 30, 2015. Updated October 2016.

Table of Contents

OVERVIEW	2
1. INDIVIDUAL RISK FACTORS	3
1.1 THERMAL.....	3
1.2 RESERVOIRS	7
1.3 SEISMIC.....	13
1.4 UTILIZATION	17
2 COMBINED RISK FACTORS.....	22
2.1 OVERVIEW OF THREE COMBINATIONS OF RISK	22
2.2 UNCERTAINTY OF RISK FACTORS AND UNCERTAINTY FOR COMBINED RISK MAPS.....	22
2.3 ALL RISK FACTORS COMBINED.....	25
2.3.1 <i>Average</i>	25
2.3.2 <i>Geometric Mean</i>	28
2.3.3 <i>Minimum</i>	32
2.4 GEOLOGY ONLY.....	34
2.4.1 <i>Average</i>	34
2.4.2 <i>Geometric Mean</i>	36
2.4.3 <i>Minimum</i>	38
2.5. NO RESERVOIRS.....	40
2.5.1. <i>Average</i>	40
2.5.2 <i>Geometric Mean</i>	42
2.5.3 <i>Minimum</i>	43
3 ROBUSTNESS OF COMBINING FUNCTIONS	45
4 POTENTIAL PROJECT LOCATIONS.....	46
5 REFERENCES CITED.....	50

DISCLAIMER

The information, data, or work presented herein was funded in part by an agency of the United States Government. Neither the United States Government nor any agency thereof, nor any of their employees, makes any warranty, express or implied, or assumes any legal liability or responsibility for the accuracy, completeness, or usefulness of any information, apparatus, product, or process disclosed, or represents that its use would not infringe privately owned rights. Reference herein to any specific commercial product, process, or service by trade name, trademark, manufacturer, or otherwise does not necessarily constitute or imply its endorsement,

recommendation, or favoring by the United States Government or any agency thereof. The views and opinions of authors expressed herein do not necessarily state or reflect those of the United States Government or any agency thereof.

Overview

This document outlines detailed calculations and extended results for the individual risk factor maps and the combined risk factor (common risk segment, CRS) maps. Individual risk factors are addressed first. For each individual risk factor the values (thresholds, minimum, and maximum) used in converting the risk factor to the common play fairway favorability scale, the frequency distribution of the scaled risk factor, and the play fairway scaled risk factor maps (3- and 5-color versions) are shown. Some risk factors have additional challenges or assumptions that were used in processing and these are also discussed.

The second section outlines the methods used to combine the individual risk factor maps into a single play fairway map (CRS map). Results are presented for combining the 3- and 5-color maps separately, including the distribution of the combined play fairway metric for the whole map. The combinations are completed separately and presented for all four risk factors, for the three geologic risk factors (thermal, seismic, and reservoirs), and for a “no reservoir” set (utilization, thermal, and seismic).

The next section discusses the uncertainty in the maps. Although uncertainty maps are presented near their related maps, this section gives the details of those calculations. The two main issues discussed are the methods used to derive uncertainty of each individual risk factor play fairway map and the uncertainty of each combined map.

The last two sections show the robustness of the methods of combining the risk factors, and show some results for specific project locations. The robustness is illustrated by plotting the results of different combined play fairway metrics against each other. Project-specific results show the individual risk factors for a set of locations thought to be of interest for Phase 2.

Some common terms used throughout this report are defined below.

Play Fairway Metric (PFM): A formula used to generate an aggregate measure of how favorable a place (site, raster cell) is based on input risk factors.

Scaled Risk Factor (SRF): A value for an individual risk factor (RF) that has been converted to the play fairway scale of [0,3] or [0,5], depending on the map.

Thresholds: Values used to assign an input risk factor to the range [0,3] or [0,5], depending on the map. These thresholds delineate different color groups on the maps and represent boundaries of favorability.

Further explanations and treatment of most of this material can be found in Whealton (2016).

1. Individual Risk Factors

Individual risk factors are presented in the following sections. If there were special considerations when calculating the risk factor, these are outlined as well. Generally, each input risk factor was converted into the play fairway metric by linearly scaling its continuous value between the selected thresholds. If an unscaled value was greater than the selected maximum on the play fairway scale for that risk factor, it was assigned the maximum (3 or 5). Similarly, if an unscaled value was less than the selected minimum on the play fairway scale for that risk factor, it was assigned the minimum (0). On the map figures, areas colored white are areas with no data for the calculation. These are areas where the risk factor could not be evaluated at that location (e.g. no information), or areas outside of the region. Histograms show the selected thresholds with respect to the original, unscaled input risk factor map.

1.1 Thermal

The depth to 80 °C is used as the map for the thermal risk factor as per the Statement of Project Objectives (SOPO) requirements. The thresholds are based on the memo titled “Assignment of Thresholds for Depth-to-Temperature and Temperature-at-Depth Maps” (August 25, 2016). Table 1 provides the scaling values and thresholds, Figure 1 shows the histogram of the input risk factor map. Figures 2 and 4 show the 3- and 5-color maps for the scaled values.

There were no special calculation considerations for this risk factor. All conversions used a linear scale.

The uncertainty was estimated using the mean and standard error of prediction. The distribution was assumed to be normal, with mean and standard deviation defined from the mean and standard error of prediction. After this, the methods discussed in the uncertainty section were used to derive the uncertainty maps shown in Figures 3 and 5.

Table 1: Table of minimum, maximum, and favorability thresholds used in scaling the thermal map (depth to 80 °C [m]). The scale is reversed so that high values are unfavorable because shallow depths should result in a reduced cost.

Min	5000
Max	1000
3-Color Thresholds	{3750, 2350}
5-Color Thresholds	{4000, 3000, 2500, 2000}

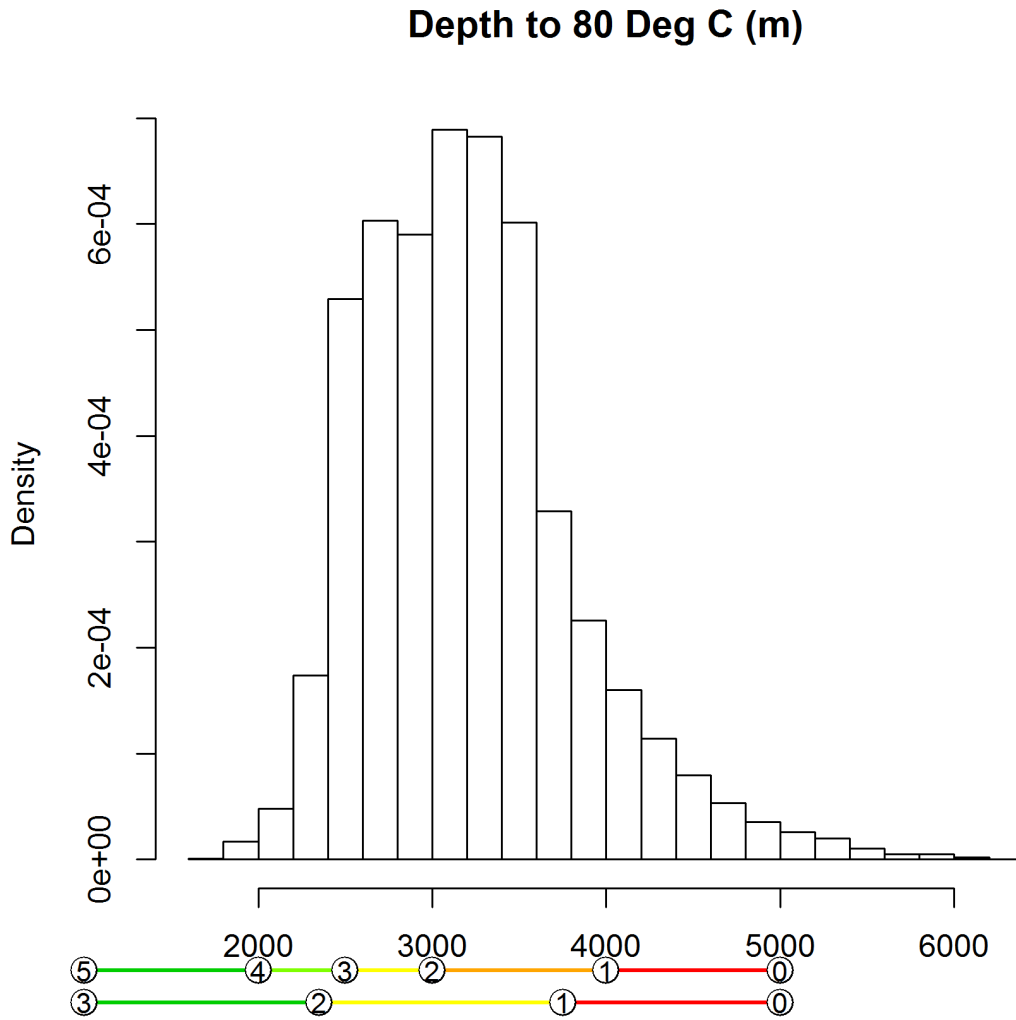


Figure 1: Histogram of the thermal risk factor with the 3- and 5-color thresh-olds noted. Points beyond the minimum and maximum of the scale are assigned the minimum and maximum of the scale, respectively (e.g. 0, and 3 or 5). Density is proportional to the frequency or count in the bins, but the values have been rescaled so the total area of the histogram is 1.

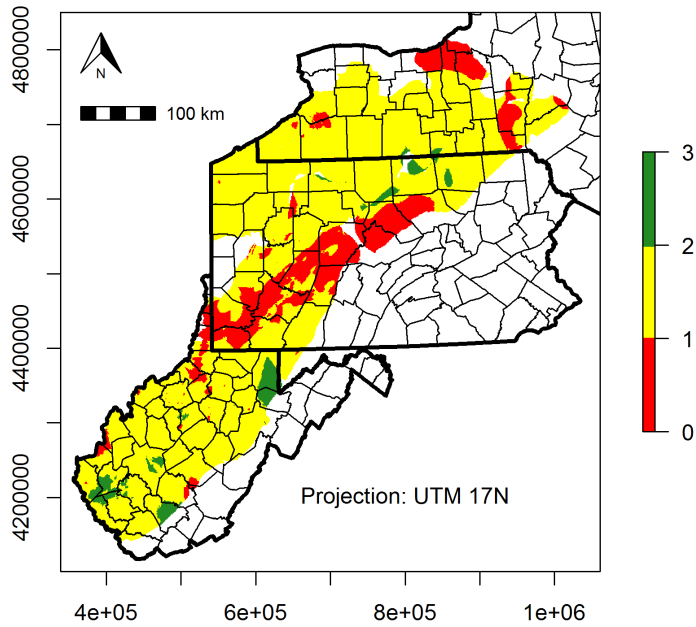


Figure 2: Map of the thermal risk factor with a 3-color scheme. Red areas are unfavorable and green areas are favorable values of the scaled risk factor.

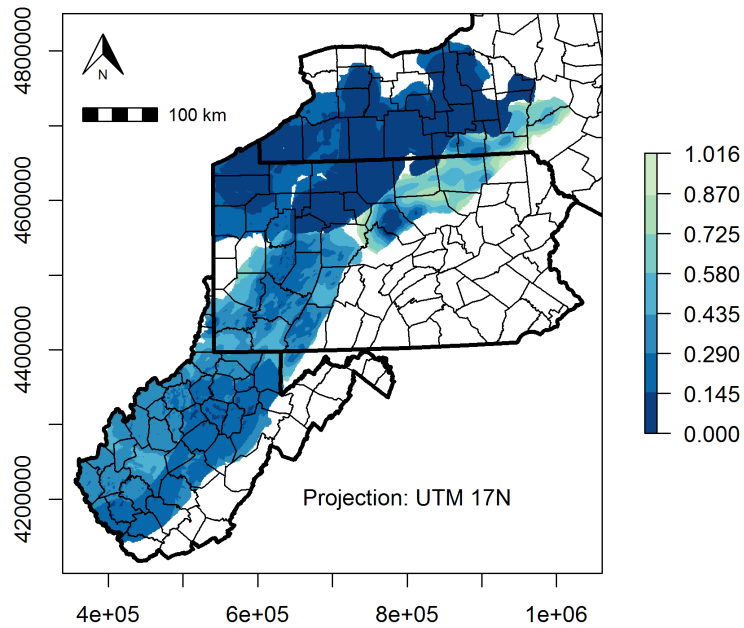


Figure 3. Map of the standard deviation of the scaled thermal risk factor with a 3-color scheme. Dark colors are more certain and light colors are less certain.

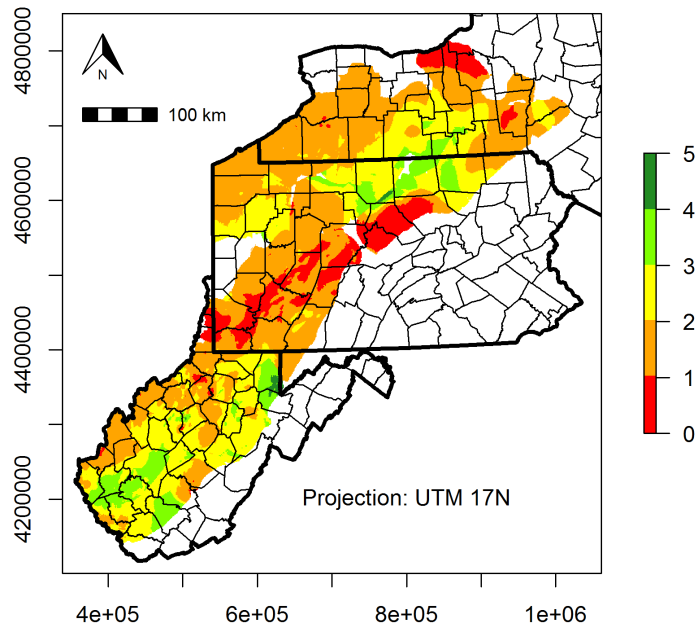


Figure 4. Map of the thermal risk factor with a 5-color scheme. Red areas are unfavorable and green areas are favorable values of the scaled risk factor.

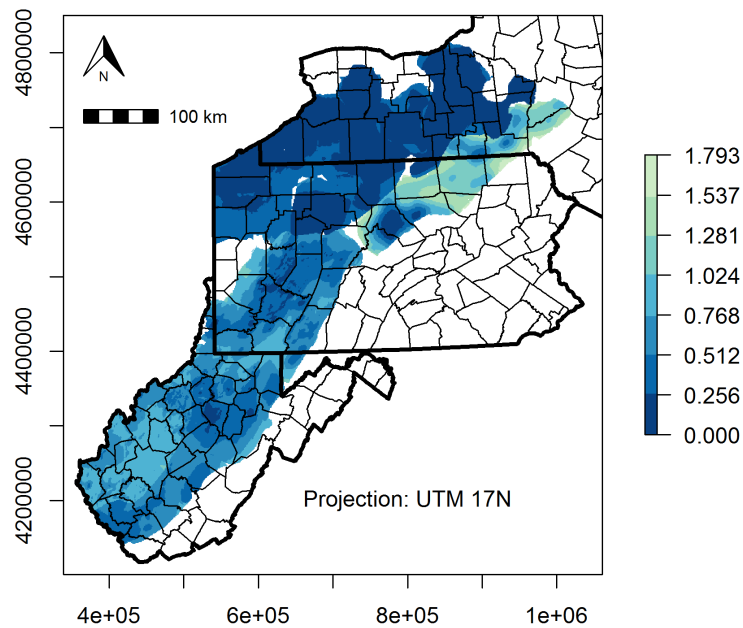


Figure 5. Map of the standard deviation of the scaled thermal risk factor with a 3-color scheme. Dark colors are more certain and light colors are less certain.

1.2 Reservoirs

The reservoir play fairway risk is in terms of Reservoir Productivity Indices for water as a working fluid (RPI_w) and for supercritical carbon dioxide as a working fluid (RPI_g), measured in units of kg/MPa-s, as well as another metric that expresses only the natural *in situ* capacity to hold fluids, the Reservoir Fluid Capacity metric (RFC). These reservoir quality indices are the calculated expressions of the reservoir's favorability for geothermal applications. More information is available in the memo "Natural Reservoirs Task Methodology". The reservoir data were divided into 500 m depth slices, with the shallowest slice being 1000-1500 m and the deepest being 3500-4000 m. These depth slices were combined into a single risk factor map by taking the maximum (high values are good) value at each spatial location. Reservoirs shallower than 1000 m were ignored in the combination because they will likely not meet the minimum temperature requirements for our projects.

A point of reference for the selection of thresholds at which to divide RPI_w into a non-dimensional reservoir metric is the anticipated need to achieve the equivalent of 30 kg/sec flow rate for a water-based geothermal well. Assuming that the greatest pressure drop would be 3 MPa, the RPI_w threshold for the reservoir which could achieve 30 kg/sec flow with no reservoir stimulation is approximately 10 kg/MPa-s. A conversion of potential heat transfer and transport by supercritical carbon dioxide to this water-based flux provides a basis for determining that the thresholds for RPI_g should be approximately the same as for RPI_w. Table 2 gives the thresholds, and Figure 6 gives the histograms of all three reservoir productivity indices (transformed to base-10 log). Figures 7a, 8a, and 9a plot the 3-color maps of RPI_w, RPI_g, and RFC factors converted to the 3-point scale, respectively. Figures 10a, 11a, and 12a plot the 5-color maps of the play fairway conversion for RPI_w, RPI_g, and RFC.

Table 2 gives the thresholds, and Figure 6 gives the histograms of all three reservoir productivity indices (transformed to base-10 log). Figures 7a, 8a, and 9a plot the 3-color maps of RPI_w, RPI_g, and RFC risk factors converted to the 3-point scale, respectively. Figures 10a, 11a, and 12a plot the 5-color maps of the play fairway conversion for RPI_w, RPI_g, and RFC.

The thresholds are defined mainly for orders of magnitude, so the conversion was linear on a logarithmic scale. The steps in this analysis were first to convert the raster of the maximums by taking the base-10 log of the values. Similarly, the thresholds were converted to base-10 logs. Once the raster and the thresholds were converted, the conversion was linear.

Because the reservoir data are limited to a subset of the study area, regions with no reservoir data in this project's compilation appear on the maps as white zones. These white zones portray no significance relative to the existence or not of potential reservoirs for geothermal heat extraction. Yet they do portray a high degree of risk because the lack of data.

The uncertainty of the reservoir map was calculated by assuming that the provided mean and coefficient of variation defined a log-normal distribution. The parameters were specified in real-space, not log-space, so they had to be converted. The log-space variance, σ^2 , can be solved for from the real space coefficient of variation, CV, as shown in Equation 1. The log-space mean, μ , can be solved using the real-space mean, m , and the log-space variance, σ^2 , as shown in Equation

2. The uncertainty of the individual maps was then calculated based the methods discussed in the uncertainty section of this document and the results are shown in Figures 7b, 8b, 9b, 10b, 11b and 12b.

$$\sigma^2 = \ln(1 + CV^2) \quad (1)$$

$$\mu = \ln(m) - \frac{\sigma^2}{2} \quad (2)$$

Table 2: Table of minimum, maximum, and favorability thresholds used in scaling the reservoir map. RPIw, RPIg, and RFC can each be considered as a measure of risk for the reservoir risk factor.

	RPIw (kg/MPa-s)	RPIg (kg/MPa-s)	RFC (mD-m)
Min	1×10^{-4}	1×10^{-4}	1×10^{-3}
Max	10	10	1×10^4
3-Color Thresholds	{0.1, 1}	{0.1, 1}	{10, 100}
5-Color Thresholds	{0.001, 0.01, 0.1, 1}	{0.001, 0.01, 0.1, 1}	{1,10,100,1000}

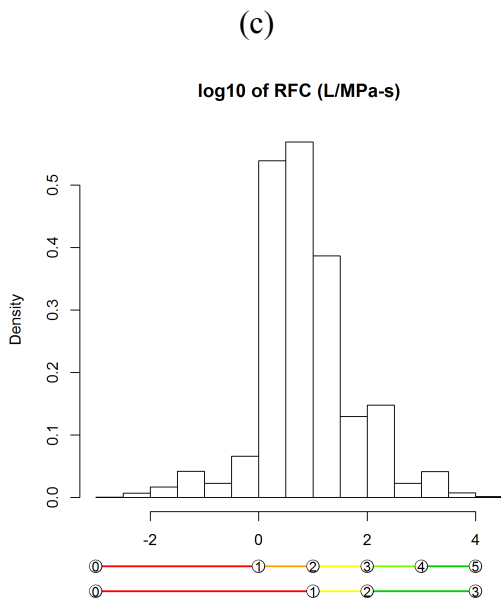
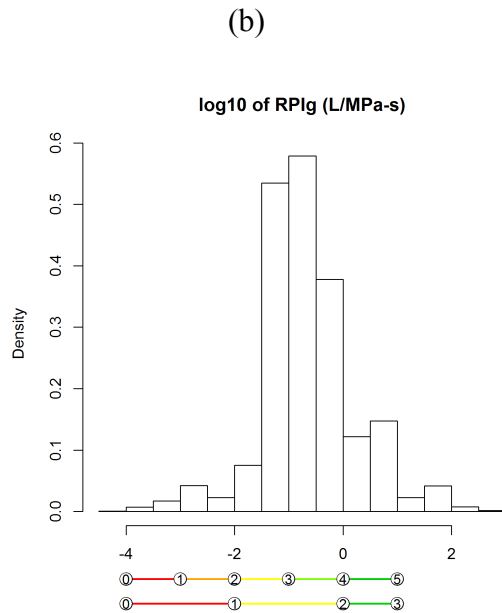
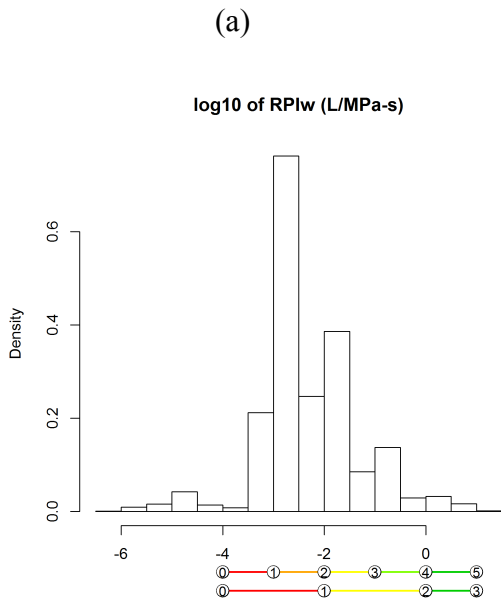


Figure 6: Histograms of the reservoir risk factors with the 3- and 5-color thresholds noted in Table 2. Points beyond the minimum and maximum of the scale are assigned the minimum and maximum of the scale, respectively (e.g. 0, and 3 or 5). Density is proportional to the frequency or count in the bins, but the values have been rescaled so the total area of the histogram is 1. a) for RPIw; b) for RPIg; c) for RFC.

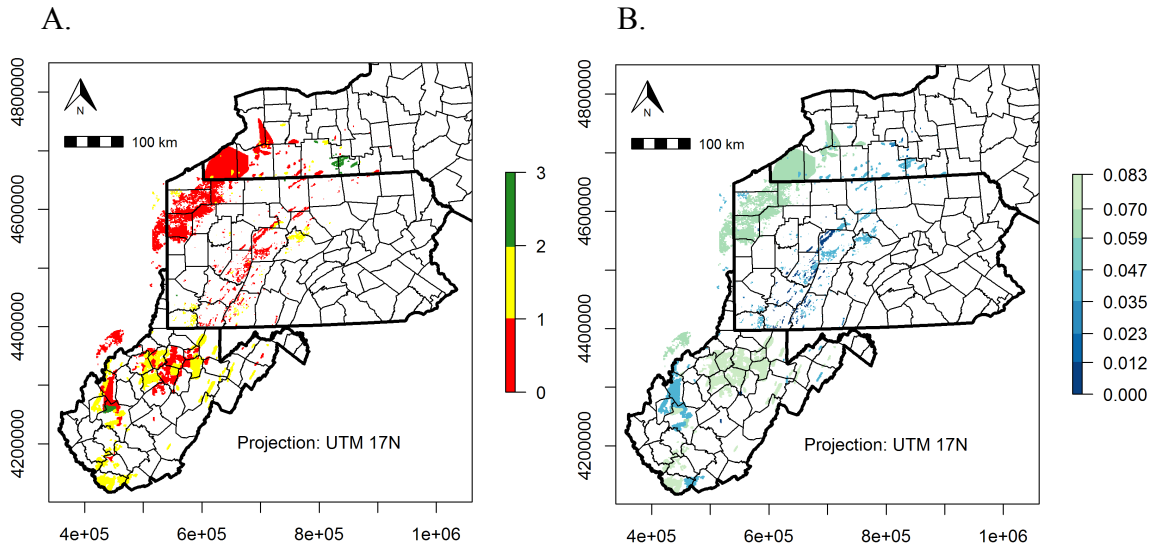


Figure 7. a) Map of the reservoir risk factor RPIw with a 3-color scheme. Red areas are unfavorable and green areas are favorable values of the scaled risk factor. b) Map of the standard deviation of the scaled risk factor for reservoirs for a 3-color scheme. Dark colors are more certain and light colors are less certain.

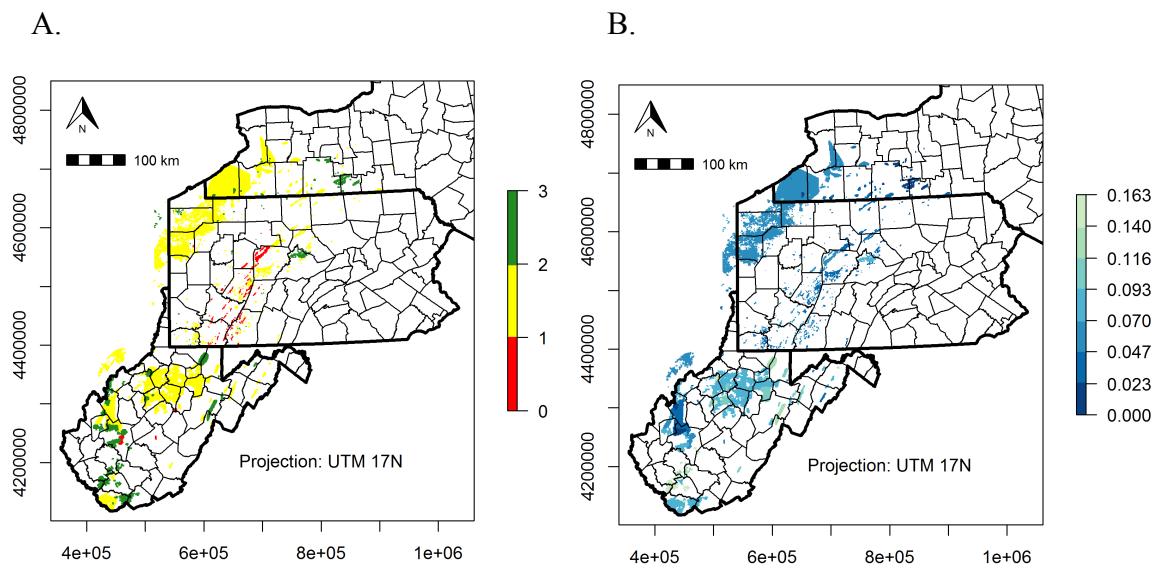


Figure 8. a) Map of the reservoir risk factor RPIg with a 3-color scheme. Red areas are unfavorable and green areas are favorable values of the scaled risk factor. b) Map of the standard deviation of the scaled risk factor for reservoirs for a 3-color scheme. Dark colors are more certain and light colors are less certain.

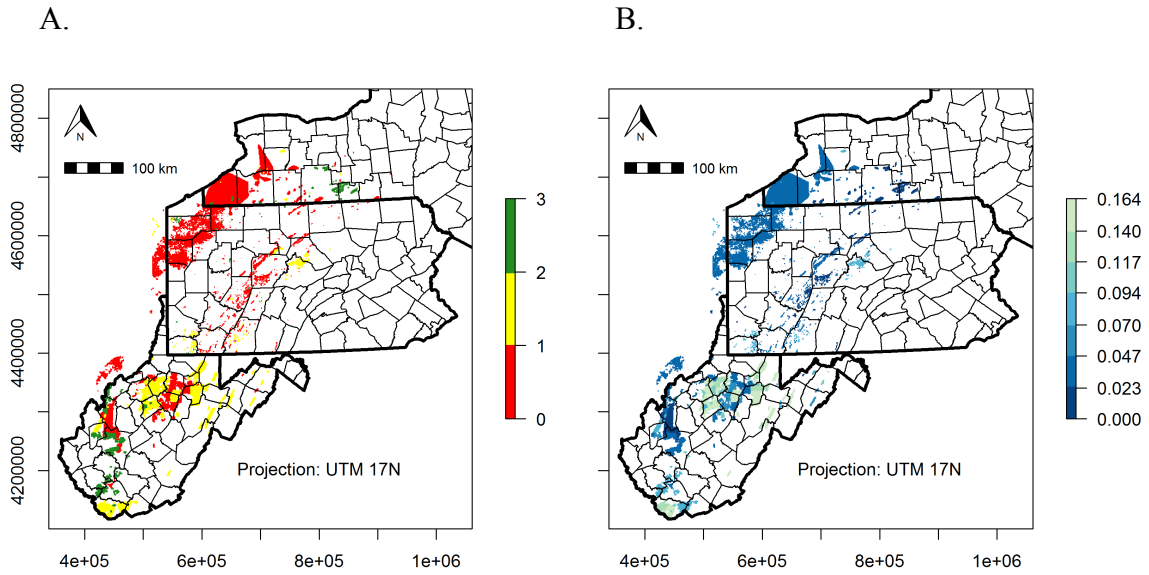


Figure 9. a) Map of the reservoir risk factor RFC with a 3-color scheme. Red areas are unfavorable and green areas are favorable values of the scaled risk factor. b) Map of the standard deviation of the scaled risk factor for reservoirs for a 3-color scheme. Dark colors are more certain and light colors are less certain.

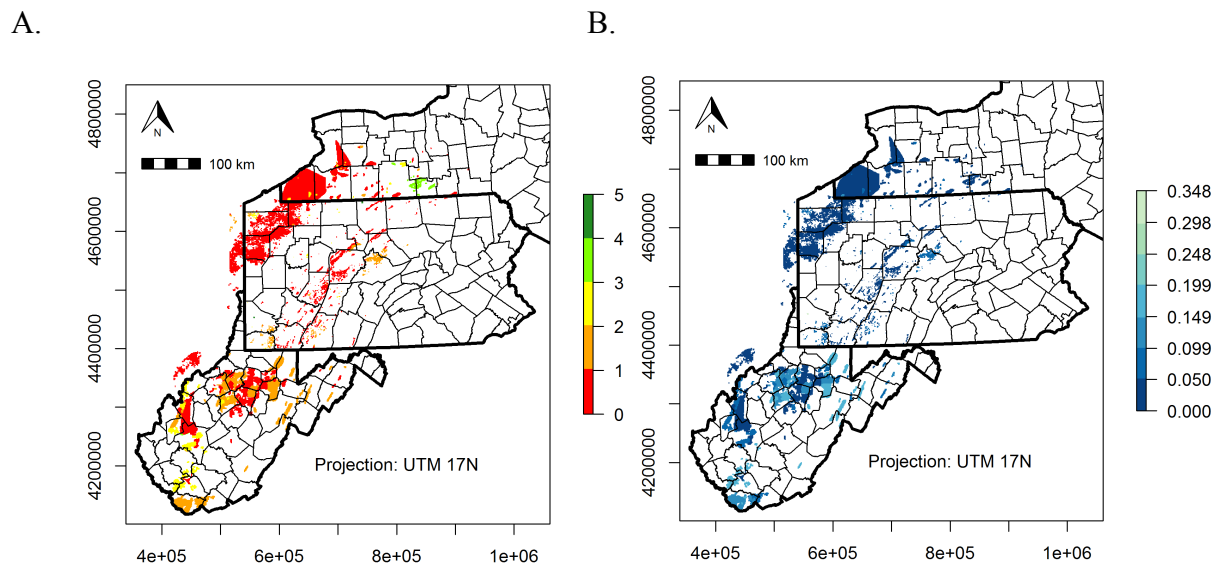
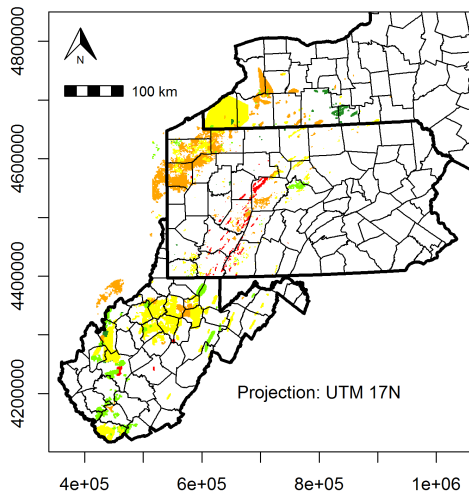


Figure 10. a) Map of the reservoir risk factor RPIw with a 5-color scheme. Red areas are unfavorable and green areas are favorable values of the scaled risk factor. b) Map of the standard deviation of the scaled risk factor for reservoirs for a 5-color scheme. Dark colors are more certain and light colors are less certain.

A.



B.

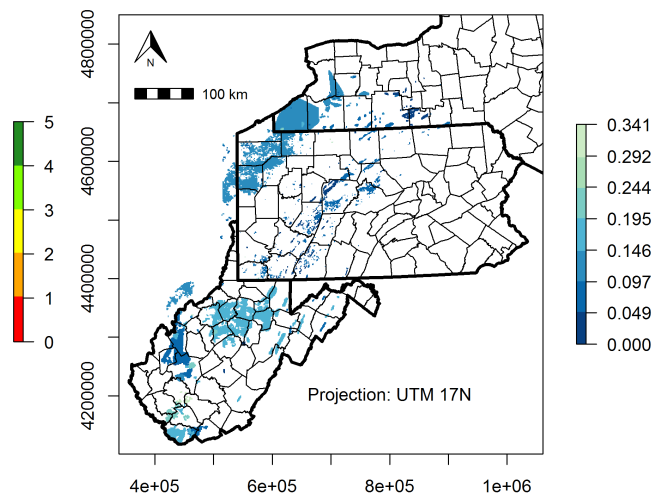
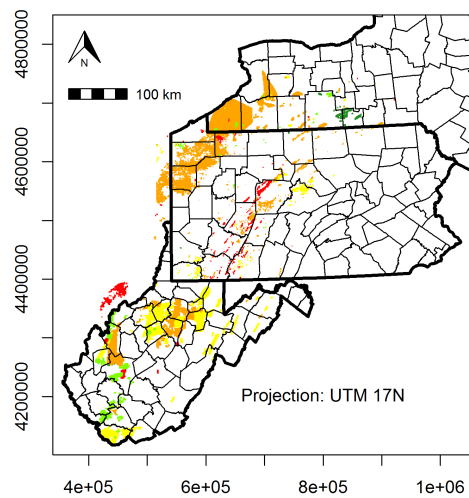


Figure 11. a) Map of the reservoir risk factor RPIg with a 5-color scheme. Red areas are unfavorable and green areas are favorable values of the scaled risk factor. b) Map of the standard deviation of the scaled risk factor for reservoirs for a 5-color scheme. Dark colors are more certain and light colors are less certain.

A.



B.

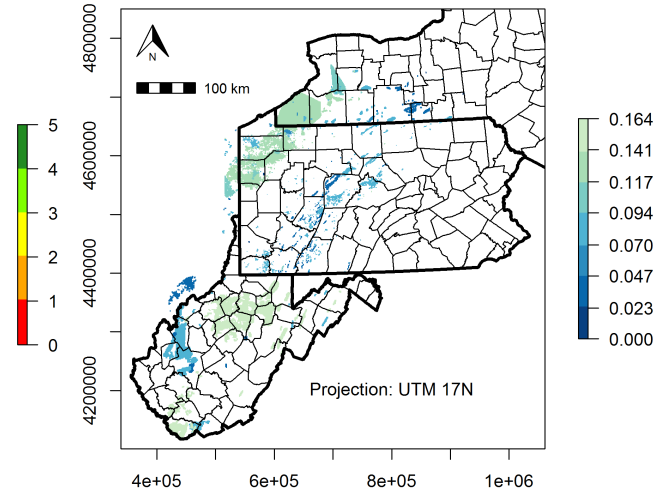


Figure 12. a) Map of the reservoir risk factor RFC with a 5-color scheme. Red areas are unfavorable and green areas are favorable values of the scaled risk factor. b) Map of the standard deviation of the scaled risk factor for reservoirs for a 5-color scheme. Dark colors are more certain and light colors are less certain.

1.3 Seismic

The seismic risk factor had two separate measures of risk: one for proximity to earthquakes and one for orientation of “worms” to the stress field. These were considered separate estimates of the risk, so they were averaged to create a seismic risk map. Both were converted into the play fairway scale before averaging. The stress map has values calculated as the minimum angle between the “worms” and the stress field failure angle according to Byerlee’s Law for failure of preexisting fractures. The earthquake map uses proximity to earthquakes and has units of meters.

Table 3 presents the thresholds used in creating the maps and Figure 13 plots the histograms of the earthquake- and stress-based risks. Figures 14a and 15a are the earthquake based risk maps for 3- and 5-color schemes, Figures 16a and 17a are the stress based risk maps for 3- and 5-color schemes, and Figures 18a and 19a are the averaged seismic risk map for the 3- and 5-color schemes. The same scale is used in the averaged map as in the input maps. The averaged seismic maps show that the areas with earthquakes are still high risk, but many of the “worms” with favorable orientation but no earthquakes nearby have been discounted in the average.

The uncertainty for the earthquake-based map was calculated by assuming a normal distribution with mean and standard deviation given as the prediction and the error, respectively. Because being 1 km from a worm should be equivalent to being -1 km from a worm, the absolute value was taken. The methods described in the uncertainty section were used to develop uncertainty maps, which are shown in Figures 14b and 15b.

The uncertainty for the stress-based map was calculated by assuming that the mean and standard deviation defined a normal distribution. Because being 1° from a critical failure orientation should be equivalent to being -1° from a critical failure orientation, the absolute value was taken. All angles were converted to $[0^\circ, 180^\circ]$ because the critical angles were calculated in this domain. The two critical orientations are 65.2° and 114.8° on $[0^\circ, 180^\circ]$. The risk factor was calculated by finding the smallest angle to one of the critical angles. The methods described in the uncertainty section were used to develop uncertainty maps for this metric, which are shown in Figures 16b and 17b.

When the two stress maps were averaged (multiplied by 0.5 each), the variance of the average could be calculated by summing the two individual variance uncertainty maps and multiplying the total by a value of 0.25. The results are given in Figures 18b and 19b. Generally, the earthquake-based maps have much higher certainty than the stress angle-based maps (more details in the memos “Identifying Potentially Activatable Faults for the Appalachian Basin Play Fairway Analysis” and “Conversion of Seismic Risk Data to Risk Maps”).

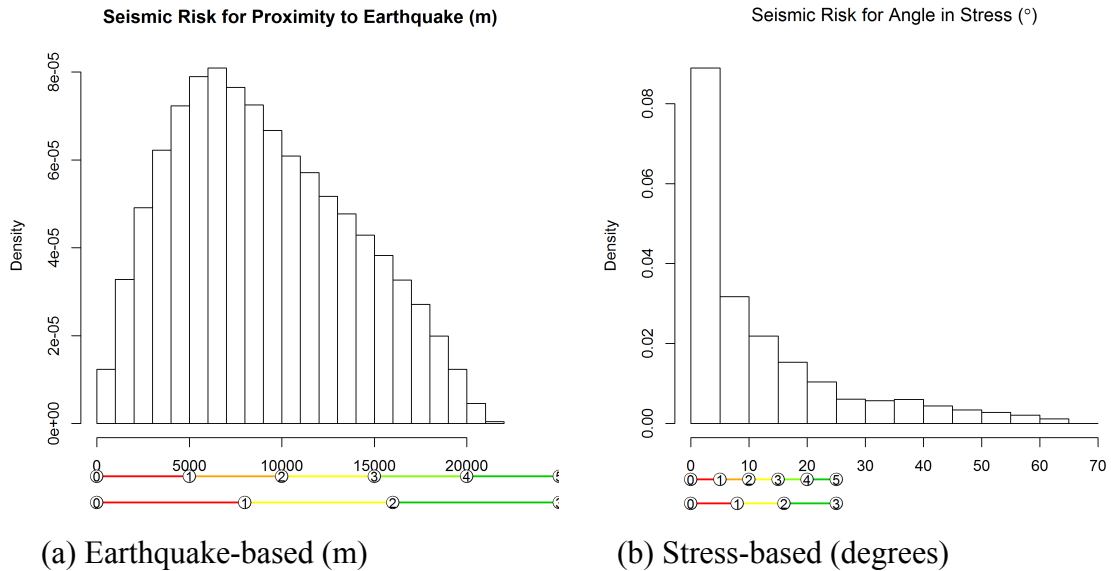
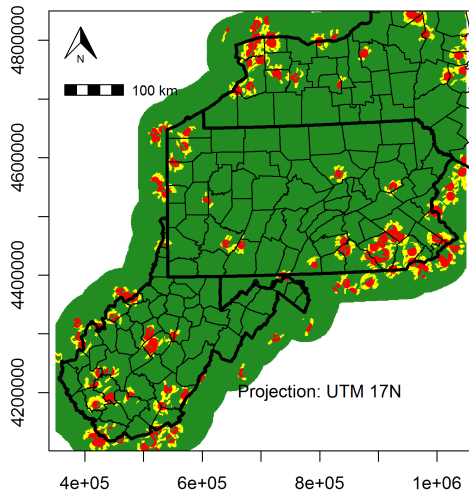


Figure 13. Histograms of the seismic risk factor for earthquakes and stress with the 3- and 5-color thresholds noted. Points beyond the minimum and maximum of the scale are assigned the minimum and maximum of the scale, respectively (e.g. 0, and 3 or 5). Density is proportional to the frequency or count in the bins, but the values have been rescaled so the total area of the histogram is 1.

Table 3: Table of minimum, maximum, and favorability thresholds used in scaling the seismic maps. Earthquake units are in meters and stress units are in degrees. Minimum values were not set to zero to avoid possible numerical problems.

Scaling	Earthquake (m)	Stress Angle (°)
Min	0.1	0.001
Max	25000	25
3-Color Thresholds	{8000, 16000}	{8, 16}
5-Color Thresholds	{5000, 10000, 15000, 20000}	{5, 10, 15, 20}

A.



B.

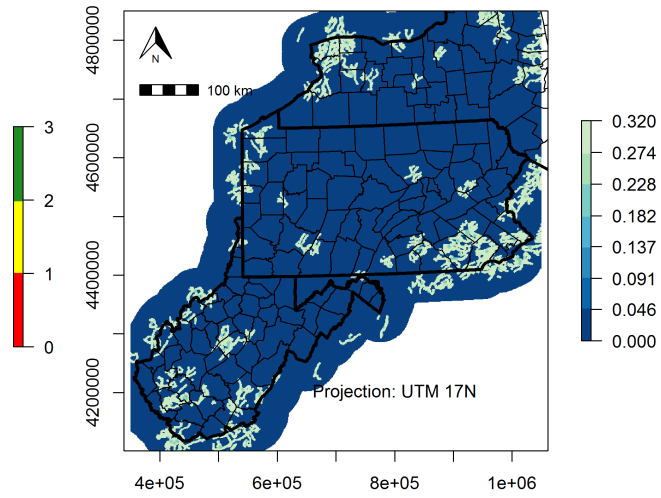
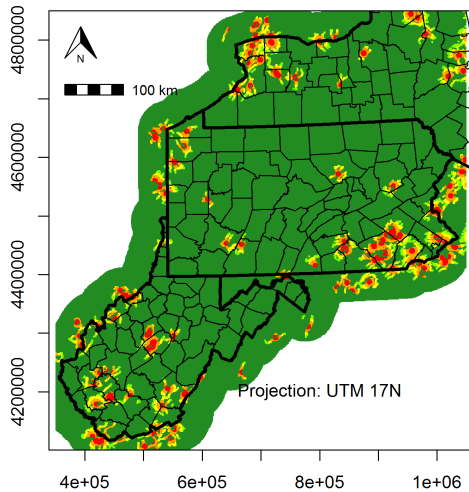


Figure 14. a) Map of the seismic risk factor for earthquakes with a 3-color scheme. Red areas are unfavorable and green areas are favorable values of the scaled risk factor. b) Standard deviation of the scaled earthquake-based seismic risk factor for a 3-color scheme. Dark colors are more certain and light colors are less certain.

A.



B.

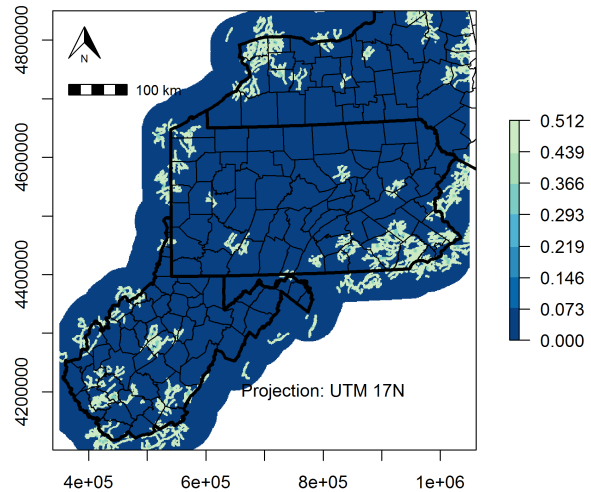
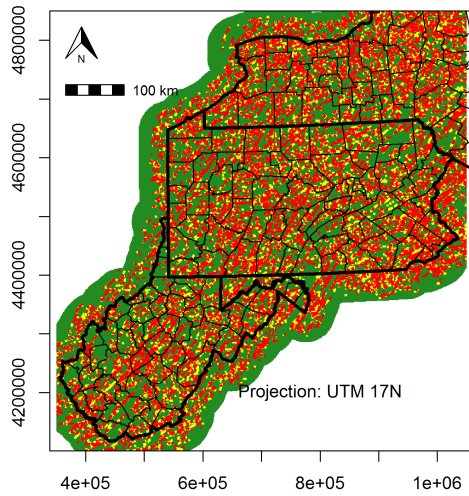


Figure 15. a) Map of the seismic risk factor for earthquakes with a 5-color scheme. Red areas are unfavorable and green areas are favorable values of the scaled risk factor. b) Standard deviation of the scaled earthquake-based seismic risk factor for a 5-color scheme. Dark colors are more certain and light colors are less certain.

A.



B.

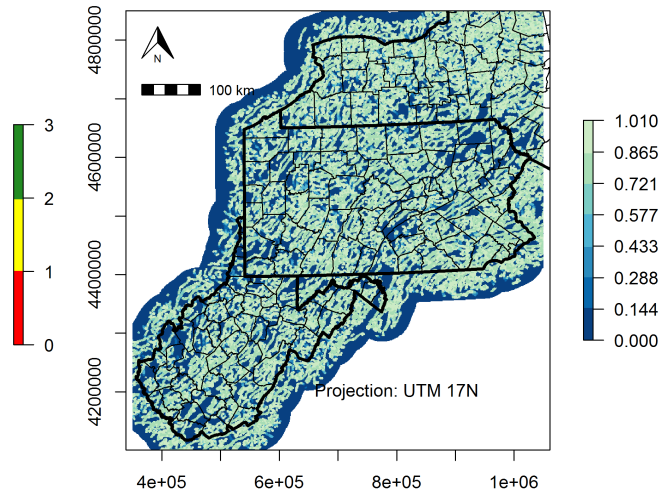
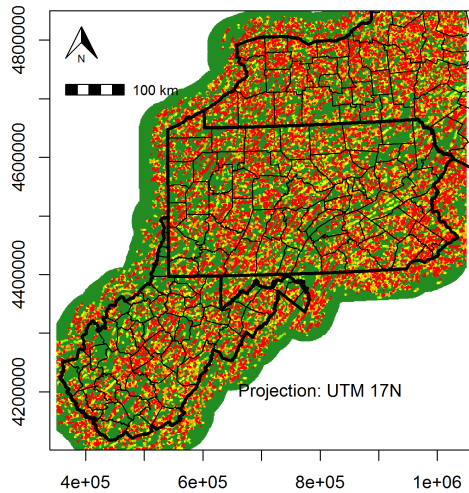


Figure 16. a) Map of the seismic risk factor for slip tendency in the regional stress field with a 3-color scheme. Red areas are unfavorable and green areas are favorable values of the scaled risk factor. b) Map of the standard deviation of the scaled risk factor for slip tendency in the regional stress field with a 3-color scheme. Dark colors are more certain and light colors are less certain.

A.



B.

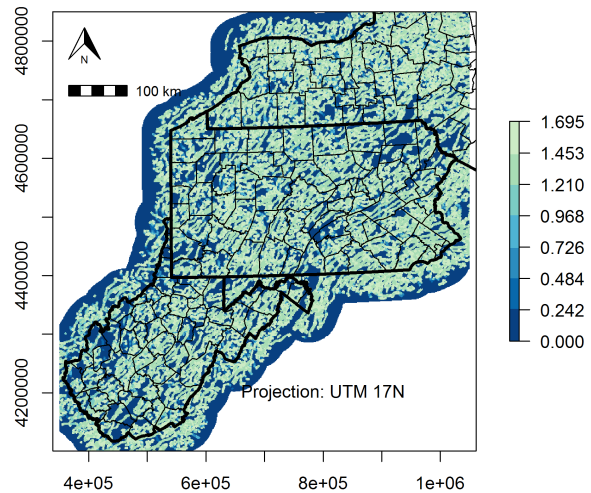
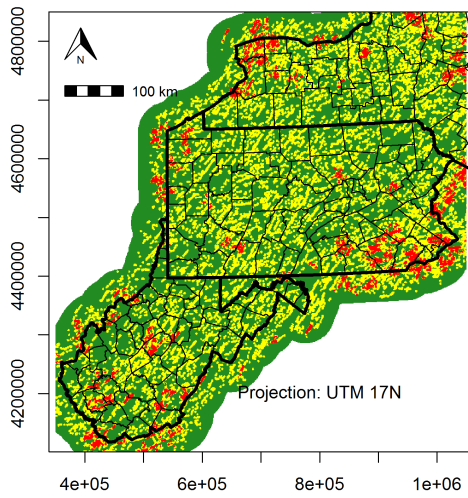


Figure 17. a) Map of the seismic risk factor for stress-based assessment with a 5-color scheme. Red areas are unfavorable and green areas are favorable values of the scaled risk factor. b) Map of the standard deviation of the scaled risk factor for slip tendency in the regional stress field with a 5-color scheme. Dark colors are more certain and light colors are less certain.

A.



B.

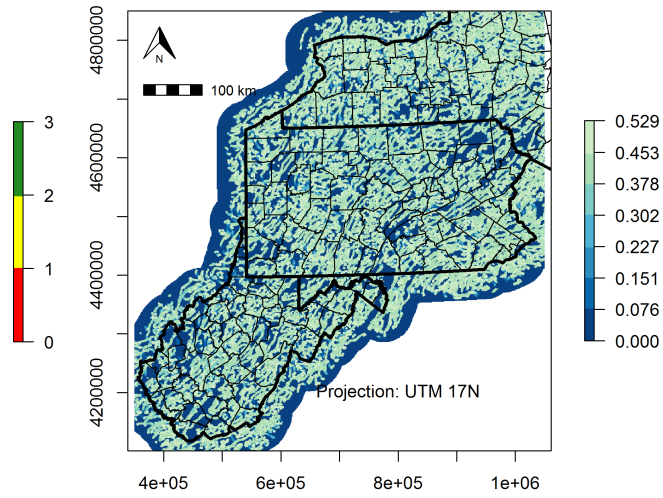
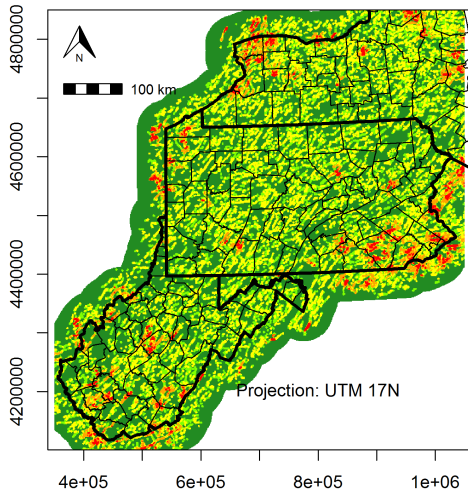


Figure 18. a) Map of the seismic risk factor (averaged stress-based and earthquake proximity-based) with a 3-color scheme. Red areas are unfavorable and green areas are favorable values of the scaled risk factor. b) Map of the standard deviation of the scaled risk factor for averaged seismic risk factor with a 3-color scheme. Dark colors are more certain and light colors are less certain.

A.



B.

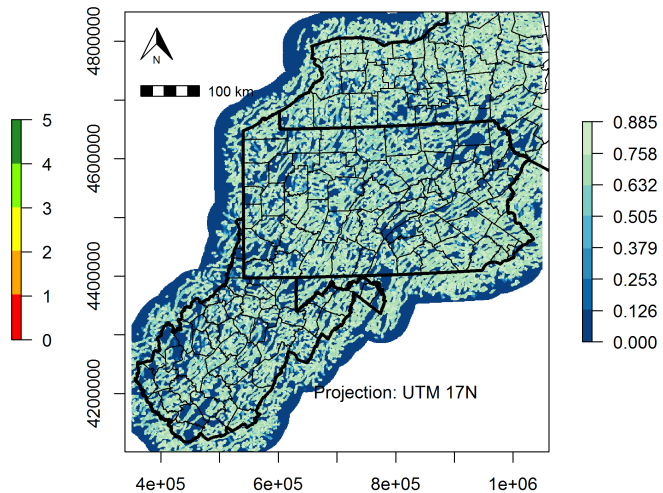


Figure 19. a) Map of the seismic risk factor (averaged stress and earthquake) with a 5-color scheme. Red areas are unfavorable and green areas are favorable values of the scaled risk factor. b) Map of the standard deviation of the scaled risk factor for averaged seismic risk factor with a 5-color scheme. Dark colors are more certain and light colors are less certain.

1.4 Utilization

The utilization risk factor is based on the surface levelized cost of heat (SLCOH, \$/MMBTU),

which was calculated using methods described in the utilization methodology section. The calculations are based on district heating only, not other potential direct-use applications. There were several special considerations. Because this analysis focused on geothermal district heating systems, the communities must be of sufficient size to afford the upfront capital cost associated with the project. Therefore, places with fewer than 4,000 people had the SLCOH set to an arbitrary value, 100 \$/MMBTU, to represent that a district heating system of sufficient size to be of interest for this project would be infeasible for this population.

Occasionally a place with fewer than 4,000 people was located adjacent to a place with enough people such that the sum of the two places was greater than 4,000 people. As a result of this finding, all census places with fewer than 4,000 people were merged with available adjacent places within 100 m. Places were merged until the combined population was greater than or equal to 10,000 people. After a set of places reached 10,000 people, the resulting set only gained those places that were adjacent to it and had populations fewer than 4,000 people.

Our project requires co-location of the utilization location with the reservoirs, but it is reasonable to assume that the utilization location can be a small distance from the location of the reservoir. Therefore, the input utilization map was buffered. All pixels (raster cells) whose center was within 5 km of the center of the middle cell were included in the buffer. The best utilization value (lowest SLCOH) among these cells was assigned to only the center value. Figure 20 shows an example of the cells considered in the calculation.

The 3-color thresholds are based on recommendations from the utilization team, including K. Welcker, Z. Frone, and M. Richards. Based on these values, the 5-color thresholds were assigned. The minimum and maximum values were assigned as well.

Table 4 summarizes the thresholds, Figure 21 gives the histogram of the utilization risk factor (only values less than \$100/MMBTU are plotted), Figures 22 and 23 give the utilization map converted into the 3- and 5-color play fairway scheme without buffering to account for the utilization distance, whereas Figures 24 and 25 illustrate the utilization map with the buffers.

No uncertainty was assigned by the utilization team to their calculations or model prior to these calculations being made.

Table 4: Table of minimum, maximum, and thresholds used in scaling the utilization map. The measure of risk is the surface levelized cost of heat (\$/MMBTU). The scale is reversed because high SLCOH is unfavorable.

Min	25
Max	5
3-Color Thresholds	{13.5,16}
5-Color Thresholds	{12,13.5, 16, 20}

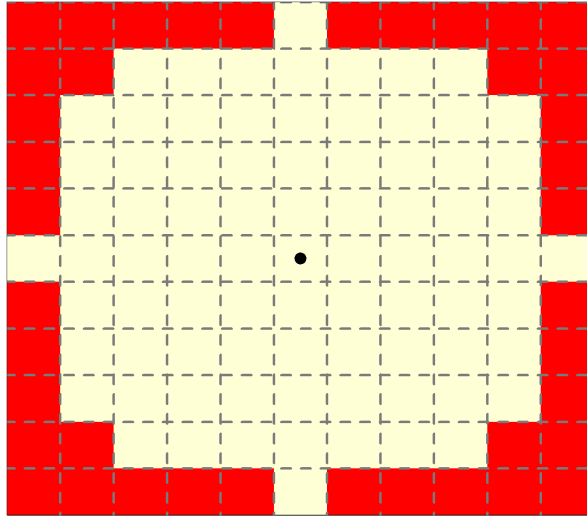


Figure 20. Weighting matrix used when evaluating the best utility for the pixel (raster cell). The maximum of the neighboring pixels within a certain distance is taken (best of cells in yellow). Cells whose center is farther than 5 km from the center (black dot) are not considered and are marked as red.

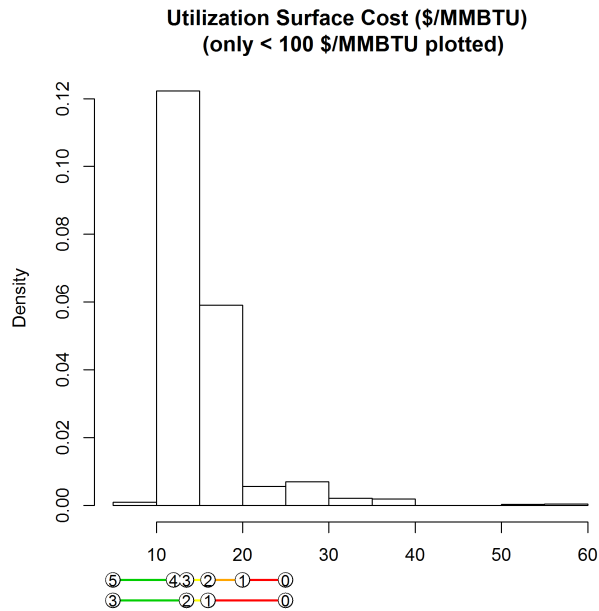


Figure 21. Histogram of the utilization risk factor with the 3- and 5-color thresholds noted. Points beyond the minimum and maximum of the scale are assigned the minimum and maximum of the scale, respectively (e.g. 0, and 3 or 5). Only values less than 100 are plotted to avoid large distortions in the scale. Density is proportional to the frequency or count in the bins, but the values have been rescaled so the total area of the histogram is 1.

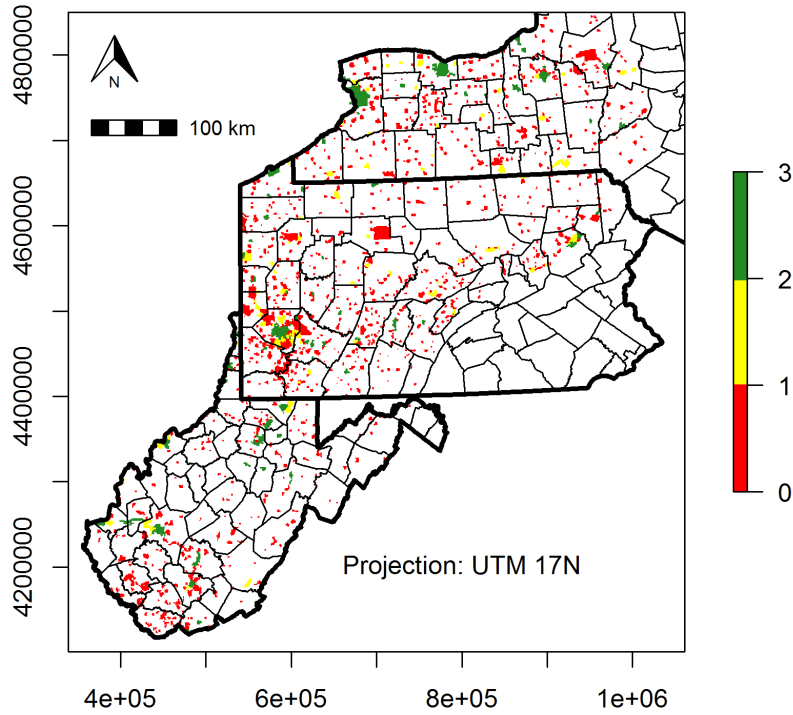


Figure 22. Map of the utilization risk factor with a 3-color scheme with no buffer. Red areas are unfavorable and green areas are favorable values of the scaled risk factor.

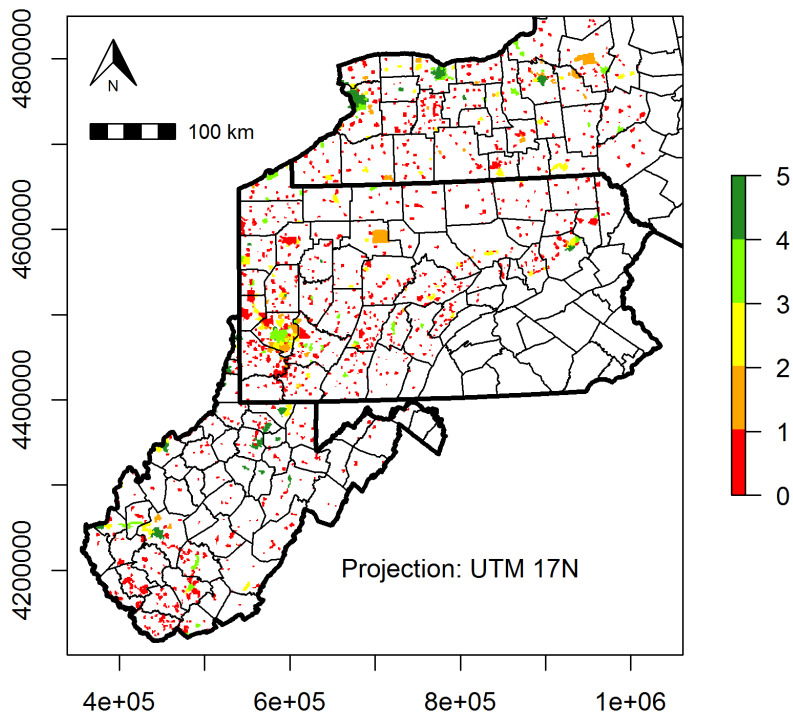


Figure 23. Map of the utilization risk factor with a 5-color scheme with no buffer. Red areas are unfavorable and green areas are favorable values of the scaled risk factor.

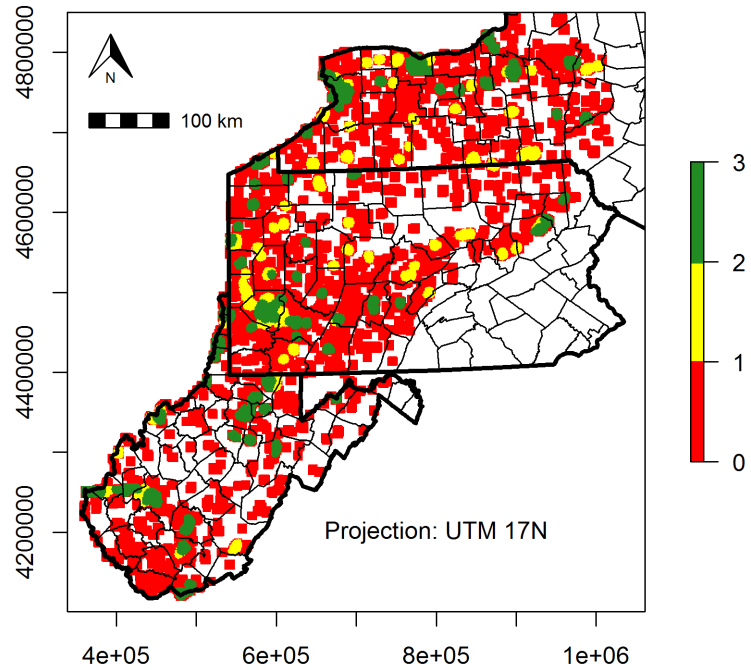


Figure 24. Map of the utilization risk factor with a 3-color scheme with a 5 km radial buffer. Red areas are unfavorable and green areas are favorable values of the scaled risk factor.

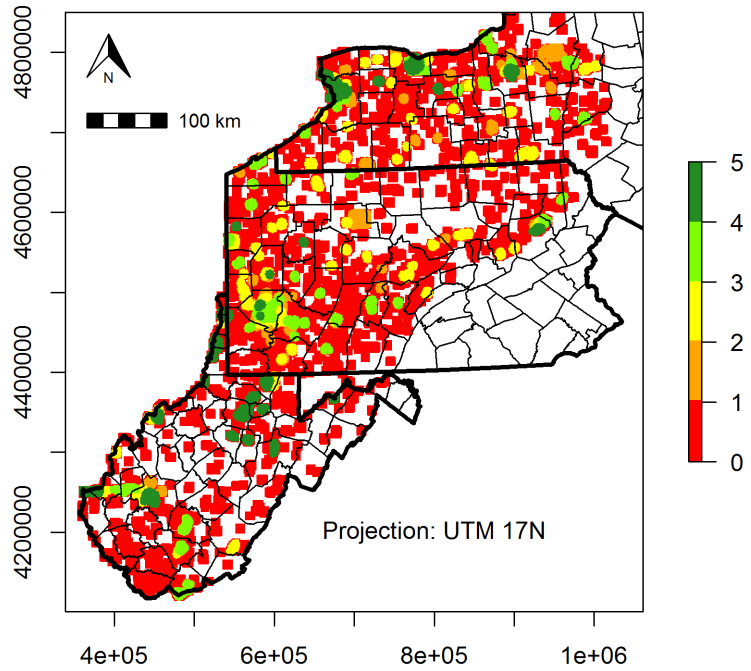


Figure 25. Map of the utilization risk factor with a 5-color scheme with a 5 km radial buffer. Red areas are unfavorable and green areas are favorable values of the scaled risk factor.

2 Combined Risk Factors

The following sections outline extended results for combining risk factors. The results for all risk factors are presented first, followed by geology variables only (no utilization), and then the results without reservoirs (potentially enhanced geothermal systems [EGS]).

2.1 Overview of Three Combinations of Risk

The risk factors can be combined in several ways. We considered taking the average, geometric mean, or minimum value. Equations 3 to 5 show the formulas used, where PFM is the combined play fairway metric, SRF_i is the i^{th} risk factor scaled into the play fairway system (e.g. 0 to 3, or 0 to 5), n is the number of risk factors, and (j, k) is the raster cell location. Areas without a risk factor defined appear as white in the final map, indicating insufficient data to evaluate the PFM at that location.

The following subsections present the results for 3- and 5-color maps for each method of combining the maps (Figures 26-34).

Table 5: Table of thresholds for the different methods of combining risk factors.

Scaling	3-Color	5-Color
Average		
Geometric Mean	{0,1,2,3}	{0, 1, 2, 3, 4, 5}
Minimum		

$$PFM_{avg} = \frac{1}{n} \sum_{i=1}^n SRF_i(j, k) \quad (3)$$

$$PFM_{gm} = \prod_{i=1}^n SRF_i^{1/n}(j, k) \quad (4)$$

$$PFM_{min} = \min\{SRF_1, SRF_2, \dots, SRF_n\}(j, k) \quad (5)$$

2.2 Uncertainty of Risk Factors and Uncertainty for Combined Risk Maps

We are not only interested in the mean value of the play fairway metric, but also the uncertainty. Each group working on a geologic risk factor submitted an uncertainty map. The uncertainty

sometimes is statistically based, and in other cases based on the professional judgment of members in the group. The first objective was to convert the uncertainty in a risk factor into the uncertainty of the scaled risk factor (risk factor converted into the play fairway scheme), and display these results in a map. The second objective was to use the uncertainties in the scaled risk factors to estimate the uncertainty in the combined play fairway metric.

There are two main methods of approximating the variance (uncertainty) of a function given the uncertainty in the inputs: Taylor series approximations and Monte Carlo simulation. Both are used in this analysis of uncertainty.

The Taylor series approximation is given in Equation 6. This equation is used to approximate the uncertainty variance of the PFM at each pixel. Here PFM is the combined play fairway metric (e.g. average or geometric mean), RF_i is the i^{th} risk factor (e.g. thermal or seismic), SRF_i is the i^{th} scaled risk factor (scaled to the play fairway system using the favorability thresholds), $Var(\cdot)$ is a variance, μ_{RF} is the mean value of risk factor RF at the pixel, and n is the number of risk factors. This approach is useful for many applications, but in our case the function used to map RF_i to SRF_i based on the thresholds has many kinks and is often constant over large ranges. The kinks make the partial derivative discontinuous, and the constant areas make the derivative equal to zero; however, we still anticipate some uncertainty in SRF_i . One advantage of the Taylor Series approach is that it could be completed with the existing rasters fairly easily [Note: Equation 6 assumes that there is no covariance between the risk factors].

$$Var(PFM) \approx \sum_{i=1}^n \left[\frac{\partial PFM(\mu_{SRF})}{\partial SRF_i} \right]^2 \left[\frac{\partial SRF_i(\mu_{RF})}{\partial RF_i} \right]^2 Var(RF_i) \quad (6)$$

The Monte Carlo simulation approach to calculating the variance of the PFM is to generate a random sample from the distribution of each risk factor at a pixel (raster cell) and then calculate the variance of the resulting distribution of the PFM. In principle this should be more accurate, but using a separate Monte Carlo trial for each pixel becomes challenging computationally. This approach is also limited in accuracy by the distribution (e.g. normal, lognormal) used to generate replicates (random values) of each risk factor.

We used a hybrid procedure that used both Taylor Series and Monte Carlo analysis to quantify the uncertainty in PFM_{avg} and PFM_{gm} . The uncertainty addressed with this method was only based on the mean (typical value) and uncertainty (variance, coefficient of variation) of the risk factors and not based on propagating uncertainty in variables used to calculate each risk factor. Table 6 shows the risk factor model (left-most column) that was the source of the uncertainty, the method used to estimate the uncertainty, the assumed distribution of the data, and the assumed distribution model for the Monte Carlo analysis of scaled risk factors.

In order to evaluate the uncertainty variance in the scaled risk factors (SRFs), we built an interpolation table of the SRF variance. This interpolation table was referenced by the mean (rows) and uncertainty (columns) of the unscaled RFs. The interpolation table mean values and uncertainty values were based on the range (minimum to maximum over the region) of inputs for the unscaled RF of interest. A separate interpolation table was made for each RF. The resolution

in each table was at least 13% of the range in each dimension. 100,000 replicates were used to build the interpolation table. Next, based on the mean and uncertainty of each unscaled RF at each pixel in the map, we linearly interpolated in the table for the uncertainty values of the RF to estimate the resulting variance of the SRF, $Var(SRF)$. Next, we used the Taylor series approximation in equation 7 to quickly approximate the variance in each PFM based on the Taylor series expansion, where PFM_{gm} and PFM_{avg} were substituted for PFM. The computations for the geometric mean were done in log space (described below), and the computations for the average were done in real space.

Table 6: Risk factor uncertainties and distributions used in propagating uncertainty in the combined risk analysis. The uncertainties can arise from several sources. The right most column provides the distributions used in the Monte Carlo analysis described in the uncertainty analysis section.

SRF Uncertainty source	Uncertainty Estimation	Distribution	SRF Uncertainty Model
Thermal			
Spatial Interpolation	Kriging Standard Error	normal	normal
Reservoirs			
Permeability (κ)	Expert Judgment	log-normal	log-normal
Thickness (η)	Expert Judgment	triangular	
Viscosity (μ)	Expert Judgment	normal	
Area Factor (f_a)	Expert Judgment	triangular	
Seismic based on Stress Field and Edge Orientations			
Stress Map Interpolation and Edge Orientation	From Resolution of Data	von Mises	folded normal
Seismic Based on Earthquake Proximity to Edges			
Hypocenter Location Error	Typical Error from Catalog	normal	normal
Utilization			
Approximations of Piping and Network and other Infrastructure	Professional Judgment	normal	normal

$$Var(PFM) \approx \sum_{i=1}^n \left[\frac{\partial PFM(\mu_{SRF})}{\partial SRF_i} \right]^2 Var(\widehat{SRF}_i) \quad (7)$$

The uncertainty is expressed as the standard deviation for the average of all the risk factors in Figures 27d, e, f and 28d, e, f.

The expansion of the geometric mean could be completed either in terms of PFM_{gm} (real-space) or $\ln(PFM_{gm})$ (log-space). Both have advantages and disadvantages. In real-space, the variances of the SRFs are always defined, but for small values of the geometric

mean (close to zero) the expansion becomes undefined or unstable. In log-space, the variance of the SRFs is not defined if the distribution of the variable includes any real-space zeros; however, in log-space the geometric mean is a simple average and the variance of an average of independent uncertainties is just the sum of the variances with their weights squared.

We used a log-space method for the geometric mean, and in our Monte Carlo analysis we also generated the variance of the logarithms of the four SRFs. To avoid issues of undefined log-space variances, if any generated value of a SRF was less than 0.2 in the Monte Carlo analysis, it was set to 0.2. Such areas will likely not be of great interest because they have low favorability, and it allowed the analysis to proceed. Because seismic was the average of two factors, the log-space variance was estimated from a Taylor series expansion based on the real-space variance of those two factors. To avoid numerical problems, when the average of the seismic variables was less than 0.2 the average was set to 0.2. After developing the log-space variance of the geometric mean, it was transformed to real-space using a Taylor series.

The uncertainty expressed as standard deviation for the combination of all the risk factors by geometric mean is displayed in Figure 30d, e, f and 31d, e, f.

The uncertainty in the minimum of several random variables (risk factors) is more complicated. The variance of the minimum should not be approximated using the Taylor series equations above. The minimum function is very poorly approximated by the Taylor series if the risk factor that defines the minimum is not always the same (e.g. always utilization). As a result of this complication, we opted to Monte Carlo the uncertainty of the minimum using the same distributions for each RF as provided in Table 6. We used 10,000 replicates for computational time savings relative to 100,000 replicates. We also only made minimum uncertainty maps for the 5 color scheme for computational time savings.

The uncertainty expressed as standard deviation for the combination of all the risk factors by minimum is displayed in Figure 34d, e, f.

2.3 All Risk Factors Combined

This subsection gives the results for combining all four risk factors. The results are given for combinations based on the average, the geometric mean, and the minimum of the individual risk factors. For each combination function, histograms of the distribution of combined play fairway metric values are also provided.

2.3.1 Average

The following results are for averaging the individual risk factors. The thresholds are given in Table 5. Figure 26 shows the histograms (specific to RPIw as the reservoir metric) for the 5-color map. Figures 27 and 28 show the 3- and 5-color maps, respectively, for all combinations of four categories of risk factors, solved three times to utilize the three different reservoir metrics.

Average of All Risk Factors with RPIw for Reservoirs

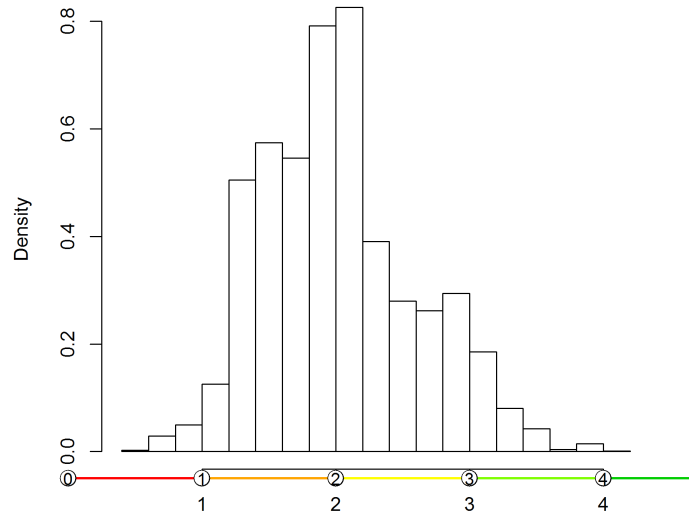


Figure 26. Histogram of the combined risk metric for RPIw as the reservoir metric using an average with 5-color schemes. Density is proportional to the frequency or count in the bins, but the values have been rescaled so the total area of the histogram is 1.

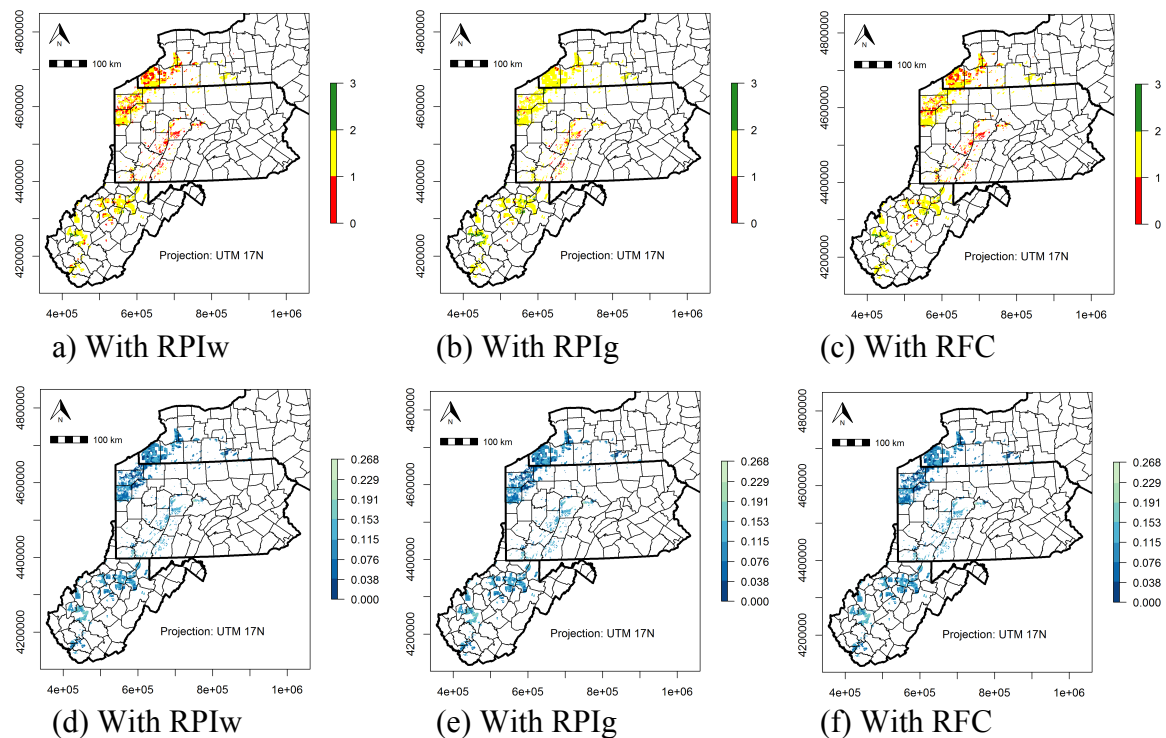


Figure 27. Maps of the combined risk with a 3-color scheme using averaging. Red areas are unfavorable and green areas are favorable values of the play fairway metric. a) For reservoir quality described by RPIw. b) For reservoir quality described by RPIg. c) For reservoir quality described by RFC. d) Standard deviation on the average of all four individual risk categories, using RPIw as the reservoir quality metric. e) Standard deviation on the average of all categories, using RPIg as the reservoir quality metric. f) Standard deviation on the average of all categories, using RFC as the reservoir quality metric.

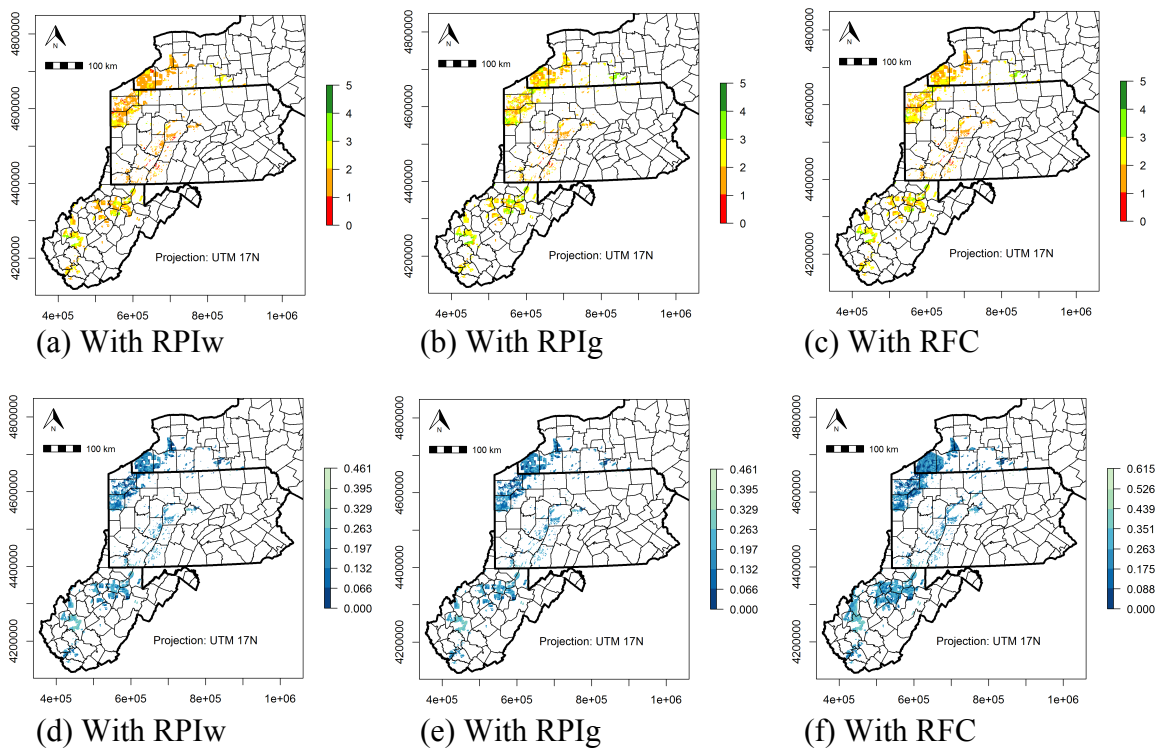


Figure 28. Maps of the combined risk with a 5-color scheme using the average. Red areas are unfavorable and green areas are favorable values of the play fairway metric. a) For reservoir quality described by RPIw. b) For reservoir quality described by RPIg. c) For reservoir quality described by RFC. d) Standard deviation on the average of all four individual risk categories, using RPIw as the reservoir quality metric. e) Standard deviation on the average of all categories, using RPIg as the reservoir quality metric. f) Standard deviation on the average of all categories, using RFC as the reservoir quality metric.

2.3.2 Geometric Mean

The following results are for taking the geometric mean of the risk factors. The thresholds are given in Table 5. The histogram for the 5-color map (specific to RPIw as the reservoir metric) is given in Figure 29, and the 3- and 5-color maps for all three reservoir metrics are given in Figures 30 and 31, respectively. The geometric mean of the four categories of risk is shown three times, once for each of the choices of reservoir metrics. Note that there is a large portion of the data at zero mainly because the utilization values gave many zeros, which set the geometric mean to zero.

**Geometric Mean of All Risk Factors
with RPIw for Reservoirs**

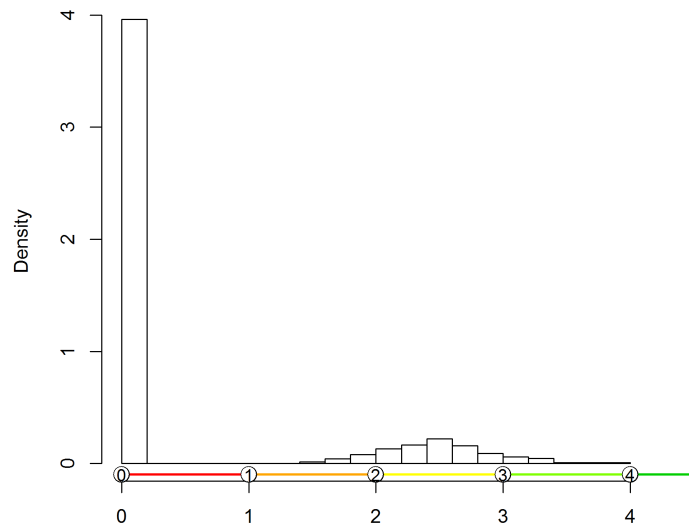


Figure 29. Histogram of the combined risk metric for RPIw as the reservoir metric using a geometric mean with the 5-color schemes. Density is proportional to the frequency or count in the bins, but the values have been rescaled so the total area of the histogram is 1.

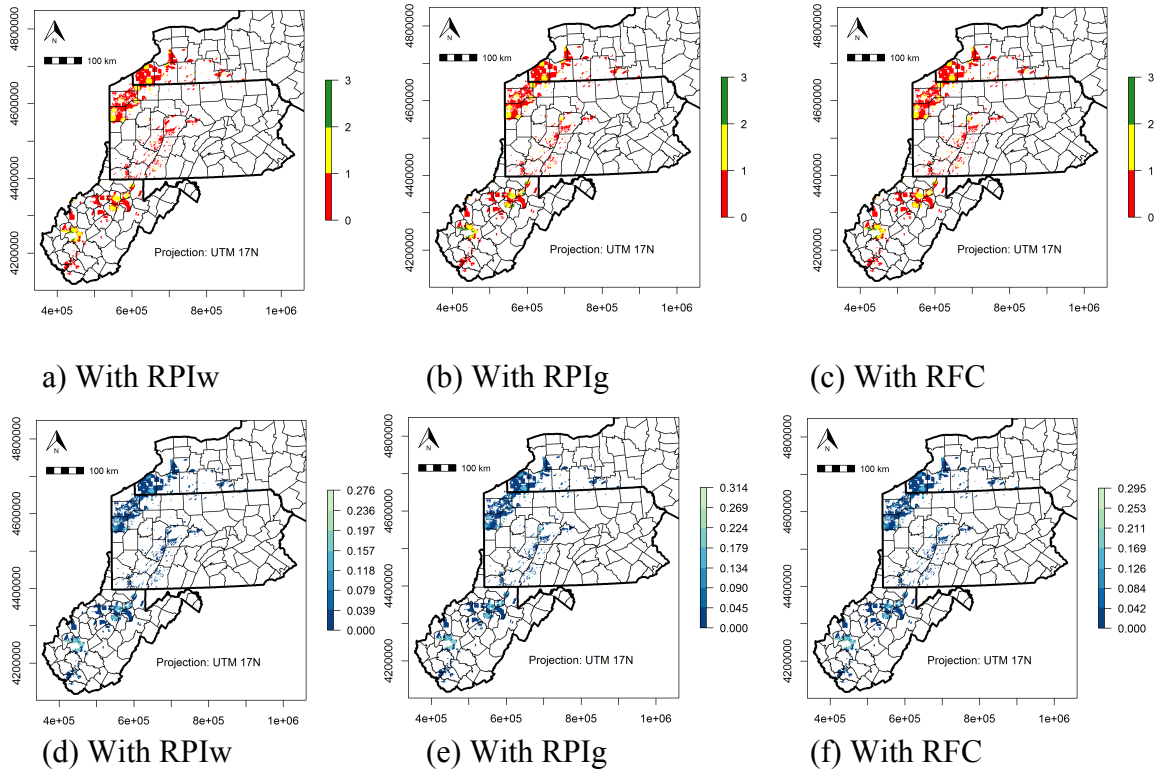


Figure 30. Map of the combined risk map with a 3-color scheme using geometric mean. Red areas are unfavorable and green areas are favorable values of the play fairway metric. a) For reservoir quality described by RPIw. b) For reservoir quality described by RPIg. c) For reservoir quality described by RFC. d) Standard deviation on the geometric mean of all categories, using RPIw as the reservoir quality metric. e) Standard deviation on the geometric mean of all categories, using RPIg as the reservoir quality metric. f) Standard deviation on the geometric mean of all categories, using RFC as the reservoir quality metric.

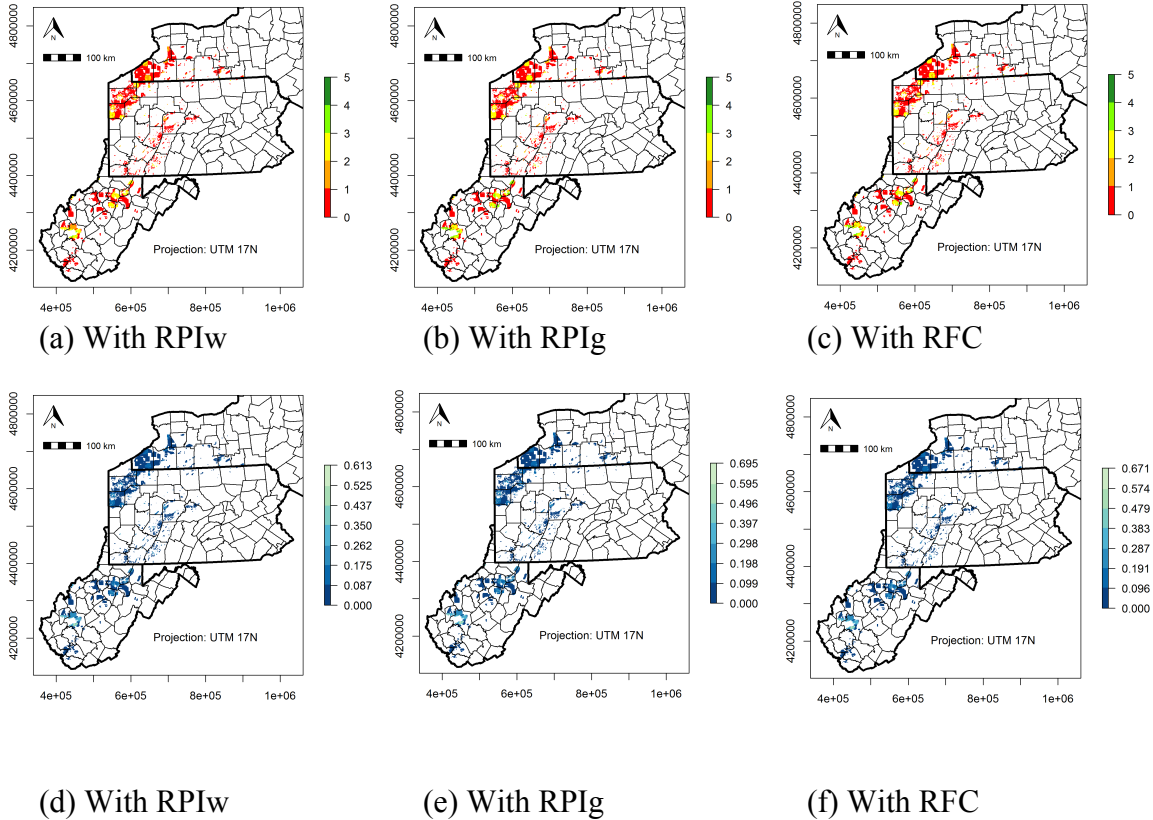


Figure 31. Maps of the combined risk with a 5-color scheme using geometric mean. Red areas are unfavorable and green areas are favorable values of the play fairway metric. a) For reservoir quality described by RPIw. b) For reservoir quality described by RPIg. c) For reservoir quality described by RFC. d) Standard deviation on the geometric mean of all categories, using RPIw as the reservoir quality metric. e) Standard deviation on the geometric mean of all categories, using RPIg as the reservoir quality metric. f) Standard deviation on the geometric mean of all categories, using RFC as the reservoir quality metric.

2.3.3 Minimum

The following results are for taking the minimum of the risk factors. The thresholds are given in Table 5. The thresholds are based on the original scale of the colors, so green would mean that the lowest risk metric is green at that location (very good). Because of the choice of scale, the area is dominated by reds. Figure 32 plots the histogram for the 5-color map (specific to RPIw as the reservoir metric). Figures 33 and 34 plot the 3- and 5-color maps, respectively, of the combined risk of the four risk factors, solved three times to utilize each of the reservoir metrics. The large number of zeros is because many of the utilization locations did not meet the requirement of 4,000 people, so they had the high SLCOH assigned, which in turn means that their scaled risk factor value was zero.

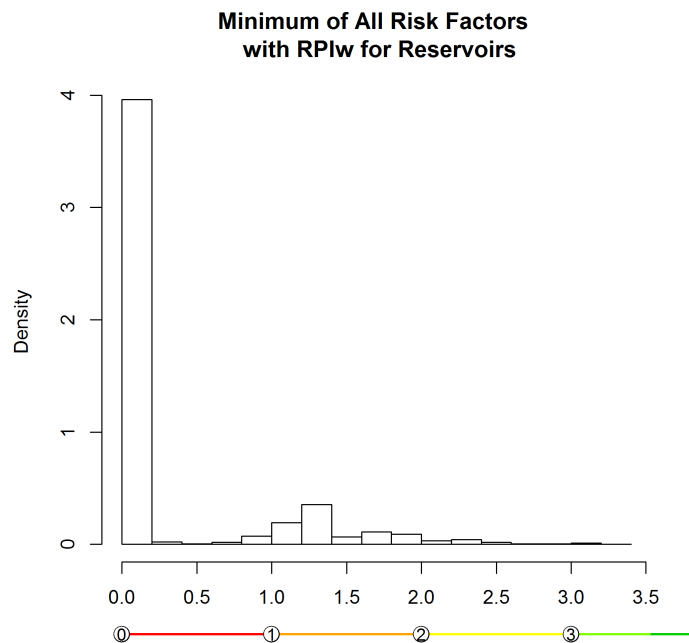


Figure 32. Histogram of the combined risk metric for RPIw as the reservoir metric, for a combination based on using a minimum, with the 5-color schemes. Density is proportional to the frequency or count in the bins, but the values have been rescaled so the total area of the histogram is 1.

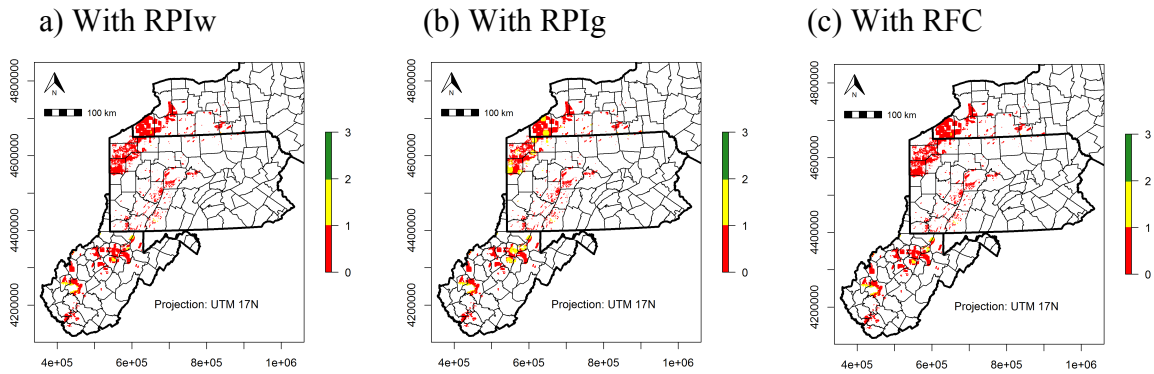


Figure 33. Map of the combined risk map with a 3-color scheme using minimums. Red areas are unfavorable and green areas are favorable values of the play fairway metric. a) For reservoir quality described by RPIw. b) For reservoir quality described by RPIg. c) For reservoir quality described by RFC.

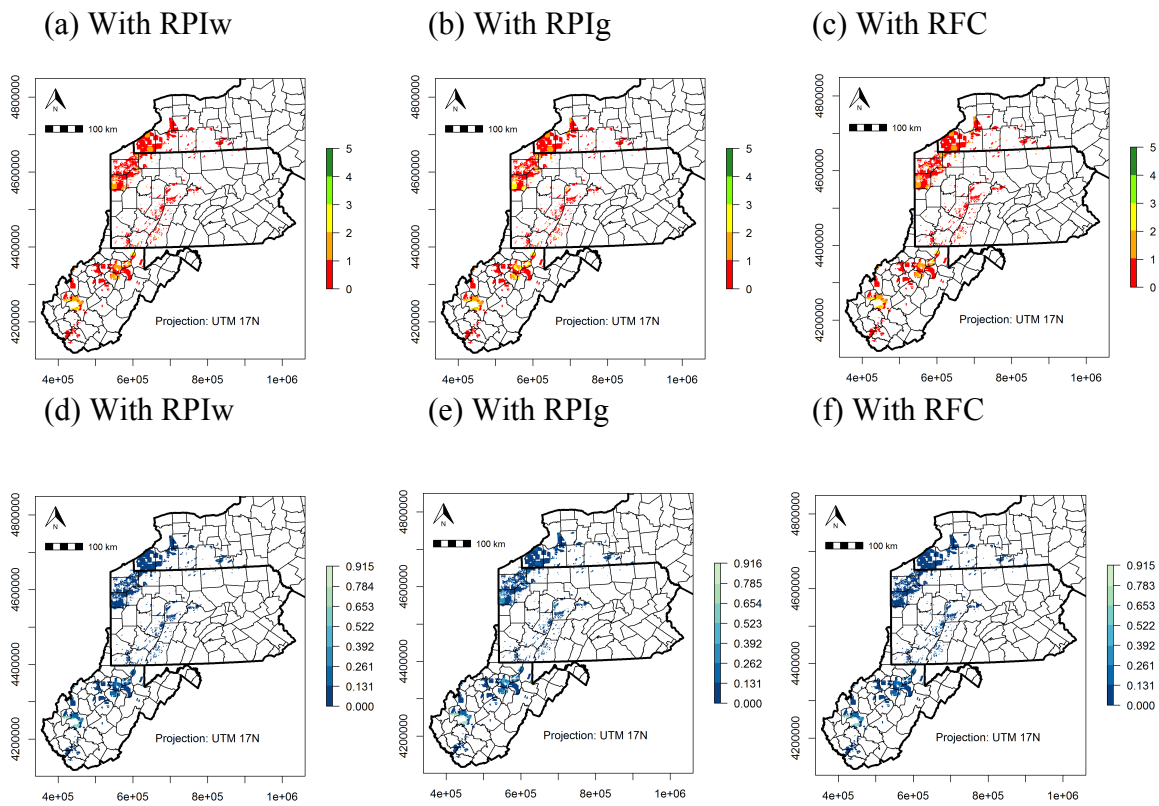


Figure 34. Maps of the combined risk with a 5-color scheme combined based on minimums. Red areas are unfavorable and green areas are favorable values of the play fairway metric. a) For reservoir quality described by RPIw. b) For reservoir quality described by RPIg. c) For reservoir quality described by RFC. d) Standard deviation on the minimum of all categories, using RPIw as the reservoir quality metric. e) Standard deviation on the minimum of all categories, using RPIg as the reservoir quality metric. f) Standard deviation on the minimum of all categories, using RFC as the reservoir quality metric.

2.4 Geology Only

This section presents the results for combining the three risk categories that relate to geology only. No utilization factor is included. Furthermore, only the natural properties of the reservoir rather than the design of a well field and extraction process are to be included, thus RFC is the reservoir metric used. This would represent the best areas to develop the resources independent of the current location of population centers and the engineering design of an extraction project. The results are given for combinations based on the average, the geometric mean, and the minimum of the three individual risk factors. For each combination function, histograms of the distribution of combined play fairway metric values are also provided.

2.4.1 Average

The following results are for averaging the geologic risk factors. The thresholds are given in Table 5. Figure 35 shows the histogram for the 5-color map of the resulting metric, and Figures 36 and 37 show the 3- and 5-color maps, respectively.

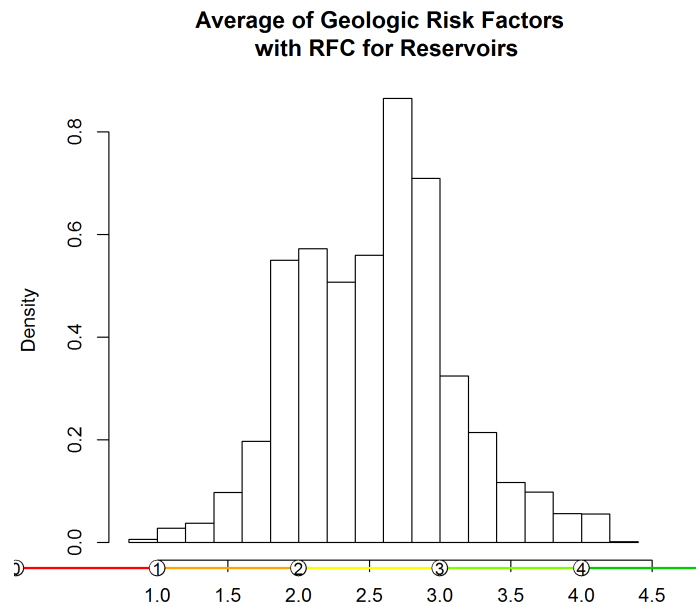


Figure 35. Histograms of the combined risk metric using an average with the 5-color scheme for geology only. Density is proportional to the frequency or count in the bins, but the values have been rescaled so the total area of the histogram is 1.

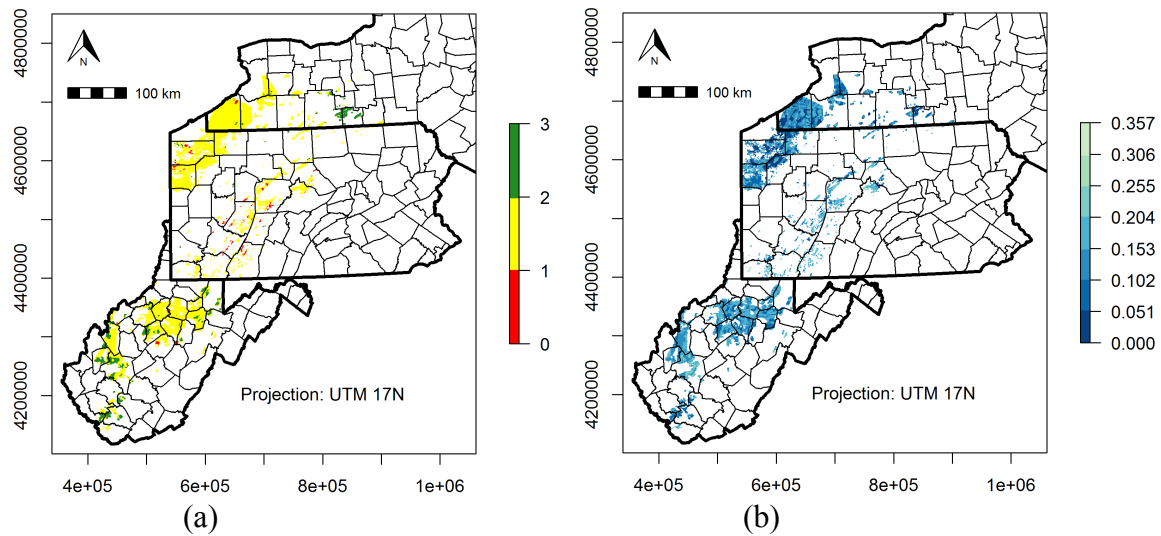


Figure 36. a) Map of the combined risk with a 3-color scheme using an average for geology only, and using RFC as the reservoir quality metric. Red areas are unfavorable and green areas are favorable values of the play fairway metric. b) Map of the standard deviation of the uncertainty related to computing the combined risk by averaging. Dark tones indicate a high degree of certainty, and light tones a low degree of certainty.

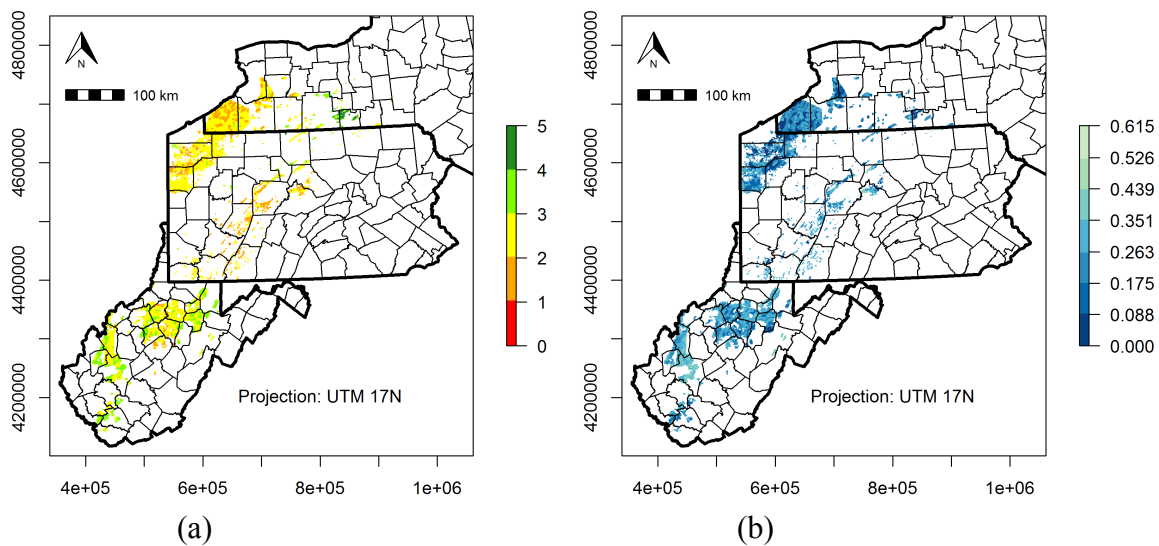


Figure 37. a) Map of the combined risk with a 5-color scheme using an average for geology only, and using RFC as the reservoir quality metric. Red areas are unfavorable and green areas are favorable values of the play fairway metric. b) Standard deviation on the average of the three geological categories, using RFC as the reservoir quality metric. Dark tones indicate a high degree of certainty, and light tones a low degree of certainty.

2.4.2 Geometric Mean

The following results are for taking the geometric mean of the risk factors. The thresholds are given in Table 5. The histogram for the 5-color map is given in Figure 38 and the 3- and 5-color maps are given in Figures 39 and 40, respectively.

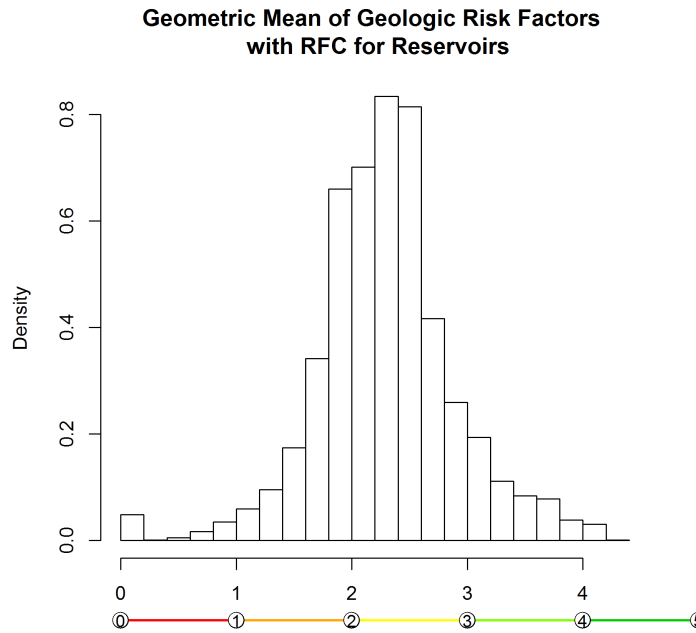


Figure 38. Histogram of the combined risk metric using a geometric mean with the 5-color scheme for geology only. Density is proportional to the frequency or count in the bins, but the values have been rescaled so the total area of the histogram is 1.

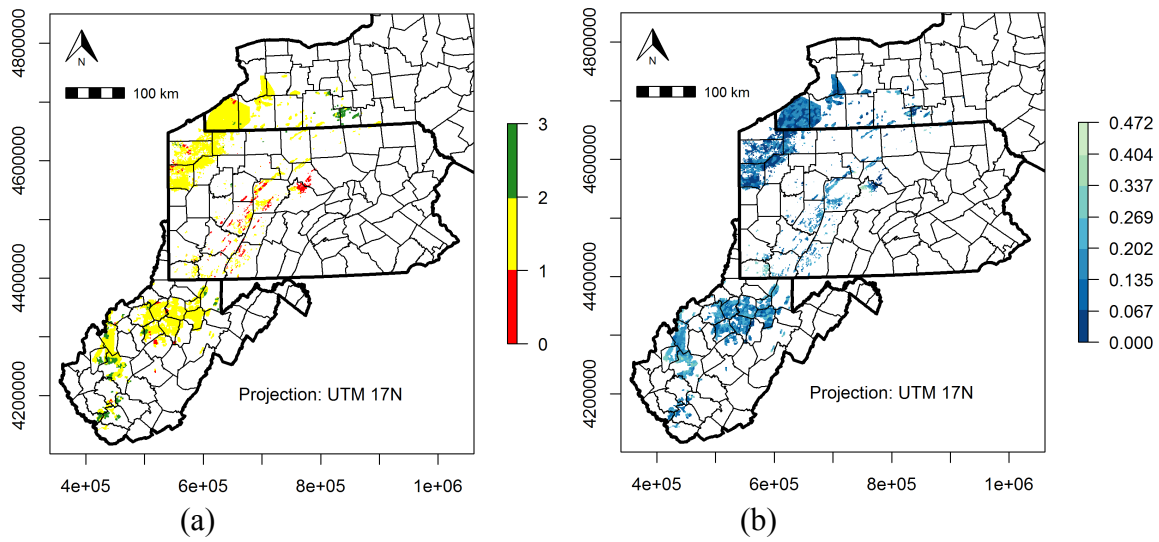


Figure 39. a) Map of the combined risk with a 3-color scheme using a geometric mean for geology only, and using RFC as the reservoir quality metric. Red areas are unfavorable and green areas are favorable values of the play fairway metric. b) Map of the standard deviation of the uncertainty based on a combination by geometric mean. Dark tones indicate a high degree of certainty, and light tones a low degree of certainty.

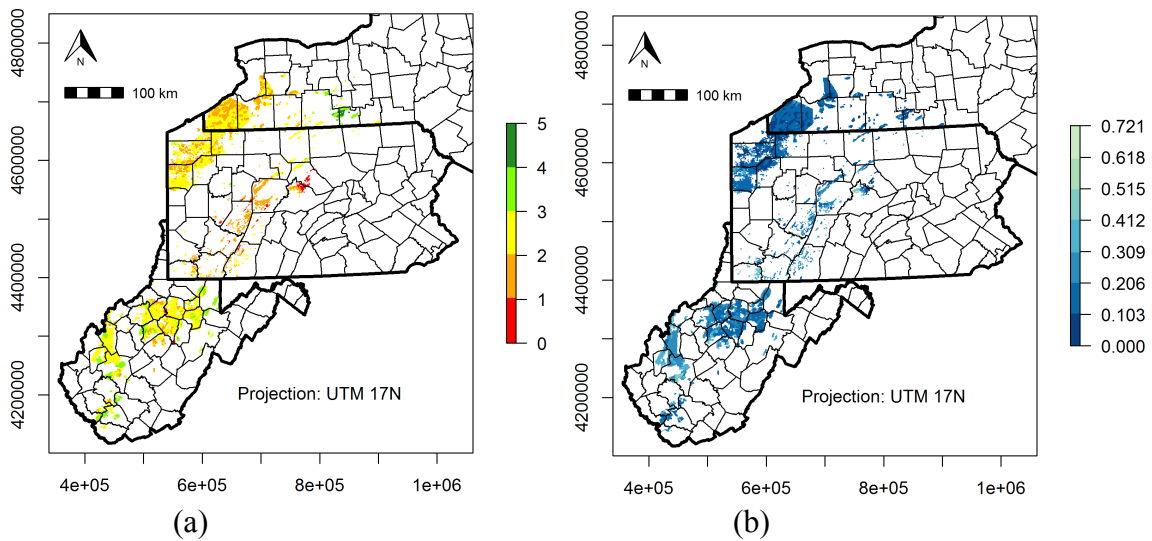


Figure 40. a) Map of the combined risk with a 5-color scheme using minimum for geology only, and using RFC as the reservoir quality metric. Red areas are unfavorable and green areas are favorable values of the play fairway metric. b) Standard deviation on the minimum of the three geological categories, using RFC as the reservoir quality metric. Dark tones indicate a high degree of certainty, and light tones a low degree of certainty.

2.4.3 Minimum

The following results are for taking the minimum of the risk factors. The thresholds are given in Table 5. The thresholds are based on the original scale of the colors, so green would mean that the lowest risk metric is green at that location (very good). Because of the choice of scale, the area is dominated by reds. Figure 41 plots the histogram for the 5-color map and Figures 42 and 43 plot the 3- and 5-color maps, respectively.

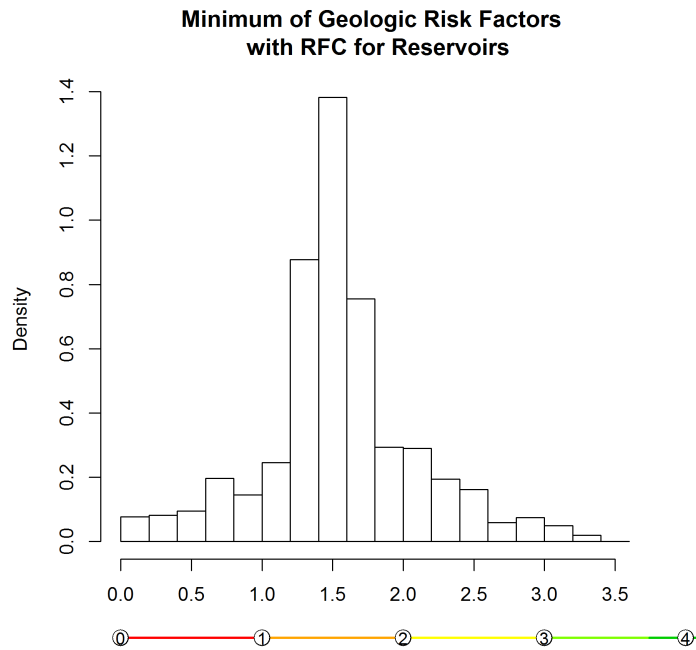


Figure 41. Histogram of the combined risk metric using a minimum with the 5-color scheme for geology only. Density is proportional to the frequency or count in the bins, but the values have been rescaled so the total area of the histogram is 1.

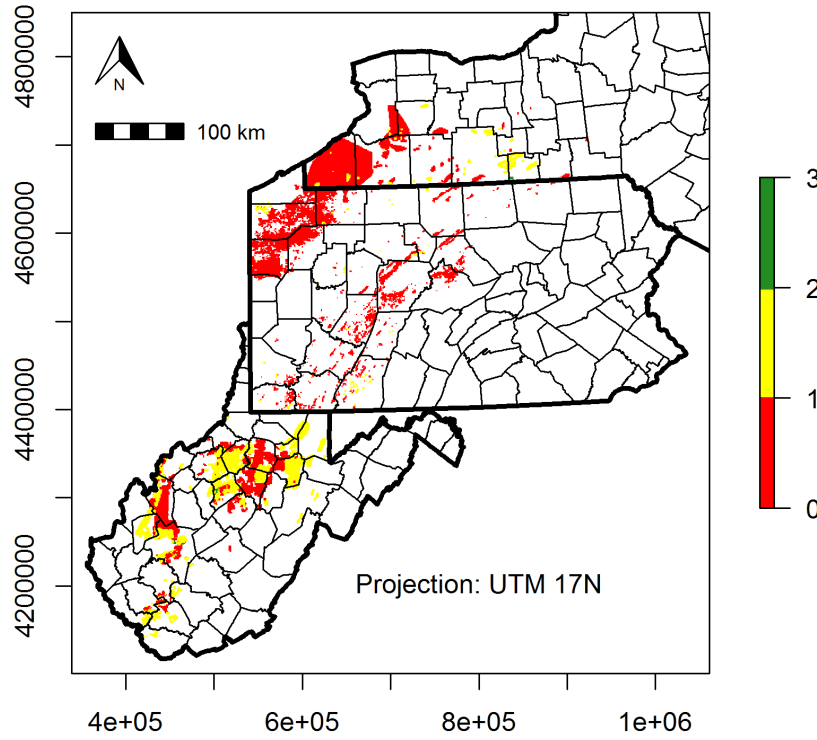


Figure 42. Map of the combined risk map with a 3-color scheme using minimums for geology only, and using RFC as the reservoir quality metric. Red areas are unfavorable and green areas are favorable values of the play fairway metric.

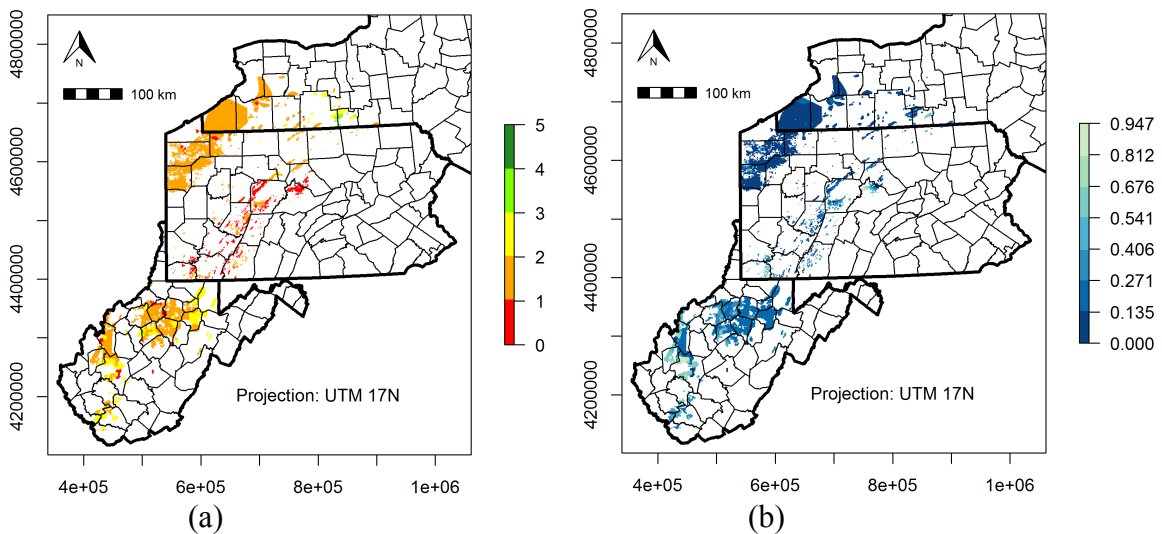


Figure 43. a) Map of the combined risk map with a 5-color scheme using minimums for geology only, and using RFC as the reservoir quality metric. Red areas are unfavorable and green areas are favorable values of the play fairway metric. b) Standard deviation on the minimum of the three geological categories, using RFC as the reservoir quality metric. Dark tones indicate a high degree of certainty, and light tones a low degree of certainty.

2.5. No Reservoirs

This section presents the results for combining three categories of risk (thermal, utilization, induced seismicity) but omitting reservoirs. This analysis is intended to inform consideration of the regional variability of opportunities for enhanced geothermal systems (EGS), in which a reservoir is produced by engineering rather than provided by natural conditions. The results are given for combinations based on the average, the geometric mean, and the minimum of the individual risk factors. For each combination function, histograms of the distribution of combined play fairway metric values are also provided.

2.5.1. Average

The following results are for averaging the three risk factors. The thresholds are given in Table 5. Figure 44 shows the histograms for the 3- and 5-color maps, respectively, of the resulting metric and Figures 45 and 46 show the 3- and 5-color maps, respectively.

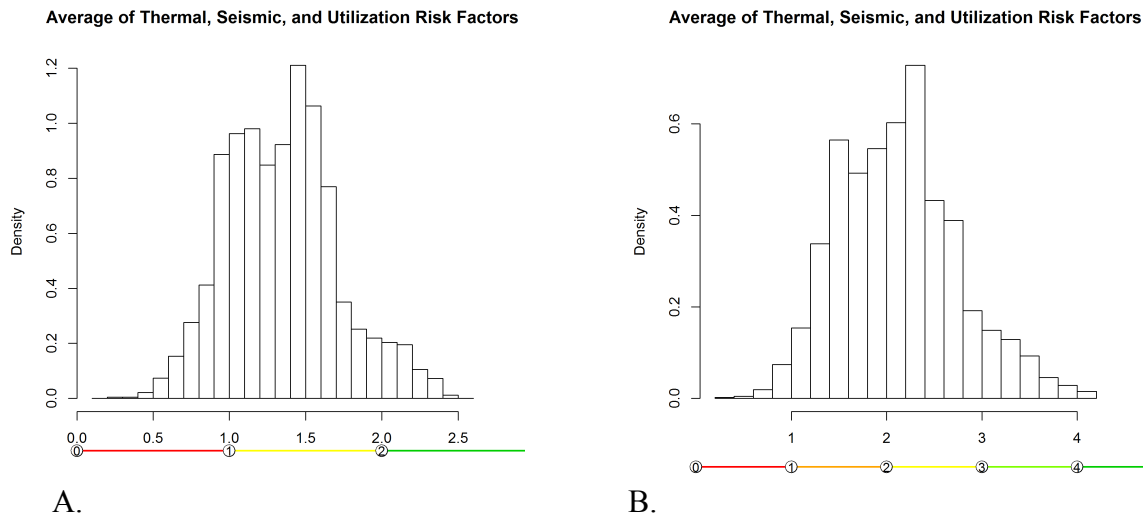


Figure 44. Histograms of the combined risk metric using an average with a) 3- and b) 5-color schemes for the thermal, seismic and utilization risk factors (no natural reservoirs). Density is proportional to the frequency or count in the bins, but the values have been rescaled so the total area of the histogram is 1.

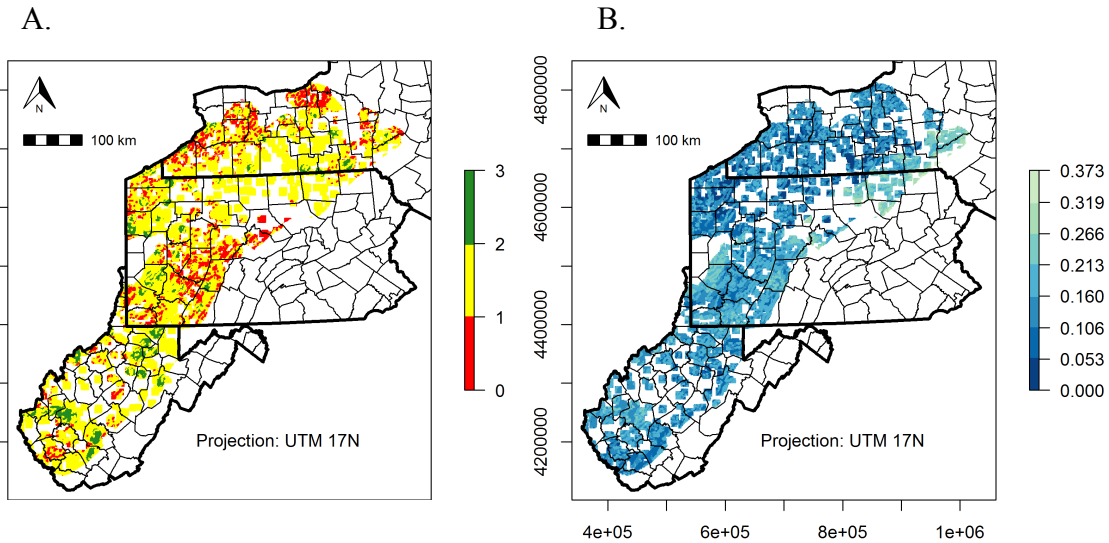


Figure 45. a) Map of the combined risk map with a 3-color scheme using an average for all risk factors except natural reservoirs. Red areas are unfavorable and green areas are favorable values of the play fairway metric. b) Map of the standard deviation of the combined risk computed by averaging. Dark tones indicate a high degree of certainty, and light tones a low degree of certainty.

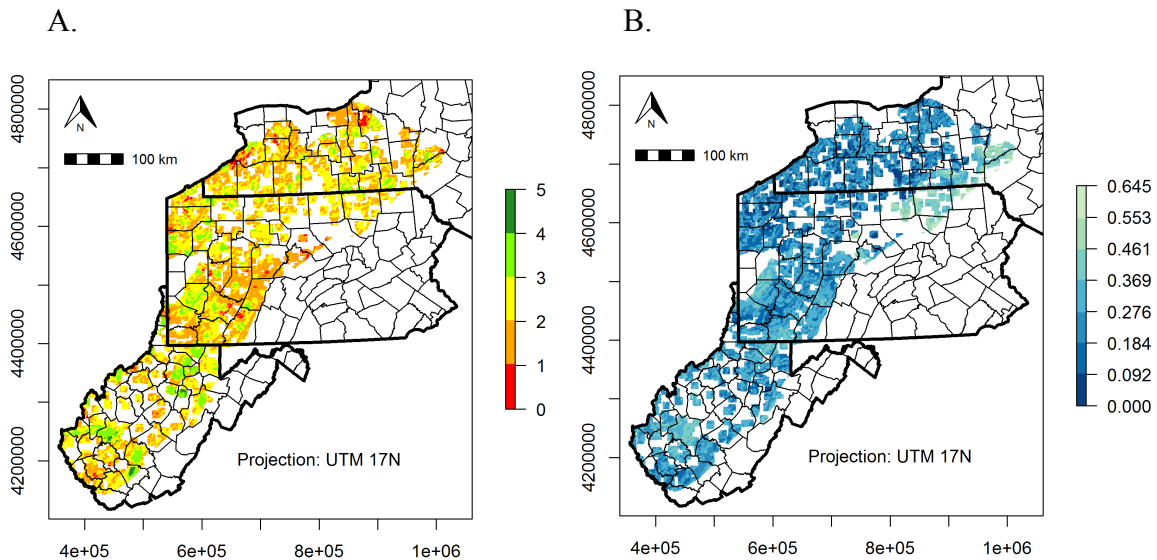


Figure 46. a) Map of the combined risk map with a 5-color scheme using an average for all risk factors except natural reservoirs. Red areas are unfavorable and green areas are favorable values of the play fairway metric. b) Map of the standard deviation of the combined risk computed by averaging. Dark tones indicate a high degree of certainty, and light tones a low degree of certainty.

2.5.2 Geometric Mean

The following results are for taking the geometric mean of the risk factors. The thresholds are given in Table 5. The histograms for the 3- and 5-color maps are given in Figure 47 and the 3- and 5-color maps are given in Figures 48 and 49, respectively.

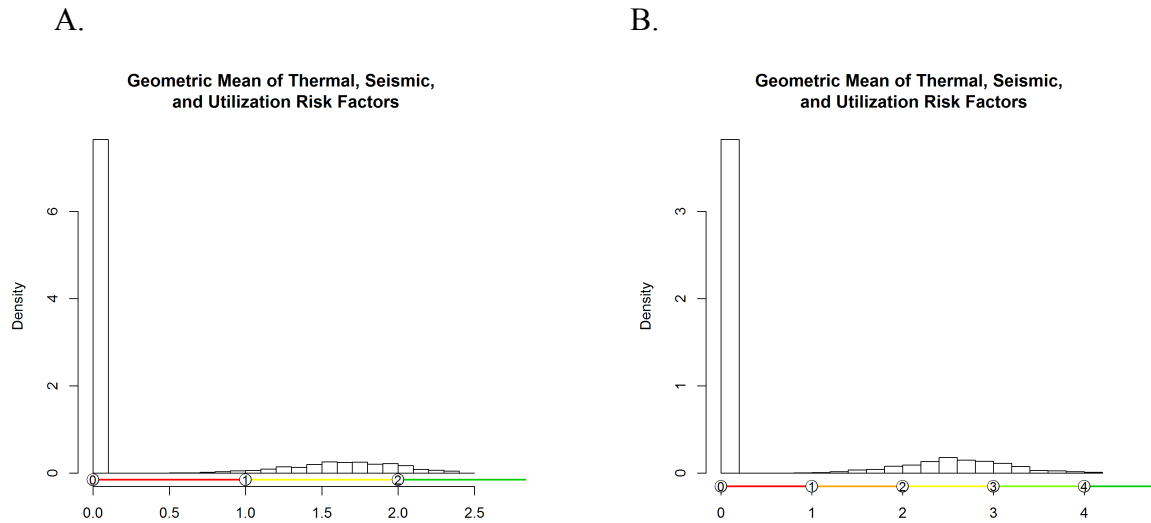


Figure 47. Histograms of the combined risk metric using a geometric mean with a) 3- and b) 5-color schemes for all risk factors except natural reservoirs. Density is proportional to the frequency or count in the bins, but the values have been rescaled so the total area of the histogram is 1.

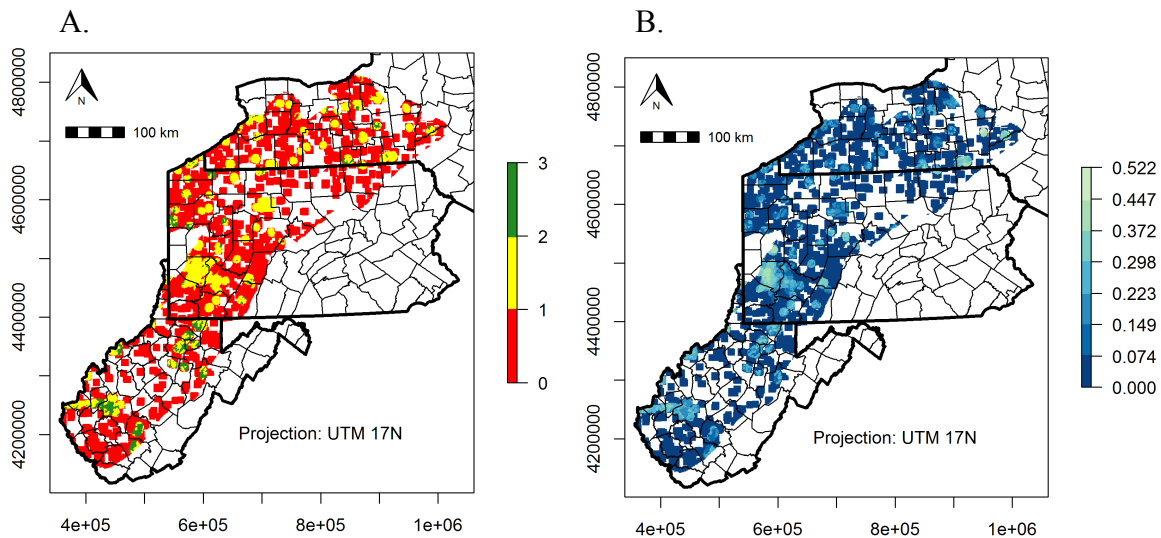


Figure 48. a) Map of the combined risk map with a 3-color scheme using a geometric mean of all risk factors except natural reservoirs. Red areas are unfavorable and green areas are favorable values of the play fairway metric. b) Map of the standard deviation of the combined risk computed using the geometric mean. Dark tones indicate a high degree of certainty, and light tones a low degree of certainty.

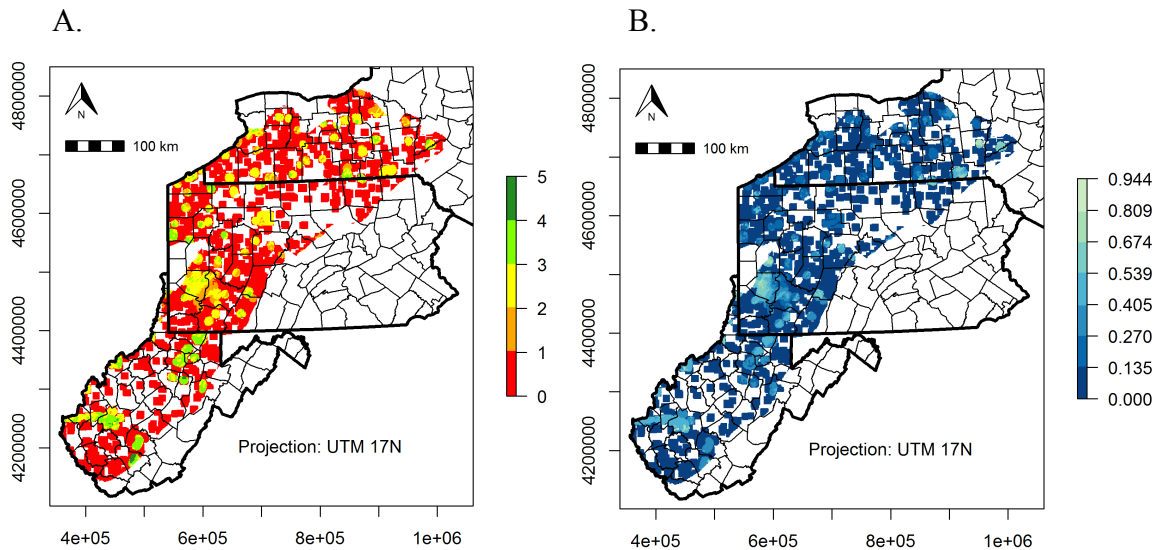


Figure 49. a) Map of the combined risk map with a 5-color scheme using a geometric mean of all risk factors except natural reservoirs. Red areas are unfavorable and green areas are favorable values of the play fairway metric. b) Map of the standard deviation of the combined risk computed using the geometric mean. Dark tones indicate a high degree of certainty, and light tones a low degree of certainty.

2.5.3 Minimum

The following results are for creating the Play Fairway Metric by taking the minimum of the three non-reservoir risk factors. The thresholds are given in Table 5. The thresholds are based on the original scale of the colors, so green would mean that the lowest risk metric is green at that location (very good). Because of the choice of scale, the area is dominated by reds. Figure 50 plots the histograms for the 3- and 5-color maps and

Figure 51 presents the 3- and 5-color maps. The large number of zeros is because many of the utilization locations did not meet the requirement of 4,000 people, so they had the high SLCOH assigned, which in turn means that their scaled risk factor value was zero.

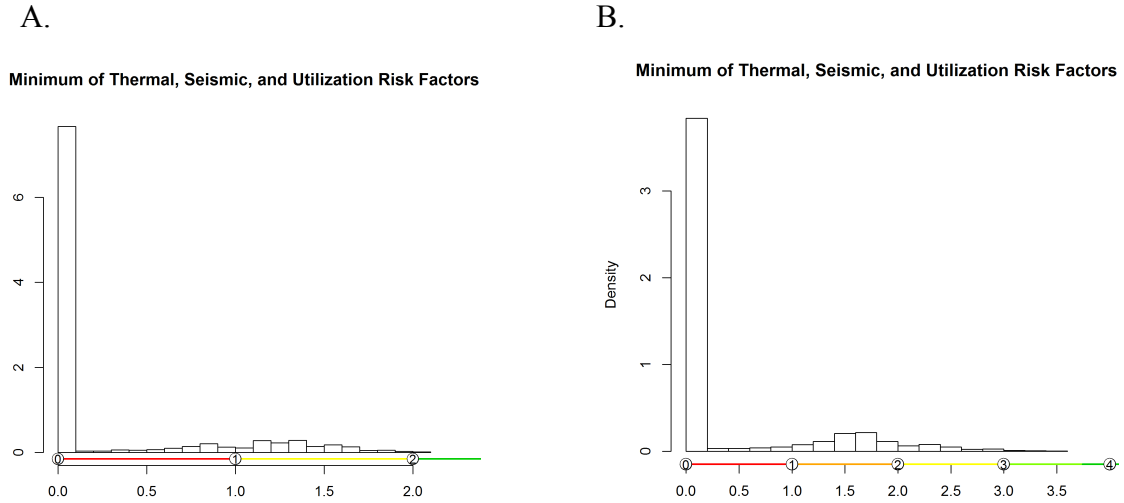


Figure 50. Histograms of the combined risk metric using a minimum with 3- and 5-color schemes for all risk factors except reservoirs. Density is proportional to the frequency or count in the bins, but the values have been rescaled so the total area of the histogram is 1.

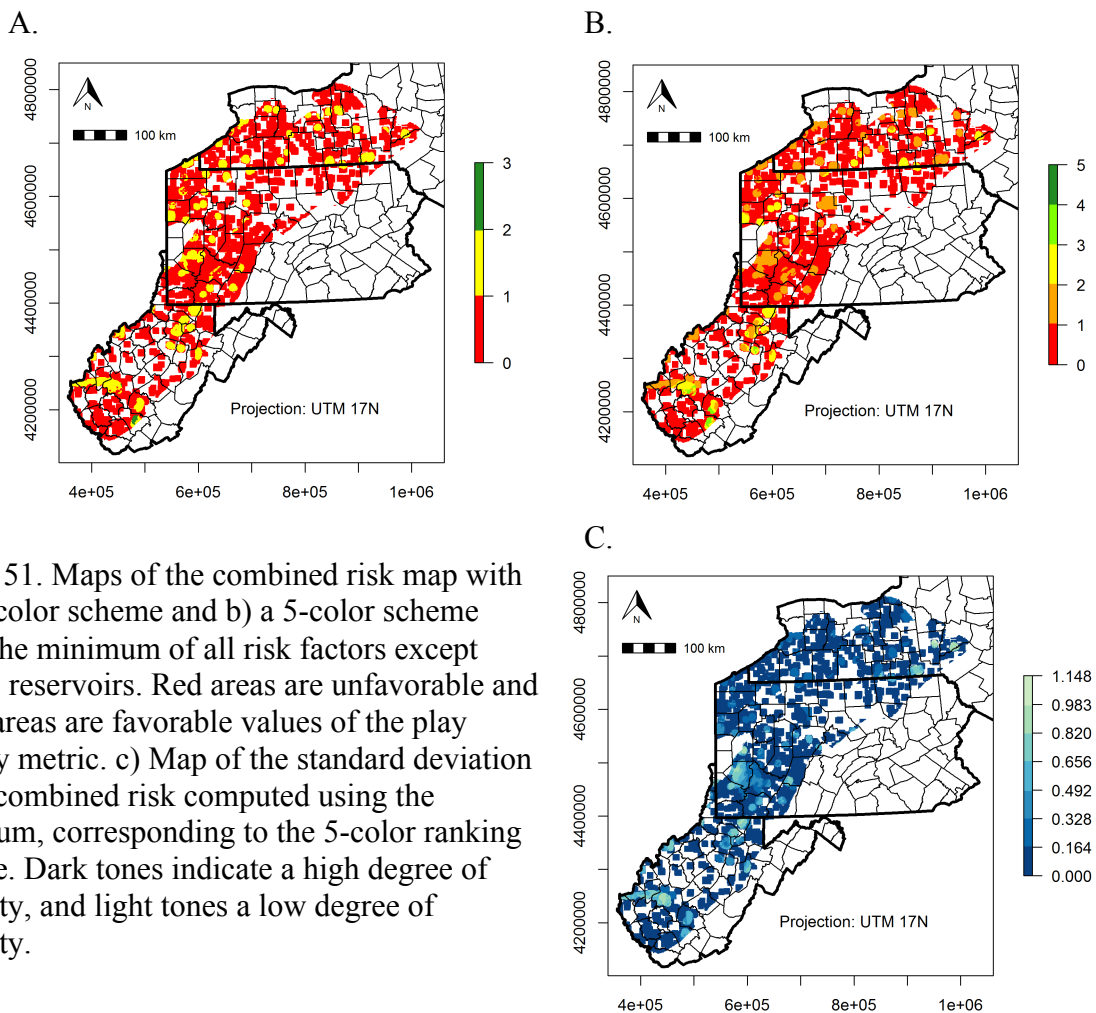


Figure 51. Maps of the combined risk map with a) a 3-color scheme and b) a 5-color scheme using the minimum of all risk factors except natural reservoirs. Red areas are unfavorable and green areas are favorable values of the play fairway metric. c) Map of the standard deviation of the combined risk computed using the minimum, corresponding to the 5-color ranking scheme. Dark tones indicate a high degree of certainty, and light tones a low degree of certainty.

3 Robustness of Combining Functions

It is not clear which method of combining the risk factors is best. Therefore, the consistency of the different methods of combining the risk factors should be investigated. If the methods are fairly similar, then locations with a high value for the average should also have a high value for the geometric mean, for example. The locations of US Census places were found and then the 5-color average, geometric mean, and minimum PFMs were sampled at those locations using the function *extract* from the Raster package in R. The combined play fairway metrics were for the 5-color scheme. Figure 57 plots the comparison of the metrics, provided that all points had all risk factors defined and the minimum value was greater than zero (105 total points).

Generally, the metrics seem to match fairly well provided that all of the values are greater than zero. This could be a reasonable indication that the metrics would tend to give the same relative rankings. The coloring scheme is discrete, so the maps could look significantly different even if the relative rankings are the same.

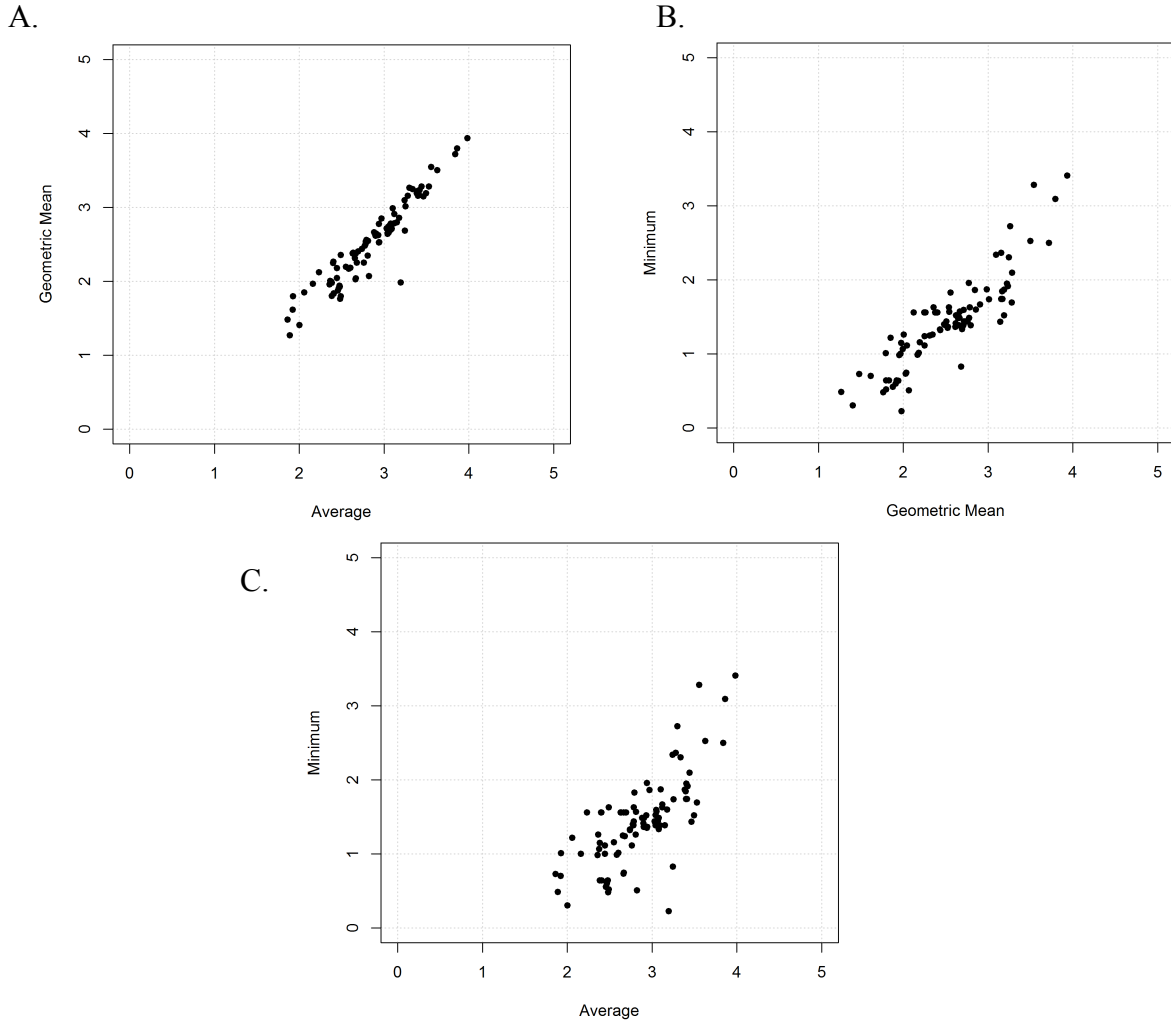


Figure 53. Scatter plots comparing the play fairway metric for the three different functions (average, geometric mean, minimum) when combining all four risk factors for areas with non-zero utilization scaled risk factor values. (a) Compares the geometric mean to the average. (b) Compares the minimum to the geometric mean. (c) Compares the minimum to the average.

4 Potential Project Locations

In addition to the maps, we can also consider a specific set of project locations and show the risk factors in more detail for these sites. Locations selected for this scrutiny are listed in Table 7, selected mainly because the geological factors are fairly favorable with a reasonable population or other special demand for heat.

The processing used to obtain values was that the values at the center of each raster cell were obtained using the *extract* function in the R package 'raster'. The raster was defined on the UTM 17N projection. The locations of each place in Table 7 were converted into the NAD83, UTM17N projection, and the distance between each of the raster cell centers and the project

locations was calculated. Next, the cells within 10 km of the project locations were considered as representing reasonable locations near the project location. The maximum value of the combined risk map of all four risk factors was used to select the values for the project location. If multiple sites had the same value, the site with the smallest variance was selected. If multiple sites had the same variance, the site closest to the project location was selected.

Figures 54 and 55 plot the combined metrics by the average method and their uncertainty for these locations. The uncertainty for the geologic risk factor combination using RFC as the reservoir metric is represented by boxplots (Figure 54). These are a representation of the data that indicate the center and general spread of the data. The distributions of the geologic risk factors are also illustrated as violin plots for the average, geometric mean, and minimum combination method (Figure 55). There are clear differences in the symmetry and spread of the distributions among sites, and also for each metric. The geometric mean and the minimum plots have long lower tails as a result of zeros.

Figure 56 is a parallel axis plot of the project locations. The lines are color-coded by location. This plot illustrates that there can be trade-offs between locations, so a more favorable value in one risk factor might mean you have to accept a less favorable value in another.

Table 7. Sites selected for location-specific examination

Town/City/Area	State
Corning/Elmira	NY
Jamestown	NY
Mansfield College	PA
Meadsville	PA
Sayre	PA
Charlestown	WV
Morgantown	WV
Pineville	WV

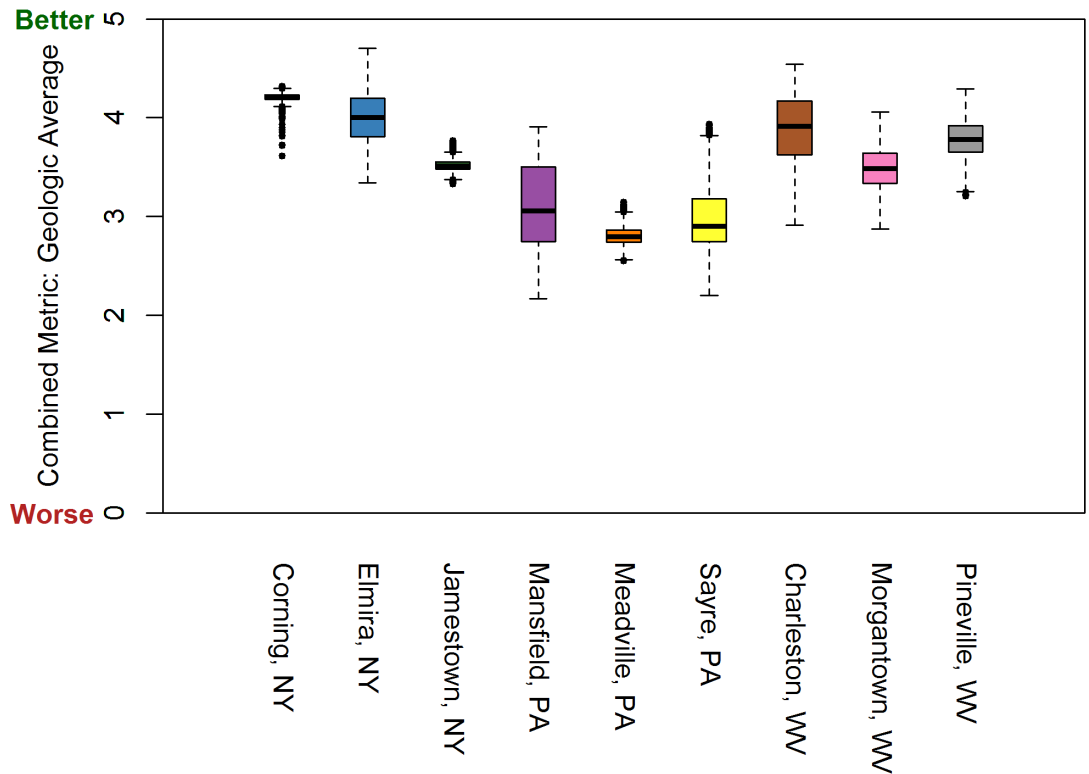


Figure 54. Boxplots showing the Monte Carlo distribution of the combined play fairway metric (PFM) for the average of the geologic risk factors, using RFC as the reservoir metric. The box extends from the 25th to 75th percentiles with a line at the median. The whiskers extend to the most extreme point that is within 1.5 times the interquartile range (25th to 75th percentiles distance). Points beyond the whiskers are plotted individually. High values are favorable.

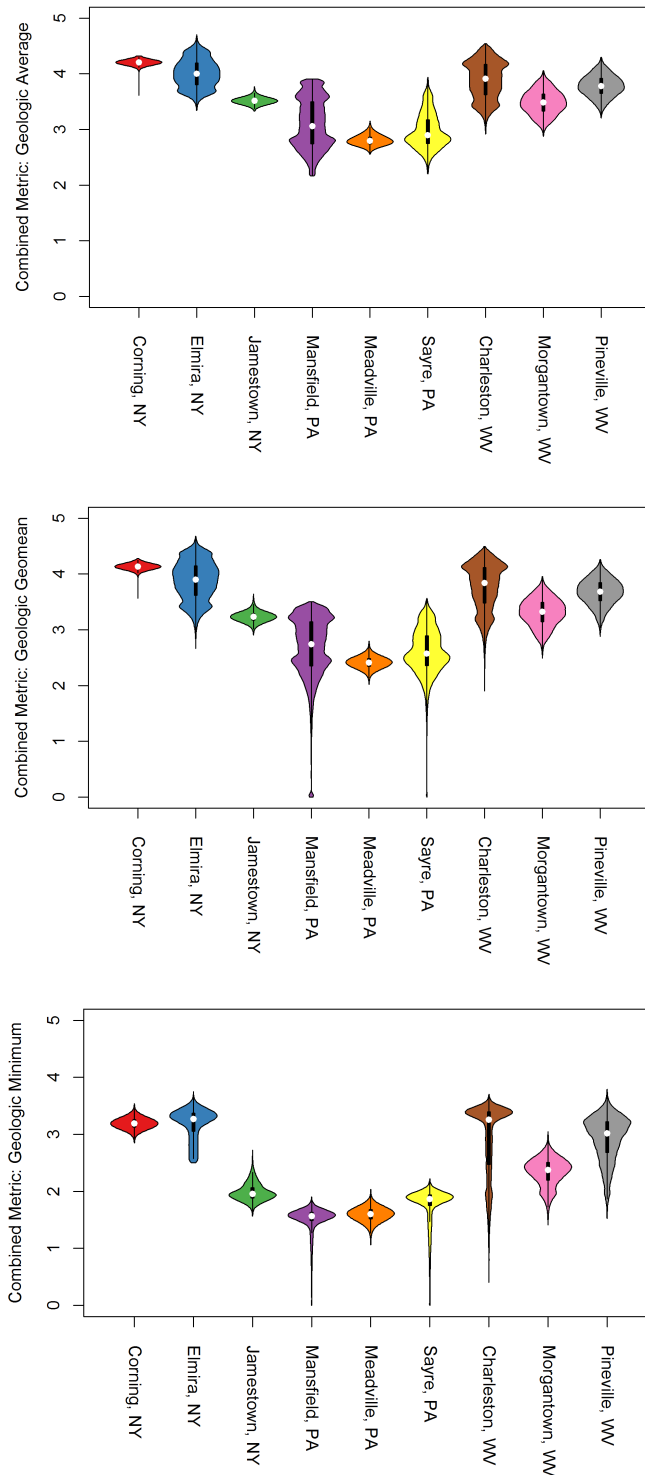


Figure 55. Violin plots showing the Monte Carlo distribution of the combined play fairway metric (PFM) for the average (top) geometric mean (middle) and minimum (bottom) of the geologic risk factors, using RFC as the reservoir metric. The violins show a smoothed density function of the data. The interior of the violins is a boxplot with a white circle at the median. High values are favorable.

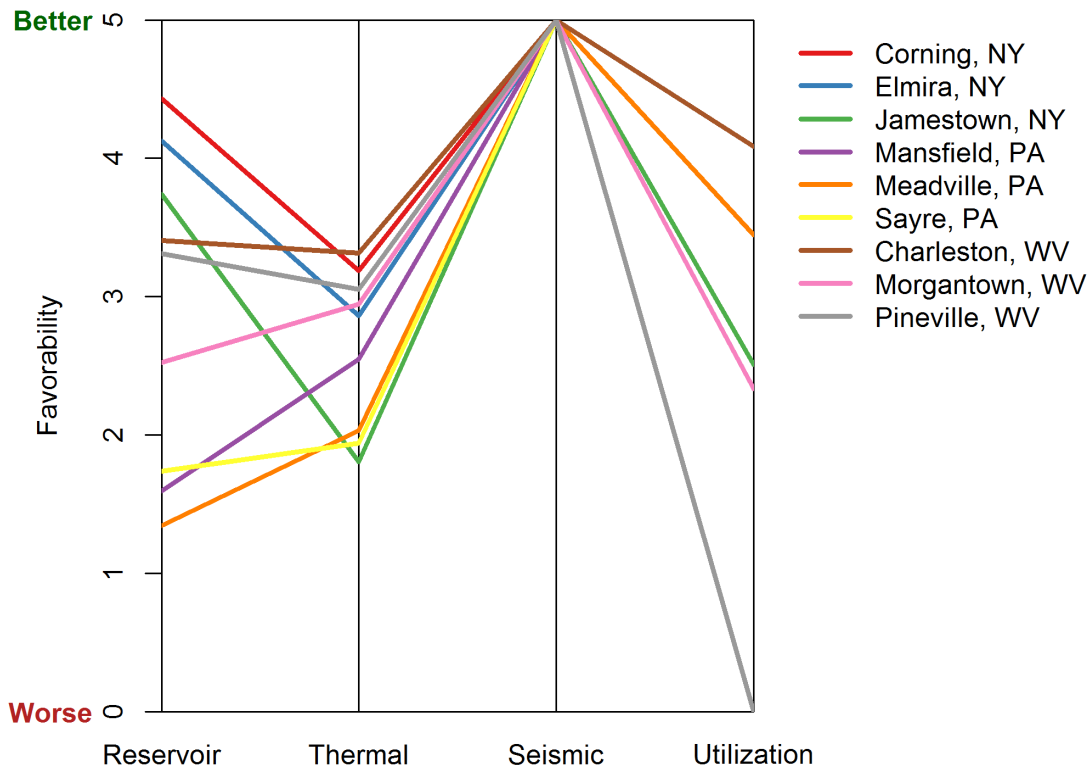


Figure 56. Parallel axis plot for nine illustrative site locations. The reservoir metric illustrated is RFC and the risk factor combination method is the average. The lines are color-coded by location. High values are favorable and low values are unfavorable.

5 References cited

Whealton, C. A., 2016, Statistical Data Analysis, Global Sensitivity Analysis, and Uncertainty Propagation Applied to Evaluating Geothermal Energy in the Appalachian Basin: Cornell University, Ithaca, NY, USA, Ph.D. dissertation, 250 pp.

Memo 18: Permits for Geothermal District Heating Project in GPFA-AB

Memo on Permits for Geothermal District Heating Project

Before we start the permitting process at the state or local level during Phase 2, it will be important for us to begin discussing our projects at a local level to educate the public on the project and more broadly on geothermal energy, geothermal district heating, and how these compare/contrast to geothermal heat pump applications and oil and gas production. Marian Higgins' PhD research (TAMU, December 2015) in Matagorda County, Texas, observed that geothermal energy development was received more favorably if the local community understood the expectations and had an opportunity to ask questions and discuss concerns (Figure 1). There are currently only geothermal heat pumps in use in New York, Pennsylvania and West Virginia. These three States do not yet have established laws on the geothermal mineral right for larger projects such as geothermal district heating or electrical generation from a geothermal reservoir that utilizes former and gas fields. Therefore, an effort to establish and lead grassroots discussions to educate the public about higher temperature geothermal consumption, and include the concerns about drilling, injection, building codes, etc. will be necessary in order to alleviate the potential for negative campaigns as is occurring related to hydraulic fracturing. This effort will be part of the effort of the Phase 2 permitting team's time and expenses.

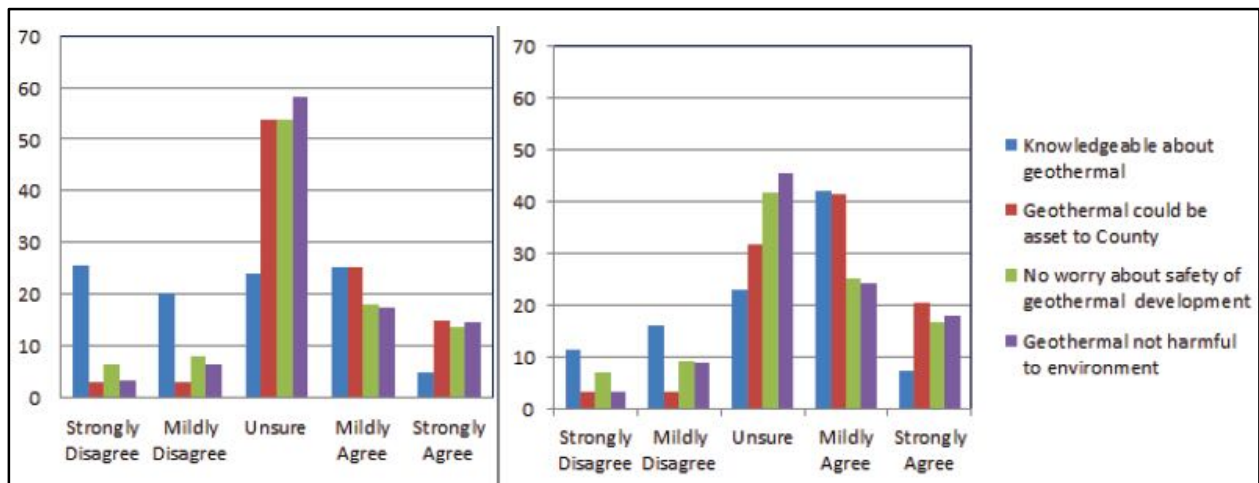


Figure 1. Charts showing the opinions of citizens in Matagorda County, Texas at *beginning* and *end* of grassroots effort to educate them on possible geothermal projects (Higgins, SMU Power Plays Conference, 2015).

During Phase 2 of this project, a combination of Federal, State and Local permits will be required for any new wells we plan to drill. Permits are also required for performing tests of an existing well. Local contractors with existing permits for entering an oil/gas well will be hired to perform these tests, thus reducing the permitting timeline, and reducing out-of-pocket expenses for permits.

Additional permits will be necessary during Phase 3 of the project. When we are working on a site to convert it over to geothermal district heating, there will be building and plumbing permits required. The

owner of the property will most likely be the entity who applies for these related permits. Being aware of all the permits required from start to end of a project, regardless of who is responsible for their submission, will be important to keep the development on a tight timeline for us to complete it within the timeframe of the DOE allocations.

This memo reviews the permitting process starting with the Federal Government permits and then outlines the permits for each of the three States. There are many overlapping requirements between the Federal and State permits. Considerable work will be needed to keep track of all the different forms and requirements, along with the timelines and fees associated with each permit.

Federal Permits

Geothermal projects may be subject to the following Federal Laws:

- National Environmental Policy Act (NEPA)
- Clean Air Act of 1970
- Clean Water Act of 1987
- Endangered Species Act
- National Historic Preservation Act.

We are expecting to have to hire a specialist to complete reconnaissance of the National Environmental Policy Act (NEPA) documentation. Other Federal policies to be reviewed are the Clean Water Act of 1987, Endangered Species Act, and National Historic Preservation Act.

Pursuant to the Geothermal Steam Act of 1970 (Title 30 U.S.C. Chapter 23), as amended, the Bureau of Land Management (BLM), an agency of the U.S. Department of the Interior, leases federal lands and reviews permit applications for geothermal development on those lands. The U.S. Forest Service, an agency of the U.S. Department of Agriculture, manages federal public lands in national forests and grasslands. Allegany National Forest in PA and the Monongahela National Forest in WV fall within our study area but these are not expected to have the required heat demand for a project in the near future. The Federally owned land within the NY, PA, and WV Appalachian Basin vicinity are typically related to military bases (Figure 2). There are many of them, but the total land holdings by the federal government is small.

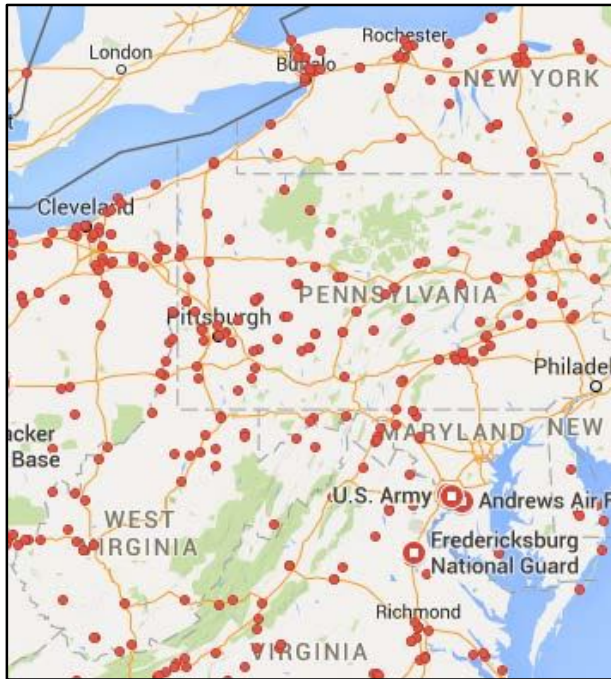


Figure 2. The US Federal Land sites for military facilities in New York, Pennsylvania and West Virginia shown as red dots.

Federal law, however, does not preempt state water laws and even on Federal land, all state laws must be met. The exact steps that are required to permit a geothermal resource vary depending upon where it is located and the land use at the time of development. Generally the steps can be summarized as follows:

- Gain access to lands.
- Contact local and state agencies to determine the requirements for local land use laws including zoning, land use, and building permits.
- Contact federal agencies, if required.
- Secure water rights, if applicable.
- Secure mineral rights as needed.
- Prepare environmental review as required by the National Environmental Policy Act or state environmental laws.
- Obtain well construction permit.
- Drill exploration wells.
- Identify the composition of the resource, which may affect the level of environmental impacts, waste disposal, etc.
- Determine fluid disposal plan and obtain permits for underground injection or surface disposal.
- Contact state agricultural department or state fish and wildlife agency if developing an aquaculture project.
- Drill production and injection wells.
- Drill monitoring wells if required.

As geothermal projects involve many notification forms, permits, and licenses to be submitted, the process can take months to a year to get all approvals required. There is the OpenEI website for some

Western US States that is helpful for us to understand the potential Federal requirements for geothermal sites in the Appalachian Basin (<http://en.openei.org/wiki/RAPID/Geothermal>).

There are fees for Federal Land Permits. According to the 2012 documentation by Witherbee et al. (2013) the fees will be approximately \$1500 (Table 1).

According to the Flowchart for the Geothermal Development Process completed in 2012 by the Regulatory Roadmap Committee, it can take three to five years for all the exploration and permitting processes to be completed. The goal of this project is to speed up this timeline by working with private individual/corporation/federal sites where they own both land surface and mineral rights and are capable of using the produced heated fluids.

Table 1. BLM Fees for Processing Geothermal and Oil and Gas Documents and Applications on BLM and USFS lands as of 2012 (Witherbee et al., 2013).

Geothermal and Oil and Gas Application / Document ²	FY 13
Geothermal Drilling Permit (GDP) – <i>Geothermal only</i>	\$0
Application for Permit to Drill (APD) – <i>Oil and Gas only</i>	\$6,500
Noncompetitive lease application (From #)	\$390
Competitive lease application	\$150
Assignment and transfer of record title or operating right	\$85
Name change, corporate merger or transfer to heir/devisee	\$205
Lease consolidation	\$430
Lease reinstatement	\$75
Nomination of land – <i>Geothermal only</i>	\$110
Plus per acre nomination fee – <i>Geothermal only</i>	\$0.11
Site license application – <i>Geothermal only</i>	\$60
Assignment or transfer of site license – <i>Geothermal only</i>	\$60

¹ 43 CFR § 3200.12

² Note: with the exception of drilling permit fees, most other fees are the same for geothermal as for oil and gas.

Native American Lands

As Sovereign Nations, tribes have inherent authority over their land. Their approval must be obtained to use or lease tribal resources, e.g., land, water, and minerals. Tribes are not subject to state regulation; they can negotiate with state and local governmental agencies. Permitting for a project on Indian land may take different paths and will be through the Tribal Agency and the Department of Interior.

Figure 3. Map of Native American reservations in the study area and adjacent states, also showing county boundaries. New York has 8 federally recognized reservations, whereas West Virginia and Pennsylvania have none. Tribal lands codes: 6 – Allegany; 33 – Cattaraugus; 165 – Oil Springs; 167 – Oneida; 168 – Onondaga; 253 – St. Regis; 265 –Tonawando; 274 – Tuscarora.



State Permits and Licenses

The following are examples of types of permits and licenses a geothermal developer may have to obtain from the state:

- Conditional use
- Exploration
- Well construction and drilling
- Water rights
- Air emissions
- Fluid disposal
- Building construction
- Power facility
- Hazardous waste disposal
- License for direct uses
- Endangered species.

Permits for Geothermal in Local Communities

In addition to state agencies, a developer must also contact local and county agencies to determine the licenses and permits they may require. Relevant local and county agencies include:

- Local land use boards
- Local planning commissions
- Zoning boards
- County boards of commissioners

- Local sewer and water districts
- Regional boards, e.g., air pollution and water control districts.

New York Geothermal Permitting

In New York State, geothermal wells deeper than 500 feet are permitted in the same manner as oil and gas wells. There are required permits for water withdrawal for sites producing more than 100,000 gpd. There is also a permit for brine injection wells following the US EPA regulations.

The permitting authority is the New York Division of Mineral Resources within the Department of Environmental Conservation.

NYSDEC
 Division of Mineral Resources
 625 Broadway
 3rd Floor
 Albany NY 12233-6500
 518-402-8056
oilgas@dec.ny.gov

The DEC website is very helpful. The main site for oil and gas is <http://www.dec.ny.gov/energy/205.html>

There are links from there to all the other information and forms required.

Drilling Permit

Application for drilling can be made through an onsite paper form or online submission if outside the area. The application consists of the following steps:

- 1) **Oil and Gas Organization Report** - to be notarized, submitted and approved before the permit application is submitted.
 - a. This report includes: contact information, person(s) responsible for correspondence, and type of well drilled (geothermal is listed as a choice).
- 2) **Financial Security** documents – there is a worksheet to calculate the amount. You can chose between A. Bond, B. Cash, C. Escrow account, D. Irrevocable letter of credit, E. Certificate of Deposit
- 3) **Drilling Permit** application form and the following:
 - three copies of a plat (i.e. a survey map)
 - three copies of a map of the proposed spacing unit (for geothermal there will be at least two wells)
 - Affirmation of Acreage Control and Rights in Target Formation
 - the proposed drilling program (note there are casing requirements)
 - fee: examples 4000 ft = \$1620, 6000 ft = \$2380, 8000 ft = \$3140
 - Division of Mineral Resources' well permitting Environmental Assessment Form

- Includes information about the physical setting of the proposed project, the general character of the land and land use, the size of the area disturbed and the length of time the drilling rig will be on the site. The applicant must also describe the procedures that will be used to construct the access road, supply water for drilling, contain and dispose of wastes and how to reclaim the site.
- Note: Drilling must be performed by a drilling contractor registered with the NY Division of Mineral Resources.
- Note: The operations must be commenced within the 180 day permit period.

Drilling Permit Fees

As stated above, fees are based on well depth (eg. 4000 ft. = \$1620, 6000 ft. = \$2380, 8000 ft. = \$3140).

Water Withdrawal Permits

The forms for Water Withdrawal Permits are found on the DEC website

- <http://www.dec.ny.gov/lands/94327.html>. Applications for "New Permits" are submitted to the Division of Environmental Permits in the DEC region where the water extraction will be located. Projects expected to produce at least 100,000 gpd are required to submit a permit.

Injection Well Permits

A well permit is required from the Division of Mineral Resources for any brine disposal well deeper than 500 feet. Also a Class IID Underground Injection Control permit must be obtained from the Region II Office of the USEPA before operating any well for brine disposal. EPA staff review proposed operations with respect to protection of groundwater aquifers. Parameters reviewed by the EPA may include well construction and plugging plans, proposed injection rate and pressure, injectate composition, and proposed injectate and groundwater monitoring plans. The EPA contact for New York permits is:

Ms. Nicole Foley Kraft
 USEPA Ground Water Compliance Section
 290 Broadway, 20th Floor
 New York, NY 10007-1866
 (212) 637-3093 Fax: (212) 637-3953

County/City Building Permits

There is a State of New York 2010 Building Codes and Energy Code that all buildings must meet. Depending on the county size and city size, there may be local building permits. For example, the city of Ithaca, NY requires a building permit if changes occur to building plumbing. The usual permitting process approval/rejection timeframe for Ithaca is 30 days. Whereas, the county of Steuben has a planning office that will provide technical assistance to local municipalities in land use planning and regulation, economic development and environmental protection. If there are not specific requirement for permits related to construction, buildings, drilling, etc., then zoning requirements will need to be followed along with all the state codes.

Pennsylvania Geothermal Permitting

Pennsylvania Department of Environmental Protection (PADEP) is the agency overseeing the permitting of the Oil and Gas Industry. As there are no established mineral rights for geothermal energy in Pennsylvania, our project well depth falls most closely within the permits of this agency.

Oil and gas exploration is regulated under the state's oil and gas laws (Oil and Gas Act, Coal and Gas Resource Coordination Act, and Oil and Gas Conservation Law) and the environmental protection laws that include the Clean Streams Law, the Dam Safety and Encroachments Act, the Solid Waste Management Act, the Water Resources Planning Act and the Community Right to Know Act. As we develop a geothermal district heating system, the wells drilled for production and injection will be regulated under these laws.

http://www.portal.state.pa.us/portal/server.pt/community/laws%2C_regulations_guidelines/20306

Drilling Permit

With so many permits required, Pennsylvania has an online tool to help determine which type of permits, bonds, licenses are needed. It is called the Permit Application Consultation Tool (PACT) <http://www.ahs.dep.pa.gov/PACT/>. There is a Pre-Application Conference with PADEP to discuss and verify project results and permit coordination.

Once the required specific documentation is determined, we will find them in the Permit/Authorization Packages in the e-Library. Forms and information for the Oil and Gas Industry can be found at <http://www.elibrary.dep.state.pa.us/dsweb/View/Collection-8294>.

Tracking the progress of permits through Pennsylvania's Environment Facility Application Compliance Tracking System (eFACTS) is possible through the website <http://www.ahs.dep.pa.gov/eFACTSWeb/default.aspx>. It is also possible to receive updates from PADEP's Electronic Notification System (eNOTICE). This will be helpful for confirming the project permits are staying on the designated timeframe.

Note – In Pennsylvania there is a lot of underground coal mining so this is something they look at closely when a permit is submitted.

During Phase 1 of this project, our team has held two meetings with the Pennsylvania Department of Conservation and Natural Resources (PADCNR) to discuss their existing well data and to update them on our results. We plan on working with them throughout the permitting process as they provide valuable input and can help liaise with PADEP. In the most recent meeting in August 2015, PADCNR were especially interested in working with us to find locations we could develop for geothermal district heating. The permitting process with their assistance will take time, but is expected to have a workable solution to fit the considerations of geothermal drilling into the oil and gas regulations.

Drilling Permit Fees

Fees are calculated using drill depth. For example, 5000 feet = \$650, 10,000 feet = \$1650

Water Withdrawal Permits

In general, there is no comprehensive legal or institutional approach to water use in Pennsylvania. The Department of Environmental Protection Bureau of Water Supply Management grants allocation permits to public water systems that use surface water. We will contact this agency to see if they require a permit for our project.

Reinjection Wells

In Pennsylvania, deep injection wells or brine disposal wells are regulated by the Environmental Protection Agency through the Underground Injection Control Program (UIC). The US EPA took over the task of permits, inspections and enforcement from state regulators in 1985.

County/City Building Permits

Pennsylvania has a statewide building code, the Uniform Construction Code (UCC), which falls under the Department of Labor and Industry. The UCC is administered and enforced locally and at the state level. Municipalities within PA can opt-in or opt-out. The status of municipalities is available from <http://www.portal.state.pa.us/portal/server.pt?open=514&objID=553835&mode=2>.

As we move into Phase 2 of the Play Fairway Analysis Project and narrow down the locations of most interest for development in Phase 3, the city/county required permits and codes can be determined.

West Virginia Geothermal Permitting

In West Virginia, geothermal wells are not yet established as a specific category. There are no legislative rulings on how geothermal projects will be classified or how the royalties associated with extracting geothermal fluids from the ground will be linked with the mineral rights owner or the surface owner. To get around this potential barrier of no legislative predetermination of geothermal rights, the focus for West Virginia will look to locations where the surface and mineral right owner is the same entity and there is a large enough tract of land to contain both the production and injection wells.

Drilling Permit

The depth of the wells we are anticipating to drill for this project are similar to those in the oil and gas industry. Therefore as a starting place the permits for drilling and exploration fall within the West Virginia Department of Environmental Quality Office of Oil and Gas. The details for permitting can be found through their website <http://www.dep.wv.gov/oil-and-gas/Pages/default.aspx>.

West Virginia has many documents rather than a combined few to submit. A check list for all the filings required is provided (see list below). For a new well, the requirements include the same items as New York, with the addition of surface and royalty owner signatures needed and a worker's comp plan established.

Table of West Virginia Check List of forms to submit for Permitting a well.

- WW-2B
- WW-2B signed off by inspector
- WW-2A
- Certified Mail Receipts or affidavit of personal service
- Surface Owner Waiver
- Coal Owner/Lessee/Operator Waiver
- WW-2A (1) including page and book and royalty percentage
- WW-2B (1) (If sources to be tested –names, addresses and location on topo listed as water testing)
- WW-9 (page 1 and 2)
- Inspector Signature on WW-9
- Reclamation Plan
- Mylar Plat
- Topography Map of the proposed location

- _____ Database for Coal Depths, Permits, Boundaries
- _____ Bond Agreements
- _____ A check for \$650.00 shallow well, \$900.00 Deep well
- _____ Workers Comp/Employ/Registered with the SOS.

Drilling Permit Fees

As stated above, fees are based on well depth with a fee of \$650.00 for shallow wells (wells drilled and completed in a formation above the top of the uppermost member of the "Onondaga Group"), and \$900.00 for deep wells (wells drilled and completed in a formation at or below the top of the uppermost member of the "Onondaga Group").

Water Withdrawal Permits

There are permits for withdrawal of water from surface streams, lakes, etc. and drinking water aquifers, that our project will not fall under. The brine fluids expected to be produced in this district heating project will be from formations deeper than potable water sources.

Reinjection Wells

There is a permit for a geothermal reinjection well under the code for the UIC Industrial Commercial Septic Application. This is expected to be only for geothermal heat pumps and not for the larger district heating project brine injection wells. There is also a permit for brine injection wells with a set of permits to submit through the Office of Oil and Gas, which has developed a comprehensive permit package to assist in the preparation of a UIC permit application. Our geothermal district heating project will be under the category of WV Code 1479 Solution Mining wells (3S) that includes recovery of geothermal energy to produce electric power from geothermal injection wells. Although not generating power from the well fluids, the size and flow rates for the wells are more closely tied to electric generation than geothermal heat pumps. For a detailed description and required forms see the document: [Underground Injection Control \(UIC\) Permit Application Package Class 2 & 3](#). The application fee of \$550.00 is submitted with the completed documentation to:

West Virginia Department of Environmental Protection
Office of Oil and Gas
Underground Injection Control (UIC)
601 57th Street, SE
Charleston, WV 25304

<http://www.dep.wv.gov/oil-and-gas/GI/Forms/Documents/UIC%20APPLICATION%20PACKAGE%2006-25-2014.pdf>

There is a form for Oil and Gas companies injecting more than 300,000 gallons of water to hydrofrac a well. They are concerned about the flowback and thus disposal of that water. The water produced in this project will be contained within the pipes and be injected properly into a permitted injection well.

County/City Building Permits

The State of West Virginia follows the 2012 International Building Code, 2012 International Plumbing Code, and the 2009 International Energy Conservation Code. Depending on the county size and city size, there may be additional local building permits and fees. For example, the county of Kanawha does not require any additional permits related to construction, buildings, drilling, etc., but it does have the Kanawha County Commission Department of Planning and Development with additional requirements for oil and gas well drilling pertaining to floodplains. The Kanawha County Health Department has an

Environmental Division, which oversees water (typically well or surface water), who are an example of a group to contact as part of the effort for grassroots education on geothermal development. For locations with no specific requirement for additional permits then we will need to be follow all the state codes.

References

- Battocletti, Liz, 2005, An Introduction to Geothermal Permitting, Bob Lawrence and Associates, Inc., online documentation http://www.geothermal-biz.com/Docs/Intro_to_geo_permitting.pdf.
- OpenEI – Geothermal Regulations and Permitting Information Desktop Toolkit, accessed 2015 online documentation <http://en.openei.org/wiki/RAPID/Geothermal>
- Levine, Aaron; Young, Katherine, 2014. Geothermal Development and the Use of Categorical Exclusions Under the National Environmental Policy Act of 1969, GRC Transactions.
- Witherbee, Kermit; Young, Katherine; Levine, Aaron, 2013. Funding Mechanisms for Federal Geothermal Permitting, GRC Transactions.
- Young, Katherine R.; Witherbee, Kermit; Levine, Aaron; Keller, Adam; Balu, Jeremy; Bennett, Mitchell, 2014. Geothermal Permitting and NEPA Timeline Analysis, GRC Transactions.
- Young, Katherine R.; Levine, Aaron, 2014. Geothermal National Environmental Policy Act Database on Open Energy Information, GRC Transactions.
- Young, Katherine R.; Levine, Aaron, 2014. Regulatory and Permitting Information Desktop (RAPID) Toolkit, GRC Transactions.